



*Using De Geer moraines to reconstruct ice sheet retreat in high resolution*

RIVERS, Gwyneth Evelyn

Available from the Sheffield Hallam University Research Archive (SHURA) at:

<https://shura.shu.ac.uk/36015/>

## A Sheffield Hallam University thesis

This thesis is protected by copyright which belongs to the author.

The content must not be changed in any way or sold commercially in any format or medium without the formal permission of the author.

When referring to this work, full bibliographic details including the author, title, awarding institution and date of the thesis must be given.

Please visit <https://shura.shu.ac.uk/36015/> and <http://shura.shu.ac.uk/information.html> for further details about copyright and re-use permissions.

# Using De Geer moraines to reconstruct ice sheet retreat in high resolution

Gwyneth Evelyn Rivers

A thesis submitted in partial fulfilment of the requirements of  
Sheffield Hallam University  
for the degree of Doctor of Philosophy

March 2025

## Candidate Declaration

I hereby declare that:

1. I have not been enrolled for another award of the University, or other academic or professional organisation, whilst undertaking my research degree.
2. None of the material contained in the thesis has been used in any other submission for an academic award.
3. I certify that this thesis is my own work. The use of all published or other sources of material consulted have been properly and fully acknowledged.

The data presented in chapter 6 was obtained in collaboration with Professor Antti E.K. Ojala, Dr Joni Mäkinen, and Camilla Holmroos from the University of Turku, Finland / Geological Survey of Finland, during the fieldwork campaign of June 2023. I played a major role in the preparation and execution of the investigation, the data analysis and interpretation. Sedimentological investigations were undertaken by project collaborators Professor Antti E.K. Ojala, Dr Joni Mäkinen and Camilla Holmroos from the University of Turku and Geological Survey of Finland. Contributions from collaborators, such as diagrams or calibrations, are explicitly referenced in the text.

4. The work undertaken towards the thesis has been conducted in accordance with the SHU Principles of Integrity in Research and the SHU Research Ethics Policy, and ethics approval has been granted for all research studies in the thesis.
5. The word count of the thesis is 70,390.

<b>Name</b>	Gwyneth Evelyn Rivers
<b>Date of Submission</b>	March 2025
<b>Award</b>	PhD
<b>Research Institute</b>	Social and Economic (SERI)
<b>Director of Studies</b>	Dr Robert D. Storrar

## Abstract

This thesis explores the spatiotemporal properties of De Geer moraines (DGMs) in southwest Finland and assesses their utility as high-resolution ice margin indicators. This research provides new insights into DGM formation mechanisms, ice margin geochronometric potential, and discusses implications relative to ice sheet reconstructions. Key findings from this study include the development of a new Python-based ArcGIS toolbox for automated 3D morphometric analyses, quantified morphometric and internal architectural insights, and temporal associations with local clay-varved chronologies, producing an annual-resolution ice margin reconstruction of the southwest Finnish sector of the Fennoscandian Ice Sheet (FIS).

A total of 3 966 DGMs were mapped across southwest Finland and were subdivided into prominent (2 581) and intermediate (1 385) moraines. Morphometric analyses find DGMs to be slightly sinuous and asymmetric in profile. Internal architecture of DGMs located across 4 sites in southwest Finland present proximal to distal transitions whereby proximal sides are characterised by compact laminae and thrust plane structures, and distal sides are characterised by poorly compact diamicton reworked by proglacial water currents. These findings support DGM formation at the grounding line of water-terminating ice margins and provide evidence to accurately position them within a wider ice sheet context. In addition, spatial analyses reveal DGM-subtypes, namely regularly spaced prominent DGMs and irregularly spaced intermediate DGMs, that depict interseasonal variations during formation. Specifically, regularly spaced prominent DGMs are suggested to form via push during winter readvances, whereas irregularly spaced DGMs are suggested to form during periods of summer retreat.

Connections with local clay-varved chronologies show close alignment with annual rates of retreat and demonstrate that an annual signal can be established within De Geer terrain (DGT) enabling annual DGM isochrones to be constructed. The DGM-derived reconstruction in this study presents an annual 714 year long ice margin retreat pattern across southwest Finland between 11 615 – 10 901 cal. years BP, characterised by retreat rates ranging between  $\sim 500 - 2\,000\text{ m/yr}^{-1}$ . This is a significant refinement to that of the current highest resolution (e.g. annual compared to 100-year resolution) and provides detailed insights into grounding line processes whereby interrelationships between temperature, water depth and topography drive ice margin retreat. Specifically, the dynamic fluctuations of ice margin retreat observed at annual timescales infer hinge-driven calving processes as a result of thinning ice, increasing water depths and smooth, shallow-gradient bed topography.

The findings from this study demonstrate that DGMs may be used as valuable ice margin proxies and can capture retreat rates at very high resolution. Furthermore, this work demonstrates how DGMs may offer valuable insight relative to grounding line forcing mechanisms at annual to centennial timescales. Insights produced from this study are particularly valuable for understanding ice sheet retreat dynamics at societally relevant timescales and may assist with projecting changes in contemporary ice sheets. Moreover, this study provides a methodological framework and foundation for future studies that aim to utilise DGMs as ice margin indicators and reveal detailed insights into complex grounding line processes.



## Acknowledgements

*I would like to acknowledge and thank Sheffield Hallam University, the Royal Geographical Society and the Quaternary Research Association for providing funding support for the undertaking of this project.*

*I extend my deepest gratitude to my Director of Studies, Dr Robert Storrar, for his unwavering support, attention to detail, insightful critiques and shared enthusiasm throughout my research journey. His consistent supervision and subject passion have been inspiring and have significantly shaped this work. I am equally thankful to my supervisor Dr Andrew Jones for his insight, constructive feedback and essential suggestions that have significantly enhanced the quality of my work. The support from both Rob and Andrew extends far beyond my thesis, having been a part of my academic journey since undergraduate. It is a privilege to know you.*

*I would like to extend my warmest thanks to Prof. Antti Ojala for such an enjoyable collaboration, and for his consistent enthusiasm, support and knowledge throughout this project. Thank you also for tolerating my over-excitable Finnish over the past few years - se on ollut ilo!*

*I would also like to acknowledge Naomi Holmes. Whilst only briefly supervising this project, Naomi was a key member during fieldwork and provided valuable constructive feedback on my work during the first stages of this project. I would similarly like to thank Joni Mäkinen and Camilla Holmroos who also worked collaboratively on parts of this project.*

*My appreciation also goes out to various staff members in the Department of Natural & Built Environment at Sheffield Hallam University, whose inclusion, support and encouragement have positively influenced and inspired my academic experience. Dr Natasha Dowey and Dr Elizabeth Laycock, I am particularly grateful for your support alongside Rob during some challenging fieldwork whilst out in Iceland. I would also like to thank the technical staff in the Norfolk Resources Department whose flexibility and readiness to assist have helped greatly with the smooth running of various fieldwork and admin related tasks throughout my studies.*

*I would also like to acknowledge my peers (including the PGR SERI Admin Team), for their support, camaraderie, snack sharing and insightful discussions that have inspired (and kept me sane!) throughout this journey. Their support and encouragement have been invaluable to my research experience.*

*Finally, I would like to extend my most heartfelt gratitude to, Steve, who has been with me every step of the way, and without whom the completion of this project would not have been possible. I really can't describe in words what your support has given me; perhaps being lost for words says the most.*

# Contents

Candidate Declaration .....	ii
Abstract .....	iii
Acknowledgements .....	iv
Contents .....	v
List of Tables & Figures .....	xiii
<b>1. Chapter 1: Introduction .....</b>	<b>1</b>
1.1 Rationale .....	1
1.2 Project aim, research questions & objectives .....	3
1.2.1 Research questions .....	4
1.2.2 Research objectives .....	4
1.3 Thesis structure .....	4
<b>2. Chapter 2: Literature Review .....</b>	<b>6</b>
2.1 Importance of ice sheet reconstructions .....	6
2.2 Spatial & temporal resolutions of ice sheet reconstructions .....	9
2.2.1 Increase the input geomorphological dataset .....	11
2.2.2 Increase frequency of absolute chronological ages .....	12
2.2.3 Seek out alternative landforms .....	12
2.3 Geomorphological indicators in ice sheet reconstructions .....	14
2.3.1 Ice marginal features .....	14
2.3.1.1 Outwash fans .....	14

2.3.1.2	Grounding zone wedges.....	16
2.3.1.3	Trough mouth fans.....	17
2.3.1.4	Corrugation ridges.....	18
2.3.1.5	Ice-marginal moraines.....	20
2.3.1.6	Ice-dammed lakes.....	21
2.3.1.7	Ice-marginal meltwater channels.....	22
2.3.1.8	Thrust-block moraines.....	25
2.4	A review of the literature on DGM formation.....	27
2.4.1	DGM formation hypothesis (1).....	29
2.4.2	DGM formation hypothesis (2).....	31
2.4.3	DGMs in ice sheet reconstructions.....	35
2.5	Crevasse-squeeze ridges.....	35
2.5.1	CSR formation.....	37
2.5.2	CSRs in ice sheet reconstructions.....	38
2.6	Ice sheet evolution since the Last Glacial Maximum.....	38
2.6.1	The Fennoscandian Ice Sheet.....	42
2.7	Summary.....	45
<b>3.</b>	<b>Chapter 3: Method overview and key study areas.....</b>	<b>47</b>
3.1	Introduction.....	47
3.2	Methods.....	47
3.2.1	Remote sensing & geomorphological mapping.....	47
3.2.1.1	Morphometric analysis.....	49
3.2.2	Sedimentology & Ground Penetrating Radar (GPR).....	49

3.2.3	Ice margin reconstruction.....	50
3.3	Study areas.....	51
3.3.1	Southwest Finland.....	51
3.3.2	Northwest Territories, Canada.....	56
4.	<b>Chapter 4: Method Development – A Python-based ArcGIS toolbox to automatically generate 3D morphometric data of elongated landscape features at user-defined transect-segmented intervals</b> .....	59
4.1	Introduction.....	60
4.1.1	Morphometry studies.....	60
4.1.2	Remotely sensed high-resolution DEM data.....	60
4.1.3	Morphometric quantification.....	61
4.1.4	Challenges in morphometric analysis.....	61
4.2	The toolbox.....	62
4.2.1	Data preparation.....	63
4.2.2	Toolbox operation and required inputs.....	63
4.2.2.1	The primary tool.....	63
4.2.2.1	The secondary tool.....	64
4.2.3	Geoprocessing methods and morphometry calculation.....	64
4.2.4	Generated outputs.....	69
4.2.4.1	Primary tool ‘3D Morphometry Tool’.....	69
4.2.4.2	Secondary tool ‘Average Feature Morphometry Tool’.....	70
4.2.5	Quality control checks.....	70
4.2.6	Script execution.....	71
4.2.7	Software requirements and availability.....	72

4.3	Example application.....	72
4.3.1	Target geomorphology & study area.....	72
4.3.2	Feature digitisation / mapping.....	75
4.3.3	Tool execution.....	76
4.3.3.1	Primary tool execution '3D-Morphometry-Tool'.....	76
4.3.3.2	Generated outputs (primary tool).....	76
4.3.3.3	Quality control.....	80
4.3.3.4	Secondary tool execution 'Average-Feature-Morphometry'....	80
4.3.3.5	Generated outputs (secondary tool).....	80
4.3.4	Further analysis.....	80
4.3.4.1	Data visualisation.....	80
4.3.4.2	Statistical tests.....	81
4.4	Wider applications.....	83
4.5	Additional advice & comments.....	84
4.6	Conclusions.....	85
5.	<b>Chapter 5: 3D morphometry of De Geer Moraines and Crevasse-Squeeze Ridges: Differentiating between pushing and squeezing mechanisms from remotely sensed data.....</b>	<b>86</b>
5.1	Introduction.....	87
5.2	Formation of DGMs & CSRs.....	88
5.2.1	De Geer moraines.....	88
5.2.2	Crevasse-squeeze ridges.....	91
5.3	Study areas.....	94
5.3.1	Southwest Finland (DGMs).....	94

5.3.2	Northwest Territories, Canada (CSRs)	95
5.4	Methods	97
5.4.1	Data collection	97
5.4.2	Quality control: relative accuracy	97
5.4.3	Morphometric calculations	98
5.5	Results	98
5.5.1	Summary statistics	98
5.5.2	Statistical tests	103
5.5.3	Landform summary	105
5.5.4	Spatial observations	107
5.5.4.1	Single feature variability	107
5.5.4.2	Macroscale variations	109
5.6	Discussion	112
5.6.1	Glacial dynamics – the importance of DGMs & CSRs	112
5.6.2	CSR morphometry indicates crevasse in-filling	113
5.6.3	Lateral continuity of DGMs indicates ice-marginal formation	114
5.6.4	DGM asymmetry indicates ice-marginal advance	115
5.6.5	Wider spatial variability of prominent DGM morphometry	115
5.6.6	Wider spatial variability of CSR morphometry	116
5.6.7	Intermediate De Geer moraines	116
5.7	Conclusions	117
6.	<b>Chapter 6: De Geer moraine internal architecture based on sedimentological and geophysical investigations and implications for ice marginal reconstructions</b>	<b>118</b>

6.1	Introduction.....	119
6.2	Study sites & general characteristics of DGMs in southwest Finland.....	122
6.3	Methods.....	126
6.3.1	Sedimentological Investigations.....	126
6.3.2	Geophysical Investigations and radar facies identification.....	128
6.3.3	Uncrewed aerial vehicle field observations.....	129
6.4	Results and interpretation.....	129
6.4.1	Site (1) UT1 (Uimarannatie, Haaro, Perniö (60.249°N; 23.283°E)).....	129
6.4.2	Site (1) UT2 (Uimarannatie, Haaro, Perniö (60.248°N; 23.283°E)).....	137
6.4.3	Site (2) Makarla, Ylönkylä (60.169°N; 22.977°E).....	144
6.4.4	Site (3) Kurajoki, Porkka (60.482°N; 23.258°E).....	146
6.3.5	Site (4) Suorsala, Mynämäki (60.700°N; 21.813°E).....	148
6.5	Discussion.....	150
6.5.1	DGM internal architecture.....	150
6.5.2	Proposed conceptual model.....	152
6.5.3	Implications for ice marginal reconstructions.....	157
6.6	Conclusions.....	158
7.	<b>Chapter 7: An annual ice margin reconstruction and investigation of grounding line mechanics in the southern Baltic Sea Ice Lobe area of the Finnish sector of the Fennoscandian Ice Sheet using De Geer moraines as geochronometric indicators.....</b>	<b>160</b>
7.1	Introduction.....	161
7.2	Study Area.....	166
7.3	Methods.....	168
7.3.1	DGM mapping.....	168

7.3.2	Isochrone construction.....	169
7.3.3	Geochronological anchoring.....	172
7.3.4	Analysis of grounding line forcing mechanisms.....	174
7.4	Results.....	176
7.4.1	Grounding line variables.....	180
7.4.1.1	20-year resolution results.....	180
7.4.1.2	Annual resolution results.....	184
7.5	Discussion.....	192
7.5.1	Deglaciation chronology and ice margin characteristics.....	192
7.5.2	Grounding line forcing mechanisms during deglaciation.....	193
7.5.2.1	11 615 – 11 531 cal. yr BP.....	193
7.5.2.2	11 530 – 11 350 cal. yr BP.....	193
7.5.2.3	11 349 – 11 150 cal. yr BP.....	194
7.5.2.4	11 149 – 11 000 cal. yr BP.....	194
7.5.2.5	10 999 – 10 901 cal. yr BP.....	195
7.5.2.6	Grounding line forcing mechanisms.....	195
7.5.3	Precision & limitations.....	198
7.6	Conclusions.....	200
<b>8.</b>	<b>Chapter 8: Discussion.....</b>	<b>202</b>
8.1	Research questions.....	202
8.2	Research objectives.....	202
8.3	RQ1: How do DGMs form, and how do they reflect the position of ice margins? .....	202



8.3.1	Key morphometry & spatial distribution findings.....	203
8.3.2	Key internal architecture findings.....	203
8.4	RQ2: At what timescales do DGMs form? .....	208
8.4.1	Key findings.....	208
8.5	RQ3: How does increased spatial and temporal resolutions in ice sheet reconstructions help to improve the current understanding of ice sheet retreat rate and grounding line processes?.....	210
8.5.1	Key findings.....	210
8.6	Limitations.....	214
8.6.1	Methodological challenges.....	214
8.6.2	Analyses & cumulative errors.....	215
8.6.3	Implications & comparability.....	215
8.7	Directions for future research.....	216
8.7.1	Expand spatial analysis.....	216
8.7.2	Investigate calving processes.....	216
8.7.3	Investigate slope as a grounding line variable.....	216
8.7.4	Temporal refinement.....	217
8.7.5	Experimentation with numerical modelling.....	217
8.8	Summary.....	218
<b>9.</b>	<b>Chapter 9: Conclusions .....</b>	<b>220</b>
	References.....	223
	Appendices.....	293

## LIST OF TABLES & FIGURES

**TABLE 4.1.** *Geoprocessing steps and calculation methods for each morphometric.*

**TABLE 4.2.** *Reference table showing the generated 'Transect\_Morphometry.shp' attribute table field names and relative morphometrics.*

**TABLE 4.3.** *Reference table showing the generated 'Av\_Feature\_Morphometry.shp' attribute table field names and relative morphometrics.*

**TABLE 5.1.** *Summary statistics of quantified prominent DGM morphometrics (Rivers et al., 2023).*

**TABLE 5.2.** *Summary statistics of quantified intermediate DGM morphometrics. (Rivers et al., 2023).*

**TABLE 5.3.** *Summary statistics of quantified CSR morphometrics. (Rivers et al., 2023).*

**TABLE 5.4.** *Z-test results table summarising each tested morphometric. (Rivers et al., 2023).*

**TABLE 5.5.** *Landform summary table providing a taxonomic generalisation of prominent DGMs, intermediate DGMs and CSRs. (Rivers et al., 2023).*

**TABLE 6.1.** *Summary of interpreted radar facies based on correlations with UT1 and UT2 lithofacies as presented in Appendices Figures 2 & 8.*

**FIGURE 1.1.** *Hillshaded LiDAR DEM showing examples of DGM fields located in Finland. A) Ruokojärvi, Kuovola; B) Kortistonkulma, Hyvinkää; C) Etu-Holsti, Porvoo; D) Kituranta, Jämijärvi [source: Ojala, 2016].*

**FIGURE 2.1.** *Corrugation ridges on the mid-Norwegian margin. A) Map showing high-resolution bathymetric data coverage and corrugation ridge spacing along measured transects in study; b) Corrugation ridges in mid-Trænadjupe; c) Corrugation ridges in inner Sklinnadjupe; d) Corrugation ridges in inner Sklinnadjupe [source: Batchelor et al., 2023].*

**FIGURE 2.2.** Outwash plain, Charlesbreen, Svalbard [source: Taylor, 2024].

**FIGURE 2.3.** Diagram illustrating the formation controls of GZWs at high-latitude continental margins [source: Batchelor & Dowdeswell, 2015].

**FIGURE 2.4.** conceptual models of high-gradient (A) and low-gradient (B) trough mouth fans [source: Rydningen et al., 2015].

**FIGURE 2.5.** Conceptual sketches illustrating formation mechanisms for corrugation ridges [source: Jakobsson et al., 2011].

**FIGURE 2.6.** Location map showing the major end moraines around Fennoscandia. Black box indicates the location of the First, Second and Third Salpausselkäs in southern Finland [source: Lunkka et al., 2020].

**FIGURE 2.7.** Image showing the extent and position of the former Baltic Ice Lake and White Sea Ice Lake at approximately (~12 300 – 11 600 ka BP (Donner, 2010)) positioned along the southeast margins of the former Scandinavian Ice Sheet (SIS) [source: Lunkka, 2023].

**FIGURE 2.8.** Palaeo-ice-marginal meltwater channel in the summer areas of Hazelton Mountains [source: Margold et al., 2013].

**FIGURE 2.9.** Proglacial moraine complex characterised by thrust-block moraines at the margin of the Leverett Glacier, western Greenland [source: Waller, 2013].

**FIGURE 2.10.** Digital Elevation Model capturing distinct and regular De Geer moraine landforms situated in SW Finland: A) Södra Vallgrund, B) Koskela, C) Kaidanpää, D) Ruokojärvi [source: Ojala et al., 2015].

**FIGURE 2.11.** Schematic diagram of DGM formation hypothesis (1). A sub-aqueous ice-marginal process by which subglacial sediment is advected toward and deposited at the grounding line.

**FIGURE 2.12.** Schematic diagram of DGM ‘crevasse-squeeze ridge’ formation hypothesis (2). Diagram illustrates the squeezing of sediments into subglacial crevasses formed behind the ice margin.

**FIGURE 2.13.** Schematic diagram of DGM ‘channelised meltwater conduit’ formation theory. Diagram illustrates meltwater drainage via surface crevasses. Sediments are then deposited within basal crevasses behind the ice margin via sediment-laden meltwater conduits.

**FIGURE 2.14.** Aerial images of CSR landforms (arrows indicate ice flow direction). A) Kjerulfbreen, Trygghamna, Svalbard; B) Brúarjökull, Iceland; C) submarine geometric ridges, Wahlenbergbreen, Yoldiabukta, Svalbard; and D) Sefströmbreen, Brevika, Svalbard [source: Ben-Yehoshua, 2017].

**FIGURE 2.15.** The marine oxygen isotope record from the NorthGRIP ice core showing warming and cooling events over the last 125 ka [source: Lowe & Walker, 2014].

**FIGURE 2.16.** Glacial ice extent at approximately 20 000 ka BP [source: Gowan et al., 2021].

**FIGURE 2.17.** Reconstruction of the Eurasian Ice Sheet at ~20 ka BP showing ‘minimum’ (black dotted lines), ‘maximum’ (black dashed) and ‘most credible’ (solid white line and shaded white area) extents [source: Hughes et al., 2016].

**FIGURE 2.18.** Map showing large Salpausselkä moraines (SS I, II & III) that can be traced north eastwards through southeast Finland, Russian Karelia and the Kola peninsula [source: Saarnisto & Saarinen, 2001].

**FIGURE 3.1.** Study area for investigations of DGMs located across southwest Finland.

**FIGURE 3.2.** Post YD independent ice lobe formations situated across Finland. North Karelian Ice Lobe (NKIL), Näsijärvi Ice Lobe (NJIL), Finnish Lake District Ice Lobe (FLDIL), Baltic Sea Ice Lobe (BSIL): A) Inset map showing the most prominent Younger-Dryas age end moraines in Fennoscandia; B) Ice lobe formations and Salpausselkä moraines extending across Finland [source: Lunkka et al., 2019].

**FIGURE 3.3.** Location map showing the subdivision of the Baltic Sea Ice Lobe. Pink area represents the Loimaa sublobe, characterised by murtoo geomorphology, the green area represents the Southern sublobe, characterised by DGM geomorphology [figure edited from Mäkinen et al., 2023]. NB: Inset Fig. B not shown.

**FIGURE 3.4.** Location of the former Baltic Ice Lake (BIL) extending from SE Finland in a south-westerly direction toward SE Sweden. The BIL was characterised by distinct developmental stages that responded to ice advance/retreat phases and continental adjustments [source: Stroeven et al., 2016].

**FIGURE 3.5.** The North American Ice Sheet Complex (NAISC: comprising the Innuitian, Cordilleran and Laurentide ice sheets) [source: Dalton et al., 2023].

**FIGURE 3.6.** Study area chosen for CSR data collection; a 20 km<sup>2</sup> section of the former Great Slave Lake Ice Stream, located in the Northwest Territories, Canada [ice stream data source: Margold et al., 2015]. Location map shows the study area situated inside of the shear margin of the palaeo-ice stream.

**FIGURE 4.1.** A) Oblique view of digitised landform and generated transects. Basic morphometrics are calculated from outlines and crestlines (e.g. length, sinuosity and footprint area). B) Cross-sectional view of a digitised landscape feature highlighting the three elevation points along each transect. Asymmetry is calculated along each transect at the point of crestline intersection. A mean average base terrain elevation is calculated from the 'Base Terrain Elevation Points' (e.g. the two end points of each transect located on the crestline). The height is calculated from the difference between the 'Mean Base Elevation' and the 'Crestline Elevation'. Width is calculated based on the extent of the digitised outlines. C) Oblique view of a digitised landscape feature with derived metrics. Cross-sectional area is calculated based on the principles of a triangular prism (e.g.  $0.5 \times \text{width (transect length)} \times \text{height}$ ). Cross-sectional volume is calculated for each 'transect segment' (e.g.  $\text{cross-sectional area} \times \text{segment length (transect interval)}$ ). See calculation table (TABLE 1) for each morphometric reference.

**FIGURE 4.2.** Schematic workflow illustrating ArcMap tool integration and 3D morphometric calculations.

**FIGURE 4.3.** Example of a digitised feature. Note, a section of the feature is quite sinuous. Depending on the digitised outline placement, this can result in transects that do not intercept the feature outline and therefore are not clipped to the feature extent. As such, careful digitisation with close alignment to the identified feature is important to maximise accuracy. Distorted transects can be easily identified by a visual assessment of transect

placement and by reviewing the attribute table for any anomalous results. In addition, a transect has been removed to rectify anomalous height values - this procedure can be repeated for the distorted transects.

**FIGURE 4.4.** A series of aerial photographs showing CSRs located in the Northwest Territories, Canada [photographs courtesy of Roger Paulen, Geological Survey of Canada].

**FIGURE 4.5.** DEM (Hillshade) of CSR landforms located in the Northwest Territories, Canada. CSRs are orientated transverse to former ice flow direction (southeast to northwest). [DEM source: ArcticDEM - Porter et al., 2018].

**FIGURE 4.6.** Study area selected for mapping crevasse-squeeze ridges. Location: Great Slave Lake palaeo-ice stream, Northwest Territories, Canada [ice stream data source: Margold et al., 2015].

**FIGURE 4.7.** Example of a manually digitised crestline (pink) and outline (blue) of an identified target feature (CSR). A) Slope rendered DEM to accurately identify central and lateral slope breaks in the feature; B) Hillshade rendered DEM to identify the target feature [DEM source: ArcticDEM - Porter et al., 2018].

**FIGURE 4.8.** Example of generated transects upon execution of the primary tool '3D-Morphometry-Tool' with inset attribute table showing calculated morphometrics per transect. Transects are oriented  $90^{\circ}$  to the feature crestline and are spaced at 10 m intervals [slope rendered DEM source: ArcticDEM - Porter et al., 2018].

**FIGURE 4.9.** Series of automatically generated summary histograms providing a graphical representation of the initial calculated transect morphometry. A) cross-sectional volume, B) asymmetry, C) cross-sectional area, D) average slope, E) height and F) width.

**FIGURE 4.10.** Example transect morphometry visualisation showing transects generated at 10 m intervals. The 'cross-sectional area' calculated along each transect are shown and colour-graded to represent high (red) - low (blue) values. This is a powerful method in which to analyse variations along single features. This method can be repeated for each morphometric as required. In addition, the wider scale visualisation of calculated morphometrics at each transect segment is a useful method to explore any spatial clustering as demonstrated in this example. [DEM source: ArcticDEM - Porter et al., 2018].

**FIGURE 4.11.** Example results of 'Getis-Ord Gi\* Hot Spot Analysis' conducted on the 'TOTAL\_VOL' attribute of the 'Av\_Feature\_Morphometry.shp' file. Results show a statistically significant clustering in CSR volumes (central clustering of higher values and southward clustering of lower values). [DEM source: ArcticDEM - Porter et al., 2018].

**FIGURE 4.12.** Wider spatial coverage results of 'Getis-Ord Gi\* Hot Spot Analysis' conducted on the 'TOTAL\_VOL' attribute of the 'Av\_Feature\_Morphometry.shp' file. Results show a statistically significant clustering in CSR volumes. An inset histogram is provided to summarise feature volume of the dataset [DEM source: ArcticDEM - Porter et al., 2018; Ice stream flow direction source: Margold et al., 2015].

**FIGURE 5.1.** Digital Elevation (DEM) with multi-directional hillshade (MDOW) and oblique aerial drone imagery capturing distinct and regularly spaced De Geer moraine formations situated in SW Finland. Intermediate De Geer moraines can also be in image C. A) Torholankulma, Salo; B) Kurimäki, Salo; C) Konnonperä, Isokyrö; D) Palpuro, Hyvinkää; E) Haaro, Perniö and F) Suorsalantie, Mynämäki [DEM source: ©National Land Survey of Finland, LiDAR digital elevation mode, 2/2023] (Rivers et al., 2023).

**FIGURE 5.2.** A) Series of aerial photographs of CSR landforms located in the Northwest Territories, Canada [courtesy of Roger Paulen]. B) Hillshaded DEM showing example CSRs identified across a section of the former Great Slave Lake ice stream, northwest Territories, Canada [DEM source: ArcticDEM – Porter et al., 2018].

**FIGURE 5.3.** Study area selected for DGM data collection in southwest Finland. The location of De Geer moraines fields has been adapted from Ojala (2016) and Baltic Sea Ice Lobe boundary and Salpausselkä moraine positions are based on Palmu et al., (2021). The study area encompasses DGMs that are positioned northwest of the second Salpausselkä moraine (Rivers et al., 2023).

**FIGURE 5.4.** A) Study area chosen for CSR data collection; a 20 km<sup>2</sup> section of the former Great Slave Lake Ice Stream, Northwest Territories, Canada [ice stream data source: Margold et al., 2015]. Location map shows the study area situated inside of the shear margin of the palaeo-ice stream. B) Hillshaded DEM indicating mapping extent of CSRs at the study area. Imagery shows ridges arranged in a linear and cross-cutting configuration. [DEM source: ArcticDEM – Porter et al., 2018] (Rivers et al., 2023).

**FIGURE 5.5.** A series of boxplots presenting comparative summary statistics of quantified prominent DGM, intermediate DGM and CSR morphometry data. A) Transect Height, B) Transect Width, C) Transect Average Slope, D) Transect Asymmetry, E) Feature Length, F) Feature Sinuosity, G) Average Width Standard Error, and H) Average Cross-Sectional Area Standard Error. The lower and upper whiskers represent the minimum and maximum values of the data respectively with outliers residing outside of each whisker limit, the box represents the interquartile range (IQR) (e.g. 50% of the data) with the lower limit representing the lower quartile (Q1) and the upper limit representing the upper quartile (Q3). The central interquartile line represents the median value of the dataset. The white + symbol represents the mean average value. Extreme values that extended far beyond the general dataset were removed. (Rivers et al., 2023).

**FIGURE 5.6.** Schematic figure of Landform Summary Table 5.5, showing generalised morphometric differences between prominent DGMs, intermediate DGMs and CSRs. Prominent DGMs show as slightly more sinuous and asymmetrical in profile, whereas CSRs appear generally larger and straighter. NB: Prominent DGMs are typically the longest landforms across the groups; however, due to laterally discontinuity and mapping strategy, results may not always reflect this.

**FIGURE 5.7.** Transect morphometry visualisation showing transects generated at 20 m intervals for each landform group: A) prominent DGMs; B) intermediate DGMs, and C) CSRs. The cross-sectional area calculated along each transect are shown and colour-graded to represent high (red) to low (blue) values. [DEM sources: A & B: ®National Land Survey of Finland, LiDAR digital elevation model, 6/2023; C: ArcticDEM – Porter et al., 2018]. (Rivers et al., 2023).

**FIGURE 5.8.** Results of 'Getis-ord  $G_i^*$  hotspot analysis'. A) prominent DGMs total feature volume; B) prominent DGMs average feature width; and C) prominent DGMs average feature height (Rivers et al., 2023).

**FIGURE 5.9.** Results of 'Getis-ord  $G_i^*$  hotspot analysis'. A) CSR total feature volume; B) CSR average feature width; and C) CSR average feature height (Rivers et al., 2023).

**FIGURE 6.1.** Location map indicating selected sites across southwest Finland for data acquisition: 1 = Uimarannatie, Haaro, Perniö – sedimentology and GPR; 2 = Makarla, Salo



– GPR; 3 = Kurajoki, Salo – GPR; 4 = Suorsala, Mynämäki - GPR. Note the blue area marks the extent of the Baltic Sea Ice Lobe (BSIL) in which the investigated De Geer moraines are associated.

**FIGURE 6.2.** Hillshaded digital elevation model (DEM) imagery depicting different DGM field types across southwest Finland. A. Kurkela (Salo) - regular, only prominent DGMs. B. Pehtsalo (Laitila) - regular DGMs interspersed with irregular DGMs. C. Pohiperä (Uusikaupunki) - only irregular/more scattered DGMs with a less distinct rhythmic distribution (DEM source: ©National Land Survey of Finland, LiDAR digital elevation model, 2/2023).

**FIGURE 6.3.** Location of excavated sediment exposures at Site (1) Uimarannatie, Haaro, Perniö (see FIGURE 6.1). A. Hillshaded DEM highlighting prominence of DGMs and positioning of sediment excavations. B. Oblique photograph of excavated sediment exposures facing southwest.

**FIGURE 6.4.** Imagery of UT1 excavated sediment exposure. Excavation dimensions: length ~28 m; depth ~2 m. A. Hillshaded DEM indicating location of sediment exposure and GPR profiles along UT1 ridge at site 1 (DEM Source: ©National Land Survey of Finland, LiDAR digital elevation model, 2/2023). B. Photograph viewed from proximal to distal. C. Photograph viewed from distal to proximal. D. Photograph viewed from distal to proximal.

**FIGURE 6.5.** Exposure sketch of UT1 with the original subsurface (bottom) and interpreted (middle) GPR data. GPR data were acquired along the excavation bottom to allow subsurface investigations. Locations of sediment logs are shown (e.g. UT1\_2023\_log1, UT1\_2023\_log2 and UT1\_2023\_log3) which are presented in FIGURE 6.6. Locations of clast macrofabric measurements are indicated, with data presented in rose diagrams and stereonet. Stereonets are plotted on the lower hemisphere of a Schmidt diagram. Lithofacies units are labelled accordingly presented in sediment logs shown in FIGURE 6.6.

**FIGURE 6.6.** Sediment logs presented from UT1 showing unit thickness, composition and internal structures. Lithofacies are interpreted using standardised coding (Evans & Benn 2004). Rose diagrams and stereonet supplement identified units where applicable. Lithofacies codes: Dmm = matrix-supported, massive diamicton; Dms = matrix-supported massive diamicton with shearing structures; Dml = matrix-supported, laminated

*diamicton; Gm = massive gravel, Gs = gravel with shearing structures; Sm = massive sand; Sld = horizontal and draped laminated sand with dropstones; Smd = massive sand with dropstones; Fld = fine laminated silt and clay often with minor fine sand and very small ripples and with dropstones; Fmd = massive silt and clay with dropstones.*

**FIGURE 6.7.** A. Depositional units from the middle part of UT1 excavation. This shows the main ridge composition of the silty-to-sandy diamicton Unit 3a which is draped by the fine-grained and highly fissile/sheared Unit 4. Unit 5 forms the mantle of the ridge composed of bouldery diamicton. B. Strongly sheared and fissile structures of Unit 4. C. View towards the proximal section of the UT1 De Geer ridge. Note the deformed clay layers between Units 3a and 5. White arrows indicate ice flow direction.

**FIGURE 6.8.** Photographs of UT2 excavated sediment exposure. Excavation dimensions: length ~28 m; depth ~2 m. A. Hillshaded DEM showing location of sediment exposure and GPR profiles along UT2 ridge at site 1 (DEM Source: ®National Land Survey of Finland, LiDAR digital elevation model, 2/2023). B. Photograph viewed from distal to proximal. C. Photograph viewed from proximal to distal.

**FIGURE 6.9.** Exposure sketch of UT2. Locations of sediment logs are shown (e.g. UT2\_2023\_log4 and UT2\_2023\_log5); logs are presented in Fig. 10. Clast macrofabric measurement locations are indicated with data presented in both rose diagrams and stereonet (clast macrofabric sample sizes = 50). Stereonets are plotted on the lower hemisphere of a Schmidt diagram. Lithofacies units are labelled accordingly and described in the sediment logs as presented in FIGURE 6.10.

**FIGURE 6.10.** Sediment logs presented from UT2 showing unit thickness, composition and structures. Lithofacies are interpreted using standardised coding (Evans & Benn 2004). Rose diagrams and stereonet accompany identified units where applicable. Lithofacies codes: Dmm = matrix-supported massive diamicton; Dms(s) = matrix-supported massive diamicton with shearing structures; Dml = matrix-supported laminated diamicton; Dcs = clast-supported stratified diamicton; Gm = massive gravel; Gs = gravel with shearing structures; Gcs = clast-supported gravels with shearing; Sm = massive sand; Sld = horizontal and draped laminated sand with dropstones; Smd = massive sands with dropstones.

**FIGURE 6.11.** A. Depositional units from the middle section of UT2 excavation. Note the deformed, sandy sorted sediments of Unit 2 truncated by Unit 3a that forms the main part of the proximal side of the ridge. B. Downslope dipping bedding structures in distal parts of Unit 3b. C. Strongly sheared and fissile structures of Unit 4, similar to UT1, but present only in proximal parts of UT2. White arrows indicate ice flow direction.

**FIGURE 6.12.** Hillshaded DEM showing position of GPR profiles along surveyed ridge at site 2 (DEM Source: ©National Land Survey of Finland, LiDAR digital elevation model, 2/2023).

**FIGURE 6.13.** Radargram #1 at Makarla, Ylönkylä (GPR profiles #2 and #3 are presented in Appendices Figures 14 & 15). Identified radar facies and connected lithofacies are detailed in TABLE 1.

**FIGURE 6.14.** Hillshaded DEM showing position of GPR profiles along surveyed ridge at site 3 (DEM Source: ©National Land Survey of Finland, LiDAR digital elevation model, 2/2023).

**FIGURE 6.15.** Radargram #1 acquired at Kurajoki, Porkka (GPR profiles #2 and #3 are presented in Appendices Figures 16 & 17). Identified radar facies and connected lithofacies are detailed in TABLE 1.

**FIGURE 6.16.** Hillshaded DEM showing position of GPR profiles along surveyed ridge at site 4 (DEM Source: ©National Land Survey of Finland, LiDAR digital elevation model, 2/2023).

**FIGURE 6.17.** Radargram #1 from Suorsala, Mynämäki (GPR profiles #2 and #3 are presented in Appendices Figures 18 & 19). Identified radar facies and connected lithofacies are detailed in TABLE 1.

**FIGURE 6.18.** Proposed conceptual model of inter-seasonal De Geer ridge forming processes. A) Late spring/early summer: fine-grained materials settle out at GL (Unit 2). Ice may depress into bed during temporary stabilisations resulting in coarser-grained sediment extrusion (Unit 3). B) Late summer/early autumn: increased subglacial meltwater transports coarser-grained material to grounding line. Possible proximal compaction may occur due to buoyant flexure of overriding ice (Units 3a/4). Calving

processes occur creating a series of irregularly spaced ridges. C) Late autumn/early winter: ice margin retreated to winter position. Aggregation of glaciofluvial material at grounding line. Possible proximal compaction from buoyant flexure of overriding ice. Release of debris from overriding ice. D) Late winter/early spring: ice re-advance over deposited material. Proximal thrusting and significant shearing deform most notably upper proximal units of ridge (Units 4/5) however, deformation could occur throughout sediment package. Release of debris from overriding ice. E) “De Geer terrain” characterised by regular (winter) and irregular (summer) ridges. Interdistances between winter ridges indicate annual rate of retreat.

**FIGURE 7.1.** Location map showing DGT across southwest Finland within the southern sector of the Baltic Sea Ice Lobe. Salpausselkä moraines indicated by black polygons (SS I, SS II & SS III). Deltas are indicated by blue dots; red line (dotted line - speculative) depicts the position of Baltic Sea water drop estimated at between ~11 620 – 11 560 cal. years BP (Andrén et al., 2002; Donner, 2010; Saarnisto & Saarinen, 2001; Stroeven et al., 2015).

**FIGURE 7.2.** Hillshaded DEM imagery showing ice margin isochrone construction from designated moraines across varied DGT configuration [DEM source: ©National Land Survey of Finland, LiDAR digital elevation model, 2/2023]. 7.2A & B) show regular, prominent moraines only; panels 7.2C & D) show regular, prominent DGMs interspersed with irregular DGMs; and 7.2E & F) show irregular moraine only. In areas characterised by DGT as shown in 7.2C, D, E & F, prominent moraines were primarily used and the number of irregular moraines used were informed by the number required from the local varve chronology (Strömberg, 2005) to derive an annual reconstruction.

**FIGURE 7.3.** Images illustrating geochronological anchoring for the DGM-derived reconstruction. A) Hillshaded DEM showing correlation between regularly spaced mapped DGMs and varve / interpreted calendar years; B) Hillshaded DEM showing DGMs without mapped polylines; C) Map showing location of study area and selected varve sites from (Strömberg, 2005); D) Map showing selected varve sites and DGMs located across southwest Finland. Selected clay varved sites were used from the established local chronology across southwest Finland (Strömberg, 2005). DGMs were connected to varve sites by closest proximity. The number of successive DGMs were counted and matched to varve dates between sites in direction of deglaciation.

**FIGURE 7.4.** Map (7.4A) and method sketch (7.4B). 7.4A) shows mapped DGMs presented in blue and relative constructed isochrones presented in pink. Varve sites depicted by purple dots. Deglaciation flow lines are shown in white and were used to derive average retreat distance and grounding line variable datasets along each intersected isochrone. 7.4B) illustrates methods for data extraction and calculations are illustrated in the method sketch.

**FIGURE 7.5.** Annual DGM-derived reconstruction with colour-graded isochrones delineating rate of retreat ( $\text{m/yr}^{-1}$ ). The reconstruction is subdivided in spatiotemporal segments as outlined above: 1) 11 615 – 11 531, 2) 11 530 – 11 350, 3) 11 349 – 11 150, 4) 11 149 – 11 000, 5) 10 999 – 10 901.

**FIGURE 7.6.** Annual ice margin reconstruction of the southwest Finnish sector of the Fennoscandian Ice Sheet between 11 615 – 10 901 cal. years BP, derived from DGMs located across the study area (pink isochrones). The reconstruction is subdivided into spatiotemporal segments 1-5 as defined in FIGURE 7.5. 100-year isochrones between 11.6 – 10.7 ka BP are overlaid for context and comparison (blue isochrones) (Stroeven et al., 2016).

**FIGURE 7.7.** Line plots comparing estimated retreat rate across southwest Finland between DGM-derived annual reconstruction (grey line plot) and 100-yr reconstruction (blue line plot) (Stroeven et al., 2016). The plots are subdivided into the spatiotemporal segments 1-5 as defined in FIGURE 7.5. NB: the retreat rate from Stroeven et al. (2016) was compared between 11 400 – 10 900 cal. yr BP based on the spatial extent of mapped DGMs, and deglaciation flow lines as shown in FIGURES 7.4A & 7.6.

**FIGURE 7.8.** Scatter plots presenting correlations between A) 20-year avg. NGRIP temperature ( $^{\circ}\text{C}$ ) (Vinther et al., 2009), 2) slope ( $^{\circ}$ ), and 3) water depth (m) vs retreat rate ( $\text{m/20-yr}$ ). NB: for the purposes of fair correlation with the 20-year average NGRIP temperature records, retreat rate, slope and water depth data were also converted to 20-year average.

**FIGURE 7.9.** Line plots showing grounding line variables at 20-year averages: A) retreat rate ( $\text{m/20-yr}$ ); B) water depth (m); C) 20-yr avg. NGRIP temperature ( $^{\circ}\text{C}$ ); D) slope ( $^{\circ}$ ) vs

time (cal. years BP); E) elevation (m) vs distance (m) across study area in direction of deglaciation. Panels mark time segments 1) 11 615 – 11 531, 2) 11 530 – 11 350, 3) 11 349 – 11 150, 4) 11 149 – 11 000, 5) 10 999 – 10 901 and correspond with the grounding line variable maps presented in FIGURE 7.5.

**FIGURE 7.10.** Annual resolution reconstruction maps presented with colour-graded isochrones relative to each variable: A) retreat rate ( $\text{m/yr}^{-1}$ ), B) slope ( $^{\circ}$ ), C) 20-yr avg. NGRIP temperature ( $^{\circ}\text{C}$ ), and D) water depth (m). Panels mark time segments - 1: 11 615 – 11 531, 2: 11 530 – 11 350, 3: 11 349 – 11 150, 4: 11 149 – 11 000, 5: 10 999 – 10 901.

**FIGURE 7.11.** Box plots showing: A) retreat rate ( $\text{m/yr}^{-1}$ ), B) water depth (m), C) 20-yr avg. NGRIP temp ( $^{\circ}\text{C}$ ), D) slope ( $^{\circ}$ ), and E) elevation (m) across each time segment; 1) 11 615 – 11 531, 2) 11 530 – 11 350, 3) 11 349 – 11 150, 4) 11 149 – 11 000, 5) 10 999 – 10 901 (FIGURE 7.5). NB: Boxes represent interquartile range, upper and lower bounds of boxes denote upper and lower quartiles respectively, black line within boxes represent median values, 'X' within boxes represent mean average values including outliers, whiskers denote minimum and maximum values excluding outliers.

**FIGURE 7.12.** Annual resolution histograms showing water depth (m) vs retreat rate ( $\text{m/yr}^{-1}$ ). Each histogram represents time segments - A: 11 615 – 11 531, B: 11 530 – 11 350, C: 11 349 – 11 150, D: 11 149 – 11 000, E: 10 999 – 10 901 and correspond with the grounding line variable maps presented in FIGURE 7.5.

**FIGURE 7.13.** Annual resolution scatterplots showing retreat rate ( $\text{m/yr}^{-1}$ ) vs slope ( $^{\circ}$ ). Each scatterplot represents time segments - A: 11 615 – 11 531, B: 11 530 – 11 350, C: 11 349 – 11 150, D: 11 149 – 11 000, E: 10 999 – 10 901 and correspond with the grounding line variable maps presented in FIGURE 7.5.

**FIGURE 7.14.** Annual resolution line plots: A) retreat rate ( $\text{m/yr}^{-1}$ ), B) water depth (m), C) 20-yr avg. NGRIP temperature ( $^{\circ}\text{C}$ ), D) slope ( $^{\circ}$ ), vs time (cal. years BP); and E) elevation (m) vs distance (km). Spatiotemporal segments are represented by pink dashed lines to correspond with the time segments shown in FIGURE 7.5 - 1: 11 615 – 11 531, 2: 11 530 – 11 350, 3: 11 349 – 11 150, 4: 11 149 – 11 000, 5: 10 999 – 10 901.

**APPENDICES TABLE 1.** *Presenting quantified annual resolution data and descriptive statistics (total (retreat distance only), % change between successive segments in direction of deglaciation, minimum, maximum, median, mean, standard deviation and variance) for retreat distance (m/yr), water depth (m), 20-yr avg. temperature NGRIP (°C), slope (°), and elevation (m), across segments A-E as defined in FIGURE 7.5 (chapter 7).*

**APPENDICES FIGURE 1.** *Boxplot presenting calculated transect height difference captured from LiDAR and ArcticDEM data. A sample of 573 transects were compared. A Wilcoxon signed-rank test indicated a significant difference between the two datasets ( $z = -12.8$ ,  $p < .001$ ,  $r = -0.5$ ), with an average difference of 0.79 m. [DEM sources: National Land Survey of Finland, 6/2023; ArcticDEM – Porter et al., 2018].*

**APPENDICES FIGURE 2.** *Correlation between excavated sediment exposure and neighbouring GPR profile #3 at Site (1) UT1 (see Supplementary FIGURE 1). Radar facies are presented in TABLE 1 within the main manuscript.*

**APPENDICES FIGURE 3.** *Location 1, UT1 GPR Radargram #1.*

**APPENDICES FIGURE 4.** *Location 1, UT1 GPR Radargram #2.*

**APPENDICES FIGURE 5.** *Location 1, UT1 GPR Radargram #3.*

**APPENDICES FIGURE 6.** *Trench locations of grain size curves for location 1, UT1.*

**APPENDICES FIGURE 7.** *Grain size curves for location 1 UT1. Diamicton curves shown in black. Sand and gravel curves shown in brown.*

**APPENDICES FIGURE 8.** *Correlation between excavated sediment exposure and neighbouring GPR profile #1 at Site (1) UT2 (see Supplementary FIGURE 8). Comparisons with UT1 show the same lithofacies in the same order within the exposure. This is reflected in the radar facies TABLE 1, presented in the main manuscript.*

**APPENDICES FIGURE 9.** *Location 1, UT2 GPR Radargram #1.*

**APPENDICES FIGURE 10.** *Location 1, UT2 GPR Radargram #2*

**APPENDICES FIGURE 11.** *Location 1, UT2 GPR Radargram #3.*

*APPENDICES FIGURE 12. Trench locations of grain size curves for location 1 UT2.*

*APPENDICES FIGURE 13. Grain size curves for location 1 UT2. Diamicton curves shown in black. Sand and gravel curves shown in brown.*

*APPENDICES FIGURE 14. Location 2, GPR Radargram #2.*

*APPENDICES FIGURE 15. Location 2, GPR Radargram #3.*

*APPENDICES FIGURE 16. Location 3, GPR Radargram #2.*

*APPENDICES FIGURE 17. Location 3, GPR Radargram #3.*

*APPENDICES FIGURE 18. Location 4, GPR Radargram #2.*

*APPENDICES FIGURE 19. Location 4, GPR Radargram #3.*

*APPENDICES ATTACHMENT 1. Ethics approval*



# Chapter 1: Introduction

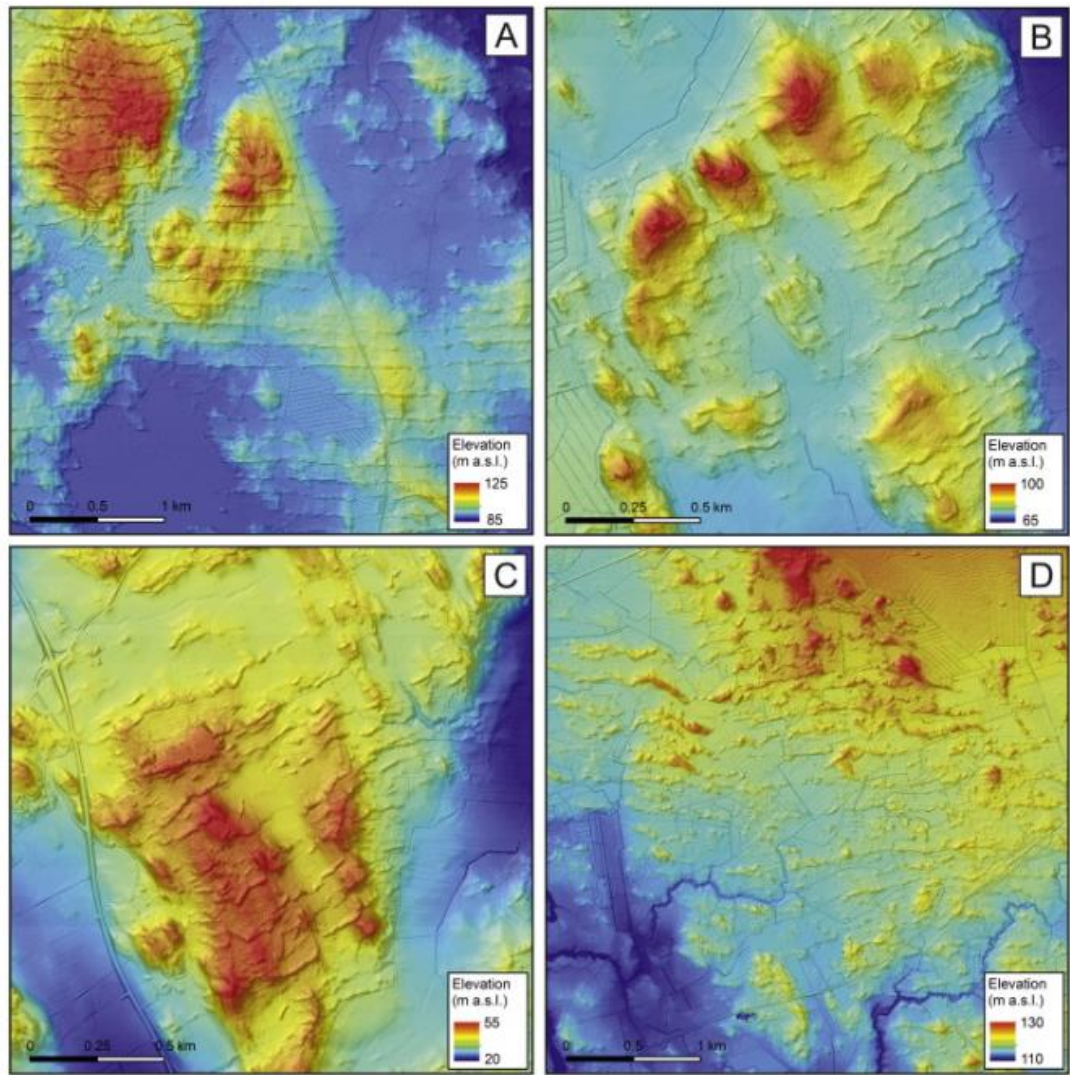
## 1.1 Rationale

Ice sheets are a core component of the global climate system and a sensitive indicator of environmental change (Fyke *et al.*, 2018; Meredith *et al.*, 2019). One of the major concerns surrounding anthropogenic climate change is rising sea levels due to melting glacier ice and thermal expansion (Alley *et al.*, 2005; Benn & Evans, 2010; Carlson *et al.*, 2019). The greatest uncertainty associated with projecting future sea level rise resides in the responses of Earth's contemporary ice sheets (Alley & Joughin, 2012; Carlson *et al.*, 2019). Ice sheets are highly dynamic systems capable of very rapid responses to climate change; however, there are many interconnected variables that can influence such responses which can be difficult to observe in contemporary settings (Alley & Joughin, 2012; Benn & Evans, 2010; Clark, 1994). Reconstructions of palaeo-ice sheets can allow a deeper understanding of ice sheet response to climate change and can act as effective climate-proxies over long periods of time (Alley *et al.*, 2005). By understanding how ice sheets responded to past climate change, we are better equipped to understand how they may respond in the future (Alley *et al.*, 2005; Benn & Evans, 2010; Pearce *et al.*, 2017).

Typically, ice sheet reconstructions aim to capture ice margin retreat rate, configuration, and flow dynamics (Benn & Evans, 2010; Pearce *et al.*, 2017). Retreat rate is usually presented as time-slice intervals, determined by the availability of landscape evidence (e.g. geomorphology such as end moraines) that capture the spatial position of the ice margin at a specific point in time. These spatiotemporal intervals define the resolution of an ice sheet reconstruction which currently range from > 1 000 to 100 years (Dalton *et al.*, 2023; Hughes *et al.*, 2016; Stroeven *et al.*, 2016). These timescales, whilst helpful for delineating long-term retreat, highlight a gap in knowledge at shorter timescales (e.g. annual to centennial) due to limited landscape datasets and uncertainties associated with radiometric dates (Walker, 2005). By working to increase resolutions, we can improve the current understanding of ice margin retreat dynamics across shorter timescales and potentially produce more accurate and tangible models that can be extrapolated to contemporary ice sheets.

Primary elements for ice sheet reconstructions comprise geomorphological observations combined with numerical dating methods. Contemporarily, geomorphological observations are often acquired via remote sensing methods (although field observations have historically been, and can be, a common approach) whereby remotely sensed imagery is visually assessed for glacially derived land features. The success of this method is determined by the spatial resolution of the remotely sensed imagery itself (Chandler *et al.*, 2018; Clark, 1997; Smith *et al.*, 2006). Recent advances in remote sensing instrumentation, and subsequently image resolutions, have enabled more subtle landscape features to be identified, which may be constructed at more regular timescales (Bouvier *et al.*, 2015; Ojala *et al.*, 2015; Ojala, 2016). This presents an opportunity for new geomorphological evidence to be collected as a means for refining the resolutions of palaeo-ice sheet reconstructions.

De Geer moraines (DGMs) are relatively subtle glaciologically derived landscape features that typically present as a series of regularly spaced, low-relief, elongated ridges, often resembling a washboard like appearance across low-lying terrains (Benn & Evans, 2010; Bouvier *et al.*, 2015; De Geer, 1889 & 1940; Golledge & Phillips *et al.*, 2008; Ojala *et al.*, 2015; Ojala, 2016). The regular appearance of these ridges suggests a cyclical nature during formation thereby highlighting a potential utility as indicators of ice margin retreat patterns.



**FIGURE 1.1.** Hillshaded LiDAR DEM showing examples of DGM fields located in Finland. A) Ruokojärvi, Kuovola; B) Kortistonkulma, Hyvinkää; C) Etu-Holsti, Porvoo; D) Kituranta, Jämsijärvi [source: Ojala, 2016].

## 1.2 Project aim, research questions & objectives

This project aims to explore the potential utility of DGMs as high-resolution ice margin indicators by investigating their internal architecture and origin, large-scale morphometry, and spatiotemporal relationship with former ice margins. Subsequently, a refined ice margin reconstruction of the southwest Finnish sector of the Fennoscandian Ice Sheet (FIS) is produced. The outputs from this work can be used to improve understanding of past ice sheet behaviour in response to climate change, which in turn may assist with improving projections of contemporary ice sheet evolution by providing more reliable information for numerical models.

### **1.2.1 Research questions**

- 1) How do DGMs form, and how do they reflect the position of ice margins?
- 2) At what timescales do DGMs form?
- 3) How does increasing spatial and temporal resolutions of ice sheet reconstructions help to improve the current understanding of ice sheet retreat rate and grounding line processes?

### **1.2.2 Research objectives**

To address the aim of this project and answer the identified research questions, three key objectives have been developed:

- 1) Constrain DGM formation processes via triangulation of morphometric, sedimentological, and geophysical datasets.
- 2) Constrain the timescale of DGM formation by comparing established varve chronologies to DGM distribution.
- 3) Produce a refined palaeo-ice marginal reconstruction at very high (potentially annual) spatiotemporal resolutions based on the quantification of, and reconciliation between, geomorphological evidence and geochronological/palaeo-climate records.

## **1.3 Thesis structure**

Chapter 2 provides a detailed review of the literature on glacially derived ice marginal landforms, with a focus on DGMs, and discusses this in the wider context of palaeo-ice sheet reconstructions. A detailed description of the study area is also provided. Chapter 3 presents an overview of the different methods used throughout the study, with more specific methods presented in the results chapters respectively (chapters 5-7). Chapter 4 presents the development of a new method in the form of a Python-based ArcGIS toolbox for the purposes of automated calculation of 3D morphometry. Chapters 5 – 7 present the results. Chapter 5 presents the results of a detailed remotely sensed morphometry study, using the toolbox outlined in chapter 4. Chapters 4 and 5 were published as a single research paper; however, to achieve a more logical structure within the thesis, this paper

has been divided into method development (chapter 4) and results of morphometric investigations (chapter 5). Chapter 6 presents the results from a detailed sedimentological and geophysical study exploring the internal architecture of DGMs to better understand formation properties. Chapter 7 presents a refined reconstruction of the southwest Finnish sector of the former Fennoscandian Ice Sheet (FIS) using DGMs as geochronometric ice margin indicators, and subsequently explores grounding line forcing mechanisms relative to rates of retreat. Chapter 8 draws together the results and discusses the findings in the context of the overall aim of the thesis. The main conclusions of the thesis are presented in chapter 9.

## Chapter 2: Literature Review

This chapter reviews the current literature on DGMs, focusing on their use as geochronometric ice margin indicators. The importance of ice sheet reconstructions is outlined prior to focusing on DGMs to provide context and rationale for the purpose of the study. More specifically, spatiotemporal resolutions of ice sheet reconstructions are discussed, highlighting gaps in the current understanding at shorter timescales (e.g. annual to centennial). Common ice margin geomorphology is summarised and briefly described to illustrate the methods and evidence used to reconstruct ice margin extent and evolution, and highlights under-utilised geomorphology such as DGMs which may provide a more detailed record of ice margin retreat. A detailed review of DGMs is then provided, discussing the current knowledge and ideas surrounding spatial and temporal formation properties, as well as current utility within ice sheet reconstructions. Similarities between DGMs and Crevasse-Squeeze Ridges (CSRs) are highlighted which have historically presented challenges when attempting to constrain DGM formation. As such, CSRs are also discussed in detail, of which comparative analyses between DGMs and CSRs are later presented in chapter 4. Finally, a review of the extent and evolution of the former FIS since the Last Glacial Maximum (LGM) is outlined, along with a more detailed contextualisation of the specific study area, southwest Finland.

### 2.1 Importance of ice sheet reconstructions

Ice sheets and glaciers collectively comprise the cryosphere, a key component of the integrated Earth system, and are a sensitive (albeit complex) indicator of climate change (Benn & Evans, 2010; Knight, 1999; Passchier, 2018; Vaughn, 2009). Ice sheets are the largest ice masses within the cryosphere and impose direct controls over sea level fluctuations and climate (Knight, 1999; Passchier, 2018; Sinet *et al.*, 2023 & 2024). These are dynamic systems influenced by a number of interdependent controls such as: eustatic and isostatic sea level change, local and regional climate, natural and anthropogenic climate forcings, ocean tides, bedrock lithology, and topographic relief (Benn & Evans, 2010; Knight, 1999). Ice sheet configuration generally comprises a central region of greater mass, whereby major flow patterns are mostly controlled by ice flow properties rather than topographic constraints, and outer regions that are characterised by thinner,

faster moving ice flows that are more sensitive to localised topography and climate controls (Benn & Evans, 2010; Knight, 1999). Generally, the outer sectors of ice sheets can be classified into either ice streams or glacial outlet lobes that are interspersed with areas of slower ice flows depending on topography and bedrock lithology (Benn & Evans, 2010; Hambrey, 1994; Knight, 1999).

Contemporary ice sheets have continued to retreat and lose mass in response to oceanic and climatic warming since the early Holocene (Anderson *et al.*, 2002; Alley *et al.*, 2010; Passchier, 2018). In more recent years, climatic warming and subsequent ice sheet retreat has accelerated instigating large research efforts to understand and project future impacts (IPCC, 2023). Whilst observations of contemporary ice sheets are critical for attempting to constrain responses to climatic warming, observations of palaeo-ice sheets can provide detailed information over much longer timescales which is useful for improving understanding of historic ice mass evolution, and for providing context to observed contemporary changes (Clark *et al.*, 2022).

As ice sheets melt and disintegrate, they leave behind landscape evidence that preserves evolution across large areas (Benn & Evans, 2010; Embleton & King, 1968). This evidence can be used to reconstruct the behaviour of palaeo-ice masses through space and time using a glacial-inversion method (Kleman & Borgström, 1996; Kleman *et al.*, 2006; Pearce *et al.*, 2017; Stokes *et al.*, 2015) which can be used to make inferences about changes in ice volume, ice-margin extent, configuration, flow and retreat dynamics. As such, reconstructions of palaeo-ice sheets have become an important analogue in which to understand deglaciation dynamics, and in turn can be used to inform numerical models allowing more accurate assessments of changes in contemporary ice masses to be derived (Batchelor *et al.*, 2019; Boulton *et al.*, 1985; Boyes *et al.*, 2023; Clark *et al.*, 2022; Ely *et al.*, 2015; Gandy *et al.*, 2018; Gowan *et al.*, 2021; Hughes *et al.*, 2016; Kleman *et al.*, 1997 & 2006; Stokes *et al.*, 2015; Stroeve *et al.*, 2016).

It should be noted that ice sheet reconstructions differ in scale and purpose, with local reconstructions offering detailed insights into specific dynamic processes, while wider reconstructions focus on regional ice extent and overall retreat patterns. Local studies, such as those by Szuman *et al.* (2024) and Ploeg & Stroeve (2025), reveal nuanced behaviours like ice streaming and complex retreat sequences in regions like the Baltic Ice

Stream Complex, shedding light on subglacial hydrology, ice-flow reorganization, and faulting. Similarly, research by Regnéll *et al.* (2023) and Lunkka (2023) explores the role of ice-dammed lakes in central Jämtland and southern Finland, respectively, linking lake drainage events to dynamic ice margin fluctuations. These reconstructions contrast with wider-scale syntheses (e.g. Hughes *et al.*, 2016; Saarnisto & Saarinen, 2001; Stroeve *et al.*, 2016), which map large-scale ice sheet configurations and margins. Localised studies are critical for refining models of deglaciation and for understanding the complex, heterogeneous nature of ice sheet retreat.

In addition to understanding changes in ice volume and ice margin extent, palaeo-ice sheet reconstructions are also critical for understanding the mechanisms associated with sea-level fluctuations, glacio-isostatic adjustment, oceanic circulation and freshwater forcings of climate change (Berends *et al.*, 2021; Bradley *et al.*, 2023; Carlson, 2011; Carlson & Clark, 2012; Stokes *et al.*, 2015). For example, Carlson & Clark (2012) used geological records, estimated glacial isostatic adjustment effects, and model derived ice-equivalent sea levels, to examine the history of meltwater discharge and freshwater routings for Northern Hemisphere and Antarctic ice sheets. This allowed relationships to be investigated relative to periods of abrupt climate change and enabled timings and magnitude of sea level rise to be constrained. Inversely, global ice volume can be informed by fluctuations in sea level (Berends *et al.*, 2021; Bradley *et al.*, 2023; Carlson, 2011). Bradwell *et al.* (2023) demonstrate how relative sea level records can be tested against various plausible ice thickness estimates to distinguish between different glaciation scenarios and used to test ice sheet reconstructions. These integrated ice sheet-sea level reconstructions, when reconciled with palaeo-climate records, can provide very well-constrained information relative to interconnected dynamics within the cryospheric-oceanic-climatic system.

A second valuable attribute of palaeo-ice sheet reconstructions is related to the role of ice streams. Given the importance of high-velocity ice streaming to ice sheet mass balance and stability, palaeo-ice streams have become a vital parameter within ice sheet reconstructions and numerical models (Stokes & Clark, 2001; Gandy *et al.*, 2018; Hemming, 2004; Clark *et al.*, 2012; Margold *et al.*, 2015). Reconstructions of palaeo-ice stream activity can provide new insights into the long-term behaviour of ice streams and



their potential forcings on overall ice sheet reduction (Gandy *et al.*, 2018; Stokes *et al.*, 2015). For example, investigations of ice stream indicative geomorphology have enabled abrupt changes in the trajectory of palaeo-ice streams, known as ‘flow switching’, to be identified, which has been attributed to internal changes in ice-sheet dynamics and sustained sediment deposition (Dowdeswell *et al.*, 2006; Winsborrow *et al.*, 2012). This ‘flow switching’ mechanism has been linked to bed topography constraints and may modulate grounding line responses to changes in sea level. Furthermore, this mechanism is suggested to be an important control on the long-term behaviour of marine-based ice streams and outlet glaciers in contemporary ice sheets (Winsborrow *et al.*, 2012) and may provide valuable information when assessing areas of vulnerability.

A third example illustrating the importance of palaeo-ice sheet reconstructions is the potential that they can offer in terms of assessing the duration and magnitude of ice sheet instabilities (Gandy *et al.*, 2018; Kleman & Applegate, 2014; Stokes *et al.*, 2015). Such instabilities include Marine Ice Sheet Instability (MISI) (Schoof, 2007; Weertman, 1974) and Marine Ice Cliff Instability (MICI) (Benn *et al.*, 2019; Crawford *et al.*, 2021). The idea of MISI can be understood whereby if the grounding line retreats across an adverse slope, the thinning rate will increase, because the thickness of the ice at a retreating grounding line must increase (Schoof, 2007; Stokes *et al.*, 2015; Weertman, 1974). This subsequently gives rise to the possibility of a grounding-line instability. Recent years have seen an increased focus on improving the modelling accuracy of MISI where the bed is substantially grounded below sea level (Schoof, 2007; Nick *et al.*, 2010; Docquier *et al.*, 2011; Feldmann *et al.*, 2014). An important aspect of grounding-line modelling is quantifying the thickness of ice sheets in the past to constrain grounding line position, migration and volume. If palaeo-ice sheet thickness records are accurately constrained, these can be integrated with numerical models and physical law-based formulas (e.g. the Schoof flux formula (Schoof, 2007) and ‘calving laws’ (Benn *et al.*, 2007; Nick *et al.*, 2010)) to calculate flux and identify potential instabilities (e.g. MISI) within contemporary ice sheets.

## **2.2 Spatial & temporal resolutions of ice sheet reconstructions**

The primary aims of ice sheet reconstructions are to constrain ice mass extent and volume, rates of ice mass fluctuation, flow dynamics, and relative palaeo-climate

parameters (Pearce *et al.*, 2017; Stokes *et al.*, 2015). This presents a spatiotemporal challenge that can only be resolved via the integration of geomorphological and geochronological evidence (Benn & Evans, 2010; Chandler *et al.*, 2018). Resolutions of ice sheet reconstructions are an important consideration and can present challenges in both spatial and temporal domains.

Geomorphological mapping provides a foundational framework for establishing the spatial extent and evolution of palaeo-ice sheets (Chandler *et al.*, 2018). Observations of contemporary glaciers demonstrate that they produce a wide range of geomorphology that can be used as proxies for ice extent and behaviour. Landforms that are particularly useful for this purpose include ice-marginal features, which delineate ice extent, and subglacial bedforms, which indicate flow patterns, behaviour, and direction (Pearce *et al.*, 2017). In addition, the study of landform assemblages allows depiction of more detailed flow pattern configurations (Ely, 2015; Ely *et al.*, 2017; Ely *et al.*, 2023; Hughes *et al.*, 2014; Mangerud *et al.*, 2019). Following geomorphological mapping, an ice sheet can be reconstructed using a 'glacial inversion model', which refers to a set of assumptions that allow palaeo-glaciological inferences to be made from the geomorphological record (Clark *et al.*, 2012; Kleman & Borgström, 1996; Pearce *et al.*, 2017; Stokes & Clark, 1999; Stokes *et al.*, 2009).

Once the spatial extent of ice sheets has been determined from landform evidence, a chronology of formation must be developed to delineate evolution through time. This involves using a variety of numerical dating methods, such as; absolute dating techniques, which may include radiocarbon dating and cosmogenic nuclide exposure-age dating to quantify an exposure/burial date, and/or relative dating techniques such as lichenometry, palaeomagnetic dating and/or principles of landform superposition to produce flowsets that constrain passage of time (Davies, 2022; Walker, 2005; Stokes *et al.*, 2009). This allows both the spatial and temporal extents of ice to be accurately reconstructed. Significantly, these spatiotemporal constraints can be reconciled with palaeo-climate records (e.g. the Greenland ice core records and sea level reconstructions), which enable correlation between ice evolution and climatic change (Hughes *et al.*, 2016; Stroeve *et al.*, 2016). This is extremely valuable for understanding and projecting the evolution of contemporary ice sheets.

The spatial and temporal resolutions of ice sheet reconstructions are critical and determine the quality of our understanding of important processes such as ice streaming (Bennett, 2003; Clark *et al.*, 2003; Robel & Tziperman, 2016) and instabilities (e.g. MISI) (Passchier, 2018; Schoof, 2007; Rignot *et al.*, 2014; Weertman, 1974), and their roles relative to deglaciation. As discussed in section 2.1, ice streaming and ice shelf instabilities can be understood and potentially projected by integrating empirical evidence with numerical modelling (Gandy *et al.*, 2018). One of the challenges when attempting to constrain these processes is the disparities in resolutions between datasets. Contemporary observations demonstrate that ice streaming and instability processes occur and evolve across a range of timescales (e.g. annual and decadal, as well as centennial and millennial), and therefore insights derived from palaeo-reconstructions may be limited by their resolution. For example, resolutions of ice sheet reconstructions may vary between >2 000 – 100 years depending on the availability of geomorphological evidence (Clark *et al.*, 2022; Gowan *et al.*, 2021, Greenwood & Clark, 2009; Hughes *et al.*, 2016; Stroeve *et al.*, 2016). As such, it may be difficult to reconcile observational data at annual resolutions with palaeo-data constrained to >100-year intervals, thus highlighting the need to increase resolutions of palaeo-ice sheet reconstruction.

Increasing resolutions of palaeo-ice sheet reconstructions presents a difficult challenge to overcome, with solutions often relating to absolute dating and numerical modelling methods (Dalton *et al.*, 2020; Ely *et al.*, 2024). Given the fundamental requirement of a geomorphological framework, additional solutions would be to: (1) increase the input geomorphological dataset (increasing spatial resolution) (2) increase frequency of absolute chronological ages, and (3) to seek out alternative landforms that can delineate ice margin retreat at more regular time intervals (increasing temporal resolution). Each of these approaches are discussed below.

### **2.2.1 Increase the input geomorphological dataset**

Historically, geomorphological data have been acquired via field mapping and aerial photography (Chandler *et al.*, 2018; Clark, 1997). These methods are generally expensive, time-consuming, and often limited by inaccessibility, resulting in small and under-representative datasets that are more suited to specific research focuses (Clark, 1997). Reconstructions have been developed using such data, producing largely accurate

reconstructions; yet they can lack nuance and detail (Prest *et al.*, 1968). This has been a limiting factor for wider scale ice sheet reconstructions; however, advances in technology (e.g. remote sensing instrumentation) have provided a means to overcome these limitations. Satellite imagery and Digital Elevation Models (DEMs) that were developed in late 20<sup>th</sup> century have enabled the acquisition of geomorphological evidence across large areas with relative ease, and at low cost (Chandler *et al.*, 2018; Clark, 1997; Johnson *et al.*, 2015). This has proved very successful and has reinvigorated research in glacial geomorphology and understanding of palaeo-ice sheets (Boulton & Clark, 1990; Clark, 1993; Clark, 1997; Dulfer *et al.*, 2022; Hughes *et al.*, 2014; Kleman *et al.*, 2010; Margold *et al.*, 2018; Stroeve *et al.*, 2016; Winsborrow *et al.*, 2010); however, the spatial resolution of remote imagery determines the accuracy of landform observations. This presents an additional obstacle when trying to develop very detailed ice marginal reconstructions.

Over the past decade, continued advancements in image sensors have resulted in the production of Digital Elevation Model (DEM) data characterised by very high spatial resolutions (e.g. 2 m LiDAR (Light Detection and Ranging)) (Chandler *et al.*, 2018; Johnson *et al.*, 2015). This has enabled researchers to collect and analyse geomorphological data in much finer detail than ever before (Bouvier *et al.*, 2015; Eilertsen *et al.*, 2015; Greenwood *et al.*, 2015; Johnson *et al.*, 2015; Öhrling *et al.*, 2018; Ojala *et al.*, 2015 & 2016;). In addition, developments in Geographical Information Systems (GIS) have resulted in sophisticated analysis methods that can provide more robust and nuanced insights into geomorphic processes (Chandler *et al.*, 2018).

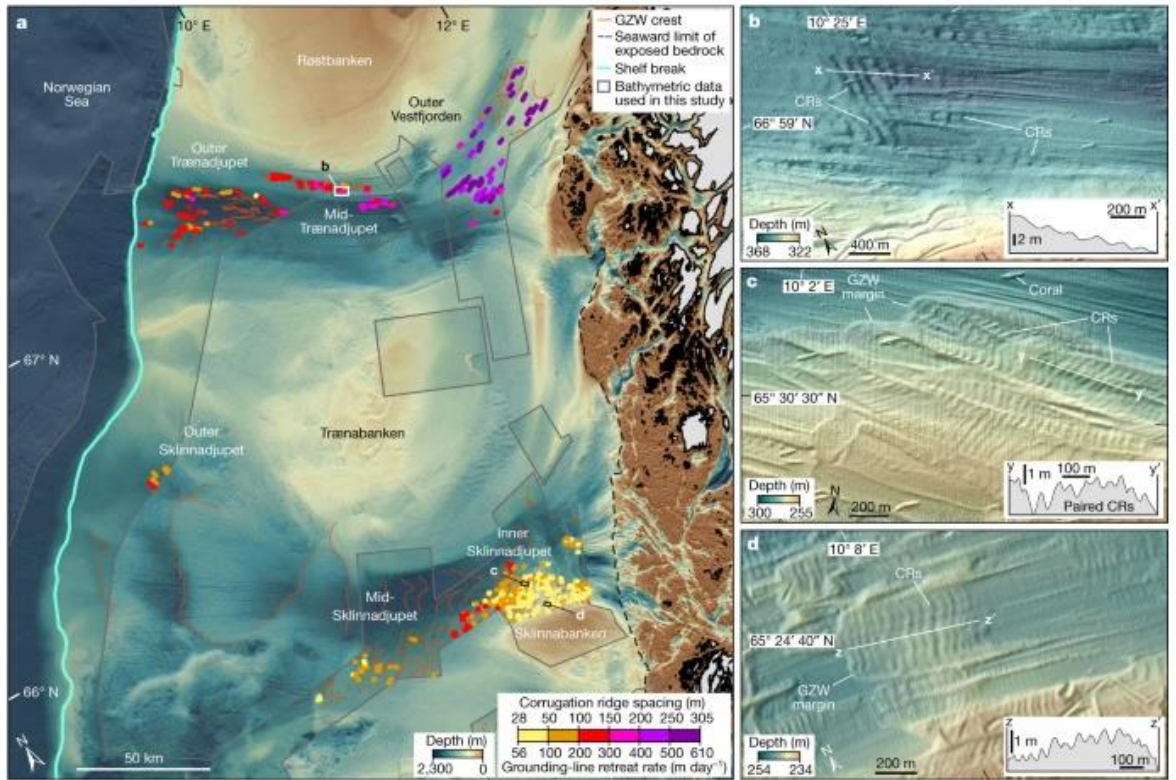
### **2.2.2 Increase frequency of absolute chronological ages**

Increasing the frequency/spatial density of absolute chronological ages has proved very effective for constraining the temporal resolutions of ice sheet reconstructions (e.g. Dalton *et al.*, 2020 & 2023, Hughes *et al.*, 2016; Stroeve *et al.*, 2016). Essentially, absolute chronological dating can provide a numerical-age estimate for a landform (Hubbard & Glasser, 2005; Walker, 2005). There are several techniques for acquiring absolute chronological ages; although each of these techniques typically involves the collection of field samples followed by laboratory analyses (Walker, 2005). As such, the work involved for absolute dating can be labour intensive, depending on the required

field samples and accessibility of study areas, and expensive when considering laboratory costs - particularly if the goal is to establish many ages. Another complication with absolute dating methods is that the precision of dates is typically limited to a few centuries, at best, which is amplified by the additional uncertainties associated with age-estimate errors (Walker, 2005). This reverts to the original issue of restricted temporal resolutions within ice sheet reconstructions.

### **2.2.3 Seek out alternative landforms**

Ice-marginal landforms such as moraines, proglacial outwash fans and ice-dammed lakes are particularly informative for ice sheet reconstructions because they delineate ice extent. To maximise the utility of such evidence, it is important to be able to distinguish between the vast range of ice-marginal landforms and understand how they relate to the ice margin through time. Currently, the dominant ice marginal landforms used in ice sheet reconstructions are large-scale major moraine belts (e.g. Stroeve *et al.*, 2016), and often, other less-prominent ice marginal landforms such as DGMs (that are known to occur in some locations with a high degree of regularity) are overlooked and not used to inform ice margin evolution. The detailed information that less-prominent landforms can provide is demonstrated in a study by Batchelor *et al.*, (2023), whereby corrugation ridges (FIGURE 2.1) have been shown to record retreat rates at very high-resolution diurnal timescales.



**FIGURE 2.1.** Corrugation ridges on the mid-Norwegian margin. A) Map showing high-resolution bathymetric data coverage and corrugation ridge spacing along measured transects in study; b) Corrugation ridges in mid-Trænadjupe; c) Corrugation ridges in inner Sklinnadjupe; d) Corrugation ridges in inner Sklinnadjupe [source: Batchelor *et al.*, 2023].

By focusing efforts to increase both spatial and temporal resolutions of ice margin reconstructions, it may be possible to reconstruct former ice sheets at unprecedented resolutions, particularly by exploiting more subtle landforms (Batchelor *et al.*, 2023; Hogan *et al.*, 2023). This will not only improve the current understanding of former ice mass evolution but may also provide more reliable constraints for models of contemporary ice sheet change.

### 2.3 Geomorphological indicators in ice sheet reconstructions

There are a variety of landforms that are used as extent and flow indicators within ice sheet reconstructions. These are generally subcategorised into either subglacial or ice marginal features, with each feature providing unique glaciological information relative to its mode of formation. This section focuses on ice marginal features only to retain relevance and focus within the scope of this project, and provides a brief description and overview of the key landforms used in ice margin reconstructions.

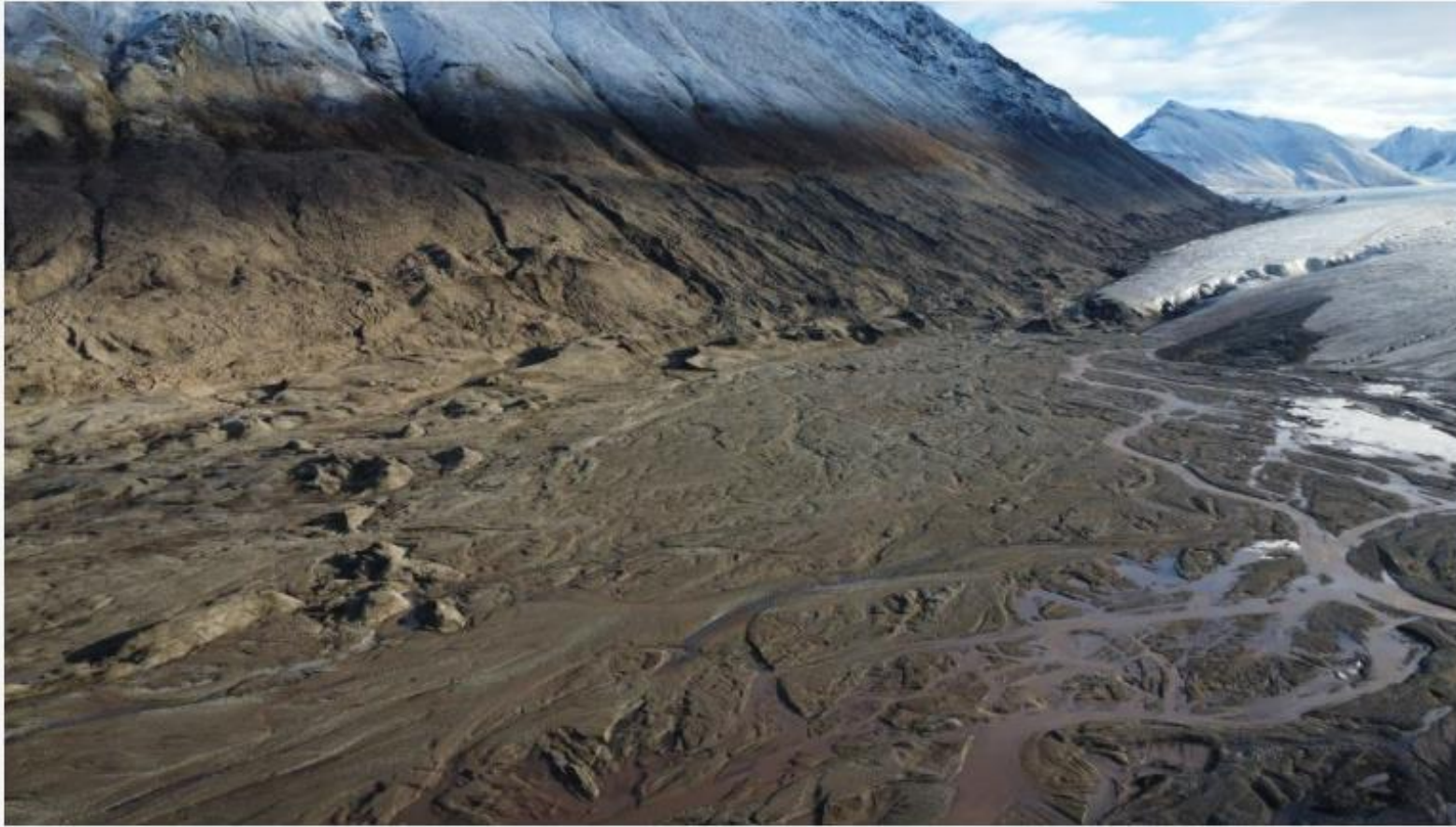
### **2.3.1 Ice marginal features**

At the margins of glacial ice, sediments are deposited and eroded through a variety of processes (Benn & Evans, 2010; Embleton & King, 1968). As ice-marginal sediments accumulate, landforms develop that generally preserve the extent and configuration of the ice margin at a given moment in time. Ice-marginal formations can preserve both the lateral and frontal extent of glacial ice which in turn can provide key information regarding retreat patterns. Ice marginal features vary considerably, ranging from grounding-line fans and shorelines to channels and moraines. Whilst ice marginal landforms are useful for delineating ice margin extent and evolution, challenges associated with ice margin readvances, overriding and preservation potential should also be acknowledged.

#### **2.3.1.1 Outwash fans**

Meltwater flowing from glaciers, often in the form of braided stream networks, deposit sediment as outwash fans beyond the ice margin within proglacial areas (Kruger, 1997; Taylor, 2014) (FIGURE 2.2). Extensive outwash fans (aka. sandar) are typically fed by high energy streams from beneath the ice. These are often composed of coarse-grained sediments in their proximal parts (closest to the source of deposition) such as pebbles, cobbles and boulders; and finer-grained sediments such as sands, silts and clays in the distal parts as transportation energy decreases (Krüger, 1997). Extensive outwash fans such as these can provide a record of long-term accumulation of proglacial outwash and can impose significant influence over proglacial drainage patterns and development of proglacial landform-assemblages (Evans & Orton, 2015).





*FIGURE 2.2. Outwash plain, Charlesbreen, Svalbard [source: Taylor, 2024].*

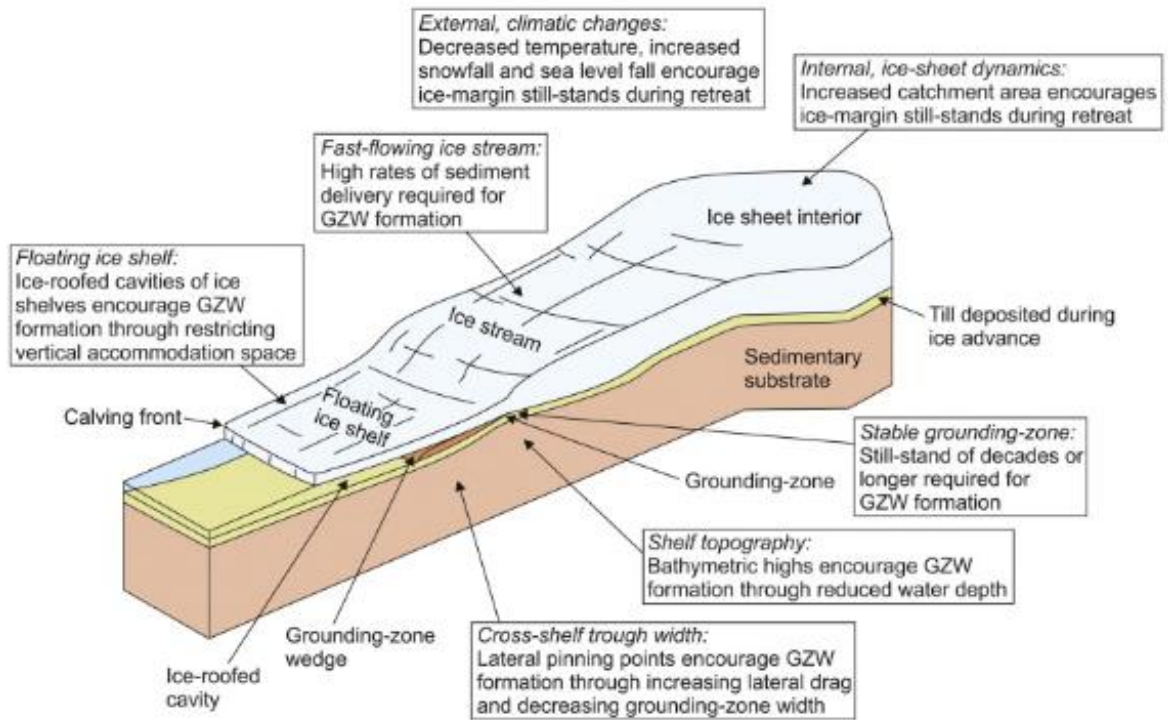


In contrast, minor outwash fans fed by supraglacial streams tend to lack the proximal-to-distal transition described above and tend to yield finer-grained sediments due to a lower transportation capacity (Kjær *et al.*, 2004; Krüger, 1997). Minor outwash fans (aka. hochsander fans) are said to be characteristic of advancing or stationary glaciers, and formation is likely to cease during periods of retreat (Kjær *et al.*, 2004; Krüger, 1997). Studies have shown that the vertical texture variations and sedimentation rates in outwash fans can reflect processes such as changes in influx of rainwater and ablation (Krüger, 1994 & 1997).

#### **2.3.1.2 Grounding zone wedges**

Grounding zone wedges (GZWs) are asymmetric depositional landforms which form via rapid accumulation of subglacial tills at the grounding zone of marine-terminating ice sheets during standstills in retreat (Batchelor & Dowdeswell, 2015; Dowdeswell *et al.*, 2016; Konal & Worster, 2020; Mosola & Anderson, 2006; Dowdeswell & Fugelli, 2012). They are typically tens of metres thick and tens of kilometres in length. The wedges thin in an ice-proximal direction and usually form subdued transverse-to-flow ridges. These landforms can usually be distinguished from other similar transverse ridges formed at the grounding zone (e.g. moraine ridges and ice-proximal fans) by their subdued appearance due to constrained vertical accommodation space by floating ice shelves immediately beyond the grounding zone (Batchelor & Dowdeswell, 2015).

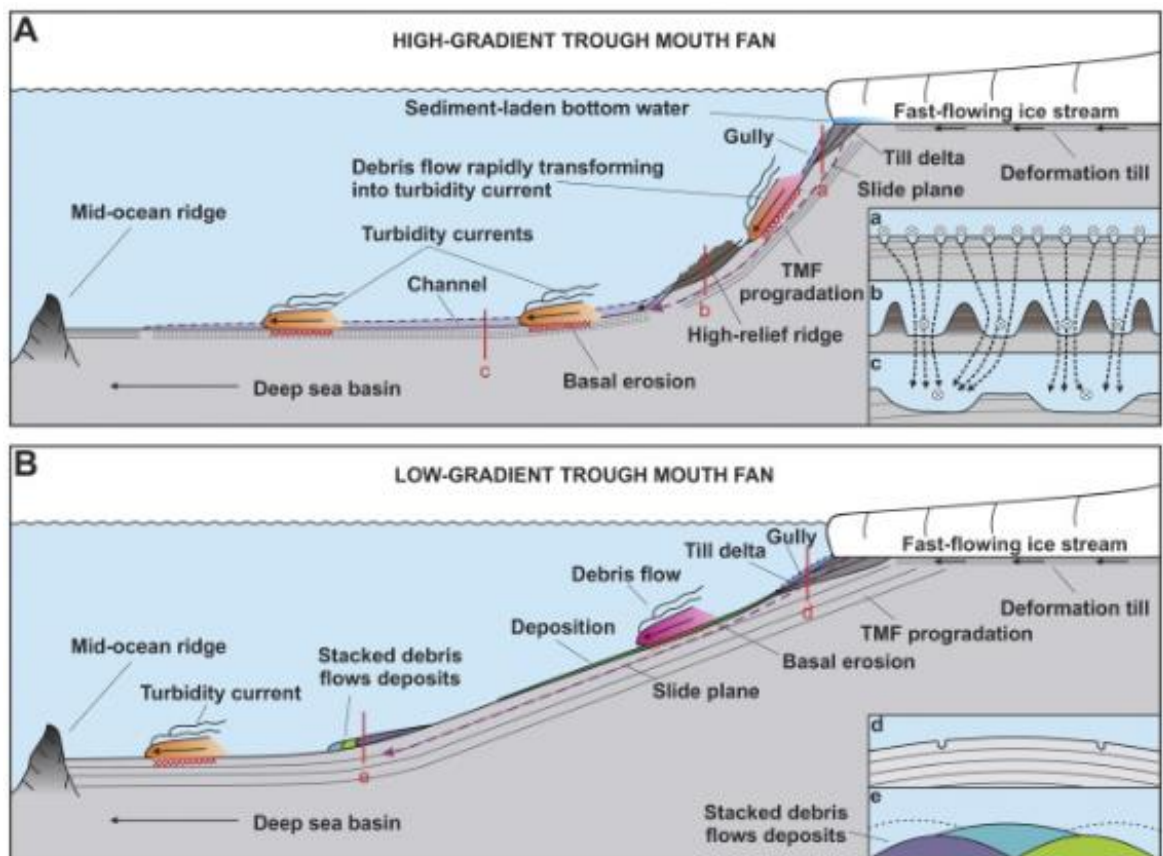
GZWs are suggested to require high rates of sediment delivery to a relatively stable fast-flowing ice margin (Batchelor & Dowdeswell, 2015). As such they have often been attributed to typical ice-stream landform assemblages and may provide insights relative to flow and retreat dynamics, as well as continental shelf geometry (Batchelor & Dowdeswell, 2015; Dowdeswell & Fugelli, 2012). In addition, the asymmetric geometry of GZWs (e.g. steeper distal side) enables the former direction of ice flow to be established (Batchelor & Dowdeswell, 2015). It is also suggested that the development of GZWs may provide stability against rapid ice margin retreat (Alley *et al.*, 2007; Dowdeswell *et al.*, 2016) (FIGURE 2.3).



**FIGURE 2.3.** Diagram illustrating the formation controls of GZWs at high-latitude continental margins [source: Batchelor & Dowdeswell, 2015].

### 2.3.1.3 Trough mouth fans

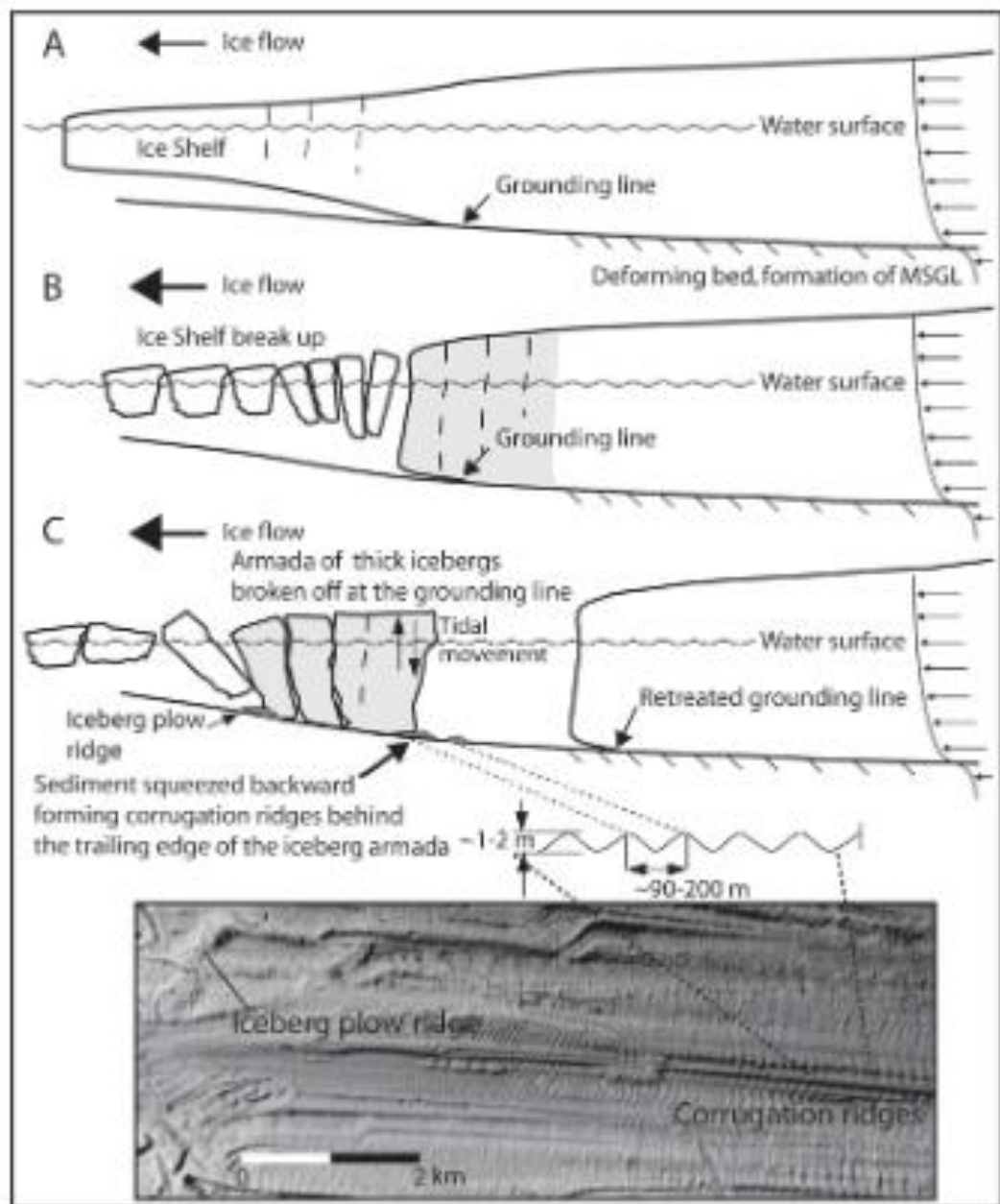
Trough mouth fans (TMFs) are fans at the mouth of transverse troughs/channels on glaciated continental shelves formed by glaciogenic sediment delivery from fast-flowing outlets (Bellwald *et al.*, 2020; Dowdeswell & Elverhøi, 2002; Rydningen *et al.*, 2015; Vorren *et al.*, 1988, 1989, 1997). TMFs are products of repeated glaciogenic sediment delivery, and it is suggested that the number of debris-flow units within these fans record the number of shelf break-positions of ice sheet margins (Bellwald *et al.*, 2020; Rydningen *et al.*, 2015; Vorren *et al.*, 1989 & 1997). As such, TMFs can act as relatively high-resolution palaeo-climate and ice sheet monitors, and have proven particularly important when reconstructing pre-Weichselian glaciations and understanding glacial-interglacial cycles (Bellwald *et al.*, 2020 (FIGURE 2.4).



**FIGURE 2.4.** conceptual models of high-gradient (A) and low-gradient (B) trough mouth fans [source: Rydningen *et al.*, 2015].

#### 2.3.1.4 Corrugation ridges

Corrugation ridges are extremely regular, low-amplitude (<1.5 m high) landforms formed at the grounding lines of retreating ice shelves (Batchelor *et al.*, 2023; Hogan *et al.*, 2023; Jakobsson *et al.*, 2011; Jakobson & Anderson, 2016; Graham *et al.*, 2013.) (FIGURE 2.5).



**FIGURE 2.5.** Conceptual sketches illustrating formation mechanisms for corrugation ridges [source: Jakobsson *et al.*, 2011].

Several formation mechanisms have been explored for corrugation ridges; however, the extreme regularity of these ridges has been suggested to rule out formation as seasonal recessional moraines or DGMs (Jakobsson *et al.*, 2011; Jakobson & Anderson, 2016). The sediment cores of corrugation ridges comprise poorly sorted glacial diamicton and glacial marine sandy clays, indicating that a current-influenced formation may also be excluded (Jakobsson *et al.*, 2011; Jakobson & Anderson, 2016; Graham *et al.*, 2013). Due

to their identification within iceberg plough marks and furrows, the ridges were thought to have been formed at the trailing edge of mega-icebergs moving up and down in response to tides while ploughing the seafloor (Andreassen *et al.*, 2014; Graham *et al.*, 2013; Jakobsson & Anderson, 2016; Jakobsson *et al.*, 2011). More recently, Hogan *et al.* (2023) proposed three formation models for corrugation ridges at tidally migrating grounding lines whereby each ridge is formed by either: constant till flux to the grounding line, till extrusion from beneath the grounding line, or the resuspension and transport of grains from the grounding zone bed. Whilst corrugation ridges may form in slightly different environments, for example behind icebergs or beneath a fractured ice stream, it is the vertical and rhythmic tidal motion that is the common denominator for formation (Jakobsson & Anderson, 2016). As these ridges are a product of tidally induced accumulation of sediments at the grounding line, these ridges can provide very high-resolution records of grounding line motion at subdiurnal to diurnal timescales (Batchelor *et al.*, 2023 & Hogan *et al.*, 2023).

#### **2.3.1.5 Ice-marginal moraines**

Ice-marginal moraines can be subclassified as: 1) proglacial glaciotectonic landforms; 2) push and squeeze moraines; 3) dump moraines and ice-marginal aprons; and 4) latero-frontal fans and ramps (Benn & Evans, 2010; Knight, 1999). A moraine ridge formed at the outermost terminal margin of glacial ice is often referred to as an end or terminal moraine (e.g. Salpausselkä moraines (FIGURE 2.6)), with similar smaller moraines associated with retreating ice often referred to as recessional moraines (Benn & Evans, 2010; Chandler *et al.*, 2016; Simkins *et al.*, 2018). As sediments are typically deposited during readvances, or periods of quiescence, if there are several parallel frontal moraines that are interspersed with lower-relief areas of non-deposition, the assemblage can be used to reconstruct patterns and rates of ice margin retreat (Chandler *et al.*, 2016; Simkins *et al.*, 2018). That being said, accurate distinction between different types of ice marginal ridges is critical due to the different processes from which they originate (Benn & Evans, 2010; Embleton & King, 1968).



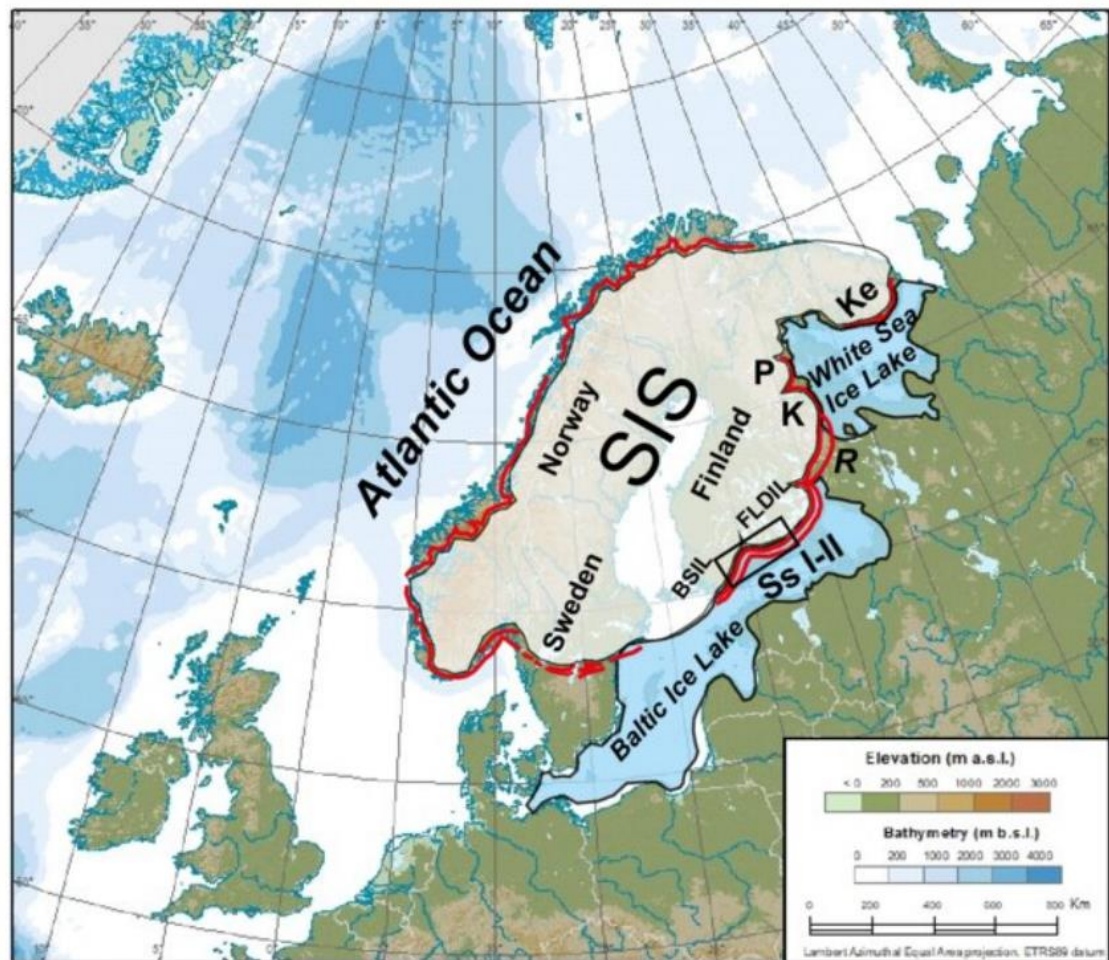
**FIGURE 2.6.** Location map showing the major end moraines around Fennoscandia. Black box indicates the location of the First, Second and Third Salpausselkäes in southern Finland [source: Lunkka *et al.*, 2020].

#### 2.3.1.6 Ice-dammed lakes

Ice-dammed lakes are formed where ice margins block the natural drainage of proglacial outlets (Benn & Evans, 2010). The lifespan of an ice-dammed lake is dictated by the presence of ice with drainage occurring upon ice retreat. Evidence of former ice-dammed lakes may present in the form of erosional/depositional shorelines, grounding-line fans, and overflow channels, and can be used as indicators for reconstructing ice marginal retreat patterns (Stroeven *et al.*, 2016; Lundqvist, 1972; Teller, 2003). Notable examples of large palaeo ice-dammed lakes are shown in FIGURE 2.7, namely the Baltic Ice Lake (BIL) and the White Sea Ice Lake (WSIL) that developed along the south-eastern margins



of the former FIS (also sometimes referred to as the Scandinavian Ice Sheet (SIS)) (Björk, 1995; Regnéll *et al.*, 2023).



**FIGURE 2.7.** Image showing the extent and position of the former Baltic Ice Lake and White Sea Ice Lake at approximately (~12 300 – 11 600 ka BP (Donner, 2010)) positioned along the southeast margins of the former Scandinavian Ice Sheet (SIS) [source: Lunkka, 2023].

### 2.3.1.7 Ice-marginal meltwater channels

Meltwater produced at the surface of ice, as well as rainfall, can drain to glacier margins either supraglacially, englacially, or subglacially. Eventually the meltwater will reach the ice margin where it drains along the margins between ice and elevated ground (Stroeven *et al.*, 2016). This ice marginal drainage usually occurs within the ablation area of glaciers and is commonly associated with polythermal and/or cold-based ice when meltwater drainage to the bed is restricted (Benn & Evans, 2010; Davies, 2020). These meltwater channels may track the lateral and terminal margins of the ice, therefore preserving a

record of retreat (FIGURE 2.8) (Greenwood *et al.*, 2007; Margold *et al.*, 2013; Benn & Evans, 2010).





*FIGURE 2.8. Palaeo-ice-marginal meltwater channel in the summer areas of Hazelton Mountains [source: Margold et al., 2013].*

#### 2.3.1.8 Thrust-block moraines

Thrust-block moraines (also referred to as composite ridges) are ice-marginal proglacial tectonic landforms, whereby proglacial and submarginal sediments are displaced due to stresses imposed by glacial ice, usually involving ductile and/or brittle deformation (FIGURE 2.9) (Benn & Evans, 2010; Benediktsson *et al.*, 2009; Evans, 1991). These landforms can be described as imbricated ridges composed of contorted bedrock and unconsolidated sediments that have been thrust upwards in a stacked configuration (Benn & Evans, 2010). These ridges are commonly inter-layered and overlain by glaciofluvial sediments (Benn & Evans, 2010; Benediktsson *et al.*, 2009; Evans, 1991). The processes involved in the formation of thrust-block moraines are generally characterised by unidirectional bulldozing and/or pushing (Benn & Evans, 2010). As these ridges are formed at the ice margin by proglacial and sub-marginal tectonic processes, they may provide an indication of glacier readvances and standstills; although individual ridges do not record the precise location of an ice margin in the same way that push moraines do (Benn & Evans 2010).



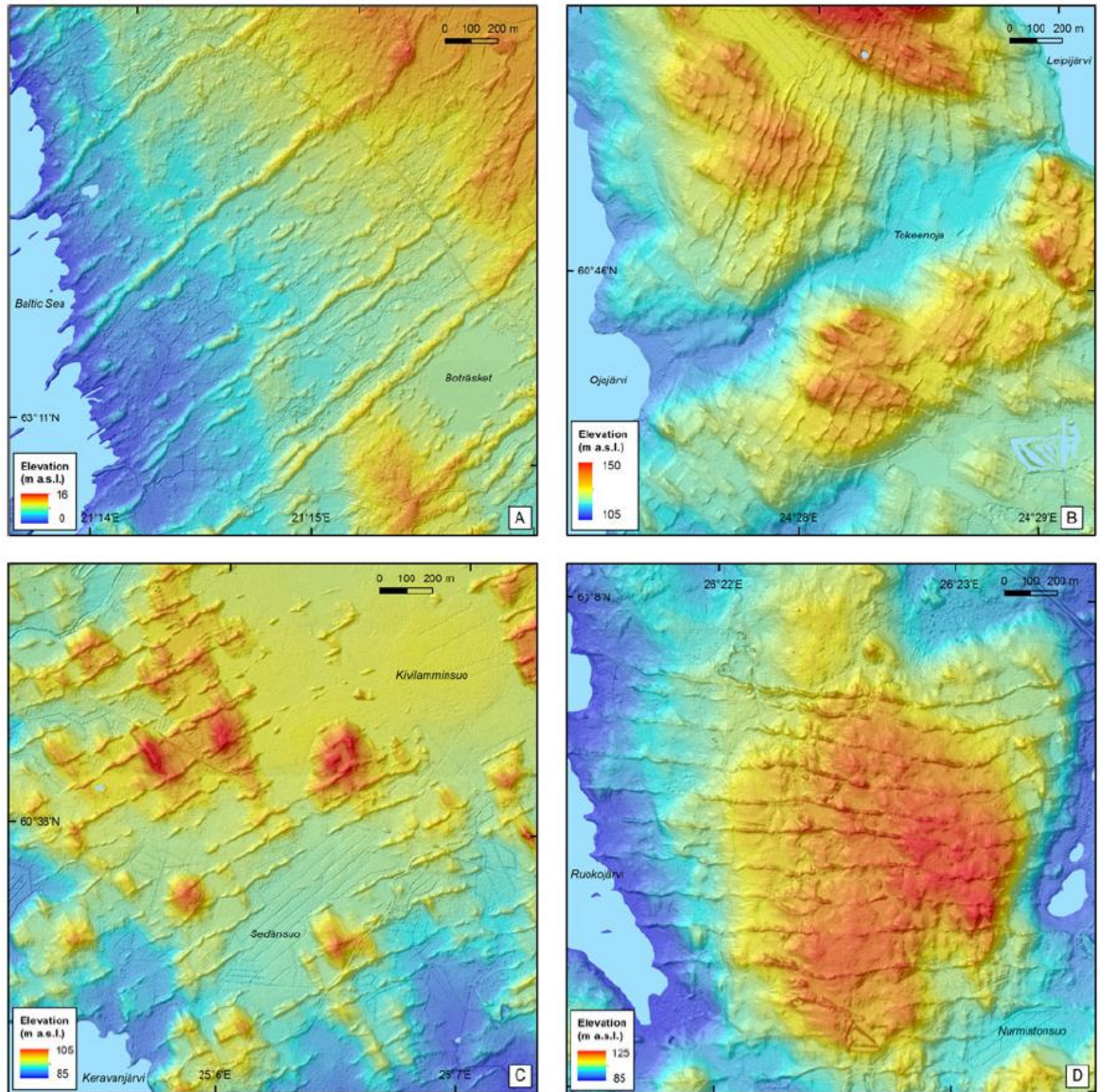
**FIGURE 2.9.** Proglacial moraine complex characterised by thrust-block moraines at the margin of the Leverett Glacier, western Greenland [source: Waller, 2013].

## 2.4 A review of the literature on DGM formation

DGMs are the central focus of this project due to their regular appearance and suggested ice margin depositional environment. These narrow and elongate ridges were first observed in Sweden by De Geer in 1889 (De Geer, 1889 & 1940). They typically occur in successive swarms, with either regular or irregular arrangements (FIGURE 2.10) and are often separated by varved silt and clay (Ojala *et al.*, 2015 & 2016). DGMs are most common in low-lying terrains, below the highest shoreline of proglacial lakes/seas (Hoppe, 1959; Embleton & King, 1968; Lindén & Möller, 2005; Ojala *et al.*, 2015 & 2016; Larsen *et al.*, 1991; Bouvier *et al.*, 2015; Finlayson *et al.*, 2007; Lundqvist, 1981); although observations have also been made in mountainous-valley, lacustrine environments (Borgström, 1979; Golledge & Phillips, 2008).

Regarding geomorphological appearance, DGMs can generally be subclassified as prominent (regular) and intermediate (irregular) moraines when observed relative to each other (Bouvier *et al.*, 2015; Ojala *et al.*, 2015; Ojala, 2016). Prominent DGMs are generally found to be larger and more regularly spaced (FIGURE 2.10B, C & D), whereas intermediate DGMs are lower amplitude, less sinuous and irregularly spaced (FIGURE 2.10A). NB: considerations should however be made for factors such as postglacial reworkings and topographical controls.





**FIGURE 2.10.** Digital Elevation Model capturing distinct and regular De Geer moraine landforms situated in SW Finland: A) Södra Vallgrund, B) Koskela, C) Kaidanpää, D) Ruokojärvi [source: Ojala *et al.*, 2015].

DGM morphometrics are generally reported as: 0.5-3 m (<15) in height, 5-25 m in width (can be up to 50 m wide (Sollid, 1989)), and 50-1 000 m in length (although can reach up to several km) (Ojala *et al.*, 2015; Zilliacus, 1989; Benn & Evans, 2010; Hoppe, 1959). Individual ridges can manifest as linear, concave, or convex in profile, depending on local topographic controls, and have been observed with both cross-sectional symmetric and asymmetric properties, often displaying a steeper distal side (Hoppe, 1959; Golledge & Phillips *et al.*, 2008; Ojala *et al.*, 2015).

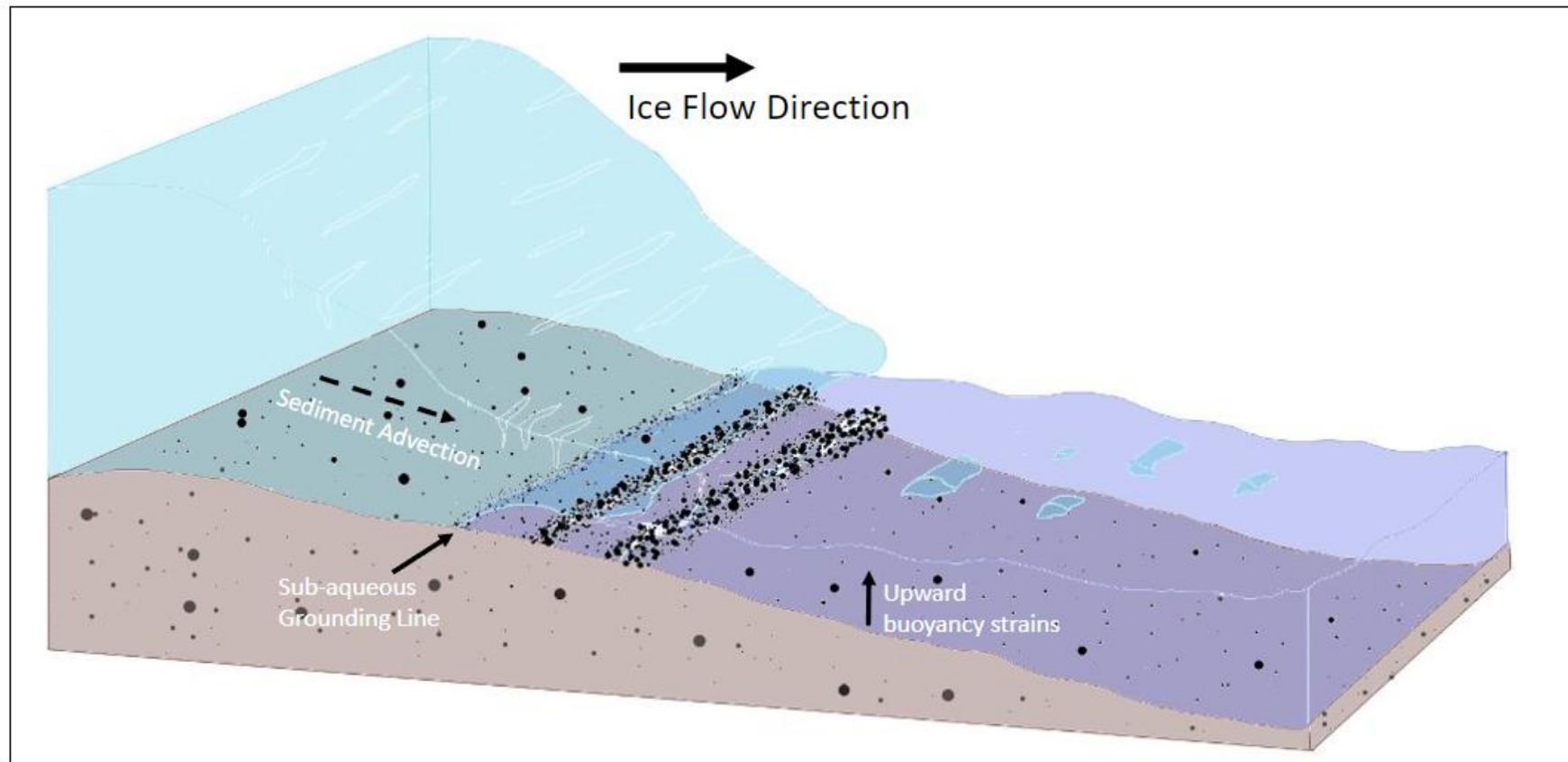
The sedimentological composition of DGMs has been suggested to comprise large diamicton units (unconsolidated / unsorted material), with some interspersions of stratified laminations of sand, silt, and gravel (Blake, 2000; Golledge & Phillips, 2008; Lindén & Möller, 2005; Larsen *et al.*, 1991). DGMs can also be observed with a veneer of ablation till, which can prove problematic for landform identification (Ojala *et al.*, 2015).

Cross-sectional analyses report variability in both sedimentological composition and fabric between proximal and distal edges, which has been suggested to reflect the different formation mechanics across a single ridge (Beaudry & Prichonnet, 1991 & 1995). For example, internal sedimentary architecture can show evidence of pressurised deformation mechanics (Lindén & Möller, 2005; Golledge & Phillips, 2008; Embleton & King, 1968; Beaudry & Prichonnet, 1991 & 1995; Larsen *et al.*, 1991), whilst intercalated sedimentary laminations have been suggested to be influenced by proximity to meltwater streams and fluvial dynamics (Blake, 2000).

The origin of DGMs has been extensively debated since their first description, with both spatial and temporal characteristics heavily contended. A review of existing literature highlights two dominant formation methods which are described below.

#### **2.4.1 DGM formation hypothesis (1)**

This formation hypothesis can be described as a sub-aqueous, ice-marginal process characterised by the advection and push of basal till to the grounding-line during seasonal advances. Upward buoyancy strains on the ice lead to calving thus preserving deposited material (Smith, 1982; Smith & Hunter, 1989; Blake, 2000; Finlayson *et al.*, 2007; Larsen *et al.*, 1991; Lindén & Möller, 2005; Borgström, 1979; Golledge *et al.*, 2008; Aartolahti *et al.*, 1995; Dix & Duck, 2000) (FIGURE 2.11). This theory suggests that DGMs may provide a detailed record of ice marginal retreat.

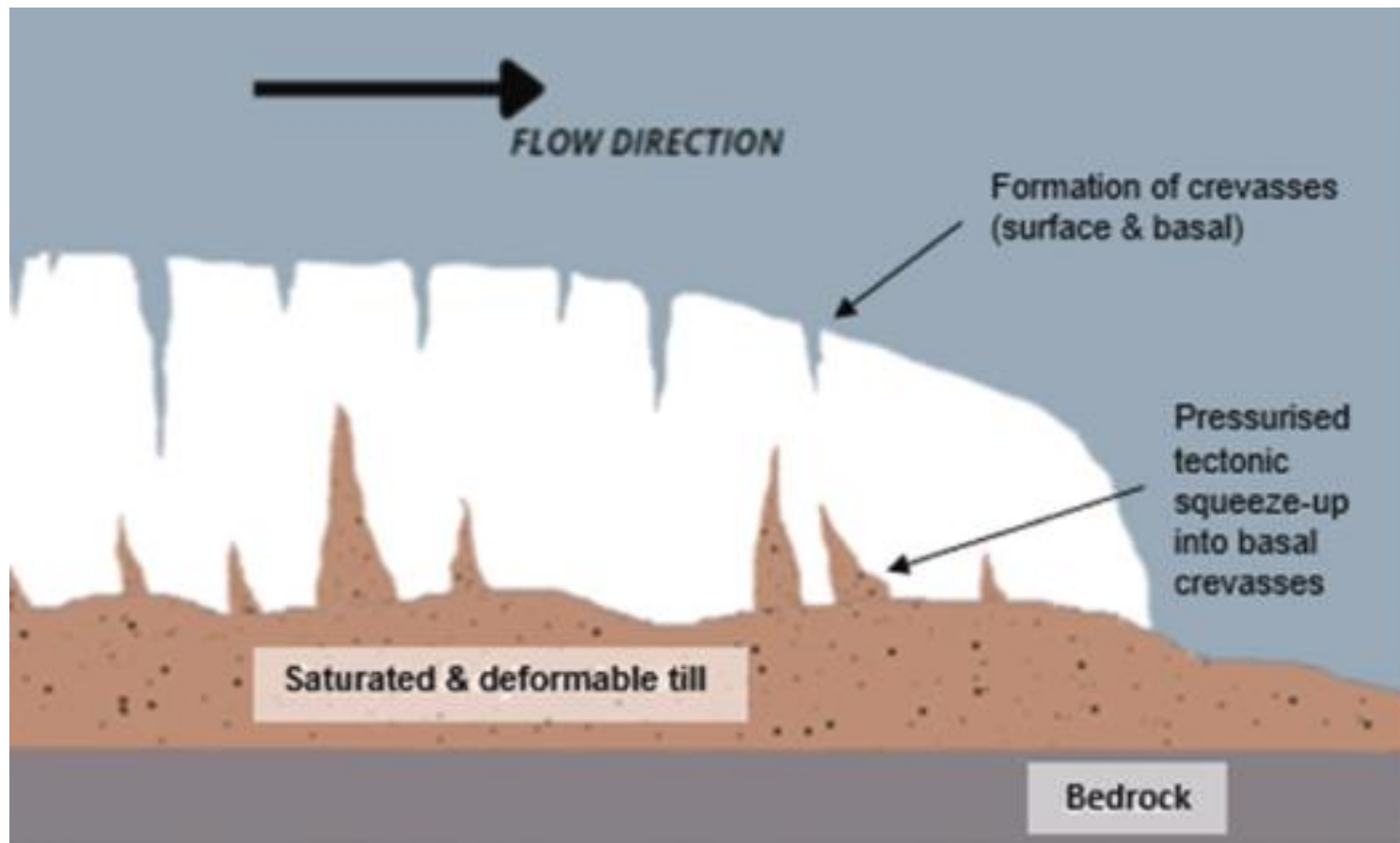


**FIGURE 2.11.** Schematic diagram of DGM formation hypothesis (1). A sub-aqueous ice-marginal process by which subglacial sediment is advected toward and deposited at the grounding line.

#### 2.4.2 DGM formation hypothesis (2)

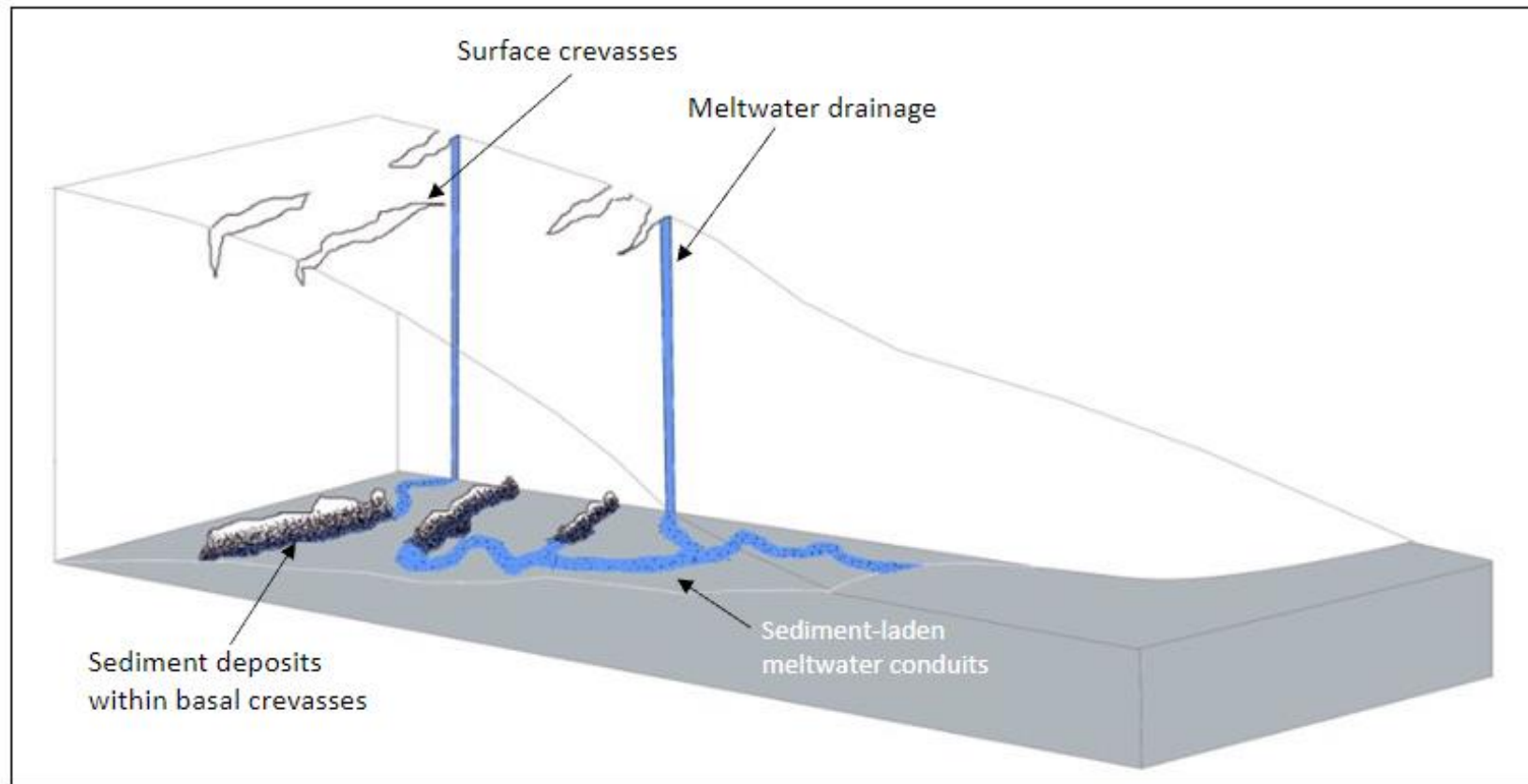
This formation hypothesis can be described as a sub-glacial process characterised by the squeezing of sediments into basal or full-depth crevasses (Beaudry & Prichonnet, 1991 & 1995; Sharp, 1985; Strömberg, 1965; Zilliacus, 1989) (FIGURE 2.12). This method suggests that crevasses are formed behind the ice margin due to enhanced flow and basal sediments are squeezed up into the crevasses, thus forming landforms referred to as 'crevasse-squeeze ridges' (CSRs). Preservation of these landforms would require the surrounding ice to be either lifted from the bed, proceeded by calving, or by rapid down-wasting. Significantly, this formation method implies synchronous formation between ridges, and therefore nullifies any temporal attributes relative to ice margin dynamics.





**FIGURE 2.12.** Schematic diagram of DGM 'crevasse-squeeze ridge' formation hypothesis (2). Diagram illustrates the squeezing of sediments into subglacial crevasses formed behind the ice margin.

A variation of the crevasse infill method (DGM formation hypothesis (2)) is the injection of sediment-laden meltwater which transports and deposits material into basal crevasses via meltwater conduits (Beaudry & Prichonnet 1991 & 1995; Evans *et al.*, 2022; Sollid, 1989) (FIGURE 2.13). It is likely, however, that these types of ridges are equifinal, forming via a combination of pressurised squeeze-up and injection processes.



**FIGURE 2.13.** Schematic diagram of DGM 'channelised meltwater conduit' formation theory. Diagram illustrates meltwater drainage via surface crevasses. Sediments are then deposited within basal crevasses behind the ice margin via sediment-laden meltwater conduits.

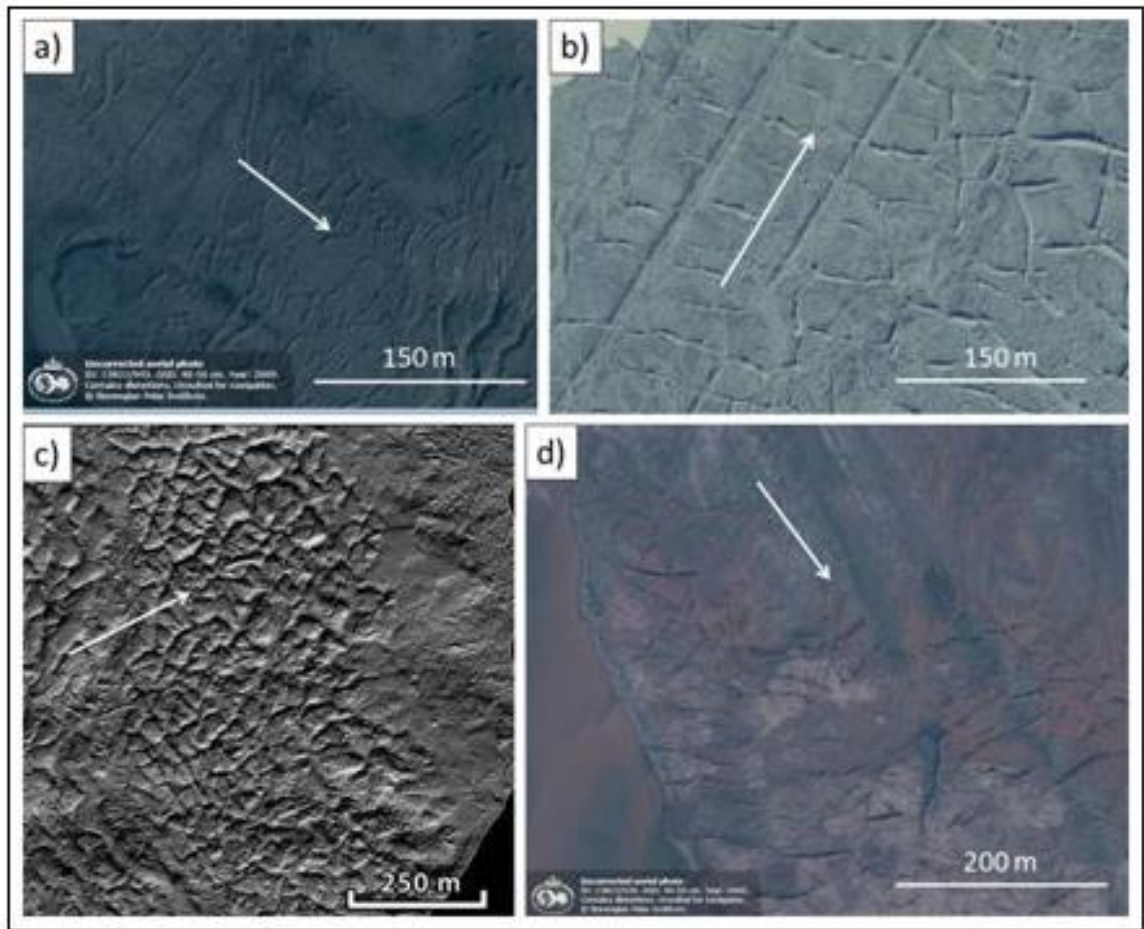
The contrasting formation hypotheses highlight the difficulty in distinguishing between DGM and CSR landforms. Whilst some researchers may lean toward a specific hypothesis, many studies suggest a degree of equifinality, whereby DGMs may be formed via a combination of methods (Bouvier *et al.*, 2015; Larsen *et al.*, 1991; Smith & Hunter, 1989; Möller, 1962; Hoppe, 1959; Lundqvist, 1981). In addition, temporal properties of DGMs remain highly ambiguous. Some studies suggest annual formation, with a single ridge being formed during a winter readvance (Bouvier *et al.*, 2015; De Geer, 1940; Smith, 1982; Sollid & Carlsson, 1984); whilst others suggest sub-annual formation whereby multiple ridges may form within a single season (Blake, 2000; Bouvier *et al.*, 2015; Larsen *et al.*, 1991; Smith & Hunter, 1989; Möller, 1962). Despite this, previous correlative studies between varved clay-based deglaciation and DGM interdistances indicate that annual rates of deglaciation and proglacial water-depths are likely to be involved in the DGM forming process (Ojala *et al.*, 2015; Ojala, 2016); however, more thorough comparative work was suggested.

#### **2.4.3 DGMs in ice sheet reconstructions**

DGMs are significantly under-utilised within ice sheet reconstructions. Whilst some reconstructions acknowledge DGM evidence, due to the uncertainties surrounding genesis, utility is often limited to delineate spatial patterns of retreat only (Hughes *et al.*, 2016; Stroeve *et al.*, 2016). To our knowledge, DGMs have not been used as geochronometric ice margin indicators. As highlighted, these landforms are a potential rich source of both spatial and temporal information due to their regularity, and thereby affirm the value in accurately constraining these landforms to maximise reconstruction utility.

#### **2.5 Crevasse-squeeze ridges**

CSRs are deposits formed within fractured ice, often preserving the spatial pattern of crevassing (Benn & Evans, 2010). CSRs can provide important information concerning subglacial processes, which can be extrapolated to assist with understanding contemporary ice sheet behaviour (Evans *et al.*, 2016; Rea & Evans, 2011) (FIGURE 2.14).



**FIGURE 2.14.** Aerial images of CSR landforms (arrows indicate ice flow direction). A) Kjerulfbreen, Trygghamna, Svalbard; B) Brúarjökull, Iceland; C) submarine geometric ridges, Wahlenbergbreen, Yoldiabukta, Svalbard; and D) Sefströmbreen, Brevika, Svalbard [source: Ben-Yehoshua, 2017].

CSRs can be described as relatively low-relief, straight, narrow, and sharp-crested ridges. They pertain a highly variable spatial distribution that can range from distinct geometrical, rhombohedral, cross-cutting/intersecting patterns (Lovell *et al.*, 2015; Solheim, 1991; Ottesen & Dowdeswell, 2006; Ottesen *et al.*, 2008), to linear ridges orientated oblique to former ice flow (Clapperton, 1975; Sharp, 1985). As CSRs are suggested to be a preservation of the spatial extent of crevasse cavities, it should be noted that crevasses evolve and deform with ice flow and therefore CSR comparisons with contemporary crevassing studies may reflect this process (Price & Whillans, 2001; Whillans & van der Veen, 2001).

Environmental parameters appear to play a role in both preservation potential and spatial distribution. CSR observations in marine settings tend to be larger in morphometry, particularly in height, which is suggested to be due to protection from subaerial exposure and postglacial reworkings (Lovell *et al.*, 2014; Farnsworth *et al.*, 2016; Ottesen *et al.*, 2016; Boulton *et al.*, 1996; Ottesen *et al.*, 2008; Rea & Evans, 2011). In addition, ice dynamic settings (i.e. surge vs ice streaming) have revealed subordinate CSR patterns which may be useful in delineating ice flow dynamics (Evans *et al.*, 2016).

Sedimentological composition is typically reported as very dense, compact, poorly sorted, matrix-supported diamicton (Ben-Yehoshua, 2017; Lovell *et al.*, 2015; Johnson, 1975). Till fabric analyses report no significant internal structure or preferred orientation of clasts (Johnson, 1975). Sedimentological composition has been reported to be both homogeneous with and heterogeneous to underlying lithology, thereby indicating a possibility of ridge transportation following deposition (Ben-Yehoshua, 2017; Sobota *et al.*, 2016). This may be problematic when attempting to capture the spatial variability of stress and flow regimes from CSR spatial distribution.

### 2.5.1 CSR formation

The prerequisites for CSR formation are the fracturing of glacial ice and the availability of sediment. Many sedimentological studies suggest that CSR material originates from the bed, thus access to the glacier bed must be permitted via full-depth or basal crevassing (Rea & Evans, 2011).

Formation hypotheses vary slightly, with the most-common referred to as a tectonic, squeeze-up process due to changes in stress regimes and basal hydrological pressures (Ben-Yehoshua, 2017; Sharp, 1985; Benn & Evans, 2010) (FIGURE 2.12). Recent studies suggest a channelised infilling process whereby sediment-laden meltwater injects material into crevasse cavities (Evans *et al.*, 2016) (FIGURE 2.13). These variations relate to differences between active vs quiescent infilling processes (Johnson, 1975; Orlowska, 2022; Boulton *et al.*, 1996; Sharp, 1985; Lovell *et al.*, 2015), whereby infilling can be synchronous with ice fracturing processes, or asynchronous, post-fracturing during stagnation, whereby infilling arises from ice depression and supraglacial debris infill.

It is suggested that the variations in spatial distribution and patterning can provide valuable insight into formation mechanisms and thereby glacial processes (Evans *et al.*, 2016). Rhombohedral patterns have been inferred to represent stress regimes dominated by longitudinal stresses (i.e., extensional and compressive strain regimes), whilst chaotic patterning has been inferred to be representative of stresses characterised by thrust-style displacements and hydrofracturing due to basal water and sediment pore pressure overburden (Lovell *et al.*, 2015). Regardless, once CSRs have been formed, preservation requires a rapid down-wasting of the surrounding ice to prevent the ridges being destroyed (Evans *et al.*, 2016; Johnson, 1975; Ben-Yehoshua, 2017).

### **2.5.2 CSRs in ice sheet reconstructions**

CSRs have historically been indicative of surging ice dynamics (Ben-Yehoshua, 2017); however, more recently have been used as indicators of ice streaming environments (Evans *et al.*, 2016). This is important as ice streams play a significant role in reducing ice sheet volume (Stokes, 2000; Stokes & Clark, 2001; Stokes, 2018; Bennett, 2003). Ice stream surface crevassing patterns and CSR observations have inferred significant similarities between the palaeo-ice streams of the LIS and contemporary ice streams in Antarctica; however, the spatiotemporal properties of these palaeo-ice streams remain poorly constrained (Margold *et al.*, 2015; Angelis & Kleman, 2005). As such, many researchers have begun to focus efforts in these areas due to the value of being able to extrapolate information from palaeo-ice streams and improve understanding of contemporary ice streaming processes (Margold *et al.*, 2018; Evans *et al.*, 2016; Bennett, 2003; Angelis & Kleman, 2005; Stokes & Clark, 2001; Winsborrow *et al.*, 2010a).

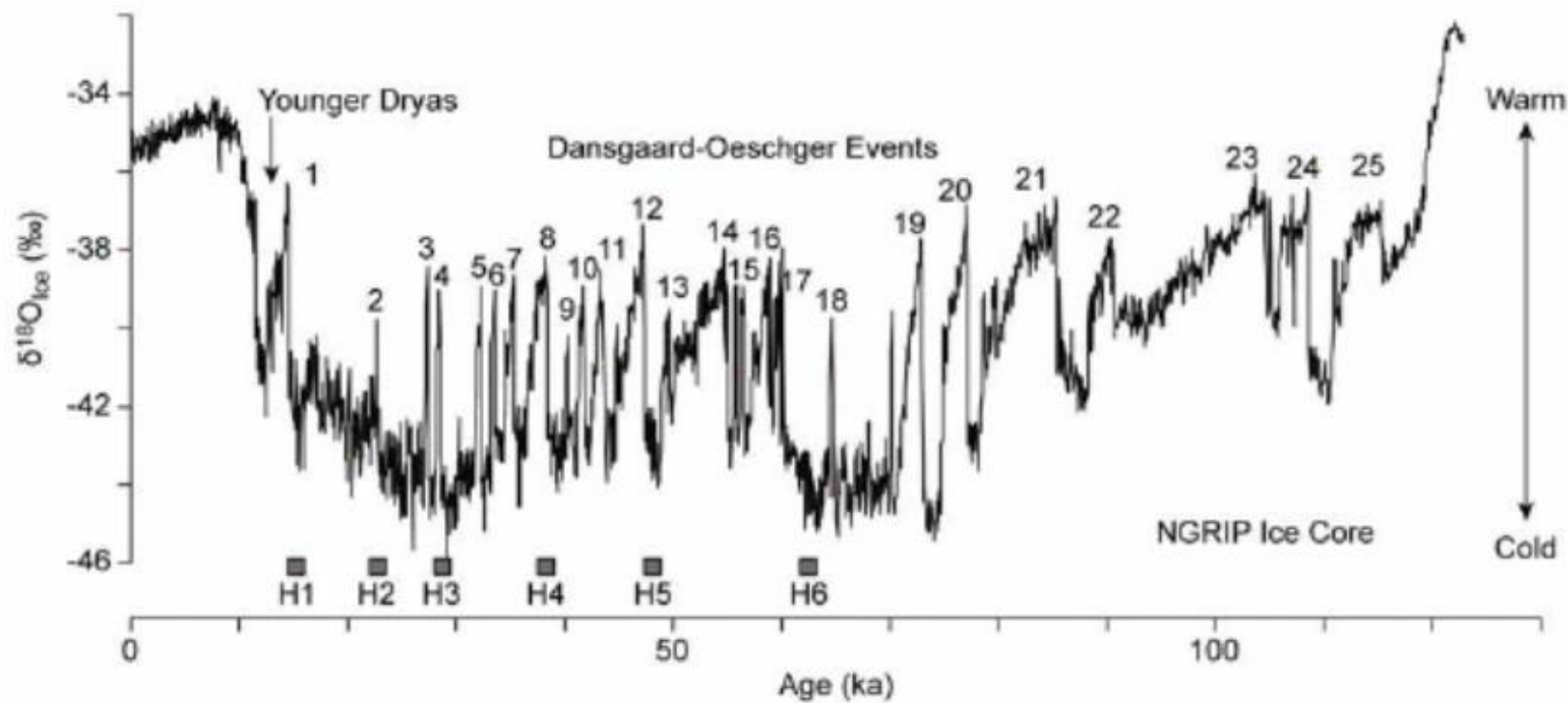
Whilst it is evident that DGMs and CSRs are morphometrically similar, the comparative review of literature highlights the different processes involved during formation and thereby the different utilities within palaeo-ice sheet reconstructions. Furthermore, accurate distinction between these landforms must be determined to validate the premise that DGMs may be used as effective ice marginal indicators.

## **2.6 Ice sheet evolution since the Last Glacial Maximum**

The Quaternary (the period spanning the last 2.6 million years) has been marked by several climate oscillations alternating between glacial and interglacial conditions (FIGURE

2.15) (Lisiecki & Raymo, 2005; Lowe & Walker, 2014). The LGM occurred ~23-21 ka BP (Clark *et al.*, 2009), during which time glacial ice occupied substantially more of the Earth's surface compared with today (FIGURE 2.16; Gowan *et al.*, 2021). In the northern hemisphere, the Greenland ice sheet was much more extensive, extending south-westwards, coalescing with the Laurentide, Cordilleran and Innuitian ice sheets, referred to collectively as the North American Ice Sheet Complex (NAISC) (Dalton *et al.*, 2020 & 2023). The NAISC covered almost all of Canada and large areas of North America (Dalton *et al.*, 2020 & 2023; Gowan *et al.*, 2021). In addition, Iceland was entirely covered by ice (Ingólfsson *et al.*, 2010), and a large ice sheet complex occupied Fennoscandia and most parts of northern Europe (Clark *et al.*, 2022; Hughes *et al.*, 2016; Stroeve *et al.*, 2016). In the southern hemisphere, large ice masses were present across Patagonia and the Antarctic ice sheet was also much more extensive than today (Gowan *et al.*, 2021).





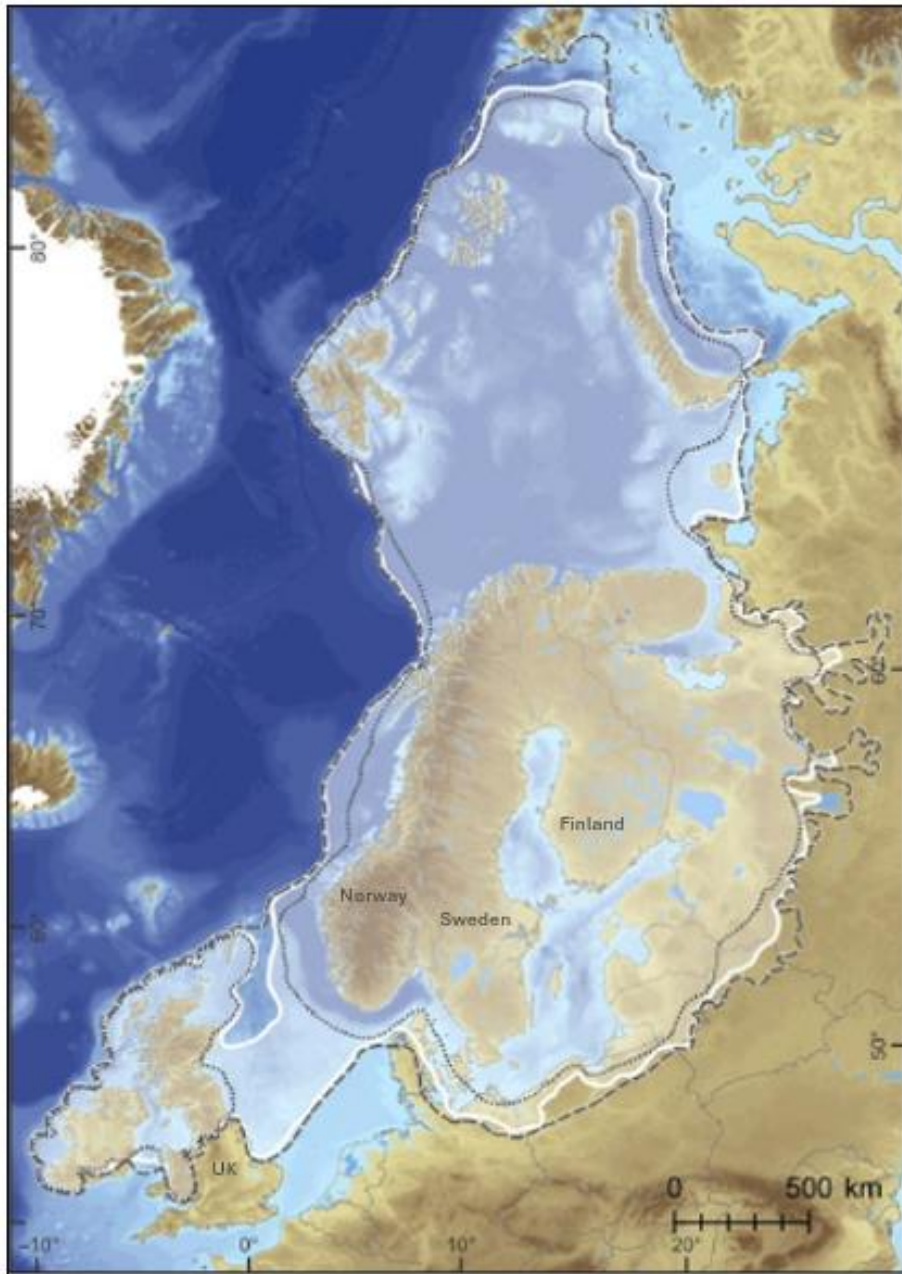
**FIGURE 2.15.** The marine oxygen isotope record from the NorthGRIP ice core showing warming and cooling events over the last 125 ka [source: Lowe & Walker, 2014].



Following the LGM, the climate warmed, instigating a general (although time-transgressive) retreat across northern hemispheric ice masses; this was interspersed with short intervals of cooling and ice readvance. These cooling events include the Younger Dryas (YD) stadial (~12 900 – 11 700 yr BP (Cheng *et al.*, 2020; Velay-Vitow *et al.*, 2024)) and the Preboreal Oscillation (PBO) (11 400 – 11 100 yr BP (Fisher *et al.*, 2002; Rasmussen *et al.*, 2007; Velay-Vitow *et al.*, 2024)). From ~11 000 yr BP, the climate generally returned to a state of stabilised warming and northern hemisphere ice masses gradually retreated until reaching the current extent of today. This study specifically focuses on the FIS, the evolution of which, following the LGM, is discussed in more detail below.

### 2.6.1 The Fennoscandian Ice Sheet

During the LGM (also referred to in Scandinavia as the Weichselian maximum), the FIS extended outwards from the Swedish mountains, covering Scandinavia and large parts of northern Europe (Hughes *et al.*, 2016; Lunkka, 2023; Ploeg & Stroeve, 2025; Regnéll *et al.*, 2023; Saarnisto & Saarinen, 2001; Sarala *et al.*, 2022; Stroeve *et al.*, 2016). Whilst there is uncertainty regarding the extent of this ice complex, minimum and maximum models have been proposed (Hughes *et al.*, 2016). The minimum model suggests that the eastern margins reached the central part of the Kola peninsula, the border between Karelia and Finland, and extended south-eastwards to the Baltic Sea gulfs and westward to the Kattegat, covering the Scandinavian peninsula (Hughes *et al.*, 2016) (FIGURE 2.17 (black dotted lines)). The maximum model proposes a much wider extent whereby the FIS coalesced north-eastward with the Svalbard-Barents-Kara Ice Sheet (SBKIS) and south-westwards with the British-Irish Ice Sheet (BIIS), with southern margins reaching northern Germany, Poland, and Belarus (Hughes *et al.*, 2016; Stroeve *et al.*, 2016) (FIGURE 2.17 (black dashed lines)).



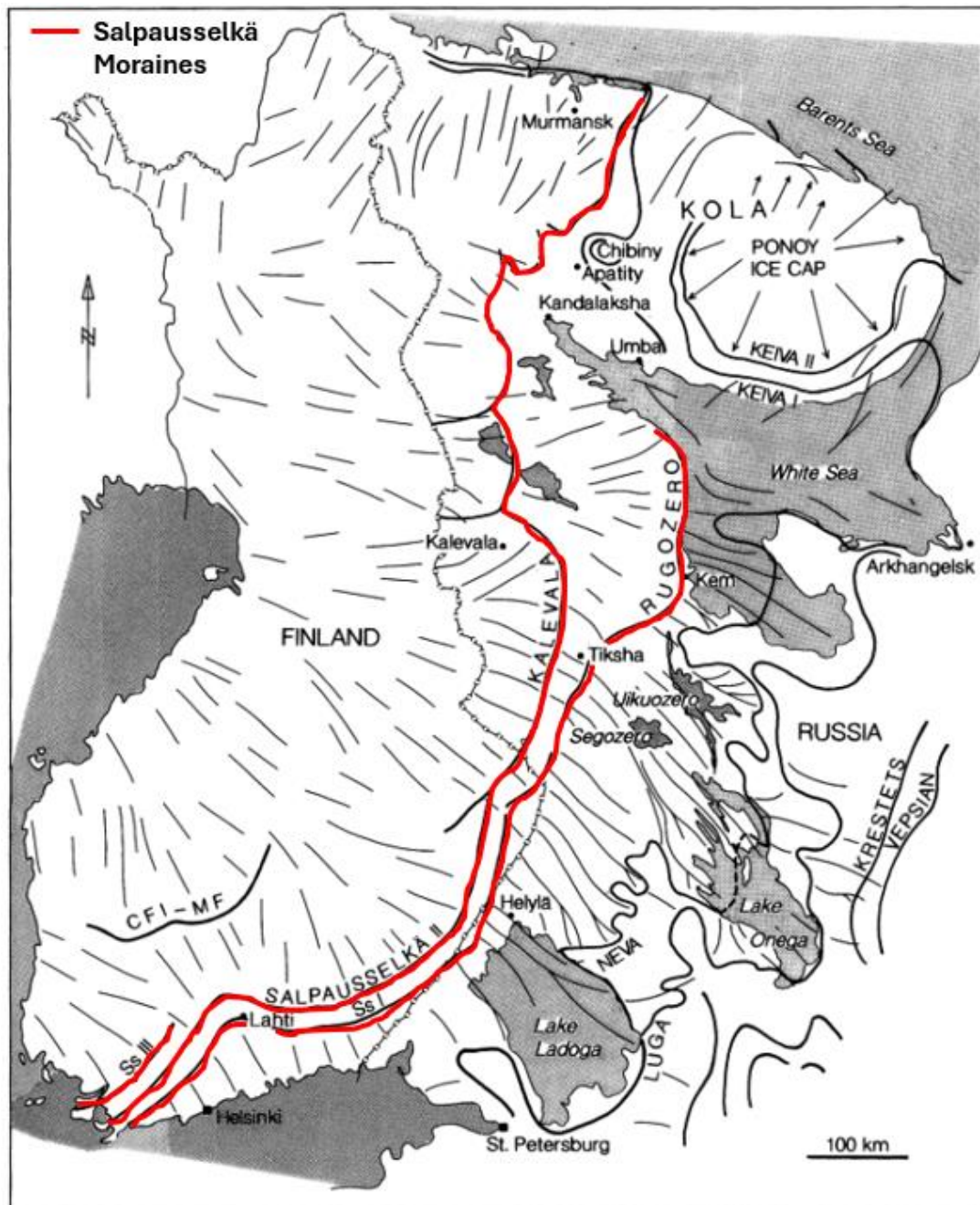
**FIGURE 2.17.** Reconstruction of the Eurasian Ice Sheet at ~20 ka BP showing ‘minimum’ (black dotted lines), ‘maximum’ (black dashed) and ‘most credible’ (solid white line and shaded white area) extents [source: Hughes *et al.*, 2016].

Following the LGM (based on the most-credible model (Hughes *et al.*, 2016)), by ~18-17 ka BP, the FIS and BIIS had become disconnected and by ~15 ka BP, the connection between the FIS and SBKIS had also ceased, rendering the FIS as the largest ice mass across Scandinavia and northern Europe. By ~13-12 ka BP the FIS had retreated from northern Europe, occupying Fennoscandia only. The south-eastern margins extended from southern Norway and Sweden to the southeast of Finland. This period was

characterised by the short-lived readvance of the YD (~12.9 – 11.7 ka BP) (Carlson, 2013) as evidenced by large moraine formations, known as the Salpausselkä moraines (SS I & II), which can be traced north-eastwards through the Scandinavian peninsula, south-east Finland, Russian Karelia and the Kola Peninsula (FIGURE 2.18) (Donner, 2010; Glückert, 1995; Lunkka *et al.*, 2021; Rainio *et al.*, 1995; Rinterknecht *et al.*, 2004; Saarnisto & Saarinen, 2001; Tschudi *et al.*, 2000; Putkinen *et al.*, 2011). In the northwest, the margin generally followed the west coastline of Sweden.

A return to warming after the YD instigated a return to retreat during which time the south-eastern ice margin maintained a relatively steady retreat north-westwards. At ~11.4 ka BP, another temporary (~200-300 year) cooling event (e.g. the PBO/11.4 ka event) (Rasmussen *et al.*, 2007) led to a short-lived readvance/standstill which is suggested to be marked by SS III located in Finland (FIGURE 2.6) (Salonen, 1990). By ~10 ka BP, the ice mass had retreated completely from Finland and occupied only Norway and the Swedish mountains (Hughes *et al.*, 2016).





**FIGURE 2.18.** Map showing large Salpausselkä moraines (SS I, II & III) that can be traced north eastwards through southeast Finland. NB. While the Finnish Salpausselkä moraines extend northward into Russian Karelia and the Kola peninsula, these are classified separately and have their own distinct nomenclature [source: Saarnisto & Saarinen, 2001].

## 2.7 Summary

Palaeo-ice sheet reconstructions are important as they help to improve understanding of glacial ice response to climatic change over long periods of time. Temporal resolutions of ice sheet reconstructions are limited to > 1 000 – 100-year intervals at best; however, technological advancements in remote sensing instrumentation present an opportunity

to refine these resolutions by enabling more subtle, regularly formed, low-relief geomorphology to be observed and integrated.

DGMs are low-relief landforms that are suggested to be formed regularly (potentially annually), at the ice margin. As such, it is plausible that DGMs could be an excellent landform candidate to refine ice margin reconstructions. Due to the ambiguity regarding formation, thorough investigations must be undertaken to accurately constrain spatiotemporal properties and differentiate them from similar landforms (e.g. CSRs). If formation properties are accurately constrained, and DGMs are found to be annual formations, these landforms could provide very high-resolution ice marginal geochronometric indicators which would significantly improve the resolutions of ice-margin reconstructions. In turn, the information from such high-resolution reconstructions may be used to better inform numerical modelling and predictions of contemporary ice sheets. This would be a valuable and constructive development on the previous work conducted by Ojala *et al.*, (2015 & 2016), whereby DGMs were mapped across southwest Finland and compared with local varve chronologies and BIL water depths. This study aims to provide a more detailed investigation of DGM formation in southwest Finland and explore the potential utility of DGMs as ice margin indicators.

## Chapter 3: Method overview and key study areas

This chapter provides a brief introduction to the methods used throughout the study and the strategic approach taken to achieve the research objectives stated in section 1.2.2. A description of the key study areas is also provided.

### 3.1 Introduction

The approach to methods in this study is primarily guided by the research objectives (see section 1.2.2) and determined by practicality of resource availability. Given that DGM formation properties must first be constrained prior to utility as ice margin indicators, a tiered approach is adopted whereby firstly, a large scale preliminary remote sensing study is undertaken which allows for a practical and cost-effective morphometric assessment of DGMs, and valuable comparison to the similar landform – CSRs. These investigations will also provide a first pass (albeit very detailed) indication of DGM formation properties and address the long-standing debate between DGM and CSR landform groups. Secondly, arising from the results of the first method investigations, a ground truthing method is undertaken whereby a more detailed investigation of DGM internal architecture is assessed to test the inferences made from the remote sensing investigations and provide stronger, more robust evidence of DGM formation. Finally, on the basis that DGM formation is proved to be at the grounding line of a subaqueous ice margin, isochrones can be reconstructed from the DGMs, utilising the remote sensing data acquired from the first investigations. A brief introduction of the methods used is provided below and more detail utility is provided in each result chapter respectively.

### 3.2 Methods

#### 3.2.1 Remote sensing & geomorphological mapping

A key foundation for this study is the acquisition of geomorphological data (Chandler *et al.*, 2018; Kleman & Borgström, 1996; Pearce *et al.*, 2017; Stokes & Clark, 1999;). Geomorphological data can be used to: constrain the spatial characteristics of landforms (Butcher *et al.*, 2020; Frydrych, 2022; Storrar *et al.*, 2014), differentiate between similar landforms (Rivers *et al.*, 2023), and, pertinent to this study, provide ice marginal proxies



from the relative spatial positioning of landforms (Bradwell *et al.*, 2021; Chandler *et al.*, 2016; Clark *et al.*, 2012; Dulfer *et al.*, 2022; Mangerud *et al.*, 2019; Rowan *et al.*, 2022).

Remotely sensed imagery has become a powerful medium for acquiring geomorphological data, particularly across large spatial areas. The applicability of using remotely sensed imagery is underpinned by three key factors: spatial resolution, temporal resolution and spectral resolution. Spatial resolution can be viewed from two perspectives; firstly, the extent of spatial coverage (e.g. does the sensor pass over the entirety of the chosen study area), and secondly, the clarity of detail in the imagery (e.g. pixel resolution). Temporal resolution is determined by how frequent the sensor obtains imagery of a certain area. Spectral resolution refers to how sensitive the sensor is to the variety of wavelengths in the electromagnetic spectrum. Currently, no single sensor satisfies all three domains (Al-Wassai & Kalyankar, 2013; Dubovik *et al.*, 2021). This can result in a trade-off when choosing imagery that may inhibit the scope of research depending on the required data. Concerning geomorphological mapping, spatial resolution is critical for determining accuracy. Again, there can be a trade-off here, whereby the spatial coverage or 'swath footprint' of an area may be limited although advantageously characterised by highly detailed imagery; or vice versa, whereby imagery pertains a large spatial coverage, but characterised by a low pixel resolution.

When a study area with suffice imagery has been selected, geomorphological features can be mapped using Geographical Information Software (GIS). This involves a careful manual scanning of the imagery to identify target features followed by tracing the crestline of each target landform, accompanied by the outer perimeter, depending on the morphometric data desired. This process takes time, depending on the extent of the study area and the number of landforms to be mapped, and requires a good understanding of the target landform along with a well-articulated mapping strategy to mitigate errors.

Due to the time involved with studies of this nature, machine learning has become a popular area of development for automated mapping (Barnes *et al.*, 2024; Brigham & Crider, 2022; Giaccone *et al.*, 2021; Lewington *et al.*, 2019; van Asselen & Seijmonsbergen, 2006). Such automated methods, however, can be limited in accuracy and better utilised to provide complementary data for manual studies (Dyba, 2024; Houser *et al.*, 2022; Lewington *et al.*, 2019). As such, manual mapping methods currently remain the most

reliable to assure quality, and to enable more accurate identification and understanding of landform evolution and wider glaciological implications.

For this study, due to practicality and availability of data, remote sensing was deemed an appropriate method in which to begin investigations. Specific remote sensing methods are presented in more detail in chapter 5.

### **3.2.1.1 Morphometric analysis**

Morphometric analysis refers to the assessment of form and geometric properties of a given landform. Geographical Information Software (GIS), such as ArcGIS (ESRI), provide a plethora of sophisticated techniques for analysing geospatial data and morphometry. At its core, geospatial analysis entails identifying specific information requirements from spatial data (e.g. length and width of a landform) and executing an appropriate GIS 'tool' in fulfilment of such. This process can be complex and time-consuming depending on the desired information, data sizes and tool availability. It may be, for example, that numerous tools need to be executed successively and therefore warrant the development of a more tailored geoprocessing sequence. This can present challenges when attempting to achieve functional outputs and inevitably, render such methods favourable to more experienced GIS users. Considering this study, it is required to acquire very detailed morphometric information across large datasets and therefore to improve data analysis efficiency, a new geoprocessing method was developed in the form of a Python-based ArcGIS toolbox. This is presented in chapter 4.

### **3.2.2 Sedimentology & Ground Penetrating Radar (GPR)**

Studying the sediment structure and composition of a landform is an effective method in which to observe and understand the processes involved during formation. This can be done via sediment exposure investigations (e.g. glacial sedimentology) (Evans, 2004; Lindholm, 1987), and/or via geophysical methods (e.g. ground penetrating radar (GPR)) (Bristow & Jol, 2003). Glacial sedimentology is the most reliable method for elucidating landform genesis as it involves direct observation of sedimentary facies and structures that can be used to test formation hypotheses (Evans, 2004). These studies can, however, be labour-intensive, highly selective in observations and measurements, and destructive if new exposures are to be excavated.

In contrast, geophysical methods such as Ground Penetrating Radar (GPR) are a relatively quick and non-intrusive approach to investigate the internal structures of landforms. This method works by using pulses of electromagnetic waves to image the subsurface of the ground, therefore removing the need for sediment exposures (Harrison *et al.*, 2022; Lally *et al.*, 2023; Stoker *et al.*, 2021; Ruffell *et al.*, 2013; Neal, 2004; Harrison *et al.*, 2022). This enables greater observational capacity and concurrently increases dataset representativity in contrast to sedimentological investigations. The outputs from geophysical methods can be difficult to interpret however, and subsurface visualization can be restricted by the presence of specific sediments (e.g. clay) and/or high-water contents (Neal, 2004). An advantageous solution to overcoming each of the method-specific limitations is to combine sedimentological and geophysical investigations. This combined is the approach taken in this study and is presented in chapter 6.

### 3.2.3 Ice margin reconstruction

Palaeo-ice sheet reconstructions rely on geomorphological indicators to constrain spatial ice extent, combined with a variety of dating/geochronological methods to constrain ice evolution through time (Hughes *et al.*, 2016; Stroeven *et al.*, 2016; Clark *et al.*, 2022; James *et al.*, 2019; Dalton *et al.*, 2023). Ice extent indicators are usually acquired via geomorphological mapping (see section 2.3). Pertinent to dating, there are a vast number of methods that can be used to constrain the timing of ice extent. These include radiometric methods, based on the decay of unstable chemical elements; incremental methods, involving the measurements of regular accumulations of materials through time; and age-equivalent methods based on contemporaneous stratigraphic horizons across different sedimentary sequences (Lowe & Walker, 2014). Each method has advantages and limitations, with the most appropriate method being determined by factors such as the type of material being dated, the dating range of the method, and the reliability of dates from which the method can provide (e.g. ‘*accuracy*’ (the degree of correspondence between the true age and that obtained by the dating method) vs ‘*precision*’ (the statistical uncertainty that is attached to any physical or chemical element) (Lowe & Walker, 2014)).

Incremental dating methods are unique in that they can provide potentially annual successive time records of glacial retreat. Annually accumulated glaciolacustrine

sediments are referred to as ‘*varves*’, and their use as annual geochronological indicators was first recognised by Gerard De Geer as early as 1878. In 1912, De Geer presented the first compilation of an extensive glaciogenic varve sequence from the southernmost to central parts of Sweden spanning a 12,000-year time-period (De Geer, 1912). Since then, numerous varve studies have been undertaken gathering greater, more detailed insights into deglaciation history (Ringberg & Rudmark, 1985; Saarnisto, 1985; Mörner, 1977; Sauramo, 1923; Strömberg, 2005; Breckenridge *et al.*, 2020; Ridge *et al.*, 2012). Whilst it is now acknowledged that not all sediment is supplied on a seasonal basis, and error margins within varve chronologies should be carefully assessed (Ojala & Tiljander, 2003; Holmquist & Wohlfarth, 1998), varve chronologies remain an unparalleled tool for depicting deglaciation at very high-resolution timescales (Avery *et al.*, 2020).

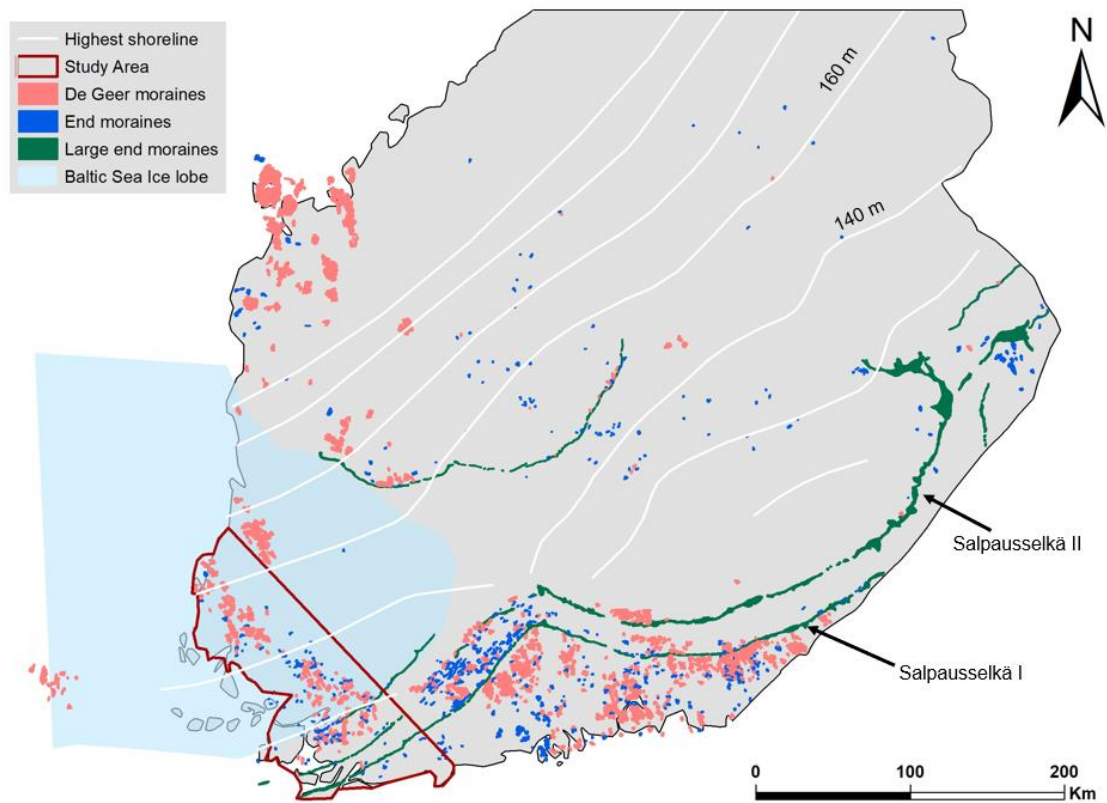
Based on the annual resolution of varve sequences, this provides the most appropriate geochronological dataset for determining the frequency of DGM formation. For example, a single De Geer ridge can be linked to the nearest varve site, with occurrences of ridges between each site counted, and compared to the floating varve dates to determine whether ridges form at an annual basis. Whilst the varve chronologies are ‘floating’, these dates can be more accurately anchored using dates derived from cosmogenic nuclide sampling in the local area.

Once timescales have been constrained, isochrones can be constructed via lateral extension of DGM ridges across the study area. This will provide an ice marginal reconstruction characterised by highly accurate ice margin configuration and potentially unprecedented annual rates of retreat. Ice marginal reconstructions of this calibre provide a much deeper, nuanced insight of ice margin retreat rates and grounding line dynamics. In turn, this information can be used to improve our understanding of contemporary ice margin dynamics and deglaciation. This work is presented in chapter 7.

### **3.3 Study areas**

#### **3.3.1 Southwest Finland**

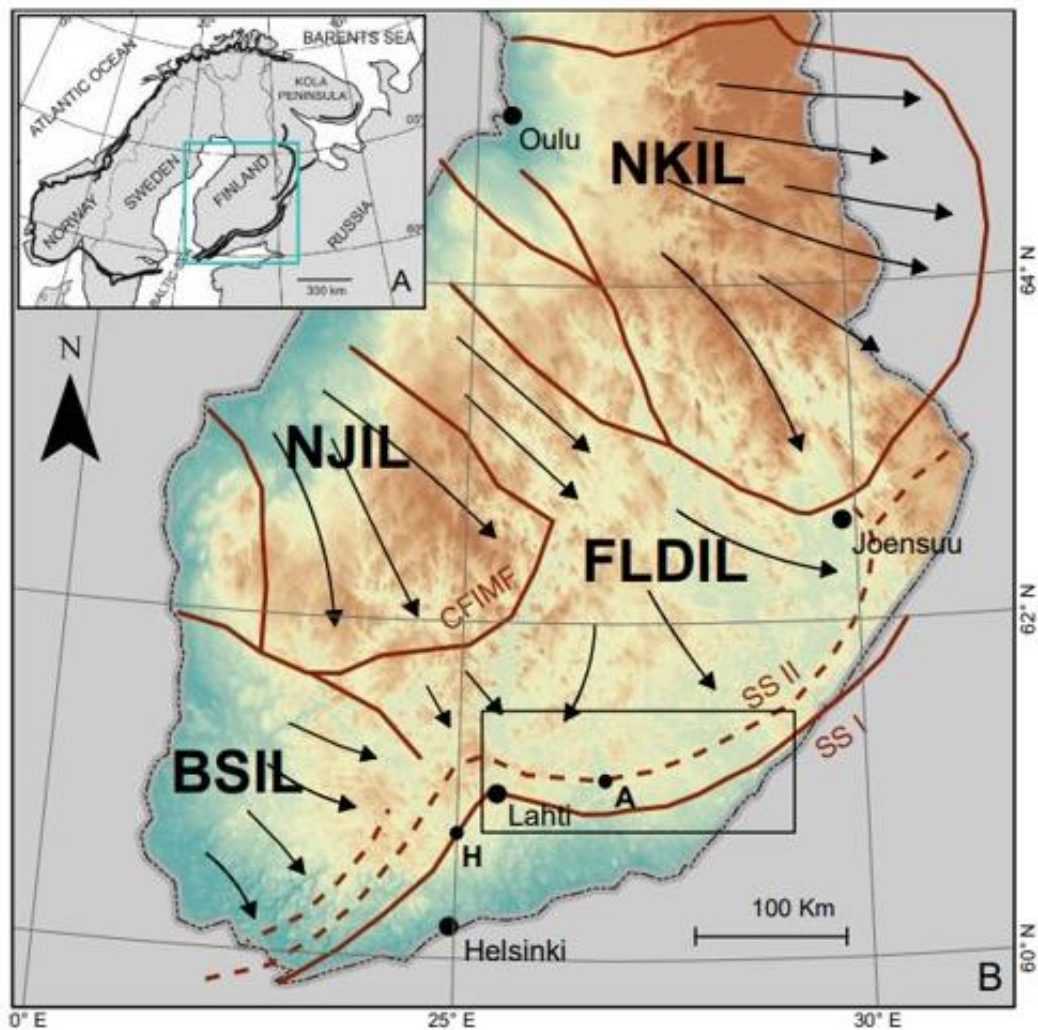
A key component of this project is to constrain the spatiotemporal properties of DGMs. These landforms are particularly abundant and prominent across southwest Finland (Ojala *et al.*, 2015; Ojala, 2016) and therefore was deemed a valuable study area for investigation FIGURE 3.1.



**FIGURE 3.1** Study area for investigations of DGMs located across southwest Finland.

During the LGM, Finland was completely covered by glacial ice, and at ~13-12 ka BP, the ice margin had reached southern coastal Finland (Hughes *et al.*, 2016; Stroeven *et al.*, 2016). Between ~12.9-11.7 ka BP, the ice margin remained stationary, or re-advanced, during the YD cooling event, resulting in the formation of SS I and SS II (Glückert, 1995; Rainio *et al.*, 1995; Rinterknecht *et al.*, 2004; Saarnisto & Saarinen, 2001; Tschudi *et al.*, 2000) (FIGURE 2.19). After the YD, a rapid retreat led to significant crenulation of the ice margin and resulted in the development of independent ice lobes (FIGURE 3.2) (Punkari, 1980; Johansson *et al.*, 2011). These ice lobes were more sensitive to localised factors such as bedrock, topography, proglacial water depth, and local climate, and therefore became more independent in retreat dynamics (Lunkka *et al.*, 2019; Lunkka *et al.*, 2021). The ice lobes were bordered either by each other, or by more passive areas of ice. The boundary zones (interlobate areas) are often characterised by large eskers and/or glaciofluvial interlobate complexes (Punkari, 1980; Lundqvist & Saarnisto, 1995). It is suggested that the ice lobes developed as a result of localised terrain, regional differences

in ice accumulation, and subglacial hydrology (Ojala *et al.*, 2021; Kurimo, 1982; Punkari, 1980).



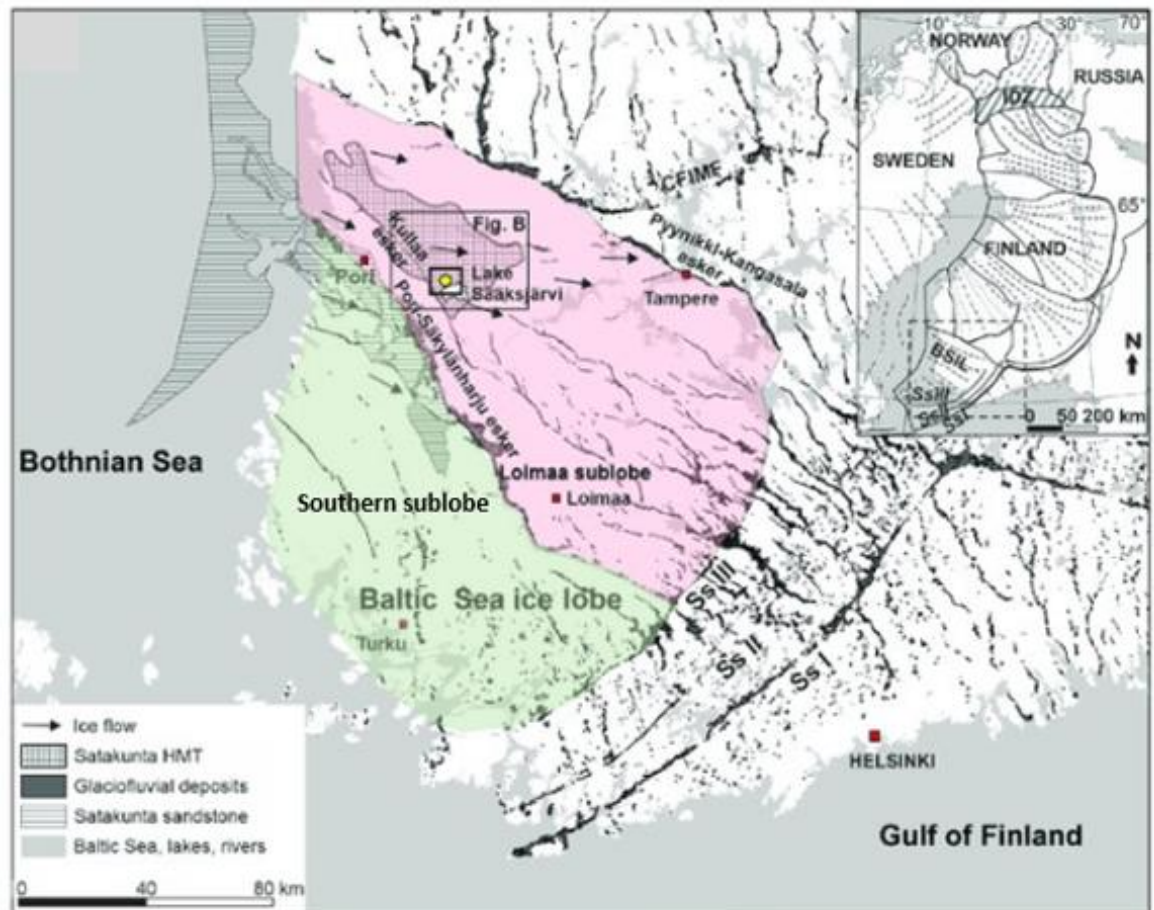
**FIGURE 3.2.** Post YD independent ice lobe formations situated across Finland. North Karelian Ice Lobe (NKIL), Näsijärvi Ice Lobe (NJIL), Finnish Lake District Ice Lobe (FLDIL), Baltic Sea Ice Lobe (BSIL): A) Inset map showing the most prominent Younger-Dryas age end moraines in Fennoscandia; B) Ice lobe formations and Salpausselkä moraines extending across Finland [source: Lunkka *et al.*, 2019].

The ice lobe that was situated across southwest Finland is referred to as the ‘Baltic Sea Ice Lobe’ (BSIL) (Punkari, 1980; Lunkka, 2019), the extent of which is marked by the position of SS III and was adjacent to the Finnish Lake District Ice Lobe (FLDIL) (FIGURES 3.2 & 3.3). Whilst dates have been regularly revised with technological advances in dating techniques and availability (Saarnisto & Saarinen, 2001; Tschudi *et al.*, 2000; Rinterknecht

*et al.*, 2004), the most recent estimations suggest that SS I was formed at the coalesced margins of the BSIL and FLDIL at approximately  $\sim 13.4 \pm 600$  ka BP (Lunkka *et al.*, 2021; Cuzzone *et al.*, 2016). A date of  $11.4 \pm 600$  ka BP is proposed for the formation of SS II (Cuzzone *et al.*, 2016), and it is postulated that SS III was formed  $\sim 300$  years after the beginning of the Holocene, coinciding with the PBO/11.4 ka event ( $\sim 11.4 - 11.1$  ka BP) (Donner, 2010; Rasmussen *et al.*, 2007; Salonen, 1990).

The BSIL was further subdivided into two sub-lobes; northern sub-lobe (Loimaa sub-lobe) and the southern sub-lobe that were divided by an interlobate esker (FIGURE 3.3) (Mäkinen *et al.*, 2023). Geomorphological evidence suggests disparities between the sub-lobe processes whereby the northern Loimaa sub-lobe is characterised by rich subglacial meltwater routes, as indicated by murtoo formations (Mäkinen *et al.*, 2023; Ojala *et al.*, 2021), and the southern sub-lobe is characterised by abundant DGM formations (Ojala *et al.*, 2015; Ojala, 2016). NB: The appearance of DGMs in similar sub-aqueous environments across the FIS is not uncommon, with many observations made around the eastern coastal areas of Sweden (Bouvier *et al.*, 2015), western Norway (Larsen *et al.*, 1991).



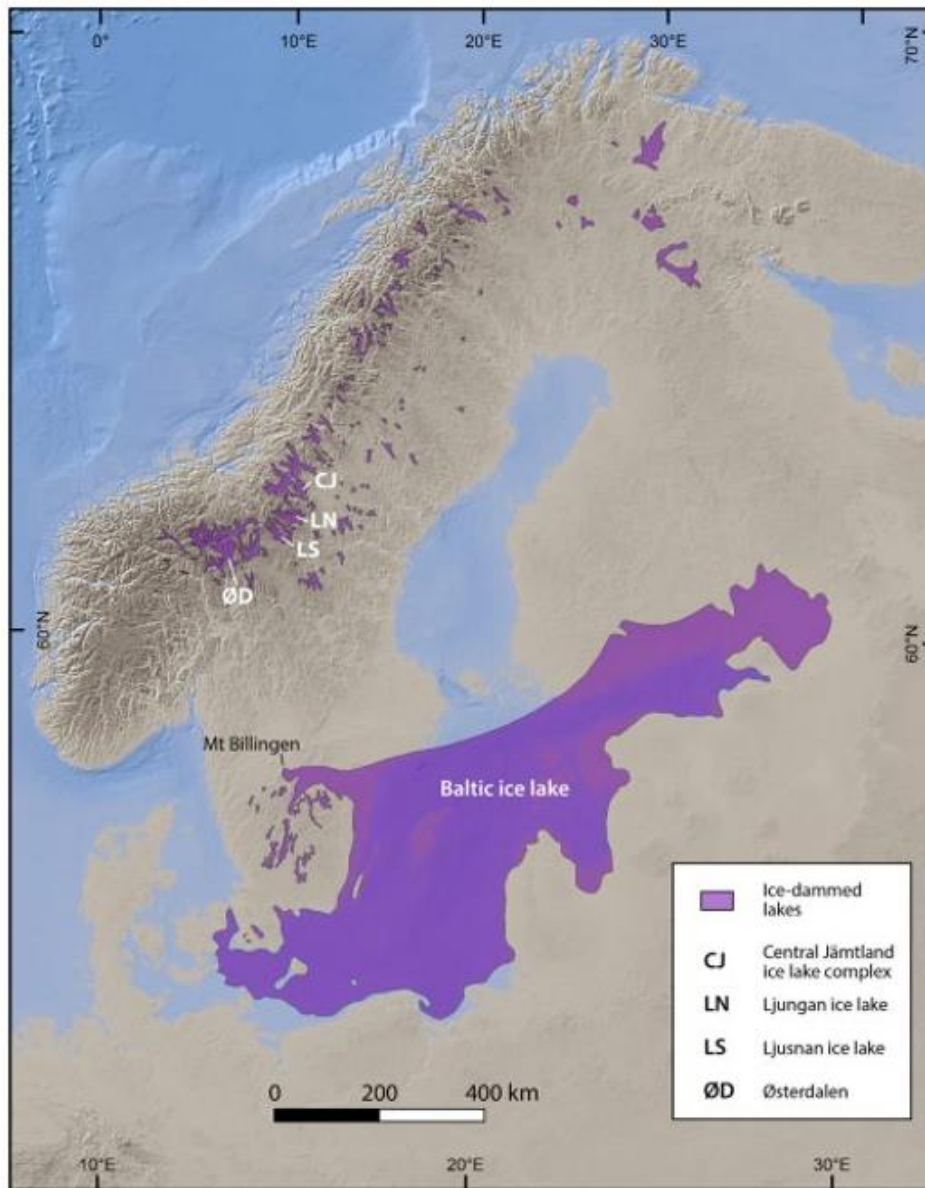


**FIGURE 3.3.** Location map showing the subdivision of the Baltic Sea Ice Lobe. Pink area represents the Loimaa sublobe, characterised by murtoo geomorphology, the green area represents the Southern sublobe, characterised by DGM geomorphology [figure edited from Mäkinen *et al.*, 2023]. NB: Inset Fig. B not shown.

In addition to direct ice controls, the geographical location of southwest Finland (and particularly the location of the BSIL southern sub-lobe) dramatically increased sensitivity to the evolving balances and feedback mechanisms between ice mass redistribution, sea level, and continental rebound (Eronen *et al.*, 2001). Due to the large ice mass occupying Finland ~12.9 – 11.7 ka BP, most of the southwest coast was submerged below sea level. During this time, the Baltic Sea area was disconnected in the west from the North Sea via the Öresund area between Sweden and Denmark (Andrén *et al.*, 2011; Björck, 2008), forming the Baltic Ice Lake (BIL) (FIGURE 3.4). Subsequent deglaciation, sedimentation, and differential uplift resulted in a variable ‘opening and closing’ of the western drainage area in Öresund which forced the evolution of the BIL to the Baltic Sea (Andrén *et al.*, 2011; Björck, 2008). Each of these interconnected processes- deglaciation, continental



uplift, fluctuating water depths, would have imposed significant controls over geomorphological development across SW Finland (Lunkka *et al.*, 2019; Ojala *et al.*, 2013).

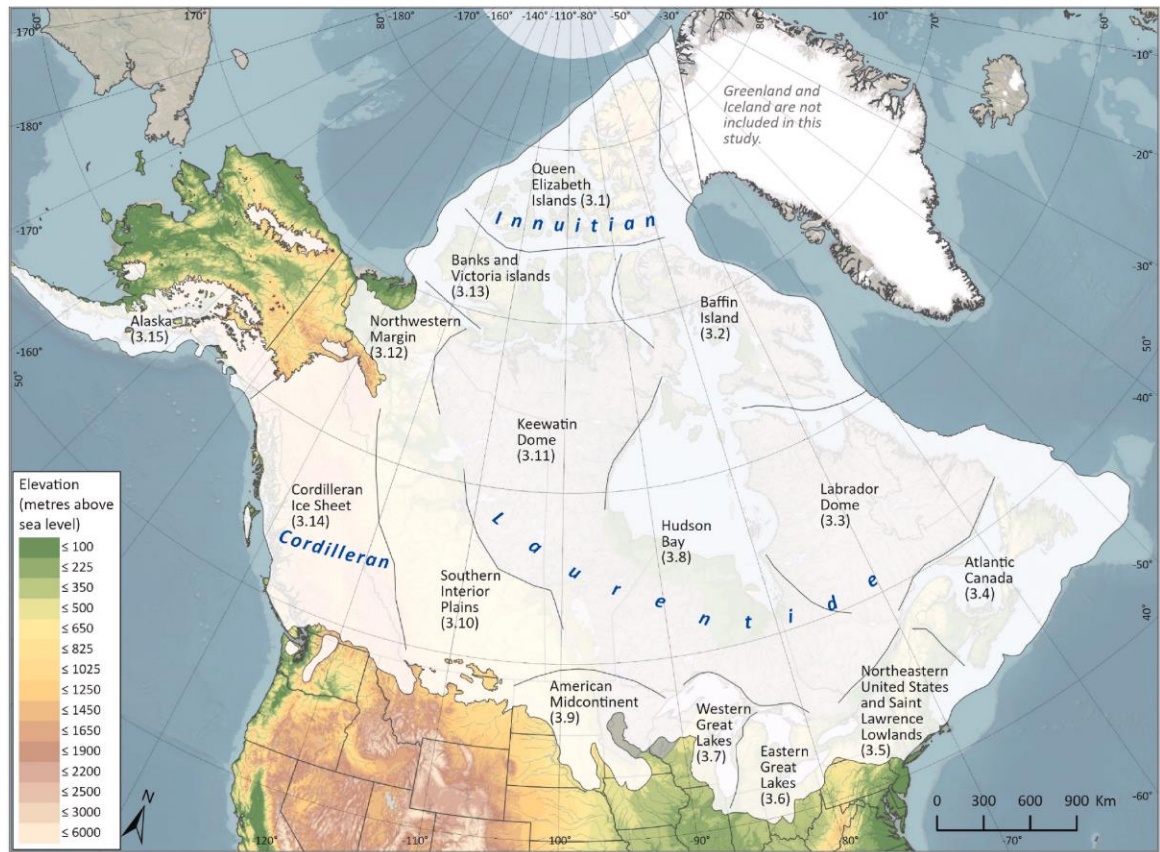


**FIGURE 3.4.** Location of the former Baltic Ice Lake (BIL) extending from SE Finland in a south-westerly direction toward SE Sweden. The BIL was characterised by distinct developmental stages that responded to ice advance/retreat phases and continental adjustments [source: Stroeven *et al.*, 2016].

### 3.3.2 Northwest Territories, Canada

Western Canada was one of several countries host to the second largest global ice complex during the LGM (Daltin *et al.*, 2023). This ice complex included a coalescence of

the Cordilleran ice sheet (CIS), the Laurentide ice sheet (LIS), the Innuitian ice sheet (IIS) and the Greenland ice sheet (GrIS) (Dalton *et al.*, 2023) (FIGURE 3.5). In this area, this most recent glacial period is often referred to as the Late Wisconsinian glaciation where ice reached its maximum extent (although time-transgressively) between ~25 – 20 ka BP (Dyke *et al.*, 2002; Stokes *et al.*, 2017; Dalton *et al.*, 2023). This was then proceeded by a significant recession and decoupling of the coalesced ice sheets (Stokes *et al.*, 2017).

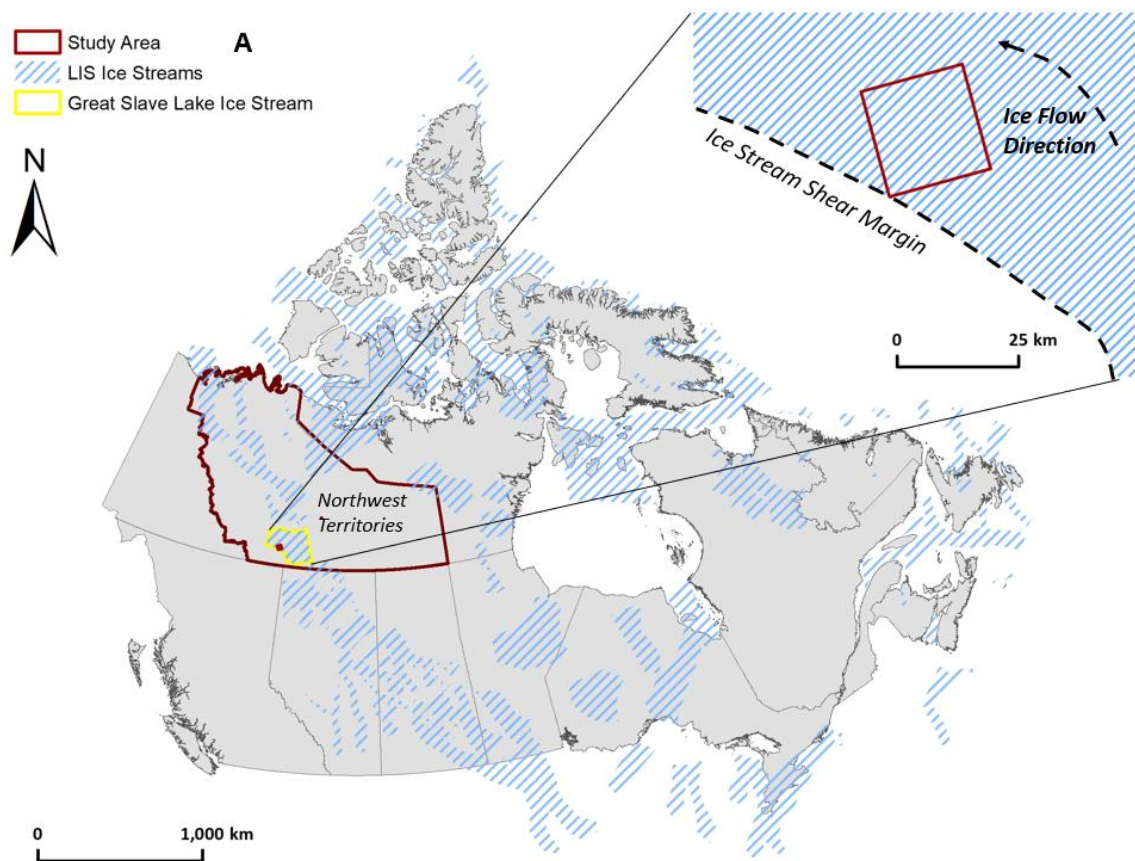


**FIGURE 3.5.** The North American Ice Sheet Complex (NAISC: comprising the Innuitian, Cordilleran and Laurentide ice sheets) [source: Dalton *et al.*, 2023].

In the west, at the CIS / LIS intersection, was a corridor defined by low-lying, relatively flat terrain located S-SE of the Mackenzie and Rocky Mountain belt. It is suggested that between 12.8 ka BP and 11 ka BP, rapid ice recession led to a decoupling of the CIS and LIS which resulted in an ice-free corridor, referred to as the 'Interior Plains' (Stokes *et al.*, 2017; Gowan, 2013). Furthermore, this area was characterised by a transition in bedrock lithology, from metamorphic/plutonic to sedimentary (Margold *et al.*, 2015). As a result of these topographical and geological disparities, much of this area was dominated by a dense ice streaming network (Margold *et al.*, 2015) which has been interpreted through

the underlying geomorphology, particularly with the presence of streamlined landforms diagnostic of ice streaming (e.g. CSRs).

The CSRs sampled in this study area associated with the former Great Slave Lake Ice Stream (Margold *et al.*, 2015), located in the interior plains of the Northwest Territories, Canada (FIGURE 3.6). The ridges located at this site exhibit clear geometric networks with evidence of cross-cutting, oblique and contrasting orientations that consistent with well-documented observations of typical CSRs elsewhere (Ankerstjerne *et al.*, 2015; Cline *et al.*, 2015; Evans *et al.*, 2016; Norris *et al.*, 2018; Ó Cofaigh *et al.*, 2010; Ross *et al.*, 2009). Not only will study area this provide a valuable dataset for DGM comparative analyses but will also provide the opportunity to develop and improve our understanding of ice stream dynamics.



**FIGURE 3.6.** Study area chosen for CSR data collection; a 20 km<sup>2</sup> section of the former Great Slave Lake Ice Stream, located in the Northwest Territories, Canada [ice stream data source: Margold *et al.*, 2015]. Location map shows the study area situated inside of the shear margin of the palaeo-ice stream.

## Chapter 4: Method Development- A Python-based ArcGIS toolbox to automatically generate 3D morphometric data of elongated landscape features at user-defined transect-segmented intervals

**Toolbox Repository:** [https://github.com/gwynrivers/3D\\_Morphometry\\_Toolbox](https://github.com/gwynrivers/3D_Morphometry_Toolbox)

**Citation:** Rivers, G.E., Storrar, R.D., Jones, A.H., Ojala, A.E.K. (2023). 3D morphometry of De Geer Moraines and Crevasse-Squeeze Ridges: Differentiating between pushing and squeezing mechanisms from remotely sensed data. *Quaternary Science Reviews*, 321C. DOI: <https://doi.org/10.1016/j.quascirev.2023.108383>

This chapter outlines the development of a new Python-based ArcGIS toolbox for the purposes of automatically extracting and calculating 3D morphometric data from large datasets, and demonstrates its use. The development of this method enabled the analysis of DGM morphometry as outlined in chapter 5 and contributed to addressing research objective (1).

### Abstract

A large body of research pertains to understanding and quantifying the morphology of elongated, positive (e.g. ridges), or negative (e.g. channels) geomorphological features. 3D morphometric analysis is a useful method by which to constrain feature morphology, thereby improving our understanding of landform genesis and evolution. Unfortunately, morphometric analyses, particularly when dealing with large datasets, can be both complex and time-consuming. To mitigate this, a new method was developed in the form of a user-friendly, Python-based ArcGIS toolbox, that efficiently extracts and calculates 3D morphometric data at user-defined transect intervals along the profile of a given landscape feature. This allows for a highly detailed assessment of elongated features and provides users with a robust dataset for further analysis if required. It is intended that this toolbox will provide an effective means by which to analyse large-scale datasets for the purposes of detailed landform morphometric quantification.



## 4.1 Introduction

A large body of research pertains to understanding and quantifying elongated landforms such as: eskers (e.g. Storrar *et al.*, 2015; Butcher *et al.*, 2016; Butcher *et al.*, 2019; Frydrych, 2022), river channels (Li *et al.*, 2022; Sarif *et al.*, 2021; Soar *et al.*, 2017; Xie *et al.*, 2018), moraines (Finlayson & Bradwell, 2008; Dunlop, 2004; Kaufman *et al.*, 1988), crevasse squeeze ridges (Ben-Yehoshua, 2017; Evans *et al.*, 2016), inverted fluvial channels (Valla *et al.*, 2010), palaeochannels (Re *et al.*, 2018), tectonic landforms such as volcanic structures (Scheidegger, 2002; Stretch *et al.*, 2006; Székely & Karátson, 2004; White *et al.*, 2002) and wrinkle ridges (Bethell *et al.*, 2022; Karagoz *et al.*, 2022; Kreslavsky & Basilevsky, 1998; Plescia, 1993). To date, these studies have employed a wide range of techniques to extract morphometric data. Below, several morphometric studies previously undertaken are highlighted and some of the challenges associated with data collection and morphometric quantification are described. The toolbox is then described in detail, explaining function and providing an example of use.

### 4.1.1 Morphometry studies

Morphometry deals with the measurement of form and is an integral aspect of geomorphological studies (King, 1982; Evans, 2012; Pike, Evans & Hengl, 2009). Quantifying morphometry enables a deeper understanding of form and process to be developed, and allows for the differentiation of different landform types, which can facilitate the development of classification criteria, landscape evolution models (LEMs) and process-form models (Valters, 2016; Li, 2020). Typically, contemporary morphometry studies adopt a two-step approach: (1) the acquisition of remotely sensed Digital Elevation Model (DEM) data, utilised for feature identification and digitisation; and (2) the extraction and quantification of feature morphometry.

### 4.1.2 Remotely sensed high-resolution DEM data

Technological advances in remote-sensing instrumentation have provided a means to improve morphometry studies (Li *et al.*, 2020; Fu *et al.*, 2019). Freely available DEM data, characterised by high spatial resolutions (most commonly 2 m GSD, but occasionally even higher) and wider spatial coverages, has permitted the capturing of large, highly detailed, and highly representative geomorphological datasets (Napieralski *et al.*, 2013). Furthermore, the development of a wide range of GIS tools has introduced more efficient

and sophisticated analysis methods, which can provide powerful information regarding landform characteristics and landscape evolution (Otto *et al.*, 2018; Li *et al.*, 2020; Rao, 2002; Mesev, 2007). These technological developments present significant opportunities to improve morphometry studies and yield new insights into landform processes.

#### **4.1.3 Morphometric quantification**

The quantification of feature morphometry requires the accurate measurement of geometric properties. Whilst basic morphometrics (e.g. length, width, and height) of a given landscape feature may be quantified with relative ease, this quantification can become more complex when dealing with large datasets and landforms defined by high spatial variability. This is particularly pertinent to elongated landscape features (e.g. ridges or channels), whereby morphometry varies along a feature's length. Such variability might be important for interpreting the origin of a landform, or even for understanding varying conditions during its formation. In addition, more detailed 3D cross-sectional information may be required if landform type is difficult to establish. This is particularly relevant when attempting to identify ambiguous landforms (e.g. Butcher *et al.*, 2016).

To capture a more detailed 3D morphometric assessment of a given landscape feature, a segmented-transect analysis approach can be employed, whereby a larger landform is divided into subsections and a cross-sectional analysis is undertaken. This approach has been effectively demonstrated in recent studies of eskers (elongated, sinuous ridges that depict the preservation of sedimentation in glacial meltwater drainage conduits; section 2.3.1.1) whereby 3D morphometrics were calculated at set transect intervals (Butcher *et al.*, 2016; Storrar *et al.*, 2015). This method has proved successful in providing a more enhanced classification of esker landforms, whilst also improving inferential knowledge relating to process-form models and landscape evolution. Such methods are proving popular in similar geomorphological studies (Ely *et al.*, 2017; Frydrych, 2022; Butcher *et al.*, 2020; Gomez-Heras *et al.*, 2019; Sapsa *et al.*, 2020; Ojala *et al.*, 2015), thereby highlighting the need to streamline this process to enable up-scaling of sample sizes and increase user accessibility.

#### **4.1.4 Challenges in morphometric analysis**

A key challenge of morphometric analysis is the complex integration of appropriate GIS tools. The integration of multiple tools and geoprocessing methods can become time-

consuming and characterised by complex workflows. This issue becomes further amplified when dealing with large datasets.

To overcome some of the complexity, and to enable large sample-size morphometric datasets to be easily and reliably generated, a new open-access Python-based ArcGIS toolbox was developed that automatically extracts 3D morphometric data at user-specified segmented transect intervals. An example application of the toolbox is provided to demonstrate the effective quantification of elongate landscape morphology using CSRs located in Northwest Territories, Canada, as an example dataset. It is intended that this toolbox will be of use to both research and industry GIS users, ranging from novice to advanced levels, that are interested in quantifying and analysing elongated landscape features.

#### **4.1 The toolbox**

The toolbox comprises two tools: (1) a primary '3D Morphometry Tool'; and (2) a secondary 'Average Feature Tool'. The primary tool is intended to extract and calculate detailed 3D transect-segmented morphometry, at user-defined intervals, along the length of a target landscape feature. The secondary tool is available to average calculated transect morphometrics derived from the primary tool, per parent feature, to provide a whole-feature morphometric assessment. This results in a toolbox that can provide: (1) 3D morphometry at high-resolution segmented intervals, which is valuable for detailed landform analysis; and (2) a powerful method by which to compare detailed morphometrics between individual features. The ability to rapidly generate large sample sizes is also advantageous for investigating morphometric patterns in spatial distribution, either at smaller scales, along individual feature lengths, or at macroscales across wider landscape coverages. The recommended toolbox workflow is as follows:

- 1) Data preparation (digitisation of target features)
- 2) Execution of the primary tool '3D Morphometry Tool'
- 3) Undertaking of quality control checks and refining of primary output data
- 4) Execution of the secondary tool 'Average Feature Morphometry'
- 5) Undertaking further analysis of the calculated morphometry data as required

#### 4.2.1 Data preparation

Each individual target feature must first be digitised. This involves carefully tracing the outline and crestline of each individual landscape feature into an ArcGIS shapefile (a polyline shapefile for crestlines, and a polygon shapefile for outlines).

It is important to note that the quality of the input data determines the quality of the calculated morphometrics. It is advised that carefully designed rendering of DEM data is utilised during the digitisation process to avoid potential errors or biases. For example, it has been suggested that at least two different azimuths should be applied if using hillshades to identify features, to reduce shadow bias (Smith & Clark, 2005), and slope rendering can help to identify the central and lateral slope breaks of features to maximise accuracy (Chandler *et al.*, 2018). Crestlines should be smooth and extend at least to the edge of the digitised outline. Outlines should be mapped carefully to align with the lateral slope breaks of target features. Users should perform checks to ensure that input data is of sufficient quality.

#### 4.2.2 Toolbox operation and required inputs

##### 4.2.2.1 The primary tool

The primary tool '3D Morphometry Tool' requires: a polygon shapefile (.shp) containing digitised outlines of the identified target features, a polyline shapefile (.shp) containing digitised crestlines of the identified target features, a DEM of the study area (.tif), and a specified 'Output Folder' to store generated outputs. The file path to the 'Output Folder' must not contain any spaces. The 'Output Folder' should be refreshed after each tool has completed execution.

The primary tool also requires two additional user-specified parameters: (1) transect intervals (*units: meters*), which is the distance the user desires to set between each transect; and (2) transect length (*units: meters*), which is the length of each individual transect (*NB: transect lengths should be set at a length which extends beyond the entire width of the digitised outlines as these will be clipped to the outline extent upon running the tool*). Note: the run time of the tool is dependent on the size of the input dataset and the number of transects specified to be generated, as well as the specification of the computer used.



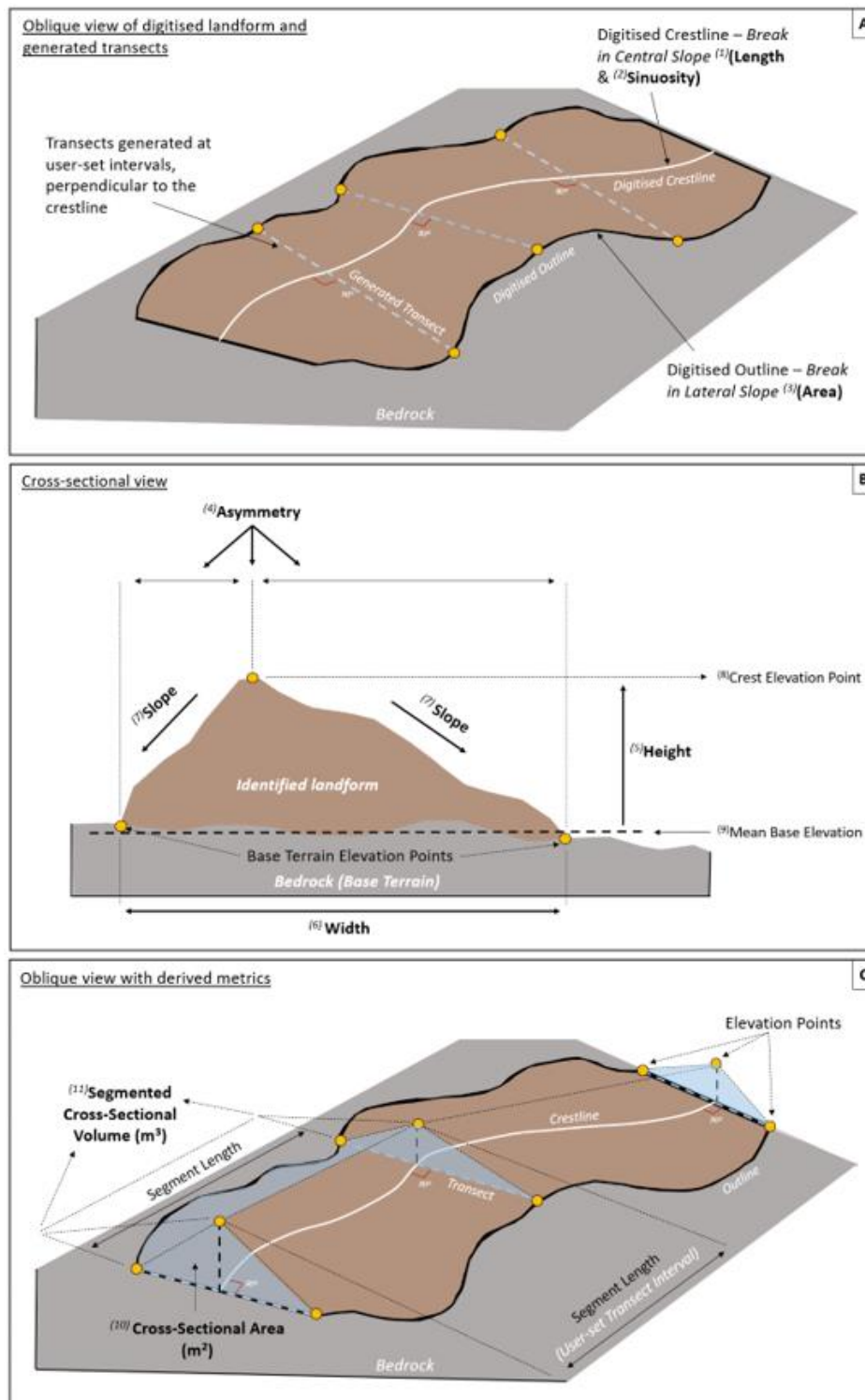
#### 4.2.2.2 The secondary tool

The secondary tool 'Average Feature Morphometry' requires: the generated '*Transect\_Morphometry.shp*' file, the generated '*Feature\_Morphometry.shp*' file, the original '*Feature Outline*' shapefile, and the file path to the specified '*Output Folder*'.

#### 4.2.3 Geoprocessing methods and morphometry calculation

Upon primary tool execution, each individually mapped crestline and outline is given a relative identification linking it to the target feature. Transects are then produced along each digitised crestline at user-defined intervals at an orientation of 90° to the crestline (FIGURE 4.1A). Elevation points are produced at three intersectional locations along each transect: at either side of the digitised outline and at the intersection of the crestline (FIGURE 4.1B).

Basic geometric information is calculated for each feature from the outline and crestline shapefiles. A footprint area is calculated from digitised outlines, and length and sinuosity are calculated from digitised crestlines (FIGURE 4.1, A). 3D morphometric data (height, width, slope, asymmetry, cross-sectional area, and cross-sectional volume) are extracted and calculated along each transect (FIGURE 4.1, B & C). The architecture of GIS tool integration can be seen in FIGURE 4.2. 3D morphometric calculations are detailed in TABLE 4.1.



**FIGURE 4.1.** A) Oblique view of digitised landform and generated transects. Basic morphometrics are calculated from outlines and crestlines (e.g. length, sinuosity and footprint area). B) Cross-sectional view of a digitised landscape feature highlighting the three elevation points along each transect. Asymmetry is calculated along each transect at the point of crestline intersection. A mean average base terrain elevation is calculated from the 'Base Terrain Elevation Points' (e.g. the two end points of each transect located

on the crestline. The height is calculated from the difference between the 'Mean Base Elevation' and the 'Crestline Elevation'. Width is calculated based on the extent of the digitised outlines. C) Oblique view of a digitised landscape feature with derived metrics. Cross-sectional area is calculated based on the principles of a triangular prism (e.g.  $0.5 \times \text{width (transect length)} \times \text{height}$ ). Cross-sectional volume is calculated for each 'transect segment' (e.g.  $\text{cross-sectional area} \times \text{segment length (transect interval)}$ ). See calculation table (TABLE 1) for each morphometric reference.

**TABLE 4.1.** Geoprocessing steps and calculation methods for each morphometric.

Morphometric Data	ArcPy Geoprocessing Tool	Calculation Methods
(1) Length	'Calculate geometry function' (unit: Meters)	Calculated along the digitised crestline of a mapped feature.
(2) Sinuosity	N/A	Calculated along the mapped crestline.
(3) Area (feature footprint)	'Calculate geometry function' (unit: Meters <sup>2</sup> )	Calculated for the outline polygon of a mapped feature.
(4) Asymmetry	'Split line at point'. Each transect is split at crestline-transect intersections.	Split transect lengths are divided by the overall transect length to give a result between 0-1.
(5) Height	N/A	'Average Base Terrain Elevation' deducted from 'Crestline Elevation' along each transect.
(6) Width	'Calculate geometry function' (unit: Meters)	Calculated based on the length of each transect.

Morphometric Data	ArcPy Geoprocessing Tool	Calculation Methods
(7) Slope	'Add Surface Information' (unit: degrees)	Calculated along each transect.
(8) Crestline Elevation	'Add Surface Information'	Calculated at each crestline-transect intersection point.
(9) Mean Base Terrain Elevation	'Add Surface Information'	A mean average elevation is calculated between the two outline-transect intersection points for each transect.
(10) Cross-sectional area	N/A	The cross-sectional area of each transect segment is calculated based on the principles of a triangular prism
(11) Cross-sectional volume	N/A	'Cross-sectional area' x length of each transect segment (e.g. user-specified transect intervals)

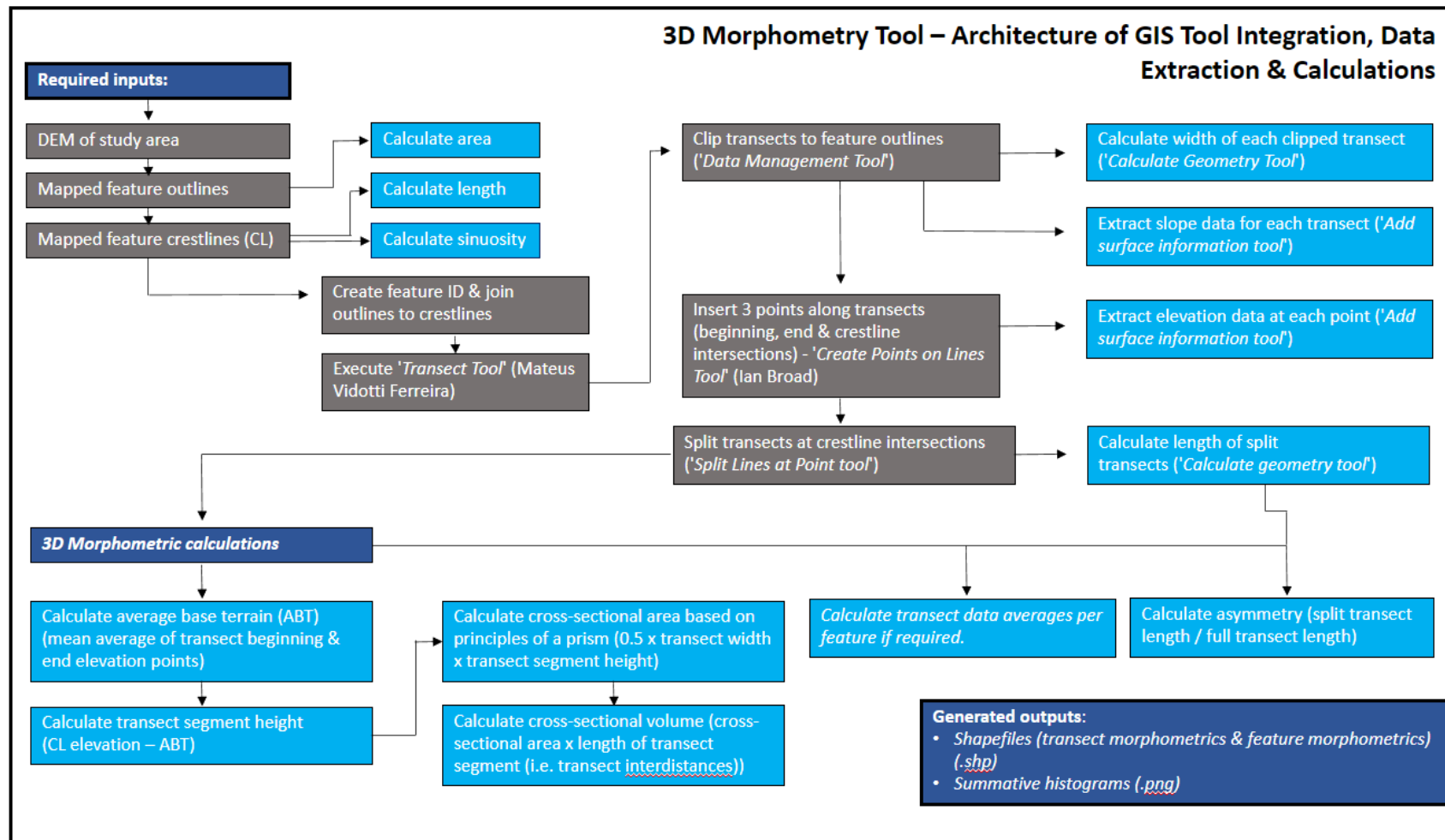


FIGURE 4.2. Schematic workflow illustrating ArcMap tool integration and 3D morphometric calculations.

#### 4.2.4 Generated outputs

##### 4.2.4.1 Primary tool '3D Morphometry Tool'

The executed primary tool provides outputs in geospatial and graphical formats.

Specific outputs include:

- 1) A shapefile ('*Transect\_Morphometry.shp*'). This file contains all calculated 3D morphometric data for each transect segment (TABLE 4.2).

**TABLE 4.2.** Reference table showing the generated '*Transect\_Morphometry.shp*' attribute table field names and relative morphometrics.

Output Code Name	Morphometric
CL_Z	<i>Crestline elevation</i>
HEIGHT	<i>Feature height</i>
AV_BASE_TE	<i>Average elevation of base terrain</i>
AVG_SLOPE	<i>Average slope along each generated transect</i>
ASYMMETRY	<i>Asymmetry along each generated transect</i>
WIDTH	<i>Width of each transect</i>
CS_AR	<i>Cross-sectional area of each transect segment</i>
CS_VOL	<i>Cross-sectional volume of each transect segment</i>
FEATURE_ID	<i>The feature to which the transects belong</i>

- 2) A shapefile containing merged outlines and crestlines ('*Av\_Feature\_Morphometry.shp*'). The attribute table of this shapefile contains morphometric information (*feature ID, length, area, and sinuosity*). Each mapped feature is given a feature identification ('*Feature\_ID*') and related crestlines, outlines and generated transects are associated accordingly.
- 3) A series of summary histograms for each calculated transect morphometric (i.e., '*Asymmetry.png*', '*Average\_Slope.png*', '*Cross\_Sectional\_Area.png*', '*Cross\_Sectional\_Volume.png*', '*Height.png*' and '*Width.png*').

#### 4.2.4.2 Secondary tool ‘Average Feature Morphometry’

The executed secondary tool calculates the mean of each transect morphometric per parent feature. This information is populated in a newly generated ‘Av\_Feature\_Morphometry.shp’ shapefile (TABLE 3.3).

**TABLE 4.3.** Reference table showing the generated ‘Av\_Feature\_Morphometry.shp’ attribute table field names and relative morphometrics.

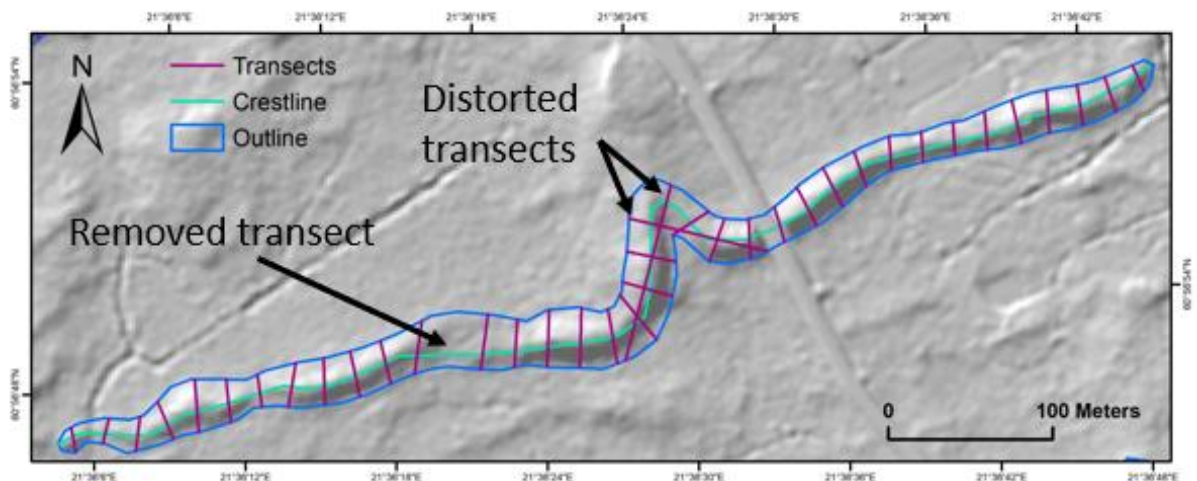
Output Code Name	Morphometric
FEATURE_ID	Identification number of each feature – linked to ‘Transect_Morphometry.shp’ file
AREA	Calculated area of each feature outline polygon
SINUOSITY	Calculated sinuosity of each feature crestline
LENGTH	Calculated length of each feature crestline
CL_Z	Calculated crestline elevation
AV_BASE_TE	Mean average base terrain elevation
AV_HEIGHT	Mean average transect height per parent feature
AV_ASYMM	Mean average transect asymmetry per parent feature
AV_SLOPE	Mean average transect slope per parent feature
AV_WIDTH	Mean average transect width per parent feature
TOTAL_VOL	Sum of each transect segment volume per parent feature

#### 4.2.5 Quality control checks

Upon primary tool execution, quality control checks should be undertaken. This involves reviewing the calculated transect morphometrics (‘Transect\_Morphometry.shp’) and observing the form and location of the transects generated by the tool.

The sign (+/-) of the morphometric variable’s height, cross-sectional area, and volume, will determine whether the feature is *positive relief* (depositional; positive values) or *negative relief* (erosional; negative values). It is advised to sort the data by one of these parameters to ensure that the values are as expected (it can be possible to digitise incorrect features, for example).

Distorted transect placements may also appear, usually as a result of manual mapping errors or highly sinuous landforms (FIGURE 4.3). These can generally be identified by anomalous values within the (*'Transect\_Morphometry.shp'*) attribute table. It is advised that any distorted results are removed from the data to mitigate influential anomalies and interpretative errors. It is important to note that once data is removed from the calculated transect morphometry shapefile, the preliminary summary histograms will no longer be accurately representative of the data.



**FIGURE 4.3.** Example of a digitised feature. Note, a section of the feature is quite sinuous. Depending on the digitised outline placement, this can result in transects that do not intercept the feature outline and therefore are not clipped to the feature extent. As such, careful digitisation with close alignment to the identified feature is important to maximise accuracy. Distorted transects can be easily identified by a visual assessment of transect placement and by reviewing the attribute table for any anomalous results. In addition, a transect has been removed to rectify anomalous height values - this procedure can be repeated for the distorted transects.

#### 4.2.6 Script execution

The tools are written in Python [v2.7] and incorporate Python libraries from 'ArcPy' [ArcGIS 10.0-10.6], *os*, 'Pandas' [McKinney *et al.*, 2010], and embeds Python code for tools, 'Transect2.0' [created by Mateus Vidotti Ferreira], and 'Create Points on Lines' [created by Ian Broad]. The toolbox needs to be downloaded from the GitHub repository ([https://github.com/gwynrivers/3D\\_Morphometry\\_Toolbox](https://github.com/gwynrivers/3D_Morphometry_Toolbox)) and imported into the general ArcGIS 'ArcToolbox' workspace prior to use.



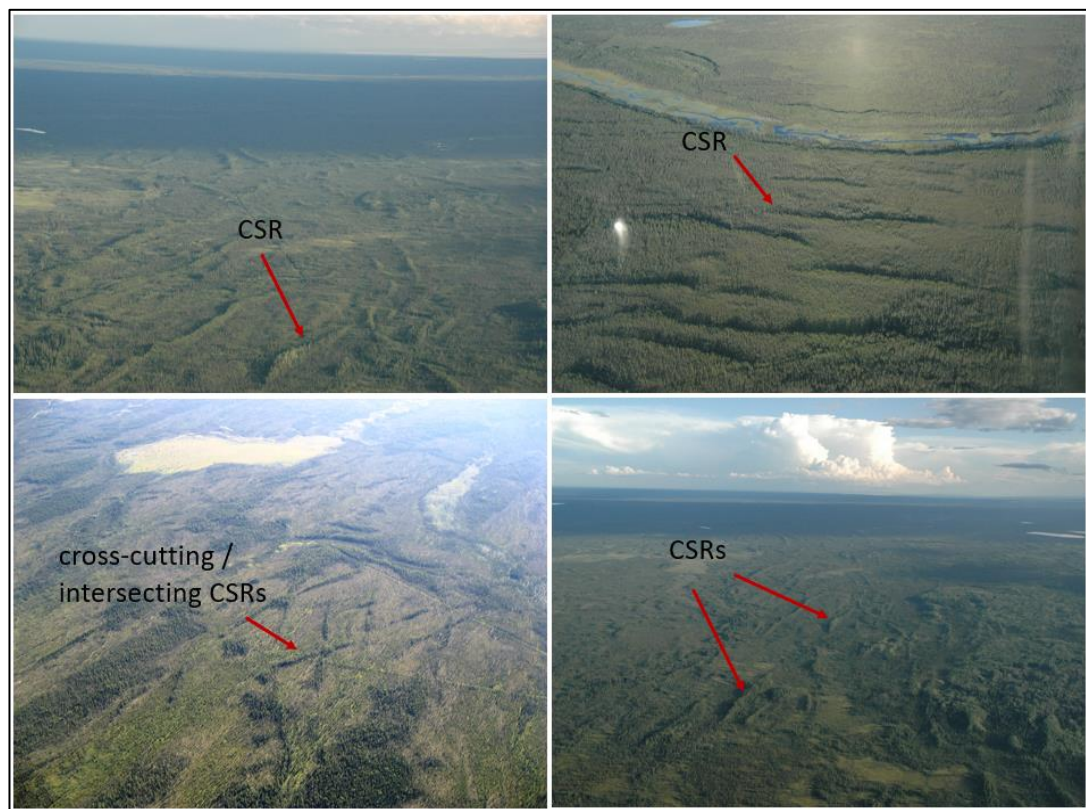
#### 4.2.7 Software requirements and availability

The toolbox is intended to work within ArcGIS 10.1 [ArcMap; ESRI, 2018] and subsequent versions (*including ArcGIS Pro [ESRI, 2020]*). A ‘3D Analyst’ and ‘Spatial Analyst’ license is required. The toolbox can be downloaded from the GitHub repository shown at the beginning of this chapter.

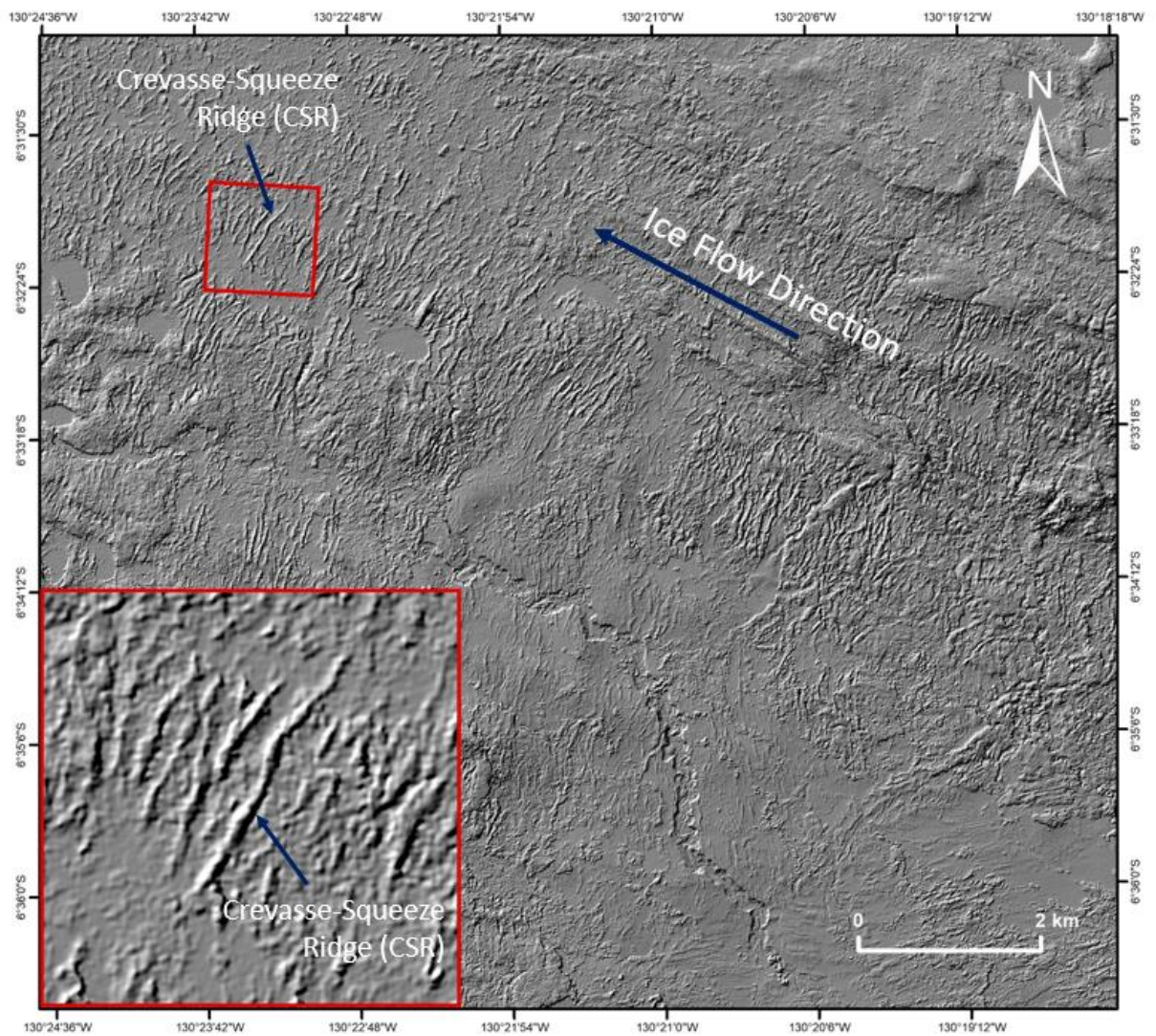
### 4.3 Example application

#### 4.3.1 Target geomorphology & study area

CSRs are used here as a demonstrative dataset for toolbox application. These landforms are deposits formed within crevasses in glacial ice, often preserving the spatial pattern of crevassing. CSRs are commonly described as straight, elongate, narrow, sharp-crested ridges, and can provide important information concerning palaeo-ice sheet subglacial processes, which can be used to better understand contemporary ice sheet behavior (Benn & Evans, 2010; Evans, Storrar & Rea, 2016; Rea & Evans, 2011) (FIGURES 4.4 & 4.5). A more detailed description of CSRs and their mode of formation can be found in section 2.5.



**FIGURE 4.4.** A series of aerial photographs showing CSRs located in the Northwest Territories, Canada [photographs courtesy of Roger Paulen, Geological Survey of Canada].

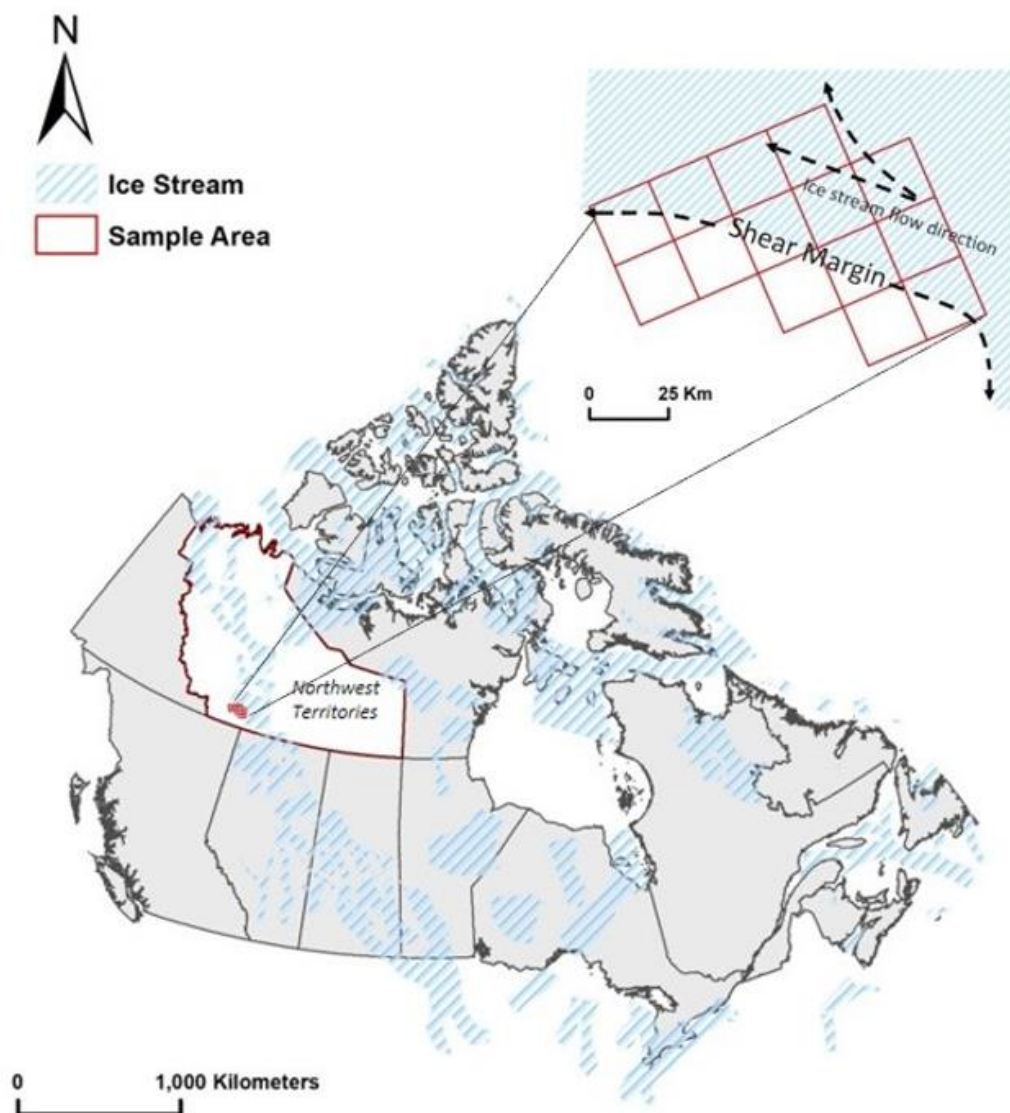


**FIGURE 4.5.** DEM (Hillshade) of CSR landforms located in the Northwest Territories, Canada. CSRs are orientated transverse to former ice flow direction (southeast to northwest). [DEM source: ArcticDEM - Porter *et al.*, 2018].

CSRs have historically been considered diagnostic of, and exclusive to, surge-type glaciers; however, contemporary studies observing palaeo-ice stream settings propose a more equifinal stance, observing subordinate infilling styles indicative of both surging and non-surging dynamics (Evans *et al.*, 2016). Given that these features are becoming more commonly observed in palaeo-ice stream settings, these landforms may provide critical information pertinent to ice stream function and evolution. This is important as ice streams are known to play a major role in reducing ice sheet volume (Stokes, 2000; Stokes



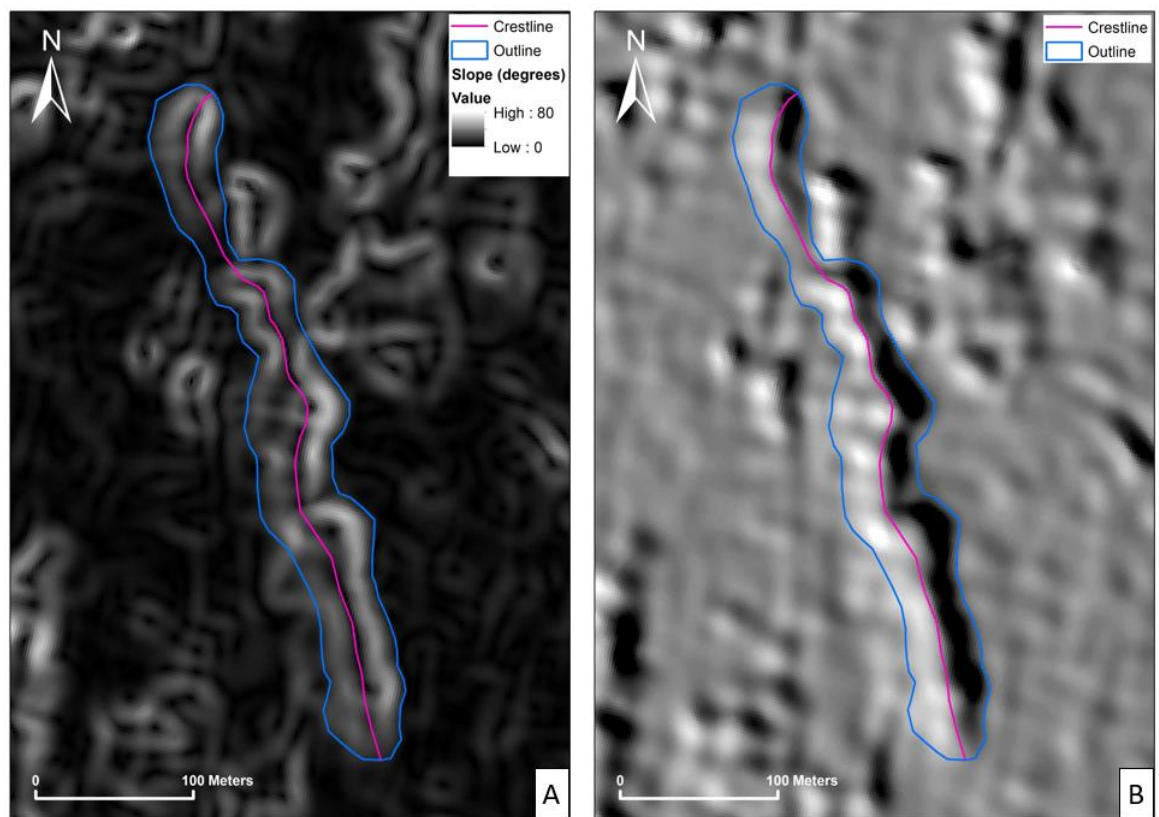
& Clark, 2001; Stokes, 2018; Bennett, 2003). As such, the assessment of CSR patterns and morphometry may provide useful data for reconstructing heterogeneous flow configurations and enabling a deeper understanding of ice stream processes. It should be noted that CSRs are not a primary focus of this PhD project; however, the outputs from this example morphometry study may be used for more thorough investigations in future work. The CSRs located across the Great Slave Lake palaeo-ice stream located in the Northwest Territories, Canada, were mapped and analysed for demonstrative purposes of the toolbox only; no interpretation is provided (FIGURE 4.6).



**FIGURE 4.6.** Study area selected for mapping crevasse-squeeze ridges. Location: Great Slave Lake palaeo-ice stream, Northwest Territories, Canada [ice stream data source: Margold et al., 2015].

#### 4.3.2 Feature digitisation / mapping

To identify the target features and maximise mapping accuracy, both hillshade and slope renderings of the DEM were produced. The rendered hillshade was used to identify target features and the slope map was used to accurately identify the break in central and lateral slopes. Crestlines and outlines of each identified feature were carefully mapped and categorised by two shapefiles, a polyline shapefile for the crestlines, and a polygon shapefile for the outlines (FIGURE 4.7). Feature mapping was conducted manually and > 11 000 CSRs were identified and digitised for the chosen study area.



**FIGURE 4.7.** Example of a manually digitised crestline (pink) and outline (blue) of an identified target feature (CSR). A) Slope rendered DEM to accurately identify central and lateral slope breaks in the feature; B) Hillshade rendered DEM to identify the target feature [DEM source: ArcticDEM - Porter et al., 2018].

### **4.3.3 Tool execution**

Once all identified features were digitised, the '3D Morphometry Toolbox' was imported into the general ArcGIS 'ArcToolbox' ready for execution. A specific 'Output Folder' was created to store generated outputs from each tool.

#### **4.3.3.1 Primary tool execution '3D-Morphometry-Tool'**

The digitised outlines, crestlines and DEM were selected in the primary tool user interface. The transect intervals were set at 10 m and the transect lengths were set at 250 m, which were sufficient to extend beyond the width extent of the mapped outlines.

#### **4.3.3.2 Generated outputs (primary tool)**

The executed primary tool generated > 48 000 transects (in the form of a shapefile '*Transect\_Morphometry.shp*'), oriented perpendicular to, and at 10 m intervals along, each mapped crestline (e.g. FIGURE 4.8).

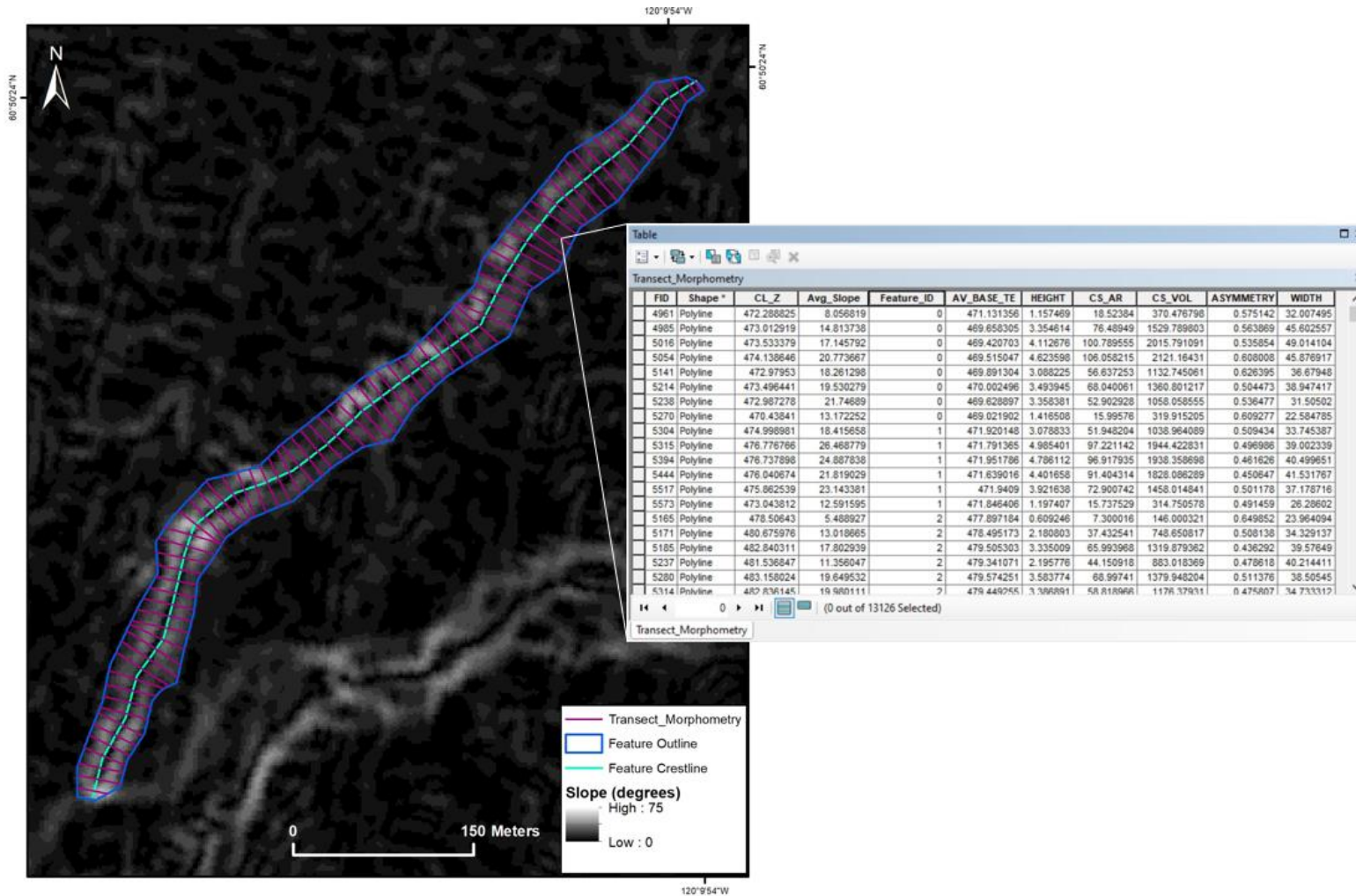
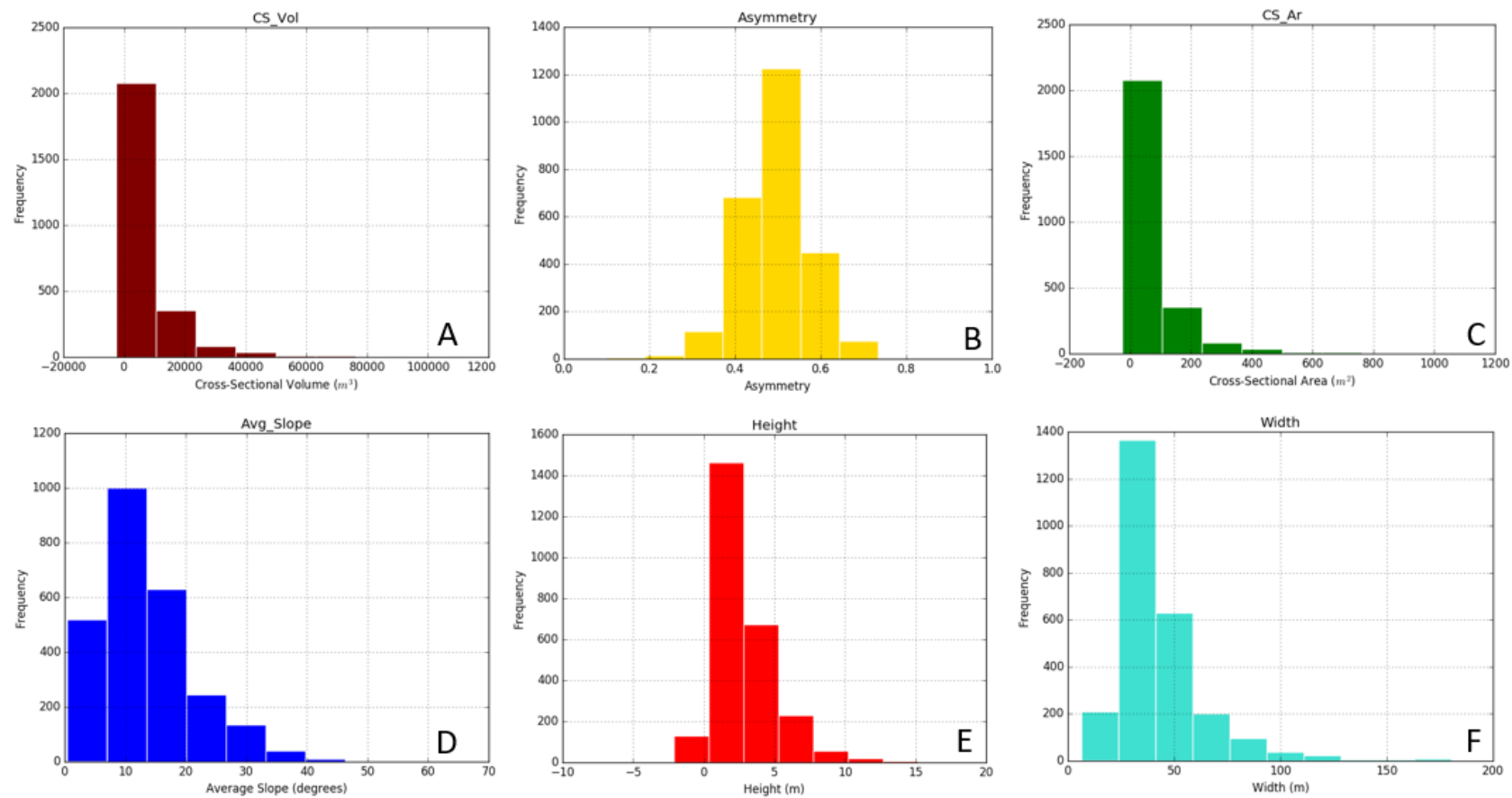


FIGURE 4.8. Example of generated transects upon execution of the primary tool '3D-Morphometry-Tool' with inset attribute table showing calculated morphometrics per transect. Transects are oriented 90° to the feature crestline and are spaced at 10 m intervals [slope rendered DEM source: ArcticDEM - Porter et al., 2018].

A series of summary histograms were also automatically generated providing a preliminary visualisation of the calculated transect morphometry data prior to performing any quality control checks (FIGURE 4.9).



**FIGURE 4.9.** Series of automatically generated summary histograms providing a graphical representation of the initial calculated transect morphometry. A) cross-sectional volume, B) asymmetry, C) cross-sectional area, D) average slope, E) height and F) width.



This quantification is useful for highlighting any preliminary inferences relative to the form and process of target features and thereby guiding further investigations. In this instance, ‘asymmetry’ is a useful morphometric, suggesting that the CSRs in this sample are generally symmetrical, consistent with their origin as deposits that are squeezed into (symmetrical) crevasses. This may be a useful morphometric for CSR identification and differentiation from superficially similar landforms in future studies.

#### **4.3.3.3 Quality control**

Quality controls checks were conducted by reviewing both the ‘*Transect\_Morphometry.shp*’ attribute table and observing the placements of the generated transects. As can be seen in the summative histograms (FIGURE 4.9E), some negative morphometric values, indicating hollows rather than ridges, were produced due to inaccuracies during the digitisation process. Given that CSRs are positive relief features, all negative values were removed. This was done by sorting the attribute table by height and removing the transects of negative values.

#### **4.3.3.4 Secondary tool execution ‘Average-Feature-Morphometry’**

Once quality control checks were complete and the output data from the primary tool was refined (e.g. negative/anomalous transects removed), the secondary tool was executed to provide averaged transect morphometry for each identified feature.

The generated ‘*Feature\_Morphometry*’ file and the refined ‘*Transect\_Morphometry*’ file were selected in the secondary tool user interface, along with the original ‘*Feature Outline*’ shapefile and ‘*Output Folder*’ to store generated outputs.

#### **4.3.3.5 Generated outputs (secondary tool)**

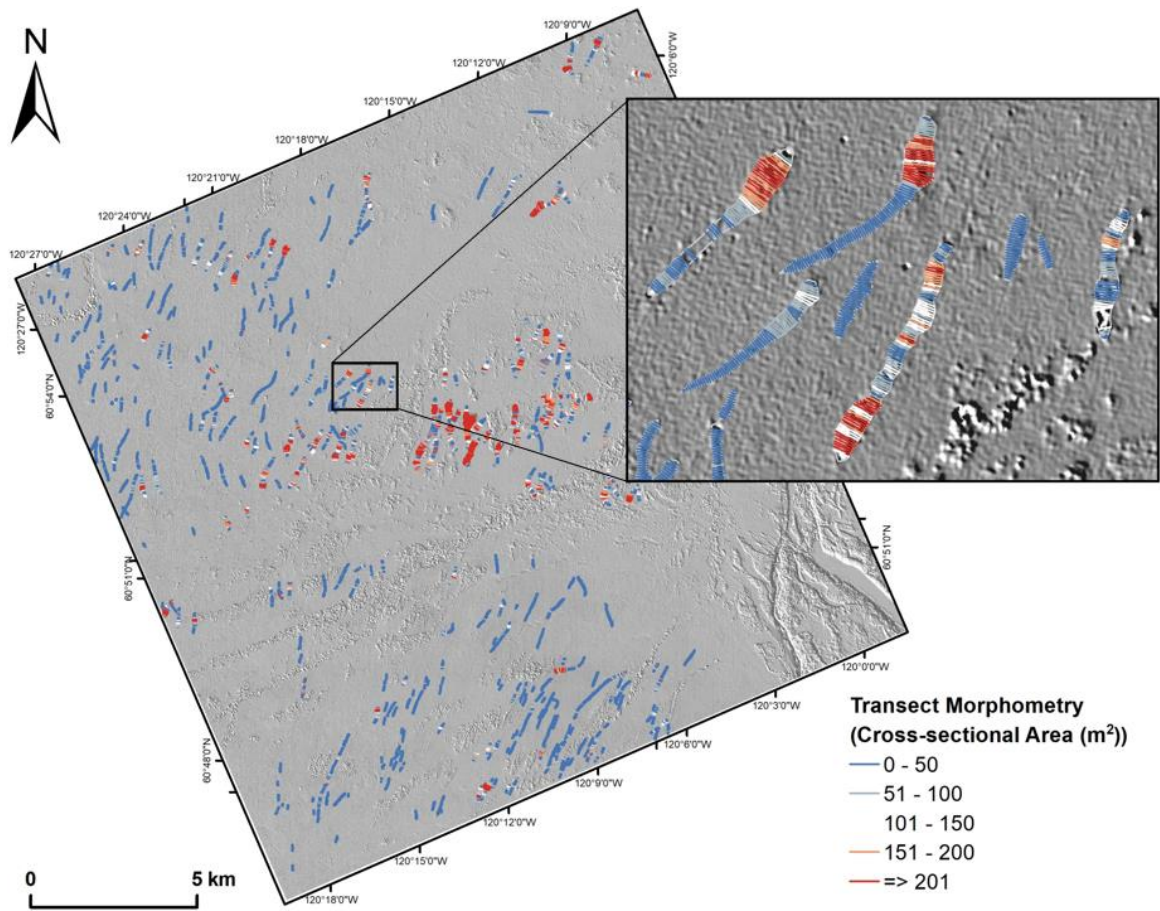
Upon execution of the secondary tool, a new output ‘*Av\_Feature\_Morphometry.shp*’ was produced which contained calculated transect morphometrics averaged across each individual parent feature.

### **4.3.4 Further analysis**

#### **4.3.4.1 Data visualisation**

Upon execution of both the primary and secondary tools, the calculated 3D morphometrics were visualised using a colour-graded scale to highlight any patterns in

feature morphometry. Patterns were also assessed at smaller scales, along individual feature lengths, and at macroscales across wider spatial areas to assess any larger distributional patterns (see example shown in FIGURE 4.10).

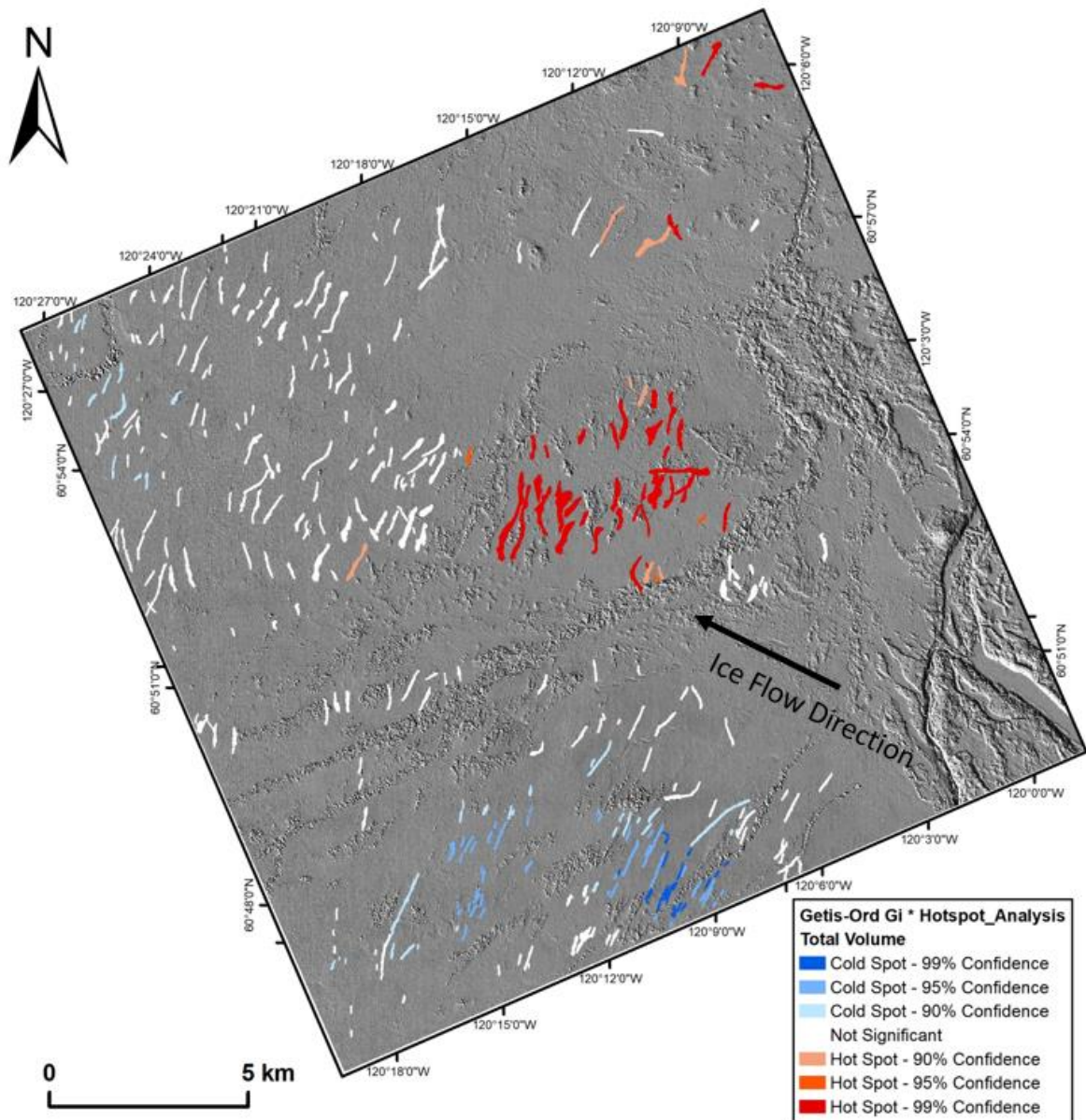


**FIGURE 4.10.** Example transect morphometry visualisation showing transects generated at 10 m intervals. The ‘cross-sectional area’ calculated along each transect are shown and colour-graded to represent high (red) - low (blue) values. This is a powerful method in which to analyse variations along single features. This method can be repeated for each morphometric as required. In addition, the wider scale visualisation of calculated morphometrics at each transect segment is a useful method to explore any spatial clustering as demonstrated in this example. [DEM source: ArcticDEM - Porter et al., 2018].

#### 4.3.4.2 Statistical tests

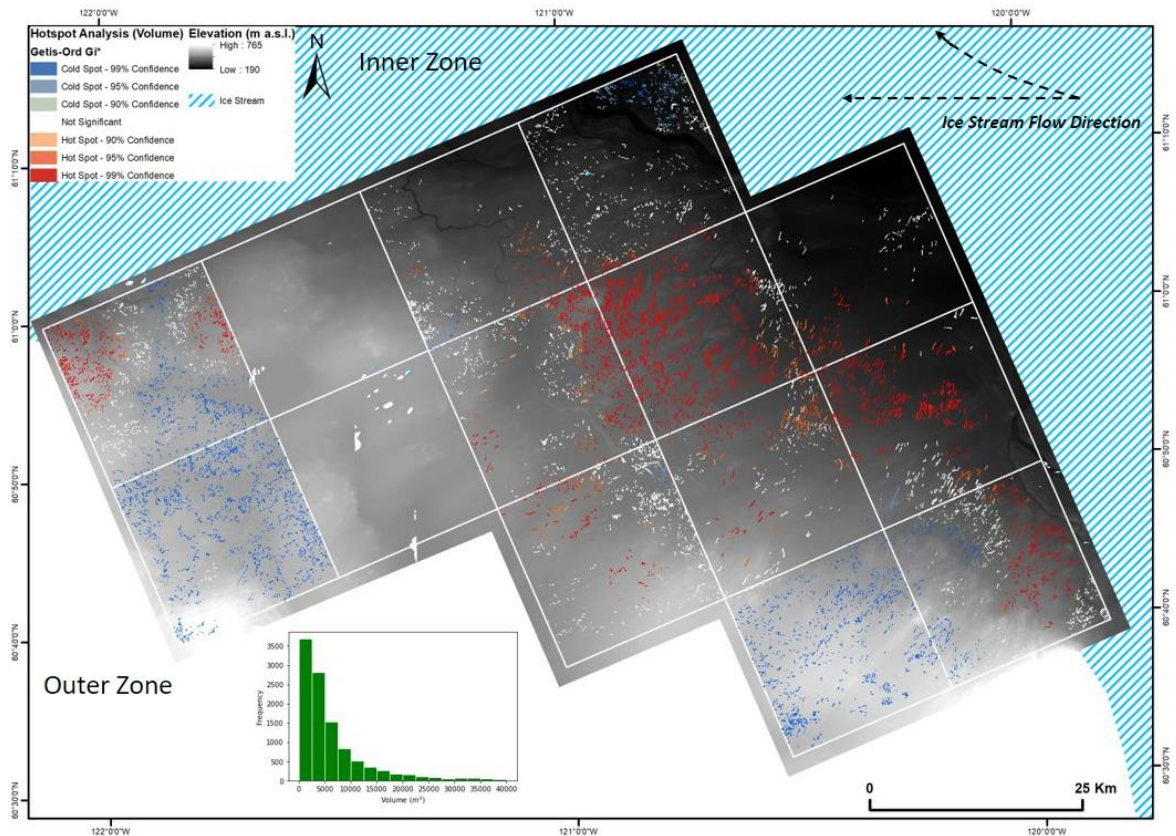
As initial data observations inferred some patterning to the spatial distribution of morphometry (FIGURE 4.10), further statistical tests were undertaken. Specifically, a ‘hot

spot analysis' test (Getis-Ord Gi\*; ArcGIS Spatial Statistics Tool) was conducted to reveal any clustering in morphometrics and test for any statistical significance in spatial distribution (FIGURES 4.11 & 4.12).



**FIGURE 4.11.** Example results of 'Getis-Ord Gi\* Hot Spot Analysis' conducted on the 'TOTAL\_VOL' attribute of the 'Av\_Feature\_Morphometry.shp' file. Results show a statistically significant clustering in CSR volumes (central clustering of higher values and southward clustering of lower values). [DEM source: ArcticDEM - Porter et al., 2018].





**FIGURE 4.12.** Wider spatial coverage results of ‘Getis-Ord  $G_i^*$  Hot Spot Analysis’ conducted on the ‘TOTAL\_VOL’ attribute of the ‘Av\_Feature\_Morphometry.shp’ file. Results show a statistically significant clustering in CSR volumes. An inset histogram is provided to summarise feature volume of the dataset [DEM source: ArcticDEM - Porter et al., 2018; Ice stream flow direction source: Margold et al., 2015].

This test could be repeated for each morphometric parameter to provide a more detailed assessment of the target features and relative spatial patterning. Furthermore, the demonstrated ‘hot spot analysis’ test provides a more robust assessment of the morphometric data and allows theoretical inferences to be made, particularly with regard to genesis and evolution. Differences in volume may relate to, for example, regional variations in sediment supply, or variations in the extent of crevassing.

#### 4.4 Wider applications

Morphometric applications are used in many areas of landscape research and environmental management, including: fluvial geomorphology (Li et al., 2022; Sarif et al., 2021; Simon et al., 2016; Re et al., 2018), glacial geomorphology (Butcher et al., 2016; Butcher et al., 2020; Storrar et al., 2015; Ely et al., 2017), tectonic landform research

(Bethell *et al.*, 2022; Karagoz *et al.*, 2022; Stretch *et al.*, 2006; White *et al.*, 2002) mountainous landscape research (Garcia-Ruiz *et al.*, 2000; Kaufman & Calkin, 1988; Valla *et al.*, 2010), geoarchaeological landscape research (Abballe & Cavalazzi, 2021; Davis, 2018), and geomorphological heritage research (Gomez-Heraz *et al.*, 2019).

This toolbox may be utilised for the measurement of any elongated landscape feature for which users require a detailed 3D morphometric assessment. As such, application is not limited by discipline area and may extend to a wide range of studies, including surveying of artificial landscape features in the built environment, such as railway embankments. Furthermore, this toolbox may be used to capture a single 3D morphometric assessment of a landscape feature, which may be useful for landform classification and/or to enhance feature diagnostic criteria. Alternatively, the toolbox may be applied as a repeated monitoring method with which to analyse evolutionary properties. This may be particularly useful in contemporary, fluvial settings, for example. The toolbox can easily be applied to negative-relief landscape features (e.g. river channels) by simply switching the sign of height, cross-sectional area and volume values.

#### **4.5 Additional advice & comments**

It is required when mapping to ensure that each identified target feature has both a single crestline and an outline. The accuracy of the output data and calculated morphometry is dependent on the accuracy of the input feature mapping. It is advised to ensure that digitised crestlines extend beyond the length of the related outlines, because these will be clipped to the extent of the outlines upon tool execution. It is also advised to set transect lengths sufficient to extend beyond the largest width of the mapped feature outlines.

Transects are placed perpendicular (90°) to crestline orientation. In rare circumstances, highly sinuous features may produce some distorted transect placements. It is advised that, once the primary tool has been executed, the user undertakes a visual quality control assessment of the transect placements to ensure that outputs are within a reasonable range/placement. Erroneous transects may be either manually removed or modified as appropriate. It should be noted that if any transects are removed, the preliminary summary histograms will no longer be accurate.

If a .csv file is required for further data manipulation, the attribute table of the .shp files may be converted to a .csv file using the ArcGIS 'conversion' toolbox. Updated summary statistics and histograms can then be produced manually from the .csv file.

#### **4.6 Conclusions**

This toolbox provides a method for the extraction and calculation of highly detailed 3D morphometric data for mapped elongated landscape features. The tool may be used for the measurement of any elongated landscape feature where users require a detailed 3D morphometric assessment. Application may extend to a wide range of studies including: fluvial geomorphology, glacial geomorphology, tectonic landform research, mountainous landscape research, geoarchaeological landscape research, geomorphological heritage research, as well as surveying of artificial landscape features in the built environment, such as railway embankments.

This toolbox may be used to capture a single 3D morphometric assessment of a landscape feature or applied as a repeated monitoring method in which to analyse dynamic changes. The toolbox may also be applied to negative-relief landscape features (e.g. river channels). It is intended that this tool be accessible for research and industry GIS users ranging from novice to advanced user levels. The 3D Morphometry Toolbox Python script is open-access and can be downloaded from the GitHub repository. The script may be further developed to meet user-specific requirements, if desired.

## Chapter 5: 3D morphometry of De Geer Moraines and Crevasse-Squeeze Ridges: Differentiating between pushing and squeezing mechanisms from remotely sensed data

**Citation:** Rivers, G.E., Storrar, R.D., Jones, A.H. & Ojala, A.E.K. (2023). 3D morphometry of De Geer Moraines and Crevasse-Squeeze Ridges: Differentiating between pushing and squeezing mechanisms from remotely sensed data. *Quaternary Science Reviews*, vol. 321(108383). DOI: <https://doi.org/10.1016/j.quascirev.2023.108383>

This chapter presents the results of a large-scale 3D morphometry study, quantifying differences and/or similarities between DGMs and CSRs, and constraining DGM formation properties. This work utilises the method outlined in chapter 3 and contributes toward research objective (1).

### Abstract

DGMs and CSRs are important landforms that can provide useful insights regarding palaeo-ice sheet processes. Specifically, these landforms can provide information regarding ice-marginal dynamics and/or subglacial processes, depending on the context in which they form. Visual similarities between DGMs and CSRs have historically proven problematic for landform differentiation and have been an area of contentious debate surrounding DGM formation. Morphometric quantification of these landform groups can help to elucidate respective formation processes and enable more accurate landform differentiation. This study presents a detailed morphometric comparative investigation of DGM and CSR landforms which accurately quantifies landform morphometrics, elucidates formation properties, and highlights differences between the landform groups that can be used as a justifiable means for differentiation and classification. Results reveal key differences in morphometric properties between the landform groups which enables a quantified foundation by which to differentiate them. Specifically, the studied CSRs are found to be higher, wider, steeper, more symmetrical, less sinuous and more voluminous than the studied prominent DGMs. In contrast, a tendency for cross-sectional asymmetry

in DGMs supports an ice-marginal push origin, rather than a basal squeeze-up into crevasses. This is further supported by CSRs being less sinuous than DGMs due to the deposits being constrained by dimension and planform of the (relative straight) host crevasses, whereas DGMs follow a more sinuous path, related to the shape of the ice margin. This study provides foundational evidence to suggest that DGMs are formed at the grounding line of subaqueous ice margins; however, further work should include sedimentological and geophysical studies to investigate DGM internal architecture and validate preliminary inferences.

## 5.1 Introduction

DGMs are low-amplitude, narrow and elongate ridges formed at the grounding line of water terminating ice margins and are orientated parallel to former ice flow direction (section 2.4). In length, they can extend up to several kilometres; heights can range from a few centimetres, resembling sediment traces, or extend up to 10 metres. Widths have been reported as generally <50 m; however, observations of up to 100s of metres have been described (Borgstrom, 1979; Finlayson *et al.*, 2007; Golledge & Phillips, 2008; Larsen *et al.*, 1991 & Ojala *et al.*, 2015).

CSRs are low-amplitude, narrow, sharp-crested ridges formed by sediments being deposited within either full depth or basal crevasses (section 2.5). These ridges tend to form in clusters, mirroring the spatial pattern of crevassing (Benn & Evans, 2010) and are broadly orientated transverse to former ice flow; however, observations have reported variable spatial distribution patterns (Evans *et al.*, 2016). Due to a subglacial origin, CSRs can provide important information regarding subglacial ice sheet processes such as subglacial hydrology and pressure regimes, which can be used to inform contemporary ice sheet behaviour (Evans *et al.*, 2016; Rea & Evans, 2011).

DGMs and CSRs share similarities in morphometry and spatial distribution and can be difficult to qualitatively distinguish and correctly classify (section 2.4- 2.5). This been a long-standing area of contention amongst researchers whereby DGM formation has remained ambiguous with extensive debates between ice marginal push versus crevasse infill methods (Beaudry & Prichonnet, 1991 & 1995; Blake, 2000; De Geer, 1940; Hoppe, 1957 & 1959; Streuff *et al.*, 2015). The differences in depositional environment and



formation processes between these landforms make accurate distinction crucial as they each provide different information relative to ice sheet dynamics.

To overcome this issue, a detailed large scale morphometry study was undertaken whereby geometries of DGMs and CSRs are compared. The aim of this was to enable any key differences in form to be revealed, improve landform classification, and help to develop a more detailed understanding of formation processes and depositional environments for each landform.

As highlighted in chapter 4, the quantification of landform morphometry requires the accurate measurement of geometric properties. The acquisition of basic measurements such as length and footprint area are relatively straight-forward; however, this can become more challenging when working with very large datasets, and with landforms that possess a high spatial variability (Storrar *et al.*, 2015). Furthermore, for the purposes of distinguishing between similar landforms, basic metrics such as length and footprint area, may not provide enough detailed information relative to formation properties and therefore more detailed metrics such as height, asymmetry and volume may be required. The development of the automated 3D morphometric toolbox outlined in chapter 3 provides a valuable solution to these issues by enabling automated calculation of very detailed 3D morphometric data for more robust comparative analyses.

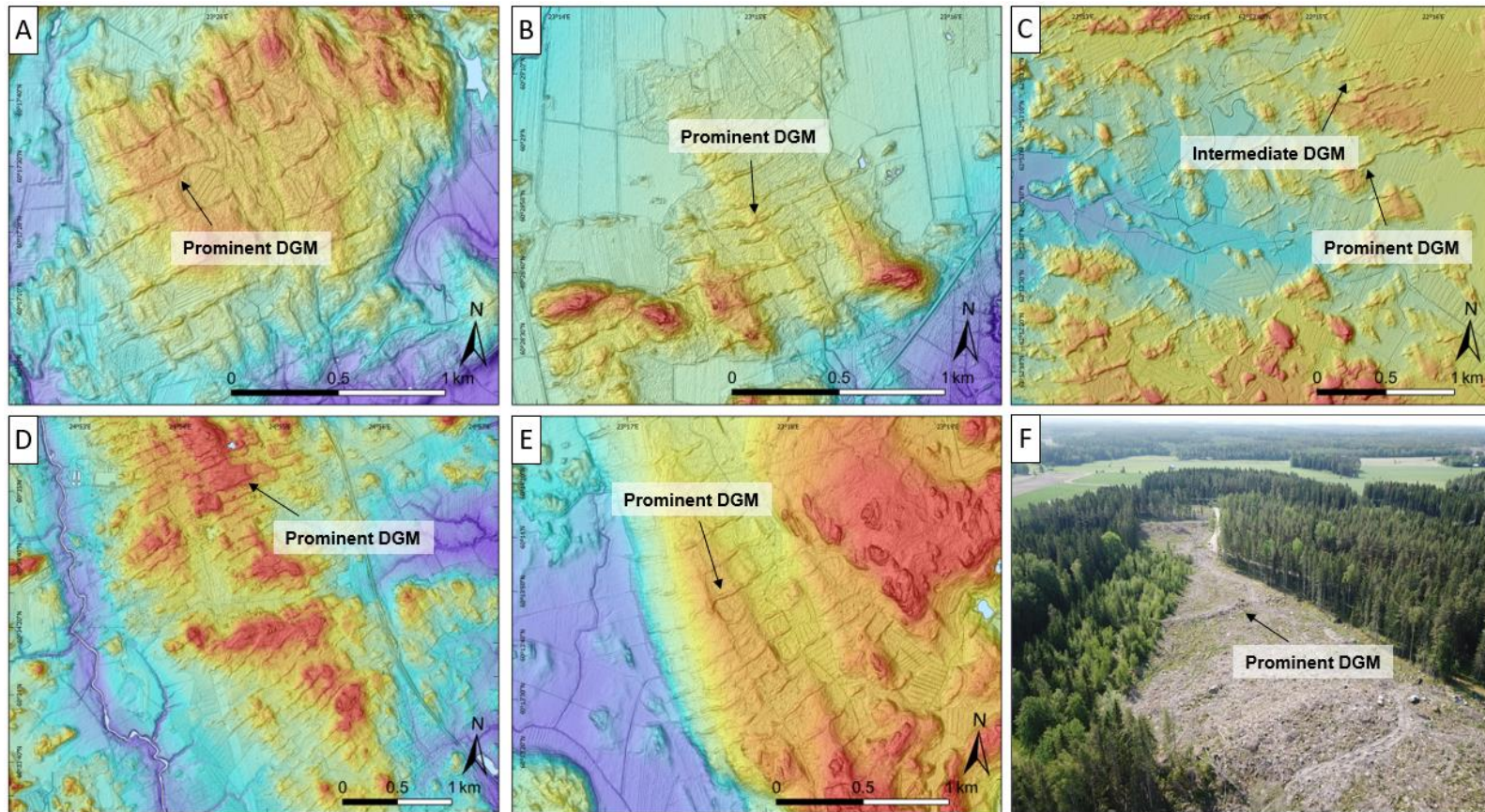
## **5.2 Formation of DGMs & CSRs**

### **5.2.1 De Geer moraines**

DGMs were first observed in Sweden and described as small, regular, frontal moraines by Gerard De Geer in 1889 (De Geer, 1889 & 1940) who interpreted them as annual moraines. In profile form, they can present as linear, concave, or convex, depending on the topographic controls, and have commonly been described as having asymmetrical properties, with a steeper distal side, although symmetrical properties have also been observed (Hoppe, 1959; Golledge & Phillips *et al.*, 2008; Ojala *et al.*, 2015). They typically occur in swarms of successive ridges, covering large tracts of terrain, exhibiting high parallel conformity, with either regular or irregular arrangements (FIGURE 5.1).

DGM observations are most common in low-relief terrain, below the highest shoreline of proglacial lakes/seas, where the grounding line was subaqueous (Bouvier *et al.*, 2015; Embleton & King, 1968; Finlayson *et al.*, 2007; Hoppe, 1959; Lindén & Möller, 2005;

Larsen *et al.*, 1991; Lundqvist, 1981; Ojala *et al.*, 2015; Ojala, 2016), although observations have also been made in mountainous-valley, lacustrine environments (Borgström, 1979; Golledge & Phillips, 2008). Preservation potential is variable and strongly influenced by topography and fluvial reworking due to the low-amplitudes and the low-relief environments in which they reside (Aartolahti, 1972). Moreover, postglacial sedimentation can create challenges with respect to masking and landform identification.



**FIGURE 5.1.** Digital Elevation (DEM) with multi-directional hillshade (MDOW) and oblique aerial drone imagery capturing distinct and regularly spaced De Geer moraine formations situated in SW Finland. Intermediate De Geer moraines can also be in image C. A) Torholankulma, Salo; B) Kurimäki, Salo; C) Konnonperä, Isokyrö; D) Palpuro, Hyvinkää; E) Haaro, Perniö and F) Suorsalantie, Mynämäki [DEM source: ©National Land Survey of Finland, LiDAR digital elevation mode, 2/2023] (Rivers et al., 2023).

DGMs have been described using a variety of terms within the literature including: calving moraines (Frödin, 1916), cross-valley moraines (Embleton & King, 1968; Hoppe, 1959), end moraines (Smith & Hunter, 1989), washboard moraines (Mawdsley, 1963, minor moraines (Smith, 1982) and transverse eskers (Virkkala, 1963), which allude to the ambiguity surrounding formation properties. A review of existing literature indicates two domination formation hypotheses which are discussed in chapter 2, section 2.4.1.

### 5.2.2 Crevasse-squeeze ridges

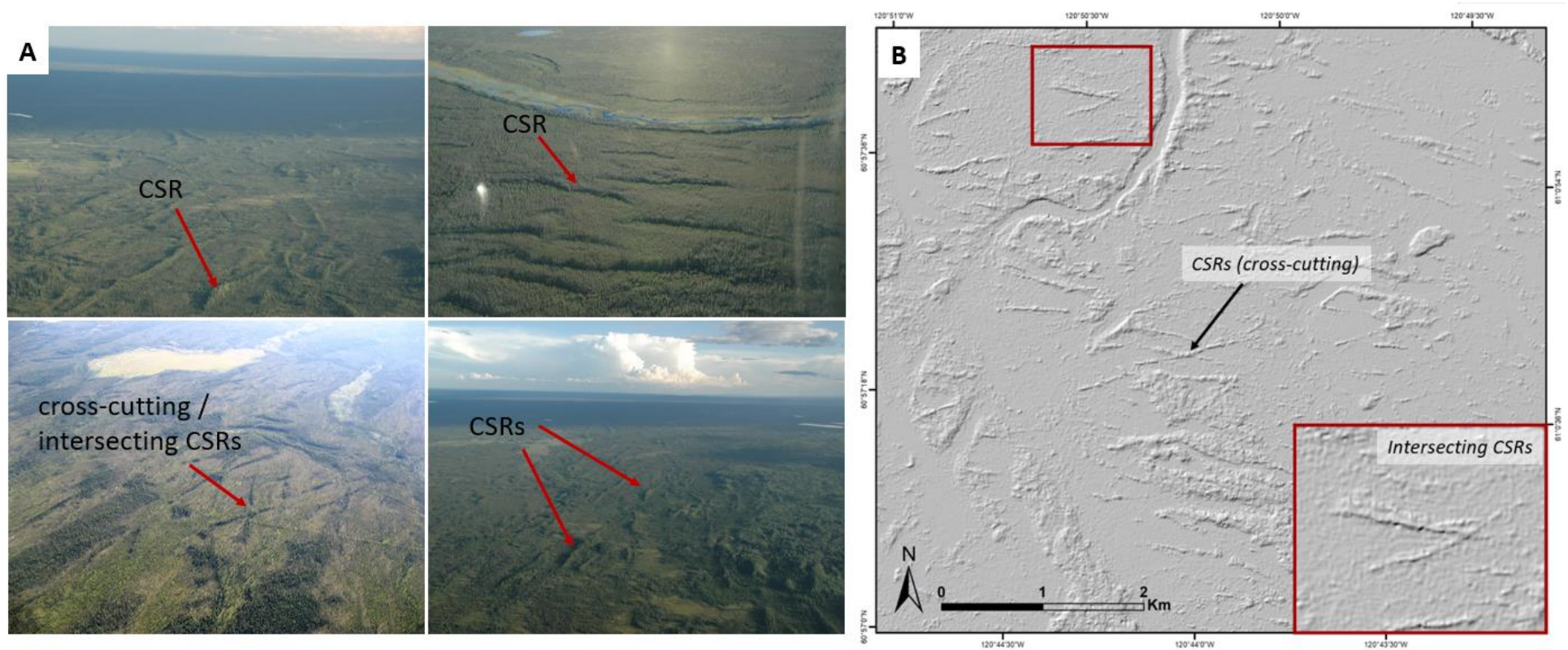
CSRs are straight, narrow, sharp-crested ridges formed by basal sediments being deposited within full depth and/or basal crevasses in glacial ice (Benn & Evans, 2010). Due to the requirement of crevasses, the spatial distribution of CSRs generally preserve the spatial pattern of crevassing. As the sediments originate from the bed of the ice, the preserved ridges can provide important information regarding subglacial processes such as pressure gradients, hydrological regimes, strain rates and fracture patterns (Evans *et al.*, 2016; Rea & Evans, 2011).

Morphometrics are variable but can be summarised as: height <1-8 m (Benn & Evans, 2010; Ben-Yehoshua, 2017; Kurjanski *et al.*, 2019; Sharp, 1985; Sobota *et al.*, 2016), width 0.5-7 m (Ben-Yehoshua, 2017; Sobota *et al.*, 2016) although have been observed of up to 270 m in submarine environments (Kurjanski *et al.*, 2019), length <100 m (Evans *et al.*, 2016; Ó Cofaigh *et al.*, 2010) although several hundred metres have also been described (Clapperton, 1975; Kurjanski *et al.*, 2019). Slope angles have been observed up to 70-80° (Lovell *et al.*, 2015); however, it should be noted that extent and slope of these ridges are highly dependent on preservation potential, whereby slope decreases with sustained subaerial exposure (Ben-Yehoshua, 2017). Moreover, interstitial ice content is a characteristic which increases susceptibility to melt-out reworkings.

The spatial distribution, size and patterning of CSRs are highly variable due to the various stress patterns produced in different topographic and ice dynamic settings. Some studies describe distinct geometrical ridge networks, with rhombohedral, cross-cutting/intersecting patterns (Lovell *et al.*, 2015; Ottesen and Dowdeswell, 2006 & 2008; Solheim, 1991), others describe patterns of linear ridges orientated transverse to sub-parallel to former ice flow (Clapperton, 1975; Kurjanski *et al.*, 2019; Sharp, 1985), some describe networks as a branched ridge system (Ben-Yehoshua, 2017), and others

have described more chaotic-like patterns with attenuated ridges that have no preferred orientation (Lovell *et al.*, 2015) (FIGURE 5.2).





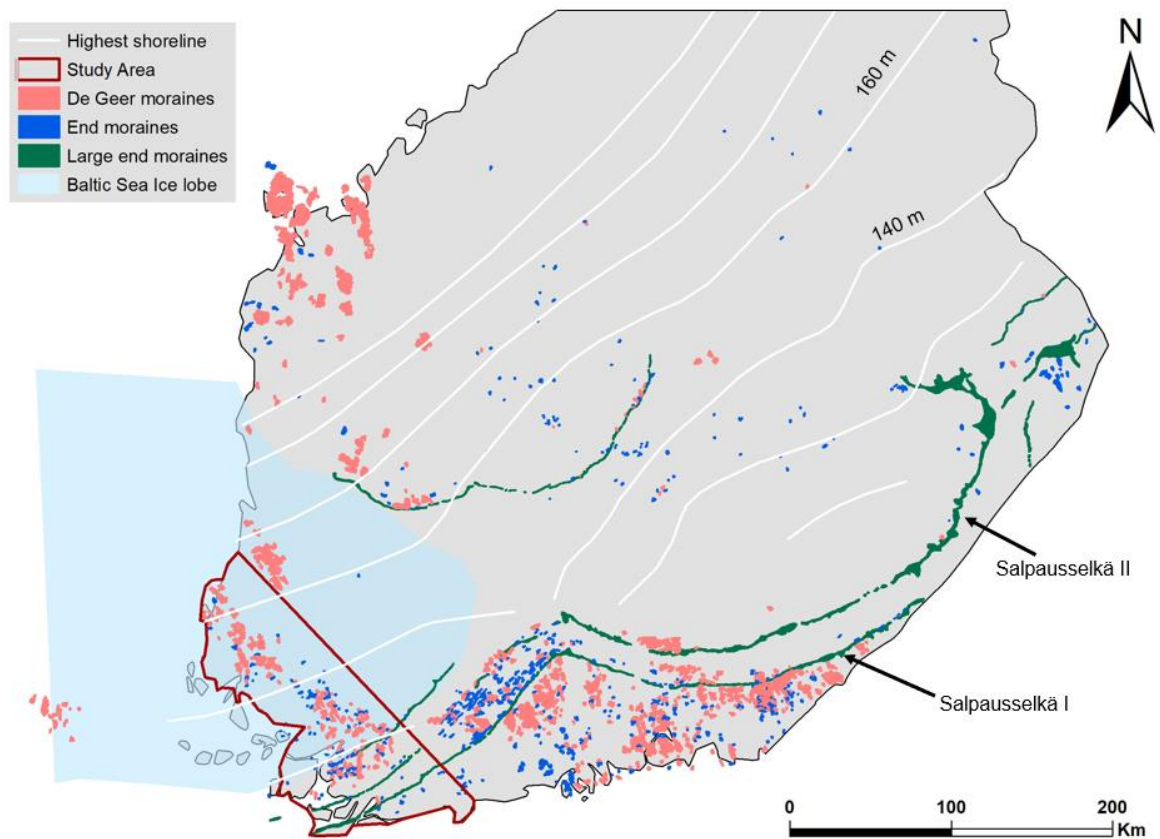
**FIGURE 5.2.** A) Series of aerial photographs of CSR landforms located in the Northwest Territories, Canada [courtesy of Roger Paulen]. B) Hillshaded DEM showing example CSRs identified across a section of the former Great Slave Lake ice stream, northwest Territories, Canada [DEM source: ArcticDEM – Porter et al., 2018].

The contrasting formation theories of DGMs and CSRs emphasise the need to accurately differentiate between the two landform groups. Moreover, if DGMs are to be used as ice marginal indicators, their formation properties must be correctly constrained. As such, this study seeks to acquire large-sample 3D morphometric data of both DGM and CSR landform groups to enable differentiation and gain insights into formation processes. This specific investigation aims to address research objective 1; ‘constrain DGM formation processes via triangulation of morphometric, sedimentological, and geophysical datasets’.

### 5.3 Study Areas

#### 5.3.1 Southwest Finland (DGMs)

DGMs are particularly abundant across southwest Finland as artefacts from the former FIS during the Weichselian deglaciation (Mäkinen *et al.*, 2007; Ojala, 2016). By the end of the Weichselian, the eastern margins of the FIS stretched across Finland forming the Salpausselkä moraines. At this point, the ice margin became crenulated and resulting in the formation of several independent ice lobes which operated time-transgressively (Boulton *et al.*, 1996; Mangerud *et al.*, 2022). The DGMs in southwest Finland reside within the southern sector of the Baltic Sea Ice Lobe (section 3.3.1), mostly up-ice from the First and Second Salpausselkäs (FIGURE 5.3). This area contains the classical DGM fields- the Eura-Lavia, the Mynämäki-Pyhämää and the Halikko-Suomusjärvi (Mäkinen *et al.*, 2007; Ojala, 2016; Zilliacus, 1989) – that present distinct and rhythmic patterns characteristic of DGMs. Due to the abundance and distinct regularity of DGMs, this location was deemed advantageous for offering a sufficiently large and representative dataset in which to study morphometry and spatial distribution.

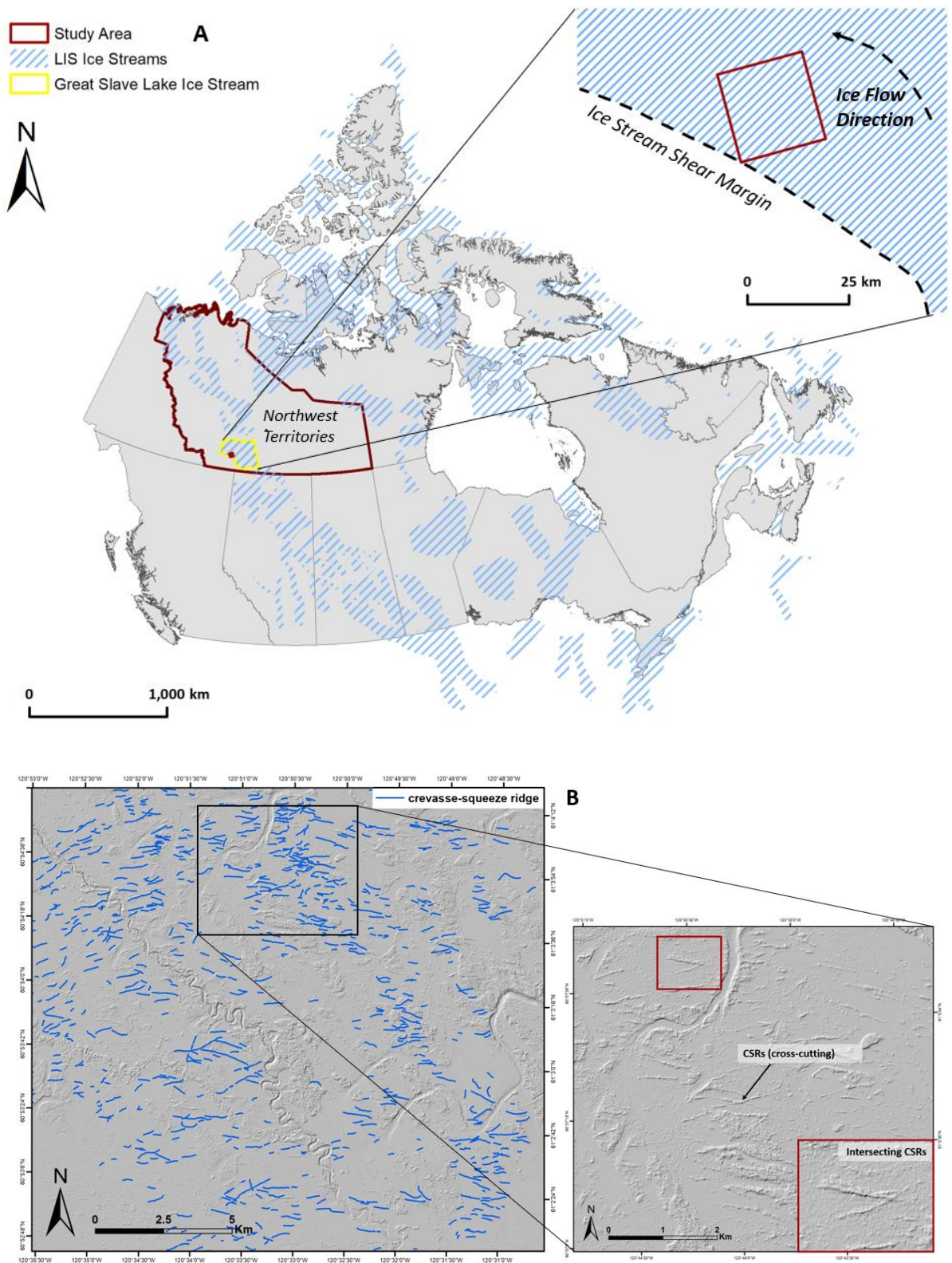


**FIGURE 5.3.** Study area selected for DGM data collection in southwest Finland. The location of De Geer moraines fields has been adapted from Ojala (2016) and Baltic Sea Ice Lobe boundary and Salpausselkä moraine positions are based on Palmu *et al.*, (2021). The study area encompasses DGMs that are positioned northwest of the second Salpausselkä moraine (Rivers *et al.*, 2023).

### 5.3.2 Northwest Territories, Canada (CSRs)

The CSRs sampled in this study area associated with the former Great Slave Lake Ice Stream (Margold *et al.*, 2015), located in the interior plains of the Northwest Territories, Canada (FIGURE 5.4A). CSR spatial distribution in this area present as a linear swarm, spanning a section inside of the ice stream shear margin (FIGURE 5.4A). Ridges exhibit clear geometric networks with evidence of cross-cutting, oblique and contrasting orientations (FIGURE 5.4B), consistent with well-documented observations of typical CSRs elsewhere (Ankerstjerne *et al.*, 2015; Cline *et al.*, 2015; Evans *et al.*, 2016; Norris *et al.*, 2018; Ó Cofaigh *et al.*, 2010; Ross *et al.*, 2009). In addition, their occurrence at the shear margin, a region characterised by high extension stress regimes, is also consistent with a crevasse origin. An area of 20 km<sup>2</sup> was sampled.





**FIGURE 5.4.** A) Study area chosen for CSR data collection; a 20 km<sup>2</sup> section of the former Great Slave Lake Ice Stream, Northwest Territories, Canada [ice stream data source: Margold et al., 2015]. Location map shows the study area situated inside of the shear margin of the palaeo-ice stream. B) Hillshaded DEM indicating mapping extent of CSRs at

the study area. Imagery shows ridges arranged in a linear and cross-cutting configuration. [DEM source: ArcticDEM – Porter *et al.*, 2018] (Rivers *et al.*, 2023).

## 5.4 Methods

### 5.4.1 Data collection

In this study, ridges were subcategorised into prominent and intermediate DGMs as defined by successive regularity, lateral continuity and height (see section 5.2.1). CSRs were not sub-categorised. DEMs with 2 m horizontal resolution were obtained for each study area (LiDAR, National Land Survey of Finland, 6/2023; ArcticDEM – Porter *et al.*, 2018).

Data was acquired manually by carefully scanning each DEM for evidence of target landforms (e.g. ridges that could be qualitatively interpreted as DGMs and CSRs). A dual rendering of each DEM was performed producing a hillshade two different azimuths applied to reduce shadow bias and accurately identify target landforms (Smith & Clark, 2005), and a slope rendering to maximise the identification of central and lateral slope breaks for each feature (Chandler *et al.*, 2018). Crestlines and outlines of each identified landform were traced using ArcMap (ArcGIS, ESRI) and stored as two separate shapefiles; a polyline shapefile for the crestlines, and a polygon shapefile for the outlines.

### 5.4.2 Quality control: relative accuracy

The *absolute* vertical accuracy of Finnish LiDAR data is  $\pm 0.1$  m (National Land Survey of Finland, 6/2023) and 1.6 m for the ArcticDEM (Natural Resources Canada, 2015). In this study, however, the *absolute* accuracy (i.e. correct spatial positions) are not important; rather, it is the *relative* accuracy (the reliability of internal measurements from the DEM) that determine the reliability of the data. The differences in *relative* vertical accuracy between the two datasets were determined by conducting a preliminary test prior to data analysis to compare calculated height across a set of mapped DGMs in southwest Finland using both DEM sources. 573 transects were compared across an area of  $\sim 4$  km<sup>2</sup>. A Wilcoxon signed-rank test showed a small (relative to the feature height) but statistically significant mean difference of 0.79 m between the two datasets ( $z = -12.8$ ,  $p < .001$ ,  $r = -0.05$ ) (Appendices Figure 1). The results showed that 76% of the calculated LiDAR heights were greater than those calculated from the ArcticDEM data.

### 5.4.3 Morphometric calculations

Once all target landforms had been mapped, morphometrics were calculated. The automated python-based ArcGIS 3D morphometric toolbox was used to automatically calculate detailed 3D morphometrics of each sampled landform group (chapter 4). This automated toolbox functions by firstly placing transects along each mapped crestline (orientated 90° to the crestline) at user-defined intervals to obtain detailed segmented cross-sectional morphometrics; and secondly, by averaging the morphometrics per landform to provide a whole-feature morphometric assessment (Rivers *et al.*, 2023). This enabled both individual feature and between feature analyses. Calculated morphometrics include: length, sinuosity, area, slope, height, width, asymmetry, cross-sectional area, and volume. For this study, transects were set at 20 m intervals, which was deemed appropriate given the general length of the mapped landforms. Additional quality control checks upon tool execution were also performed as recommended in chapter 4 to remove any distorted transects.

## 5.5 Results

2 581 prominent DGMs and 1 385 intermediate DGMs were identified and mapped across southwest Finland. 1 159 CSRs were identified and mapped across the area defined in the Northwest Territories, Canada. 27 753 transects were generated across the prominent DGM features, 6 118 transects across the intermediate DGMs feature, and 18 564 transects across the CSR features (post quality control checks). It should be noted that some intermediate DGMs were found to be very low amplitude which reduced accurate identification of landform perimeters. This inevitably limited analysis of wider spatial distribution for intermediate DGMs; however, the acquired data remains valuable for comparative morphometric assessments and single feature variability analysis.

Once the 3D morphometric data had been generated for each dataset, comparative assessments were undertaken. Transect data was used to assess height, width, slope and asymmetry. Average feature data was used to assess length and sinuosity. Extreme values that deviated greatly from the overall dataset were removed to mitigate significant skews.

### 5.5.1 Summary statistics

Summary statistics of each quantified landform are provided in TABLE 5.1, TABLE 5.2, TABLE 5.3 and FIGURE 5.5, followed by a description of each metric in turn.

**TABLE 5.1.** Summary statistics of quantified prominent DGM morphometrics (Rivers et al., 2023).

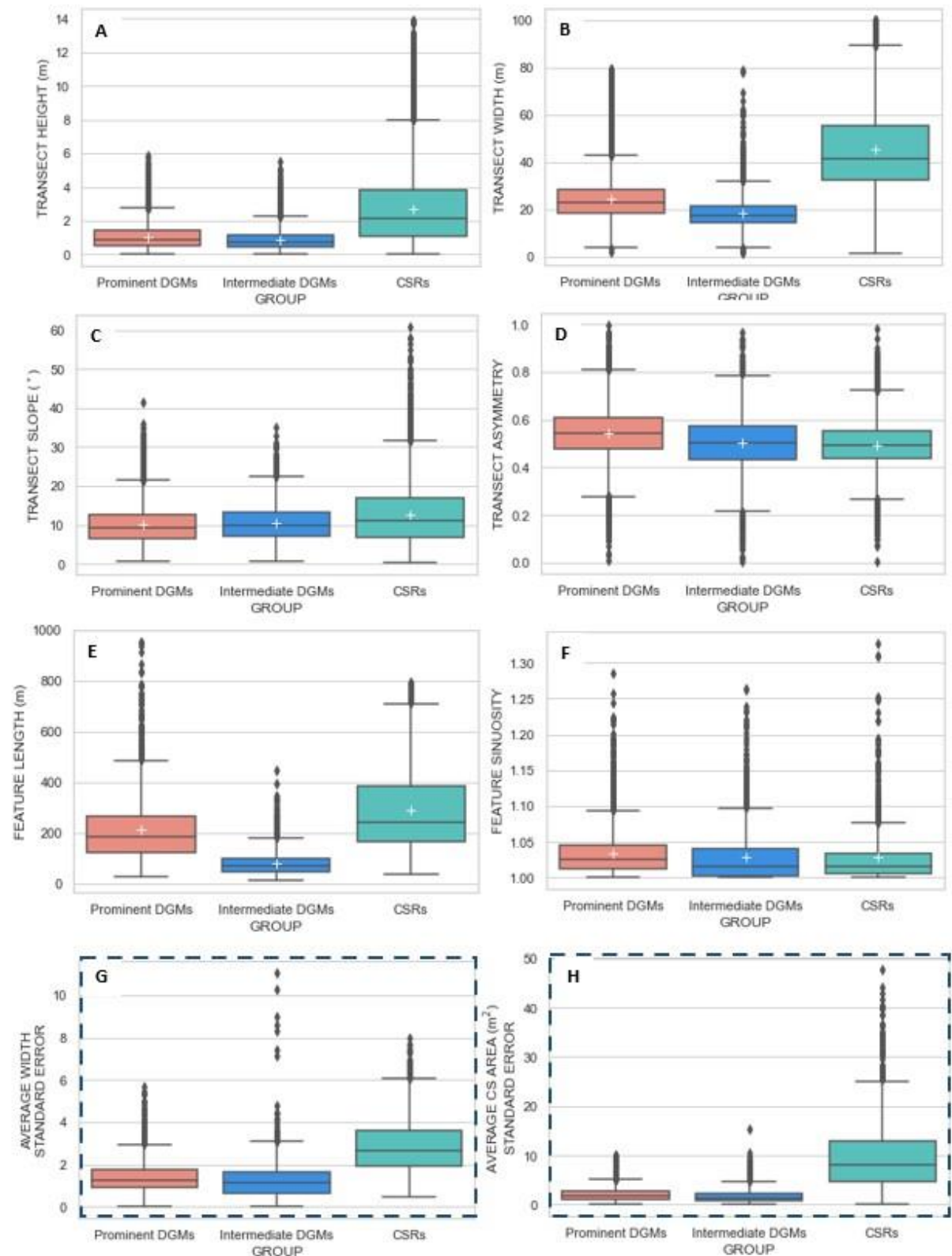
	Height (m)	Width (m)	Slope (°)	Asymmetry	Length (m)	Sinuosity
Mean	1.05	24.33	10.07	0.54	213.49	1.034
Median	0.89	22.62	9.22	0.55	184	1.025
Min	0.1	1.99	0.72	0.009	28	1
Max	5.87	79.52	41.53	1	953	1.29
Std. Dev	0.72	8.92	4.75	0.10	127.45	0.03
Kurtosis	2.32	4.48	1.16	0.28	3.85	8.12
Skewness	1.30	1.60	0.98	-0.12	1.63	2.34
Variance	0.52	79.62	22.55	0.01	16242.39	0.001

**TABLE 5.2.** Summary statistics of quantified intermediate DGM morphometrics. (Rivers et al., 2023).

	Height (m)	Width (m)	Slope (°)	Asymmetry	Length (m)	Sinuosity
Mean	0.87	18.38	10.55	0.50	82.45	1.029
Median	0.72	17.46	9.89	0.51	69	1.0152
Min	0.1	1.08	0.57	0.002	12	1
Max	5.54	78.86	35.19	0.97	448	1.26
Std. Dev	0.64	6.37	4.63	0.11	51.99	0.04
Kurtosis	3.92	7.79	0.63	0.65	5.98	7.05
Skewness	1.56	1.66	0.78	-0.11	1.99	2.35
Variance	0.41	40.62	21.47	0.01	2703.10	0.001

**TABLE 5.3.** *Summary statistics of quantified CSR morphometrics. (Rivers et al., 2023).*

	Height (m)	Width (m)	Slope (°)	Asymmetry	Length (m)	Sinuosity
Mean	2.73	45.30	12.62	0.49	288.66	1.028
Median	2.17	41.55	11.14	0.50	245	1.016
Min	0.1	1.10	0.24	0.004	39	1
Max	13.90	99.99	60.90	0.98	794	1.33
Std. Dev	2.18	18.44	7.53	0.09	164.69	0.04
Kurtosis	2.05	0.23	1.35	0.75	0.38	13.42
Skewness	1.33	0.74	1.05	-0.03	1	3.16
Variance	4.77	340.16	56.74	0.01	27122.15	0.002



**FIGURE 5.5.** A series of boxplots presenting comparative summary statistics of quantified prominent DGM, intermediate DGM and CSR morphometry data. A) Transect Height, B) Transect Width, C) Transect Average Slope, D) Transect Asymmetry, E) Feature Length, F) Feature Sinuosity, G) Average Width Standard Error, and H) Average Cross-Sectional Area

*Standard Error. The lower and upper whiskers represent the minimum and maximum values of the data respectively with outliers residing outside of each whisker limit, the box represents the interquartile range (IQR) (e.g. 50% of the data) with the lower limit representing the lower quartile (Q1) and the upper limit representing the upper quartile (Q3). The central interquartile line represents the median value of the dataset. The white + symbol represents the mean average value. Extreme values that extended far beyond the general dataset were removed. (Rivers et al., 2023).*

Results from each landform group across all morphometrics are positively skewed, except for asymmetry, which shows a negative skew across all landform groups (prominent DGM -0.12; intermediate DGMs -0.11; CSRs -0.03). Whilst asymmetry is similar across all landform groups, prominent DGMs appear slightly more asymmetrical; this can be seen by comparison of the IQR where prominent DGMs show slightly greater median and mean values, and the third quartile exceeds 0.6 (FIGURE 5.5).

CSRs show a positive skewness for width, that is less positively skewed than height. Across all landform groups, CSRs show the most variability across all morphometrics, with the exception of asymmetry and sinuosity- this is highlighted in the standard error results (FIGURE 5.5G and H). Intermediate DGMs overall have the lowest values and least variability across each morphometric, particularly for length, width, and height.

Sinuosity values are similar between prominent and intermediate DGMs, however, the IQR of intermediate DGMs extends lower than prominent DGMs showing that 50 % of the intermediate DGM sample are less sinuous than prominent DGMs. CSRs are the least sinuous landform across each group.

CSRs appear to be the greatest in length across all landform groups with the most variability. However, this could be due to the discontinuous nature of prominent DGMs, which commonly consist of multiple fragments with small gaps, which would be significantly longer if taken together. The same is not true of CSRs.

Overall, the results show that the prominent DGMs are more sinuous, and slightly more asymmetrical than CSRs. CSRs are wider, higher, straighter, and more symmetrical. Intermediate DGMs are shorter, narrower, and less sinuous than prominent DGMs, but more sinuous than CSRs.

The differences in calculated height between the DGMs and CSRs are substantially greater than the mean difference between the different DEM sources as reported above (i.e. 0.79 m; section 5.4.2) (Appendices Figure 1), confirming that the differences are genuine and not an artefact of the underlying data.

### 5.5.2 Statistical tests

Following the primary comparative assessments, a parametric, two-tailed, z-test was conducted against each morphometric to test for any statistically significant differences between mean averages across each landform group. The results are presented in TABLE 5.4.

**TABLE 5.4.** *Z-test results table summarising each tested morphometric. (Rivers et al., 2023).*

Height			
	Z Statistic (critical value: 1.96)	Result	Comments
Prominent DGMs vs CSRs	-101.04	Significant difference	CSRs greater in height
Intermediate DGMs vs CSRs	103.13	Significant difference	CSRs greater in height
Prominent DGMs vs Intermediate DGMs	19.2	Significant difference	Prominent DGMs greater in height
Width			
	Z Statistic (critical value: 1.96)	Result	Comments
Prominent DGMs vs CSRs	-144.11	Significant difference	CSRs greater in width
Intermediate DGMs vs CSRs	170.41	Significant difference	CSRs greater in width
Prominent DGMs vs Intermediate DGMs	60.98	Significant difference	Prominent DGMs greater in width



Slope			
	Z Statistic (critical value: 1.96)	Result	Comments
Prominent DGMs vs CSRs	-41.04	Significant difference	CSRs greater slope angles
Intermediate DGMs vs CSRs	25.5	Significant difference	CSRs greater slope angles
Prominent DGMs vs Intermediate DGMs	-7.4	Significant difference	Intermediate DGMs slightly greater slope
Length			
	Z Statistic (critical value: 1.96)	Result	Comments
Prominent DGMs vs CSRs	-13.80	Significant difference	CSRs greater in length
Intermediate DGMs vs CSRs	40.99	Significant difference	CSRs greater in length
Prominent DGMs vs Intermediate DGMs	45.6	Significant difference	Prominent DGMs greater in length
Asymmetry			
	Z Statistic (critical value: 1.96)	Result	Comments
Prominent DGMs vs CSRs	54.26	Significant difference	Prominent DGMs greater asymmetry
Intermediate DGMs vs CSRs	-5.14	Significant difference	Intermediate DGMs greater asymmetry
Prominent DGMs vs Intermediate DGMs	26.76	Significant difference	Prominent DGMs greater asymmetry
Sinuosity			
	Z Statistic (critical value: 1.96)	Result	Comments
Prominent DGMs vs CSRs	4.4	Significant difference	Prominent DGMs greater sinuosity
Intermediate DGMs vs CSRs	-0.47	No significant difference	Similar in sinuosity
Prominent DGMs vs Intermediate DGMs	4.13	Significant difference	Prominent DGMs greater in sinuosity

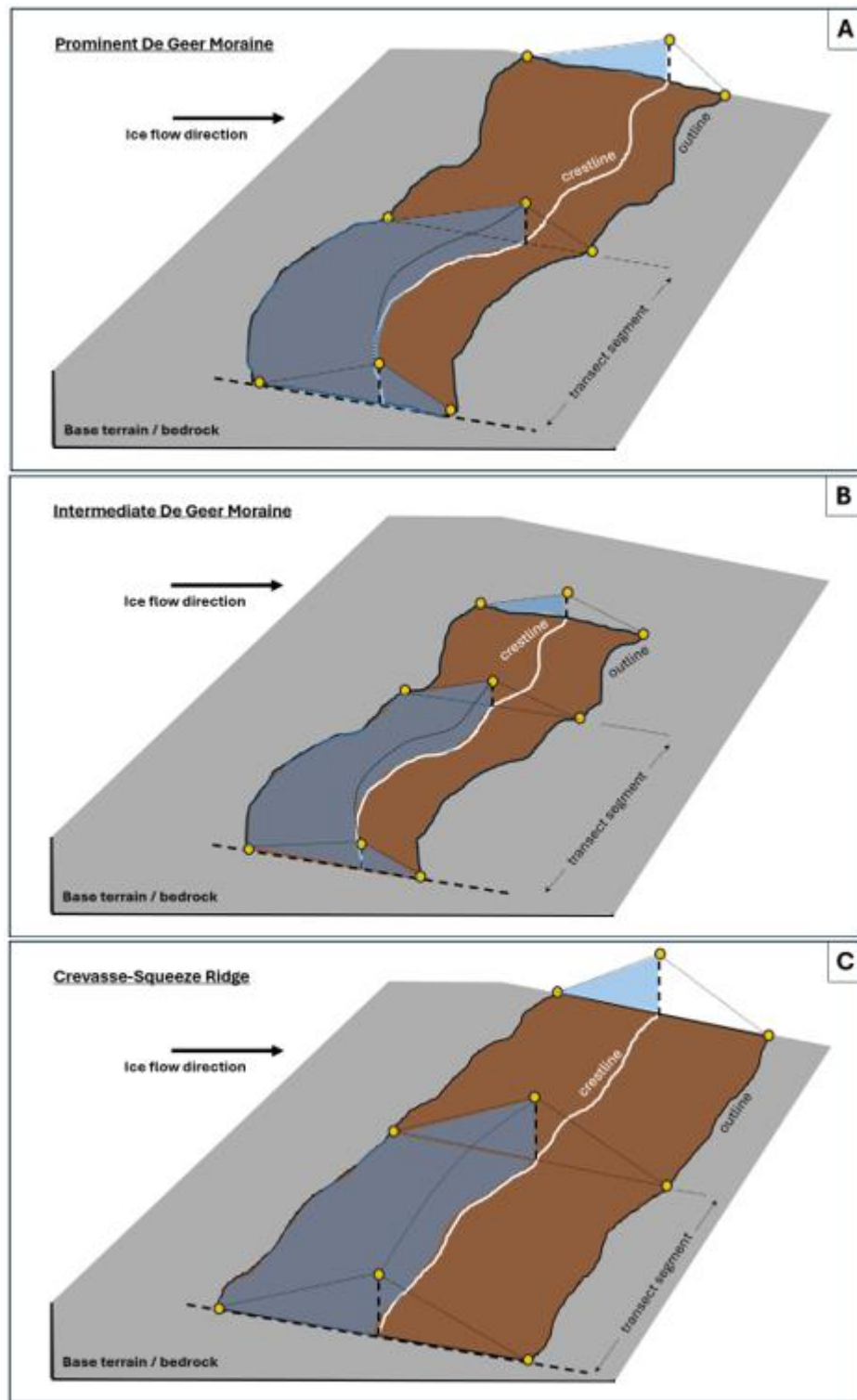
The results from the statistical tests confirm that there is a statistically significant difference between each of the landform groups, with the exception of sinuosity, whereby intermediate DGMs and CSRs show no statistically significant difference. This is particularly important, as whilst the summary statistics showed that some metrics had only slight differences (e.g. asymmetry), these differences are significant and provide a substantive means by which to differentiate between each landform group. Furthermore, a statistically significant difference in asymmetry, with prominent DGMs being the most asymmetrical of the landform groups, provides a justified means by which to infer formational properties, and a scientific basis by which to correctly interpret and position these landforms within a wider glacial context.

### 5.5.3 Landform summary

Based on quantified morphometry, a summary table has been created (TABLE 5.5), providing a taxonomic generalisation of each landform. Each metric range has been taken from the lower and upper whiskers presented in the summary boxplots (FIGURE 5.5).

**TABLE 5.5.** *Landform summary table providing a taxonomic generalisation of prominent DGMs, intermediate DGMs and CSRs. (Rivers et al., 2023).*

	Prominent DGMs	Intermediate DGMs	CSRs
Height (m)	0.1-2.7	0.1-2.3	0.1-8
Width (m)	3.7-43	3.7-32	1.1-89
Length (m)	28-486	12-182	39-710
Slope (°)	0.7-21.6	0.6-22.5	0.2-31.7
Asymmetry	0.3-0.8	0.2-0.8	0.3-0.7
Sinuosity	1-1.09	1-1.1	1-1.09
Volume (m <sup>3</sup> )	29-8067	7-2206	73-58841

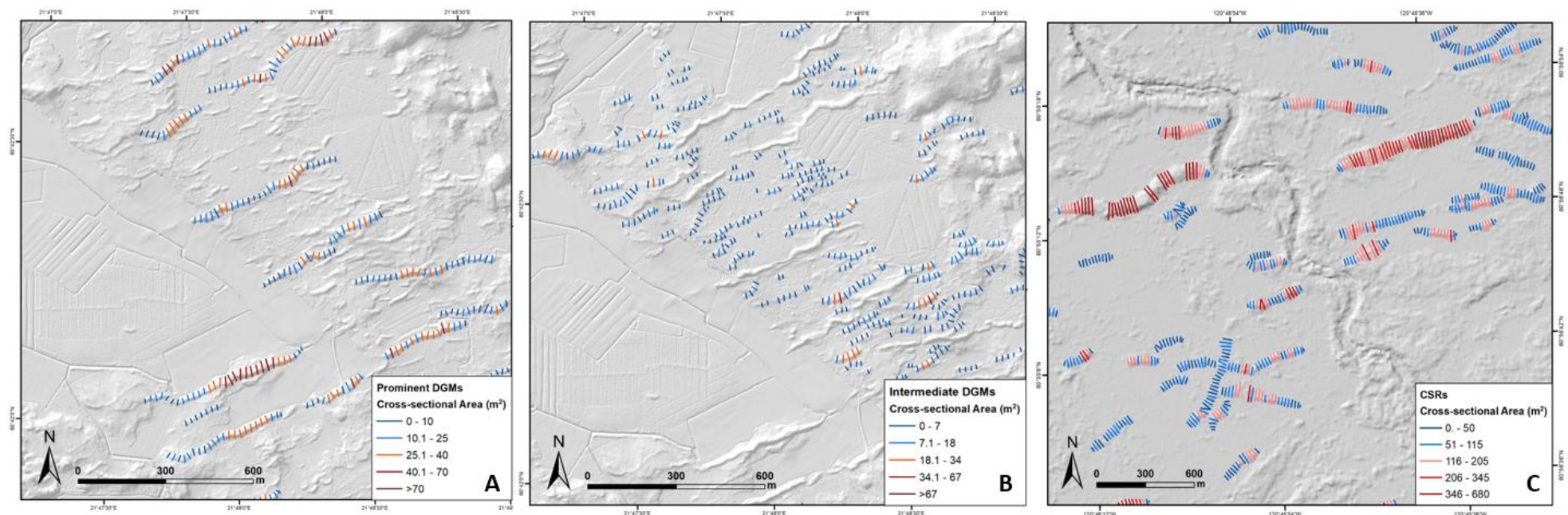


**FIGURE 5.6.** Schematic figure of Landform Summary Table 5.5, showing generalised morphometric differences between prominent DGMs, intermediate DGMs and CSRs. Prominent DGMs show as slightly more sinuous and asymmetrical in profile, whereas CSRs appear generally larger and straighter. NB: Prominent DGMs are typically the longest landforms across the groups; however, due to laterally discontinuity and mapping strategy, results may not always reflect this.

## **5.5.4 Spatial observations**

### **5.5.4.1 Single feature variability**

The calculated cross-sectional area for each transect is visualised using a colour-graded scale (high values in red, low values in blue) to assess spatial variations and/or patterns in morphometry along a single feature's length for each landform group (FIGURE 5.6A, B & C). Values were categorised using the ArcGIS automated natural breaks (Jenks). The results reveal some along-profile variability across all landform datasets; however, the variability of CSRs appears to be greatest compared to the other landform groups (FIGURE 5.6C). This is reflected in the standard error results (FIGURE 5.5G and H).

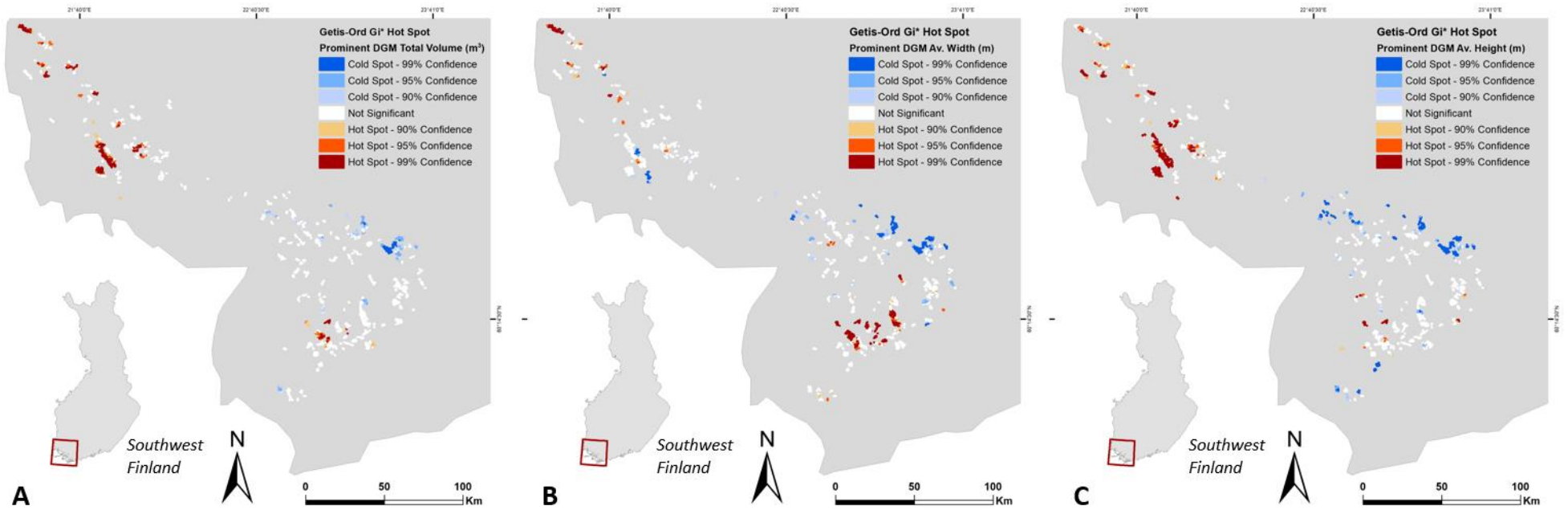


**FIGURE 5.7.** Transect morphometry visualisation showing transects generated at 20 m intervals for each landform group: A) prominent DGMs; B) intermediate DGMs, and C) CSRs. The cross-sectional area calculated along each transect are shown and colour-graded to represent high (red) to low (blue) values. [DEM sources: A & B: ©National Land Survey of Finland, LiDAR digital elevation model, 6/2023; C: ArcticDEM – Porter et al., 2018]. (Rivers et al., 2023).

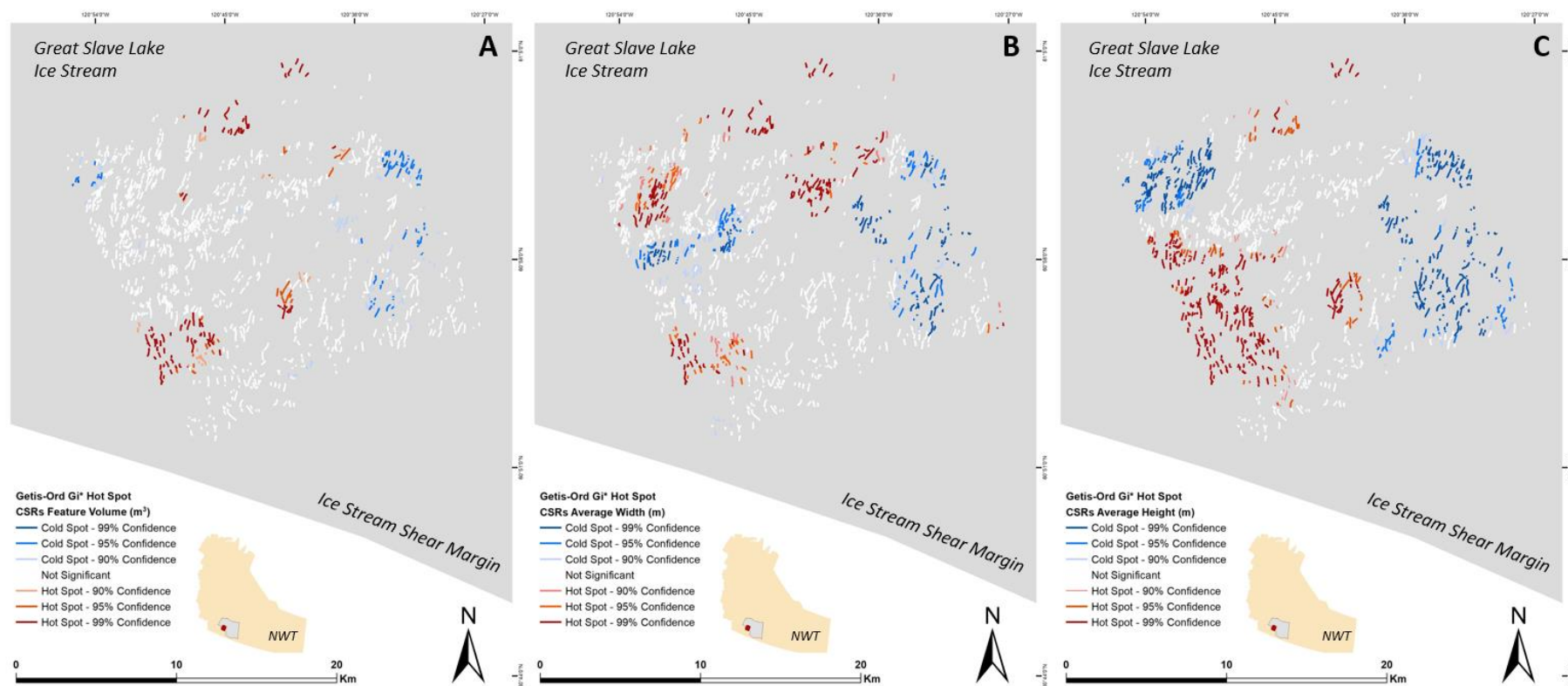
A closer assessment of single feature variability shows that, in some cases, the ridges are greater in size centrally along the feature profile, with values decreasing laterally (FIGURE 5.6A and C). This is likely a representation of sustained subaerial exposure and lateral erosion. However, with respect to CSRs, it could also be a preservation of the form of the crevasse in which the CSR was deposited, and may also be an indicator of the removal of lateral support following any interstitial melt and down-wasting of the surrounding ice (Rea & Evans, 2011). Generally, profile variability appears irregular across prominent DGMs, with sometimes greater values clustered to one side of the feature, or a section located centrally along the feature profile (FIGURE 5.6A). Intermediate DGMs present the least profile variability, showing generally uniform, low-relief metrics with occasional, sporadic cross-sections of greater values (FIGURE 5.6B).

#### **5.5.4.2 Macroscale variations**

To investigate wider spatial characteristics, and to test whether there are any patterns in landform distribution relative to key morphometric variables, a Getis-Ord  $G_i^*$  cluster analysis was conducted (ArcGIS, ESRI). Hot spots (represented in red) show significant clustering of high values and cold spots (represented in blue) show significant clustering of low values. This test was performed on the total volume, average width, and average height metrics for prominent DGMs (FIGURE 5.7) and CSRs (FIGURE 5.8). This test was not conducted on intermediate DGMs because of the difficulties in mapping landform outlines across the entire study area due to very low relief features.



**FIGURE 5.8.** Results of 'Getis-ord  $G_i^*$  hotspot analysis'. A) prominent DGMs total feature volume; B) prominent DGMs average feature width; and C) prominent DGMs average feature height (Rivers et al., 2023).



**FIGURE 5.9.** Results of 'Getis-ord  $G_i^*$  hotspot analysis'. A) CSR total feature volume; B) CSR average feature width; and C) CSR average feature height (Rivers et al., 2023).



The results for prominent DGM total volume reveal a clustering of larger features in the northwest of the study area and minor clusters of both smaller and larger DGMs in the southeast (FIGURE 5.7A). A comparison between width (FIGURE 5.7B) and height (FIGURE 5.7C) show the variations of morphometrics across southwest Finland, with wider DGMs located in the southeast and higher DGMs located in the northwest.

The results for CSR total volume show a cluster of larger CSRs situated in the southwest of the study area, closer to the ice stream shear margin (FIGURE 5.8A). Clusters of smaller CSRs appear to be located further into the ice stream northeast of the study area, with minor clusters of larger CSRs located north-northwest (FIGURE 5.8A). A comparison between width (FIGURE 5.8B) and height (FIGURE 5.8C) shows differences in spatial distribution. Clusters of wider CSRs (FIGURE 5.8B) appear to be situated in the north – northeast of the study area, with large clusters of narrower CSRs located both to the south and east. CSR height clusters appear to be larger and more distinctive than CSR width, with taller CSRs situated in the southwest and shorter CSRs situated to both the east and west of the study area.

## 5.6 Discussion

### 5.6.1 Glacial dynamics- the importance of DGMs and CSRs

DGMs and CSRs are useful for providing insights regarding palaeo-glacial processes. Specifically, they can reveal information regarding spatiotemporal ice-marginal dynamics, ice-margin direction and/or subglacial processes. The review of literature highlights distinct similarities of morphology and distribution between DGMs and CSRs and brings attention to the issue of misinterpretation between these landforms (section 2.4 – 2.5).

As CSRs preserve the spatial extent of crevasses, it should be noted that crevasses evolve and deform with ice flow. Considering contemporary crevassing studies, authors report that particularly in ice stream shear zones, crevasses can undergo a cycle of formation and rotation (Price and Whillans, 2001; Whillans and van der Veen, 2001), often described as a ‘chaotic crevasse network’ in contrast to the linear and geometric arrangements described in previous CSR studies (Evans *et al.*, 2016). This chaotic assemblage has generally been related to ice stream shear margin environments and evidence of this may be found with more detailed analyses of variations in spatial distribution.

CSR observations have been made in both terrestrial and submarine settings of surge-type glaciers. This variability appears to play a role in both preservation potential and spatial distribution. CSRs observed in marine settings tend to be larger, particularly in height, which is likely due to protection from subaerial exposure and postglacial reworking (Boulton *et al.*, 1996; Farnsworth *et al.*, 2016; Lovell *et al.*, 2015; Ottesen and Dowdeswell, 2006; Ottesen *et al.*, 2008; Rea and Evans, 2011). In addition, investigations of different ice dynamics (i.e. surging ice vs ice streams) have revealed subordinate CSR patterns which may be useful in delineating ice flow dynamics (Evans *et al.*, 2016). This supports the inference that variations in spatial distribution may reflect englacial/subglacial processes, such as stress regimes and hydrological pressures that would control fracturing processes (Rea and Evans, 2011). It is possible that these processes may be reflected in the hotspot analysis whereby morphometrics vary across the study area (FIGURE 5.8). Further mapping across the entire ice stream would be valuable to investigate how the spatial distribution of CSRs may vary across the wider palaeo-ice stream area.

DGMs have also been observed in different environmental settings; however, in contrast to CSRs, DGM observations infer that a sub-aqueous environment is a fundamental requirement (e.g. marine or lacustrine) (Finlayson *et al.*, 2007; Golledge and Phillips, 2008; Sinclair *et al.*, 2018). DGM metrics from this study are slightly larger than those reported from a valley, lacustrine setting (Golledge and Phillips, 2008), thus reflecting the marine depositional environment of southwest Finland.

### **5.6.2 CSR morphometry indicates crevasse in-filling**

Morphometrics of the CSRs are of a similar range to those reported from previous studies (e.g. Ben-Yehoshua (2017) reported CSR metrics of 1–7 m wide, 5–45 m long and 0.5–2 m high; Cline *et al.* (2015) reported CSR heights ranging from 0.5 to 2.5 m; and O'Cofaigh *et al.* (2010) reported heights of 1–4.5 m (based on field observations) and lengths of 400–1000 m (based on Google Earth imagery), with some individual ridges extending up to 5000 m long). Some of the CSRs from this study extend slightly larger than those reported from Ben-Yehoshua (2017) and Cline *et al.* (2015), showing more similarity to those described from the Maskwa Ice Stream (Evans *et al.*, 2016).

The greater width and height of CSRs compared with DGMs likely reflect controls of sediment supply and availability of accommodation space within the host crevasse cavity. Furthermore, the greater slope angles likely represent better preservation, as well as the nature of the material (e.g. angle of repose). Whilst postglacial erosional processes such as subaerial exposure and interstitial ice melt-out can degrade CSRs (Ben-Yehoshua, 2017; Evans and Rea, 1999; Sharp, 1985), generally preservation potential is high due to ice stagnation and rapid down-wasting (Evans *et al.*, 2016), or flotational passive retreat (Kurjanski *et al.*, 2019). The greater width, height and slope of CSRs indicate an environment whereby depositional processes exceed erosion (e.g. crevasse infilling), in contrast to a subaqueous ice-marginal environment that may be exposed to glaciofluvial reworking. The lesser amplitude of DGMs supports the inference of a minor pushing formation, for example a minor winter readvance. The differences between the two landforms support the hypothesis that DGMs are ice-marginal features and not crevasse infills.

In addition, the results show that CSRs possess a much greater variability, both between and within features, in their width, height and slope compared to DGMs (FIGURES 5.5G & H, 5.7 & 5.8). This is likely a reflection of the variable crevasse morphology in which they were formed, permitting a wider variability in the resultant fill ridges (Evans *et al.*, 2016; Price and Whillans, 2001; Whillans and van der Veen, 2001). For example, crevasses are likely to be wider in the centre, pinching out at each end, thus providing variable accommodation space (FIGURE 5.5G and H; FIGURE 5.6C). In contrast, deposition in the ice-marginal environment would be characterised by relatively consistent width, which is controlled by the relatively uniform pushing of material.

### **5.6.3 Lateral continuity of DGMs indicates ice-marginal formation**

The results show that CSRs appear to be longer than DGMs; however, this is unlikely to be a true feature of the data, as the mapped DGMs are smaller fragments of more continuous ridges. As such, lateral discontinuity is reflected in our morphometric results. If prominent DGMs segments were mapped continuously, it is likely that the results would reflect prominent DGMs that are greater in length compared to CSRs. CSRs would be restricted in length relative to their hosting crevasse, whereas DGM length would, assuming an ice-marginal pushing formation, be determined by ice marginal curvature,

dynamics and reworking, which may result in lateral discontinuity and/or crenulation (Aartolahti, 1972; Lindén and Möller, 2005; Ottesen *et al.*, 2008).

The length of CSRs, in contrast to DGMs, has previously been used as a characteristic of identification, whereby authors have described CSRs to not follow a continuous lateral trend similar to DGMs, instead terminating sharply and offset with respect to each other (Kurjanski *et al.*, 2019).

#### **5.6.4 DGM asymmetry indicates ice-marginal advance**

Both DGMs and CSRs have been described with either symmetrical or asymmetrical properties (Borgstrom, 1979; Rea and Evans, 2011). However, there is a large body of research that describe DGMs with asymmetric cross-sections, characterised by a steeper distal side, which has been related to a unidirectional push process during formation, whereby material is pushed forwards and then falls to form a shallow proximal slope and steep distal slope (Blake, 2000; Finlayson *et al.*, 2007; Golledge and Phillips, 2008; Linden and Moller, 2005; Ojala *et al.*, 2015).

In contrast, CSRs have been described to have symmetrical cross-sections based on 3D seismic data (Kirkham *et al.*, 2021) and sedimentological data (Ankerstjerne *et al.*, 2015; Sharp, 1985). This simply reflects the typically symmetrical cross-section of the crevasse cavity. Our data support these ideas, showing a slight, but statistically significant, difference in asymmetry between DGMs and CSRs, with DGMs presenting slightly more asymmetrical cross-sections. It should be acknowledged that each of these landforms can display both symmetrical and asymmetrical cross-sections; however, our large-scale dataset support an ice-marginal formation of DGMs, although sedimentological data will be important to validate this. This is presented and discussed later in chapter 6.

#### **5.6.5 Wider spatial variability of prominent DGM morphometry**

The variability in overall volume of prominent DGMs (FIGURE 5.7A) across the wider study area may highlight several controlling factors such as: topographic controls, sediment availability, preservation potential, postglacial clay masking, water depth, elevation, rate of retreat, ice margin configuration or flow dynamics. The differences between width and height (FIGURE 5.7B and C) could also be indicative of each of the controls described above. For example, wider, lower DGMs in the southeast may reflect a restricted sediment supply and/or differences ice configuration/flow compared to the northwest of the study

area. It may also reflect greater erosional processes and slope degradation due to differences in postglacial reworkings and sub-aerial exposure.

#### **5.6.6 Wider spatial variability of CSR morphometry**

The spatial distribution and cluster analysis of CSRs may indicate controls related to the ice stream shear margin. The results from this study show a large cluster of more voluminous CSRs closer to the shear margin. This is similar to CSR spatial distributions reported from previous studies (Lovell *et al.*, 2015). As the study area is not situated directly across the shear margin, it is possible that CSR spatial distribution may reflect ice stream shear margin migration (Haseloff, 2015; Stokes, 2000). The clustered CSR spatial distribution may also highlight other controls relating to ice stream bed characteristics such as: sediment availability, topography, roughness, and lithology (Stokes, 2000). Each of these would influence stress regimes, fracturing processes, and hydrological pressures within and beneath the ice. CSRs transportation should also be acknowledged, whereby CSRs are formed within a crevasse which is then transported englacially before final deposition (Ben-Yehoshua, 2017; Sobota *et al.*, 2016). The CSRs in this study were not mapped for the purpose of spatial pattern analysis. Whilst some observations can be made from our data, given the various possible controls on spatial distribution, extended mapping would be required to investigate CSRs and ice stream/shear margin dynamics further.

#### **5.6.7 Intermediate De Geer moraines**

Regarding geomorphological appearance, there are many different types of DGM fields in Finland and intermediate DGMs are not always present (Ojala, 2016). These intermediate DGM ridge-types are observed either 1) in the spaces between regularly spaced prominent DGMs (FIGURE 5.1A), or 2) in separate fields that have no regularly spaced prominent DGMs. The morphometric results show that these intermediate ridges are different to prominent DGMs, generally presenting as lower relief features. In addition, these intermediate DGMs show less asymmetry than that of prominent DGMs which could indicate a different formation process. It could be, for example, that they are subdued versions of prominent DGMs, or it could be that they are crevasse infills formed behind the grounding line that is marked by the prominent DGM. This warrants further investigation whereby sedimentological and geophysical data would be valuable. It should

also be noted that the characteristic 'regularly spaced' properties of DGMs usually refers to prominent DGMs. Intermediate DGMs are typically positioned irregularly within the spaces between prominent DGMs. Therefore, if any temporal investigations were to be undertaken, differences between prominent and intermediate DGMs should be considered.

## **5.7 Conclusions**

DGMs and CSRs are important landforms that can provide useful insights regarding palaeo-ice sheet processes. Specifically, these landforms can provide information regarding ice-marginal dynamics and/or subglacial processes, depending on the context in which they form. Visual similarities between DGMs and CSRs have historically proven problematic for landform differentiation and have been an area of contentious debate surrounding DGM formation. This study presents a detailed morphometric comparative investigation of DGM and CSR landforms to accurately quantify landform morphometrics, elucidate formation properties and identify any differences between the landform groups that can be used as a justifiable means for differentiation.

Results reveal key differences in morphometric properties between the landform groups which enables a quantified foundation by which to differentiate them. Specifically, the CSRs are found to be higher, wider, steeper, more symmetrical, less sinuous and more voluminous than the prominent DGMs. In contrast, a tendency for cross-sectional asymmetry in DGMs supports an ice-marginal push origin, rather than a basal squeeze-up into crevasses. This is further supported by CSRs being less sinuous than DGMs due to the deposits being constrained by dimension and planform of the (relative straight) host crevasses, whereas DGMs follow a more sinuous path, related to the shape of the ice margin. Further work should include sedimentological and geophysical studies to constrain DGM internal architecture and validate the inferred formation processes.

## Chapter 6: De Geer moraine internal architecture based on sedimentological and geophysical investigations and implications for ice marginal reconstructions

**Citation:** Rivers, G.E., Storrar, R.D., Ojala, A.E.K., Mäkinen, J., Holmroos, C. & Holmes, N. (2024). De Geer moraine internal architecture based on sedimentological and geophysical investigations and implications for ice marginal reconstructions. *Boreas*. DOI: <https://doi.org/10.1111/BOR.12692>

This chapter presents findings from a sedimentological and geophysical study of the DGMs located in southwest Finland investigating formation properties. This work develops on the previous morphometry study outlined in chapter 5 and contributes to research objectives (1 & 2).

### Abstract

DGMS may act as valuable ice margin indicators; however, to date, their variable mode of formation has presented challenges for this utility. Morphometric investigations provide useful insights into formation processes, which can be developed using sedimentological and geophysical methods. Here, sedimentological and Ground Penetrating Radar (GPR) data of DGMs located in southwest Finland is presented. Individual lithofacies were identified and interpreted using sediment architectural elements. These were correlated with neighbouring GPR radargrams and extrapolated across the wider study area. Generally, internal architecture presents a multi-phase structure with lower units representing subglacial traction till and ice margin infill deposits, truncated by a larger prominent push unit, which is then successively deformed via the overriding of active ice. Significantly, there are notable differences between proximal and distal structures, with proximal sides characterised by silts, clays, and diamicton with laminae, stratification and thrust planes, and distal sides characterised by poorly consolidated diamicton and proglacial water current reworkings. Internal architecture of both prominent and intermediate ridges is the same, with slight differences, reflecting similar formation processes, with inter-seasonal variations. Based on these findings, an integrated conceptual model for the genesis of DGMs is presented whereby inter-seasonal ridge

forming processes occur within a sub-aqueous ice marginal environment. The model highlights that DGMs can be subcategorised as, i) sediment deposition at an unstable margin during summer calving, and/or ii) sediment pushing at a stabilised margin during a winter readvance. No evidence indicative of crevasse filling as a mechanism for DGM formation is found. A new landform assemblage classification is proposed whereby 'De Geer terrain' (DGT) is used to describe series of parallel ridges arranged in a typical washboard-like configuration. This classification identifies all DGMs derived within a sub-aqueous ice marginal environment, whilst also capturing the equifinal characteristics between individual DGM ridge-types.

## 6.1 Introduction

Palaeo-ice sheet reconstructions can provide valuable information regarding the extent and evolution of past ice sheets (Boulton *et al.*, 1984; Dyke *et al.*, 2002; Hughes *et al.*, 2016; Stroeve *et al.*, 2016; Gowan *et al.*, 2021; Clark *et al.*, 2022). This is important as it enables us to understand how the cryosphere responds to global/hemispheric climate and environmental change, and how glacial ice behaves under different localised conditions. Ice sheet reconstructions are typically produced by a "glacial inversion model" (Kleman *et al.*, 1997), allowing inferences to be made from the integration between geomorphological evidence, numerical dating and modelling (Clark, 1997; Stokes *et al.*, 2015; Pearce *et al.*, 2017; Gowan *et al.*, 2021; Dalton *et al.*, 2023). Modern palaeo-ice sheet reconstructions provide time-slice resolutions of between 1000 – 100 years (Hughes *et al.*, 2016; Stroeve *et al.*, 2016; Clark *et al.*, 2022); however, as remotely sensed data improves (e.g. LiDAR derived digital elevation models (DEMs)), it is possible that lower-relief geomorphology may be identified and used to improve these resolutions.

DGMs are low-relief landforms and can be characterised as long, narrow, elongated ridges that are orientated transverse to former ice flow direction. These ridges often occur in swarms, closely spaced, parallel to the ice margin with either regularly spaced and laterally continuous, or irregularly spaced and laterally discontinuous configurations, typically resembling a washboard-like appearance (De Geer, 1889; Hoppe, 1959; Benn & Evans, 2010; Ojala *et al.*, 2015; Ojala, 2016). DGMs are moderately sinuous and often display asymmetric cross-profiles with a steeper distal side, although symmetric ridges have also been observed (Todd *et al.*, 2007; Rivers *et al.*, 2023). DGMs commonly occur



below the highest shoreline of proglacial lakes/seas (Prest *et al.*, 1968; Ojala *et al.*, 2015; Ojala, 2016). However, observations have also been made in mountainous-valley, lacustrine environments (Golledge & Phillips, 2008; Regnéll *et al.*, 2023).

Since the first observations in Sweden (De Geer, 1889), several conceptual models of DGM formation have been considered, with two overarching hypotheses historically debated (see also section 2.4). The first constitutes formation at the grounding line of water terminating ice margins (De Geer, 1889, 1940; Sollid & Carlsson, 1984; Sollid, 1989; Larsen *et al.*, 1991; Blake, 2000; Lindén & Möller, 2005; Golledge & Phillips, 2008; Bouvier *et al.*, 2015; Sinclair *et al.*, 2018). The second hypothesis can be described as a crevasse cavity infilling process whereby saturated and deformable sediments at the bed of the ice are squeezed up into full depth and/or basal crevasses (Andrews, 1963; Strömberg, 1965; Zilliacus, 1989; Beaudry & Prichonnet, 1991, 1995). This crevasse infilling process occurs up ice, behind the grounding line and is similar to the formation process of CSRs but presents different spatial patterns (e.g. “washboard” terrain instead of geometric ridge networks) and potentially without the squeezing that is inherent in CSRs (Benn & Evans, 2010; Rea & Evans, 2011; Evans *et al.*, 2016). The morphological similarities between DGMs and CSRs has been the cause of debate regarding DGM origin; however, the hypothesis that DGMs are formed at the grounding line of water terminating ice margins is most widely accepted (Larsen *et al.*, 1991; Blake, 2000; Golledge & Phillips, 2008; Bouvier *et al.*, 2015; Rivers *et al.*, 2023).

When reviewing DGM formation at the grounding line, different seasonal models have been proposed, with suggestions of ridge formation during winter readvances and/or during summer retreat (De Geer, 1889, 1940; Frödin, 1916; Möller, 1962; Sollid & Carlson, 1984; Larsen *et al.*, 1991; Blake, 2000; Lindén & Möller, 2005; Bouvier *et al.*, 2015; Sinclair *et al.*, 2018;). In the winter model, ridges are constructed via glacial and glaciofluvial deposition and/or settling at the grounding line, and later deformed as the ice margin advances (De Geer, 1940; Larsen *et al.*, 1991; Blake, 2000; Golledge & Phillips, 2008; Bouvier *et al.*, 2015; Sinclair *et al.*, 2018). It should be noted that some authors place less emphasis on push deforming processes but instead consider DGM formation as lodgement of till at the ice margin during either readvances or standstills (Sollid & Carlsson, 1984). In the summer model, ridges are formed by the advection of subglacial

sediments to the grounding line during temporary halts in retreat, preferentially driven by calving processes (Lindén & Möller, 2005).

Distinction between the different seasonal formation processes is important as they present different implications for grounding line dynamics. A winter readvance push formation would infer that ridges form on a periodical basis, with ridge interdistances relating closely to annual rates of ice margin retreat (De Geer, 1940; Möller, 1962; Zilliacus, 1981; Larsen *et al.*, 1991; Lindén & Möller, 2005; Bouvier *et al.*, 2015; Sinclair *et al.*, 2018). In contrast, ridges formed during summer would depict irregular patterns associated with a calving ice margin (Frödin, 1916; Möller, 1962; Zilliacus, 1981; Lindén & Möller, 2005; Bouvier *et al.*, 2015). The cycle of deposition and calving throughout the summer season would likely repeat, allowing several ridges to be constructed within a single year (Zilliacus, 1981; Lindén & Möller, 2005). Essentially, winter ridges would delineate glacier dynamics associated with mass balance, and summer ridges would be more representative of sporadic grounding line forcing mechanisms such as calving intensity and thinning (Benn *et al.*, 2007; Ritchie *et al.*, 2008). The summer and winter models are not mutually exclusive, and the potential alternations between winter and summer ridges introduces complexities regarding preservation potential, as ridges constructed during the summer may be overridden or destroyed during a subsequent winter readvance (Lindén & Möller, 2005; Sinclair *et al.*, 2018).

The identification of, and distinction between, “summer” and “winter” DGMs has been discussed in previous studies, with suggestions that regularly spaced, high relief, and laterally continuous ridges represent annual winter readvances, and irregularly spaced, low relief ridges denote summer retreat patterns (Möller, 1962; Zilliacus, 1981; Lindén & Möller, 2005; Bouvier *et al.*, 2015). The use of LiDAR in recent years has better enabled distinction between regular and irregular DGM ridges, allowing the complexities in DGM formation to be observed across large areas (Bouvier *et al.*, 2015; Ojala *et al.*, 2015; Ojala, 2016; Rivers *et al.*, 2023).

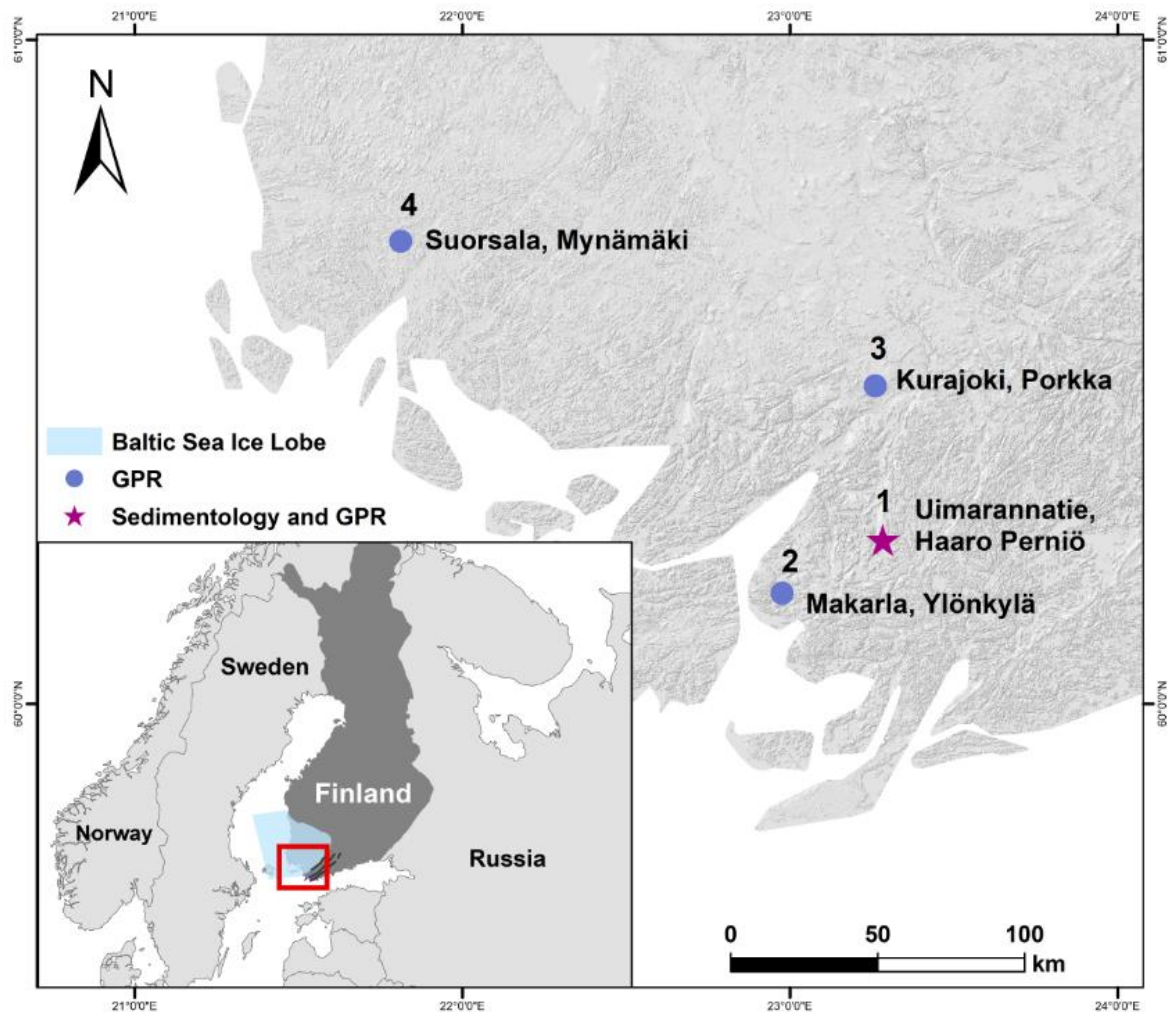
To current knowledge, explicit comparative field investigations between winter and summer DGMs within the same environment do not yet exist. As such, this study aims to explore the internal architecture of DGMs to investigate differences and/or similarities in prominence and regularity, with a view to increase understanding of DGM formation. The

existing morphometry studies in southwest Finland provide valuable detailed insights that may be used to elucidate DGM formation (Ojala *et al.*, 2015; Ojala, 2016; Rivers *et al.*, 2023). As detailed in chapter 5, it was found that in Finland ridge morphology indicated that DGMs are dissimilar to CSRs; however, these findings may be further improved upon with supportive field investigations. As such, this study aims to address two questions: (i) what are the main sediment units within both prominent and intermediate DGMs, and how do these relate to ridge-forming processes, and (ii) does the sedimentology and structure of the exposed ridges allow the various processes suggested above to be distinguished? This study aims to improve the current understanding of DGM formation, particularly regarding different formation processes between ridges, and ultimately assess their validity as geochronometric ice marginal indicators during the FIS deglaciation.

## **6.2 Study sites & general characteristics of DGMs in southwest Finland**

Southwest Finland is a relatively low-relief depositional setting that was completely overridden by the FIS during the LGM (~23-21 ka BP) (Svendsen *et al.*, 2004; Clark *et al.*, 2009; Johansson *et al.*, 2011; Hughes *et al.*, 2016; Stroeven *et al.*, 2016; Lunkka *et al.*, 2021). Much of the Earth's crust in Finland was isostatically depressed leaving southwest Finland submerged below sea level during deglaciation. The ice margin position of the FIS during the YD ~12.9-11.7 ka BP is particularly well preserved in southeast Finland by the notable Salpausselkä moraines (Glückert, 1995; Rainio *et al.*, 1995; Tschudi *et al.*, 2000; Saarnisto & Saarinen, 2001; Rinterknecht *et al.*, 2004). After the YD, a rapid retreat led to significant crenulation of the ice margin and the development of several independent ice lobes across Finland (Lunkka *et al.*, 2021). Southwest Finland was host to the Baltic Sea Ice Lobe (BSIL) which was further subdivided into the northeastern Loimaa sub-lobe and the remaining southwestern main lobe which terminated into the Baltic Ice Lake (BIL) (Lunkka *et al.*, 2021) (see section 3.3.1 & FIGURES 3.2, 3.3 & 3.4).

The geographical setting of the southwestern sector of the BSIL is unique in that the interconnected processes between deglaciation, continental rebound, and fluctuating water depths would have imposed significant controls over geomorphological development (Ojala *et al.*, 2013, 2016; Lunkka *et al.*, 2019) (FIGURE 6.1), resulting in a landscape characterised by abundant DGMs.



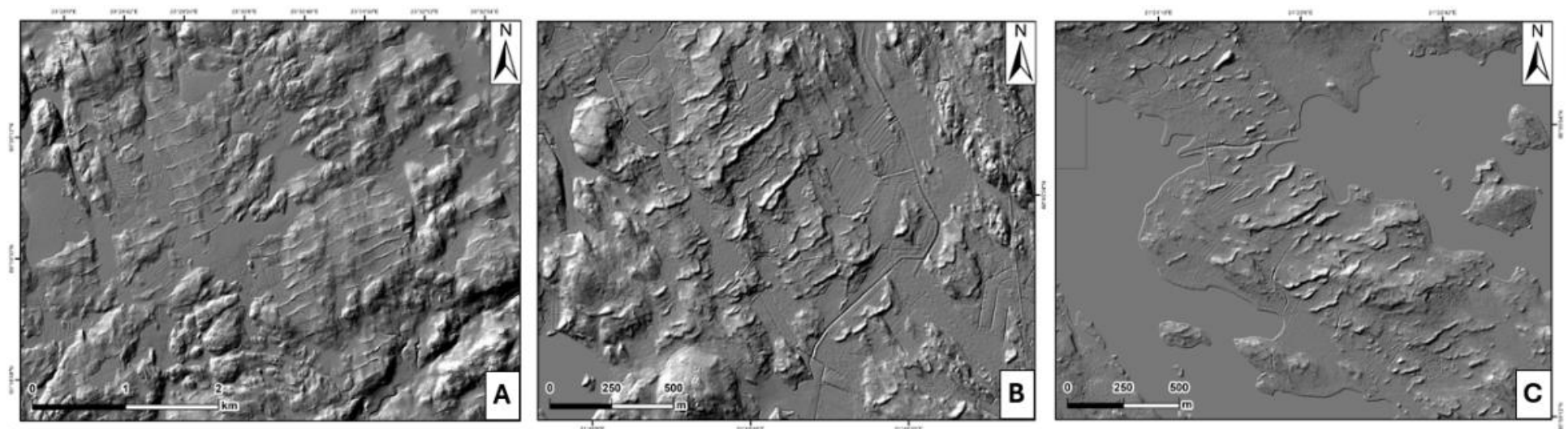
**FIGURE 6.1.** Location map indicating selected sites across southwest Finland for data acquisition: 1 = Uimarannatie, Haaro, Perniö – sedimentology and GPR; 2 = Makarla, Salo – GPR; 3 = Kurajoki, Salo – GPR; 4 = Suorsala, Mynämäki - GPR. Note the blue area marks the extent of the Baltic Sea Ice Lobe (BSIL) in which the investigated De Geer moraines are associated.

The study outlined in chapter 5, investigated DGM morphometry across southwest Finland, building on previous studies undertaken by Ojala *et al.* (2015, 2016). Morphometrics of both prominent (regularly spaced) and intermediate (irregularly spaced) DGMs were compared to those of typical CSRs located in the Northwest Territories, Canada. The findings revealed statistically significant differences between DGM and CSR morphometries, with DGMs presenting lower-amplitude, more sinuous, and slightly more asymmetrical geometries. Importantly, the study highlighted that sinuous and slightly asymmetric cross-profile tendencies support the notion that DGMs

located in southwest Finland are formed at the ice margin via unidirectional push processes, rather than via a crevasse cavity squeeze-up process.

Within this study, the morphometry of prominent (high-relief and regularly spaced) and intermediate DGMs (low-relief and irregularly spaced) was compared, finding intermediate DGMs to be lower-relief, less sinuous and more symmetric than prominent DGMs. It was suggested that intermediate DGMs could be lower amplitude versions of more prominent DGMs, formed via ice marginal push, or formed by alternative processes, such as crevasse infilling behind the grounding line. This reiterates the problem of careful morphometric distinction between DGM ridges of differing geometries and highlights the necessity of further investigation to improve understanding.

In southwest Finland, DGMs vary greatly in their distribution and relief pattern (Zilliacus, 1981; Ojala *et al.*, 2015; Ojala, 2016; Rivers *et al.*, 2023). The appearance of DGMs may be configured in one of three ways: i) only regular prominent ridges, ii) regular ridges interspersed with irregular/intermediate ridges, or iii) only irregular ridges (FIGURE 6.2). Generally, size can range between 0.1 – 3 m height, 25 – 500 m width, 4 – 45 m length for prominent DGMs, and 0.1 – 2.5 m height, 10 – 200 m length, 4 – 35 m width for intermediate DGMs (Rivers *et al.*, 2023). DGM morphometry is also shown to vary across wider areas highlighting controls such as topography, sediment availability and water depth (Ojala, 2016; Rivers *et al.*, 2023).



**FIGURE 6.2.** Hillshaded digital elevation model (DEM) imagery depicting different DGM field types across southwest Finland. A. Kurkela (Salo) - regular, only prominent DGMs. B. Pehtsalo (Laitila) - regular DGMs interspersed with irregular DGMs. C. Pohiperä (Uusikaupunki) - only irregular/more scattered DGMs with a less distinct rhythmic distribution (DEM source: ®National Land Survey of Finland, LiDAR digital elevation model, 2/2023).

From these starting points, the sites of specific investigation in southwest Finland are given in FIGURE 6.1. The selection of sites was based on LiDAR DEMs and preliminary field reconnaissance during spring 2023.

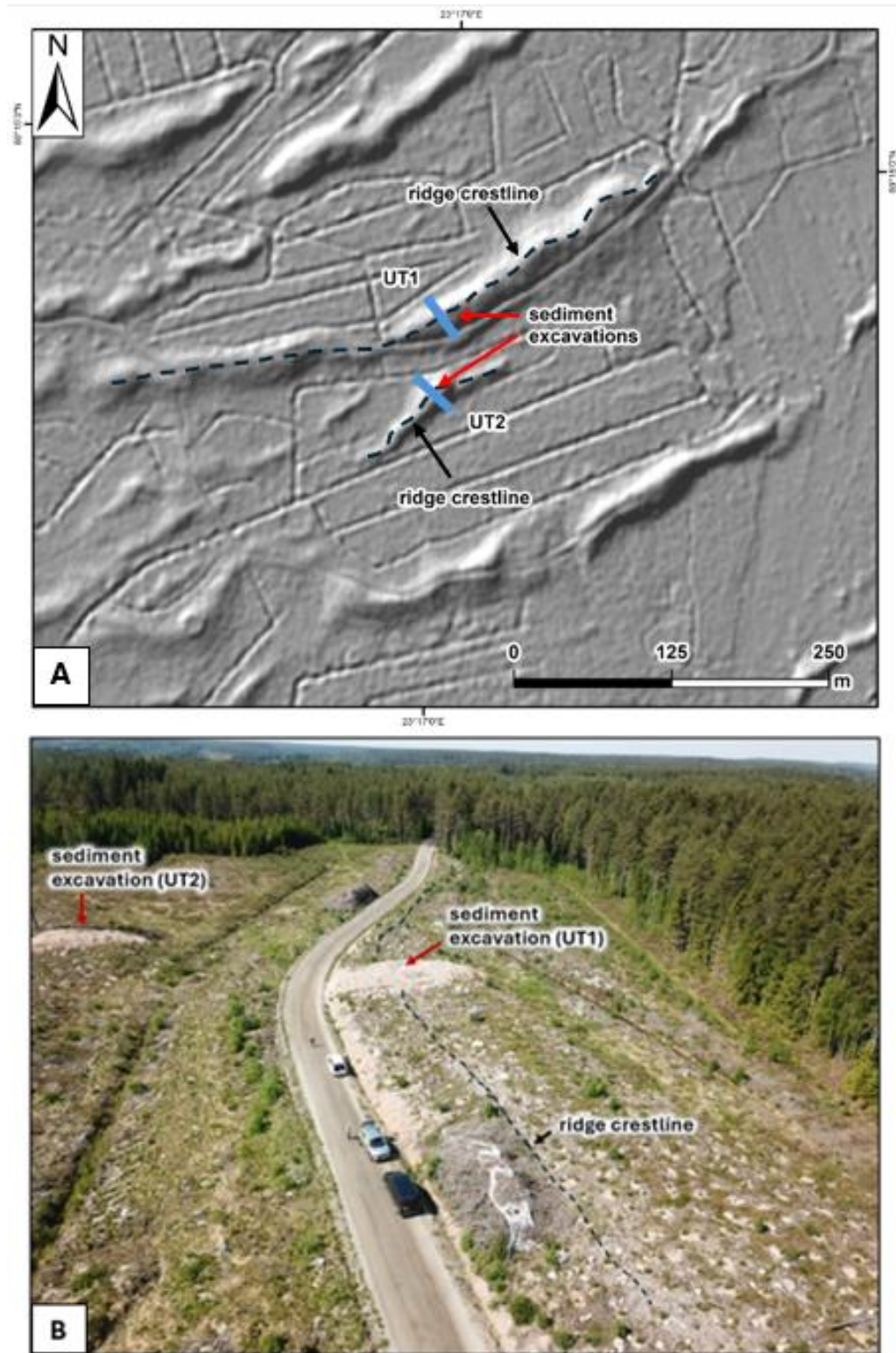
### **6.3 Methods**

Sedimentological and GPR data were acquired at Uimarannatie, Haaro, Perniö (Site 1 in FIGURE 6.1), and independent GPR data were acquired at three additional sites (2, 3 and 4 in FIGURE 6.1). Ridges are identified as either prominent (large and regular ridges) or intermediate (small and irregular ridges) based on the subclassifications outlined in chapter 5 (Rivers *et al.*, (2023)).

#### **6.3.1 Sedimentological investigations**

For this study, sediment exposures were obtained via excavations across the mid-sections of one prominent (UT1) and one intermediate (UT2) DGM at Uimarannatie, Haaro, Perniö at right angles to the ridge crestlines (FIGURE 6.3). Vertical sections of the trenches were photographed and logged for lithological units and sediment structural characteristics. Descriptions of vertical sections at UT1 and UT2 trenches were supplemented with site-specific logs: UT1\_2023\_log1, UT1\_2023\_log2, UT1\_2023\_log3, UT2\_2023\_log4 and UT2\_2023\_log5, where lithofacies unit characteristics were delineated in more detail. Sedimentological logging of units included grain-size, degree of sorting, matrix composition and clast lithology, with lithofacies codes applied to each unit (Evans & Benn 2004). Altogether, nine clast macrofabric samples (50 clasts, a-axis azimuth and dip) were acquired and plotted in rose diagrams and stereonetts using Orient software (Vollmer 2023). In addition, we subsampled different lithological units for grain-size distribution (10 samples from UT1 and six samples from UT2) that were dry sieved in the laboratory and measured for grain-size distribution (>0.063 mm) (Appendices Figures 6, 7, 12, 13).





**FIGURE 6.3.** Location of excavated sediment exposures at Site (1) Uimarannatie, Haaro, Perniö (see FIGURE 6.1). A. Hillshaded DEM highlighting prominence of DGMs and positioning of sediment excavations. B. Oblique photograph of excavated sediment exposures facing southwest.



### 6.3.2 Geophysical investigations and radar facies identification

GPR has become an increasingly popular approach for investigating the internal architecture of glaciogenic landforms (Neal, 2004; Livingstone *et al.*, 2017; Stoker *et al.*, 2021; Harrison *et al.*, 2022; Lally *et al.*, 2023). Whilst there is a degree of subjectivity in GPR interpretations, this method provides a valuable alternative and/or supplementary approach to sedimentological analyses whereby the internal architecture of landforms can be investigated non-intrusively and relatively easily, allowing more representative datasets to be acquired. Subjectivity in interpretation can be overcome by 'ground truthing' GPR interpretation with sediment exposures, where possible.

GPR data in this study were collected using a 32-bit MALÅ GroundExplorer (GX) 160-MHz shielded antenna mounted on a rough terrain skid plate and connected to a MALÅ GX controller. Profiles were acquired using a wheel acquisition mode with traces recorded every 0.05 m. A velocity of  $0.1 \text{ m ns}^{-1}$  was used based on antenna frequency and lithology, providing an estimated penetration depth of  $\sim 5 \text{ m}$ , although this depth will be restricted by the presence of conductive silts and clays (Jol, 1995; Jol & Bristow, 2003; Livingstone *et al.*, 2017; Stoker *et al.*, 2021; Lally *et al.*, 2023).

GPR data were processed using REFLEXW v7.5.9 (proprietary software of Karl-Josef Sandmeier). A standard processing sequence, close to those used in similar studies (e.g. Stoker *et al.*, 2021; Lally *et al.*, 2023) was applied across all profiles. This comprised: static correction of time-zero drift, removal of low frequency signal saturation (DEWOW), application of gain to increase visibility of reflectors at depth, and 3D topographic profile correction. Radargrams were visualised and interpretations were presented using Adobe Illustrator. For transparency, we present unannotated radargrams alongside our interpretations.

Radar facies were determined by identifying variations in reflector motif (e.g. reflector strength, length, shape, amplitude, and pattern). Radar facies were compared with the lithofacies observed in the trenches at Site (1) UT1 and UT2 between the excavated sediment exposures and neighbouring GPR profiles to ensure an accurate basis for GPR interpretation (see TABLE 6.1, Appendices Figures 2, 8). This was then extrapolated and used to interpret radargrams acquired at the additional locations across the study area, where sediment sections were not available (FIGURE 6.1). It should be noted that we have

interpreted facies at Sites (2, 3 and 4) based on the exposures at Site (1). Whilst we can observe similar radar facies between sites, we cannot be certain that the facies at Sites (2, 3 and 4) are directly related to the observed exposures at Site (1). It is possible that there may be other units/facies that are not described from the exposures at Site (1). However, we believe that the exposures at Site (1) provide enough evidence for reasonable interpretation.

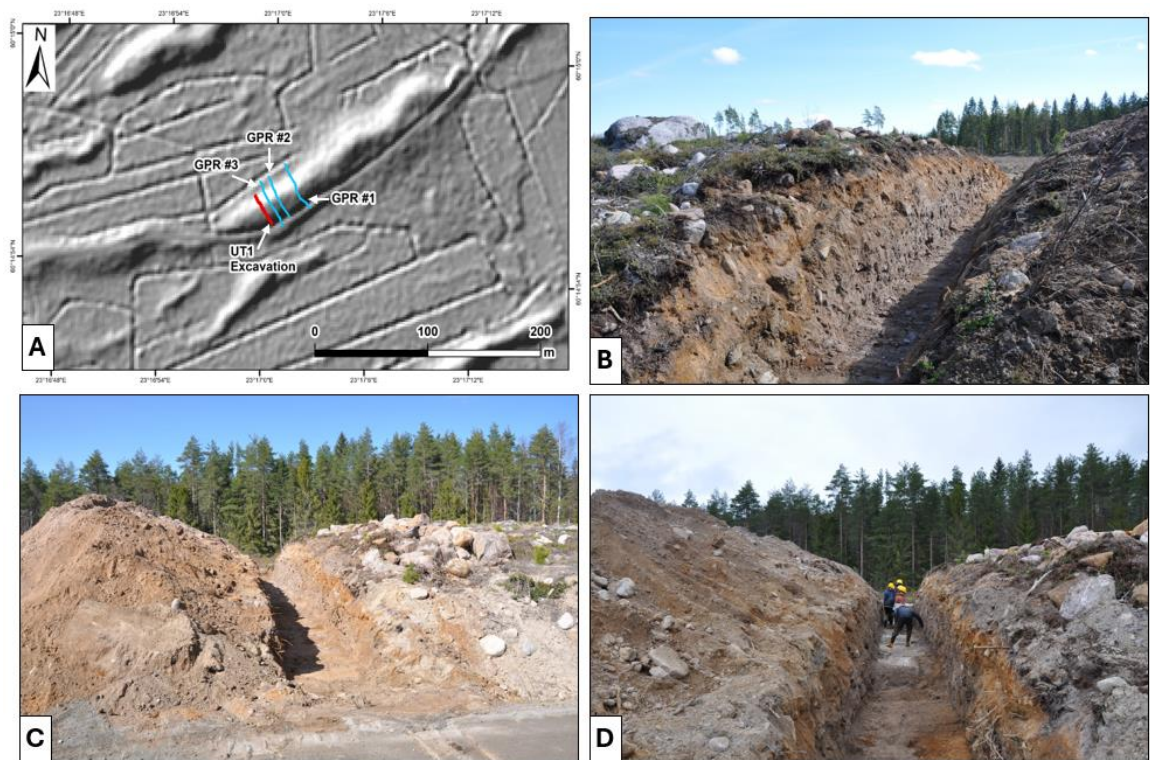
### **6.3.3 Uncrewed aerial vehicle field observations**

A high resolution (7 cm) DEM and orthomosaic of the study area were produced using UAV-based Structure from Motion photogrammetry. A DJI Mavic Pro was used to collect overlapping photographs, and 10 ground control points, evenly distributed across the area, were surveyed using a Trimble R10 GNSS. Images were processed using Agisoft Metashape v1.8.1 (Agisoft, 2022). The orthophoto and DEM were used for field observations and topographic corrections of GPR profiles.

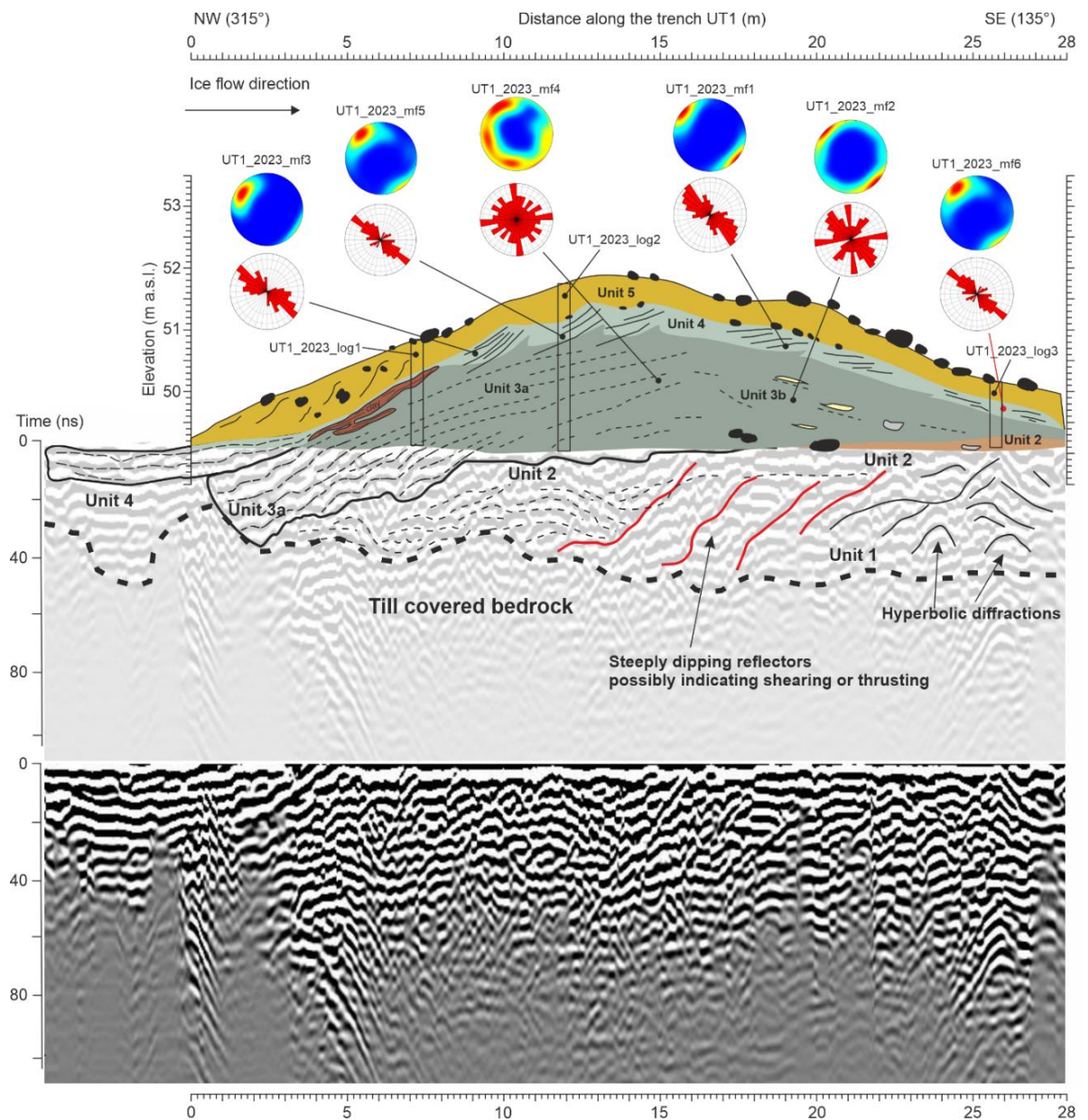
## **6.4 Results and interpretation**

### **6.4.1 Site (1) UT1 (Uimarannatie, Haaro, Perniö (60.249°N; 23.283°E))**

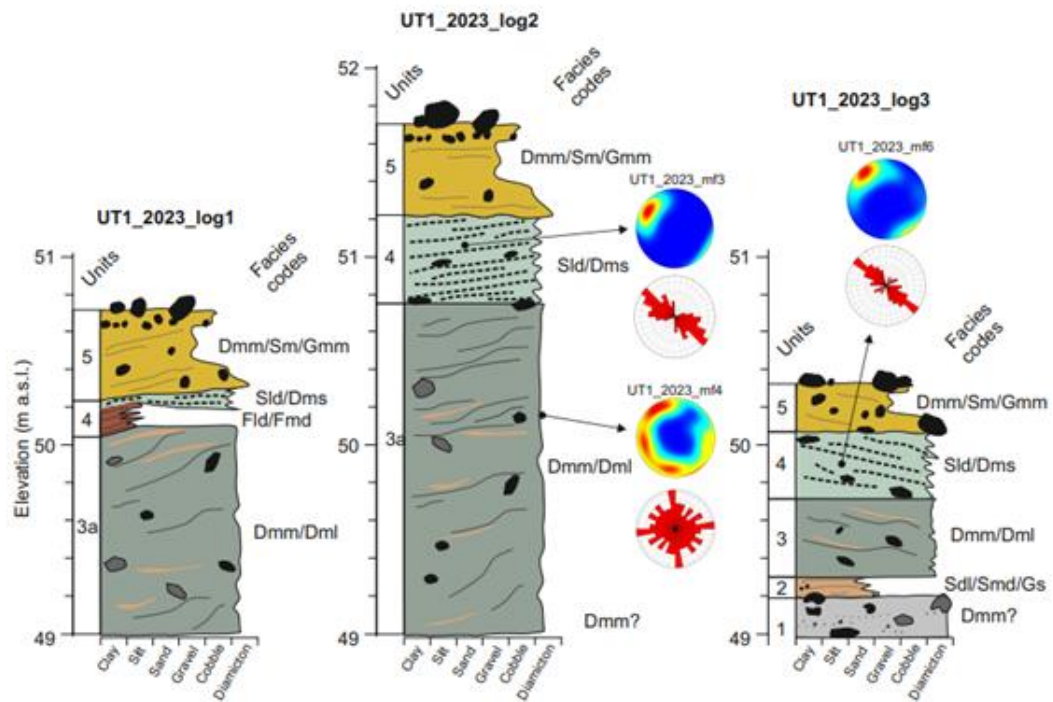
One trench was excavated, and three GPR-lines were acquired at Site (1) UT1 (FIGURE 6.4). The DGM at UT1 is a large, prominent ridge, ~485 m long, ~2 m high and ~40 m wide. It should be noted that the sediment exposure did not reach bedrock, however, GPR data was used to identify this. The logged sections (FIGURE 6.5) and sediment exposure combined with the GPR profiles (TABLE 6.1, Appendices Figures 2, 3, 4, 5) revealed five main lithofacies:



**FIGURE 6.4.** Imagery of UT1 excavated sediment exposure. Excavation dimensions: length ~28 m; depth ~2 m. A. Hillshaded DEM indicating location of sediment exposure and GPR profiles along UT1 ridge at site 1 (DEM Source: ®National Land Survey of Finland, LiDAR digital elevation model, 2/2023). B. Photograph viewed from proximal to distal. C. Photograph viewed from distal to proximal. D. Photograph viewed from distal to proximal.

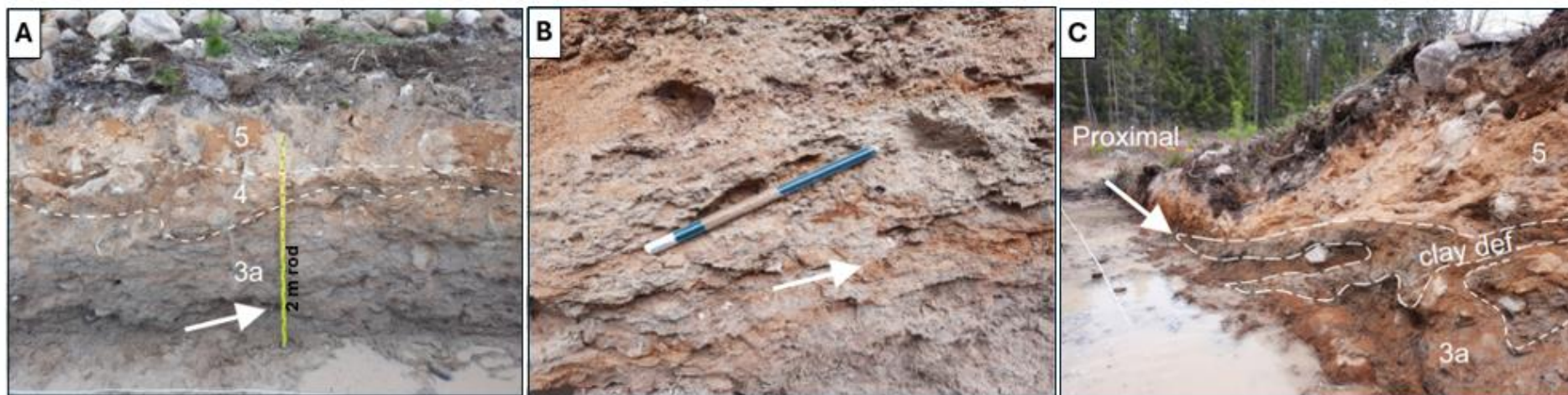


**FIGURE 6.5.** Exposure sketch of UT1 with the original subsurface (bottom) and interpreted (middle) GPR data. GPR data were acquired along the excavation bottom to allow subsurface investigations. Locations of sediment logs are shown (e.g. UT1\_2023\_log1, UT1\_2023\_log2 and UT1\_2023\_log3) which are presented in FIGURE 6.6. Locations of clast macrofabric measurements are indicated, with data presented in rose diagrams and stereonets. Stereonets are plotted on the lower hemisphere of a Schmidt diagram. Lithofacies units are labelled accordingly presented in sediment logs shown in FIGURE 6.6.



**FIGURE 6.6.** Sediment logs presented from UT1 showing unit thickness, composition and internal structures. Lithofacies are interpreted using standardised coding (Evans & Benn 2004). Rose diagrams and stereonet plots supplement identified units where applicable. Lithofacies codes: Dmm = matrix-supported, massive diamicton; Dms = matrix-supported massive diamicton with shearing structures; Dml = matrix-supported, laminated diamicton; Gm = massive gravel, Gs = gravel with shearing structures; Sm = massive sand; Sld = horizontal and draped laminated sand with dropstones; Smd = massive sand with dropstones; Fld = fine laminated silt and clay often with minor fine sand and very small ripples and with dropstones; Fmd = massive silt and clay with dropstones.





**FIGURE 6.7.** A. Depositional units from the middle part of UT1 excavation. This shows the main ridge composition of the silty-to-sandy diamicton Unit 3a which is draped by the fine-grained and highly fissile/sheared Unit 4. Unit 5 forms the mantle of the ridge composed of bouldery diamicton. B. Strongly sheared and fissile structures of Unit 4. C. View towards the proximal section of the UT1 De Geer ridge. Note the deformed clay layers between Units 3a and 5. White arrows indicate ice flow direction.

Unit 1 sits within the distal regions, at the base of the ridge, likely overlying till-covered bedrock, as identified by GPR. Interpreted steep thrust planes dip up-ice, towards the proximal side of the ridge. Hyperbolic diffractions and parallel to sub-parallel reflectors suggest stratified deposits interspersed with boulders (TABLE 6.1 RF1, FIGURE 6.6 Unit 1).

Unit 2 is located on the distal side of the exposure (FIGURE 6.5), however, based on our radar facies interpretation it stretches across to the proximal side of the ridge. This unit was only partially exposed, with the majority only observable in the radar profile. We interpret the unit to range from horizontal and deformed laminated sands, to massive gravel and medium to coarse-grained sands, interspersed with silt, fine-grained sands and granule gravel lens. The radar profile shows steep dipping reflectors which may represent thrust-planes. This unit is truncated and deformed with a diffuse upper contact boundary to Unit 3.

Unit 3 comprises most of the ridge morphometry (FIGURES 6.5, 6.6) and is divided into two subunits: Unit 3a, located in the proximal part of the ridge and Unit 3b, located within the distal part. Unit 3a can be defined as poorly sorted massive to matrix-supported diamicton containing weak laminations. The supporting matrix is composed mainly of silt and medium to fine-grained sands. Clast morphology is variable, with clasts ranging from subangular to subrounded. Medium-angle ( $330/20^{\circ}$ ) thrust plane structures are present and dipping in alignment with slope direction (i.e. up-ice). Fissility is well-developed particularly in the upper part of the unit. Unit 3b is generally similar to proximal unit 3a, however contrasts with downslope dipping, low-angle shear structures. The unit shows weak fissility, however, this improves over large clasts. The unit is interspersed with patches of sand and contains elongated rafts of compact sediment.


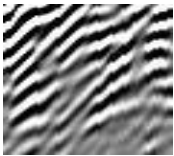


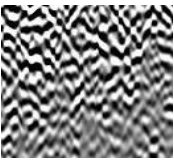
Unit 4 drapes the entire ridge with a sharp lower contact boundary to the underlying Unit 3. Its composition ranges from massive to laminated silts and clays, to a sandy fine-grained diamicton. The unit shows strong shearing aligned to the direction of ice flow (FIGURE 6.7B). The proximal side of the unit is composed of laminated to massive deformed silty clay, separated by a wedge of coarse sand and gravel (FIGURE 6.7B). This then transitions to sandy, fine-grained diamicton characterised by laminae (lenses of fine to medium sand) interspersed with pebbles. The orientation of pebble clasts follows laminae structures which conformably overlie gravel clasts. Gravel clasts are mainly

subrounded. The upper contact boundary is mainly diffuse, although sharp/erosional in some places.

Unit 5 is the uppermost unit, mantling the ridge. The unit is composed of massive to matrix supported sandy diamicton, clast-rich, with boulders, and containing crude clast layers (one-clast thick). The unit thickens downslope on the proximal side. The lower proximal slope comprises massive medium to very coarse sand, interspersed with granule lens and pebbles. In the upper parts, this passes into a loose massive to matrix-supported sandy gravel and medium to coarse-grained sand. Clasts are mainly rounded to sub-rounded. GPR data show similar structures across all acquired profiles from this ridge. In particular, interpreted sheared structures within RF3a and RF4 are distinctive features in the upper parts of the radar profiles as indicated by long and continuous reflectors, representing lithofacies Units 3a and 4.



**TABLE 6.1.** Summary of interpreted radar facies based on correlations with UT1 and UT2 lithofacies as presented in Appendices Figures 2 & 8.

Radar facies no.	RF example	Reflector motif	Correlated lithofacies	Lithological Description
4		Long and continuous with high reflectivity. Parallel to sub-parallel and slightly wavy arrangement.	4	UT1: Fld, Fmd, Sld, Dms UT2: Sld, Dms
3a		Medium to long, with medium continuity. Medium to weak reflector strength with parallel to sub-parallel arrangement.	3a	Dmm, Dml
3b		Short to medium in length with medium continuity to discontinuous. High to medium reflectivity. Wavy and sometimes overlapping.	3b	UT1: Dmm, Dml, Dcs UT2: Dcs, Gcs
2		Medium to long, with medium continuity, although sometimes discontinuous. Strong reflectivity with parallel to sub-parallel arrangement.	2	UT1: Sld, Smd, Gs UT2: Sld, Smd, (g)Smd, Gs
1		Very short, very discontinuous with high to medium reflectivity. Wavy, sometimes overlapping with hyperbolic diffractions. Interpretation of coarse diamicton with boulders.	1	Unknown. Not exposed within sediment excavation; partly exposed in UT2. Hyperbolic diffractions may suggest coarse, poorly sorted, bouldery diamicton, or fractured bedrock.

Unit 1 is interpreted as a buried bouldery sediment ridge with proximal thrust planes, overlying till-covered bedrock. This unit forms the core of the De Geer ridge. Similar ridge-like architecture can be seen in some of the GPR profiles from the Uimarannantie site (Appendices Figures 3, 4, 5).

Unit 2 is interpreted as glaciofluvial material, deposited either at the ice margin or behind the ice margin via shallow distributed canals as suggested by composition, degree of sorting and presence of laminations (Bennett *et al.* 2000; Bennett & Glasser 2009). The presence of steep thrusting structures at the root of the ridge suggest deformation by ice movement either syn-depositionally and/or during the later stages of ridge bulldozing (e.g. formation of Unit 3a).

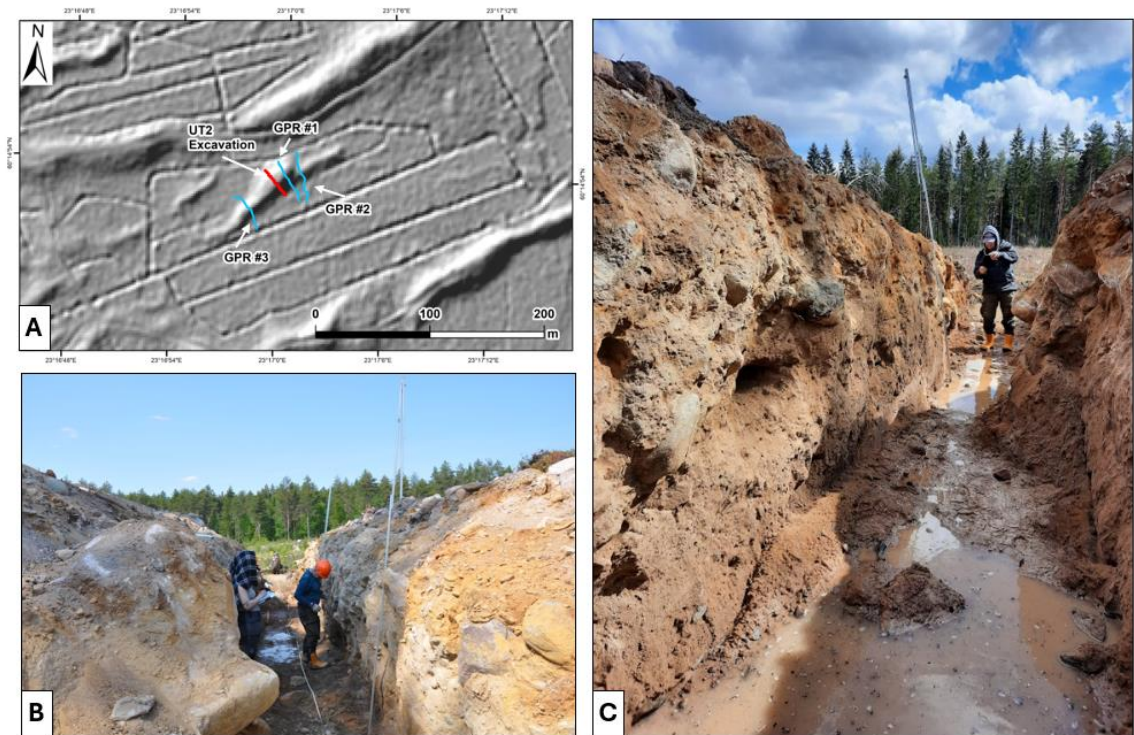
Units 3a/b are interpreted as the main body of the ridge whereby coarser subglacial material is deposited via bulldozing at the grounding line. An initial subglacial origin of the material is supported by clast form (e.g. subangular to subrounded) (Benn & Ballantyne 1994). The pushing/bulldozing of this material is evidenced by the presence of compressional up-ice dipping thrust planes and compact fissile textures located within the proximal regions of the unit (e.g. Unit 3a) (Evans *et al.* 2006).

Unit 4 is characterised by strong shearing structures and a distinct clast orientation to ice flow direction indicating overriding of ice. The extent of overriding may vary, potentially overriding only as far as the ridge crestline as suggested by Lønne & Nemec (2011).

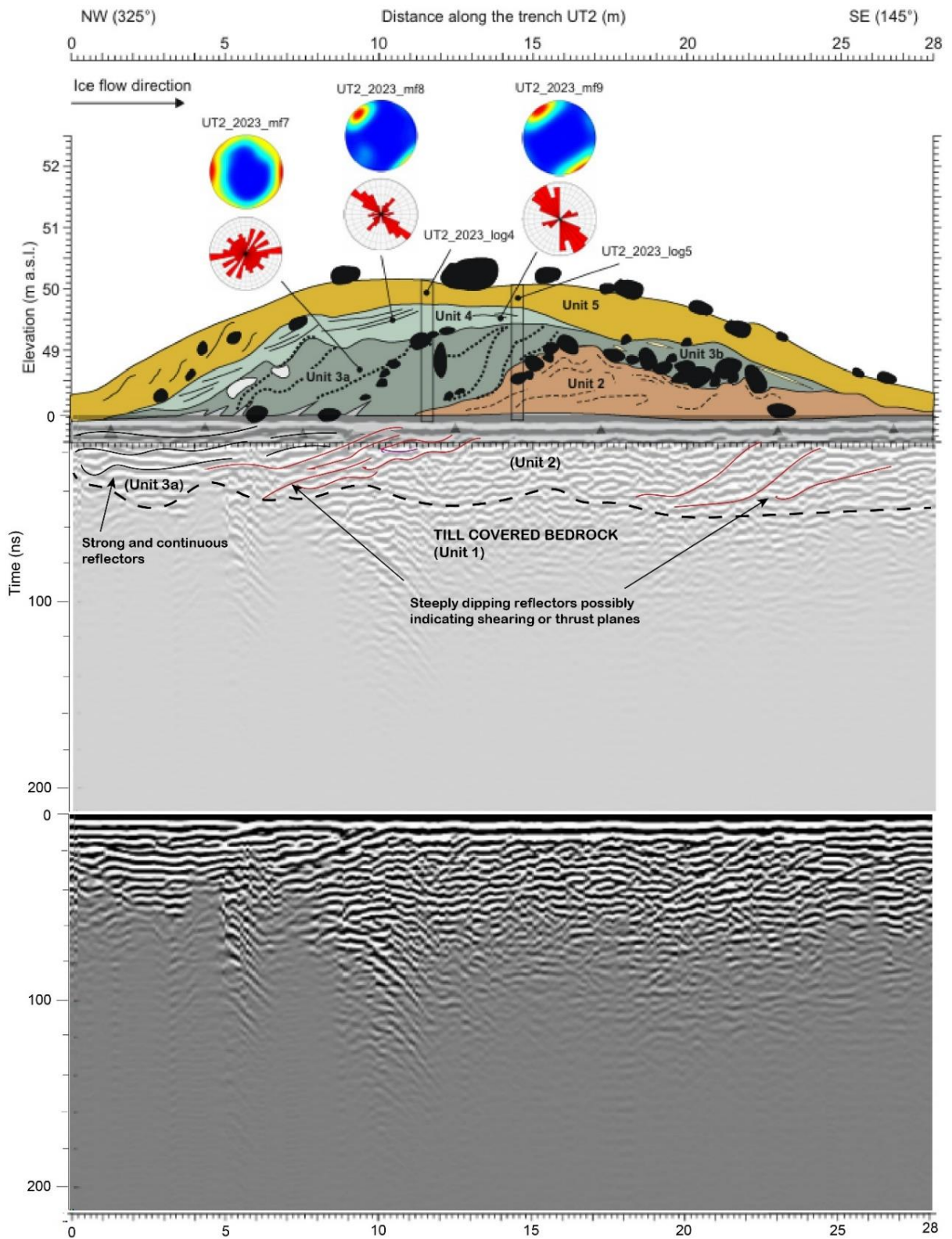
Unit 5 is interpreted as basal till that has melted out from the bottom of the ice during the final melting of the ice sheet. This has been subsequently reworked by shore sedimentation and proximally transitions to beach deposits. This material is also modified by frost heave, root zone and soil development but the exact process is not clear. This type of diamicton is also typical for murtoos and exists in areas not influenced by shoreline processes (Mäkinen *et al.* 2023).

#### **6.4.2 Site (1) UT2 (Uimarannantie, Haaro, Perniö (60.248°N; 23.283°E))**

One trench was excavated, and three GPR-lines were acquired at Site (2) UT2 (FIGURE 6.8). The DGM at UT2 is a lower amplitude, intermediate ridge, ~100 m long and ~25 m wide. The sediment exposure revealed five main lithofacies units (FIGURES 6.9, 6.10).

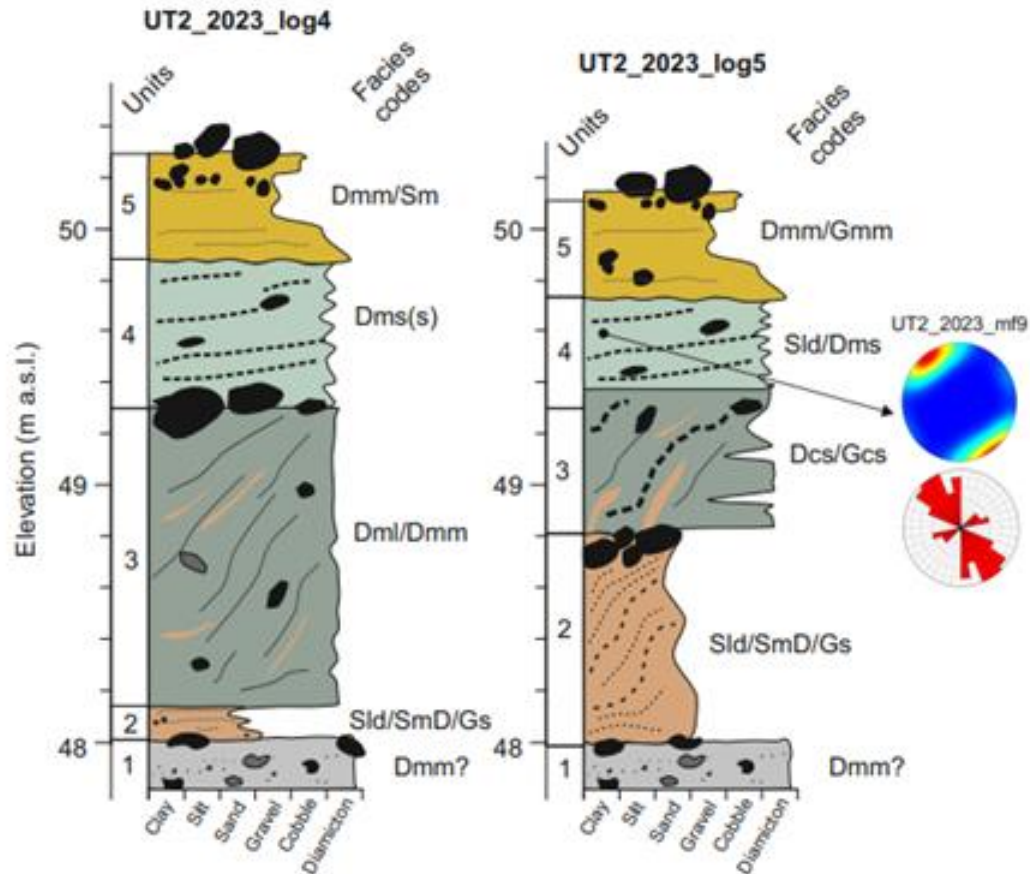


**FIGURE 6.8.** Photographs of UT2 excavated sediment exposure. Excavation dimensions: length ~28 m; depth ~2 m. A. Hillshaded DEM showing location of sediment exposure and GPR profiles along UT2 ridge at site 1 (DEM Source: ©National Land Survey of Finland, LiDAR digital elevation model, 2/2023). B. Photograph viewed from distal to proximal. C. Photograph viewed from proximal to distal.



**FIGURE 6.9.** Exposure sketch of UT2. Locations of sediment logs are shown (e.g. UT2\_2023\_log4 and UT2\_2023\_log5); logs are presented in Fig. 10. Clast macrofabric measurement locations are indicated with data presented in both rose diagrams and

stereonet (clast macrofabric sample sizes = 50). Stereonets are plotted on the lower hemisphere of a Schmidt diagram. Lithofacies units are labelled accordingly and described in the sediment logs as presented in FIGURE 6.10.



**FIGURE 6.10.** Sediment logs presented from UT2 showing unit thickness, composition and structures. Lithofacies are interpreted using standardised coding (Evans & Benn 2004). Rose diagrams and stereonet accompany identified units where applicable. Lithofacies codes: Dmm = matrix-supported massive diamicton; Dms(s) = matrix-supported massive diamicton with shearing structures; Dml = matrix-supported laminated diamicton; Dcs = clast-supported stratified diamicton; Gm = massive gravel; Gs = gravel with shearing structures; Gcs = clast-supported gravels with shearing; Sm = massive sand; Sld = horizontal and draped laminated sand with dropstones; Smd = massive sands with dropstones.





**FIGURE 6.11.** A. Depositional units from the middle section of UT2 excavation. Note the deformed, sandy sorted sediments of Unit 2 truncated by Unit 3a that forms the main part of the proximal side of the ridge. B. Downslope dipping bedding structures in distal parts of Unit 3b. C. Strongly sheared and fissile structures of Unit 4, similar to UT1, but present only in proximal parts of UT2. White arrows indicate ice flow direction.

Unit 1 is located at the base of the ridge and comprises matrix-supported massive diamicton with large boulders (NB: only the upper surface of the unit was exposed). This unit is likely overlying bedrock.

Unit 2 is situated on top of Unit 1 in the distal part of the ridge. This unit comprises stratified massive gravel and medium to coarse-grained sand (clast form subangular to subrounded), mantled by boulder clast horizons. Partly preserved patches of silty, fine-grained sand were observed in the lowest part of the unit. The unit is thicker and more prominent compared to a similar unit at site (1) UT1.

Unit 3 is situated across the entire ridge and truncates Unit 2 with an erosional to diffuse and deformed contact boundary (FIGURE 6.11A). This unit is sub-classified into Units 3a and 3b, whereby Unit 3a is located toward the proximal regions of the ridge, and Unit 3b is located toward the distal side. Unit 3a is composed of massive / matrix-supported and laminated diamicton. The matrix is poorly sorted silt and fine to coarse-grained sand. Clasts are subangular to subrounded. This unit contains steeply dipping thrust planes (some nearly vertical) (FIGURE 6.9) and sediment rafts/blocks. The lower part contains pebbly sand beds (~5 cm thick). This unit is grey in colour and showed weak fissility in places. Unit 3b comprises clast-supported, stratified diamicton and gravel. This unit also contains large boulders/a boulder horizon, and patches of sand with downslope dipping crude bedding (FIGURE 6.11B). In contrast to the proximally located unit 3a, this unit has a higher sand/gravel content, a higher degree of sorting, and is light grey to yellow in colour.

Unit 4 is situated in the proximal to central regions of the ridge and overlays Units 3a/b with a diffuse and deformed contact boundary. Material comprises horizontal/draped laminated sands and diamicton. Significant shearing structures are present, similar to those observed in Unit 4 UT1; however, these are only present in the proximal part of the ridge (FIGURE 6.9).

Unit 5 mantles the entire ridge, overlying Units 4 and 3b with sharp, erosional contact boundaries. This unit shows similarities to Unit 5 in UT1, comprising clast-supported massive gravel and matrix-supported massive diamicton, with shearing structures.

Additional radargrams acquired at UT2 highlight some internal variations across the ridge. GPR Profiles #1 and #3 (Appendices Figures 9 & 11, respectively) show what we interpret to be thrust planes within the proximal part of the ridge. In contrast, profile #2 (Appendices Figure 10) shows less evidence of thrusting, although some interpreted stratification can be seen.

We interpret Unit 1 to be subglacial till overlying bedrock.

Unit 2 is interpreted as glaciofluvial material, originally deposited either at or behind the grounding line and/or in crevasses behind the grounding line via distributed or channelised subglacial flow. The mantling boulder clast horizons may represent a sediment horizon deposited during downwasting of surrounding ice or could be related to erosional lag affected by deformation processes. Also, this unit is subsequently deformed by proximal (and/or submarginal) thrusting likely caused by stress exerted by moving ice. This is supported by the presence of thrust planes and steeply dipping clast orientations in the proximal part of the ridge, combined with sediment rafts.

Unit 3 is interpreted as the main body of the ridge and is subdivided into Units 3a (proximal) and 3b (distal). The high silt content and presence of laminations in the proximal side (Unit 3a) likely reflect the settling out of suspended fine-grained material at the grounding line during a short quiescent phase, which is then later deformed during the onset of ice activity. We interpret that the coarser distal side sediments (Unit 3b) were deposited from beneath the ice at the grounding line into the basin with currents (Golledge & Phillips 2008; Bennett & Glasser 2009; Lønne & Nemec 2011).

Unit 4 is interpreted as ice-marginal deposits subsequently deformed by ice advance, a similar origin to that of UT1, as evidenced by the highly variable matrix composition and significant shearing structures.

Unit 5 is interpreted as basal till reworked by shore processes and proximally replaced by beach deposits, similar to that of UT1. This unit also shows modification by frost heave, root zone and soil development.

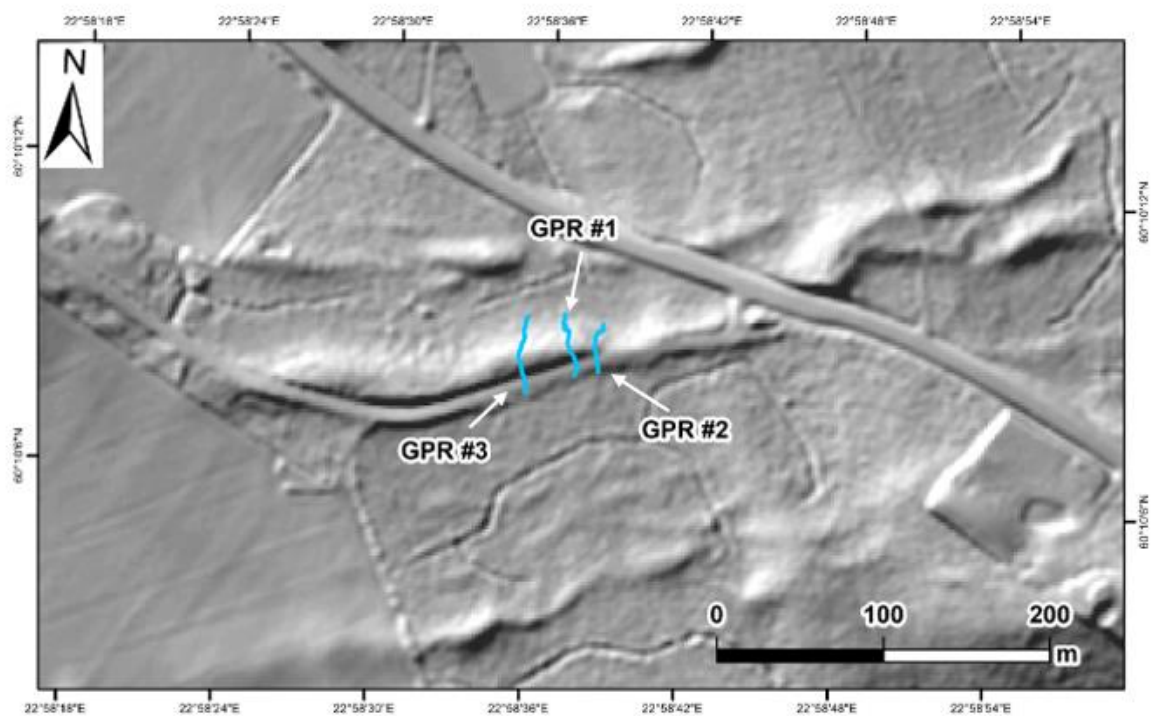
The internal variations observed along the ridge (Appendices Figures 9, 10, 11) appear to coincide with ridge amplitude as shown in the hillshaded DEM (FIGURE 6.8A). GPR



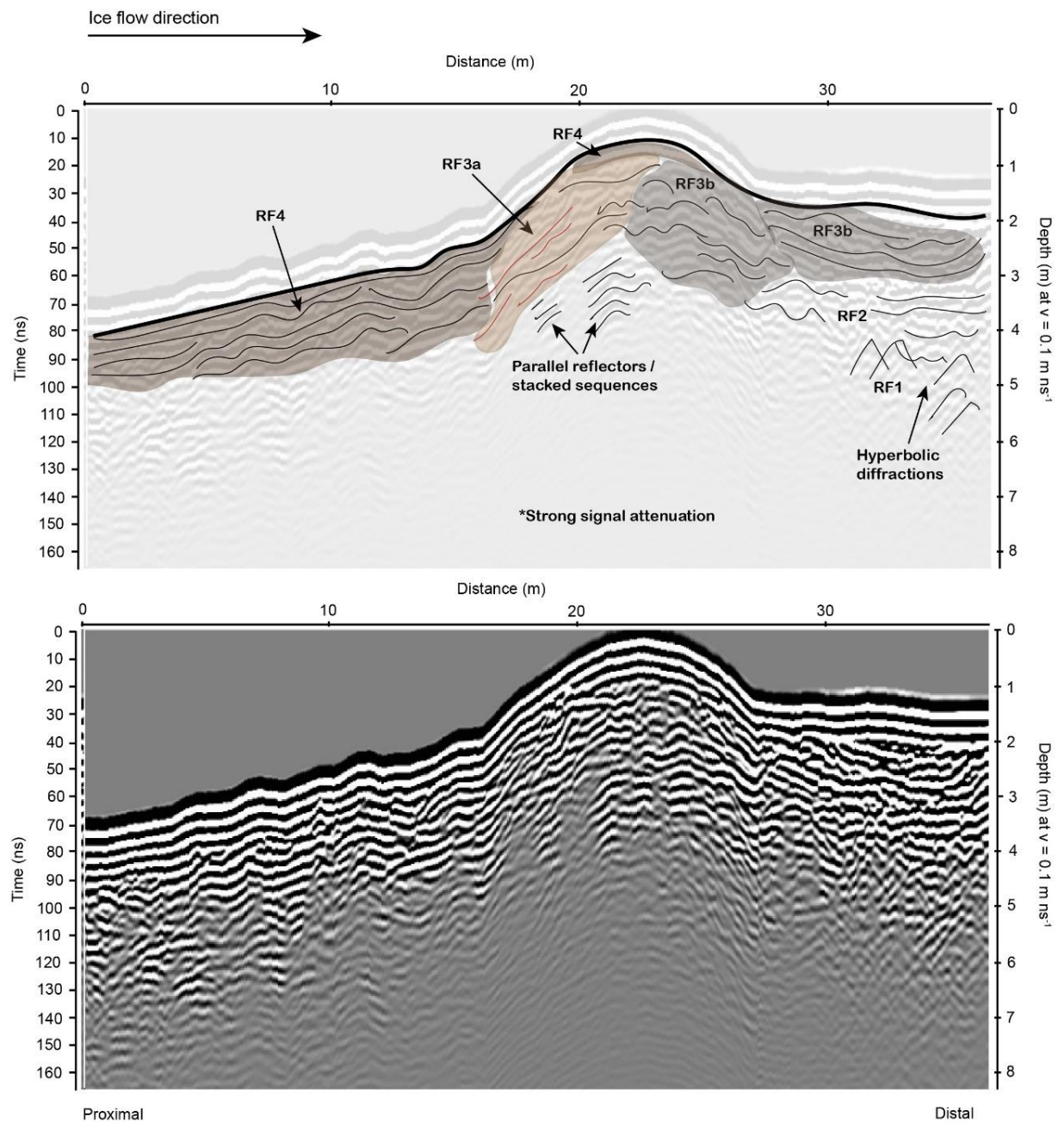
profiles #1 and #3 (Appendices Figures 9 and 11, respectively) are situated within larger sections of the ridge, where interpreted thrust/shearing planes are observed, whereas profile #2 (Appendices Figure 10) is situated along a smaller section which shows comparatively less evidence of thrusting/shearing. It may be that the ridge comprises two separate formations, whereby the larger section of the ridge overrides a previously formed smaller ridge. This may explain the origin of the lower Units 1 and 2.

#### 6.4.3 Site (2) Makarla, Ylönkylä (60.169°N; 22.977°E)

GPR results are presented for site 2 below. DGMs in this area can be characterised as large prominent ridges interspersed with smaller, intermediate ridges. The DGM observed is identified as a prominent ridge with metrics of ~300 m long, ~33 m wide and ~1.56 m high. Along ridge locations for acquired GPR profiles are presented in FIGURE 6.12. GPR data is presented in FIGURE 6.13 (additional radargrams are available in Appendices Figures 14 & 15).



**FIGURE 6.12.** Hillshaded DEM showing position of GPR profiles along surveyed ridge at site 2 (DEM Source: ©National Land Survey of Finland, LiDAR digital elevation model, 2/2023).



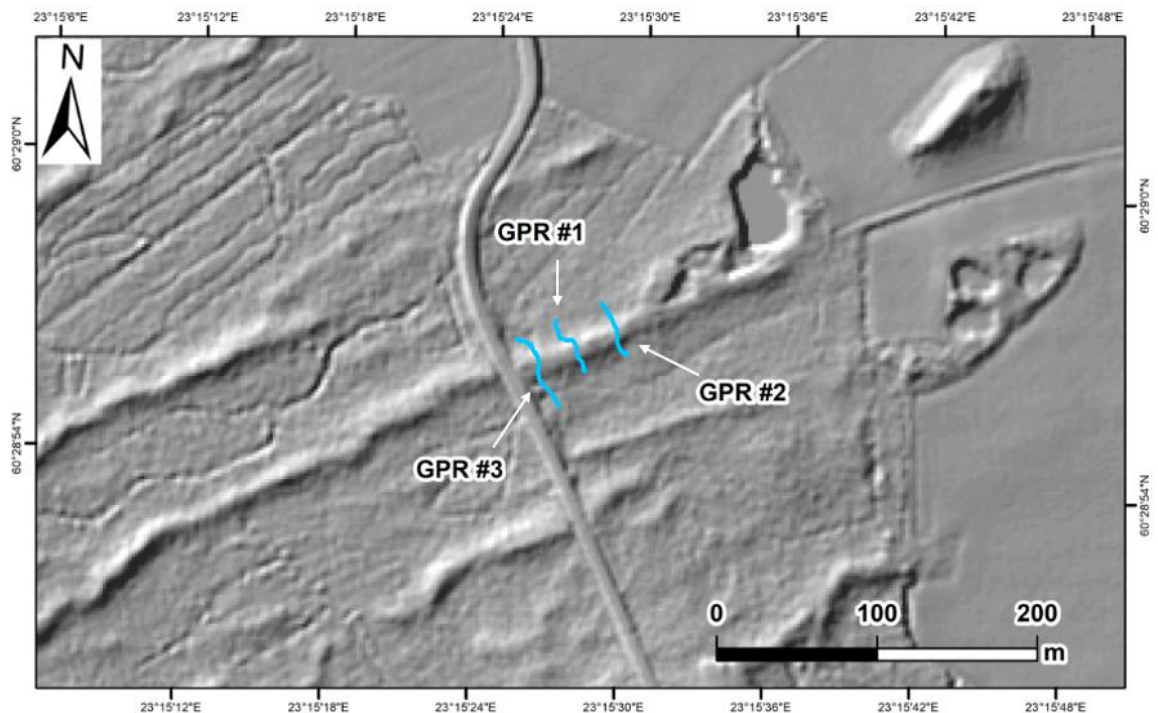
**FIGURE 6.13.** Radargram #1 at Makarla, Ylönkylä (GPR profiles #2 and #3 are presented in Appendices Figures 14 & 15). Identified radar facies and connected lithofacies are detailed in TABLE 1.

Proximal regions of the ridge are strongly dominated by RF4 and RF3a, providing evidence of what we interpret to be compaction/laminae and thrusting/shearing that was described in both UT1 and UT2 excavations. Parallel alignment of reflectors may also signify sequences of stacked sediments. RF3b is located within the distal regions and RF2 and 1 are located at the distal foot of the ridge, containing hyperbolic diffractions which

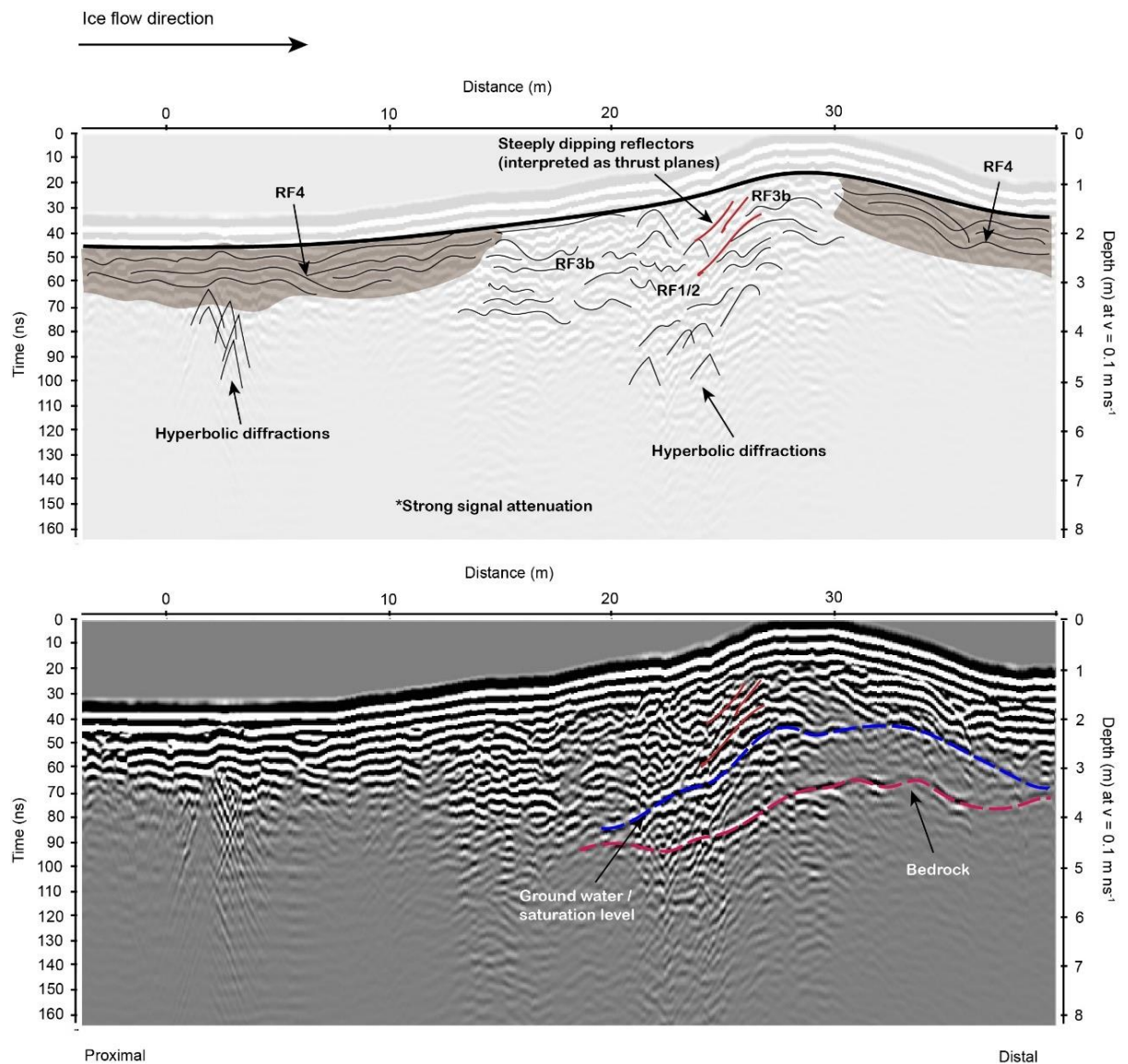
is interpreted as the presence of boulders. The coarseness of these distal units may signify gravity driven flow deposits and/or current reworkings whereby finer sediment is removed and coarser material is deposited (Bennett & Glasser, 2009). This ridge shows characteristic structures of a grounding line/push depositional process (Bennett & Glasser, 2009; Lønne & Nemec, 2011).

#### 6.4.4 Site (3) Kurajoki, Porkka (60.482°N; 23.258°E)

GPR results are presented for site 3 below. DGMs in this area comprise regular, prominent ridges interspersed with irregular, intermediate ridges. The DGM observed is identified as a prominent ridge due to lateral continuity and regularity between ridges in the wider terrain; however, is the lowest amplitude of all observed ridges with metrics of ~745 m long, 1.06 m high and ~24 m wide. Along ridge locations for acquired GPR profiles are presented in FIGURE 6.14. GPR data is presented in FIGURE 6.15 (additional radargrams are available in Appendices Figures 16 & 17).



**FIGURE 6.14.** Hillshaded DEM showing position of GPR profiles along surveyed ridge at site 3 (DEM Source: ©National Land Survey of Finland, LiDAR digital elevation model, 2/2023).



**FIGURE 6.15.** Radargram #1 acquired at Kurajoki, Porkka (GPR profiles #2 and #3 are presented in Appendices Figures 16 & 17). Identified radar facies and connected lithofacies are detailed in TABLE 1.

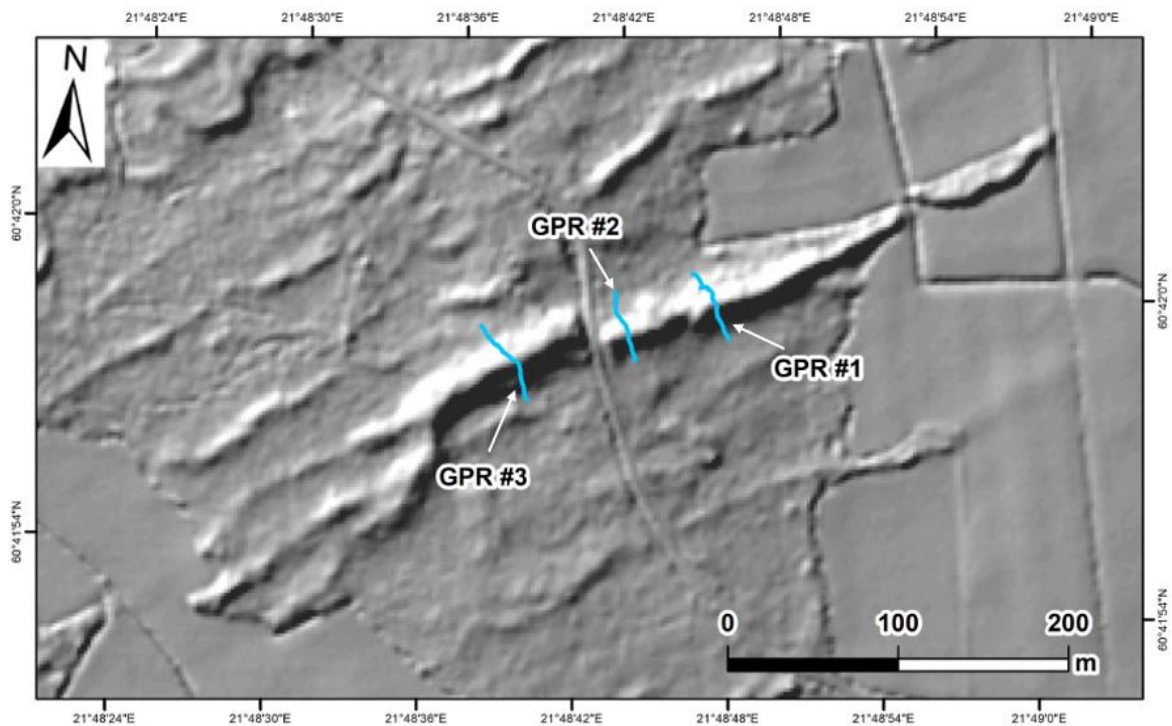
The radar facies architecture is different when compared to those previously presented. The ridge is generally overlain by a veneer of long and continuous reflectors (RF4) which may be interpreted as compaction and/or laminations and shearing across the upper part similar to Unit 4 in the UT1 excavation, however, there appears to be little evidence of thrusting structures within the proximal regions. Instead, there appears to be what could be interpreted as the remains of a pre-existing ridge or hummock of coarse, poorly sorted, boulder-filled material within the proximal side, against the interpreted bedrock, as suggested by short, wavy, discontinuous reflectors and hyperbolic diffractions



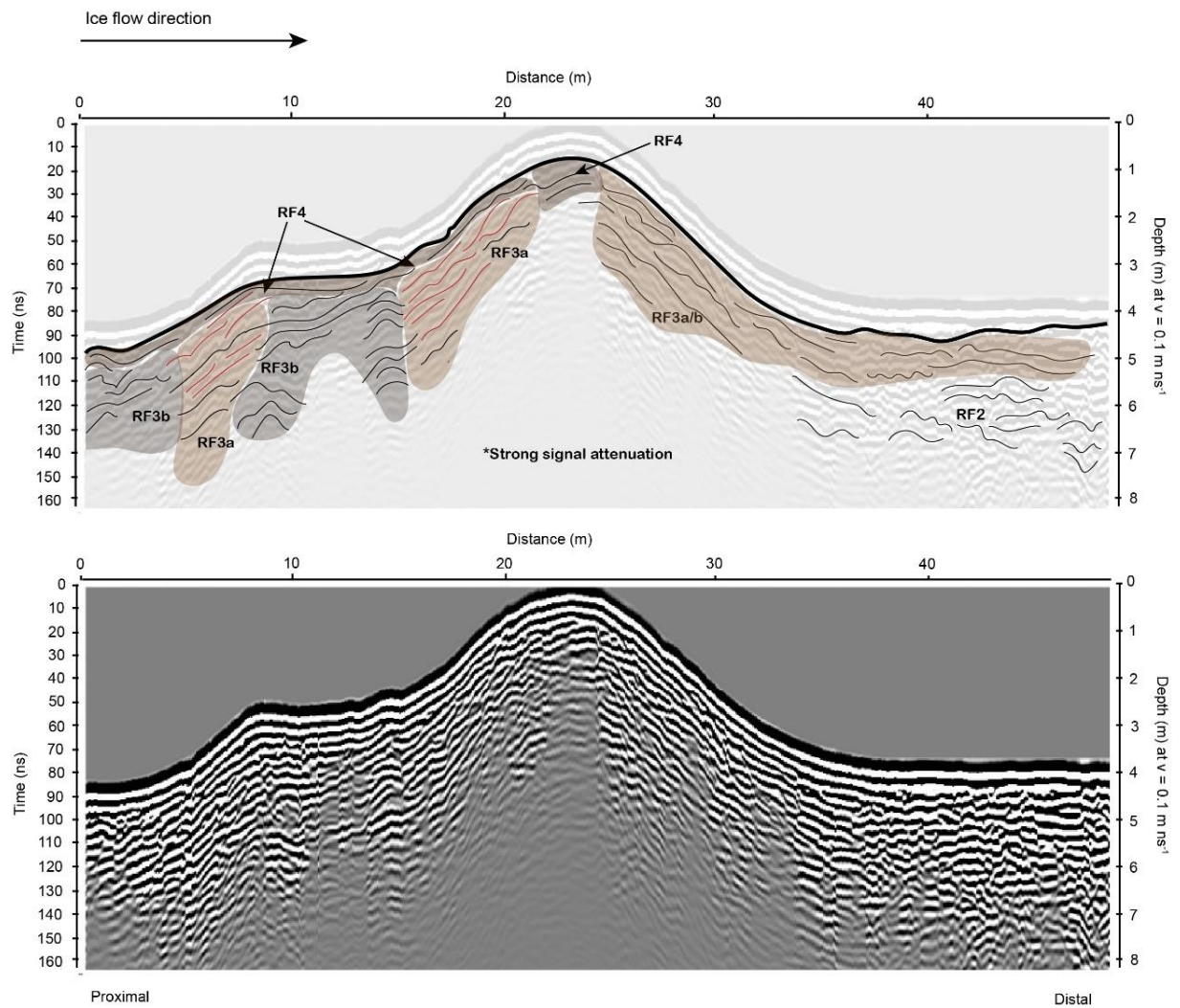
(RF1 and 2), sandwiched between a looser diamicton (RF3b). The upper distal part shows strong evidence of compaction/stratification by long and continuous reflectors (RF4) which may be interpreted as shearing from the deposits being completely overridden by ice. Silt and clay are present throughout most of the ridge, as indicated by strong signal attenuation. When examining the ridge structure, it seems to follow the orientation of the bedrock. Sediments distal to the bedrock knob are different to the proximal ones indicating a strong influence of bedrock over grounding line processes. As signal attenuation is particularly strong in this profile, it is difficult to form an accurate architectural assessment, however, we can observe that the bedrock has affected DGM formation in this area.

#### 6.4.5 Site (4) Suorsala, Mynämäki (60.700°N; 21.813°E)

GPR results are presented for site 4 below. DGMs in this area comprise prominent ridges interspersed with intermediate ridges. The DGM observed is identified as a prominent ridge with metrics of ~454 m long, ~2.04 m high and ~25 m wide. Along ridge locations for acquired GPR profiles are presented in FIGURE 6.16. GPR data is presented in FIGURE 6.17 (additional radargrams are available in Appendices Figures 18 & 19).



**FIGURE 6.16.** Hillshaded DEM showing position of GPR profiles along surveyed ridge at site 4 (DEM Source: ©National Land Survey of Finland, LiDAR digital elevation model, 2/2023).



**FIGURE 6.17.** Radargram #1 from Suorsala, Mynämäki (GPR profiles #2 and #3 are presented in Appendices Figures 18 & 19). Identified radar facies and connected lithofacies are detailed in TABLE 1.

The proximal regions of the ridge comprise a combination of RF3a and RF3b as detected in UT1 excavation, with some longer, continuous reflectors in the upper parts which we interpret as compaction/shearing. The alternations between RF3a, representing thrusting, and 3b, representing looser diamicton, infers a more gradual/staggered ice marginal push process. The distal side of the ridge comprises parallel to sub-parallel reflectors dipping in the direction of ice flow. Similar to all other ridges, signal attenuation

within lower regions is observed indicating high water, silt and/or clay content. This ridge is interpreted to be a typical ice marginal push formation, comparable to UT1; however, formed in two stages before the formation of Unit 4.

## **6.5 Discussion**

### **6.5.1 DGM internal architecture**

The findings show that both larger, prominent and smaller, intermediate ridges comprise the same sediment facies and architectural structures; however, slight variations can be observed. The main insights can be confined to:

- Lower Units 1 and 2 are composed of either buried bouldery ridges with deformed sediments showing proximal thrust plane structures (Site (1) UT1, Unit 1) or basal till (Site (1) UT2, Unit 1) and glaciofluvial sand/gravel interpreted as waterlain deposition either at the ice margin during summer, or possibly via shallow distributed canals up ice of the margin (Unit 2). Generally, thrusting structures are located within the proximal- to mid-sections of the ridges (Unit 3a); however, these structures are also observed within the lower Units 1 and 2 of UT1 (FIGURE 6.5). These structures may be formed syn-depositionally, or post-depositionally during the formation of Unit 3a. If formed syn-depositionally, this may infer that material was deposited subglacially in crevasse cavities behind the grounding line via shallow distributed canals, which was then overridden by ice and later amalgamated at the grounding line as the ice margin retreated and aligned with the original deposits. The height and prominence of Unit 2 in the UT2 ridge compared to the UT1 ridge is the main architectural difference that we have observed between intermediate and prominent DGMs, in addition to the deformed and rafted clays in the proximal part of UT1 that were likely deposited during a quiescent period in winter (FIGURES 6.5, 6.7C). Furthermore, Unit 2/RF2 may not always be present (see Site (1), UT2, GPR #2 and #3, Appendices Figures 9 & 10), or may be very thin, possibly mixed with the overlying Unit 3 and therefore not easily identifiable within the GPR data. Without being able to observe in the exposure, it is difficult to make any accurate interpretations.

- Units 3a/b constitute most of the ridge and are interpreted as a grounding line push/bulldozing material. This is particularly notable from proximally located clay slabs pushed onto the ridge (FIGURES 6.5, 6.7C) and from transitions between compression structures in the proximal side and coarser material in the distal part (Lønne & Nemec, 2011). As such, irrespective of the origin of the lower Units 1 and 2 (e.g. basal cavity, subglacial meltwater, or grounding line deposits), Units 3a/b represent a true grounding line formation and therefore support the idea that DGM ridges may be used as ice marginal indicators.
- Unit 4 is indicative of overriding active ice, evidenced by strong shearing structures at the surface. We suggest that this unit in both UT1 and UT2 has a similar origin, whereby meltwater flow becomes limited, and deposition of fine-grained sediments takes place, while ice continues to retreat at the margin. Note the deformed winter clays associated with this unit in UT1 indicate ice flow reactivation in spring over the ridge. Differences in unit extent between UT1 and UT2 suggest variability in the extent of ice advance, e.g. overriding ice may extend only as far as the ridge crest as shown in UT2 and are dependent upon factors such as ice thickness and water depth (Lønne & Nemec, 2011). Good preservation of ridges suggests that ice is unlikely to advance significantly beyond the ridge crest.
- Unit 5 can be interpreted as basal till that has melted out from the bottom of the ice during the final melting of the ice sheet. This diamicton has then been washed by littoral processes and modified by frost heave and root zone (Mäkinen *et al.*, 2023).

When comparing internal architecture between the presently studied ridges, it appears that the prominence of thrusting and shearing structures positively correlates with ridge amplitude where the ridges with greater relief (e.g. prominent ridges) show more evidence of thrusting. Furthermore, lower-amplitude ridges (e.g. the observed ridge at site 3; FIGURE 6.15, Appendices Figures 16, 17) appear to comprise mostly coarser-grained material and present less evidence of stratification and shearing characteristics. These between-ridge variations may denote the seasonal stage at which the deposits are made, as well as the availability and type of material being pushed at the margin, and the



prominence of bedrock controls. For example, if deposits are formed during summer when meltwater discharge is high, the deposits may be coarser in texture and the size of the unit may be greater as observed in UT2. Moreover, if the ice margin is unstable in a state of calving/retreat deposits may be subject to less proximal compaction than would be expected from a more stable advancing ice margin.

When comparing our results to existing models, we must consider the influence of proglacial water depth and local to regional bedrock topography. Lønne & Nemec (2011) illustrate the variability of grounding line depositional systems relative to water depth. Ice terminating in shallow water (<175 m) tends to be relatively thin with a low erosional capacity and therefore subglacial influence is largely restricted to the proximal sides of marginal ridges; however, ice protrusion may form and partly, or fully, override deposits. In very shallow water (<50 m), ice advances over a low-relief seabed and any deposits would be easily overridden, therefore moraines may present a sheet-like geometry. These shallow-water ridges described by Lønne & Nemec (2011) are similar to our observations and correspond to the shallow proglacial water depths at the study area (Ojala *et al.*, 2013). Furthermore, correlations between DGM interdistances and water depth have been found whereby DGM interdistances are greater in greater water depths (Ojala, 2016). In relation to bedrock topography, the differences in architecture at the Porkka region (site 3) demonstrate how bedrock topography influences DGM formation.

Lønne & Nemec (2011) also highlight other factors for consideration, namely the configuration of how well the ice bottom is in contact with the underlying till surface (smooth vs undulating) and the preservation potential of shallow water deposits due to a limited erosional capacity. These factors can be seen in the DGM morphometry study outlined in chapter 5, whereby DGMs tend to be lower-relief and more laterally continuous when formed in shallow water, and higher-amplitude with greater lateral discontinuity as water depths increase.

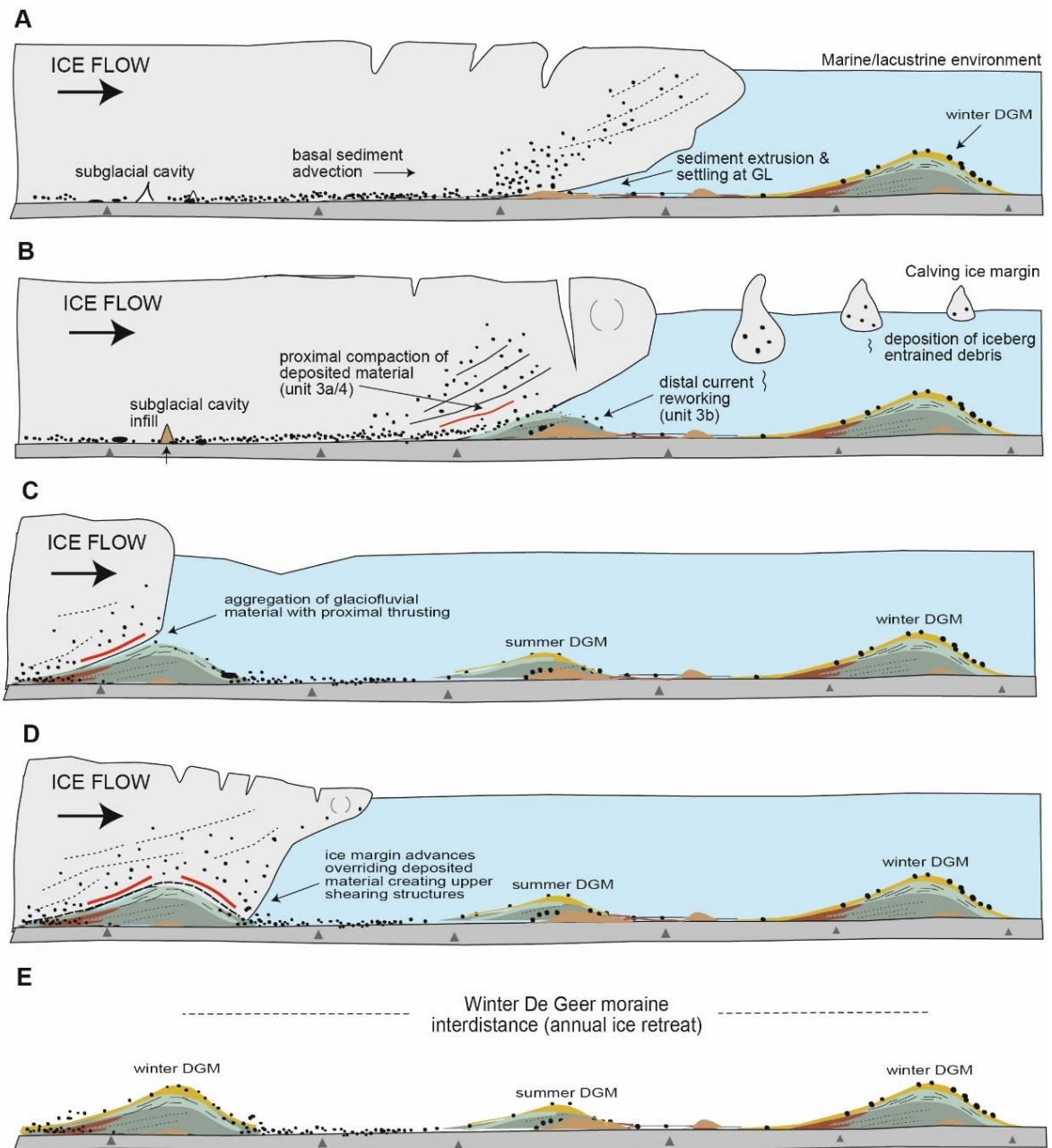
### **6.5.2 Proposed conceptual model**

The results reveal that DGMs situated across southwest Finland are grounding line formations that can vary in size and internal structure depending on the seasonal stage of formation, bedrock topography, sediment availability and water depth. The field

observations do not show evidence of crevasse infilling as a mechanism for DGM formation. Based on the findings and those reported from previous studies, an integrated conceptual model is presented whereby DGMs are formed in the same way but with slight variations depending on the seasonal stage of deposition. These variations can be subcategorised as (FIGURE 6.18):

- Summer calving retreat (FIGURE 6.18A, B). Saturated and deformable subglacial sediments are advected toward and deposited at the grounding line via subglacial meltwater and/or extrusion from beneath the margin during late summer/early autumn. Deposited sediments may be subject to proximal compaction from overriding ice and distal reworkings from proglacial water currents (Bennett & Glasser, 2009; Lønne & Nemec, 2011). The ice margin subsequently undergoes calving, the grounding line retreats, and the deposited sediments are preserved (Lindén & Möller, 2005); calving may lead to loss of buoyancy which may result in further deformation processes as the margin depresses. After calving, the ice margin may remain stationary or continue to advance, and if enough time allows new sediments will accrue at the margin, however, as the margin is in an unstable state of retreat, the amount of material deposited will likely be less than that during winter advances (Möller, 1962). This process would repeat throughout the summer and result in a series of irregularly spaced ridges, which we refer to as intermediate DGM ridges such as UT2 (Rivers *et al.*, 2023). As calving processes exert significant forcing over grounding line position resulting in an unstable ice margin (Haseloff & Sergienko, 2022), summer ridges would be smaller and more reflective of grounding line forcing dynamics such as water depth relative to ice thickness (Simkins *et al.*, 2018).
- Winter and spring push advance (FIGURE 6.18C, D). Saturated and deformable subglacial sediments are advected toward and deposited at the grounding line via subglacial meltwater during late summer/early autumn (e.g. the same processes occurring in summer calving retreat processes). During winter/early spring, however, the ice margin re-advances (Boulton, 1986; Ottesen & Dowdeswell, 2006), depositing additional material at the grounding line via bulldozing and deforming pre-existing material (this is represented by the larger Units 3a and 3b),

similar to the originally proposed formation by De Geer (1940). This results in a larger, more continuous ridge that is likely formed once per season; however, it should be considered that size and lateral continuity would inevitably be determined by other factors such as ice-moraine contact configuration, water depth and sediment availability (Lønne & Nemec, 2011). These ridges, such as UT1, are considered as regular, prominent DGMs. Furthermore, as the ridge is formed via winter push processes, the position of the ridge would relate more closely to mass balance compared to the grounding line dynamics of summer calving ridges. As ice continues to retreat, a series of similarly formed winter and summer ridges are preserved on the landscape (FIGURE 6.18E).



**FIGURE 6.18.** Proposed conceptual model of inter-seasonal De Geer ridge forming processes. A) Late spring/early summer: fine-grained materials settle out at GL (Unit 2). Ice may depress into bed during temporary stabilisations resulting in coarser-grained sediment extrusion (Unit 3). B) Late summer/early autumn: increased subglacial meltwater transports coarser-grained material to grounding line. Possible proximal compaction may occur due to buoyant flexure of overriding ice (Units 3a/4). Calving processes occur creating a series of irregularly spaced ridges. C) Late autumn/early winter: ice margin retreated to winter position. Aggregation of glaciofluvial material at grounding line. Possible proximal compaction from buoyant flexure of overriding ice. Release of debris

*from overriding ice. D) Late winter/early spring: ice re-advance over deposited material. Proximal thrusting and significant shearing deform most notably upper proximal units of ridge (Units 4/5) however, deformation could occur throughout sediment package. Release of debris from overriding ice. E) “De Geer terrain” characterised by regular (winter) and irregular (summer) ridges. Interdistances between winter ridges indicate annual rate of retreat.*

The complexity in depositional processes between different DGMs gives rise to a potential ambiguity regarding the term “De Geer moraine”. Lundqvist (2000) highlights that the term “De Geer Moraine” is often extended to similar landforms (e.g. cross-valley moraines, washboard moraines), and even when the term “De Geer moraine” is used very strictly (e.g. only to those moraines originally described by Gerard De Geer), there can be more than one formation mechanism. In contrast, Bouvier *et al.*, (2015) suggests that DGMs are an example of equifinality. Ojala (2016) classified De Geer moraine fields into five maturity classes based on their spatial regularity and distinct ridge-type appearance. Given that the term De Geer moraine is thus neither strictly descriptive, nor genetic, it is proposed that these distinctive fields of ice marginal ridges could be called “De Geer terrain (DGT)”. This captures the equifinality of DGMs and the range of landforms described based on their appearance (fields of parallel ridges resembling a washboard), whereby different inter-seasonal ridge forming processes may occur within the same environment.

When viewing the integrated model (FIGURE 6.18), wider DGT configuration can be considered. As previously highlighted (FIGURE 6.2), DGT can be configured in one of three ways; i) only regular ridges, ii) regular ridges interspersed with irregular ridges, or iii) only irregular ridges. Based on this model, DGT configuration would elucidate which inter-seasonal ridge forming processes are most dominant relative to grounding line dynamics (Lønne & Nemec, 2011). For example, DGT comprising only lower amplitude irregular ridges may suggest that calving processes are most dominant and thus signify increased water depths (Simkins *et al.*, 2018). This is not to suggest that evidence of winter readvance deposits are absent, rather that summer calving is more prominent and therefore ridges of this origin are more plentiful. Equally, the reverse would be true of DGT characterised by more prominent regular ridges, suggesting that calving processes

are limited, or pre-existing summer ridges have been destroyed, and therefore assemblages are more indicative of regular winter readvance deposits. It should be acknowledged that this is a general rule for De Geer ridge formation, and additional local complexities such as bedrock topography may impose significant influences over formation processes.

### **6.5.3 Implications for ice marginal reconstructions**

As defined in the model (FIGURE 6.18), it is found that DGT assemblages may contain bi-seasonal signals which may in some instances be identified by the size and regularity of the ridges. This signifies that an annual signal is present, however, the annual regularity of ridges must be carefully identified when considering whether they can be used as annual ice marginal indicators. As highlighted in previous studies, the variability in DGT appearance and distribution support the notion that no single model is appropriate for the genesis of all De Geer ridges (Ojala, 2016). It would be reasonable to assume that the regularity of ridges in DGT provides some guidance to distinguish between inter-seasonal signals (e.g. regularly spaced ridges are likely to be more indicative of winter readvances), however, external influences must also be accounted for such as: calving intensity, bedrock topography, sediment availability, ice-moraine contact, water depth etc. Regardless of formation process, both winter push and summer calving ridges denote ice margin spatial positioning. However, for use as retreat rate indicators, the seasonal timing of deposition must be identified.

Previous studies have attempted to address this problem, finding positive correlations between regularly spaced push ridges and annual rates of retreat (De Geer, 1940; Bouvier *et al.*, 2015; Ojala, 2016; Sinclair, 2018). However, the slight variations between inter-seasonal formation processes can make this correlation difficult to establish (Hoppe, 1959; Möller, 1962; Zilliacus, 1981, 1989; Sollid, 1989; Lindén & Möller, 2005). This study provides an integrated conceptual model for the different seasonal types of De Geer ridge that can form in a grounding line/calving environment. Future work, as demonstrated in chapter 7, could use this model to begin to reconstruct detailed ice margin behaviour in Finland and further afield where DGT evidence is present.

## 6.6 Conclusions

DGMs may act as valuable ice marginal indicators; however, to date, their variable mode of formation has presented challenges for this utility. This study develops upon existing morphometry studies, using sedimentological and GPR methods, to refine the current understanding of how DGMs are formed. More specifically, this study compares the internal structures of regular and irregular DGMs, revealing that subtly different ridge forming processes can occur within the same environment.

The DGMs studied suggest an overall multi-phase structure, with lower units representing ice marginal extrusion and/or basal cavity infill deposits, truncated by a larger prominent push/bulldozed unit, which is subsequently deformed by overriding ice. Significant disparities between proximal and distal structures are notable, with proximal parts characterised by laminae, stratification and thrust planes, and distal parts characterised by looser diamicton and erosional effects caused by local topography, calving processes and current reworkings. Generally, the internal architecture of both prominent and intermediate ridges is the same; however, the main architectural differences observed are the extent of Unit 2 which is more extensive in the observed intermediate ridge, as well as the presence of proximally located deformed clays within prominent ridges likely deposited during quiescent periods in winter. No evidence indicative of crevasse infilling as a mechanism for DGM formation is found.

This study presents an integrated conceptual model whereby all De Geer ridges are formed in the same way with slightly different inter-seasonal formation processes occurring within the same sub-aqueous ice marginal environment. These slight variations can be subcategorised as: i) sediment deposition at an unstable margin during summer calving, and ii) sediment bulldozing/pushing at a stabilised margin during a winter readvance. In addition, a new landform classification is proposed whereby “De Geer Terrain” may be used as an alternative to “De Geer moraines” to describe series of parallel ridges arranged in a typical washboard-like configuration. This alternative classification is considered to be helpful and clearer when describing fields of similar ridges that are formed by different inter-seasonal processes.



Previous studies conducted in Sweden have found that prominent, regularly spaced ridges appear to coincide with independently determined margin-retreat rates. This is suggested to be an important direction for future research in Finland and is explored in chapter 7.

## **Chapter 7: An annual ice margin reconstruction and investigation of grounding line mechanics in the southern Baltic Sea Ice Lobe area of the Fennoscandian Ice Sheet using De Geer moraines as geochronometric indicators**

Rivers, G.E., Storrar, R.D., Ojala, A.E.K. & Jones, A.H. (in prep). An annual ice margin reconstruction and investigation of grounding line mechanics in the southern Baltic Sea Ice Lobe area of the Fennoscandian Ice Sheet using De Geer moraines as geochronometric indicators.

This chapter presents a refined, annual ice margin reconstruction of the southern Baltic Sea Ice Lobe area of the FIS. In addition, this chapter presents analyses of grounding line variables to better understand ice margin retreat dynamics in the area. This work contributes to research objectives (1, 2 & 3) and is the final production of the overall aims of this research.

### **Abstract**

Observations and projections of ice mass loss are an important area of research due to the rapidly warming climate. Reconstructions of past continental ice sheets, such as the FIS, provide a valuable means by which to elucidate ice sheet behaviour and improve understanding of how ice sheets respond to long periods of climatic change. To date, ice margin reconstructions delineate retreat rates at millennial to centennial resolutions. DGMs have the potential to increase these resolutions to annual timescales if their temporal properties can be accurately constrained. Using the established local clay-varved chronology in the Baltic Sea Ice Lobe region of the FIS, the chronology of DGMs in the area is constrained to provide an ice margin reconstruction at ~annual resolution between 11 615 to 10 901 calendar years BP. Temperature, proglacial water depth and bed slope are evaluated to assess the impact on grounding line retreat rate across the study area. The results reveal highly dynamic fluctuations in patterns of annual retreat, compared to a uniform retreat pattern presented in previous work at 100-year resolution.

Investigations of grounding line forcing mechanisms show that no single variable dominates control of ice margin retreat; instead, complex and interconnected relationships between temperature, water depth and topography can be observed, whereby the dominance of each forcing mechanism varies over space and time. The results show that rates of ice margin retreat increase with greater temperatures and water depths, and when the grounding line migrates across smooth, shallow-gradient bed topography. In addition to increased rates of retreat, these variables also lead to significant grounding line instability as shown by increased fluctuations in annual retreat, which are likely driven by buoyancy-driven hinge calving processes. These processes are the result of surface thinning due to greater temperatures which allow the ice margin to reach flotation thickness, relative to proglacial water depth, creating an upward bending moment that results in calving at the ice margin. The retreat rates observed in this study range between  $\sim 500 - 2\,000 \text{ m/yr}^{-1}$ . The higher-end retreat rates are similar to those observed in contemporary settings at Peterman Glacier, Greenland ( $1\,250 \text{ m/yr}^{-1}$ ) and Thwaites Glacier, West Antarctica ( $2\,100 \text{ m/yr}^{-1}$ ), whereby increased retreat rates coincide with grounding line migration across adverse bed slope topography, or past topographic pinning points. This study demonstrates the utility of DGMs as ice margin geochronometric indicators and highlights the valuable information that can be derived relative to grounding line processes. The refined reconstruction presented in this study contributes to a deeper understanding of deglaciation processes at annual to centennial timescales which may be extrapolated to assist with projecting changes in contemporary ice sheets at societally relevant timescales.

## 7.1 Introduction

Observations and projections of ice mass loss are an important area of research due to the rapidly warming climate and uncertainties over rates of future sea level rise (IPCC, 2023). At the margins of ice sheets, where ice extends into the ocean, ice mass loss is regulated by external forcings from the ocean and atmosphere (Bamber *et al.*, 2007; Dawson *et al.*, 2022; Fyke *et al.*, 2018). These areas are notoriously difficult to observe in contemporary settings due to inaccessibility and the relatively limited time window of available satellite observations (e.g.  $\sim 50$  years). For example, Park *et al.* (2013) observed retreats rates of  $\sim 0.95 \text{ km yr}^{-1}$  at Pine Island Glacier, West Antarctica; however,

observations were limited between 1992 and 2011. Similarly, Milillio *et al.* (2019) observed retreat rates of  $0.8 \text{ km yr}^{-1}$  at Thwaites Glacier, West Antarctica between 1992 to 2017. Brancato *et al.* (2020) observed a 5.4 km retreat of Denman Glacier, East Antarctica between 1996 and 2018. Antropova *et al.* (2024) measured retreat rates of  $\sim 55 \text{ m yr}^{-1}$  at Milne Glacier, Ellesmere Island, Canada between 1966 to 2023. The temporal limitations of these studies highlight a gap in understanding at decadal to centennial timescales. Reconstructions of past continental ice sheets, such as the FIS, provide a means to overcome these issues, offering insights that can improve our knowledge of contemporary ice sheet behaviour in response to longer periods of climatic change (Clark *et al.*, 2022; Dalton *et al.*, 2023; Gowan *et al.*, 2021; Hughes *et al.*, 2016; Ó Cofaigh *et al.*, 2014; Stroeve *et al.*, 2016).

Within ice marginal zones, the ‘grounding line’ refers to a sensitive boundary where grounded and floating ice intersect (Benn & Evans, 2010; Brunt *et al.*, 2010; Bradley & Hewitt, 2024; Friedl *et al.*, 2020; Schoof, 2007; Powell & Alley, 1997). Motion at the grounding line occurs across a range of timescales. At shorter time scales (e.g. subdiurnal to diurnal), motion is tidally forced; at much longer timescales (centennial to millennial), forcings are more complex, involving interdependent feedback mechanisms between ice, climate, land and ocean (Hager *et al.*, 2024; Hogan *et al.*, 2023; Lowry *et al.*, 2019; Sejrup *et al.*, 2022; Shackleton *et al.*, 2019). Investigating grounding line motion across the range of timescales is important as it enables us to understand different forcing mechanisms and their impact on rates of deglaciation. For example, if an ice sheet continues to retreat over a retrograde bed slope, it is postulated to lead to significant instability; the concept referred as Marine Ice Sheet Instability (MISI) (Schoof, 2007; Weertman, 1974). This concept comes from the notion that ice flux across the grounding line increases with thickness. As such, retreat on a retrograde bed slope into deeper water, characterised by regions of greater ice thickness, facilitate a self-perpetuating retreat dynamic that can drive the grounding line past a critical threshold from which it cannot easily recover (Hill *et al.*, 2023; Pattyn & Morlighem, 2020; Schoof, 2007; Weertman, 1974).

MISI is often discussed in relation to the sensitivity of the West Antarctic Ice Sheet and the potential risk of collapse if the grounding line retreats past areas of topographic

stabilisation (Book *et al.*, 2022; Yu *et al.*, 2018). Specifically, this has been demonstrated by Reese *et al.* (2023), whereby modelling of Amundsen Sea glaciers shows an evolution of irreversible retreat from centennial to millennial timescales, leading to eventual collapse and a sea level rise of 2.7 to 3.5 m. This affirms the importance of observing ice sheet retreat processes across various timescales in order to understand how they emerge and evolve over time, and to establish the magnitude of instabilities (England *et al.*, 2022; Rignot *et al.*, 2014; Scambos *et al.*, 1994; Schoof, 2007; Sergienko, 2022; Siegert *et al.*, 2003; van Aalderen *et al.*, 2024; Weertman, 1974; Winter *et al.*, 2018).

When sediments are deposited at the grounding line, resultant landforms can mark the position of the ice margin and provide a geomorphologically informed record of glacier retreat and advance (Benn & Evans, 2010). This has become a well-established method for reconstructing and exploring ice margin position and oscillation at both short and long-term timescales. At shorter timescales (e.g. subdiurnal to diurnal), existing studies have used high-resolution bathymetry data to investigate low-amplitude grounding line ridges (also referred to as corrugation ridges) formed by tidally induced motion (Batchelor *et al.*, 2023; Hogan *et al.*, 2023). These studies observed rapid retreat rates of up to between 55 – 610 m day<sup>-1</sup> as a result of dominant buoyancy-driven forcing mechanisms across shallow-gradient beds.

At longer timescales (e.g. centennial to millennial), palaeo-ice sheet studies utilise very large ice marginal complexes, such as the Salpausselkä moraines in Finland, to reconstruct ice margin position (Lunkka *et al.*, 2022). These large moraine complexes, whilst significantly less regular than the diurnally formed corrugation ridges, can be used as ice sheet scale geochronological anchoring points for timing of deglaciation by dating their formation. This enables ice margin retreat to be delineated over much longer time periods; for example, depicting ice maximum extent to ultimate demise at time intervals of > 1,000 – 100 years (Clark *et al.*, 2022; Dalton *et al.*, 2023; Donner, 2010; Hughes *et al.*, 2016; Rinterknecht *et al.*, 2004; Saarnisto & Saarinen, 2001; Stroeve *et al.*, 2016). It is important to note, however, that at these timescales, even areas considered to be well constrained still hold uncertainties of between ~100 – 500 years (Stroeve *et al.*, 2016), potentially missing valuable information regarding ice margin retreat dynamics.

Studies of varied temporal resolutions in reconstructions at short and long-term timescales illustrate the sensitivity of ice sheet margins to a wide range of grounding line forcing mechanisms; in addition, they also highlight a gap in understanding at intermediate timescales (e.g. annual to centennial) (Batchelor *et al.*, 2023). These are critical timescales in which to understand ice margin retreat as they are more societally appropriate for contemporary ice sheet projections.

Similar to the diurnally formed ‘corrugation ridges’ (Batchelor *et al.*, 2023; Hogen *et al.*, 2023), DGMs are low-amplitude, regularly spaced, parallel ridges, formed at the grounding line of water terminating ice margins (Blake, 2000; Bouvier *et al.*, 2015; De Geer, 1889 & 1940; Golledge & Phillips, 2008; Larsen *et al.*, 1991; Lindén & Möller, 2005; Rivers *et al.*, 2024; Sinclair *et al.*, 2018; Sollid & Carlsson, 1984; Sollid, 1989) (see section 2.4). These ridges often present in ‘washboard-like’ fields and have been referred to collectively as De Geer terrain (DGT) to encapsulate different formation processes between individual ridges (see chapter 6; Rivers *et al.*, 2024). The regularity of ridge occurrence within DGT suggests a rhythmic temporal pattern (potentially annual) of deposition (Bouvier *et al.*, 2015; De Geer, 1940; Ojala, 2016; Sinclair *et al.*, 2018); however, accurate timescale quantification has generally remained uncertain due to the presence of more ridges than required by independently determined rates of ice margin retreat, or their often complex geomorphological appearance, thus hindering their use as ice marginal indicators (Hoppe, 1959; Möller, 1962; Zilliacus, 1981 & 1989; Sollid, 1989; Lindén & Möller, 2005).

Generally, individual ridge occurrence within DGT can vary, and can be confined to; 1) regularly spaced prominent ridges, 2) regularly spaced prominent ridges interspersed with irregular ridges, or 3) irregularly spaced ridges only (Ojala *et al.*, 2015; Ojala, 2016; Rivers *et al.*, 2023; Rivers *et al.*, 2024, Zilliacus, 1981). The occurrence of irregularly spaced ridges poses challenges when attempting to constrain the timing of formation, as it presents a degree of deviation from the regular formation pattern. Previous studies undertaken in Sweden have suggested these irregularly spaced ridges to be reflective of inter-seasonal variations during formation (Bouvier *et al.*, 2015; Lindén & Möller, 2005; Möller, 1962; Zilliacus, 1981). This can be seen more explicitly in chapter 6 whereby investigations of DGM internal architecture, comparing regular and irregular spaced

ridges, found that generally, regularly spaced prominent DGMs and irregular DGMs have the same formation properties, with slight variations that can be attributed to different inter-seasonal formation processes (Rivers *et al.*, 2024). Congruent with ideas suggested in previous studies (Blake, 2000; Bouvier *et al.*, 2015; De Geer, 1889 & 1984; Frödin, 1916; Möller, 1962; Sollid & Carlsson, 1984; Larsen *et al.*, 1991; Lindén & Möller, 2005; Sinclair *et al.*, 2018), the integrated DGM formation model presented in chapter 5 (section 6.5.2; FIGURE 6.18) depicts bi-seasonal changes in behaviour at the ice margin that reflect subtly different formation processes between regular and irregular ridges. Specifically, irregular ridges are suggested to form during periods of summer calving and retreat, and regular ridges are suggested to form during a late winter/early spring readvance, thereby reflecting an annual periodicity. This integrated model encompasses variable DGT configuration and validates the premise that DGMs may be used as effective annual ice margin indicators, provided that the regularly spaced ‘annual’ ridges can be accurately disentangled from the wider terrain.

The chronology of DGM formation in southwest Finland can be tested by comparing the spatial occurrences of ridges with an established annual clay varve-based deglaciation chronology (Strömberg, 2005); similar to those undertaken previously in Sweden and Finland (Bouvier *et al.*, 2015; De Geer, 1940; Ojala, 2016). If ages can be accurately constrained, DGMs may then be used as a basis for isochrone construction, which would in theory provide an annually refined ice margin reconstruction of the southwest Finnish sector of the FIS. Furthermore, the annual signal that is potentially present within DGT will also enable grounding line forcing mechanisms to be explored at intermediate timescales (e.g. centennial to annual), which is currently under-investigated (Batchelor *et al.*, 2023).

The purpose of this study is to: (i) investigate the extent to which DGMs are annual by using a locally established clay-varve chronology to constrain their relative age, (ii) test whether an annual ice margin reconstruction can be developed in the Baltic Sea Ice lobe (BSIL) area of the FIS during Late Weichselian to Early Holocene deglaciation using DGMs as geochronometric indicators, and (iii) investigate grounding line forcing mechanisms at intermediate timescales (e.g. annual to centennial) that are predominantly driving the rate of deglaciation in the area.

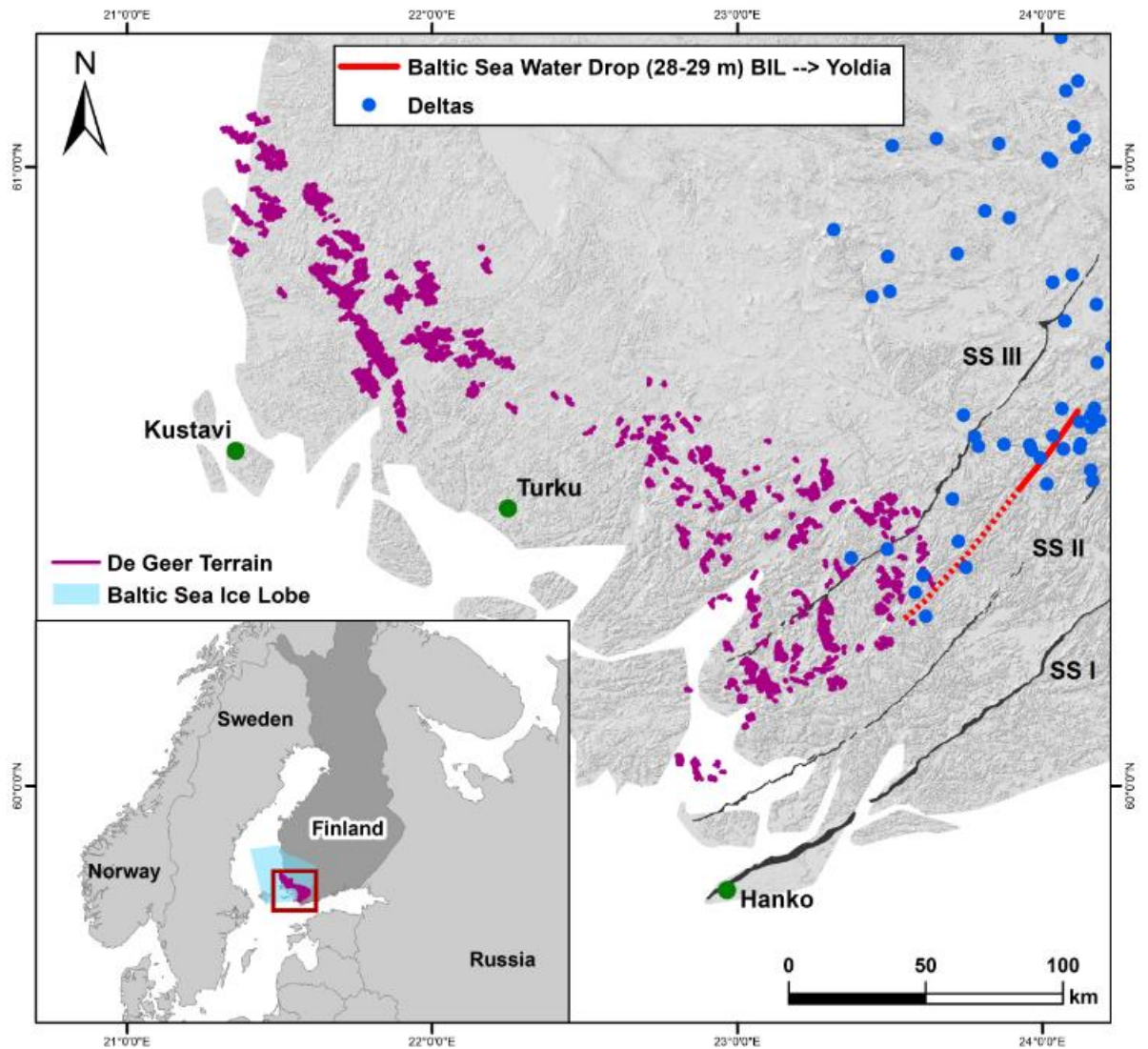
## 7.2 Study Area

Following the LGM ~20 ka BP (Clark *et al.*, 2009), the FIS underwent rapid retreat until a short-lived readvance during the YD ~12.9 – 11.7 ka BP (Donner, 2010; Rinterknecht *et al.*, 2004; Saarnisto & Saarinen, 2001) (see section 3.3). The ice margin extent during the YD is marked by the position of the First and Second Salpausselkä ice marginal complexes that can be traced north-eastwards from the Scandinavian Peninsula through southeast Finland and Russian Karelia to the Kola Peninsula (NB: While the Finnish Salpausselkä moraines extend northward into Russian Karelia and the Kola peninsula, these are classified separately and have their own distinct nomenclature) (Donner, 2010; Glückert, 1995; Lunkka *et al.*, 2021; Rainio *et al.*, 1995; Rinterknecht *et al.*, 2004; Saarnisto & Saarinen, 2001; Tschudi *et al.*, 2000; Putkinen *et al.*, 2011). Following the YD, the ice margin became crenulated, resulting in the formation of independent ice lobes (although these may have already existed before the YD) (Ahokangas & Mäkinen, 2014; Putkinen *et al.*, 2017; Punkari, 1980; Kurimo, 1982; Johansson *et al.*, 2011), with southwest Finland being host to the southern sector of the BSIL (FIGURE 7.1). These ice lobes behaved time-transgressively and were complex in retreat dynamics due to an increased sensitivity to localised conditions. Such complexities can obscure understanding of deglaciation; however, it is generally accepted that after the YD, the ice margin returned to a relatively stable state of retreat, with a temporary standstill denoted by the Third Salpausselkä ridge (FIGURE 7.1) (Donner, 1995; Hughes *et al.*, 2016; Johansson *et al.*, 2011; Lunkka *et al.*, 2004 & 2021; Okko, 1962; Rainio *et al.*, 1995; Stroeve *et al.*, 2016). As such, pertinent to this study, from the end of YD (~11.7 ka BP), it can be assumed that no significant readvance occurred that may have overridden pre-existing formations, and thus DGMs after this period (e.g. up-ice of SS II), can be considered successive, thereby depicting a relatively undisturbed record of ice margin retreat.

DGT is abundant across the BSIL area in southwest Finland, as a relic of the complex environment created by dynamic relationships between topography, fluctuations in proglacial water depth, ice mass redistribution and isostatic adjustment (Andrén *et al.*, 2011; Eronen *et al.*, 2001; Fyfe, 1990; Glückert, 1991; Larson *et al.*, 2009; Lunkka *et al.*, 2019; Ojala, 2016; Sharma, 1984; Szuman *et al.*, 2024). Due to the complexity of ice lobe setting and oscillation, deglaciation dynamics in southwest Finland after the YD are not



precisely delineated nor absolutely dated (Lunkka *et al.*, 2021). It is evident in the area that proglacial water depth became generally suitable for the formation of DGMs only after the 25-28 m drop of the Baltic Ice Lake to the Yoldia Sea water level when a sudden and catastrophic drainage into the North Atlantic occurred (e.g. Andrén *et al.*, 2002). This can be seen by the onset of DGT formation whereby it is only observable northwest of the drainage boundary (FIGURE 7.1). This drainage event has been dated to 11 590  $\pm$ 100 cal. years BP by Saarnisto & Saarinen (2001), 11 560 cal. years BP by Andrén *et al.* (2002), 11 620  $\pm$ 100 cal. years BP by Stroeve *et al.* (2015) and 11 570 cal. years BP by Donner (2010), i.e. occurring very soon after the formally defined Pleistocene/Holocene boundary 11 700  $\pm$ 99 years b2k (i.e., 11 650  $\pm$ 100 cal. years BP) (Walker *et al.*, 2019). In the Finnish varve chronology by Sauramo (1923, 1929) the zero year ( $\pm$ 0) marks the drainage of the Baltic Ice Lake into the Yoldia Sea when the ice margin had retreated inside the Salpausselkä II. In a corrected varve chronology Sauramo's  $\pm$ 0 year corresponds to varve year -1480 (Strömberg, 2005).



**FIGURE 7.1.** Location map showing DGT across southwest Finland within the southern sector of the Baltic Sea Ice Lobe. Salpausselkä moraines indicated by black polygons (SS I, SS II & SS III). Deltas are indicated by blue dots; red line (dotted line - speculative) depicts the position of Baltic Sea water drop estimated at between ~11 620 – 11 560 cal. years BP (Andrén *et al.*, 2002; Donner, 2010; Saarnisto & Saarinen, 2001; Stroeve *et al.*, 2015).

### 7.3 Methods

#### 7.3.1 DGM mapping

This work utilised the DGT dataset developed in chapter 5 (Rivers *et al.*, 2023), whereby high-resolution, 2 m LiDAR data was used to identify and map all DGMs across southwest Finland. Based on automated 3D morphometric and statistical analyses, DGMs were subdivided into regular (prominent), and irregular (intermediate) ridge types determined

by prominence, lateral extent and successive regularity between individual ridges. A total of 3 966 DGM landforms were mapped across the study area: 2 581 regular/prominent and 1 385 irregular/intermediate ridges. The identification and utility of both prominent and intermediate ridges was critical to allow an annual signal to be accurately identified across the wider terrain. It should be noted that in some instances, it was difficult to accurately differentiate between prominent and intermediate ridges due to formation controls such as strength of ice margin oscillation, sediment availability and preservation potential. As such, for the purposes of this study, both prominent and intermediate ridges were utilised, with a primary use of prominent ridges where possible; however, in more complex DGT, intermediate ridges were also utilised.

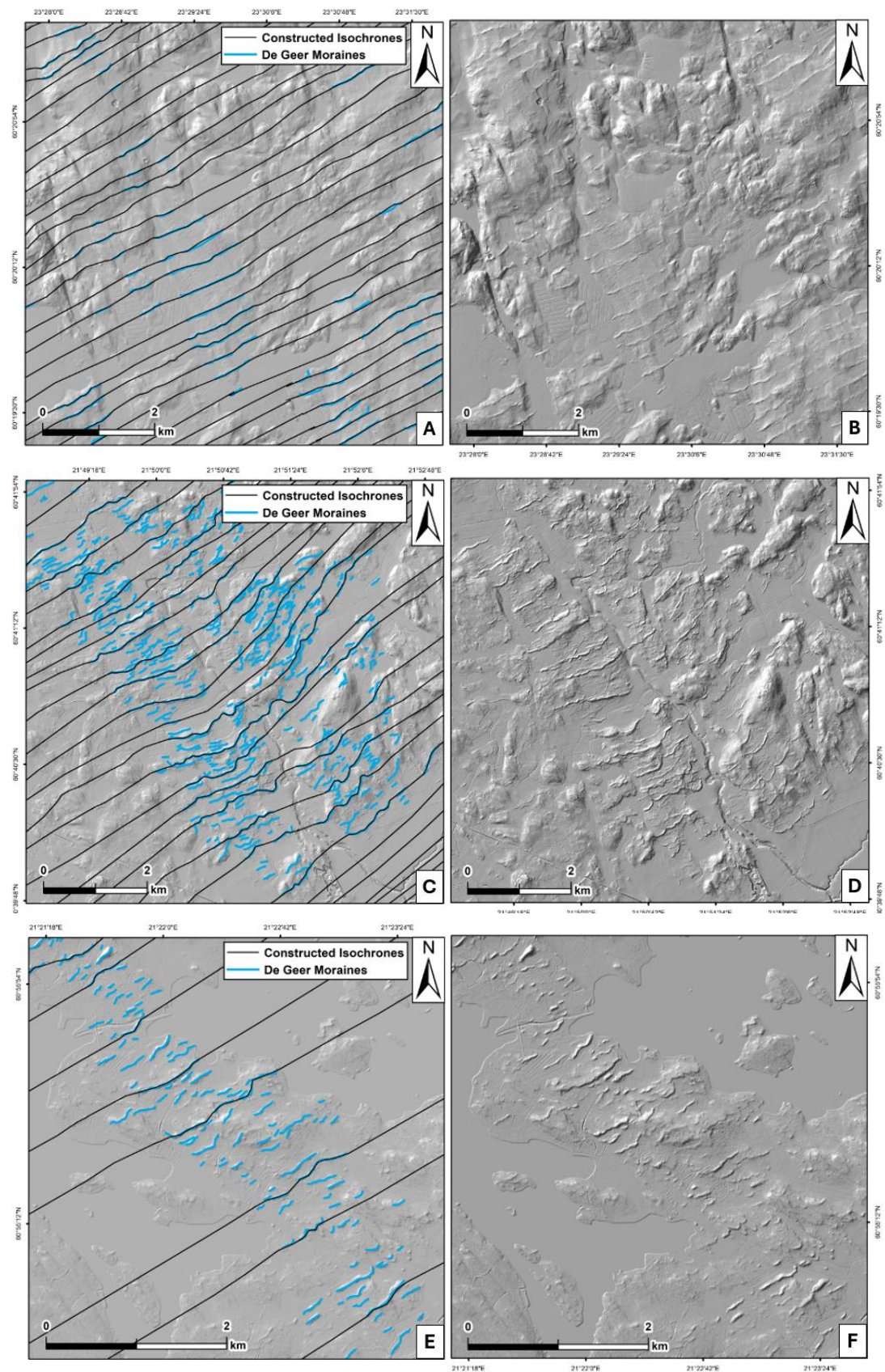
### **7.3.2 Isochrone construction**

Individual DGMs were extended laterally across the study area, adjoining neighbouring ridges where possible, and guided by topographical inclination using dual azimuth hillshade rendered LiDAR imagery (LiDAR 6/23, National Land Survey of Finland). Each laterally extended moraine was designated as a single isochrone providing an indication of former grounding line position (FIGURE 7.2).

In areas characterised by regular prominent DGMs, all ridges were extended as isochrones and compared with the local varved clay chronology (FIGURE 7.2A & B) (Strömberg, 2005). In areas of combined regular prominent and irregular ridges (FIGURE 7.2C & D), and only irregular ridges (FIGURE 7.2E & F), selected ridges representing annual ice margin retreat comprise prominent ridges whenever possible, combined with irregular ridges if the number of ridges required by the varve chronology was greater than the number of observable prominent ridges (Strömberg, 2005) (see section 7.3.3, FIGURE 7.3). This method leant on the premise that DGMs are formed annually (Bouvier *et al.*, 2015; De Geer, 1940; Ojala, 2016; Rivers *et al.*, 2024; Sinclair *et al.*, 2018).

It is expected that not all moraines appearing in DGT would serve as annual formations due to the bi-seasonal characteristics (Bouvier *et al.*, 2015; Lindén & Möller, 2005; Möller, 1962; Zilliacus, 1981; Rivers *et al.*, 2024) (see chapter 6); as such, a degree of subjectivity and uncertainty in the rate of annual deglaciation in areas of more complex DGT must be accepted. It should also be considered that in some areas DGT may be undetectable due

to postglacial sedimentation. For this reconstruction, all detectable ridges were considered successive, even across relatively large distances, despite the likelihood that some ridges may be absent. This will inevitably be reflected in the data showing greater retreat distances than what may reasonably be expected in some areas; however, due to the abundance of DGT in the area, we expect these anomalies to be minimal.



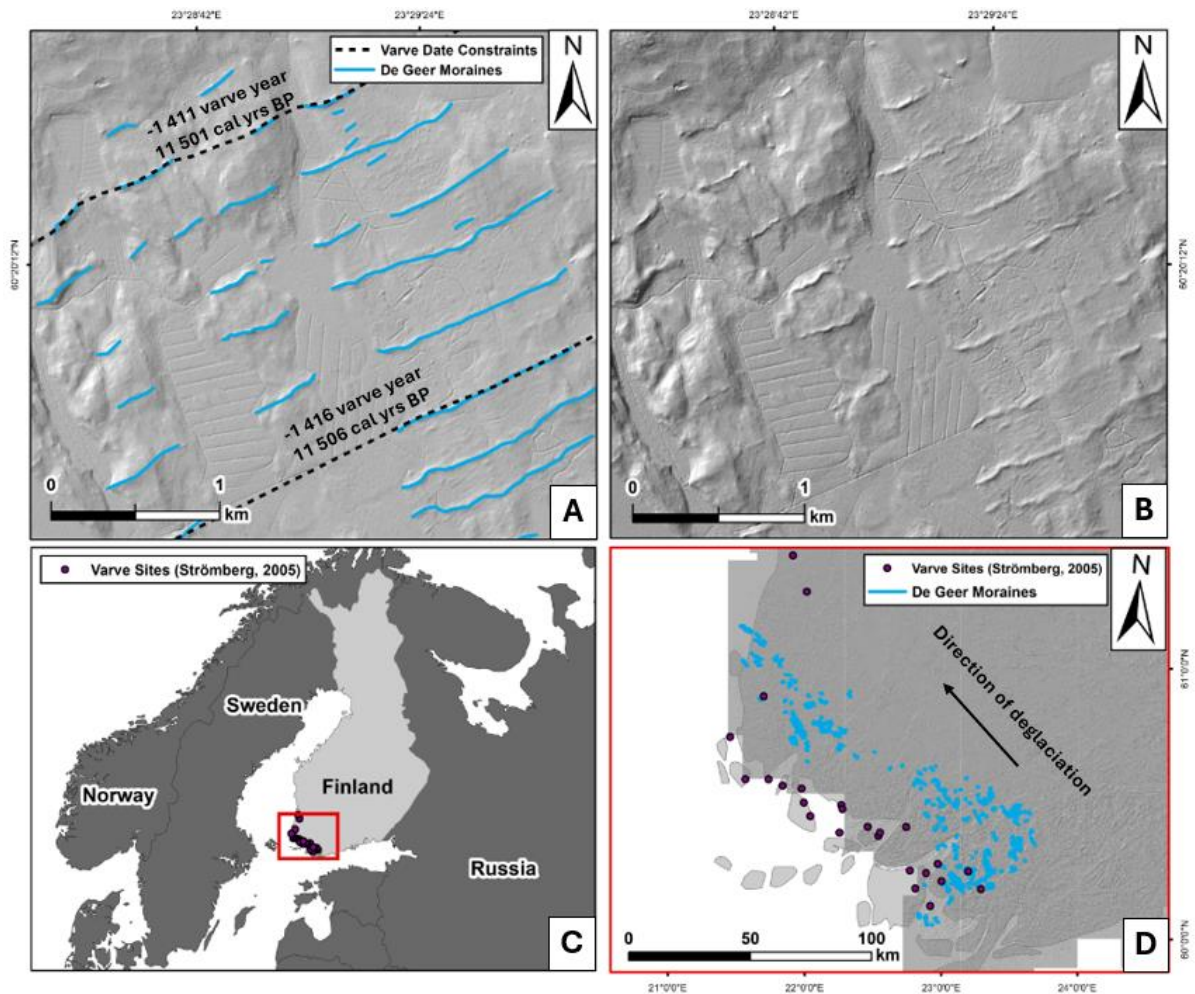
**FIGURE 7.2.** Hillshaded DEM imagery showing ice margin isochrone construction from designated moraines across varied DGT configuration [DEM source: ®National Land



*Survey of Finland, LiDAR digital elevation model, 2/2023]. 7.2A & B) show regular, prominent moraines only; panels 7.2C & D) show regular, prominent DGMs interspersed with irregular DGMs; and 7.2E & F) show irregular moraine only. In areas characterised by DGT as shown in 7.2C, D, E & F, prominent moraines were primarily used and the number of irregular moraines used were informed by the number required from the local varve chronology (Strömberg, 2005) to derive an annual reconstruction.*

### **7.3.3 Geochronological anchoring**

The existing clay varve chronology across southwest Finland between Salpausselkä II and Kustavi was used as a floating time constraint for correlation with DGM frequency (Strömberg, 2005). Ridges were connected to the nearest varve site and individual ridge occurrence between each varve site was counted and matched against the floating dates (FIGURE 7.3). This provided an effective means by which to compare an annual rate of deglaciation between DGMs and the existing varve chronology (Strömberg, 2005), and by which to accurately quantify the timescale of DGM formation. Varve sites were selected based on, 1) proximity to ridges and 2) dates successively decreased between varve sites from a southeast to north-westerly direction (e.g. in the direction of deglaciation).



**FIGURE 7.3.** Images illustrating geochronological anchoring for the DGM-derived reconstruction. A) Hillshaded DEM showing correlation between regularly spaced mapped DGMs and varve / interpreted calendar years; B) Hillshaded DEM showing DGMs without mapped polylines; C) Map showing location of study area and selected varve sites from (Strömberg, 2005); D) Map showing selected varve sites and DGMs located across southwest Finland. Selected clay varved sites were used from the established local chronology across southwest Finland (Strömberg, 2005). DGMs were connected to varve sites by closest proximity. The number of successive DGMs were counted and matched to varve dates between sites in direction of deglaciation.

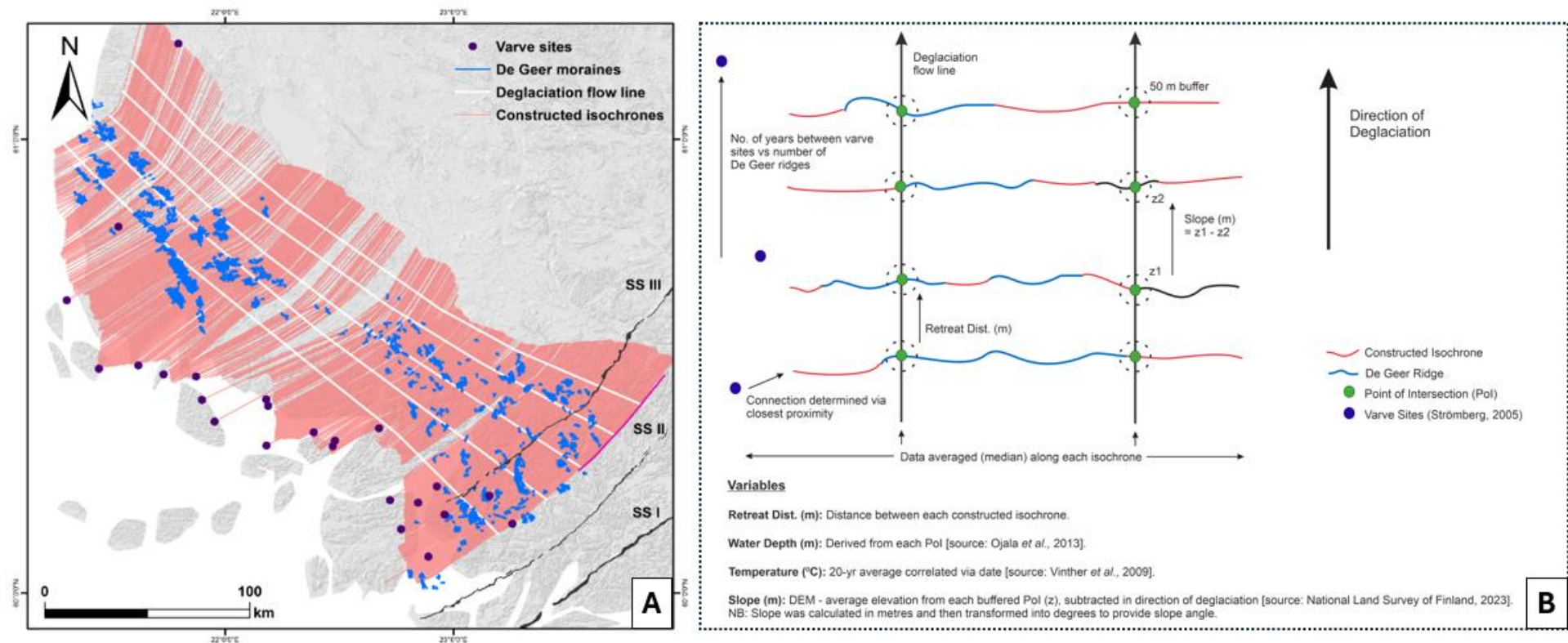
Here, we use the corrected varve chronology by Strömberg (2005) which was updated from the older Finnish varve chronology produced by Sauramo (1923) and connected to the ‘Swedish Time Scale’. Whilst this chronology is floating, calendar year time constraints were correlated based on the estimated date of the final drainage of the Baltic Ice Lake at

11 620 cal. yr BP according to Stroeve *et al.* (2015), which corresponds to -1480 in floating varve years by Strömberg (2005). This allowed the reconstruction of time steps for ice margin positions and comparison of DGM-based rate of deglaciation with NGRIP temperatures (Vinther *et al.* 2009).

#### **7.3.4 Analysis of grounding line forcing mechanisms**

To determine annual retreat rate, five deglaciation flow lines were positioned perpendicular to constructed isochrones and were distributed evenly across the study area to obtain an average rate of retreat between each annually estimated isochrone (FIGURE 7.4). Distance of retreat analysis was then undertaken to test whether retreat rate correlated with, 1) temperature (using the NGRIP 20-year average temperature data (Vinther *et al.* 2009)), 2) topographic controls (i.e. slope and elevation), and 3) water depth (Ojala *et al.*, 2013), to investigate the strength and spatiotemporal variability of grounding line forcing mechanisms (FIGURE 7.4). NB: slope was analysed overall and separately by 'type' (e.g. adverse vs normal). Slope in this instance is considered more representative of terrain roughness, whereas elevation profiles provide an indication of bed slope direction (e.g. adverse vs normal). Other retreat rate variables such as proglacial water temperature and ice surface slope were not analysed in this study; however, influences from these variables should be acknowledged.

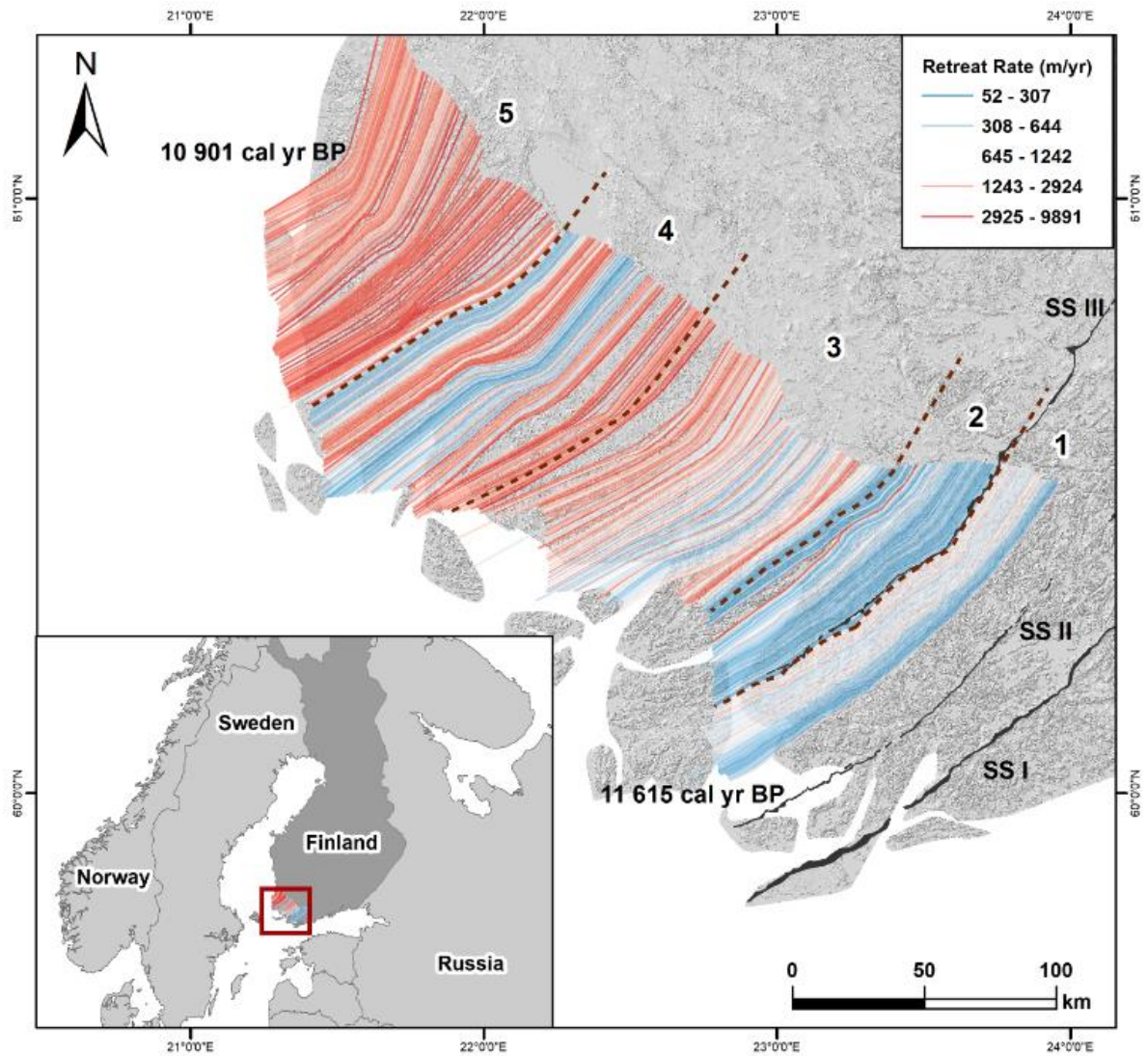




**FIGURE 7.4.** Map (7.4A) and method sketch (7.4B). 7.4A) shows mapped DGMs presented in blue and relative constructed isochrones presented in pink. Varve sites depicted by purple dots. Deglaciation flow lines are shown in white and were used to derive average retreat distance and grounding line variable datasets along each intersected isochrone. 7.4B) illustrates methods for data extraction and calculations are illustrated in the method sketch.

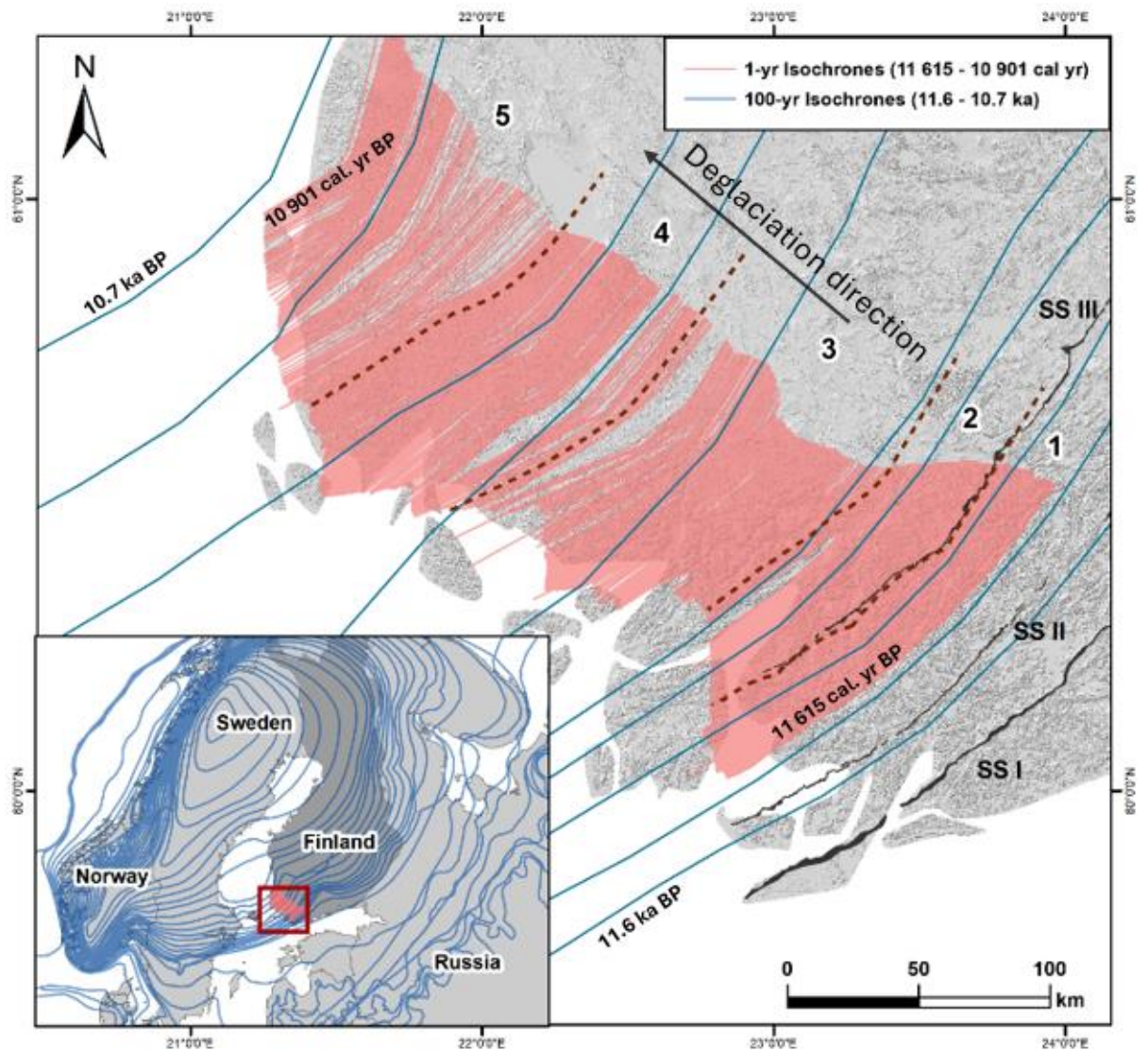
## 7.4 Results

A 714 yearlong annual ice margin reconstruction was developed across the study area based on DGM derived isochrones between 11 615 – 10 901 cal. yr BP. FIGURE 7.5 presents constructed isochrones that are colour-graded to coincide with annual retreat rate. The reconstruction is subdivided into five spatiotemporal segments based on interesting variations in retreat: 1) a period of increasing retreat up to the Salpausselkä III moraine, 2) a decline in retreat rate, 3) a return to a gradual increase, 4) a period of fluctuating retreat rates, and 5) a return to increased retreat rates. The overall shape and pattern of DGM derived isochrones were compared to the current highest resolution reconstruction in the area (e.g. 100-year intervals; Stroeven *et al.*, 2016) (FIGURE 7.6). This enabled testing of the plausibility of results and to establish the degree of refinement achieved. This comparison is also presented as line plots (FIGURE 7.7) whereby annual and 100-year (Stroeven *et al.*, 2016) ice margin retreat rates are compared. Overall, broadly similar patterns are observed between the two, with retreat rate increasing through time from 250 up to 2 000 m/yr<sup>-1</sup> (FIGURE 7.7).

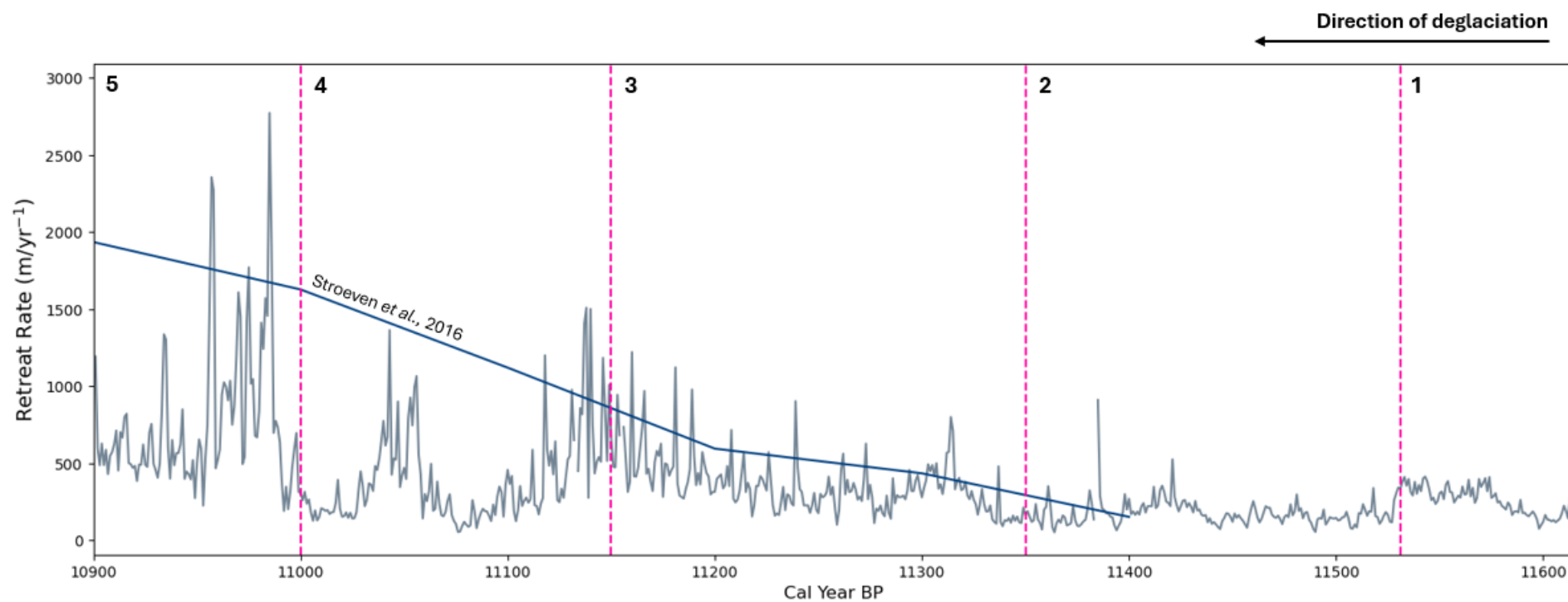


**FIGURE 7.5.** Annual DGM-derived reconstruction with colour-graded isochrones delineating rate of retreat ( $\text{m/yr}^{-1}$ ). The reconstruction is subdivided in spatiotemporal segments as outlined above: 1) 11 615 – 11 531, 2) 11 530 – 11 350, 3) 11 349 – 11 150, 4) 11 149 – 11 000, 5) 10 999 – 10 901.





**FIGURE 7.6.** Annual ice margin reconstruction of the southwest Finnish sector of the Fennoscandian Ice Sheet between 11 615 – 10 901 cal. years BP, derived from DGMs located across the study area (pink isochrones). The reconstruction is subdivided into spatiotemporal segments 1-5 as defined in FIGURE 7.5. 100-year isochrones between 11.6 – 10.7 ka BP are overlaid for context and comparison (blue isochrones) (Stroeve et al., 2016).



**FIGURE 7.7.** Line plots comparing estimated retreat rate across southwest Finland between DGM-derived annual reconstruction (grey line plot) and 100-yr reconstruction (blue line plot) (Stroeve et al., 2016). The plots are subdivided into the spatiotemporal segments 1-5 as defined in FIGURE 7.5. NB: the retreat rate from Stroeve et al. (2016) was compared between 11 400 – 10 900 cal. yr BP based on the spatial extent of mapped DGMs, and deglaciation flow lines as shown in FIGURES 7.4A & 7.6.

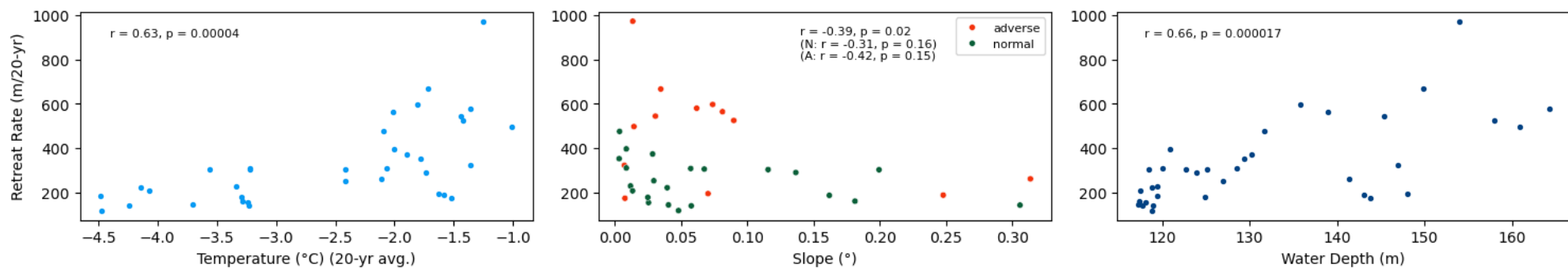
Overall, the two reconstructions show strong similarities between the general ice margin configuration and pattern of retreat (FIGURE 7.6). This provides a reasonable indication of accuracy and means of quality control for the DGM-derived reconstruction. FIGURE 7.7 presents a more detailed comparison between estimated retreat rates showing a significantly more detailed and nuanced retreat pattern compared to the 100-year resolution. This is particularly notable when visualising fluctuations between annual rates of retreat (e.g. segments 4 & 5, FIGURE 7.7). In the DGM-derived reconstruction, within segments 3 & 4, it should be noted that some of the observed gaps/increased distances of retreat may be due to less evidence of DGT (FIGURES 7.5 & 7.6). This is likely attributed to postglacial sedimentation. Nevertheless, despite these uncertainties, the DGM-derived reconstruction, still shows significant improvements of estimated ice margin retreat characteristics compared to the that of the 100-year reconstruction (Stroeven *et al.*, 2016) (FIGURES 7.6 & 7.7).

#### **7.4.1 Grounding line variables**

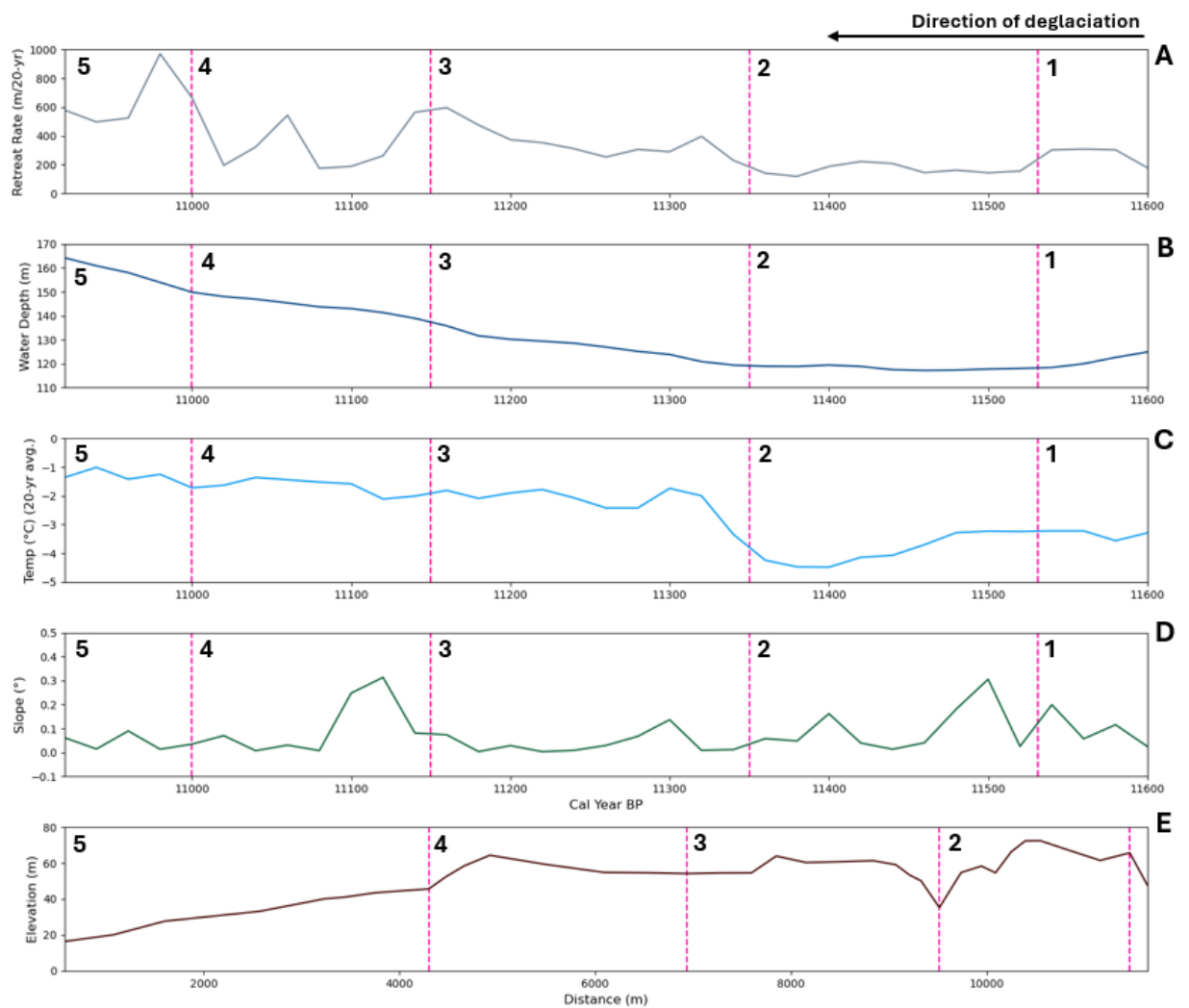
Grounding line variables temperature (Vinther *et al.*, 2009), proglacial water depth (Ojala *et al.*, 2013), and slope (from LiDAR DEM) were analysed to investigate relationships with retreat rate. Results are presented as 20-year average resolution in section 7.4.1.1, to enable more accurate comparisons with the 20-year average NGRIP temperature records (Vinther *et al.* 2009), and annual resolution in section 7.4.1.2, to enable more detailed analysis derived from the annual DGM dataset.

##### **7.4.1.1 20-year resolution results**

Scatter plots are presented below measuring the strength of correlation between retreat rate (m/20-yr) and grounding line variables, temperature (°C) (FIGURE 7.8A), slope (°) (FIGURE 7.8B) and water depth (m) (FIGURE 7.8C), using 20-year averaged datasets. Line plots are presented in FIGURE 7.9 showing retreat rate (m/20-yr) (FIGURE 7.9A), water depth (m) (FIGURE 7.9B), temperature (°C) (FIGURE 7.9C), and slope (°) vs time (cal. yr BP) (FIGURE 7.9D). An elevation profile (FIGURE 7.9E) is also presented to compare gradient across the entire study area in the direction of deglaciation. NB: extreme outliers in retreat rate due to lack of DGM evidence were removed to mitigate any influential inaccuracies when undertaking statistical analyses. Results are outlined for each defined time segment in turn.



**FIGURE 7.8.** Scatter plots presenting correlations between A) 20-year avg. NGRIP temperature (°C) (Vinther et al., 2009), 2) slope (°), and 3) water depth (m) vs retreat rate (m/20-yr). NB: for the purposes of fair correlation with the 20-year average NGRIP temperature records, retreat rate, slope and water depth data were also converted to 20-year average.



**FIGURE 7.9.** Line plots showing grounding line variables at 20-year averages: A) retreat rate (m/20-yr); B) water depth (m); C) 20-yr avg. NGRIP temperature ( $^{\circ}\text{C}$ ); D) slope ( $^{\circ}$ ) vs time (cal. years BP); E) elevation (m) vs distance (m) across study area in direction of deglaciation. Panels mark time segments 1) 11 615 – 11 531, 2) 11 530 – 11 350, 3) 11 349 – 11 150, 4) 11 149 – 11 000, 5) 10 999 – 10 901 and correspond with the grounding line variable maps presented in FIGURE 7.5.

**1) 11 615 – 11 531 cal. yr BP:** During this period, retreat rate is slow with a slight increase between  $\sim 11\,615$  to  $\sim 11\,575$  cal. yr BP, which then levels to steady retreat rate of 300 m/20-yr. Water depth, whilst relatively low at this stage, decreases slightly across this time period. Temperature shows a similar pattern whereby a slight decrease is observed but generally this variable remains low and stable. Slope and elevation are relatively stable, characterised overall by a normal bed slope direction.



**2) 11 530 – 11 350 cal. yr BP:** Overall, this period is characterised by the slowest retreat rate as a continuation from the previous segment, including a slight decrease up to ~11 450 cal. yr BP, then transitioning to a slight increase. Temperature remains low and stable and then decreases from ~11 475 cal. yr BP. Water depth continues to decrease. Terrain continues to increase in roughness during the beginning of this time period and stabilises from ~ 11 450 cal. yr BP onwards. This is also the stage at which bed slope direction transitions from normal to adverse, which coincides with the slight increase in retreat rates toward the end of this time period.

**3) 11 349 – 11 150 cal. yr BP:** The increased trajectory of temperature and retreat rate observed from ~11 400 cal. yr BP continues from the previous segment, whereby the relationship between these two variables is most prominent. A general increase in retreat rate is observed across the whole time period which also corresponds with the continual increase in water depth. Terrain becomes smoother during this this time period, characterised by a relatively flat bed topography.

**4) 11 149 – 11 000 cal. yr BP:** Retreat rate is the most dynamic within this time period in contrast to those previously described. Temperature and water depth maintain a gradual increase during this time; however, terrain roughness increases, characterised by a normal bed slope direction. This appears to coincide with decreased retreat rates. Slope then transitions sharply to an adverse bed slope direction, followed by a sustained period of smoother terrain.

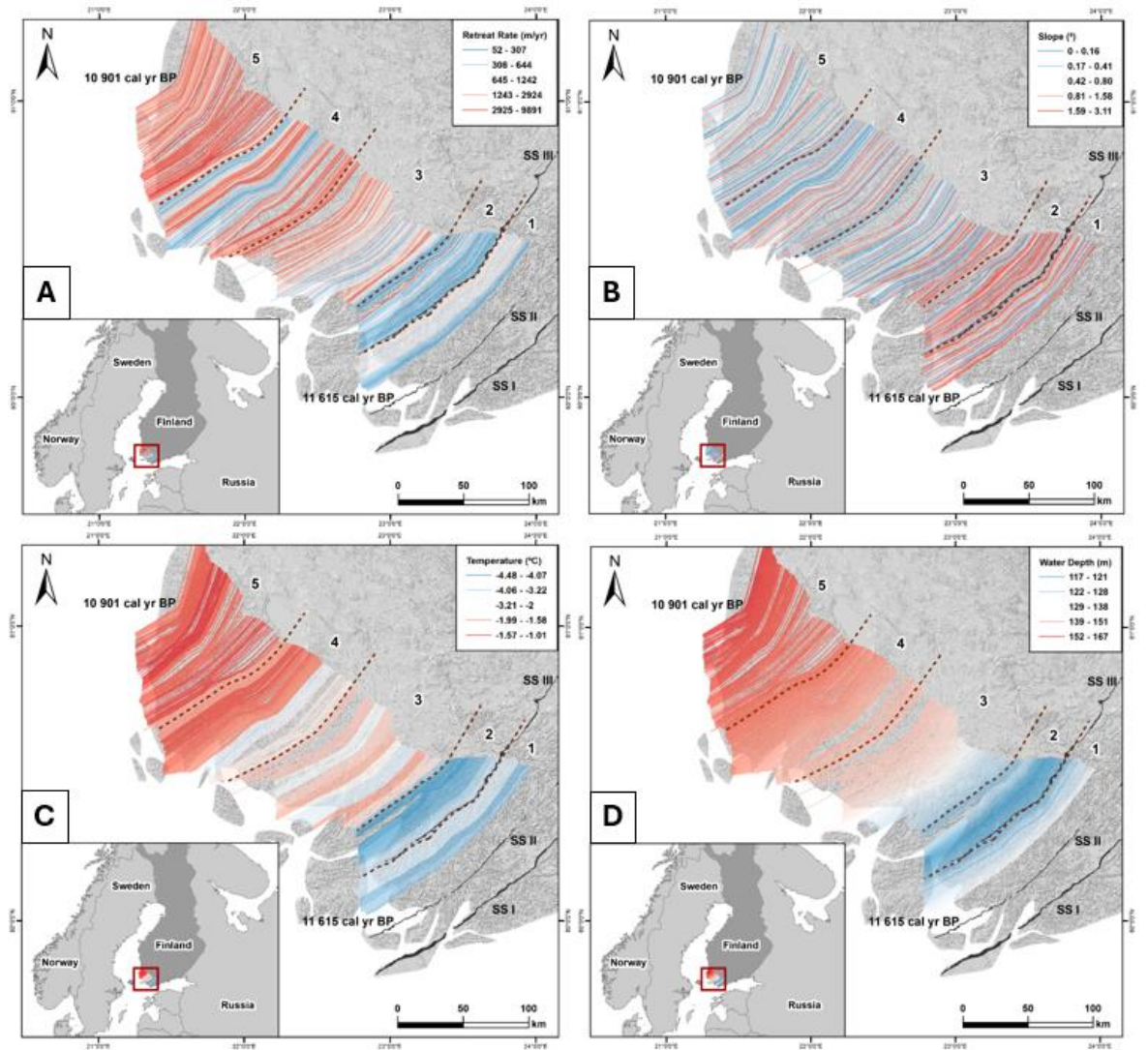
**5) 10 999 – 10 901 cal. yr BP:** This period is characterised by strong fluctuations in retreat rate. During this time period, water depth continues to rapidly increase. Temperatures remain relatively high gradually increasing. Terrain roughness is relatively smooth; however, overall bed slope direction is adverse. The spike in retreat rate at the beginning of this time period denote the highest retreat rates observed from the data. NB: interpretations of very high retreat rates should be taken with the caveat that these may coincide with limited DGT evidence that can produce similar results.

Statistical analyses in FIGURE 7.8 show moderate and significant positive correlations between retreat rate, temperature and water depth (temperature:  $r = 0.63$ ,  $p < 0.05$ ; water depth:  $r = 0.66$ ,  $p < 0.05$ ). Based on the line plot visualisation in FIGURE 7.9, it is

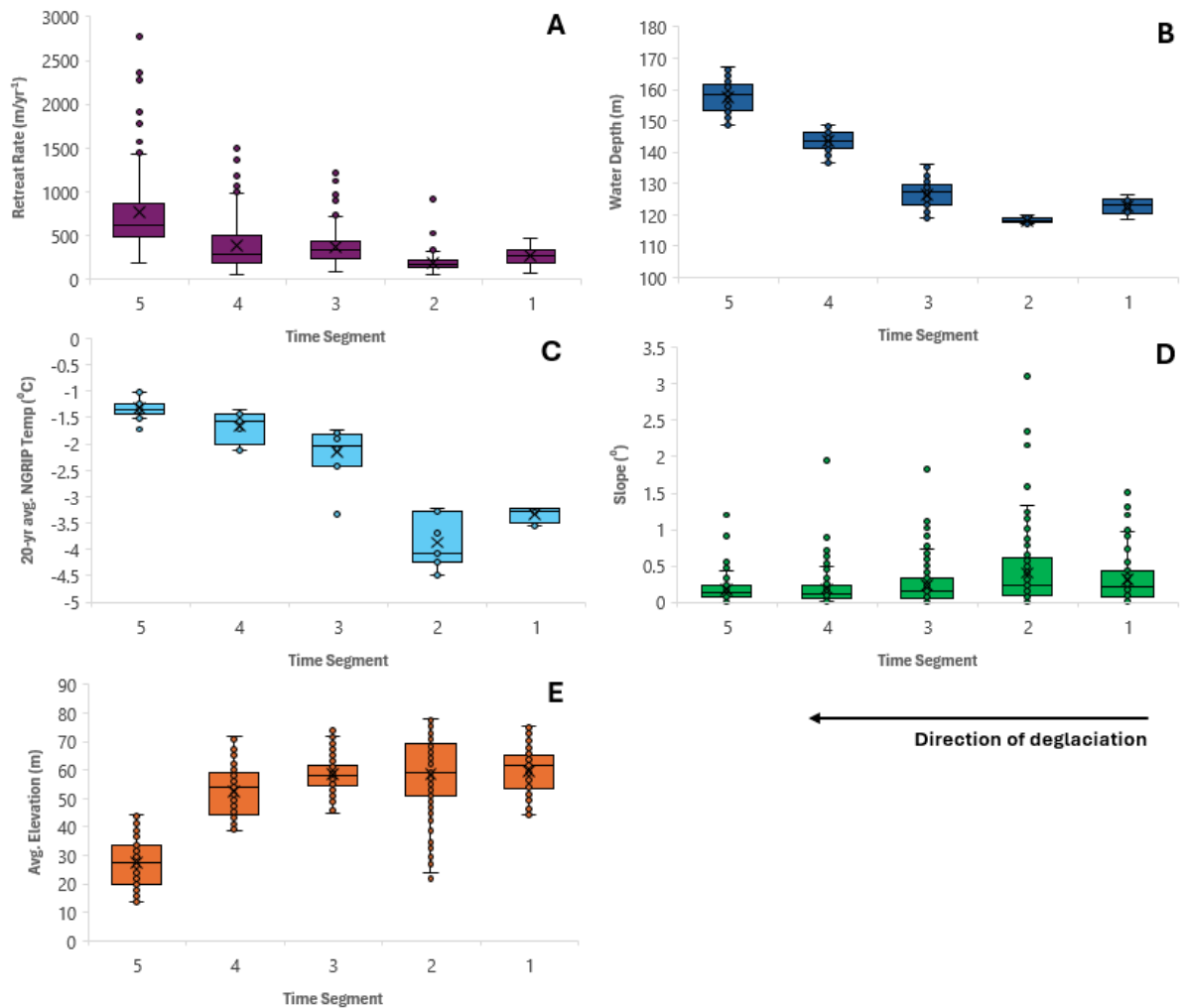
apparent that these variables correlate across the entire study area, with a varying degree of strength throughout. Slope was analysed both with and without distinction between slope type (e.g. normal vs adverse). Without distinction, slope shows a slight statistically significant weak negative correlation with retreat rate (slope:  $r = -0.39$ ,  $p < 0.05$ ). In contrast, when distinguishing between slope type, the data shows no statistically significant correlation for either (normal:  $r = -0.31$ ,  $p > 0.05$ , adverse:  $r = -0.42$ ,  $p > 0.05$ ). Whilst the overall correlation between slope and retreat rate is weak, based on visual observations presented in FIGURE 7.9, it would be reasonable to argue this variable does influence retreat rate to some degree, even at shallow-gradients; however, due to the dominance of water depth and temperature, and given that slope extent is relatively minimal across the study area, it is difficult to precisely extricate the relationship with this variable.

#### 7.4.1.2 Annual resolution results

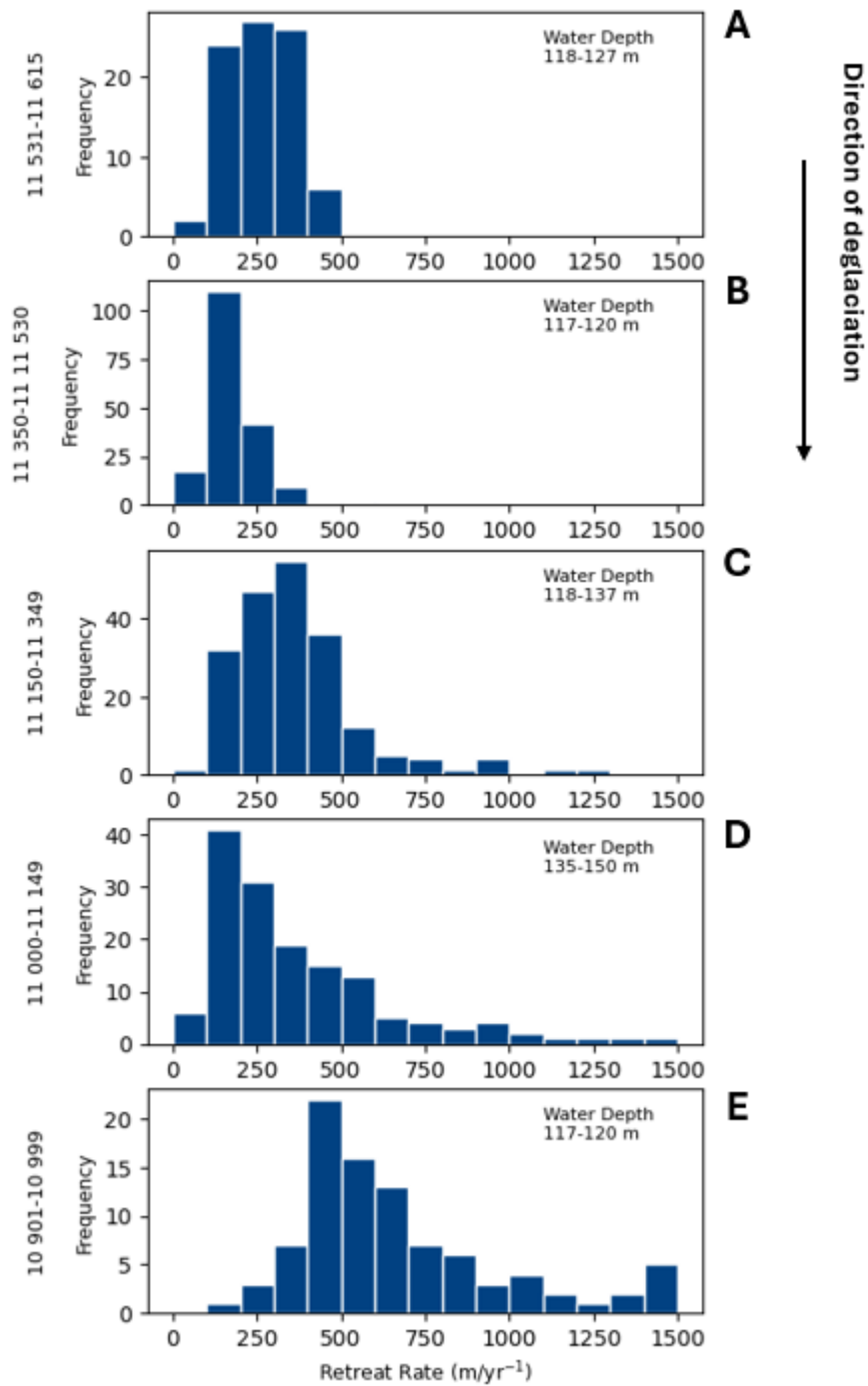
Results derived from annual datasets are presented below. FIGURE 7.10 presents colour-graded isochrone maps relative to each variable: retreat rate ( $\text{m/yr}^{-1}$ ) (7.10A), slope ( $^{\circ}$ ) (7.10B), 20-yr avg. NGRIP temperature ( $^{\circ}\text{C}$ ) (7.10C) and water depth (m) (7.10D). FIGURE 7.11 presents quantified data as box and whisker plots showing annual retreat rate ( $\text{m/yr}^{-1}$ ) (FIGURE 7.11A), water depth (m) (FIGURE 7.11B), 20-yr avg. temperature ( $^{\circ}\text{C}$ ) (FIGURE 7.11C), slope ( $^{\circ}$ ) (FIGURE 7.11D) and elevation (m) (FIGURE 7.11E). This data can also be found tabulated in Appendices Table 1. Histograms and scatterplots are presented showing the relationship between retreat rate ( $\text{m/yr}^{-1}$ ), water depth (m) (FIGURE 7.12) and slope ( $^{\circ}$ ) (FIGURE 7.13). NB: temperature is excluded from correlative scatterplots at annual resolution due to the dataset being 20-year average (Vinther *et al.*, 2009). Line plots are presented in FIGURE 7.14 showing: A) retreat rate ( $\text{m/yr}^{-1}$ ), B) water depth (m), C) temperature (20-yr avg.) ( $^{\circ}\text{C}$ ), and D) slope ( $^{\circ}$ ) vs time (cal. yr BP), and E) elevation vs distance (m) across the study area. Line plots are subdivided by pink dashed lines that correspond with the spatiotemporal segments defined in FIGURE 7.5.



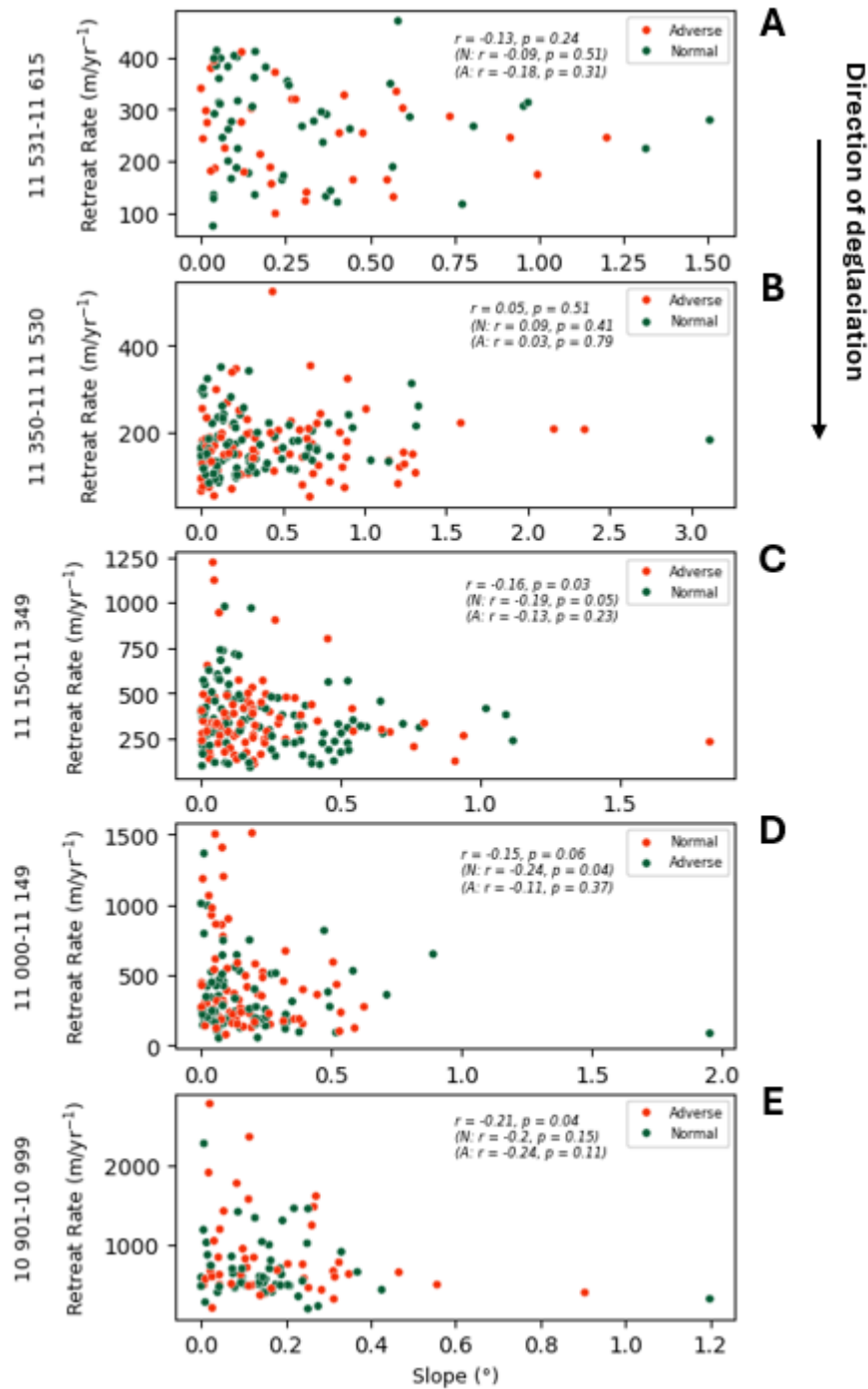
**FIGURE 7.10.** Annual resolution reconstruction maps presented with colour-graded isochrones relative to each variable: A) retreat rate ( $\text{m/yr}^{-1}$ ), B) slope ( $^{\circ}$ ), C) 20-yr avg. NGRIP temperature ( $^{\circ}\text{C}$ ), and D) water depth (m). Panels mark time segments - 1: 11 615 – 11 531, 2: 11 530 – 11 350, 3: 11 349 – 11 150, 4: 11 149 – 11 000, 5: 10 999 – 10 901.



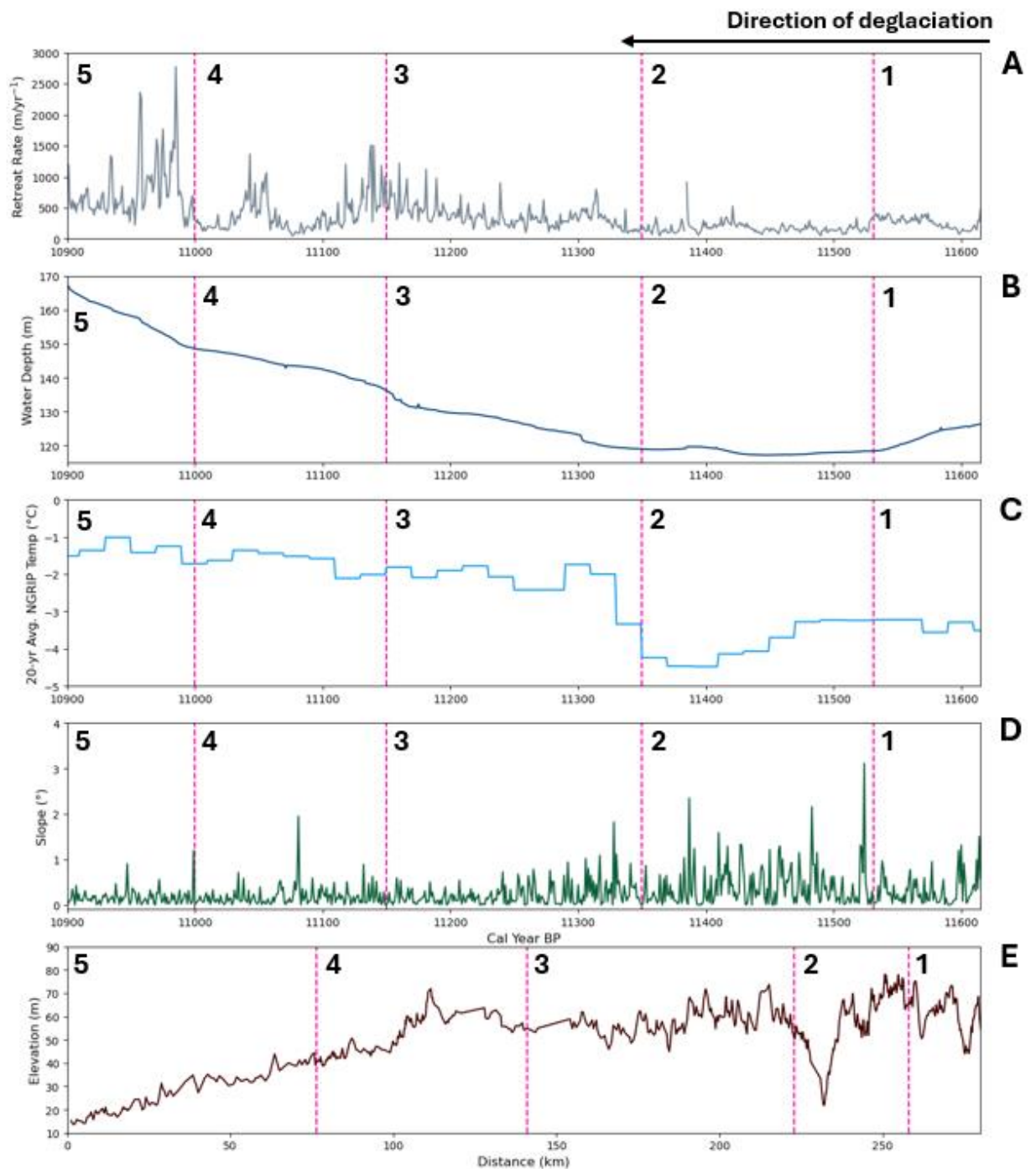
**FIGURE 7.11.** Box plots showing: A) retreat rate (m/yr<sup>-1</sup>), B) water depth (m), C) 20-yr avg. NGRIP temp (°C), D) slope (°), and E) elevation (m) across each time segment; 1) 11 615 – 11 531, 2) 11 530 – 11 350, 3) 11 349 – 11 150, 4) 11 149 – 11 000, 5) 10 999 – 10 901 (FIGURE 7.5). NB: Boxes represent interquartile range, upper and lower bounds of boxes denote upper and lower quartiles respectively, black line within boxes represent median values, 'X' within boxes represent mean average values including outliers, whiskers denote minimum and maximum values excluding outliers.



**FIGURE 7.12.** Annual resolution histograms showing water depth (m) vs retreat rate (m/yr<sup>-1</sup>). Each histogram represents time segments - A: 11 615 – 11 531, B: 11 530 – 11 350, C: 11 349 – 11 150, D: 11 149 – 11 000, E: 10 999 – 10 901 and correspond with the grounding line variable maps presented in FIGURE 7.5.



**FIGURE 7.13.** Annual resolution scatterplots showing retreat rate ( $\text{m/yr}^{-1}$ ) vs slope ( $^{\circ}$ ). Each scatterplot represents time segments - A: 11 615 – 11 531, B: 11 530 – 11 350, C: 11 349 – 11 150, D: 11 149 – 11 000, E: 10 999 – 10 901 and correspond with the grounding line variable maps presented in FIGURE 7.5.



**FIGURE 7.14.** Annual resolution line plots: A) retreat rate ( $\text{m/yr}^{-1}$ ), B) water depth (m), C) 20-yr avg. NGRIP temperature ( $^{\circ}\text{C}$ ), D) slope ( $^{\circ}$ ), vs time (cal. years BP); and E) elevation (m) vs distance (km). Spatiotemporal segments are represented by pink dashed lines to correspond with the time segments shown in FIGURE 7.5 - 1: 11 615 – 11 531, 2: 11 530 – 11 350, 3: 11 349 – 11 150, 4: 11 149 – 11 000, 5: 10 999 – 10 901.

1) 11 615 – 11 531 cal. yr BP: Retreat rate is relatively low during this time period, with a slight increase from ~11 550 cal. yr BP. In addition, annual fluctuations in retreat

rate are minimal during this stage, reflecting a relatively stable ice margin (FIGURES 7.10A & 7.14A). Water depth is relatively low characterised by a decreasing trend (FIGURES 7.10D & 7.14B). Temperatures are relatively low and stable (7.10C & 7.14C). Slope as an indicator of terrain roughness shows a moderate roughness (FIGURES 7.10B & 7.14D) characterised overall by a normal bed slope direction; however, some relatively significant alternations in bed slope direction can be observed in this period (FIGURE 7.14E).

**2) 11 530 – 11 350 cal. yr BP:** This period is characterised by the slowest retreat rates; however, annual fluctuations begin to increase slightly in contrast to the previous time period (FIGURES 7.10A, 7.11 & 7.14A). Water depth is also lowest during this period, which begins to increase slightly from ~11 425 cal. yr BP (FIGURES 7.10D, 7.12B & 7.14B). Temperature continues to remain stable as a continuation from the previous time period and decreases from ~11 475 cal. yr BP (FIGURES 7.10C, 7.11 & 7.14C). Terrain roughness is greatest at this stage (FIGURES 7.10B & 7.14D), characterised overall by an adverse bed slope direction (FIGURE 7.14E).

**3) 11 349 – 11 150 cal. yr BP:** Retreat rate continues to increase during this stage along with progressively increasing annual fluctuations (FIGURES 7.10A, 7.11 & 7.14A). Water depth continues to increase (FIGURES 7.10D, 7.11B & C, & 7.14B). Temperature continues to increase from the previous time period, decreasing slightly from ~11 290 cal. yr BP and returning to a steady increase from ~11 275 cal. yr BP (FIGURE 7.10C, 7.11 & 7.14C). Terrain becomes smoother during this time period (FIGURES 7.10B & 7.14D), characterised by a relatively flat bed topography (FIGURE 7.14E).

**4) 11 149 – 11 000 cal. yr BP:** General and annual fluctuations in retreat rate become more prominent during this period (FIGURES 7.10A, 7.11 & 7.14A). Water depths continue to increase (FIGURES 7.10D, 7.12C & D, & 7.14B), and temperatures remain relatively high (FIGURES 7.10C, 7.11 & 7.14C). Terrain continues to become smoother as a continuation from the previous time period, with a slight increase in roughness at ~11 080 cal. yr BP (FIGURES 7.10B, 7.11 & 7.14D), which coincides with a change in bed slope direction from normal to adverse (FIGURE 7.14E). General fluctuations in retreat rates appear to align with bed slope topography (FIGURE 7.14A & E).



**5) 10 999 – 10 901 cal. yr BP:** Retreat rates continue to increase from the previous time period and annual fluctuations increase dramatically at this stage reflecting an increasingly unstable ice margin (FIGURES 7.10A, 7.11 & 7.14A). Water depths continue to increase at a relatively high rate (FIGURES 7.10D, 7.11, 7.12 D & E, & 7.14B). Temperature remains high (FIGURES 7.10C, 7.11 & 7.14C). Terrain is smoothest during this period (FIGURES 7.10C & 7.14D), characterised overall by an adverse bed slope direction (FIGURE 7.14E).

The annual resolution line plot results (FIGURE 7.14) mirror the general relationships as described from the 20-year average data (section 7.4.1.1), whereby retreat rate increases with greater water depths (FIGURES 7.9A & C), higher temperatures (FIGURE 7.9A & C), and flatter terrain (FIGURE 7.9A, D & E). However, when visualising the data at annual resolution, detailed fluctuations between years can be observed (FIGURE 7.14A). Overall, variability in annual retreat rate increases progressively from time segments (1) to (5) (FIGURE 7.14A) and denotes a more unstable ice margin.

At annual resolution, the relationship between retreat rate and water depth is well defined in FIGURE 7.12, whereby comparisons across each of the time segments show that as water depth increases, occurrences of greater retreat distances can also be observed. When assessing slope as an indicator of terrain roughness, an inverse pattern can be observed, whereby retreat rates increase as terrain becomes smoother, despite statistical analyses revealing only weak correlations, and statistical significance in only some time periods (FIGURE 7.13C & E). Nevertheless, visual observations at annual resolution (FIGURES 7.10 & 14) more clearly depict how terrain facilitates the forcing mechanisms of water depth and temperature. Furthermore, terrain roughness (FIGURE 7.14D), in conjunction with bed slope direction as depicted from the elevation data (FIGURE 7.14E), demonstrates the control of bed topography, whereby increased bed friction and topographic pinning points act to stabilise the ice margin and decrease rates of retreat (FIGURE 7.14A, D & E). Similarly, when bed slope direction is adverse, this acts to enhance rates of retreat (FIGURE 7.14A & E). Overall, the results show that water depth, temperature and topography, as an interconnected dynamic system, provide favourable conditions for an increasingly unstable ice margin as deglaciation progresses.

## 7.5 Discussion

### 7.5.1 Deglaciation chronology and ice margin characteristics

The overall shape and configuration of the DGM-derived reconstruction shows strong similarities to the current highest resolution (100-year; Stroeve *et al.*, 2016), providing an important means of quality control. The DGM-derived reconstruction provides more nuanced information regarding ice margin retreat characteristics and presents a significant improvement to that of the current 100-year resolution (Stroeve *et al.*, 2016) (FIGURES 7.5, 7.6 & 7.7). Furthermore, the refined reconstruction enables more accurate rates of retreat to be quantified.

Considering that DGMs are reflective of ice margin characteristics, based on the formation processes outlined in chapters 5 and 6 (Rivers *et al.*, 2023 & 2024), changes in DGT configuration can be assessed across the study area to make inferences regarding processes at the margin. Regular prominent DGMs are more dominant in the southeast of the study area, just after Salpausselkä III (e.g. segments 1 & 2, FIGURE 7.5), whereas irregular DGMs become more dominant toward the northwest. If prominent DGMs are considered reflective of winter readvances and irregular DGMs are reflective of summer retreat/calving events (Blake, 2000; Bouvier *et al.*, 2015; De Geer, 1889 & 1940; Frödin, 1916; Möller, 1962; Rivers *et al.*, 2024; Sollid & Carlsson, 1984; Larsen *et al.*, 1991; Lindén & Möller, 2005; Sinclair *et al.*, 2018), the regular prominent DGMs in the southeast of the study area may be reflective of a more stable ice margin promoting prominent DGM formation (see chapter 6, section 6.5.2; FIGURE 6.18; Rivers *et al.*, 2024). In contrast, irregular DGM formations may be restricted in these areas due to unfavourable calving conditions imposed by shallower water depths (Benn *et al.*, 2007; Boyce *et al.*, 2007; Ojala *et al.*, 2023; Ojala, 2016; Warren & Kirkbride, 2003). Concurrently, as water depth increases to the northwest of the study area, it can be inferred that calving processes become more prevalent, as reflected by a greater abundance of irregular DGMs and increased retreat rates (FIGURE 7.5). In addition, the good preservation of regular prominent DGMs in the southeast of the study area support the notion that deglaciation was not interrupted by readvances shortly after Salpausselkä III (e.g. segments 1 & 2, FIGURES 7.5 & 7.6).

The DGM-derived reconstruction provides valuable insights into the spatiotemporal properties of ice sheet retreat and margin characteristics. At an annual resolution, sub-ice lobe scale glacier-terminus changes can be reconstructed which is important for delineating glacial dynamics, e.g. stepwise retreat of the grounding line. In addition, the shape and configuration of the ice margin can be assessed very precisely due to the formation processes of DGT. This is important for local studies of deglaciation and shoreline processes. In addition, this study provides additional evidence, combined with double-deltas (FIGURE 7.1), for deciphering the history of the Baltic Sea level, since the onset of DGMs in the study area mark the ice sheet position when drainage to the Yoldia sea level occurred (FIGURE 7.1).

### **7.5.2 Grounding line forcing mechanisms during deglaciation**

The results show that there is no single forcing mechanism driving retreat across the study area. Instead, changes through time can be observed, driven by climate, water depth, and topography. Significantly, evolving strengths and interplay between each of the assessed grounding line mechanisms can be observed across the defined time segments.

#### **7.5.2.1 11 615 – 11 531 cal. yr BP**

During this period, retreat rate is relatively low, although slightly faster than segment (2), with each of the variables acting to suppress ice margin retreat (FIGURES 7.10 & 7.14); namely, low water depths, low temperatures and moderate terrain roughness. Considering bed slope direction, however, whilst this time period is characterised overall by a normal slope direction, there are some moderate to significant alternations between normal and adverse at annual resolution. Despite these alternations, retreat rates do not appear as responsive to these topographic influences when compared with later time periods. This suggests that water depth and temperature are slightly more dominant controls during this time.

#### **7.5.2.2 11 530 – 11 350 cal. yr BP**

This time period is characterised by the slowest retreat rate, shallowest water depths, lowest temperatures and greatest terrain roughness (FIGURE 7.10 & 7.14). Concerning terrain, bed slope direction is overall adverse, with the largest fluctuations in elevation. A slight response in retreat rate to bed slope direction is observed toward the latter end

of this time period, whereby retreat rates increase slightly as adverse bed slope becomes more prominent (FIGURE 7.14A & E). However, the other assessed grounding line variables (water depth, temperature and terrain roughness) appear to provide conditions acting to stabilise the ice margin (7.14A, B, C & D).

#### **7.5.2.3 11 349 – 11 150 cal. yr BP**

Retreat rate continues to increase concurrently with water depth and temperature during this time period (FIGURES 7.10 & 7.14). In addition, topography begins to decrease in roughness and bed slope in general becomes relatively flat. The period between 11 349 to 11 275 cal. yr BP denotes some strong similarities between retreat rate and temperature whereby a slight increase in both variables can be observed; suggesting a greater strength in forcing mechanism at this stage (FIGURE 7.14A & C). As time progresses, the similarities in the trajectory of increase between retreat rates and water depth from ~11 275 cal. yr BP, reflect a possible transition in strength of forcing mechanism from temperature, which appears to stabilise at this point, to water depth (FIGURE 7.14A & B). Similar decreasing trends are observed in terrain roughness during this time, depicting an increasing strength in this variable which acts to facilitate increased retreat rates (FIGURE 7.14A & D).

#### **7.5.2.4 11 149 – 11 000 cal. yr BP**

During this time the ice margin transitions to a much more dynamic and unstable state, characterised by greater fluctuations between years (FIGURES 7.10 & 7.14A). Temperatures remain relatively high, and water depth continues to increase (FIGURE 7.14C & B). Terrain is relatively smooth overall, with some spikes in roughness observed at ~ 11 075 cal. yr BP (FIGURE 7.14D). Patterns of fluctuations in retreat rate can be observed at both annual and decadal-centennial timescales (FIGURES 7.10 & 7.14A). From 11 149 to 11 075 cal. yr BP, bed slope direction changes from normal to adverse, which coincides with a spike in terrain roughness (FIGURE 7.14D & E). As bed slope direction is normal, retreat rates at decadal to centennial timescales slow and then speed up at the point of transition to adverse (FIGURE 7.14A & E). Retreat rate then decreases again as bed slope direction begins to level. This suggests that the alternation between normal to adverse, along with the spike in terrain roughness, may have acted

as a pinning point to stabilise the ice margin. As the ice margin retreated past this point, retreat rates increased. At annual timescales, greater fluctuations in retreat rate appear to coincide with increased water depths and smoother terrain, illustrating an acute responsiveness to more favourable retreat conditions.

#### **7.5.2.5 10 999 – 10 901 cal. yr BP**

Retreat rate overall continues to increase during this time period and is characterised by dramatic fluctuations at annual timescales (FIGURE 7.14A). At this stage, temperatures remain relatively high, and water depth continues to increase at a more rapid rate (FIGURE 7.14C & B). Terrain is smooth during this time period, characterised overall by an adverse bed slope (FIGURE 7.14D & E). Whilst sustained high temperatures provide favourable conditions to facilitate retreat; given the similarities of increasing trajectory between retreat rate, water depth, and bed slope direction (FIGURE 7.14A, B & E), it is reasonable to infer that water depth and terrain are the most dominant controls driving retreat during period. Annual fluctuations in retreat rate are most notable during this period, increasingly so from the previous time segment. Whilst some of the spikes in retreat rate may coincide with limited DGM evidence; water depth and bed slope direction show strong increases during this time period, suggesting that some of the fluctuations are a true insight from the date. This illustrates how increased water depths and adverse bed slopes can elicit a highly dynamic response ice margin retreat. The specific functions of water depth and bed slope are discussed in more detail below (section 7.5.2.6).

#### **7.5.2.6 Grounding line forcing mechanisms**

As highlighted previously, temperature is lowest during time period 11 530 – 11 350 cal. yr BP, which continues to decrease from ~11 500 to 11 400 cal. yr BP, and then returns to period of warming (FIGURES 7.10C & 7.14C). The period of decreased temperatures appears to correspond with the estimated timings of the Preboreal Oscillation (PBO) ~11 500 – 11 150 cal. yr BP (Fisher *et al.*, 2002; Björck *et al.*, 1998; Rasmussen *et al.*, 2007), which spatially coincides with Salpausselkä III and beyond, in direction of deglaciation (FIGURE 7.10). This is important as it has previously been questioned whether the PBO should be attributed to the formation of Salpausselkä III, or whether it should be attributed to the formation Salpausselkä II as a delayed readvance from the YD

(Strömberg, 2005). The data provides evidence to support that Salpausselkä III likely denotes the PBO event (FIGURE 7.10A & C).

The significance of water depth as a driver of retreat has been shown in previous studies whereby Batchelor *et al.* (2023) observed rapid, tidally induced, buoyancy driven retreat rates of up to 610 m/day<sup>-1</sup>. It should be noted that calving rates are an order of magnitude greater in tidewater compared to freshwater environments (Benn *et al.*, 2007; Boyce *et al.*, 2007; Warren *et al.*, 1992; Warren *et al.*, 2001; Warren & Kirkbride, 2003); nevertheless, a positive correlation with water depth and retreat rate is observed across the study area, resulting in high-magnitude retreat rates (e.g. > 1 000 m/yr<sup>-1</sup>) (FIGURE 7.12); a similar relationship to that found by Ojala (2016).

Whilst water depth is considered to be an important control on calving processes (Warren *et al.*, 2001), this relationship is suggested to be a more complex interplay between ice thickness vs water depth (Van der Veen, 1996 & 2002). Whilst tidally influenced buoyancy stresses are irrelevant in our study area due to minimal tidal flexure and wave action in the Baltic Sea basin; when considering calving dynamics at freshwater termini, the results may be reflective of buoyancy-driven hinge-calving caused by surface thinning, which allows the ice margin to reach flotation thickness. This flotation can create an upward bending moment at the margin resulting in calving (Benn *et al.*, 2007; Boyce *et al.*, 2007; Van der Veen, 1996 & 2002; Vieli *et al.*, 2001; Warren *et al.*, 2001). The magnitude of such calving is, however, dependent on how quickly upward bending stresses are imposed and whether they are subsequently relaxed by ice creep (Boyce *et al.*, 2007).

Undercutting by subaqueous melting is another factor also attributed to increased calving at freshwater termini (Benn *et al.*, 2007; Kirkbride & Warren, 1999; Mallalieu *et al.*, 2020; Purdie & Fitzharris, 1999; Warren & Kirkbride, 2003; Haresign & Warren, 2005). The combination of increased surface thinning and subaqueous melting would account for the positive correlations between increased temperatures, greater water depths and increased rates of retreat (FIGURES 7.10A, C & D, 7.11A, B & C & 7.14A, B & C). Other calving controls should also be considered such as sedimentation and topographic pinning points that may reduce calving (Benn *et al.*, 2007; Boyce *et al.*, 2007; Vieli, 2001 & 2002; Warren *et al.*, 1992). Calving controls imposed by bedrock

topography have been observed in DGM internal architecture in the Kurajoki, Porkka region of southwest Finland (see chapter 6; Rivers *et al.*, 2024), thus reinforcing the connection between DGM morphology and ice margin characteristics. Whilst some of the large spikes observed in retreat rate (FIGURE 7.14A) may be attributed to lack of DGT evidence and/or subjectivity of individual DGM designation, they may also be representative of significant calving events. This is particularly noticeable in segment 5, 10 999 – 10 901 cal. yr BP (FIGURE 7.14A).

The interplay between surface thinning due to increased temperatures, greater water depths and topography may be the reason that a strong statistical correlation between retreat rate and individual variables alone cannot be seen (FIGURE 7.8); rather the results reflect the processes from the variables combined. The results show that irregular DGMs may have the potential to inform us of calving dynamics (e.g. a greater abundance of irregular DGMs in areas characterised by greater water depth); however, more thorough investigations of irregular DGMs should be undertaken to accurately ascertain how calving processes specifically relate to irregular DGM formation.

The results from this study show that smooth, shallow-gradient bed topography facilitates increased rates of retreat (segments 4 & 5, FIGURES 7.10A & D, 7.11A, B & E & 7.14A, B & E). This is congruent with previous studies that have observed accelerated retreat rates across similar shallow-gradient bed topography, due to less stability provided by friction and knickpoints, and enhanced buoyancy effects (Batchelor *et al.*, 2023; Catania & Felikson, 2022; Roman *et al.*, 2024). Whilst the terrain in southwest Finland is relatively shallow gradient, the influence of bed slope direction can still be observed whereby slower retreat rates coincide with areas of normal bed slope direction and increase over areas of adverse bed slope direction. The influence of adverse bed slopes on retreat rate alludes to the issue of MISI (see section 7.1), and illustrates how, in the case of this study, shallow-gradient, adverse bed slope topography, can result in very rapid retreat rates ( $\sim 500 - 2\,000$  m/yr<sup>-1</sup> time segment (5); FIGURE 7.14). The rapid retreat rates from this study are consistent with contemporary observations from the Peterman Glacier, Greenland, whereby rates of 1 250 m/yr<sup>-1</sup> were observed along a retrograde bed grounded 500 m below sea level (Millan *et al.*, 2022). Similar rapid pulses of retreat have also been observed at Thwaites Glacier, West Antarctica whereby rates

of  $>2\ 100\ \text{m/yr}^{-1}$  were observed as the grounding zone migrated past stabilising high points (Graham *et al.*, 2022).

Whilst topography alone is unlikely to be a dominant control of ice margin retreat (Greenwood *et al.*, 2021), this study demonstrates how topographic characteristics and sufficient water depths combined can lead to a highly unstable ice margin, and highlight the potential vulnerability associated with adverse, shallow-gradient beds. The data from this study could be used to test and model retreat rates based on various water depths relative to bed slope gradients to more accurately establish the magnitude and scale of grounding line forcing based on the relationship between these two variables.

Whilst some observations and inferences have been made regarding topographic influences on retreat rates, it should be reiterated that the terrain across southwest Finland is generally low gradient, with relatively little change in relief and slope. As such, whilst the data demonstrates that shallow-gradient smooth topography contributes to increased retreat rates (FIGURES 7.10A & B, 7.11A, D & E & 7.14A, D & E), it is difficult to quantify the strength of this forcing mechanism due to minimal change in this variable. Given that ice sheet sensitivity to topographic controls increases with deglaciation and thinning (Åkesson *et al.*, 2018; Benn & Evans, 2010), it would be valuable to apply the method demonstrated in this study to other areas of more variable topography to assess the extent to which bed slope controls retreat rates at annual timescales. This would provide more robust information when considering topographic influences on contemporary ice masses.

### 7.5.3 Precision & limitations

The availability of DGT evidence determines whether, and how accurately, ice margin retreat can be reconstructed. For example, in segments 1 & 2 (FIGURE 7.5), DGT is abundant and comprises largely regularly spaced prominent ridges, resulting in a well constrained ice margin. In the central part of the study area, however, (segment 3 & 4, FIGURE 7.5), DGT becomes sparse resulting in a more subjective ice margin. Nevertheless, the ability to anchor the designated individual DGMs to the established annual clay-varve chronology (Strömberg, 2005), without imposing significant distortion to the overall pattern and configuration of the reconstruction (FIGURE 7.6), confirms that any subjectivity in this study has not resulted in unrealistic results.



Regarding availability of DGM evidence, in this study, some of the spiked increases in retreat rate coincide with limited DGM data and therefore interpretations should be taken with care. Nevertheless, based on comparability with contemporary studies, the interpretations made are not implausible and are likely representative to a reasonable extent.

When DGMs appear as regularly spaced prominent ridges, they are considered to be a true reflection of annual rates of ice margin retreat, as suggested in previous studies (Bouvier *et al.*, 2015; De Geer, 1940; Larsen *et al.*, 1991; Lindén & Möller, 2005; Möller, 1962; Rivers *et al.*, 2024; Sinclair *et al.*, 2018; Zilliacus, 1981). The results from this study support the concept of annual cycles for the formation of prominent DGMs, whereby DGM-derived isochrones are well constrained and correspond easily with the local clay varve chronology (e.g. FIGURES 7.3, 7.4, 7.5 & 7.6; segments 1 & 2). When considering the presence of irregular DGMs, these are considered to be reflective of inter-seasonal ice margin retreat patterns (e.g. periods of summer retreat/calving), as suggested in previous studies (Bouvier *et al.*, 2015; Frödin, 1916; Lindén & Möller, 2005; Möller, 1962; Rivers *et al.*, 2024); however, DGM formation controls must also be considered. If sediment availability is low, winter readvance is minimal, and postglacial reworkings are strong, 'prominent' annual DGMs may be difficult to distinguish from smaller, irregular DGMs. For these reasons, in areas of DGT comprising irregular ridges, annual isochrones may still be designated (the number of which can be informed by local varve chronology); however, this inevitably introduces a degree of subjectivity to the reconstruction.

In this reconstruction, errors are bounded between successive clay-varve sites (FIGURE 7.3), and comparisons with existing reconstructions (FIGURES 7.6 & 7.7) (e.g. Stroeve *et al.*, 2016) provide some quality control to check the plausibility of designated DGMs. Given that an annual ice margin reconstruction has been developed across southwest Finland showing good correspondence with local clay-varved chronologies and existing reconstructions, this provides very strong evidence to support that DGMs can be utilised as annual ice margin retreat indicators. Inter-seasonal DGMs in areas of more complex DGT cannot be overlooked however, and in some instances

these ridges must be integrated and designated as annual ice margin indicators but characterised by a greater uncertainty.

## 7.6 Conclusions

This chapter demonstrates the utility of DGMs as annual ice margin geochronometric indicators across the southwest Finnish sector of the FIS. A significantly improved delineation of configuration, pattern and rate of ice margin retreat across the study area is presented, along with assessments of the strength of grounding line forcing mechanisms, temperature, water depth and topography.

The results show that there is no single forcing mechanism driving retreat across the study area. Instead, it is found that different combinations of forcings dominate through time driven by climate, bed slope, water depth, and to a small degree, terrain roughness. The results show that ice retreat rate is suppressed between 11 615 – 11 300 cal. yr BP, which appears to coincide with the estimating timings of the PBO. The results show water depth to be a significant driver of ice margin retreat whereby greater water depths, facilitated by smooth, shallow-gradient topography, result in enhanced calving and ice margin retreat due to buoyancy-driven hinge-calving mechanisms. The role of topography in this study demonstrates how less resistance at the bed-ice interface and less stability provided by topographic highs and pinning points enhances ice margin retreat. Significantly, the results reflect the interconnected processes, and evolution in strength, between temperature, water depth and topography.

The DGM-derived reconstruction provides valuable insights into the spatiotemporal properties of ice margin retreat and characteristics. At an annual resolution, sub-ice lobe scale glacier-terminus changes can be reconstructed, which is important for understanding glacial dynamics, e.g. stepwise retreat of the grounding line. In addition, the preservation of DGT means that the shape and configuration of the ice margin can be delineated very precisely. This is important for local studies of deglaciation and shoreline processes. In addition, this study provides additional evidence for deciphering the history of the Baltic Sea level, since the onset of DGMs in the study area mark the ice sheet position when drainage to the Yoldia sea level occurred. Moreover, this work demonstrates that with an annual DGM-derived reconstruction, interplay between grounding line forcing mechanisms can be observed and the strength and evolution of

individual mechanisms can be quantified over space and time. As such, DGM-derived reconstructions can improve understanding of grounding line forcing mechanisms of former ice sheets and use this information to better predict changes in contemporary ice sheets.

## Chapter 8: Discussion

This chapter synthesizes the results outlined in chapters 5-7 and discusses these in the context of the research questions outlined in chapter 1 (sections 1.2.1 & 1.2.2; and reiterated below); specifically focusing on the formation of DGMs, their temporal dynamics, and their role in reconstructing ice margin positions and rates of retreat. The discussion is structured to address each research question in turn, beginning with a short, bulleted summary of key findings respectively. Limitations and directions for future research are also discussed.

### 8.1 Research questions

RQ1) How do DGMs form, and how do they reflect the position of ice margins?

RQ2) At what timescales do DGMs form?

RQ3) How does increasing spatial and temporal resolutions of ice sheet reconstructions help to improve the current understanding of ice sheet retreat rate and grounding line processes?

### 8.2 Research objectives

RO1) Constrain DGM formation processes via triangulation of morphometric, sedimentological, and geophysical datasets.

RO2) Constrain the timescale of DGM formation by comparing established varve chronologies to DGM distribution.

RO3) Produce a refined palaeo-ice marginal reconstruction at very high spatiotemporal resolutions based on the quantification of, and reconciliation between, geomorphological evidence and geochronological/palaeo-climate records.

### 8.3 RQ1: How do DGMs form, and how do they reflect the position of ice margins?

This research question was addressed through the undertaking of research objective (1), specifically, investigating DGM morphometry via remote sensing methods (chapter 5) and investigating internal architecture via sedimentological and geophysical analyses (chapter 6).

### **8.3.1 Key morphometry & spatial distribution findings (chapter 5):**

- DGMs are generally lower amplitude, more sinuous and more asymmetric in profile compared to CSRs.
- The asymmetry, sinuosity and lateral discontinuity of DGMs provide evidence to support a unidirectional push process at the ice margin, rather than crevasse infilling.
- CSRs present as generally straight landforms with symmetric profiles, reflecting deposition within basal crevasses. Variable morphology along individual CSRs likely reflects the shape of the hosting crevasse in which material was deposited.
- Comparisons between prominent and intermediate DGMs show prominent DGMs to be slightly greater in length and width, and slightly more asymmetric in profile.
- Morphometry alone does not provide enough evidence to elucidate any differences in formation properties between prominent and intermediate DGMs.
- DGM morphometry varies over wide spatial areas, likely reflective of environmental factors such as sediment/meltwater availability, topography, water depth, and ice thickness.
- DGT (e.g. larger fields of DGMs) can be classified into three subtypes; i) regularly spaced prominent DGMs only, ii) regularly spaced prominent DGMs interspersed with irregularly spaced intermediate DGMs, and iii) only irregularly spaced intermediate DGMs.

### **8.3.2 Key internal architecture findings (chapter 6):**

- The internal architecture of DGMs supports formation at the grounding line whereby proximal sides are characterised by laminae, stratification, and thrust plane structures, and distal sides comprise poorly consolidated diamicton and reworked sediments from proglacial water currents. The proximal to distal differences are indicative of unidirectional push processes at the ice margin, congruent with inferences derived from the morphometry results (chapter 5).
- Generally, prominent and intermediate DGMs comprise the same internal architecture, reflecting similar formation processes; however, prominent DGMs present stronger push deformation structures compared to intermediate DGMs,

whereas intermediate DGMs comprise larger lower glaciofluvial units compared to prominent DGMs.

- The slight differences in internal architecture between prominent and intermediate DGMs suggest seasonal variability during formation, whereby prominent DGMs are suggested to form during winter readvances and intermediate DGMs are suggested to form during periods of summer retreat. This interseasonal variability highlights the importance of identifying, differentiating between, and integrating, different DGM-subtypes when considering utility as ice margin geochronometric indicators.

The uncertainties surrounding DGM formation has presented challenges when attempting to position these landforms in a wider ice sheet context and has limited their use for understanding ice sheet dynamics. The two dominant formation hypotheses are i) formation via push at the grounding line of a subaqueous ice margin (Aartolahti *et al.*, 1995; Blake, 2000; Bouvier *et al.*, 2015; Borgström, 1979; Dix & Duck, 2000; Finlayson *et al.*, 2007; Golledge & Phillips, 2008; Larsen *et al.*, 1991; Lindén & Möller, 2005; Smith, 1982; Smith & Hunter, 1989), and ii) formation via basal sediment squeeze-up into basal crevasses (e.g. crevasse-squeeze ridges (CSRs) (Beaudry & Prichonnet, 1991 & 1995; Sharp, 1985; Strömberg, 1965; Zilliacus, 1989) (see section 2.4.1). If DGMs form at the grounding line, they would provide information relative to ice margin retreat processes and grounding line forcing mechanisms; if they form within basal crevasses, they can provide information relative to subglacial hydrology, pressure and stress regimes. These two dominant formation ideas present difficulties when differentiating between DGMs and CSRs. Whilst many studies generally lean toward DGM formation at the grounding line (Aartolahti *et al.*, 1995; Blake, 2000; Bouvier *et al.*, 2015; Borgström, 1979; Dix & Duck, 2000; Finlayson *et al.*, 2007; Golledge & Phillips, 2008; Larsen *et al.*, 1991; Lindén & Möller, 2005; Smith, 1982; Smith & Hunter, 1989), uncertainty has still prevented accurate integration and utility within ice sheet reconstructions.

The morphometry results presented in chapter 5 capture and quantify morphometric differences between DGMs mapped in southwest Finland and CSRs mapped in Northwest Territories, Canada (TABLES 5.1, 5.2, 5.3, 5.4 & 5.5; FIGURES 5.5, 5.6, 5.7 & 5.8). DGMs were generally found to be lower amplitude, slightly more sinuous and often asymmetric in profile. In contrast, CSRs were found to be relatively straight, greater in

width and height, and symmetric in profile. In addition, individual CSRs were found to be more variable across the length of individual landforms compared to DGMs, often widest centrally and narrowing laterally (FIGURE 5.6C). It should be reiterated that CSRs were found to be greater length compared to DGMs; however, this is likely due to lateral discontinuity of DGMs from postglacial reworking and ice margin properties during formation. As such, these findings are more reflective of mapping strategies rather than a true observation of the data. The asymmetric characteristics of DGMs suggest a unidirectional push process occurring at the ice margin (Blake, 2000; Finlayson *et al.*, 2007; Golledge & Phillips, 2008; Linden & Moller, 2005; Ojala *et al.*, 2015). This is further supported by sinuous and laterally discontinuous characteristics which likely reflect the shape and configuration of the ice margin during the time of formation (Aartolahti, 1972; Lindén & Möller, 2005; Ottesen *et al.*, 2008). In contrast, the variable size of CSRs observed across individual landforms, in conjunction with the straight and symmetric properties, likely reflect the shape of the hosting crevasses in which sediments are deposited (Evans *et al.*, 2016; Price & Whillans, 2001; Whillans & van der Veen, 2001). As such, the quantified morphometric characteristics from this study can be used for distinguishing between DGM and CSR landform groups, and to provide evidence for positioning DGMs at the ice margin of ice sheets.

Concerning landform differentiation, care should be taken when identifying landforms based on generalised morphometric differences. For example, the asymmetric characteristics of DGMs are reported in previous studies; however, symmetric properties have also been observed (Hoppe, 1959; Golledge & Phillips *et al.*, 2008; Ojala *et al.*, 2015). As such, a single morphometric parameter should not be used as a sole identifier of DGMs or means of differentiation from CSRs. Instead, landform identification and differentiation should be based on several morphometric attributes combined with other characteristics such as spatial distribution and environmental parameters (Chandler *et al.*, 2018).

In addition to comparisons between DGMs and CSRs, DGMs were also subdivided into regularly spaced 'prominent' ridges and irregularly spaced 'intermediate' ridges and analysed for similarities/differences (see section 5.6.7). The results show prominent DGMs to be longer, wider and slightly more asymmetric in profile compared to intermediate DGMs. Generally, height and sinuosity are similar between the two DGM

sub-types, although intermediate DGMs tend to show more variability in sinuosity compared with prominent DGMs. Prominent and intermediate DGMs can generally be distinguished by observing spatial pattern and distribution relative to one another; however, more detailed quantified morphometrics are valuable when spatial observations become more problematic due to factors such as postglacial reworking, sediment availability and ice margin dynamics. For example, if sediment availability is low, postglacial reworking is high, and the pushing capacity of the ice margin is minimal, prominent DGMs may appear smaller and similar to intermediate DGMs (Aartolahti, 1972). The observable differences in spatial distribution and morphometry between prominent and intermediate DGMs present uncertainties regarding formation processes. For example, it could be that intermediate DGMs form via similar processes to prominent DGMs at the grounding line, or via alternative processes, such as crevasse infilling up-ice behind the grounding line. Given the morphological similarities between the two DGM sub-types, the balance of probability suggests that they are formed via similar processes at the grounding line; however, observations of internal architecture are required to confirm this and are discussed below.

The sedimentological and geophysical investigations presented in chapter 6 allowed the internal architecture of DGMs to be more thoroughly investigated to better understand the formation of DGMs. In addition, these investigations enabled detailed comparative analyses between prominent and intermediate DGMs allowing mode of formation to be linked with morphometric characteristics. The general architecture of the investigated DGMs present a multi-phase structure with lower units representing subglacial traction till and ice marginal infill deposits, truncated by a larger prominent push unit, which is then successively deformed via the overriding of active ice (see section 6.5.1). The studied DGMs show notable differences between proximal and distal sides, with proximal sides characterised by laminae, stratification and thrust planes, and distal sides characterised by poorly consolidated diamicton and proglacial water current reworkings. These proximal-distal differences provide very strong evidence to support that DGMs are formed at the ice margin via unidirectional push processes (Lønne & Nemec, 2011).

The comparisons between prominent and intermediate DGMs across a number of different locations show that generally internal architecture is similar, thus reflecting



similar formation processes; however, slight differences can be observed in the height and prominence of the lower sediment Unit 2 (FIGURES 6.5 & 6.9; section 6.5.1) which comprises glaciofluvial material, and is interpreted as being deposited either at, or behind the grounding line in crevasses, or via distributed or channelised subglacial flow. Deformation structures are also observed in this unit, likely caused by exerted stress from moving ice. This unit appears larger within the observed intermediate ridges. In addition, thrust plane structures within upper units tend to correlate with amplitude whereby larger prominent DGMs show stronger push deformation structures. This is congruent with the morphometric observations outlined in chapter 5 whereby larger prominent DGMs show greater asymmetry compared to smaller intermediate DGMs. The differences observed between prominent and intermediate DGMs are interpreted to reflect inter-seasonal differences during formation which is illustrated in the bi-seasonal formation model presented in section 6.5.2 (FIGURE 6.18). This model shows that prominent DGMs are formed during a winter readvance, thus resulting in strong push characteristics, whereas intermediate DGMs are formed during summer retreat, which is supported by evidence of larger glaciofluvial units due to higher melt and less pushing structures due to the margin being in a state of retreat.

The spatial pattern and distribution of DGMs is a key attribute in which DGM land assemblages can be identified; namely, a series of regularly spaced, elongated ridges, oriented transverse to former ice flow direction, generally resembling a ‘washboard-like’ appearance (FIGURES 2.10 & 5.1) (De Geer 1889 & 1940; Hoppe 1959; Benn & Evans 2010; Ojala *et al.* 2015; Ojala 2016). As previously highlighted, morphometry of individual DGMs can vary across wide spatial areas (e.g. DGMs in northwest of SW Finland are larger compared with ridges in the southeast); however, the spatial pattern and distribution of ridges can also vary between different areas of DGT. This can be understood when distinguishing between regularly spaced prominent DGMs, and irregularly spaced, intermediate DGMs. Generally, DGT configuration can be sub-classified as; 1) only regularly spaced prominent ridges, 2) regularly spaced, prominent ridges, interspersed with irregularly spaced, intermediate ridges, and 3) only irregularly spaced intermediate ridges (FIGURE 6.2). These variations correspond with the findings presented in chapter 6, whereby regularly spaced prominent ridges represent annual cycles of winter readvance, and irregularly spaced intermediate ridges represent the ice

margin during periods of summer retreat. This means that variations in DGT configuration may inform us of inter-seasonal ice margin dynamics as well as rates of ice margin retreat. As such, it is important to be able to identify and distinguish between the two DGM sub-types as they present different implications for ice margin reconstructions.

When considering different DGT configurations, the extent to which regularly spaced prominent ridges can be easily identified ultimately determines the level of confidence to which an annual signal can be estimated. The presence of intermediate ridges introduces a degree of uncertainty; however, the utility of these ridge types is also important for the purposes of ice margin reconstructions as some intermediate ridges may also represent annual ice margin positions. The morphology and prominence of a ridge is determined by sediment and meltwater availability, topography, water depth, the pushing capacity/thickness/geometry of the ice margin, and postglacial reworking (Aartolahti, 1972; Barr & Lovell, 2014; Bennett, 2001; Lønne & Nemec 2011; Lukas, 2012; Ojala, 2016; Rettig *et al.*, 2023; Simkins *et al.*, 2018); therefore if the ice margin is in a constant state of retreat and instability, a large prominent DGM formed by ice margin readvance may not be identifiable. As the ice margin thins and continues to retreat, the size of ridges will reflect this. This can be seen in section 5.5.4.2, FIGURE 5.7, whereby DGM morphometry and configuration varies across southwest Finland with wider more regularly spaced DGMs observed in the southwest and taller more irregularly spaced DGMs observed in the northwest. As such, in areas of more complex DGT, an annual signal may not be easily identifiable by visual observations alone and may require a reliance on local clay-varve chronologies to provide a means of estimation. Moreover, DGT is not ubiquitous (as can be observed central to southwest Finland (FIGURE 7.1)) and formation may only occur if environmental parameters and ice margin dynamics are favourable. This presents additional challenges when estimating continually successive rates of retreat.

## **8.4 RQ2: At what timescales do DGMs form?**

### **8.4.1 Key findings (chapters 6 & 7)**

- Previous studies largely acknowledge that DGMs are to some extent annual formations; however, uncertainties arise due to 'additional ridges' being present

when attempting to correlate with annual chronologies. These ‘additional ridges’ likely represent intermediate DGMs that are formed during periods of summer retreat.

- A strong correspondence is observed between prominent DGMs in southwest Finland and the established local clay-varved chronology (Strömberg, 2005). In areas more abundant with intermediate DGMs, a more subjective designation of ‘annual DGMs’ is employed, guided by the local clay-varved chronology.
- The observed bi-seasonal signals within DGT are congruent with the proposed model of prominent DGMs forming during winter readvances and intermediate DGMs forming during periods of summer retreat (chapter 6).
- The temporal evidence, along with the evidence from morphometric analyses (chapter 5) and internal architecture (chapter 6), resolve the ambiguities regarding DGM spatiotemporal formation properties (RQs 1 & 2), whereby DGMs are formed bi-seasonally at the grounding line of water-terminating ice margins.

Many studies acknowledge that DGM formation may, to some extent, occur at an annual periodicity (De Geer 1940; Ojala, 2016; Möller 1962; Zilliacus 1981; Larsen *et al.* 1991; Lindén & Möller 2005; Bouvier *et al.* 2015; Sinclair *et al.* 2018); however, often a greater number of ridges are observed compared to the number required by independent chronologies (Hoppe 1959; Lindén & Möller 2005; Möller 1962; Sollid 1989; Zilliacus 1981, 1989). As highlighted in section 6.5, these ‘additional ridges’ are likely irregularly spaced intermediate DGMs, that represent summer season formations, rather than winter readvance formations.

The comparisons between DGMs in southwest Finland and the local clay-varved chronology (Strömberg, 2005) show good correspondence between the number of observed DGMs and the number required by the varve chronology; however, the quality of correspondence was dependent on DGT configuration (see chapter 7). In areas of only regularly spaced prominent DGMs, ridge occurrence corresponds very well with successive dates between clay-varve sites, thus delineating a well-constrained annual signal. In areas of more complex DGT (e.g. a greater number of irregularly spaced intermediate DGMs), confidence levels decreased and designated DGMs (the number of which was guided by the clay-varve chronology) became more subjective (section

7.3.2, FIGURE 7.2). Nevertheless, an annual DGM pattern connected to the local annual clay-varved chronology was successfully defined across the entire study area (sections 7.3 & 7.4, FIGURES 7.3 & 7.5).

Comparisons with the highest-resolution ice margin reconstruction in the area (e.g. 100-year; Stroeve *et al.*, 2016) showed strong similarities between overall pattern and shape, providing a reasonable measure of accuracy for the results. As such, building on the findings derived from the morphometric (chapter 5) and internal architecture investigations (chapter 6), the high-level of correspondence between the local clay-varved chronology and DGM occurrence in areas of well-preserved prominent ridges, along with the ability to successfully estimate an annual signal amongst irregular intermediate DGMs, provide very strong evidence to support the suggested bi-seasonality of DGT formation as proposed in section 6.5.2, FIGURE 6.18, thus resolving RQ2.

## **8.5 RQ3: How does increased spatial and temporal resolutions in ice sheet reconstructions help to improve the current understanding of ice sheet retreat rate and grounding line processes?**

### **8.5.1 Key findings (chapter 7)**

- The DGM-derived reconstruction provides a highly nuanced understanding of ice margin retreat rate and dynamics in southwest Finland and provides an annual refinement of the existing 100-year resolution reconstruction (Stroeve *et al.*, 2016).
- The refinement captures significant fluctuations in retreat rate, delineating episodic rather than uniform retreat.
- The DGM-derived reconstruction reveals interconnected controls between temperature, water depth and terrain, driving ice margin retreat.
- Greater fluctuations between annual rates of retreat likely reflect the increasing instability of the ice margin as deglaciation progresses and may correspond to significant calving events driven by surface ice thinning and increasing water depths.

- A key benefit of the DGM-derived reconstruction is the ability to delineate annual rates of retreat spanning hundreds of years in contrast to contemporary ice sheets which are often limited to decadal observations.
- Rapid retreat rates observed in this study highlight flatbed topography as a key vulnerability when considering contemporary ice sheet retreat.

The estimated annual signal identified by comparisons between DGM occurrence and local clay-varved chronology was used to develop an ice margin reconstruction across southwest Finland, whereby each ‘annual’ DGM was extended laterally and designated as an ice margin isochrone (see chapter 7, FIGURES 7.5 & 7.6). The DGM-derived reconstruction shows strong similarities between general ice margin configuration and pattern of retreat to that of the current highest resolution (100-year; Stroeve *et al.*, 2016) in the study area. When comparing rates of retreat, the DGM-derived reconstruction provides significantly more nuanced detail and greatly improves our understanding of ice margin behaviour and retreat dynamics across southwest Finland (section 7.4, FIGURES 7.6, 7.7, 7.10, 7.11 & 7.14). In addition, a more accurate quantification of retreat rate can be estimated based on the interdistances measured between each annually successive DGM isochrone. The more detailed depiction of annual fluctuations in retreat distance that can be seen in FIGURE 7.7. In contrast to the coarser resolution presented by Stroeve *et al.* (2016), this illustrates an episodic rather than uniform ice margin retreat pattern. The fluctuations depicted in the DGM-derived reconstruction infer variability in grounding line controls that can be observed at annual-centennial timescales.

The results show that there is no single grounding line forcing mechanism driving grounding line retreat across the study area. Instead, the results show interconnected dynamics of different controls that evolve through space and time. The drivers analysed in this study were, i) temperature, ii) water depth and iii) terrain (e.g. slope/roughness and elevation) (section 7.4.1). The interconnected dynamics between temperature and water depth is particularly notable whereby temperature is a more dominant driver between 11 615 – 11 300 cal. yr BP and as deglaciation continues water depth becomes a more dominant driver between from 11 300 cal. yr BP onwards (section 7.4.1, FIGURES 7.8, 7.9, 7.10, 7.11 & 7.14). The variability in driving mechanisms coincide with DGT configuration, whereby DGMs in the southwest of the study area are prominent and

regularly spaced, concomitant with temperature as a dominant control; in contrast to DGMs in the northwest of the study area, that are more irregularly spaced as water depth increases.

As described in sections 7.4.1 & 7.5.2, the relationships between temperature, water depth and grounding line retreat are complex and likely reflect processes of buoyancy-driven hinge-calving. This is caused by surface thinning due to increased temperatures which allows the ice margin to reach flotation thickness, creating an upward bending moment and inducing calving (Benn *et al.*, 2007; Boyce *et al.*, 2007; Warren *et al.*, 1992; Warren *et al.*, 2001; Warren & Kirkbride, 2003; Van der Veen, 1996 & 2002; Vieli *et al.*, 2001). Each of these factors, combined with a relatively low-gradient, smooth bed topography promote enhanced calving (Batchelor *et al.*, 2023; Benn *et al.*, 2007; Boyce *et al.*, 2007; Catania & Felikson, 2022; Roman *et al.*, 2024; Vieli, 2001 & 2002; Warren *et al.*, 1992). Whilst the DGM-derived reconstruction delineates a general increase in retreat rate across the study area (similar to that shown by Stroeve *et al.*, 2016) coinciding with increasing temperatures and water depths, the same can also be observed when assessing the extent of annual fluctuations in retreat rate (section 7.4.1, TABLE 7.1; FIGURES 7.7 & 7.11). From 11 300 cal. yr BP, annual fluctuations in retreat rate become greater and more dynamic, reflecting the increasing instability of the ice margin as deglaciation continues. As such, the greater fluctuations in retreat rate that can be observed in FIGURE 7.14 may denote significant calving events.

Considering comparability with contemporary ice sheets, studies of retreat rates across Thwaites Glacier in West Antarctica have been shown to range between > 2 100 m/yr (Graham *et al.*, 2022) to ~300 m/yr (Milillo *et al.*, 2019); however, palaeo-studies of grounding line landforms on the seafloor at the Larson continental ice shelf, western Weddell Sea, have also revealed estimated retreat rates of > 10 000 m/yr (Dowdeswell *et al.*, 2020). Retreat rates of ~95 m/yr have been observed at Pine Island Glacier, Antarctica (Park *et al.*, 2023); ~50 m/yr at Milne Glacier, northern coast of Ellesmere Island, Canada (Antropova *et al.*, 2024); 250 m/yr at Denman Glacier, East Antarctica (Brancato *et al.*, 2020); and rates of up to ~240 m/yr have been observed at Petermann Glacier, Greenland (Millan *et al.*, 2022). The DGM-derived reconstruction presented in chapter 6 shows similar variability in retreat rates ranging between 52 and 2 773 m/yr, with a mean average of 333 m/yr. The observed ranges in retreat rate are considerable

and highlight the importance of understanding the forcing mechanisms that drive such variability.

Several factors can influence rates of ice margin retreat, such as: climate, terminus environment (e.g. terrestrial, lacustrine, marine), proglacial water depth and temperature, interactions and configuration at the ice-bed-ocean interface (e.g. basal cavities, intrusion of warm seawater beneath the ice), topography, surface and basal ice melt, subglacial hydrology and pressure regimes (Baumhoer *et al.*, 2021; Benn & Evans, 2010; Clark *et al.*, 2012 & 2021; Jones *et al.*, 2021; Pollard *et al.*, 2015; Post *et al.*, 2021). Many of these factors are entangled and susceptible to amplifying feedback cycles (Albrecht *et al.*, 2024; Fyke *et al.*, 2018; Li *et al.*, 2024; Ren & Leslie, 2011). This can be seen in the DGM-derived reconstruction whereby interconnected relationships between temperature, water depth and topography govern grounding line retreat (chapter 7; FIGURES 7.11 & 7.14).

Bed topography is an important, albeit complex, control of ice margin retreat (Benn & Evans, 2010; Catania & Felikson, 2023; Goodship & Alexanderson, 2020; Greenwood *et al.*, 2021; Jones *et al.*, 2021; Knight, 1999; Post *et al.*, 2021) and is particularly notable when considering Marine Ice Sheet Instability (MISI), the concept whereby when bed topography is retrograde (e.g. sloping downward in an up-ice direction), the grounding line is unstable and predisposed to rapid retreat (Pattyn, 2018; Schoof, 2007; Weertman, 1974). The results from this study showed increased retreat rates facilitated by topography in southwest Finland, due to smooth, shallow-gradient bed characteristics that likely promoted enhanced buoyancy and less basal friction due to a lack of stabilising bed features. Similar rapid retreat rates across flat, shallow-gradient beds have been reported in previous studies (Batchelor *et al.*, 2023; Dowdeswell *et al.*, 2020). This highlights that whilst some studies demonstrate the potential vulnerabilities associated with retrograde bed slopes (Gandy *et al.*, 2018; Hill *et al.*, 2023; Schoof, 2007; Sergienko & Wingham, 2022; Reese *et al.*, 2023); flat/shallow-gradient bed topography must also be considered as a key vulnerability when assessing contemporary ice sheet retreat. As such, it would be valuable to utilise the information from this study within numerical models to investigate the magnitude of influence from flatbed topographies relative to annual rates of retreat and identify key areas of vulnerability across contemporary ice sheets. Furthermore, a key advantage of this study is that whilst

contemporary studies can observe annual rates of retreat, these can often be limited to decadal, sometimes monthly timescales (Antropova *et al.*, 2024; Brancato *et al.*, 2020; Graham *et al.*, 2022; Millan *et al.*, 2022; Milillo *et al.*, 2019; Park *et al.*, 2013; Rignot, 1998; Rignot *et al.*, 2014; Schmidt *et al.*, 2023). In contrast, this study provides an annual record of retreat spanning several hundreds of years, offering a more robust dataset for utility within numerical models to develop deglaciation simulations.

## 8.6 Limitations

Upon conducting this study, limitations have been assessed and outlined below:

### 8.6.1 Methodological challenges

- The utilisation of DGMs as ice margin indicators requires a careful approach when considering which DGMs to designate as ‘annual’. This is particularly pertinent in areas of complex DGT (e.g. fields of combined prominent and irregular ridges, and fields of only irregular ridges). The greater presence of irregular ridges increases uncertainty with respect to the reconstruction outputs.
- The study area spans a width of ~125 km, as such, laterally extending and adjoining discontinuous DGMs across large distances poses the risk of ‘spatial wandering’ and presents the potential to distort the position and configuration of the reconstructed ice margin.
- A major constraint when developing a DGM-derived ice margin reconstruction is that DGT is not ubiquitous. To establish a reasonable ice margin reconstruction, DGT must be abundant and individual DGMs must be well-preserved. As such, some estimated retreat distances between ‘successive DGMs’ may be over-estimated due to the absence, or impractical identification of DGM evidence.
- The second major constraint is anchoring an accurate chronology to constructed DGM isochrones. The most obvious and accurate geochronological datasets are local clay-varved chronologies, as demonstrated in this study, due to the annual resolution. If this study was to be repeated in areas without an established annual chronology, alternative methods may be used, such as cosmogenic nuclide dating, that can provide an estimated time anchor, and an annual chronology can be inferred from this.



- Fieldwork in this study was generally successful, and enabled DGMs to be sampled in several different locations across SW Finland; however, the study was geographically limited and poses issue of representativity from the sampled DGMs in contrast with those located further afield. As such, if funding and time permitted, a geographically wider field study characterised by a larger sample size would be advantageous.

#### 8.6.2 Analyses & cumulative errors

- Disparities in resolution between different datasets (e.g. annual clay varve chronology, annual DGMs and 20-year average NGRIP) presents challenges when attempting to associate the magnitude of impact relative to different drivers of retreat. Similarly, the cumulative error between datasets must be considered. A systematic approach to the sampling strategy was undertaken as a measure of mitigation; nevertheless, these potential errors should be acknowledged.
- The climate data in this study was derived from the NGRIP temperature records (Vinther *et al.*, 2009) and therefore an assumption was permitted that the Greenland climate was representative of southwest Finland. This is a reasonable assumption to allow, but consideration of this should also be acknowledged.

#### 8.6.3 Implications & comparability

- When comparing retreat rates observed in this study with those from contemporary studies, individual parameters of each glacier must be taken into consideration to validate comparability. For example, the southwest Finnish sector of the FIS (e.g. the southern Baltic Sea Ice Lobe) was grounded on relatively flat, shallow-gradient topography and terminated in the Baltic Ice Lake (see section 3.3.1). In contrast, for example, Thwaites Glacier is marine terminating, influenced by tidal processes and variable convection dynamics at the grounding line interface, and characterised by stabilising ridges at the bed (Anselin *et al.*, 2023; Morlighem *et al.*, 2019; Padman *et al.*, 2018; Schmidt *et al.*, 2023). As such, direct comparison between rates of retreat may not always be appropriate. Nevertheless, insights from this study may be used to inform of glacier retreat dynamics across similar environments, e.g. outlets retreating over areas of flatter topography, terminating in laterally unconstrained lacustrine environments.

## 8.7 Directions for future research

### 8.7.1 Expand spatial analysis

- Identifying key areas of DGT across the entire FIS would be valuable to develop a refined ice sheet wide reconstruction. This work may also extend to the Laurentide Ice Sheet for example, where DGM evidence is abundant in the Hudson Bay area (Josenhans & Zevenhuizen, 1990; Lajeunesse, 2008) and could potentially be extended to the margins of the Antarctic and Greenland Ice Sheets (Batchelor *et al.*, 2019; Winkelmann *et al.*, 2010). Investigating DGMs in contemporary glacial environments would complement the findings from this work by strengthening process-form understanding. This would also enable DGM comparisons across wider geographical areas and elucidate any unknown variations in spatial and temporal properties.

### 8.7.2 Investigate calving processes

- Regarding DGM investigations, most studies have focused on regularly spaced prominent DGMs, leaving irregularly spaced intermediate DGMs often overlooked and underrepresented, thus highlighting an area for further development. This may include developing on the work presented in chapter 6 (e.g. internal architecture investigations), characterised by a wider geographical study area and larger sample size. Furthermore, given the suggested formation properties of intermediate DGMs (e.g. formation via calving during periods of summer retreat) (chapter 6; Lindén & Möller, 2005), a more thorough investigation of intermediate DGMs may offer specific insights regarding calving mechanisms, ridge construction and grounding line dynamics (Benn *et al.*, 2007; Warren, 1991 & 1992).

### 8.7.3 Investigate slope as a grounding line variable

- The analysis of slope as a grounding variable in this study, revealed minimal statically significant findings; however, this is likely due to slope variability being relatively minimal across southwest Finland. Topography is a key control on moraine formation and distribution (Barr & Lovell, 2014; Boston *et al.*, 2023; Rowan *et al.*, 2022; Warren, 1991 & 1992) and introduces a layer of complexity when interpreting moraines for their palaeo-climatic significance. Whilst topography is a key research focus within contemporary glacial environments,

this is less explicitly discussed within palaeo-ice sheet reconstructions (Barr & Lovell, 2014). Previous studies have suggested that due to the topographic controls on moraine formation and spacing, moraines may be misinterpreted to carry palaeo-climatic significance that they do not have (Barr & Lovell, 2014; Boston *et al.*, 2023; Rowan *et al.*, 2022; Warren, 1991; Warren & Hulton, 1990). This highlights a significant advantage of using DGMs as palaeo-climatic indicators as DGMs require flat, low-relief environments for formation, therefore topography is less of an obscurant and allows more accurate inferences to be made. Nevertheless, the issue of misinterpreting moraines as palaeo-climatic indicators remains problematic in areas of more topographically complex terrain and therefore it would be valuable to apply the slope analysis method used in this study to areas with a greater slope variability. This could enable a quantification, or at least better understanding, of the extent to which slope controls grounding line retreat in palaeo-glacial environments. This would contribute to improving the accuracy of palaeo-ice sheet reconstructions and may offer insight when attempting to draw parallels with contemporary ice masses.

#### **8.7.4 Temporal refinement**

- Varve chronology comparisons in addition to this (chapter 7) and previous studies (Bouvier *et al.*, 2015; Ojala, 2016; Zilliacus, 1989), would strengthen the temporal interpretations of DGMs. For example, DGMs situated around the Hudson Bay area (Josenhans & Zevenhuizen, 1990; Lajeunesse, 2008) may be compared with the North American varve chronology (Ridge *et al.*, 2012). In addition, increasing absolute dating evidence is crucially valuable for better constraining timings of deglaciation and provides a more accurate geochronological anchor for DGM-derived reconstructions.

#### **8.7.5 Experimentation with numerical modelling**

- The DGM-derived reconstruction offers an annual record of retreat across hundred-year timescales. This is a significant temporal refinement of the existing 100-year interval palaeo-ice reconstruction, and an increase in the timescales at which annual rates of retreat can be delineated compared with contemporary observations that are often limited to decadal timescales. This essentially bridges

a temporal gap in understanding of ice sheet retreat dynamics. As such, it would be valuable to utilise this empirical data within numerical modelling, similar to that of the British-Irish Ice Sheet (Gandy *et al.*, 2018 & 2019), to simulate deglaciation dynamics at societally relevant timescales. This will also further validate the use of DGMs to inform the palaeo-glaciological record. Additional experimentation with modelling could include using DGM reconstructions to provide regional indicators of rates of change which may not be universally available across an entire sheet.

## 8.8 Summary

This chapter provides a summative discussion addressing the research questions outlined in chapter 1. Specifically, the results find that DGMs are formed at the grounding line of water-terminating ice margins. DGMs can be subcategorised into regularly spaced prominent ridges and irregularly spaced intermediate ridges, which denote interseasonal formation properties. Specifically, regularly spaced prominent DGMs are suggested to form via push processes during a winter readvance, whereas irregularly spaced intermediate ridges are suggested to form via calving process during periods of summer retreat. In addition, DGMs show spatial variability due to factors such as: sediment availability, meltwater availability, water depth, and ice margin thickness/configuration.

By using local clay-varve chronologies as a geochronological anchor, this study shows that DGMs can be utilised to derive highly detailed annual rates of ice margin retreat and provide insights relative to grounding line forcing mechanisms. Specifically in southwest Finland, the results show a significant refinement of the current highest resolution (100-year), depicting detailed fluctuations in rates of ice margin retreat that correspond with interconnected relationships between temperature and water depth. The DGM-derived reconstruction provides a valuable dataset whereby annual records of retreat are depicted across hundred-year timescales, in contrast to contemporary retreat rates that are often limited to decadal observations. In addition, the rapid retreat rates observed in this study across flat, shallow-gradient topography, highlights that flatbed topography must be considered a key vulnerability when assessing contemporary ice sheet retreat. This work resolves the research questions outlined in section 1.2, relative to constraining spatiotemporal properties of DGMs, and has

demonstrated the value of utilising DGMs as high-resolution geochronometric ice margin indicators.

## Chapter 9: Conclusions

Palaeo-ice sheet reconstructions are important as they help to improve understanding of glacial ice behaviour in relation to climatic change over long periods of time. Temporal resolutions of ice sheet reconstructions are limited to > 1 000 – 100-year intervals at best; however, technological advances in remote sensing instrumentation present an opportunity to refine these resolutions by enabling more subtle, low-relief geomorphology to be observed and integrated. DGMs are low-relief landforms that are suggested to form regularly (potentially annually), at the ice margin, thus highlighting potential as high resolution geochronometric indicators. However, uncertainties surrounding DGM formation has historically presented challenges for such utility.

This research provides clarity on DGM formation by investigating both spatial and temporal properties of DGMs located in southwest Finland. Investigations of spatial characteristics include analysis of morphometry, spatial distribution and internal architecture. Temporal properties were investigated by correlating local clay-varve chronologies with successive DGM occurrence across the study area.

Findings from spatial analyses show DGMs to possess slightly more sinuous and asymmetric characteristics in comparison to similar landforms, and internally comprise proximal to distal transitions with proximal compact laminae and thrust structures and distal poorly compact reworked diamicton. Morphometric properties, along with internal proximal to distal sediment transitions, infer a unidirectional push process during formation and support the idea that DGMs form at the grounding line of water-terminating ice margins. In addition, spatial analysis of DGT configuration across the study area revealed two DGM-subtypes (e.g. regularly spaced prominent DGMs and irregularly spaced intermediate DGMs). These DGM-subtypes depict interseasonal variations during formation whereby prominent DGMs form at a regular periodicity via push during winter readvances and intermediate DGMs form more irregularly via calving processes during periods of summer retreat. The distinction between prominent and intermediate DGMs for the purposes of ice margin reconstructions is critical given the different implications that each DGM-subtype represents for ice margin dynamics.

The correlation between the local clay-varved chronology in southwest Finland and DGM occurrence show close alignment with annual rates of retreat, particularly in areas of DGT abundant with prominent ridges. This enabled an annual signal to be established across the study area and concurrently for annual DGM isochrones to be constructed. In areas comprising a greater number of intermediate DGMs, the designation of ‘annual’ DGMs was guided by the number required from the clay-varved chronology. Whilst this introduced a degree of subjectivity, it enabled an annual ice margin reconstruction to be developed across the southwest Finnish sector of the FIS.

The DGM-derived reconstruction demonstrates a significant improvement to the current highest resolution in the study area (e.g. annual compared to 100-year), revealing highly detailed nuanced patterns in retreat rate and grounding line dynamics. Specifically, the findings show interconnected processes between temperature, water depth and topography, driving grounding line retreat and demonstrate how these variables evolve in strength over space and time. In addition, the nuanced fluctuations observed at annual timescales may delineate significant calving events during deglaciation and may help to improve understanding of calving related processes.

The major constraints of DGM utility as ice margin geochronometric indicators is, i) the availability of DGM evidence, and ii) accurate dating methods in which to establish an annual signal within the terrain and provide a geochronological anchor to the reconstruction. For utility as ice margin indicators, DGMs must be abundant and well-preserved. As such, postglacial reworking and sedimentation may present difficulties when attempting to identify individual DGMs. Furthermore, DGM is not ubiquitous, requiring specific depositional environments (e.g. low-relief terrain, flat, smooth, slightly raised beds), therefore ice sheet reconstruction refinement will ultimately be limited to areas of DGT evidence. The distinction between prominent and intermediate DGMs is critical, particularly when establishing an annual signal. As such, local clay-varved chronologies provide the most appropriate means of geochronological anchoring; however, other methods may be utilised, and annual signals may be inferred with a higher degree of uncertainty. Specific to this study, a well-constrained ice margin was able to be reconstructed due to the abundance of DGMs and an established clay-varve chronology in the area. Areas of less well-preserved DGMs and limited local chronologies may produce variable results.

Future work may include expansion of spatial analyses of DGMs to further contribute to the existing knowledge, and expansion of DGM utility as ice margin indicators for further refinements of ice sheet reconstructions. Similarly, additional temporal investigations would prove valuable to develop on the findings from this study. The application of the methodological framework demonstrated in this study to investigate grounding line processes such as calving would prove valuable to assess the extent to which slope drives grounding line retreat at annual timescales.

Overall, this study contributes to the existing knowledge of DGMs and offers a paradigm shift in their utility for palaeo-glaciological research. This study demonstrates the utility of DGMs as ice margin geochronometric indicators, providing an ice margin reconstruction characterised by an annual resolution across the southwest Finnish sector of the FIS. Furthermore, this study demonstrates how DGMs can be used to investigate grounding line forcing mechanisms at annual to centennial timescales of which findings are particularly valuable for understanding changes in contemporary ice sheets. Significantly, this study provides a methodological framework and foundation for the utility of DGMs as annual ice margin geochronometric indicators which can be developed upon in future work.



## References

- ®National Land Survey of Finland, LiDAR digital elevation model, 2/2023.
- Aario, R. (1977). Classification and terminology of morainic landforms in Finland. *Boreas*, vol. 6(2), pp. 87-100. DOI: <https://doi.org/10.1111/j.1502-3885.1977.tb00338.x>
- Aartolahti, T. (1972). On deglaciation in Southern and Western Finland. *Societas Geographica Fenniae*, vol. 114. Helsinki. UIN: BLL01010260022
- Aartolahti, T., Koivisto, M. & Nenonen, K. (1995). De Geer moraines in Finland. Special Paper – Geological Survey of Finland, vol. 20, pp. 67-74.
- Abballe, M. & Cavalazzi, M. (2021). Morphometric Analysis For Geoarchaeological Research: From Testing Different Methods To Results Verification In The Romagna Plain. *Archeologia a Calcolatori*, 32(1), pp. 114-136. DOI: <https://doi.org/10.19282/ac.32.1.2021.07>
- Aber, J.S. & Ber, A. (2007). Chapter 5 – Composite Ridges. *Developments in Quaternary Sciences*. Elsevier, vol. 6, pp. 59 – 82. DOI: [https://doi.org/10.1016/S1571-0866\(07\)80073-X](https://doi.org/10.1016/S1571-0866(07)80073-X). ISSN: 1571-0866
- Agisoft - Metashape (version 1.8.1). 2022: Retrieved from: <https://agisoft.com/downloads/installer/>
- Ahokangas, E. & Mäkinen, J. (2014). Sedimentology of an ice lobe margin esker with implications for the deglacial dynamics of the Finnish Lake District lobe trunk. *Boreas*, vol. 43, pp. 90-106. DOI: <https://doi.org/10.1111/bor.12023>. ISSN: 0300-9483
- Ahokangas, E. (2020). Interlobate esker aquifer characterization by high resolution seismic reflection method with landstreamer in SW Finland. *Journal of Applied Geophysics*, vol. 177. DOI: <https://doi.org/10.1016/j.jappgeo.2020.104014>
- Åkesson, H., Morlighem, M., Nisancioglu, K.H., Svendsen, J.I. & Mangerud, J. (2018). Atmosphere-driven ice sheet mass loss paces by topography: Insights from modelling the south-western Scandinavian Ice Sheet. *Quaternary Science Reviews*, vol. 195, pp. 32-47. DOI: <https://doi.org/10.1016/j.quascirev.2018.07.004>

- Albrecht, T., Bagge, M. & Klemann, V. (2024). Feedback mechanisms controlling Antarctic glacial-cycle dynamics simulated with a coupled ice sheet-solid Earth model. *The Cryosphere*, vol. 18(9), pp. 4233-4255. DOI: <https://doi.org/10.5194/tc-18-4233-2024>
- Alley, R.B. & Joughin, I. (2012). Modeling Ice-Sheet Flow. *Science*, vol. 336(6081), pp. 551-552. Retrieved from: <https://www.jstor.org/stable/41584738>
- Alley, R.B., Anandakrishnan, S., Dupont, T.K., Parizek, B.R. & Pollard, D. (2007). Effect of sedimentation on ice-sheet grounding-line stability. *Science*, vol. 315, pp. 1838-1841. DOI: <https://doi.org/10.1126/science.1138396>
- Alley, R.B., Andrews, J.T., Brigham-Grette, J., Clarke, G.K.C., Cuffey, K.M., Fitzpatrick, J.J., Funder, S., Marshall, S.J., Miller, G.H., Mitrovica, J.X., Muhs, D.R. & Otto-Bliesner, B.L. (2010). History of the Greenland Ice Sheet: paleoclimatic insights. *Quaternary Science Reviews*, vol. 29(15-16), pp. 1728-1756. DOI: <https://doi.org/10.1016/j.quascirev.2010.02.007>
- Alley, R.B., Clark, P.U., Huybrechts, P. & Joughin, I. (2005). Ice-Sheet and Sea-Level Changes. *Science*, vol. 310(5747), pp. 456-460. DOI: <https://doi.org/10.1126/science.1114613>
- Al-Wassai, F.A. & Kalyankar, N.V. (2013). Major Limitations of Satellite Images. *Journal of Global Research in Computer Science*, vol. 4(5), pp. 51-59. DOI: <https://doi.org/10.48550/arXiv.1307.2434>
- Anders, C.E., Dutton, A., Long, A.J. & Milne, G.A. (2019). PALeo constraints on SEA level rise (PALSEA): Ice-sheet and sea-level responses to past climate warming. *Quaternary Science Reviews*, vol. 212, pp. 28-32. DOI: <https://doi.org/10.1016/j.quascirev.2019.03.032>
- Anderson, J.B., Shipp, S.S., Lowe, A.L., Wellner, J.S., Mosola, A.B. (2002). The Antarctic Ice Sheet during the Last Glacial Maximum and its subsequent retreat history: A review. *Quaternary Science Reviews*, vol. 21(1-3), pp. 49-70. DOI: [https://doi.org/10.1016/S0277-3791\(01\)00083-X](https://doi.org/10.1016/S0277-3791(01)00083-X)

- Andreassen, K., Winsborrow, M.C.M., Bjarnadóttir, L.R. & R  ther. (2014). Ice stream retreat dynamics inferred from an assemblage of landforms in the northern Barents Sea. *Quaternary Science Reviews*, vol. 92, pp. 246-257. DOI: <https://doi.org/10.1016/j.quascirev.2013.09.015>
- Andreassen, K., Winsborrow, M.C.M., Bjarnadóttir, L.R., R  ther, D.C. (2014). Ice stream retreat dynamics inferred from an assemblage of landforms in the northern Barents Sea. *Quaternary Science Reviews*, vol. 92, pp. 246-257. DOI: <https://doi.org/10.1016/l.quascirev.2013.09.015>
- Andr  n, T., Bj  rk, S., Andr  n, E., Conley, D., Zill  n, L. & Anjar, J. (2011). Chapter 4 – The Development of the Baltic Sea Basin During the Last 130 ka. *The Baltic Sea Basin, Central and Eastern European Development Studies (CEEDES)*. DOI: [https://doi.org/10.1007/978-3-642-17220-5\\_4](https://doi.org/10.1007/978-3-642-17220-5_4)
- Andr  n, T., Lindeberg, G. & Andr  n, E. (2002). Evidence of the final drainage of the Baltic Ice Lake and the brackish phase of the Yoldia Sea in glacial varves from the Baltic Sea. *Boreas*, vol. 31, pp. 226-238. DOI: <https://doi.org/10.1111/j.1502-3885.2002.tb01069.x>
- Andr  n, T.U., Bj  rck, S., Andr  n, E., Conley, D.J., Zill  n, L., Anjar, J. (2011). The Development of the Baltic Sea Basin During the Last 130 k. (eds) *The Baltic Sea Basin. Central and Eastern European Development Studies (CEEDES)*. Springer, Berlin, Heidelberg. DOI: [https://doi.org/10.1007/978-3-642-17220-5\\_4](https://doi.org/10.1007/978-3-642-17220-5_4)
- Andrews, J. T. 1963: End moraines and late glacial chronology in the northern Nain-Okak section of the Labrador coast. *Geografiska Annaler* 45, 158-171, <https://doi.org/10.2307/520391>.
- Angelis, H.D. & Kleman, J. (2005). Palaeo-ice streams in the northern Keewatin Sector of the Laurentide Ice Sheet. *Annals of Glaciology*, vol. 42(1), pp. 135-144. DOI: <https://doi.org/10.3189/172756405791812925>
- Ankerstjerne, S., Iverson, N.R. & Lacroix, F. (2015). Origin of a washboard moraine of the Des Moines Lobe inferred from sediment properties, *Geomorphology*, vol. 248, pp. 452-463. DOI: <https://dx.doi.org/10.1016/j.geomorph.2015.07.019>

- Anselin, J., Reed, B.C., Jenkins, A. & Green, J.A.M. (2023). Ice Shelf Basal Melt Sensitivity to Tide-Induced Mixing Based on the Theory of Subglacial Plumes. *Journal of Geophysical Research: Oceans*, vol. 128. DOI: <https://doi.org/10.1029/2022JC019156>
- ArcMap. (1995-2018). Esri Inc. ArcGIS Desktop version 10.6.1.9270. ArcMap software by Esri. ArcGIS and ArcMapTM. [www.esri.com](http://www.esri.com).
- ArcticDEM. The Polar Geospatial Center (PGC), National Science Foundation. Porter, Claire; Morin, Paul; Howat, Ian; Noh, Myoung-Jon; Bates, Brian; Peterman, Kenneth; Keeseey, Scott; Schlenk, Matthew; Gardiner, Judith; Tomko, Karen; Willis, Michael; Kelleher, Cole; Cloutier, Michael; Husby, Eric; Foga, Steven; Nakamura, Hitomi; Platson, Melisa; Wethington, Michael, Jr.; Williamson, Cathleen; Bauer, Gregory; Enos, Jeremy; Arnold, Galen; Kramer, William; Becker, Peter; Doshi, Abhijit; D'Souza, Cristelle; Cummins, Pat; Laurier, Fabien; Bojesen, Mikkel. (2018). "ArcticDEM". DOI: <https://doi.org/10.7910/DVN/OHHUKH>, Harvard Dataverse, V1.
- Avery, R.S., Greenwood, S.L., Schenk, F., Morén, B.M., Armstrong McKay, D.I., Brunnberg, L. & Wohlfarth, B. (2020). A 725-year integrated offshore terrestrial varve chronology for southeastern Sweden suggests rapid ice retreat ~15 ka BP. *Boreas*, vol. 50(2), pp. 477-496. DOI: <https://doi.org/10.1111/bor.12490>
- Bamber, J.L., Alley, R.B. & Joughin, I. (2007). Rapid response of modern day ice sheets to external forcing. *Earth and Planetary Science Letters*, vol. 257(1-2), pp. 1-13. DOI: <https://doi.org/10.1016/j.epsl.2007.03.005>
- Barnes, T.J., Schuler, T.V., Filhol, S. & Lilleøren, K.S. (2024). A machine learning approach to the geomorphometric detection of ribbed moraines in Norway. *Earth Surface Dynamics*, vol. 12(3), pp. 801-818. DOI: <https://doi.org/10.5194/esurf-12-801-2024>
- Barr, I.D. & Lovell, H. (2014). A review of topographic controls on moraine distribution. *Geomorphology*, vol. 226, pp. 44-64. DOI: <https://doi.org/10.1016/j.geomorph.2014.07.030>
- Batchelor, C.L. & Dowdeswell, J.A. (2015). Ice-sheet grounding-zone wedges (GZWs) on high-latitude continental margins. *Marine Geology*, vol. 363, pp. 65-92. DOI: <https://doi.org/10.1016/j.margeo.2015.02.001>

- Batchelor, C.L., Christie, F.D.W., Ottesen, D., Montelli, A., Evans, J., Dowdeswell, E.K., Bjarnadóttir, L.R. & Dowdeswell, J.A. (2023). Rapid, buoyancy-driven ice-sheet retreat of hundreds of metres per day. *Nature*, vol. 617, pp. 105-110. DOI: <https://doi.org/10.1038/s41586-023-05876-1>
- Batchelor, C.L., Christle, F.D.W., Ottesen, D., Montelli, A., Evans, J., Dowdeswell, E.K., Bjarnadóttir, L.R. & Dowdeswell, J.A. (2023). Rapid, buoyancy-driven ice-sheet retreat of hundreds of metres per day. *Nature*, vol. 617. DOI: <https://doi.org/10.1038/s41586-023-05876-1>
- Batchelor, C.L., Dowdeswell, J.A., Hogan, K.A., Larter, R.D., Parsons, E. & West, O. (2019). Processes and patterns of glacier-influenced sedimentation and recent tidewater glacier dynamics in Darbel Bay, western Antarctic Peninsula. *Antarctic Science*, vol. 31(4), pp. 218-227. DOI: <https://doi.org/10.1017/S0954102019000191>
- Batchelor, C.L., Margold, M., Krapp, M., Murton, D.K., Dalton, A.S., Gibbard, P.L., Stokes, C.R., Murton, J.B. & Manica, A. (2019). The configuration of Northern Hemisphere ice sheets through the Quaternary. *Nature Communications*, vol. 10(3713). DOI: <https://doi.org/10.1038/s41467-019-11601-2>
- Baumhoer, C.A., Dietz, A.J., Kneisel, C., Paeth, H. & Claudia, K. (2021). Environmental Drivers of Circum-Antarctic Glacier and Ice Shelf Front Retreat over the Last Two Decades. *The Cryosphere*, vol. 15, pp. 2357-2381. DOI: <https://doi.org/10.5194/tc-15-2357-2021>
- Beaudry, L. M. & Prichonnet, G. (1991). Late Glacial De Geer moraines with glaciofluvial sediment in the Chapais area, Quebec (Canada). *Boreas*, vol. 20, pp. 377-394. ISSN: 0300-9483
- Beaudry, L. M. & Prichonnet, G. (1995). Formation of De Geer Moraines Deposited Subglacially, Central Quebec. *Geographie physique et Quaternaire*, vol. 49 (3), 337-361. DOI: <https://doi.org/10.7202/033059ar>
- Beaudry, L. M. & Prichonnet, G. 1991: Late Glacial De Geer moraines with glaciofluvial sediment in the Chapais area, Québec (Canada). *Boreas* 20, 337-394, <https://doi.org/10.1111/j.1502-3885.1991.tb00286.x>.

- Beaudry, L. M. & Prichonnet, G. 1995: Formation of De Geer moraines Deposited Subglacially, Central Québec. *Géographie Physique et Quaternaire* 49, 337-361, <https://doi.org/10.7202/033059ar>.
- Beaudry, L.M. & Prichonnet, G. (1991). Late Glacial De Geer moraines with glaciofluvial sediment in the Chapais area, Québec (Canada). *Boreas*, vol. 20(4), pp. 377-394. DOI: <https://doi.org/10.1111/j.1502-3885.1991.tb00286.x>
- Beaudry, L.M. & Prichonnet, G. (1995). Formation of De Geer Moraines Deposited Subglacially, Central Québec. *Géographie Physique et Quaternaire*, vol. 49(3), pp. 337-361. DOI: <https://doi.org/10.7202/033059ar>
- Bellwald, B., Planke, S., Becker, L.W.M. & Myklebust, R. (2020). Meltwater sediment transport as the dominating process in mid-latitude trough mouth fan formation. *Nature Communications*, vol. 11(4645). DOI: <https://doi.org/10.1038/s41467-020-18337-4>
- Benediktsson, Í.Ö., Ingólfsson, Ó., Schomacker, A. & Kjaer, K.H. (2009). Formation of submarginal and proglacial end moraines: implications of ice-flow mechanism during the 1963-64 surge of Brúarjökull, Iceland. *Boreas*, vol. 38, pp. 440-457. DOI: <https://doi.org/10.1111/j.1502-3885.2008.00077.x>
- Benediktsson, Í.Ö., Ingólfsson, Ó., Schomacker, A. & Kjær, K.H. (2009). Formation of submarginal and proglacial end moraines: implications of ice-flow mechanisms during the 1963-64 surge of Brúarjökull, Iceland. *Boreas*, vol. 38, pp. 440-457. DOI: <https://doi.org/10.1111/j.1502-3885.2008.00077.x>. ISSN: 0300-9483
- Benn, D. & Evans, D.J.A. (2010). *Glaciers and glaciation*, 2nd edition. Taylor & Francis Group.
- Benn, D. I. & Ballantyne, C. K. 1994: Reconstructing the transport history of glacial sediments; a new approach based on the co-variance of clast form indices. *Sedimentary Geology* 91, 215-227, [https://doi.org/10.1016/0037-0738\(94\)90130-9](https://doi.org/10.1016/0037-0738(94)90130-9).
- Benn, D. I., Warren, C. R. & Mottram, R. H. 2007: Calving processes and the dynamics of calving glaciers. *Earth-Science Reviews* 82, 143-179, <https://doi.org/10.1016/j.earscirev.2007.02.002>.

- Benn, D., & Evans, D. J. A. 2010: *Glaciers and glaciation*. 563 pp. Arnold, London.
- Benn, D.I. & Evans, D.J.A. (2010). *Glaciers & Glaciation* (2nd ed.). Routledge, Abingdon, Oxon, 734 pp. ISBN: 13: 978-0-340-90579-1.
- Benn, D.I., Hulton, N.R.J. & Mottram, R.H. (2007). 'Calving laws', 'sliding laws' and the stability of tidewater glaciers. *Annals of Glaciology*, vol. 46, pp. 123-130. DOI: <https://doi.org/10.3189/172756407782871161>
- Bennett, M. M. & Glasser, N. F. (eds). 2009: *Glacial geology: Ice sheets and landforms*. 305 pp. John Wiley & Sons, Chichester.
- Bennett, M. R., Huddart, D. & Waller, R. I. 2000: Glaciofluvial crevasse and conduit fills as indicators of supraglacial dewatering during a surge, Skeiðarárjökull, Iceland. *Journal of Glaciology* 46, 25-34, <https://doi.org/10.3189/172756500781833232>.
- Bennett, M.R. (2001). The morphology, structural evolution and significance of push moraines. *Earth-Science Reviews*, vol. 53(3-4), pp. 197-236. DOI: [https://doi.org/10.1016/S0012-8252\(00\)00039-8](https://doi.org/10.1016/S0012-8252(00)00039-8)
- Bennett, M.R. (2003). Ice streams as the arteries of an ice sheet: their mechanics, stability and significance. *Earth-Science Reviews*, vol. 61(3-4), pp. 309-339. DOI: [https://doi.org/10.1016/S0012-8252\(02\)00130-7](https://doi.org/10.1016/S0012-8252(02)00130-7)
- Bennett, M.R. (2003). Ice streams as the arteries of an ice sheet: their mechanics, stability and significance. *Earth-Science Reviews*, vol. 61, pp. 309-339. DOI: [https://doi.org/10.1016/S0012-8252\(02\)00130-7](https://doi.org/10.1016/S0012-8252(02)00130-7)
- Bennett, M.R., Huddart, D. & Waller, R.I. (2000). Glaciofluvial crevasse and conduit fills as indicators of supraglacial dewatering during a surge, Skeidrarjokull, Iceland. *Journal of Glaciology*, vol. 46 (152). DOI: <https://doi.org/10.3189/172756500781833232>
- Ben-Yehoshua, D. (2017). *Crevasse-Squeeze Ridges in Trygghamna, Svalbard*. The University Centre in Svalbard. Retrieved from: [https://skemman.is/bitstream/1946/26725/1/Crevasse-Squeeze\\_Ridges\\_in\\_Trygghamna-Svalbard\\_Daniel%20Ben-Yehoshua\\_MSc\\_Thesis.pdf](https://skemman.is/bitstream/1946/26725/1/Crevasse-Squeeze_Ridges_in_Trygghamna-Svalbard_Daniel%20Ben-Yehoshua_MSc_Thesis.pdf)

- Ben-Yehoshua, D. (2017). Crevasse-Squeeze Ridges in Trygghamna, Svalbard. University of Iceland, Faculty of Earth Science. Retrieved from <https://hdl.handle.net/1946/26725>
- Ben-Yehoshua, D., Aradóttir, N., Farnsworth, W.R., Benediktsson, Í.Ö. & Ingólfsson, Ó. (2023). Formation of crevasse-squeeze ridges at Trygghamna, Svalbard. *Earth Surface Processes and Landforms*, vol. 48(12), pp. 2334-2348. DOI: <https://doi.org/10.1002/esp.5631>
- Berends, C.J., de Boer, B. & van de Wal, S.W. (2021). Reconstructing the evolution of ice sheets, sea level, and atmospheric CO<sub>2</sub> during the past 3.6 million years. *Clim. Past.*, vol. 17, pp. 361-377. DOI: <https://doi.org/10.5194/cp-17-361-2021>
- Bethell, E.M., Ernst, R.E. & Samson, C. (2022). Analysis of Venusian Wrinkle Ridge Morphometry Using Stereo-Derived Topography: A Case Study From Southern Eistla Regio. *JGR Planets*. Vol. 127(5). DOI: <https://doi.org/10.1029/2021JE006879>
- Björck, S. (1995). A review of the history of the Baltic Sea, 13.0-8.0 ka BP. *Quaternary International*, vol. 27, pp. 19-40. DOI: [https://doi.org/10.1016/1040-6182\(94\)00057-C](https://doi.org/10.1016/1040-6182(94)00057-C)
- Björck, S. (2008). The late Quaternary development of the Baltic Sea basin. In *The BACC Author Teams (Eds.): Assessment of climate change for the Baltic Sea Basin*, Springer-Verlag Berlin Heidelberg, pp. 398-407. ISBN: 978-3-540-72785-9
- Björck, S., Rundgren, M., Ingólfsson, Ó. & Funder, S. (1998). The preboreal oscillation around the Nordic Seas: terrestrial and lacustrine responses. *Journal of Quaternary Science*, vol. 12(6), pp. 455-465. DOI: [https://doi.org/10.1002/\(SICI\)1099-1417\(199711/12\)12:6<455::AID-JQS316>3.0.CO;2-S](https://doi.org/10.1002/(SICI)1099-1417(199711/12)12:6<455::AID-JQS316>3.0.CO;2-S)
- Blake, K. P. (2000). Common origin for De Geer moraines of variable composition in Raudvassdalen, northern Norway. *Journal of Quaternary Science*, vol. 15 (6), pp. 633-644. ISSN: 0267-8179
- Blake, K. P. 2000: Common origin for De Geer moraines of variable composition in Raudvassdalen, northern Norway. *Journal of Quaternary Science* 15, 633-644, [https://doi.org/10.1002/1099-1417\(200009\)15:6<633::AID-JQS543>3.0.CO;2-F](https://doi.org/10.1002/1099-1417(200009)15:6<633::AID-JQS543>3.0.CO;2-F).



- Blake, K.P. (2000). Common origin for De Geer moraines of variable composition in Raudvassdalen, northern Norway. *Journal of Quaternary Science*, vol. 15(6), pp. 633-644. DOI: [https://doi.org/10.1002/1099-1417\(200009\)15:6<633::AID-JQS543>3.0.CO;2-F](https://doi.org/10.1002/1099-1417(200009)15:6<633::AID-JQS543>3.0.CO;2-F)
- Book, C., Hoffman, M.J., Kachuck, S.B., Hillbrand, T.R., Price, S.F., Perego, M. & Bassis, J.N. (2022). Stabilizing effect of bedrock uplift on retreat of Thwaites Glacier, Antarctica, at centennial timescales. *Earth and Planetary Science Letters*, vol. 597(11798). DOI: <https://doi.org/10.1016/j.espl.2022.117798>
- Borgstrom, I. (1979). De Geer Moraines in a Swedish Mountain Area? *Geografiska Annaler. Series A, Physical Geography*, vol. 61 (1/2), pp. 35-42. Retrieved from: <https://www.jstor.org/stable/520512>
- Borgström, I. (1979). De Geer Moraines in a Swedish Mountain Area? *Geografiska Annaler: Series A, Physical Geography*, vol. 61(1-2), pp. 35-42. DOI: <https://doi.org/10.1080/04353676.1979.11879979>
- Boston, C.M., Chandler, B.M.P., Lovell, H., Weber, P.P. & Davies, B.J. (2023). The role of topography in landform development at an active temperate glacier in Arctic Norway. *Earth Surface Processes and Landforms*, vol. 48, pp. 1783-1803. DOI: <https://doi.org/10.1002/esp.5588>
- Boulton, G. S. 1986: Push-moraines and glacier-contact fans in marine and terrestrial environments. *Sedimentology* 33, 677-698, <https://doi.org/10.1111/j.1365-3091.1986.tb01969.x>.
- Boulton, G. S., Smith, G. D. & Morland, L. W. 1984: The Reconstruction of Former Ice Sheets and their Mass Balance Characteristics using a Non-Linearly Viscous Flow Model. *Journal of Glaciology* 30, 140-152, <https://doi.org/10.3189/S0022143000005876>.
- Boulton, G.S. & Clark, C.D. (1990). A highly mobile Laurentide ice sheet revealed by satellite image of glacial lineations. *Nature*, vol. 346, pp. 813-817. DOI: <https://doi.org/10.1038/346813a0>

- Boulton, G.S., van der Meer, J.J.M., Hart, J., Beets, D., Ruegg, G.H.J., van der Wateren, F.M. & Jarvis, J. (1996). Till and moraine emplacement in a deforming bed surge – an example from a marine environment. *Quaternary Science Reviews*, vol. 15(10), pp. 961-987. DOI: [https://doi.org/10.1016/0277-3791\(95\)00091-7](https://doi.org/10.1016/0277-3791(95)00091-7)
- Boulton, G.S., van der Meer, J.J.M., Hart, J., Beets, D., Ruegg, G.H.J., van der Wateren, F.M. & Jarvis, J. (1996). Till And Moraine Emplacement In A Deforming Bed Surge- An Example From A Marine Environment. *Quaternary Science Reviews*, vol. 15, pp.961-987. DOI: [https://doi.org/10.1016/0277-3791\(95\)00091-7](https://doi.org/10.1016/0277-3791(95)00091-7)
- Bouvier, V., Johnson, M. D. & Pässe, T. 2015: Distribution, genesis and annual-origin of De Geer moraines in Sweden: insights revealed by LiDAR. *GFF* 137, 319-333, <https://doi.org/10.1080/11035897.2015.1089933>.
- Bouvier, V., Johnson, M. D. & Pässe, T. (2015). Distribution, genesis and annual-origin of De Geer moraines in Sweden: insights revealed by LiDAR. *GFF*, vol. 137 (4), pp. 319-333. DOI: <https://dx.doi.org/10.1080/11035897.2015.1089933>
- Bouvier, V., Johnson, M.D. & Pässe, T. (2015). Distribution, genesis and annual-origin of De Geer moraines in Sweden: insights revealed by LiDAR. *GFF*, vol. 137(4), pp. 319-333. DOI: <https://doi.org/10.1080/11035897.2015.1089933>
- Bouvier, V., Johnson, M.D. & Pässe, T. (2015). Distribution, genesis and annual-origin of De Geer moraines in Sweden: insights revealed by LiDAR. *GFF*, vol. 137(4), pp. 319-333. DOI: <https://doi.org/10.1080/11035897.2015.1089933>
- Boyce, E.S., Motyka, R.J. & Truffer, M. (2007). Flotation and retreat of a lake-calving terminus, Mendenhall Glacier, southeast Alaska, USA. *Journal of Glaciology*, vol. 53(181), pp. 211-224. DOI: <https://doi.org/10.3189/172756507782202928>
- Boyes, B.M., Linch, L.D., Pearce, D.M. & Nash, D.J. (2023). The last Fennoscandian Ice Sheet glaciation on the Kola Peninsula and Russian Lapland (Part 2): Ice sheet margin positions, evolution, and dynamics. *Quaternary Science Reviews*, vol. 300(107872). DOI: <https://doi.org/10.1016/j.quascirev.2022.107872>

- Bradley, A.T. & Hewitt, I.J. (2024). Tipping point in ice-sheet grounding-zone melting due to ocean water intrusion. *Nature Geoscience*. DOI: <https://doi.org/10.1038/s41561-024-01465-7>
- Bradley, S.L., Ely, J.C., Clark, C.D., Edwards, R.J. & Shennan, I. (2023). Reconstruction of the palaeo-sea level of Britain and Ireland arising from empirical constraints of ice extent: implications for regional sea level forecasts and North American ice sheet volume. *Journal of Quaternary Science*, vol. 38(6), pp. 791-805. DOI: <https://doi.org/10.1002/jqs.3523>
- Bradwell, T., Small, D., Fabel, D., Clark, C.D., Chiverrell, R.C., Saher, M.H., Dove, D., Callard, S.L., Burke, M.J., Moreton, S.G., Medialea, A., Bateman, M.D., Roberts, D.H., Golledge, N.R., Finlayson, A., Morgan, S. & Cofaigh, C.Ó. (2021). Pattern, style and timing of British-Irish Ice Sheet retreat: Shetland and northern North Sea sector. *Journal of Quaternary Science*, vol. 36(5), pp. 681-722. DOI: <https://doi.org/10.1002/jqs.3163>
- Breckenridge, A., Lowell, T.V., Peteet, D., Wattrus, N., Moretto, M., Norris, N. & Dennison, A. (2020). A new glacial varve varve chronology along the southern Laurentide Ice Sheet that spans the Younger Dryas-Holocene boundary. *Geology*, vol. 49(3), pp. 283-288. DOI: <https://doi.org/10.1130/G47995.1>
- Brigham, C.A.P. & Crider, J.G. (2022). A new metric for morphologic variability using landform shape classification via supervised machine learning. *Geomorphology*, vol. 399. DOI: <https://doi.org/10.1016/j.geomorph.2021.108065>
- Bristow, C.S. & Jol, H.M. (2003). Ground Penetrating Radar (GPR) in Sediments. Geological Society London Special Publication, vol. 211. Retrieved from: <https://www.geokniga.org/bookfiles/geokniga-groundpenetratingradarinsediments.pdf>
- Brunt, K.M., Fricker, H.A., Padman, L., Scambos, T.A. & O'Neel, S. (2010). Mapping the grounding zone of the Ross Ice Shelf, Antarctica, using ICESat laser altimetry. *Annals of Glaciology*, vol. 51(55), pp. 71-79. DOI: <https://doi.org/10.3189/172756410791392790>

- Butcher, F., Balme, M., Conway, S., Gallagher, C., Arnold, N., Storrar, R., Lewis, S. & Hagermann, A. (2020). Morphometry of a glacier-linked esker in NW Tempe Terra, Mars, and implications for sediment-discharge dynamics of subglacial drainage. *Earth and Planetary Science Letters*. Vol. 542(116325). DOI: <https://doi.org/10.1016/j.epsl.2020.116325>
- Butcher, F.E., Balme, M.R., Gallagher, C., Storrar, R.D., Conway, S.J., Arnold, N.S., Lewis, S.R. & Hagermann, A. (2019). 3D Morphometries of Eskers on Mars, and Comparisons to Eskers in Finland. In: 50th Lunar and Planetary Science Conference, 18-22 Mar 2019, The Woodlands, Houston, Texas, USA. Retrieved from [http://oro.open.ac.uk/59280/1/Butcher\\_EskerMorphometries\\_1874.pdf](http://oro.open.ac.uk/59280/1/Butcher_EskerMorphometries_1874.pdf)
- Butcher, F.E.G., Balme, M.R., Conway, S.J., Gallagher, C., Arnold, N.S., Storrar, R.D., Lewis, S.R. & Hagermann, A. (2020). Morphometry of a glacier-linked esker in NW Tempe Terra, Mars, and implications for sediment-discharge dynamics of subglacial drainage. *Earth and Planetary Science Letters*, vol. 542. DOI: <https://doi.org/10.1016/j.epsl.2020.116325>
- Butcher, F.E.G., Conway, S.J. & Arnold, N.S. (2016). Are the Dorsa Argentea on Mars eskers? *Icarus* 275, pp. 65-84. DOI: <https://doi.org/10.1016/j.icarus.2016.03.028>
- Carlson, A.E. & Clark, P.U. (2012). Ice sheet sources of sea level rise and freshwater discharge during the last deglaciation. *Reviews of Geophysics*, vol. 50(4), RG4007. DOI: <https://doi.org/10.1029/2011RG000371>
- Carlson, A.E. (2011). Ice Sheets and Sea Level in Earth's Past. *Nature Education Knowledge*, vol. 3(10), pp. 3. Retrieved from: <https://www.nature.com/scitable/knowledge/library/ice-sheets-and-sea-level-in-earth-24148940/>
- Carlson, A.E. (2013). PALEOCLIMATE | The Younger Dryas Climate Event. *Encyclopedia of Quaternary Science (Second Edition)*, pp. 126-134. DOI: <https://doi.org/10.1016/B978-0-444-53643-3.00029-7>
- Catania, G. & Felikson, D. (2022). Topographic modulation of outlet glaciers in Greenland: a review. *Annals of Glaciology*, vol. 63(87-89), pp. 171-177. DOI: <https://doi.org/10.1017/aog.2023.55>

- Chandler, B.M., Lovell, H., Boston, C.M., Lukas, S., Barr, I., Benediktsson, I., Benn, D., Clark, C., Darvill, C.M., Evans, D., Ewertowski, M., Loibl, D., Margold, M., Otto, J., Roberts, D.H., Stokes, C., Storrar, R., & Stroeven, A. (2018). Glacial geomorphological mapping: A review of approaches and frameworks for best practice. *Earth-Science Reviews*, vol. 185, pp. 806-846. DOI: <https://doi.org/10.1016/j.earscirev.2018.07.015>
- Chandler, B.M.P., Evans, D.J.A. & Roberts, D.H. (2016). Characteristics of recessional moraines at a temperate glacier in SE Iceland: Insights into patterns, rates and drivers of glacier retreat. *Quaternary Science Reviews*, vol. 135, pp. 171-205. DOI: <https://doi.org/10.1016/j.quascirev.2016.01.025>
- Chandler, B.M.P., Lovell, H., Boston, C.M., Lukas, S., Barr, I.D., Benediktsson, Í.Ö., Benn, D.I., Clark, C.D., Darvill, C.M., Evans, D.J.A., Ewertowski, M.W., Loibl, D., Margold, M., Otto, J-C., Roberts, D.H., Stokes, C.R., Storrar, R.D. & Stroeven, A.P. (2018). Glacial geomorphological mapping: A review of approaches and frameworks for best practice. *Earth-Science Reviews*, vol. 185, pp. 806-846. DOI: <https://doi.org/10.1016/j.earscirev.2018.07.015>
- Cheng, H., Zhang, H., Spötl, C., Baker, J., Sinha, A., Bartolomé, M., Moreno, A., Kathayat, G., Zhao, J., Dong, X., Li, Y., Ning, Y., Jia, X., Zong, B., Brahim, Y.A., Pérez-Mejías, C., Cai, Y., Novello, V.F., Cruz, F.W., Severinghaus, J.P., An, Z. & Edwards, R.L. (2020). Timing and structure of the Younger Dryas event and its underlying climate dynamics. *Earth, Atmospheric and Planetary Sciences*, vol. 117(38), pp. 23408-23417. DOI: <https://doi.org/10.1073/pnas.2007869117>
- Christoffersen, P., Piotrowski, J.A. & Larsen, N.K. (2005). Basal processes beneath an Arctic glacier and their geomorphic imprint after a surge, Elisebreen, Svalbard. *Quaternary Research*, vol. 64, pp. 125-137. DOI: <https://doi.org/10.1016/j.yqres.2005.05.009>
- Clapperton, C.M. (1975). The debris content of surging glaciers in Svalbard and Iceland. *Journal of Glaciology*, vol. 14(72), pp. <https://doi.org/10.3189/S0022143000021924>
- Clapperton, C.M. (1975). The Debris Content of Surging Glaciers in Svalbard and Iceland. *Journal of Glaciology*, vol. 14, (72). DOI: <https://doi.org/10.3189/S0022143000021924>

- Clark, C. D. 1997: Reconstructing the evolutionary dynamics of former ice sheets using multi-temporal evidence, remote sensing and GIS. *Quaternary Science Reviews* 16, 1067-1092, [https://doi.org/10.1016/S0277-3791\(97\)00037-1](https://doi.org/10.1016/S0277-3791(97)00037-1)
- Clark, C. D., Ely, J. C., Hindmarsh, R. C. A., Bradley, S., Ignéczi, A., Fabel, D., Ó Cofaigh, C., Chiverrell, R. C., Scourse, J., Benetti, S., Bradwell, T., Evans, D. J. A., Roberts, D. H., Burke, M. S., Callard, L., Medialdea, A., Saher, M., Small, D., Smedley, R. K., Gasson, E., Gregoire, L., Gandy, N., Hughes, A. L. C., Ballantyne, C., Bateman, M. D., Bigg, G. R., Doole, J., Dove, D., Duller, G. A. T., Jenkins, G. T. H., Livingstone, S. L., McCarron, D., Moreton, S., Pollard, D., Praeg, D., Sejrup, H. P., Van Landeghem, K. J. J., Wilson, P. 2022: Growth and retreat of the last British-Irish Ice Sheet, 31 000 to 15 000 years ago: the BRITICH-CHRONO reconstruction. *Boreas* 51, 699-758, <https://doi.org/10.1111/bor.12594>.
- Clark, C.D. (1993). Mega-scale glacial lineations and cross-cutting ice-flow landforms. *Earth Surf. Proc. Land*, vol. 18(1), pp. 1-29. DOI: <https://doi.org/10.1002/esp.3290180102>
- Clark, C.D. (1997). Reconstructing the evolutionary dynamics of former ice sheets using multi-temporal evidence, remote sensing and GIS. *Quaternary Science Reviews*, vol. 16(9), pp. 1067-1092. DOI: [https://doi.org/10.1016/S0277-3791\(97\)00037-1](https://doi.org/10.1016/S0277-3791(97)00037-1)
- Clark, C.D., Chiverrell, R.C., Fabel, D., Hindmarsh, R.C.A., Ó Cofaigh, C. & Scourse, J.D. (2021). Timing, pace and controls on ice sheet retreat: an introduction to the BRITICE-CHRONO transect reconstructions of the British-Irish Ice Sheet. *Journal of Quaternary Science*, vol. 36(5), pp. 673-680. DOI: <https://doi.org/10.1002/jqs.3326>
- Clark, C.D., Ely, J.C., Hindmarsh, R.C.A., Bradley, S., Ignéczi, A., Fabel, D., Cofaigh, C.Ó., Chiverrell, R.C., Scourse, J., Benetti, S., Bradwell, T., Evans, D.J.A., Roberts, D.H., Burke, M., Callard, S.L., Medialdea, A., Saher, M., Small, D., Smedley, R.K., Gasson, E., Gregoire, L., Gandy, N., Hughes, A.L.C., Ballantyne, C., Bateman, M.D., Bigg, G.R., Doole, J., Dove, D., Duller, G.A.T., Jenkins, G.T.H., Livingston, S.L., McCarron, S., Moreton, S., Pollard, D., Praeg, D., Serjrup, H.P., Landeghem, K.J.J.V. & Wilson, P. (2022). Growth and retreat of the last British-Irish Ice Sheet, 31 000 to 15 000 years ago: the BRITICE-CHRONO reconstruction. *Boreas*, vol. 51(4), pp. 699-758. DOI: <https://doi.org/10.1111/bor.12594>

- Clark, C.D., Ely, J.C., Hindmarsh, R.C.A., Bradley, S., Ignéczi, A., Fabel, D., Ó Cofaigh, C., Chiverrell, R.C., Scourse, J., Benetti, S., Bradwell, T., Evans, D.J.A., Roberts, D.H., Burke, M., Callard, S.L., Medialdea, A., Saher, M., Small, D., Smedley, R.K., Gasson, E., Gregoire, L., Gandy, N., Hughes, A.L.C., Ballantyne, C., Bateman, M.D., Bigg, G.R., Boole, J., Dove, D., Duller, G.A.T., Jenkins, G.T.H., Livingstone, S.L., McCarron, S., Moreton, S., Pollard, D., Praeg, D., Sejrup, H.P., van Landeghem, K.J.J. & Wilson, P. (2022). Growth and retreat of the last British-Irish Ice Sheet, 31 000 to 15 000 years ago: the BRITICE-CHRONO reconstruction. *Boreas*, vol. 51(4), pp. 699-758. DOI: <https://doi.org/10.1111/bor.12594>
- Clark, C.D., Evans, D.J.A. & Piotrowski, J.A. (2003). Palaeo-ice streams: an introduction. *Boreas*, vol. 32(1), pp. 1-3. ISSN: 0300-9483. DOI: <https://doi.org/10.1080/03009480310001182>
- Clark, C.D., Hughes, A.L., Greenwood, S.L., Jordan, C. & Sejrup, H.P. (2012). Pattern and timing of retreat of the last British-Irish Ice Sheet. *Quaternary Science Reviews*, vol. 44, pp. 112-146. DOI: <https://doi.org/10.1016/j.quascirev.2010.07.019>
- Clark, C.D., Hughes, A.L.C., Greenwood, S.L., Jordan, C. & Sejrup, H.P. (2012). Pattern and timing of retreat of the last British-Irish Ice Sheet. *Quaternary Science Reviews*, vol. 44, pp. 112-146. DOI: <https://doi.org/10.1016/j.quascirev.2010.07.019>
- Clark, G.K.C., Collins, S.G. & Thompson, D.E. (1984). Flow, thermal structure, and subglacial conditions of a surge-type glacier. *Can. J. Earth Sci*, vol. 21, pp. 232-140. DOI: <https://doi.org/10.1139/e84-024>. Retrieved from [https://www.researchgate.net/publication/237172635\\_Flow\\_thermal\\_structure\\_and\\_subglacial\\_conditions\\_of\\_a\\_surge-type\\_glacier](https://www.researchgate.net/publication/237172635_Flow_thermal_structure_and_subglacial_conditions_of_a_surge-type_glacier)
- Clark, P. U., Dyke, A. S., Shakun, J. D., Carlson, A. E., Clark, J., Wohlfarth, B., Mitrovica, J. X., Hostetler, S. W. & McCabe, A. M. 2009: The Last Glacial Maximum. *Science* 325, 710-714, <https://doi.org/10.1126/science.1172873>.
- Clark, P.U. (1994). Unstable Behaviour of the Laurentide Ice Sheet over Deforming Sediment and Its Implications for Climate Change. *Quaternary Research*, vol. 41(1), pp. 19-25. DOI: <https://doi.org/10.1006/qres.1994.1002>

- Clark, P.U., Dyke, A.S., Shakun, J.D., Carlson, A.E., Clark, J., Wohlfarth, B., Mitrovica, J.X., Hostetler, S.W. & McCabe, A.M. (2009). The Last Glacial Maximum. *Science*, vol. 325(5941), pp. 710-714. DOI: <https://doi.org/10.1126/science.1172873>
- Cline, M.D., Iverson, N.R. & Harding, C. (2015). Origin of washboard moraines of the Des Moines Lobe: Spatial analyses with LiDAR data. *Geomorphology*, vol. 246, pp. 570-578. DOI: <https://dx.doi.org/10.1016/j.geomorph.2015.07.021>
- Cuzzone, J.K., Clark, P.U., Carlson, A.E., Ullman, D.J., Rinterknecht, V.R., Milne, G.A., Lunkka, J-P., Wohlfarth, B., Marcott, S.A. & Caffee, M. (2016). Final deglaciation of the Scandinavian Ice Sheet and implications for the Holocene global sea-level budget. *Earth and Planetary Science Letters*, vol. 448, pp. 34-41. DOI: <https://doi.org/10.1016/j.epsl.2016.05.019>
- Dalton, A. S., Dulfer, H. E., Margold, M., Heyman, J., Clague, J. J., Froese, D. G., Gauthier, M. S., Hughes, A. L. C., Jennings, C. E., Norris, S. L. & Stoker, B. J. 2023: Deglaciation of the north American ice sheet complex in calendar years based on a comprehensive database of chronological data: NADI-1. *Quaternary Science Reviews* 321, 108345, <https://doi.org/10.1016/j.quascirev.2023.108345>.
- Dalton, A.S., Dulfer, H.E., Margold, M., Heyman, J., Clague, J.J., Froese, D.G., Gauthier, M.S., Hughes, A.L.C., Jennings, C.E., Norris, S.L. & Stoker, B.J. (2023). Deglaciation of the north American ice sheet complex in calendar years based on a comprehensive databse of chronological data: NADI-1. *Quaternary Science Reviews*, vol. 321(108345). DOI: <https://doi.org/10.1016/j.quascirev.2023.108345>
- Dalton, A.S., Dulfer, H.E., Margold, M., Heyman, J., Clague, J.J., Froese, D.G., Gauthier, M.S., Hughes, A.L.C., Jennings, C.E., Norris, S.L. & Stoker, B.J. (2023). Deglaciation of the north American ice sheet complex in calendar years based on a comprehensive database of chronological data: NADI-1. *Quaternary Science Reviews*, vol. 321. DOI: <https://doi.org/10.1016/j.quascirev.2023.108345>
- Dalton, A.S., Dulfer, H.E., Margold, M., Heyman, J., Clague, J.J., Froese, D.G., Gauthier, M.S., Hughes, A.L.C., Jennings, C.E., Norris, S.L. & Stoker, B.J. (2023). Deglaciation of the north American ice sheet complex in calendar years based on a comprehensive



database of chronological data: NADI-1. *Quaternary Science Reviews*, vol. 321(108345). DOI: <https://doi.org/10.1016/j.quascirev.2023.108345>

Dalton, A.S., Margold, M., Stokes, C.R., Tarasov, L., Dyke, A.S., Adams, R.S., Allard, S., Arends, H.E., Atkinson, N., Attig, J.W., Barnett, P.J., Barnett, R.L., Batterson, M., Bernatchez, P., Borns Jr., H.W., Breckenridge, A., Briner, J.P., Brouard, E., Campbell, J.E., Carlson, A.E., Clague, J., Curry, B.B., Daigneault, R.-A., Dubé-Loubert, H., Easterbook, D.J., Franz, D.A., Friedrich, H.G., Funder, S., Gauthier, M.S., Gowan, A.S., Harris, K.L., Hétu, B., Hooyer, T.S., Jennings, C.E., Johnson, M.D., Kehew, A.E., Kelley, S.E., Kerr, D., King, E.L., Kjledsen, K.K., Knaeble, A.R., Lajeunesse, P., Lakeman, T.R., Lamothe, M., Larson, P., Lavoie, M., Loope, H.M., Lowell, T.V., Lusardi, B.A., Manz, L., McMartin, I., Nixon, F.C., Occhietti, S., Parkhill, M.A., Piper, D.J.W., Pronk, A.G., Richard, P.J.H., Ridge, J.C., Ross, M., Roy, M., Seaman, A., Shaw, J., Stea, R.R., Teller, J.T., Thompson, W.B., Thorleifson, L.H., Utting, D.J., Veillette, J.J., Ward, B.C., Weddle, T.K. & Wright Jr., H.E. (2020). An updated radiocarbon-based ice margin chronology for the last deglaciation of the North American Ice Sheet Complex. *Quaternary Science Reviews*, vol. 234(106223). DOI: <https://doi.org/10.1016/j.quascirev.2020.106223>

Davies, B. (2020). Retrieved from <https://www.antarcticglaciers.org/glacial-geology/glacial-landforms/glaciofluvial-landforms/meltwater-channels/>

Davies, B.J. (2022). 4.12 – Cryospheric Geomorphology: Dating Glacial Landforms I: Archival, Incremental, Relative Dating Techniques and Age-Equivalent Stratigraphic Markers. *Treatise on Geomorphology (Second Edition)*, vol. 4, pp. 225-248. DOI: <https://doi.org/10.1016/B978-0-12-818234-5.00042-0>

Davis, D.S. (2018). Object-based image analysis: a review of developments and future directions of automated feature detection in landscape archaeology. *Archaeological Prospection*, vol. 26, issue 2, pp. 155-163. DOI: <https://doi.org/10.1002/arp.1730>

Dawson, E.J., Schroeder, D.M., Chu, W., Mantelli, E. & Seroussi, H. (2022). Ice mass loss sensitivity to the Antarctic ice sheet basal thermal state. *Nature Communications*, vol. 13, 4957. DOI: <https://doi.org/10.1038/s41467-022-32632-2>

De Geer, G. (1889). Andmoraner I trakten mellan spanga och sundbyberg [end moraines in the area between spanga and sundbyberg]. GFF, vol. 11(4), pp. 205-208. DOI: <https://doi.org/10.1080/11035898909444255>

De Geer, G. (1889). Andmoraner I trakten mellan Spanga och Sundbyberg [End moraines in the area between Spanga and Sundbyberg]. Geologiska Foreningens I Stockholm Forhandlingar, vol. 11 (4), pp. 205-208. DOI: <https://doi.org/10.1080/11035898909444255>

De Geer, G. (1912). Geochronology of the last 12000 years. International Journal of Earth Science, vol. 3, pp. 457-471. DOI: <https://doi.org/10.1007/s00531-002-0287-6>

De Geer, G. (1940). Geochronologia Suecia Principales. Kungliga Svenska Vetenskapsakademiens Handlingar, vol. 18, pp. 1-360.

De Geer, G. (1940). Geochronologia suecia principles. Kungl. Sv. Vetenskapsakad. Handl. Tredje serien., Bd, vol. 18(6).

De Geer, G. (1940). Geochronologia Suecia Principles. Kungl. Sv. Vetenskapsakad. Handl. Tredje serien., Bd 18(6)

De Geer, G. (1940). Geochronologia suecia principles. Kungl. Sv. Vetenskapsakad. Handl. Tredje serien., Bd, vol. 18(6).

De Geer, G. 1889: Ändmoränerna I trakten mellan Spånga och Sundbyberg. Geologiska Föreningens I Stockholm Förhandlingar 11, 395-397.

De Geer, G. 1940: Geochronologia Suecica Principles. Kungliga Svenska Vetenskapsakademiens Handlingar III, 18, 367.

Dewald, N., Livingstone, S.J. & Clark, C.D. (2022). Subglacial meltwater routes of the Fennoscandian Ice Sheet. J Maps, 18(2), pp. 382-396. DOI: <https://doi.org/10.1080/17445647.2022.2071648>

Dix, J.K. & Duck, R.W. (2000). A high-resolution seismic stratigraphy from a Scottish sea loch and its implications for Loch Lomond Stadial deglaciation. Journal of Quaternary Science, vol. 15(6), pp. 645-656. DOI: [https://doi.org/10.1002/1099-1417\(200009\)15:6<645::AID-JQS559>3.0.CO;2-Q](https://doi.org/10.1002/1099-1417(200009)15:6<645::AID-JQS559>3.0.CO;2-Q)

- Dix, J.K. & Duck, R.W. (2000). A high-resolution seismic stratigraphy from a Scottish sea loch and its implications for Loch Lomond Stadial deglaciation. *J. Quaternary Sci.*, vol. 15 (6), pp. 645-656. ISSN: 0267-8179
- Docquier, D., Perichon, L. & Frank, P. (2011). Representing Grounding Line Dynamics in Numerical Ice Sheet Models: Recent Advances and Outlook. *Surveys in Geophysics*, vol. 32(4-5), pp. 417-435. DOI: <https://doi.org/10.1007/s10712-011-9133-3>
- Donner, J. (1995). *Quaternary History of Fennoscandia*. Cambridge University Press, Cambridge.
- Donner, J. (1995). The Quaternary History of Scandinavia. *World and Regional Geology Series*, vol. 7. Cambridge, New York, Port Chester, Melbourne, Sydney. ISBN: 0 521 41730 9. *Geological Magazine*, vol. 133(4). DOI: <https://doi.org/10.1017/S0016756800007639>
- Donner, J. (2010). The Younger Dryas age of the Salpausselkä moraines in Finland. *Bulletin of the Geological Society of Finland*, vol. 82, pp. 69-80. Retrieved from [https://www.geologinenseura.fi/sites/geologinenseura.fi/files/donner\\_2010.pdf](https://www.geologinenseura.fi/sites/geologinenseura.fi/files/donner_2010.pdf)
- Donner, J. (2010). The Younger Dryas age of the Salpausselkä moraines in Finland. *Bulletin of the Geological Society of Finland*, vol. 82, pp. 69-80. Retrieved from: [https://www.geologinenseura.fi/sites/geologinenseura.fi/files/donner\\_2010.pdf](https://www.geologinenseura.fi/sites/geologinenseura.fi/files/donner_2010.pdf)
- Dowdeswell, J.A. & Elverhøi, A. (2002). The timing of initiation of fast-flowing ice streams during a glacial cycle inferred from glacial marine sedimentation. *Marine Geology*, vol. 188(1-2), pp. 3-14. DOI: [https://doi.org/10.1016/S0025-3227\(02\)00272-4](https://doi.org/10.1016/S0025-3227(02)00272-4)
- Dowdeswell, J.A., Batchelor, C.L., Montelli, A., Ottesen, D., Christie, F.D.W., Dowdeswell, E.K. & Evans, J. (2020). Delicate seafloor landforms reveal past Antarctic grounding-line retreat of kilometers per year. *Science*, vol. 368(6494), pp. 1020-1024. DOI: <https://doi.org/10.1126/science.aaz30559>
- Dowdeswell, J.A., Fugelli, E.M.G. & Batchelor, C.L. (2016). Grounding-zone wedges on the West Greenland shelf imaged from multibeam and seismic data. *Geological Society, London, Memoirs*, vol. 46, pp. 235-236. DOI: <https://doi.org/10.1144/m46.63>

- Dowdeswell, J.A., Ottesen, D. & Rise, L. (2006). Flow switching and large-scale deposition by ice streams draining former ice sheets. *Geology*, vol. 34(4), pp. 313-316. DOI: <https://doi.org/10.1130/G22253.1>
- Dowdeswell, J.A., Ottesen, D., Evans, J., Ó Cofaigh, C. & Anderson, J.B. (2008). Submarine glacial landforms and rates of ice-stream collapse. *Geology*, vol. 36, pp. 819-822. DOI: <https://doi.org/10.1130/G24808A.1>
- Dowdeswell, J.A. & Fugelli, E.M.G. (2012). The seismic architecture and geometry of grounding-zone wedges formed at the marine margins of past ice sheets. *GSA Bulletin*, vol. 124(11-12), pp. 1750-1761. DOI: <https://doi.org/10.1130/B30628.1>
- Dubovik, O., Schuster, G.L., Xu, F., Hu, Y., Bösch, H., Landgraf, J. & Li, Z. (2021). Grand Challenges in Satellite Remote Sensing. *Frontiers Remote Sensing*, vol. 2. DOI: <https://doi.org/10.3389/frsen.2021.619818>
- Dulfer, H.E., Margold, M., Darvill, C.M. & Stroeve, A.P. (2022). Reconstructing the advance and retreat dynamics of the central sector of the last Cordilleran Ice Sheet. *Quaternary Science Reviews*, vol. 284(107465). DOI: <https://doi.org/10.1016/j.quascirev.2022.107465>
- Dulfer, H.E., Margold, M., Darvill, C.M. & Stroeve, A.P. (2022). Reconstructing the advance and retreat dynamics of the central sector of the last Cordilleran Ice Sheet. *Quaternary Science Reviews*, vol. 281. DOI: <https://doi.org/10.1016/j.quascirev.2022.107465>
- Dunlop, P. & Clark, C.D. (2006). The morphological characteristics of ribbed moraine. *Quaternary Science Reviews*, vol. 25(13-14), pp. 1668-1691. DOI: <https://doi.org/10.1016/j.quascirev.2006.01.002>
- Dunlop, P. (2004). The characteristics of ribbed moraine and assessment of theories of their genesis. PhD Thesis, University of Sheffield. Retrieved from <https://etheses.whiterose.ac.uk/12841/>
- Dyba, K. (2024). Explanation of the influence of geomorphometric variables on the landform classification based on selected areas in Poland. *Scientific Reports, Nature*, vol. 14. DOI: <https://doi.org/10.1038/s41598-024-56066-6>

- Dyke, A. S., Andrews, J. T., Clark, P. U., England, J. H., Miller, G. H., Shaw, J. & Veillette, J. J. (2002). The Laurentide and Innuitian ice sheets during the Last Glacial Maximum. *Quaternary Science Reviews* 21, 9-31, [https://doi.org/10.1016/S0277-3791\(01\)00095-6](https://doi.org/10.1016/S0277-3791(01)00095-6).
- Eilertsen, R., Corner, G. & Hansen, L. (2015). Using LiDAR data to characterize and distinguish between different types of raised terraces in a fjord-valley setting. *GFF*, vol. 137, pp. 353-361. DOI: <https://doi.org/10.1080/11035897.2015.1111409>
- Ely, J.C. (2015). Flow Signatures on the Bed and the Surface of Ice Sheets. PhD thesis, University of Sheffield. Retrieved from <https://etheses.whiterose.ac.uk/12585/>
- Ely, J.C., Clark, C.D., Bradley, S.L., Gregoire, L., Gandy, N., Gasson, E., Veness, R.L.J. & Archer, R. (2024). Behavioural tendencies of the last British-Irish Ice Sheet revealed by data-model comparison. *Journal of Quaternary Science*, vol. 39(6), pp. 839-871. DOI: <https://doi.org/10.1002/jqs.3628>
- Ely, J.C., Clark, C.D., Spagnolo, M., Hughes, A. L.C. & Stokes, C. R. (2017). Using the size and position of drumlins to understand how they grow, interact and evolve. *Earth Surface Processes and Landforms*, vol. 43 (2). DOI: <https://doi.org/10.1002/esp.4241>
- Ely, J.C., Clark, C.D., Spagnolo, M., Hughes, A.L.C. & Stokes, C.R. (2017). Using the size and position of drumlins to understand how they grow, interact and evolve. *Earth Surface Processes and Landforms*, vol. 43(5), pp. 1073-1087. DOI: <https://doi.org/10.1002/esp.4241>
- Ely, J.C., Stevens, D., Clark, C.D. & Butcher F.E.G. (2023). Numerical modelling of subglacial ribs, drumlins, herringbones, and mega-scale glacial lineations reveals their developmental trajectories and transitions. *Earth Surface Processes and Landforms*. ISSN 0197-9337. DOI: <https://doi.org/10.1002/esp.5529>
- Embleton, C. & King, C.A.M. (1968). *Geomorphology, Glacial and Periglacial*. Hodder & Stoughton Educational. ISBN 10: 0713153776. ISBN 13: 9780713153774
- Embleton, C. & King, C.A.M. (1968). *Glacial and Periglacial Geomorphology*. Edward Arnold (Publishers) Ltd. SBN: 7131 5377 6

- England, J.H., Coulthard, R.D., Furze, M.F.A. & Dow, C.F. (2022). Catastrophic ice shelf collapse along the NW Laurentide Ice Sheet highlights the vulnerability of marine-based ice margins. *Quaternary Science Reviews*, vol. 286(107524). DOI: <https://doi.org/10.1016/j.quascirev.2022.107524>
- Ensminger, S.L., Alley, R.B., Evenson, E.B., Lawson, D.E. & Larson, G.J. (2001). Basal-crevasse-fill origin of laminated debris bands at Matanuska Glacier, Alaska, U.S.A. *Journal of Glaciology*, vol. 47 (158). DOI: <https://doi.org/10.3189/172756501781832007>
- Eronen, M., Glückert, G., Hatakka, L., van de Plassche, O., van der Plicht, J. & Rantala, P. (2001). Rates of Holocene isostatic uplift and relative sea-level lowering of the Baltic in SW Finland based on studies of isolation contacts. *Boreas*, vol. 30(1), pp. 17-30. Oslo. ISSN: 0300-9483. Retrieved from: <https://pure.rug.nl/ws/portalfiles/portal/6663240/2001BoreasEronen.pdf>
- ESRI Inc. (2020). ArcGIS Pro (Version 2.5). ESRI Inc. <https://www.esri.com/en-us/arcgis/products/arcgis-pro/overview>.
- Evans, D. (2004). *Practical guide to the study of glacial sediments*. Taylor & Francis Group.
- Evans, D. J. A. & Benn, D. I. 2004: *Practical guide to the study of glacial sediments*. 11 pp. Arnold, London.
- Evans, D. J. A., Phillips, E. R., Hiemstra, J. F. & Auton, C. A. 2006: Subglacial till: Formation, sedimentary characteristics and classification. *Earth-Science Reviews* 78, 115-176, <https://doi.org/10.1016/j.earscirev.2006.04.001>.
- Evans, D. J. A., Storrar, R. D. & Rea, B. R. 2016: Crevasse-squeeze ridge corridors: Diagnostic features of late-stage palaeo-ice stream activity. *Geomorphology* 258, 40-50, <https://dx.doi.org/10.1016/j.geomorph.2016.01.017>.
- Evans, D.J.A. & Orton, C. (2015). Heinabergsjökull and Skalafellsjökull, Iceland: active temperate piedmont lobe and outwash head glacial landsystem. *Journal of Maps*, vol. 11(3), pp. 415-431. DOI: <https://doi.org/10.1080/17445647.2014.919617>

- Evans, D.J.A. & Rea, B.R. (1999). Geomorphology and sedimentology of surging glaciers: a land-systems approach. *Annals of Glaciology*, vol. 28. International Glaciological Society. DOI: <https://doi.org/10.3189/172756499781821823>
- Evans, D.J.A. (1991). High Arctic Thrust Block Moraines. *Canadian Geographies*, vol. 35(1), pp. 93-97. DOI: <https://doi.org/10.1111/j.1541-0064.1991.tb01628.x>
- Evans, D.J.A., Ewertowski, M., Roberts, D.H. & Tomczyk, A.M. (2022). The historical emergence of a geometric and sinuous ridge network at the Hørbyebreen polythermal glacier snout, Svalbard and its use in the interpretation of ancient glacial landforms. *Geomorphology*, vol. 406. DOI: <https://doi.org/10.1016/j.geomorph.2022.108213>
- Evans, D.J.A., Ewertowski, M., Roberts, D.H. & Tomczyk, A.M. (2022). The historical emergence of a geometric and sinuous ridge network at the Horbyebreen polythermal glacier snout, Svalbard and its use in the interpretation of ancient glacial landforms. *Geomorphology*, vol. 406, 108213. DOI: <https://doi.org/10.1016/j.geomorph.2022.108213>
- Evans, D.J.A., Storrar, R.D. & Rea, B.R. (2016). Crevasse-squeeze ridge corridors: Diagnostic features of late-stage palaeo-ice stream activity. *Geomorphology*, vol. 258, pp. 40-50. DOI: <https://doi.org/10.1016/j.geomorph.2016.01.017>
- Evans, D.J.A., Storrar, R.D. & Rea, B.R. (2016). Crevasse-squeeze ridge corridors: Diagnostic features of late-stage palaeo-ice stream activity. *Geomorphology*, vol. 258, pp. 40-50. DOI: <https://doi.org/10.1016/j.geomorph.2016.01.017>
- Evans, D.J.A., Twigg, D.R. Rea, B.R. & Shand, M. (2007). Surficial geology and geomorphology of the Bruarjokull surging glacier landsystem. *Journal of Maps*, vol. 3 (1), pp. 349-367. DOI: <https://doi.org/10.1080/jom.2007.9710850>
- Evans, I.S. (2012). Geomorphometry and landform mapping: What is a landform? *Geomorphology*. Vol. 137(1), pp. 94-106. DOI: <https://doi.org/10.1016/j.geomorph.2010.09.029>

- Farnsworth, W.R., Ingólfsson, O., Retelle, M. & Schomacker, A. (2016). Over 400 previously undocumented Svalbard surge-type glaciers identified. *Geomorphology*, vol. 264, pp. 52-60. DOI: <https://dx.doi.org/10.1016/j.geomorph.2016.03.025>
- Farnsworth, W.R., Ingólfsson, Ó., Retelle, M. & Schomacker, A. (2016). Over 400 previously undocumented Svalbard surge-type glaciers identified. *Geomorphology*, vol. 264, pp. 52-60. DOI: <https://doi.org/10.1016/j.geomorph.2016.03.025>
- Feldmann, J., Albrecht, T., Khroulev, C., Pattyn, F. & Levermann, A. (2014). Resolution-dependent performance of grounding line motion in a shallow model compared with a full-Stokes model according to the MISMIP3d intercomparison. *Journal of Glaciology*, vol. 60(220), pp. 353-360. DOI: <https://doi.org/10.3189/2014JoG13J093>
- Finlayson, A. & Bradwell, T. (2008). Morphological characteristics, formation and glaciological significance of Rogen moraine in northern Scotland. *Geomorphology*, 101 (4). 607-617. DOI: <https://doi.org/10.1016/j.geomorph.2008.02.013>
- Finlayson, A., Bradwell, T., Golledge, N. & Merritt, J. (2007). Morphology and Significance of Transverse Ridges (De Geer Moraines) Adjacent to the Moray Firth, NE Scotland. *Scottish Geographical Journal*, vol. 123(4), pp. 257-270. DOI: <https://doi.org/10.1080/14702540801968477>
- Finlayson, A.G. & Bradwell, T. (2008). Morphological characteristics, formation and glaciological significance of Rogen moraine in northern Scotland. *Geomorphology*, vol. 101(4), pp. 607-617. DOI: <https://doi.org/10.1016/j.geomorph.2008.02.013>
- Finlayson, D., Bradwell, T., Golledge, N. & Merritt, J. (2007). Morphology and Significance of Transverse Ridges (De Geer Moraines) Adjacent to the Moray Firth, NE Scotland. *Scottish Geographical Journal*, vol. 123 (4), pp. 257-270. DOI: <https://doi.org/10.1080/14702540801968477>
- Fisher, T.G., Smith, D.G. & Andrew, J.T. (2002). Preboreal oscillation caused by a glacial Lake Agassiz flood. *Quaternary Science Reviews*, vol. 21(8-9), pp. 873-878. DOI: [https://doi.org/10.1016/S0277-3791\(01\)00148-2](https://doi.org/10.1016/S0277-3791(01)00148-2)



- Fisher, T.G., Smith, D.G. & Andrews, J.T. (2002). Preboreal oscillation caused by glacial Lake Agassiz flood. *Quaternary Science Reviews*, vol. 21(8-9), pp. 873-878. DOI: [https://doi.org/10.1016/S0277-3791\(01\)00148-2](https://doi.org/10.1016/S0277-3791(01)00148-2)
- Fredin, O., Bergstrøm, B., Hansen, L., Longva, O., Nesje, A. & Sveian, H. (2013). Glacial landforms and Quaternary landscape development in Norway. In book: *Quaternary Geology of Norway*, Edition: 13. Chapter: Glacial landforms and Quaternary landscape development in Norway. Geological Survey of Norway Special Publication.
- Friedl, P., Weiser, F., Fluhner, A. & Braun, M.H. (2020). Remote sensing of glacier and ice sheet grounding lines: A review. *Earth-Science Reviews*, vol. 201(102948). DOI: <https://doi.org/10.1016/j.earscirev.2019.102948>
- Frödin, G. (1916). Über einige spätglaziale Kalbungbuchten und fluvioglaziale Estuarien im mittleren Schweden. *Bull. Geol. Inst. Upsala*, 15, pp. 149-174.
- Frödin, G. 1916: Über einige spätglaziale Kalbungbuchten und fluvioglaziale Estuarien im mittleren Schweden. *Bull. Geol. Inst. Upsala* 15, 149–174.
- Frydrych, M. (2022). Morphology of eskers in Poland, southward of the Last Glacial Maximum. *Geomorphology*, vol. 412. DOI: <https://doi.org/10.1016/j.geomorph.2022.108418>
- Frydrych, M. (2022). Morphology of eskers in Poland, southward of the Last Glacial Maximum. *Geomorphology*, vol. 415. DOI: <https://doi.org/10.1016/j.geomorph.2022.108418>
- Frydrych, M. (2022). Morphology of eskers in Poland, southward of the Last Glacial Maximum. *Geomorphology*. Vol 415(108418). DOI: <https://doi.org/10.1016/j.geomorph.2022.108418>
- Fu, W., Ma, J., Chen, P & Chen, F. (2019). Remote Sensing Satellites for Digital Earth. In: Guo, H., Goodchild, M.F., Annoni, A. (eds). *Manual of Digital Earth*. Springer, Singapore. DOI: [https://doi.org/10-1007/978-981-31-9915-3\\_3](https://doi.org/10-1007/978-981-31-9915-3_3). ISBN: 978-981-32-9914-6

- Fyfe, G.J. (1990). The effect of water depth on ice-proximal glaciolacustrine sedimentation: Salpausselkä I, southern Finland. *Boreas*, vol. 19(2), pp. 147-164. DOI: <https://doi.org/10.1111/j.1502-3885.1990.tb00576.x>
- Fyke, J., Sergienko, O., Löfverström, M., Price, S. & Lenaerts, J.T.M. (2018). An Overview of Interactions and Feedbacks Between Ice Sheets and the Earth System. *Reviews of Geophysics*, vol. 56(2), pp. 361-408. DOI: <https://doi.org/10.1029/2018RG000600>
- Fyke, J., Sergienko, O., Löfverström, M., Price, S., Lenaerts, J.T.M. (2018). An overview of Interactions and Feedbacks Between Ice Sheets and the Earth System. *Reviews of Geophysics*, vol. 56(2), pp. 361-408. DOI: <https://doi.org/10.1029/2018RG000600>
- Fyke, J., Sergienko, O., Löfverström, Price, S. & Lenaerts, J.T.M. (2018). An Overview of Interactions and Feedbacks Between Ice Sheets and the Earth System. *Reviews of Geophysics*, vol. 56(2), pp. 361-408. DOI: <https://doi.org/10.1029/2018RG000600>
- Gandy, N., Gregoire, L.J., Ely, J.C., Clark, C.D., Hodgson, D.M., Lee, V., Bradwell, T. & Ivanovic, R.F. (2018). Marine ice sheet instability and ice shelf buttressing of the Minch Ice Stream, northwest Scotland. *The Cryosphere*, vol. 12(11), pp. 3635-3651. DOI: <https://doi.org/10.5194/tc-12-3635-2018>
- Gandy, N., Gregoire, L.J., Ely, J.C., Clark, C.D., Hodgson, D.M., Lee, V., Bradwell, T. & Ivanovic, R.F. (2018). Marine ice sheet instability and ice shelf buttressing of the Minch Ice Stream, northwest Scotland. *The Cryosphere*, vol. 12(11), pp. 3635-3651. DOI: <https://doi.org/10.5194/tc-12-3635-2018>
- Gandy, N., Gregoire, L.J., Ely, J.C., Cornford, S.L., Clark, C.D. & Hodgson, D.M. (2019). Exploring the ingredients required to successfully model the placement, generation, and evolution of ice streams in the British-Irish Ice Sheet. *Quaternary Science Reviews*, vol. 223(105915). DOI: <https://doi.org/10.1016/j.quascirev.2019.105915>
- Garcia-Ruiz, J.M, Gomez-Villar, A., Ortigosa, L. & Marti-Bono, C. (2000). Morphometry of glacial cirques in the central Spanish Pyrenees. *Geografiska annaler. Series A, Physical geography*, 2000, vol. 82(4), pp. 433-442.
- Giaccone, E., Oriani, F., Tonini, M., Lambiel, C. & Mariéthoz, G. (2021). Using data-driven algorithms for semi-automated geomorphological mapping. *Stochastic*

Environmental Research and Risk Assessment. DOI: <https://doi.org/10.1007/s00477-021-02062-5>

Glacier Adventure. (2024). Climate Centre, Research Blog. Retrieved from: <https://glacieradventure.is/blog/crevasse-squeeze-ridges-at-breidamerkurjokull/>

Glückert, G. (1991). The Ancyclus and Litorina transgressions of the Baltic in southwest Finland. *Quaternary International*, vol. 9, pp. 27-32. DOI: [https://doi.org/10.1016/1040-6182\(91\)90060-2](https://doi.org/10.1016/1040-6182(91)90060-2)

Glückert, G. (1995). The Salpausselkä End Moraines in southwestern Finland. *Glacial Deposits I Northeast Europe* (1st Ed.). CRC Press. ISBN: 9781003077695

Glückert, G. 1995: The Salpausselkä End Moraines in southwestern Finland. In: Elhers, J., Kosarski, S., Gibbard, P. (eds.), *Glacial Deposits in North-East Europe*. 51-56 pp. Taylor & Francis Group, London.

Glückert, G., (1986). The First Salpausselkä at Lohja, southern Finland. *Bull. Geol. Soc. Finland*, vol. 58(1), pp. 45—55. DOI: <https://doi.org/10.17741/bgsf/58.1.003>

Golledge, N. & Phillips, E. (2008). Sedimentology and architecture of De Geer moraines in the western Scottish Highlands, and implications for grounding-line glacier dynamics. *Sedimentary Geology*, vol. 208(1-2), pp. 1-14. DOI: <https://doi.org/10.1016/j.sedgeo.2008.03.009>

Golledge, N. & Phillips, E. (2008). Sedimentology and architecture of De Geer moraines in western Scottish Highlands, and implications for grounding-line glacier dynamics. *Sedimentary Geology*, vol. 208(1-2), pp. 1-14. DOI: <https://doi.org/10.1016/j.sedgeo.2008.03.009>

Golledge, N. & Phillips, E. 2008: Sedimentology and architecture of De Geer moraines in western Scottish Highlands, and implications for grounding-line glacier dynamics. *Sedimentary Geology* 208, 1-14, <https://doi.org/10.1016/j.sedgeo.2008.03.009>.

Golledge, N. R. & Phillips, E. (2008). Sedimentology and architecture of De Geer moraines in the western Scottish Highlands, and implications for grounding-line glacier dynamics. *Sedimentary Geology*, vol. 208 (1-2), pp. 1-14. DOI: <https://doi.org/10.1016/j.sedgeo.2008.03.009>

- Gomez-Heras, M., Ortega-Becerril, J.A., Garrote, J., Fort, R. & Lopez-Gonzalez, L. (2019). Morphometric measurements of bedrock rivers at different spatial scales and applications to geomorphological heritage research. *Progress in Earth and Planetary Science*, vol. 6, article, 29. DOI: <https://doi.org/10.1186/s40645-019-0275-0>
- Goodship, A. & Alexanderson, H. (2020). Dynamics of a retreating ice sheet: a LiDAR study in Värmland, SW Sweden. *GFF*, vol. 142(4), pp. 325-345. DOI: <https://doi.org/10.1080/11035897.2020.1822437>
- Gowan, E. J., Zhang, X., Khosravi, S., Rovere, A., Stocchi, P., Hughes, A. L. C., Gyllencreutz, R., Mangerud, J., Svendsen, J.- I. & Lohmann, G. 2021: A new global ice sheet reconstruction for the past 80 000 years. *Nature Communications* 12, 1199, <https://doi.org/10.1038/s41467-021-21469-w>.
- Gowan, E.J. (2013). An assessment of the minimum timing of ice free conditions of the western Laurentide Ice Sheet. *Quaternary Science Reviews*, vol. 75, pp. 100-113. DOI: <https://doi.org/10.1016/j.quascirev.2013.06.001>
- Gowan, E.J., Zhang, X., Khosravi, S., Rovere, A., Stocchi, P., Hughes, A.L.C., Gyllencreutz, R., Mangerud, J., Svendsen, J.-I. & Lohmann, G. (2021). A new global ice sheet reconstruction for the past 80 000 years. *Nature Communication*. DOI: <https://doi.org/10.1038/s41467-021-21469-w>
- Gowan, E.J., Zhang, X., Khosravi, S., Rovere, A., Stocchi, P., Hughes, A.L.C., Gyllencreutz, R., Mangerud, J., Svendsen, J.-I. & Lohmann, G. (2021). A new global ice sheet reconstruction for the past 80 000 years. *Nature Communications*, vol. 12(1199). DOI: <https://doi.org/10.1038/s41467-021-21469-w>
- Graham, A.G.C., Dutrieux, P., Vaughan, D.G., Nitsche, F.O., Gyllencreutz, R., Greenwood, S.L., Larter, R.D. & Jenkins, A. (2013). Seabed corrugations beneath an Antarctic ice shelf revealed by autonomous underwater vehicle survey: Origin and implications for the history of Pine Island Glacier. *Journal of Geophysical Research: Earth Surface*, vol. 118(3), pp. 1356-1366. DOI: <https://doi.org/10.1002/jgrf.20087>
- Graham, A.G.C., Wåhlin, A., Hogan, K.A., Nitsche, F.O., Heywood, K.J., Totten, R.L., Smith, J.A., Hillenbrand, C.-D., Simkins, L.M., Anderson, J.B., Wellner, J.S. & Larter R.D. (2022).

- Rapid retreat of Thwaites Glacier in the pre-satellite era. *Nature Geoscience*, vol. 15, pp. 706-713. DOI: <https://doi.org/10.1038/s41561-022-01019-9>
- Greenwood, S.L. & Clark, C.D. (2009). Reconstructing the last Irish Ice Sheet 2: a geomorphologically-driven model of ice sheet growth, retreat and dynamics. *Quaternary Science Reviews*, vol. 28(27-28), pp. 3101-3123. DOI: <https://doi.org/10.1016/j.quascirev.2009.09.014>
- Greenwood, S.L., Clark, C.D. & Hughes, A.L.C. (2007). Formalising an inversion methodology for reconstructing ice-sheet retreat patterns from meltwater channels: application to the British Ice Sheet. *Journal of Quaternary Science*, vol. 22(6), pp. 637-645. DOI: <https://doi.org/10.1002/jqs.1083>
- Greenwood, S.L., Clason, C.C., Mikko, H., Nyberg, J., Petersson, G. & Smith, C.A. (2015). Integrated use of LiDAR and multibeam bathymetry reveals onset of ice streaming in the northern Bothnian Sea. *GFF*, vol. 137, pp. 284-292. DOI: <https://doi.org/10.1080/11035897.2015.1055513>
- Greenwood, S.L., Clason, C.C., Nyberg, J., Jakobsson, M. & Holmlund, P. (2017). The Bothnian Sea ice stream: early Holocene retreat dynamics of the south-central Fennoscandian Ice Sheet. *Boreas*, vol. 46, pp. 346-362. DOI: <https://doi.org/10.1111/bor.12217>. ISSN 0300-9483
- Greenwood, S.L., Simkins, L.M., Winsborrow, M.C.M. & Bjarnadóttir, L.R. (2021). Exceptions to bed-controlled ice sheet flow and retreat from glaciated continental margins worldwide. *Science Advances*, vol. 7(3). DOI: <https://doi.org/10.1126/sciadv.abb6291>
- Greenwood, S.L., Simkins, L.M., Winsborrow, M.C.M. & Bjarnadóttir, L.R. (2021). Exceptions to bed-controlled ice sheet flow and retreat from glaciated continental margins worldwide. *Science Advances*, vol. 7(3). DOI: <https://doi.org/10.1126/ciadv.abb6291>
- Hager, A.O., Sutherland, D.A. & Slater, D.A. (2024). Local forcing mechanisms challenge parameterizations of ocean thermal forcing for Greenland tidewater glaciers. *The Cryosphere*, vol. 18(2), pp. 911-932. DOI: <https://doi.org/10.5194/tc-18-911-2024>

- Hambrey, M. (1994). *Glacial Environments*. UCL Press Limited, London. ISBN: 1-85728-005-9 HB; 1-85728-004-0 PB
- Haresign, E. & Warren, C.R. (2005). Melt rates at calving termini: A study at Glaciar León, Chilean Patagonia. *Geological Society Special Publication*, vol. 242, pp. 99-109. DOI: <https://doi.org/10.1144/GSL.SP.2005.242.01.09>
- Harrison, D., Ross, N., Russell, A. J. & Jones, S. J. 2022: Ground-penetrating radar (GPR) investigations of a large-scale buried ice-marginal landsystem, Skeiðarársandur, SE Iceland. *Boreas* 51, 824-846, <https://doi.org/10.1111/bor.12587>.
- Harrison, D., Ross, N., Russell, A.J. & Jones, S.J. (2022). Ground-penetrating radar (GPR) investigations of a large-scale buried ice-marginal landsystem, Skeiðarársandur, SE Iceland. *Boreas*, vol. 51(4), pp. 824-846. DOI: <https://doi.org/10.1111/bor.12587>
- Harrison, D., Ross, N., Russell, A.J. & Jones, S.J. (2022). Ground-penetrating radar (GPR) investigations of a large-scale buried ice-marginal landsystem, Skeiðarársandur, SE Iceland. *Boreas*, vol. 51(4), pp. 824-846. DOI: <https://doi.org/10.1111/bor.12587>
- Haseloff, M. & Sergienko, O. V. 2022: Effects of calving and submarine melting on steady states and stability of buttressed marine ice sheets. *Journal of Glaciology* 68, 1149-1166, <https://doi.org/10.1017/jog.2022.29>.
- Haseloff, M. (2015). *Modelling the migration of ice stream margins*. The Faculty of Graduate and Postdoctoral Studies, The University of British Columbia, Vancouver. Retrieved from [https://central.bac-lac.gc.ca/.item?id=TC-BVAU-54268&op=pdf&app=Library&oclc\\_number=1032934150](https://central.bac-lac.gc.ca/.item?id=TC-BVAU-54268&op=pdf&app=Library&oclc_number=1032934150)
- Hemming, S.R. (2004). Heinrich events: Massive late Pleistocene detritus layers of the North Atlantic and their global climate imprint. *Reviews of Geophysics*, vol. 42(1), pp. 1-43. DOI: <https://doi.org/10.1029/2003RG000128>
- Hill, E.A., Urruty, B., Reese, R., Garbe, J., Gagliardini, O., Durand, G., Gillet-Chaulet, F., Gudmundsson, G.H., Winkelmann, R., Chekki, M., Chandler, D & Langebroek, P.M. (2023). The stability of present-day Antarctic grounding lines – Part 1: No indication of ice sheet instability in the current geometry. *The Cryosphere*, vol. 17(9), pp. 3739-3759. DOI: <https://doi.org/10.5194/tc-17-3739-2023>

- Hill, E.A., Urruty, B., Reese, R., Garbe, J., Gagliardini, O., Durand, G., Gillet-Chaulet, F., Gudmundsson, G.H., Winkelmann, R., Chekki, M., Chandler, D. & Langebroek, P.M. (2023). The stability of present-day Antarctic grounding lines – Part 1: No indication of marine ice sheet instability in the current geometry. *The Cryosphere*, vol. 17(9), pp. 3739-3759. DOI: <https://doi.org/10.5194/tc-17-3739-2023>
- Hogan, K.A., Warburton, K.L.P., Graham, A.G.C., Neufeld, J.A., Hewitt, D.R., Dowdeswell, J.A. & Larter, R.D. (2023). Towards modelling of corrugation ridges at ice-sheet grounding lines. *The Cryosphere*, vol. 17(7), pp. 2645-2664. DOI: <https://doi.org/10.5194/tc-17-2645-2023>
- Hogan, K.A., Warburton, K.L.P., Graham, A.G.C., Neufeld, J.A., Hewitt, D.R., Dowdeswell, J.A. & Larter, R.D. (2023). Towards modelling of corrugation ridges at ice-sheet grounding lines. *The Cryosphere*, vol. 17, pp. 2645-2664. DOI: <https://doi.org/10.5194/tc-17-2645-2023>
- Holmquist, B. & Wohlfarth, B. (1998). An evaluation of the Late Weichselian Swedish varve chronology based on cross-correlation analysis. *GFF*, vol. 120(1), 35-46. DOI: <https://doi.org/10.1080/11035899801201035>
- Hoppe, G. (1957). Problems of Glacial Morphology and the Ice Age. *Geografiska Annaler*, vol. 39(1), pp. 1-18. DOI: <https://doi.org/10.1080/20014422.1957.11880892>
- Hoppe, G. (1959). Glacial Morphology and Inland Ice Recession in Northern Sweden. *Geografiska Annaler*, vol. 41(4), pp. 193-212. DOI: <https://doi.org/10.1080/20014422.1959.11907951>
- Hoppe, G. (1959). Glacial morphology and inland ice recession in northern Sweden. *Geografiska Annaler*, vol. 41, pp. 193-212.
- Hoppe, G. 1959: Glacial morphology and inland recession in Northern Sweden. *Geografiska Annaler* 41, 193-212, <https://www.jstor.org/stable/4626803>.
- Houser, C., Lehner, J. & Smith, A. (2022). The Field Geomorphologist in a Time of Artificial Intelligence and Machine Learning. *Annals of the American Association of*

Geographers, vol. 112(5), pp. 1260-1277. DOI:  
<https://doi.org/10.1080/24694452.2021.1985956>

Hubbard, B & Glasser, N. (2005). *Field Techniques in Glaciology and Glacial Geomorphology*. John Wiley & Sons Ltd, Chichester. ISBN: 13 978-0-470-84426-7

Hughes, A. L. C., Gyllencreutz, R., Lohne, Ø. S., Mangerud, J., Svendsen, J. I. 2016: The last Eurasian ice sheets – a chronological database and time-slice reconstruction, DATED-1. *Boreas* 45, 1-45, <https://doi.org/10.1111/bor.12142>.

Hughes, A.L.C., Clark, C.D. & Jordan, C.J. (2014). Flow-pattern evolution of the last British Ice Sheet. *Quaternary Science Reviews*, vol. 89, pp. 148-168. DOI: <https://doi.org/10.1016/j.quascirev.2014.02.002>

Hughes, A.L.C., Gyllencreutz, R., Lohne, Ø.S., Mangerud, J. & Svendsen, J.I. (2016). The last Eurasian ice sheets – a chronological database and time-slice reconstruction, DATED-1. *Boreas*, vol. 45(1), pp. 1-45. DOI: <https://doi.org/10.1111/bor.12142>

Hughes, P.D., Gibbard, P.L. & Ehlers, J. (2013). Timing of glaciation during the last glacial cycle: evaluating the concept of a global ‘Last Glacial Maximum’. *Earth-Science Reviews*, vol. 125, pp. 171-198. DOI: <https://doi.org/10.1016/j.earscirev.2013.07.003>

Ian Broad. [Create Points on Lines Tool]. Web: [www.ianbroad.com](http://www.ianbroad.com)

Ingólfsson, Ó., Benediktsson, Ö., Schomacker, A., Kjaer, K.H., Brynjólfsson, S., Jónsson, S.A., Korsgaard, N.J. & Johnson, M.D. (2016). Glacial geological studies of surge-type glaciers in Iceland – Research status and future challenges. *Earth-Science Reviews*, vol. 152, pp. 37-69. DOI: <https://doi.org/10.1016/j.earscirev.2015.11.008>

Ingólfsson, Ó., Norðdahl, H. & Schomacker, A. (2010). 4 Deglaciation and Holocene Glacial History of Iceland. *Developments in Quaternary Sciences*, vol. 13, pp. 51-68. DOI: [https://doi.org/10.1016/S1571-0866\(09\)01304-9](https://doi.org/10.1016/S1571-0866(09)01304-9)

IPCC. (2023). *Climate Change 2023: Synthesis Report. Contribution of Working Groups I, II and III to the Sixth Assessment Report of the Intergovernmental Panel on Climate Change* [Core Writing Team, H. Lee and J. Romero (eds.)]. IPCC, Geneva, Switzerland, pp. 35-115. DOI: <https://doi.org/10.19327/IPCC/AR6-9789291691647>



- IPCC. (2023). Sections. In: Climate Change 2023: Synthesis Report. Contribution of Working Groups I, II and III to the Sixth Assessment Report of the Intergovernmental Panel on Climate Change [Core Writing Team, H. Lee and J. Romero (eds.)]. IPCC, Geneva, Switzerland, pp. 35-115. DOI: <https://doi.org/10.59327/IPCC/AR6-9789291691647>
- Iverson, N.R. (1991). Morphology of glacial striae: Implications for abrasion of glacier beds and fault surfaces. *GSA Bulletin*, vol. 103(10), pp. 1308-1316. DOI: [https://doi.org/10.1130/0016-7606\(1991\)103<1308:MOGSIF>2.3.CO;2](https://doi.org/10.1130/0016-7606(1991)103<1308:MOGSIF>2.3.CO;2)
- Jakobsson, M. & Anderson, J.B. (2016). Corrugation ridges in the Pine Island Bay glacier trough, West Antarctica. *Geological Society, London, Memoirs*, vol. 46, pp. 265-266. DOI: <https://doi.org/10.1144/M46.5>
- Jakobsson, M., Anderson, J.B., Nitsche, F.O., Dowdeswell, J.A., Gyllencreutz, R., Kirchner, N., Rezwan, M., O'Regan, M., Alley, R.B., Anandakrishnan, S., Björn, E. & Kirchner, A. (2011). Geological record of ice shelf break-up and grounding line retreat, Pine Island Bay, West Antarctica. *Geology*, vol. 39(7), pp. 691-694. DOI: <https://doi.org/10.1130/G32153.1>
- James, W.H.M., Carrivick, J.L., Quincey, D.J. & Glasser, N.F. (2019). A geomorphology based reconstruction of ice volume distribution at the Last Glacial Maximum across the Southern Alps of New Zealand. *Quaternary Science Reviews*, vol. 219, pp. 20-35. DOI: <https://doi.org/10.1016/j.quascirev.2019.06.035>
- Johansson, P., Lunkka, J. P. & Sarala, P. 2011: Chapter 9 – The Glaciation of Finland. *Developments in Quaternary Sciences* 15, 105-116, <https://doi.org/10.1016/B978-0-444-53447-7.00009-X>.
- Johansson, P., Lunkka, J.P. & Sarala, P. (2011). Glaciation of Finland. In J. Ehlers, P.L. Gibbard, P.D. Hughes (eds.): *Developments in Quaternary Science*, vol. 15, pp. 105-116. DOI: <https://doi.org/10.1016/B978-0-444-53774-7.00009-X>
- Johnson, M.D., Fredin, O., Ojala, A.E.K. & Peterson, G. (2015). Unraveling Scandinavian geomorphology: the LiDAR revolution. *GFF*, vol. 137(4). DOI: <https://doi.org/10.1080/11035897.2015.1111410>

- Johnson, P.G. (1975). Recent Crevasse Filling At The Terminus Of The Donjek Glacier, St. Elias Mountains, Yukon Territory. *Quaetiones Geographicae*, vol. 2, pp. 53-59. University of Ottawa, Canada. UAM.
- Johnson, P.G. (1975). Recent Crevasse Filling At The Terminus Of The Donjek Glacier, St. Elias Mountains, Yukon Territory. *Quaetiones Geographicae*, vol. 2, pp. 53- 29. UAM.
- Jol, H. M. & Bristow, C. S. 2003: GPR in sediments: advice on data collection, basic processing and interpretation, a good practice guide. (eds) in *Ground Penetrating Radar in Sediments*. Geological Society, London, Special Publications, 211, 9-27.
- Jol, H. M. 1995: Ground penetrating radar antennae frequencies and transmitter powers compared for penetration depth, resolution and reflection continuity 1. *Geophysical Prospecting* 43, 693-709, <https://doi.org/10.1111/j.1365-2478.1995.tb00275.x>.
- Jones, R.S., Gudmundsson, G.H., Mackintosh, A.N., McCormack, F.S. & Whitmore, R.J. (2021). Ocean-Driven and Topography-Controlled Nonlinear Glacier Retreat During the Holocene: Southwestern Ross Sea, Antarctica. *Geophysical Research Letters*, vol. 48(5). DOI: <https://doi.org/10.1029/2020GL091454>
- Jonsson, S.A., Schomacker, A. Benediktsson, I.O., Ingolfsson, O. & Johnson, M.D. (2014). The drumlin field and the geomorphology of the Mulajokull surge-type glacier, central Iceland. *Geomorphology*, vol. 207, pp. 213-220. DOI: <https://dx.doi.org/10.1016/j.geomorph.2013.11.007>
- Josenhans, H.W. & Zevenhuizen, J. (1990). Dynamics of the Laurentide Ice Sheet in Hudson Bay, Canada. *Marine Geology*, vol. 92(1-2), pp. 1-26. DOI: [https://doi.org/10.1016/0025-3227\(90\)90024-E](https://doi.org/10.1016/0025-3227(90)90024-E)
- Karagoz, O., Kenkmann, T. & Wulf, G. (2022). Circum-Tharsis wrinkle ridges at Lunae Planum: Morphometry, formation, and crustal implications. *Icarus*, Vol. 374(114808). DOI: <https://doi.org/10.1016/j.icarus.2021.114808>
- Kaufman, D.S. & Calkin, P.E. (1988). Morphometric Analysis of Pleistocene Glacial Deposits in the Kigluaik Mountains, Northwestern Alaska, U.S.A. *Arctic and Alpine Research*, vol. 20(3), pp. 273-284. DOI: <https://doi.org/10.1080/00040851.1988.12002675>

- King, C.A.M. (1982). Morphometry in Glacial Geomorphology. In: Coates, D.R. (Ed.), Glacial Geomorphology. Springer, Dordrecht. DOI: [https://doi.org/10.1007/978-94-011-6491-7\\_5](https://doi.org/10.1007/978-94-011-6491-7_5)
- King, C.A.M. (1982). Morphometry in Glacial Geomorphology. In: Coates, D.R. Glacial Geomorphology. Springer, Dordrecht. DOI: [https://doi.org/10.1007/978-94-011-6491-7\\_5](https://doi.org/10.1007/978-94-011-6491-7_5)
- Kirkbride, M.P. & Warren, C.R. (1999). Tasman Glacier, New Zealand: 20th-century thinning and predicted calving retreat. *Global Planetary Change*, vol. 22(1-4), pp. 11-28. DOI: [https://doi.org/10.1016/S0921-8181\(99\)00021-1](https://doi.org/10.1016/S0921-8181(99)00021-1)
- Kirkham, J.D., Hogan, K.A., Larter, R.D., Self, E., Games, K., Huuse, M., Stewart, M.A., Ottesen, D., Arnold, N.S. & Dowdeswell, J.A. (2021). Tunney valley infill and genesis revealed by high-resolution 3-D seismic data. *The Geological Society of America*. Vol. 49, pp. 1516-1520. DOI: <https://doi.org/10.1130/G49048.1>
- Kjær, K. H., Sultan, L., Krüger, J. & Schomacker, A. (2004). Architecture and sedimentation of outwash fans in front of the Mýrdalsjökull ice cap, Iceland. *Sedimentary Geology*, vol. 172(1-2), pp. 139-163. DOI: <https://doi.org/10.1016/j.sedgeo.2004.08.002>
- Kjaer, K.H., Korsgaard, N.J. & Schomacker, A. (2008). Impact of multiple glacier surges – a geomorphological map from Bruarjokull, East Iceland. *Journal of Maps*, vol. 4 (1), pp. 5-20. DOI: <https://doi.org/10.4113/jom.2008.91>
- Kleman, J. & Borgström, I. (1996). Reconstruction of palaeo-ice sheets: The use of geomorphological data. *Earth Surface Processes and Landforms*, vol. 21(10), pp. 893-909. DOI: [https://doi.org/10.1002/\(SICI\)1096-9837\(199610\)21:10<893::AID-ESP620>3.0.CO;2-U](https://doi.org/10.1002/(SICI)1096-9837(199610)21:10<893::AID-ESP620>3.0.CO;2-U)
- Kleman, J. (1990). On the Use of Glacial Striae for Reconstruction of Paleo-Ice Sheet Flow Patterns. *Geografiska Annaler. Series A, Physical Geography*, vol. 72(3/4), pp. 217-236. DOI: <https://doi.org/10.2307/521150>
- Kleman, J., Hättestrand, C., Borgström, I. & Stroeve, A. (1997). Fennoscandian palaeoglaciology reconstructed using a glacial geological inversion model. *Journal of*

Glaciology, vol. 43(144), pp. 283-299. DOI:  
<https://doi.org/10.3189/S0022143000003233>

Kleman, J., Hättestrand, C., Borgström, I. and Stroeve, A., 1997. Fennoscandian palaeoglaciology reconstructed using a glacial geological inversion model. *Journal of glaciology*, 43, 283-299.

Kleman, J., Jansson, K., De Angelis, H., Stroeve, A.P., Hättestrand, C., Alm, G., Glasser, N. (2010). North American Ice Sheet build-up during the last glacial cycle, 115-21kyr. DOI: <https://doi.org/10.1016/j.quascirev.2010.04.021>

Knight, P. (1999). *Glaciers*. Stanley Thornes (Publishers) Ltd, Cheltenham. ISBN: 0-7487-4000-7

Kowal, K.N. & Worster, M.G. (2020). The formation of grounding zone wedges: theory and experiments. *Journal of Fluid Mechanics*, 898, A12. DOI: <https://doi.org/10.1017/jfm.2020.393>

Kreslavsky, M.A. & Basilevsky, A.T. (1998). Morphometry of wrinkle ridges on Venus: Comparison with other planets. *Journal of Geophysical Research, Planets*. Vol. 103(E5), pp. 11103-11111. DOI: <https://doi.org/10.1029/98JE00360>

Krüger, J. (1994). *Glacial processes, sediments, landforms, and stratigraphy in the terminus region of Mýrdalsjökull, Iceland*. Hans Reitzels Forlag.

Kruger, J. (1997). Development of minor outwash fans at Kötlujökull, Iceland. *Quaternary Science Reviews*, vol. 16(7), pp. 649-659. DOI: [https://doi.org/10.1016/S0277-3791\(97\)00013-9](https://doi.org/10.1016/S0277-3791(97)00013-9)

Kurimo, H. (1982). Ice-lobe formation and function during the deglaciation in Finland and adjacent Soviet Karelia. *Boreas*, vol. 11(1), pp. 59-77. DOI: <https://doi.org/10.1111/j.1502-3885.1982.tb00522.x>

Kurjański, B., Rea, B.R., Spagnolo, M., Cornwell, D.G., Howell, J., Comte, J-C., Quirós, A.G., Palmu, J-P., Oien, R.P. & Gibbard, P.L. (2021). Cool deltas: Sedimentological, geomorphological and geophysical characterization of ice-contact deltas and implications for their reservoir properties (Salpausselkä, Finland). *Sedimentology*, vol. 68(7), pp. 3057-3101. DOI: <https://doi.org/10.1111/sed.12884>

- Kurjanski, B., Rea, B.R., Spagnolo, M., Winsborrow, M., Cornwell, D.G., Andreassen, K. & Howell, J. (2019). Morphological evidence for marine ice stream shutdown, central Barents Sea. *Marine Geology*, vol. 414, pp. 64-76. DOI: <https://doi.org/10.1016/j.margeo.2019.05.001>
- Lajeunesse, P. (2008). Early Holocene deglaciation of the eastern coast of Hudson Bay. *Geomorphology*, vol. 99(1-4), pp. 341-352. DOI: <https://doi.org/10.1016/j.geomorph.2007.11.012>
- Lally, A., Ruffell, A., Newton, A. M. W., Rea, B. R., Kahlert, T., Storrar, R. D., Spagnolo, M., Graham, C. & Coleman, M. 2023: The evolution and preservation potential of englacial eskers: An example from Breiðamerkurjökull, SE Iceland. *Earth Surface Processes and Landforms*, 4), 2864-2883, <https://doi.org/10.1002/esp.5664>.
- Lally, A., Ruffell, A., Newton, A.M.W., Rea, B.R., Kahlert, T., Storrar, R.D., Spagnolo, M., Graham, C. & Coleman, M. (2023). The evolution and preservation potential of englacial eskers: An example from Breiðamerkurjökull, SE Iceland. *Earth Surface Processes and Landforms*, vol. 48(14), pp. 2864-2883. DOI: <https://doi.org/10.1002/esp.5664>
- Lally, A., Ruffell, A., Newton, A.M.W., Rea, B.R., Kahlert, T., Storrar, R.D., Spagnolo, M., Graham, C. & Coleman, M. (2023). The evolution and preservation potential of englacial eskers: An example from Breiðamerkurjökull, SE Iceland. *Earth Surface Processes*, vol. 48(14), pp. 2864-2883. DOI: <https://doi.org/10.1002/esp.5664>
- Larsen, E., Longva, O. & Follestad, B. A. (1991). Formation of De Geer moraines and implications for deglaciation dynamics. *Journal of Quaternary Science*, vol. 6 (4), pp. 263-277. ISSN: 0267-8179
- Larsen, E., Longva, O. & Follestad, B. A. 1991: Formation of De Geer moraines and implications for deglaciation dynamics. *Journal of Quaternary Science* 6, 263-277, <https://doi.org/10.1002/jqs.3390060402>.
- Larsen, E., Longva, O. & Follestad, B.A. (1991). Formation of De Geer moraines and implications for deglaciation dynamics. *Journal of Quaternary Science*, vol. 6(4), pp. 263-277. DOI: <https://doi.org/10.1002/jqs.3390060402>

- Larson, N.K., Knudsen, K.L., Krohn, C.F., Kronborg, C., Murray, A.S. & Nielsen, O.B. (2009). Late Quaternary ice sheet, lake and sea history of southwest Scandinavia – a synthesis. *Boreas*, vol. 38(4), pp. 732-761. DOI: <https://doi.org/10.1111/j.1502-3885.2009.00101.x>
- Lewington, E.L.M., Livingstone, S.J., Sole, A.J., Clark, C.D. & Ng, F.S.L. (2019). An automated method for mapping geomorphological expressions of former subglacial meltwater pathways (hummock corridors) from high resolution digital elevation data. *Geomorphology*, vol. 339, pp. 70-86. DOI: <https://doi.org/10.1016/j.geomorph.2019.04.013>
- Li, D., DeConto, R.M., Pollard, D. & Hu, Y. (2024). Competing climate feedbacks of ice sheet freshwater discharge in a warming world. *Nature Communications*, vol. 15(5178). DOI: <https://doi.org/10.1038/s41467-024-49604-3>
- Li, Y. (2020). GIS and Remote Sensing Applications in Geomorphology. *Geography*. DOI: <https://doi.org/10.1093/OBO/9780199784002-0219>. Retrieved from <https://www.oxfordbibliographies.com/view/document/obo-9780199874002/obo-9780199874002-0219.xml>
- Li, Z., Yan, C. & Boota, M.W. (2022). Review and outlook of river morphology expression. *Journal of Water and Climate Change*, vol. 13(4), pp. 1725-1747. DOI: <https://doi.org/10.2166/wcc.2022.449>
- Linden, M. & Moller, P. (2005). Marginal formation of De Geer moraines and their implications to the dynamics of grounding-line recession. *Journal of Quaternary Science*, vol. 20 (2), pp. 113-133. DOI: <https://doi.org/10.1002/jqs.902>. ISSN: 0267-8179
- Lindén, M. & Möller, P. (2005). Marginal formation of De Geer moraines and their implications to the dynamics of grounding-line recession. *Journal of Quaternary Science*, vol. 20(2), pp. 113-133. DOI: <https://doi.org/10.1002/jqs.902>
- Lindén, M. & Möller, P. 2005: Marginal formation of De Geer moraines and their implications to the dynamics of grounding-line recession. *Journal of Quaternary Science* 20, 113-133, <https://doi.org/10.1002/jqs.902>.

- Lindholm, R. C. (1987). A Practical approach to sedimentology. Allen and Unwin.
- Lisiecki, L.E. & Raymo, M.E. (2005). A Pliocene-Pleistocene stack of 57 globally distributed benthic  $\delta^{18}\text{O}$  records. *Palaeoceanography*, vol. 20(PA1003). DOI: <https://doi.org/10.1029/2004PA001071>
- Livingstone, S. J., Utting, D. J., Ruffell, A., Clark, C. D., Pawley, S., Atkinson, N. & Fowler, A. C. 2017: Discovery of relict subglacial lakes and their geometry and mechanism of drainage. *Nature Communications* 7, ncomms11767, <https://doi.org/10.1038/ncomms11767>.
- Lønne, I. & Nemec, W. (2011). The kinematics of ancient tidewater ice margins: criteria for recognition from grounding-line moraines. *Ice-Marginal and Periglacial Processes and Sediments*. Geological Society, London, Special Publications 354, 57-75, <https://doi.org/10.1144/SP354.4>.
- Lovell, H. (2014). On the ice-sediment-landform associations of surging glaciers on Svalbard. Queen Mary University of London. Retrieved from: <https://qmro.qmul.ac.uk/xmlui/handle/123456789/8552>
- Lovell, H. (2014). On the ice-sediment-landform associations of surging glaciers on Svalbard. Queen Mary University of London. Retrieved from [https://qmro.qmul.ac.uk/xmlui/bitstream/handle/123456789/8552/Lovell\\_H\\_PhD\\_Final\\_290914.pdf?sequence=1&isAllowed=y](https://qmro.qmul.ac.uk/xmlui/bitstream/handle/123456789/8552/Lovell_H_PhD_Final_290914.pdf?sequence=1&isAllowed=y)
- Lovell, H., Fleming, E.J., Benn, D.I., Hubbard, B., Lukas, S., Rea, B.R., Noormets, R. & Flink, A.E. (2015). Debris entrainment and landform genesis during tidewater glacier surges. *Journal of Geophysical Research: Earth Surface*, vol. 120(8), pp. 1574-1595. DOI: <https://doi.org/10.1002/2015JF003509>
- Lovell, H., Fleming, E.J., Benn, D.I., Hubbard, B., Lukas, S., Rea, B.R., Noormets, R. & Flink, A.E. (2015). Debris entrainment and landform genesis during tidewater glacier surges. *Journal of Geophysical Research: Earth Surface*, vol. 120, pp. 1574-1595. DOI: <https://doi.org/10.1002/2015JF003509>
- Lowe, J. J., & Walker, M. (2014). *Reconstructing quaternary environments*. Taylor & Francis Group.

- Lowe, J.J. & Walker, M.J.C. (2014). *Reconstructing Quaternary Environments*. Taylor & Francis Group.
- Lowry, D.P., Golledge, N.R., Bertler, N.A.N., Jones, R.S. & McKay, R. (2019). Deglacial grounding-line retreat in the Ross Embayment, Antarctica, controlled by ocean and atmosphere forcing. *Science Advances*, vol. 5(8). DOI: <https://doi.org/10.1126/sciadv.aav8754>
- Lukas, S. (2012). Processes of annual moraine formation at a temperate alpine valley glacier: Insights into glacier dynamics and climatic controls. *Boreas*, vol. 41(3), pp. 463-480. DOI: <https://doi.org/10.1111/j.1502-3885.2011.00241.x>
- Lundqvist, J. & Saarnisto, M. (1995). Summary of project IGCP-253. *Quaternary International*, vol. 28, pp. 9-18. DOI: [https://doi.org/10.1016/1040-6182\(95\)00046-L](https://doi.org/10.1016/1040-6182(95)00046-L)
- Lundqvist, J. (1972). Ice-lake types and deglaciation pattern along the Scandinavian mountain range. *Boreas*, vol. 1(1), pp. 27-54. DOI: <https://doi.org/10.1111/j.1502-3885.1972.tb00142.x>
- Lundqvist, J. (1981). Moraine Morphology- terminological remarks and regional aspects. *Geografiska Annaler. Series A. Physical Geography*, vol. 63 (3-4), pp. 127-138. Retrieved from <https://www.jstor.org/stable/520824>
- Lundqvist, J. (1981). Moraine Morphology. *Geografiska Annaler, Series A, Physical Geography*, vol. 63(3/4), pp. 127-138. Retrieved from: <https://www.jstor.org/stable/pdf/520824.pdf>
- Lundqvist, J. (1989). Rogen (ribbed) moraine-identification and possible origin. *Sedimentary Geology*, vol. 62(2-4), pp. 281-292. DOI: [https://doi.org/10.1016/0037-0738\(89\)90119-X](https://doi.org/10.1016/0037-0738(89)90119-X)
- Lundqvist, J. (2000). Palaeoseismicity and De Geer Moraines. *Quaternary International* 68-71, 175-186, [https://doi.org/10.1016/S1040-6182\(00\)00042-2](https://doi.org/10.1016/S1040-6182(00)00042-2).
- Lunkka, J. (2023). The morphostratigraphic imprint of the Baltic Ice Lake drainage event in southern Finland. *Bulletin of the Geological Society of Finland*, vol. 95. DOI: <https://doi.org/10.17741/bgsf/95.1.004>



- Lunkka, J., Nikarmaa, T. & Putkinen, N. (2019). Baltic Ice Lake levels and a LiDAR/DEM-based estimate of the glacio-isostatic uplift gradient of the Salpausselkä zone, SE Finland. *Bulletin of the Geological Society of Finland*, vol. 91, pp. 119-137. DOI: <https://doi.org/10.17741/bgsf/91.1.005>
- Lunkka, J., Nikarmaa, T. & Putkinen, N. 2019: Baltic Ice Lake levels and a LiDAR/DEM-based estimate of the glacio-isostatic uplift gradient of the Salpausselkä zone, SE Finland. *Bulletin of the Geological Society of Finland* 91, 119-137, <https://doi.org/10.17741/bgsf/91.1.005>.
- Lunkka, J., Palmu, J.-P. & Seppänen, A. 2021: Deglaciation dynamics of the Scandinavian Ice Sheet in the Salpausselkä zone, southern Finland. *Boreas* 50, 404-418, <https://doi.org/10.1111/bor.12502>.
- Lunkka, J., Palmu, J.-P. & Seppänen, A. (2021). Deglaciation dynamics of the Scandinavian Ice Sheet in the Salpausselkä zone, southern Finland. *Boreas*, vol. 50(2). DOI: <https://doi.org/10.1111/bor.12502>
- Lunkka, J.P., Nikarmaa, T. & Putkinen, N. (2019). Baltic Ice Lake levels and a LiDAR/DEM-based estimate of the glacio-isostatic uplift gradient of the Salpausselkä zone, SE Finland. *Bulletin of the Geological Society of Finland*, vol. 91, pp. 119-137. DOI: <https://doi.org/10.17741/bgsf/91.1.005>
- Lunkka, J.P., Palmu, J.-P. & Seppänen, A. (2021). Deglaciation dynamics of the Scandinavian Ice Sheet in the Salpausselkä zone, southern Finland. *Boreas*, vol. 50(2), pp. 404-418. DOI: <https://doi.org/10.1111/bor.12502>
- Mäkinen, J., Dow, C.F., Ahokangas, E., Ojala, A., Kajuutti, K., Kautto, J & Palmu, J.-P. (2023). Water blister geomorphology and subglacial drainage sediments: an example from the bed of the Fennoscandian Ice Sheet in SW Finland. *Journal of Glaciology*, pp. 1-17. DOI: <https://doi.org/10.1017/jog.2023.37>
- Mäkinen, J., Kajuutti, K., Ojala, A. E. K., Ahokangas, E., Tuunainen, A., Valkama, M. & Palmu, J. -P. 2023: Genesis of subglacial triangular-shaped landforms (murtoos) formed by the Fennoscandian Ice Sheet. *Earth Surface Processes and Landforms* 48, 2171-2196, <https://doi.org/10.1002/esp.5606>.

- Mallalieu, J., Carrivick, J.L., Quincey, D.J. & Smith, M.W. (2020). Calving Seasonality Associated With Melt-Undercutting and Lake Ice Cover. *Geophysical Research Letters*, vol. 47(8). DOI: <https://doi.org/10.1029/2019GL086561>
- Mangerud, J., Hughes, A.L.C., Sæle, T.H. & Svendsen, J.I. (2019). Ice-flow patterns and precise timing of ice sheet retreat across a dissected fjord landscape in western Norway. *Quaternary Science Reviews*, vol. 214., pp. 139-163. DOI: <https://doi.org/10.1016/j.quascirev.2019.04.032>
- Mangerud, J., Hughes, A.L.C., Sæle, T.H. & Svendsen, J.I. (2019). Ice-flow patterns and precise timing of ice sheet retreat across a dissected fjord landscape in western Norway. *Quaternary Science Reviews*, vol. 214, pp. 139-163. DOI: <https://doi.org/10.1016/j.quascirev.2019.04.032>
- Margold, M., Jansson, K.N., Kleman, J., Stroeve, A.P. & Clague, J.J. (2013). Retreat pattern of the Cordilleran Ice Sheet in central British Columbia at the end of the last glaciation reconstructed from glacial meltwater landforms. *Boreas*, vol. 42(4). DOI: <https://doi.org/10.1111/bor.12007>
- Margold, M., Stokes, C. R., Clark, C. D. & Kleman, J. (2015). Ice streams in the Laurentide Ice Sheet: a new mapping inventory. *Journal of Maps*, vol. 11 (3), pp. 380-395. DOI: <https://doi.org/10.1080/17445647.2014.912036>
- Margold, M., Stokes, C.R. & Clark, C.D. (2018). Reconciling records of ice streaming and ice margin retreat to produce a palaeographic reconstruction of the deglaciation of the Laurentide Ice Sheet. *Quaternary Science Reviews*, vol. 189, pp. 1-30. DOI: <https://doi.org/10.1016/j.quascirev.2018.03.013>
- Mateus Vidotti Ferreira. [Transect2.0 Tool]. Email: [mateusvidotti@yahoo.com.br](mailto:mateusvidotti@yahoo.com.br)
- Mawdsley, J.B. (1963). The wash-board moraines of the Opawica-Chibougamau area, Quebec. *Roy. Soc. Can. Trans., Ser. 3*, 30(4), pp. 9-12.
- McKinney, W., and others. (2010). Pandas- Data Structures for Statistical Computing in Python. In *Proceedings of the 9th Python in Science Conference*, vol. 445, pp. 56-61. Editors: Stefan van der Walt & Jarrod Millman. DOI: <https://doi.org/10.25080/Majora-92bf1922-00a>

- Menzies, J., van der Meer, J.J.M. & Shilts, W.W. (2018). Chapter 5 – Subglacial Processes and Sediments. *Past Glacial Environments* (Second Edition), pp. 105-158. DOI: <https://doi.org/10.1016/B978-0-08-100524-8.00004-X>
- Meredith, M., M. Sommerkorn, S., Cassotta, C., Derksen, A., Ekaykin, A., Hollowed, G., Kofinas, A., Mackintosh, J., Melbourne-Thomas, M.M.C., Muelbert, G., Ottersen, H., Pritchard, H. & Schuur, E.A.G. (2019). Polar Regions. In: IPCC Special Report on the Ocean and Cryosphere in a Changing Climate [H.-O. Pörtner, D.C., Roberts, V. Masson-Delmotte, P. Zhai, M. Tignor, E. Poloczanska, K. Mintenbeck, A. Alegría, M. Nicolai, A. Okem, J. Petzold, B. Tama, N.M. Weyer (eds.)]. Cambridge University Press, Cambridge, UK and New York, NY, USA, pp. 2013-320. DOI: <https://doi.org/10.1017/9781009157964.005>
- Mesev, V. (2007). *Integration of GIS and Remote Sensing*. John Wiley & Sons Ltd, Chichester, West Sussex. ISBN: 978-0-470-86409-8 HB
- Möller, H. (1962). Annuella och interannuella ändmoräner. *Geologiska Föreningen i Stockholm Förhandlingar*, vol. 84(2), pp. 134-143. DOI: <https://doi.org/10.1080/11035896209449211>
- Möller, H. 1962: Annuella och interannuella ändmoräner. *Geologiska Föreningen i Stockholm Förhandlingar* 84, 134-143, <https://doi.org/10.1080/11035896209449211>.
- Morlighem, M., Rignot, E., Binder, Blankenship, D., Drews, R., Eagles, G., Eisen, O., Ferraccioli, F., Forsberg, R., Fretwell, P., Goel, V., Greenbaum, J.S., Gudmundsson, H., Guo, J., Helm, V., Hoftstede, C., Howat, I., Humbert, A., Jokat, W., Karlsson, N.B., Lee, W.S., Matsuoka, K., Millan, R., Mouginot, J., Paden, K., Pattyn, F., Roberts, J., Rosier, S., Ruppel, A., Seroussi, H., Smith, E.C., Steinhage, D., Sun, B., van den Broeke, M.R., van Ommen, T.D. van Wessel, M & Young, D.A. (2019). Deep glacial troughs and stabilizing ridges unveiled beneath the margins of the Antarctic ice sheet. *Nature*, vol. 13, pp. 132-137. DOI: <https://doi.org/10.1038/s41561-019-0510-8>
- Mörner, N.-A. (1977). Varve chronology on Södertörn: Recording and dating of the “drainage” of the Baltic Ice Lake and correlation with the Finnish varve chronology. *Boreas*, vol. 99(4), pp. 423-425. DOI: <https://doi.org/10.1080/11035897709455050>

Napieralski, L., Barr, I., Kamp, U., Kervyn, M. (2013). Remote sensing and GIScience in geomorphological mapping. In Shroder, J. (Editor in Chief), Bishop, M.P. (Ed.). *Treatise on Geomorphology*. Academic Press, San Diego, CA, vol. 3, Remote Sensing and GIScience in Geomorphology, pp. 187-227. DOI: <https://dx.doi.org/10.1016/B978-0-12-374739-6.00050-6>

National Land Survey of Finland. LiDAR Digital Elevation Model, 2, 2023.

Natural Resources Canada. (2015). High Resolution Digital Elevation Model (HRDEM). Product Specifications. Edition 1.4. Government of Canada. Retrieved from: [https://ftp.maps.canada.ca/pub/elevation/dem\\_mne/highresolution\\_hauteresolution/HRDEM\\_Product\\_Specification.pdf](https://ftp.maps.canada.ca/pub/elevation/dem_mne/highresolution_hauteresolution/HRDEM_Product_Specification.pdf)

Neal, A. (2004). Ground-penetrating radar and its use in sedimentology: principles, problems and progress. *Earth-Science Reviews*, vol. 66(3-4), pp. 261-330. DOI: <https://doi.org/10.1016/j.earscirev.2004.01.004>

Neal, A. 2004: Ground-penetrating radar and its use in sedimentology: principles, problems and progress. *Earth-Science Reviews* 66, 261-330, <https://doi.org/10.1016/j.earscirev.2004.01.004>.

Nick, F.M., Van Der Veen, C.J., Vieli, A. & Benn, D.I. (2010). A physically based calving model applied to marine outlet glaciers and implications for the glacier dynamics. *Journal of Glaciology*, vol. 56(199), pp. 781-794. DOI: <https://doi.org/10.3189/002214310794457344>

Ó Cofaigh, C., Davies, B.J., Livingstone, S.J., Smith, J.A., Johnson, J.S., Hocking, E.P., Hodgson, D.A., Anderson, J.B., Bentley, M.J., Canals, M., Domack, E., Dowdeswell, J.A., Evans, J., Glasser, N.F., Hillenbrand, C.-D., Larter, R.D., Roberts, S.J. & Simms, A.R. (2014). Reconstruction of ice-sheet changes in the Antarctic Peninsula since the Last Glacial Maximum. *Quaternary Science Reviews*, vol. 100, pp. 87-110. DOI: <https://doi.org/10.1016/j.quascirev.2014.06.023>

Ó Cofaigh, C., Evans, D.J.A. & Smith, I.R. (2010). Large-scale reorganization and sedimentation of terrestrial ice-streams during a single glacial cycle. *Geological Society of America, Bulletin* 122(5-6), pp. 743-756. DOI: <https://doi.org/10.1130/b26476.1>

- Öhrling, C., Peterson, G. & Mikko, H. (2018). Detailed geomorphological analysis of LiDAR derived elevation data, Forsmark. Svensk Kärnbränslehantering AB. ISSN: 1402-3091. Retrieved from: <https://www.skb.com/publication/2492226/R-18-10.pdf>
- Ojala, A. E. K., Palmu, J.-P., Åberg, A., Åberg, S. & Virkki, H. 2013: Development of an ancient shoreline database to reconstruct the Littorina Sea maximum extension and the highest shoreline of the Baltic Sea basin in Finland. *Bulletin of the Geological Society of Finland* 85, 127–144, <https://doi.org/10.17741/bgsf/85.2.002>.
- Ojala, A. E. K. 2016: Appearance of De Geer moraines in southern and western Finland – Implications for reconstructing glacier retreat dynamics. *Geomorphology* 255, 16-25, <https://doi.org/10.1016/j.geomorph.2015.12.005>.
- Ojala, A. E. K., Putkinen, N., Palmu, J.-P. & Nenonen, K. 2015: Characterization of De Geer moraines in Finland based on LiDAR DEM mapping. *GFF* 137, 304-318, <https://doi.org/10.1080/11035897.2015.1050449>.
- Ojala, A.E.K. & Tiljander, M. (2003). Testing the fidelity of sediment chronology: comparison of varve and paleomagnetic results from Holocene lake sediments from central Finland. *Quaternary Science Reviews*, vol. 22(15-17), pp. 1787-1803. DOI: [https://doi.org/10.1016/S0277-3791\(03\)00140-9](https://doi.org/10.1016/S0277-3791(03)00140-9)
- Ojala, A.E.K. (2016). Appearance of De Geer moraines in southern and western Finland – Implications for reconstructing glacier retreat dynamics. *Geomorphology*, vol. 255, pp. 16-25. DOI: <https://doi.org/10.1016/j.geomorph.2015.12.005>
- Ojala, A.E.K. (2016). Appearance of De Geer moraines in southern and western Finland - Implications for reconstructing glacier retreat dynamics. *Geomorphology*, vol. 255, pp. 16-25. DOI: <https://doi.org/10.1016/j.geomorph.2015.12.005>
- Ojala, A.E.K. (2016). Appearance of De Geer moraines in southern and western Finland – Implications for reconstructing glacier retreat dynamics. *Geomorphology*, vol. 255, pp. 16-25. DOI: <https://doi.org/10.1016/j.geomorph.2015.12.005>
- Ojala, A.E.K., Mäkinen, J., Ahokangas, E., Kajuutti, K., Valkama, M., Tuunainen, A. & Palmu, J-P. (2021). Diversity of murtoos and murtoo-related subglacial landforms in

the Finnish area of the Fennoscandian Ice Sheet. *Boreas*, vol. 50(4), pp. 1095-1115.  
DOI: <https://doi.org/10.1111/bor.12526>

Ojala, A.E.K., Palmu, J.-P., Åberg, A., Åberg, S. & Virkki, H. (2013). Development of an ancient shoreline database to reconstruct the Litorina Sea maximum extension and the highest shoreline of the Baltic Sea basin in Finland. *Bulletin of the Geological Society of Finland*, vol. 85, pp. 127-144. Retrieved from: [https://www.geologinenseura.fi/sites/geologinenseura.fi/files/bulletin\\_vol85\\_2\\_2013\\_ojala.pdf](https://www.geologinenseura.fi/sites/geologinenseura.fi/files/bulletin_vol85_2_2013_ojala.pdf)

Ojala, A.E.K., Palmu, J.-P., Åberg, A., Åberg, S. & Virkki, H. (2013). Development of an ancient shoreline database to reconstruct the Litorina Sea maximum extension and the highest shoreline of the Baltic Sea basin in Finland. *Bulletin of the Geological Society of Finland*, vol. 85, pp. 127-144. Retrieved from: [https://www.geologinenseura.fi/sites/geologinenseura.fi/files/bulletin\\_vol85\\_2\\_2013\\_ojala.pdf](https://www.geologinenseura.fi/sites/geologinenseura.fi/files/bulletin_vol85_2_2013_ojala.pdf)

Ojala, A.E.K., Putkinen, N., Palmu, J.P. & Nenonen, K. (2015) Characterization of De Geer moraines in Finland based on LiDAR DEM mapping. *GFF*, vol. 137(4), pp. 304-318.  
DOI: <https://doi.org/10.1080/11035897.2015.1050449>

Ojala, A.E.K., Putkinen, N., Palmu, J.P. & Nenonen, K. (2015). Characterization of De Geer moraines in Finland based on LiDAR DEM mapping. *GFF*, vol. 137(4), pp. 304-318.  
DOI: <https://doi.org/10.1080/11035897.2015.1050449>

Okko, M. (1962). On the development of the First Salpausselkä, west of Lahti. *Bulletin de la Commission géologique de Finlande*, vol. 202, pp. 162.

Orlowska, A. (2022). Crevasse-fill forms – Bridging the gap in glacial geomorphology between East and West based on a case from eastern Poland. *Quaternary International*, vol. 617, pp. 59-72. DOI: <https://doi.org/10.1016/j.quaint.2021.08.004>

Orlowska, A. (2022). Crevasse-fill forms – Bridging the gap in glacial geomorphology between East and West based on a case study from eastern Poland. *Quaternary International*, vol. 617, pp. 59-72. DOI: <https://doi.org/10.1016/j.quaint.2021.08.004>

- Ottesen, D. & Dowdeswell, J. A. 2006: Assemblages of submarine landforms produced by tidewater glaciers in Svalbard. *Journal of Geophysical Research: Earth Surface* 111, <https://doi.org/10.1029/2005JF000330>.
- Ottesen, D. & Dowdeswell, J.A. (2006). Assemblages of submarine landforms produced by tidewater glaciers in Svalbard. *Journal of Geophysical Research*, vol. 111 (F01016). DOI: <https://doi.org/10.1029/2005JF000330>
- Ottesen, D., Batchelor, C.L., Bjarnadóttir, L.R., Wiberg, D.H. & Dowdeswell, J.A. (2022). Glacial landforms reveal dynamic ice-sheet behaviour along the mid-Norwegian margin during the last glacial-deglacial cycle. *Quaternary Science Reviews*, vol. 285, 107462. DOI: <https://doi.org/10.1016/j.quascirev.2022.107462>
- Ottesen, D., Canals, M., Jakobsson, M., Todd, B.J., Dowdeswell, E.K. & Hogan, K.A. (2016). The variety and distribution of submarine glacial landforms and implications for ice-sheet reconstruction. *Geological Society, London, Memoirs*, vol. 46, pp. 519-552. DOI: <https://doi.org/10.1144/M46.183>
- Ottesen, D., Dowdeswell, J.A., Benn, D.I., Kristensen, L., Christiansen, H.H., Christensen, O., Hansen, L., Lebesbye, E. Forwick, M. & Vorren, T.O. (2008). Submarine landforms characteristic of glacier surges in two Spitsbergen fjords. *Quaternary Science Reviews*, vol. 27, pp. 1583-1599. DOI: <https://doi.org/10.1016/j.quascirev.2008.05.007>
- Ottesen, D. & Dowdeswell, J.A. (2006). Assemblages of submarine landforms produced by tidewater glaciers in Svalbard. *Journal of Geophysical Research: Earth Surface*, vol. 111(F1). DOI: <https://doi.org/10.1029/2005JF000330>
- Ottesen, D., Dowdeswell, J.A., Benn, D.I., Kristensen, L., Christiansen, H.H., Christensen, O., Hansen, L., Lebesbye, E., Forwick, M. & Vorren, T.O. (2008). Submarine landforms characteristic of glacier surges in two Spitsbergen fjords. *Quaternary Science Reviews*, vol. 27(15-16), pp. 1583-1599. DOI: <https://doi.org/10.1016/j.quascirev.2008.05.007>
- Otto, J-C., Prasicek, G., Blothe, J. & Schrott, L. (2018). GIS Applications in Geomorphology. *Comprehensive Geographic Information Systems*, pp. 81-111. DOI: <https://doi.org/10.1016/B978-0-12-409548-9.10029-6>

- Padman, L., Siegfried, M.R. & Fricker, H.A. (2018). Ocean Tide Influences on the Antarctic and Greenland Ice Sheets. *Review of Geophysics*, vol. 56(1), pp. 142-184. DOI: <https://doi.org/10.1002/2016RG000546>
- Padman, L., Siegfried, M.R. & Fricker, H.A. (2018). Ocean Tide Influences on the Antarctic and Greenland Ice Sheets. *Reviews of Geophysics*, vol. 56(1), pp. 142-184. DOI: <https://doi.org/10.1002/2016RG000546>
- Palmu, J.-P., Ojala, A.E.K., Virtasalo, J., Putkinen, N., Kohonen, J., Sarala, P. (2021). Classification system of superficial (Quaternary) geological units in Finland. *Bulletin of the Geological Survey of Finland*, vol. 412, pp. 115-169. DOI: <https://doi.org/10.30440/bt412.4>
- Palmu, J.-P., Ojala, A.E.K., Virtasalo, J., Putkinen, N., Kohonen, J. (2021). Classification system of Superficial (Quaternary) Geologic Units in Finland. *Geological Survey of Finland, Bulletin 412*, pp. 115-144. Retrieved from [https://tupa.gtk.fi/julkaisu/bulletin/bt\\_412.pdf](https://tupa.gtk.fi/julkaisu/bulletin/bt_412.pdf)
- Passchier, S. (2018). Chapter 16 - Ice Sheets and Climate: The Marine Geological Record. *Past Glacial Environments (Second Edition)*, pp. 565-584. DOI: <https://doi.org/10.1016/B978-0-08-100524-8.00017-8>
- Pattyn, F. & Morlighem, M. (2020). The uncertain future of the Antarctic Ice Sheet. *Science*, vol. 367(6484), pp. 1331-1335. DOI: <https://doi.org/10.1126/science.aaz5487>
- Pattyn, F. (2018). The paradigm shift in Antarctic ice sheet modelling. *Nature*, vol. 9(2728). DOI: <https://doi.org/10.1038/s41467-018-05003-z>
- Pearce, D., Ely, J., Barr, I. D. & Boston, C. M. 2017: Glacier Reconstruction. In: *Geomorphological Techniques*. British Society for Geomorphology, 1-16, <https://e-space.mmu.ac.uk/619301/>.
- Pearce, D.M., Ely, J.C., Barr, I.D. & Boston, C.M. (2017). Glacier Reconstruction. In: *Geomorphological Techniques*. British Society for Geomorphology, pp. 1-16. Retrieved from: [https://e-space.mmu.ac.uk/619301/1/3.4.9\\_Glacier%20Reconstruction.pdf](https://e-space.mmu.ac.uk/619301/1/3.4.9_Glacier%20Reconstruction.pdf)



- Pike, R.J., Evans, I.S. & Hengl, T. (2009). Chapter 1 Geomorphometry: A Brief Guide. *Developments in Soil Science*. Vol. 33. Pp. 3-30. DOI: [https://doi.org/10.1016/S0166-2481\(08\)00001-9](https://doi.org/10.1016/S0166-2481(08)00001-9)
- Plescia, J.B. (1993). Wrinkle ridges of Arcadia Planitia, Mars. *Journal of Geophysical Research*. Vol. 98(E8), pp. 15049-15059. DOI: <https://doi.org/10.1029/93JE01324>
- Pollard, D., DeConto, R.M. & Alley, R.B. (2015). Potential Antarctic Ice Sheet retreat driven by hydrofracturing and ice cliff failure. *Earth and Planetary Science Letters*, vol. 412, pp. 112-121. DOI: <https://doi.org/10.1016/j.epsl.2014.12.035>
- Porter, C., Morin, P., Howat, I., Noh, M-J., Bates, B., Peterman, K., Keeseey, S., Schlenk, M., Gardiner, J., Tomko, K., Willis, M., Helleher, C., Cloutier, M., Husby, E., Foga, S., Nakamura, H., Platson, M., Wethington, M. Jr., Williamson, C., Bauer, G., Enos, J., Arnold, G., Kramer, W., Becker, P., Doshi, A., D'Souza, C., Cummins, P., Laurier, F., Bojesen, M. (2018). "ArcticDEM, Version 3". Harvard Dataverse, V1. DOI: <https://doi.org/10.7910/DVN/C98DVS>.
- Post, A.L., Phillips, E., Carson, C.J. & Smith, J. (2021). Antecedent control on active ice sheet retreat revealed by seafloor geomorphology, offshore Windmill Islands, Antarctica. *The Cryosphere*. DOI: <https://doi.org/10.5194/tc-2021-8>
- Powell, R.D. & Alley, R.B. (1997). Grounding-Line Systems: Processes, Glaciological Inferences and the Stratigraphic Record. *Geology and Seismic Stratigraphy of the Antarctic Margin*, 2, vol. 71. DOI: <https://doi.org/10.1029/AR071p0169>
- Prest, V. K., Grant, D. R. & Rampton, V. N. 1968: Glacial map of Canada. Geological Survey of Canada, "A" Series Map, 1253A, <https://doi.org/10.4095/108979>.
- Prest, V.K., Grant, D.R. & Rampton, V.N. (1968). Glacial map of Canada. Geological Survey of Canada, "A" Series Map, 1253A. DOI: <https://doi.org/10.4095/108979>
- Price, S. F. & Whillans, I. M. (2001). Crevasse patterns at the onset to Ice Stream B, West Antarctica. *Journal of Glaciology*, vol. 47 (156). Retrieved from <https://www.cambridge.org/core>

- Price, S.F. & Whillans, I.M. (2001). Crevasse patterns at the onset to Ice Stream B, West Antarctica. *Journal of Glaciology*, vol. 47(156), pp. 29-36. DOI: <https://doi.org/10.3189/172756501781832494>
- Punkari, M. (1980). The ice lobes of the Scandinavian ice sheet during the deglaciation in Finland. *Boreas*, vol. 9(4), pp. 307-310. DOI: <https://doi.org/10.1111/j.1502-3885.1980.tb00710.x>
- Purdie, J. & Fitzharris, B. (1999). Processes and rates of ice loss at the terminus of Tasman Glacier, New Zealand. *Global and Planetary Change*, vol. 22(1-4), pp. 79-91. DOI: [https://doi.org/10.1016/S0921-8181\(99\)00027-2](https://doi.org/10.1016/S0921-8181(99)00027-2)
- Putkinen, N., Eyles, N., Putkinen, S., Ojala, A.E.K., Palmu, J.P., Sarala, P., Väänänen, T., Räisänen, J., Saarelainen, Ahtonen, N., Rönty, H., Kiiskinen, A., Rauhaniemi, T. & Tervo, T. (2017). High-resolution LiDAR mapping of glacial landforms and ice stream lobes in Finland. *Bulletin of the Geological Society of Finland*, vol. 89(2). DOI: <https://doi.org/10.17741/bgsf/89.2.001>
- Putkinen, N., Lunkka, J.P., Ojala, A.E.K. & Kosonen, E. (2011). Deglaciation history and age estimate of the Younger Dryas end moraines in the Kalevala region, NW Russia. *Quaternary Science Reviews*, vol. 30(27-28), pp. 3812-3822. DOI: <https://doi.org/10.1016/j.quascirev.2001.09.023>
- Rainio, H., Saarnisto, M. & Ekman, I. (1995). Younger Dryas End Moraines in Finland and NW Russia. *Quaternary International*, vol. 28, pp. 179-192. DOI: [https://doi.org/10.1016/1040-6182\(95\)00051-J](https://doi.org/10.1016/1040-6182(95)00051-J)
- Rainio, H., Saarnisto, M. & Ekman, I. (1995). Younger Dryas End Moraines in Finland and NW Russia. *Quaternary International*, vol. 28, pp. 179-182. DOI: [https://doi.org/10.1016/1040-6182\(95\)00051-J](https://doi.org/10.1016/1040-6182(95)00051-J)
- Rainio, H., Saarnisto, M. & Ekman, I. 1995: Younger Dryas End Moraines in Finland and NW Russia. *Quaternary International* 28, 179-192, [https://doi.org/10.1016/1040-6182\(95\)00051-J](https://doi.org/10.1016/1040-6182(95)00051-J).

- Rao, D.P. (2002). Remote sensing application in geomorphology. *Tropical Ecology* 43(1): 49-59. ISSN: 0564-3295. Retrieved from [http://216.10.241.130/pdf/open/PDF\\_43\\_1/43105.pdf](http://216.10.241.130/pdf/open/PDF_43_1/43105.pdf)
- Rasmussen, S.O., Vinther, B., Clausen, H.B. & Anderson, K.K. (2007). Early Holocene climate oscillations recorded in three Greenland ice cores. *Quaternary Science Reviews*, vol. 26(15), pp. 1907-1914. DOI: <https://doi.org/10.1016/j.quascirev.2007.06.015>
- Rasmussen, S.O., Vinther, B.M., Clausen, H.B. & Andersen, K.K. (2007). Early Holocene climate oscillations recorded in three Greenland ice core records. *Quaternary Science Reviews*, vol. 26(15-16), pp. 1907-1914. DOI: <https://doi.org/10.1016/j.quascirev.2007.06.015>
- Re, G.L., Fuller, I.C., Sofia, G. & Tarolli, P. (2018). High-resolution mapping of Manawatu palaeochannels. *New Zealand Geographer*. Vol. 74(2), pp. 77-91. DOI: <https://doi.org/10.1111/nzg.12186>
- Rea, B. R. & Evans, D. J. A. 2011: An assessment of surge-induced crevassing and the formation of crevasse squeeze ridges. *Journal of Geophysical Research* 116, F04005, <https://doi.org/10.1029/2011JF001970>.
- Rea, B.R. & Evans, D.J.A. (2011). An assessment of surge-induced crevassing and the formation of crevasse squeeze ridges. *Journal of Geophysical Research: Earth Surface*, vol. 116(F4). DOI: <https://doi.org/10.1029/2011JF001970>
- Rea, B.R. & Evans, D.J.A. (2011). An assessment of surge-induced crevassing and the formation of crevasse squeeze ridges. *Journal of Geophysical Research: Earth Surface*, vol. 116 (F4). DOI: <https://doi.org/10.1029/2011JF001970>
- Reese, R., Garbe, J., Hill, E.A., Urruty, B., Naughten, K.A., Gagliardini, O., Durand, G., Gillet-Chaulet, F., Gudmundsson, G.H., Chandler, D., Langebroek, P.M. & Winkelmann, R. (2023). The stability of present-day Antarctic grounding lines – Part 2: Onset of irreversible retreat of Amundsen Sea glaciers under current climate on centennial timescales cannot be excluded. *The Cryosphere*, vol. 17(9), pp. 3761-3873. DOI: <https://doi.org/10.5194/tc-17-3761-2023>

- Reese, R., Garbe, J., Hill, E.A., Urruty, B., Naughten, K.A., Gagliardini, O., Durand, G., Gillet-Chaulet, F., Gudmundsson, G.H., Chandler, D., Langebroek, P.M. & Winkelmann, R. (2023). The stability of present-day Antarctic grounding lines – Part 2: Onset of irreversible retreat of Amundsen Sea glaciers under current climate on centennial timescales cannot be excluded. *The Cryosphere*, vol. 17(9), pp. 3761-3783. DOI: <https://doi.org/10.5194/tc-17-3761-2023>
- Regnéll, C., Becher, G. P., Öhrling, C., Greenwood, S. L., Gyllencreutz R., Blomdin, R., Brendryen, J., Goodfellow, B. W., Mikko, H., Ransed, G. & Smith, C. 2023: Ice-dammed lakes and deglaciation history of the Scandinavian Ice Sheet in central Jämtland, Sweden. *Quaternary Science Reviews* 312, 108219, <https://doi.org/10.1016/j.quascirev.2023.108219>.
- Regnéll, C., Becher, G.P., Öhrling, C., Greenwood, S.L., Gyllencreutz, R., Blomdin, R., Brendryen, J., Goodfellow, B.W., Mikko, H., Ransed, G. & Smith, C. (2023). Ice-dammed lakes and deglaciation history of the Scandinavian Ice Sheet in central Jämtland, Sweden. *Quaternary Science Reviews*, vol. 314. DOI: <https://doi.org/10.1016/j.quascirev.2023.108219>
- Ren, D. & Leslie, L.M. (2011). Three positive feedback mechanisms for ice-sheet melting in a warming climate. *Journal of Glaciology*, vol. 57(206), pp. 1057-1066. DOI: <https://doi.org/10.3189/002214311798843250>
- Rettig, L., Lukas, S. & Huss, M. (2023). Implications of a rapidly thinning ice margin for annual moraine formation at Gornergletscher, Switzerland. *Quaternary Science Reviews*, vol. 308(108085). DOI: <https://doi.org/10.1016/j.quascirev.2023.108085>
- Ridge, J.C., Balco, G., Bayless, R.L., Beck, C.C., Carter, L.B., Dean, J.L., Voytek, E.B. & Wei, J.H. (2012). The new north American varve chronology: A precise record of southeastern Laurentide Ice Sheet deglaciation and climate, 18.2-12.5 kyr BP, and correlations with Greenland ice core records. *American Journal of Science*, vol. 312, pp. 685-722. DOI: <https://doi.org/10.2475/07.2012.01>
- Rignot, E., Mouginot, J., Morlighem, M., Seroussi, H & Scheuchl, B. (2014). Widespread, rapid grounding line retreat of Pine Island, Thwaites, Smith, and Kohler glaciers, West

- Antarctica, from 1992 to 2011. *Geophysical Research Letters*, vol. 41(10), pp. 3502-3509. DOI: <https://doi.org/10.1002/2014GL060140>
- Rignot, E., Mouginot, J., Morlighem, M., Seroussi, H. & Scheuchl, B. (2014). Widespread, rapid grounding line retreat of Pine Island, Thwaites, Smith, and Kohler glaciers, West Antarctica, from 1992 to 2011. *Geophysical Research Letters*, vol. 41(10), pp. 3502-3509. DOI: <https://doi.org/10.1002/2014GL060140>
- Rignot, E.J. (1998). Fast Recession of a West Antarctic Glacier. *Science*, vol. 281(5376). DOI: <https://doi.org/10.1126/science.281.5376.549>
- Ringberg, B. & Rudmark, L. (1985). Varve chronology based upon glacial sediments in the area between Karlskrona and Kalmar, southeastern Sweden. *Boreas*, vol. 14(2), pp. 107-110. DOI: <https://doi.org/10.1111/j.1502-3885.1985.tb00898.x>
- Rinterknecht, V. R., Clark, P. U., Raisbeck, G. M., Yiou, F., Brook, E. J., Tschudi, S. & Lunkka, J. P. 2004: Cosmogenic  $^{10}\text{Be}$  dating of the Salpausselkä I Moraine in southwestern Finland. *Quaternary Science Reviews* 23, 2283-2289, <https://doi.org/10.1016/j.quascirev.2004.06.012>.
- Rinterknecht, V.R., Clark, P.U., Raisbeck, G.M., Yiou, F., Brook, E.J., Tschudi, S. & Lunkka, J.P. (2004). Cosmogenic  $^{10}\text{Be}$  dating of the Salpausselkä I Moraine in southwestern Finland. *Quaternary Science Reviews*, vol. 23(23-24), pp. 2283-2289. DOI: <https://doi.org/10.1016/j.quascirev.2004.06.012>
- Ritchie, J., Lingle, C., Motyka, R. & Truffer, M. 2008: Seasonal fluctuations in the advance of a tidewater glacier and potential causes: Hubbard Glacier, Alaska, USA. *Journal of Glaciology* 54, 401-411, <https://doi.org/10.3189/002214308785836977>.
- Rivers, G. E., Storrar, R. D., Jones, A. H. & Ojala, A. E. K. 2023: 3D morphometry of De Geer Moraines and Crevasse-Squeeze Ridges: Differentiating between pushing and squeezing mechanisms from remotely sensed data. *Quaternary Science Reviews* 321C(1), 108383, <https://doi.org/10.1016/j.quascirev.2023.108383>.
- Rivers, G.E., Storrar, R.D., Jones, A.H. & Ojala, A.E.K. (2023). 3D morphometry of De Geer Moraines and Crevasse-Squeeze Ridges: Differentiating between pushing and

- squeezing mechanisms from remotely sensed data. *Quaternary Science Reviews*, vol. 321, 108383. DOI: <https://doi.org/10.1016/j.quascirev.2023.108383>
- Rivers, G.E., Storrar, R.D., Ojala, A.E.K., Mäkinen, J., Holmroos, C. & Holmes, N. (2024). De Geer moraine internal architecture based on sedimentological and geophysical investigations and implications for ice-marginal reconstructions. *Boreas*. DOI: <https://doi.org/10.1111/bor.12692>
- Robel, A.A. & Tziperman, E. (2016). The role of ice stream dynamics in deglaciation. *Journal of Geophysical Research: Earth Surface*, vol. 121(8), pp. 1540-1554. DOI: <https://doi.org/10.1002/2016JF003937>
- Roman, M., Nývlt, D., Davies, B.J., Braucher, R., Jennings, S.J.A., Břežný, M., Glasser, N.F., Hambrey, M.J., Lirio, J.M., Rodés, Á. & ASTER Team. (2024). Accelerated retreat of northern James Ross Island ice streams (Antarctic Peninsula) in the Early-Middle Holocene induced to buoyancy response to postglacial sea level rise. *Earth and Planetary Science Letters*, vol. 641(118803). DOI: <https://doi.org/10.1016/j.epsl.2024.118803>
- Rowan, A.V., Egholm, D.L. & Clark, C.D. (2022). Forward modelling of the completeness and preservation of palaeoclimate signals recorded by ice-marginal moraines. *Earth Surface Process Landforms*, vol. 47(9), pp. 2198-2208. DOI: <https://doi.org/10.1002/esp.5371>
- Rowan, A.V., Egholm, D.L. & Clark, C.D. (2022). Forward modelling of the completeness and preservation of palaeoclimate signals recorded by ice-marginal moraines. *Earth Surface Processes and Landforms*, vol. 47(9), pp. 2198-2208. DOI: <https://doi.org/10.1002/esp.5371>
- Ruffell, A., McKinley, J., Robinson, M. & Bristow, C. (2013). Ground Penetrating Radar. *Geomorphological Techniques. British Society for Geomorphology Remote Sensing Workshop*, pp. 1-12. ISSN: 2047-0371
- Rydningen, T.A., Laberg, J.S. & Kolstad, V. (2015). Seabed morphology and sedimentary processes on high-gradient trough mouth fans offshore Troms, northern Norway. *Geomorphology*, vol. 246, pp. 205-219. DOI: <https://doi.org/10.1016/j.geomorph.2015.06.007>

- Saarnisto, M. & Saarinen, T. (2001). Deglaciation chronology of the Scandinavian Ice Sheet from the Lake Onega Basin to the Salpausselkä End Moraines. *Global and Planetary Change*, vol. 31(1-4), pp. 387-405. DOI: [https://doi.org/10.1016/S0921-8181\(01\)00131-x](https://doi.org/10.1016/S0921-8181(01)00131-x)
- Saarnisto, M. & Saarinen, T. (2001). Deglaciation chronology of the Scandinavian Ice Sheet from the Lake Onega Basin to the Salpausselkä End Moraines. *Global Planetary Change*, vol. 31(1-4), pp. 387-405. DOI: [https://doi.org/10.1016/S0921-8181\(01\)00131-X](https://doi.org/10.1016/S0921-8181(01)00131-X)
- Saarnisto, M. & Saarinen, T. 2001: Deglaciation chronology of the Scandinavian Ice Sheet from the Lake Onega Basin to the Salpausselkä End Moraines. *Global and Planetary Change* 31, 387-405, [https://doi.org/10.1016/S0921-8181\(01\)00131-x](https://doi.org/10.1016/S0921-8181(01)00131-x).
- Saarnisto, M. (1985). Long varve series in Finland. *Boreas*, vol. 14(2), pp. 133-137. DOI: <https://doi.org/10.1111/j.1502-3885.1985.tb00905.x>
- Salonen, V.-P. (1990). Salpausselkä III, Pertelli. In Lundqvist, J. & Saarnisto, M. (eds.) *Termination of the Pleistocene. Field conference Norway-Sweden-Finland, May 9-16, 1990. Excursion and abstracts. Geological Survey of Finland, Guide 31*, pp. 63-64.
- Sapsa, I. & Tomeniuk, O. (2020). A GIS-based approach in the morphometric analysis of incised meanders on the Dnister River (Ukraine). *European Association of Geoscientists & Engineers. Conference Proceedings, International Conference of Young Professionals*, vol. 2020, pp. 1-5. DOI: <https://doi.org/10.3997/2214-4609.20205711>
- Sarif, M.N., Siddiqui, L., Islam, M.S., Parveen, N. & Saha, M. (2021). Evolution of river course and morphometric features of the River Ganga: A case study of up and downstream of Farakka Barrage. *International Soil and Water Conservation Research*. Vol. 9(4), pp. 578-590. DOI: <https://doi.org/10.1016/j.iswcr.2021.01.006>
- Sauramo, M. (1923). Studies on the Quaternary Varve Sediments in Southern Finland. *Bulletin de la Commission Géologique de Finlande*, vol. 60. Suomen Geologinen Komissioni. ISSN: 0365-9283

- Sauramo, M. (1923). Studies on the Quaternary varve sediments in southern Finland. *Fennia*, vol. 44, pp. 164.
- Sauramo, M. (1929) The Quaternary geology of Finland. *Bull. Geol. Fin*, vol. 86, pp. 1-110.
- Scambos, T.A., Echelmeyer, K.A., Fahnestock, M.A. & Bindshadler, R.A. (1994). Development of enhanced ice flow at the southern margin of Ice Stream D, Antarctica. *Annals of Glaciology*, vol. 20, pp. 313 -318. DOI: <https://doi.org/10.3189/1994AoG20-1-313-318>
- Scheidegger, A.E. (2002). Morphometric analysis and its relation to tectonics in Macaronesia. *Geomorphology*. Vol. 46(1-2), pp. 95-115. DOI: [https://doi.org/10.1016/S0169-555X\(02\)00056-9](https://doi.org/10.1016/S0169-555X(02)00056-9)
- Schmidt, B.E., Washam, P. Davis, P.E.D., Nicholls, K.W., Holland, D.M., Lawrence, J.D., Riverman, K.L., Smith, J.A., Spears, A., Dichek, D.J.G., Mullen, A.D., Clyne, E., Yeager, B., Anker, P., Meister, M.R., Hurwitz, B.C., Quartini, E.S., Bryson, F.E., Basinski-Ferris, A., Thomas, C., Wake, J., Vaughan, D.G., Anandakrishnan, S., Rignot, E., Paden, J. & Makinson, K. (2023). Heterogeneous melting near the Thwaites Glacier grounding line. *Nature*, vol. 614, pp. 471-478. DOI: <https://doi.org/10.1038/s41586-022-05691-0>
- Schomacker, A. Benediktsson, I.O. & Ingolfsson, O. (2014). The Eyjabakkajökull glacial landsystem, Iceland: Geomorphic impact of multiple surges. *Geomorphology*, vol. 218, pp. 98-107. DOI: <https://dx.doi.org/10.1016/j.geomorph.2013.07.005>
- Schoof, C. (2007). Ice sheet grounding line dynamics: Steady states, stability, and hysteresis. *Journal of Geophysical Research: Earth Surface*, vol. 112(F3). DOI: <https://doi.org/10.1029/2006JF000664>
- Schoof, C. (2007). Ice sheet grounding line dynamics: Steady states, stability, and hysteresis. *Journal of Geophysical research: Earth Surface* (2003-2012), vol. 112(F3). DOI: <https://doi.org/10.1029/2006JF000664>
- Sejrup, H.P., Hjelstuen, B.O., Patton, H., Esteves, M., Winsborrow, M., Rasmussen, T.L., Andreassen, K. & Hubbard, A. (2022). The role of ocean and atmospheric dynamics



- in the marine-based collapse of the last Eurasian Ice Sheet. *Communications Earth & Environment*, vol. 3(119). DOI: <https://doi.org/10.1038/s43247-022-00447-0>
- Sergienko, O.V. & Wingham, D.J. (2022). Bed topography and marine ice-sheet stability. *Journal of Glaciology*, vol. 68(267), pp. 124-138. DOI: <https://doi.org/10.1017/jog.2021.79>
- Sergienko, O.V. (2022). No general stability conditions for marine ice-sheet grounding lines in the presence of feedbacks. *Nature Communications*, vol. 13(2265). DOI: <https://doi.org/10.1038/s41467-022-29892-3>
- Shackleton, C.S., Winsborrow, M.C.M., Andreassen, K., Lucchi, R.G. & Bjarnadóttir, L.R. (2019). Ice-margin retreat and grounding-zone dynamics during initial deglaciation of the Storfjordrenna Ice Stream, western Barents Sea. *Boreas*, vol. 49(1), pp. 38-51. DOI: <https://doi.org/10.1111/bor.12420>
- Sharma, P.V. (1984). The Fennoscandian uplift and glacial isostasy. *Tectonophysics*, vol. 105(1-4), pp. 249-262. DOI: [https://doi.org/10.1016/0040-1951\(84\)90206-3](https://doi.org/10.1016/0040-1951(84)90206-3)
- Sharp, M. (1985). "Crevasse-Fill" Ridges: A Landform Type Characteristic of Surging Glaciers?. *Geografiska Annaler. Series A, Physical Geography*, vol. 67(3/4), pp. 213-220. DOI: <https://doi.org/10.2307/521099>
- Sharp, M. (1985). "Crevasse-Fill" Ridges: A Landform Type Characteristic of Surging Glaciers? *Geografiska Annaler. Series A. Physical Geography*, vol. 67 (3-4), pp. 213-220. Retrieved from <https://www.jstor.org/stable/521009>
- Siegert, M.J., Payne, A.J. & Joughin, I. (2003). Spatial stability of Ice Stream D and its tributaries, West Antarctica, revealed by radio-echo sounding and interferometry. *Annals of Glaciology*, vol. 37(1), pp. 377-382. DOI: <https://doi.org/10.3189/172756403781816022>
- Simkins, L. M., Greenwood, S. L. & Anderson, J. B. 2018: Diagnosing ice sheet grounding line stability from landform morphology. *The Cryosphere* 12, 2707-2726, <https://doi.org/10.5194/tc-12-2707-2018>.

- Simkins, L.M., Greenwood, S.L. & Anderson, J.B. (2018). Diagnosing ice sheet grounding line stability from landform morphology. *The Cryosphere*, vol. 12, pp. 2707-2726. DOI: <https://doi.org/10.5194/tc-12-2707-2018>
- Simkins, L.M., Greenwood, S.L. & Anderson, J.B. (2018). Diagnosing ice sheet grounding line stability from landform morphology. *The Cryosphere*, vol. 12, pp. 2707-2726. DOI: <https://doi.org/10.5194/tc-12-2707-2018>.
- Simon, A., Castro, J. & Rinaldi, M. (2016). Channel form and adjustment: characterization, measurement, interpretation and analysis. *Tools in Fluvial Geomorphology*. Second Edition. Edited by G. Mathias Kondolf and Herve Piegay. John Wiley & Sons, Ltd. Chichester, West Sussex. ISBN: 9780470684054. DOI: <https://doi.org/10.1002/9781118648551.ch11>
- Sinclair, S. N., Licciardi, J. M., Campbell, S. W. & Madore, B. M. 2018: Character and origin of De Geer moraines in the Seacoast region of New Hampshire, USA. *Journal of Quaternary Science* 33, 225-237, <https://doi.org/10.1002/jqs.3017>.
- Sinclair, S.N. (2015). Origin of De Geer Moraines in the Seacoast Region of New Hampshire. Master's Theses and Capstones. 1062. Retrieved from: <https://scholars.unh.edu/thesis/1062>
- Sinclair, S.N., Licciardi, J.M., Campbell, S.W. & Madore, B.M. (2018). Character and origin of De Geer moraines in the Seacoast region of New Hampshire, USA. *Journal of Quaternary Science*, vol. 33(2), pp. 225-237. DOI: <https://doi.org/10.1002/jqs.3017>
- Sinet, S., Ashwin, P., von der Heydt, A.S. & Dijkstra, H.A. (2024). AMOC stability amid tipping ice sheets: the crucial role of rate and noise. *EGU, Earth System Dynamics*, vol. 15(4), pp. 859-873. DOI: <https://doi.org/10.5194/esd-15-859-2024>
- Sinet, S., von der Heydt, A.S. & Dijkstra, H.A. (2023). AMOC Stabilization Under the Interaction With Tipping Polar Ice Sheets. *Geophysical Research Letters*, vol. 50(2). DOI: <https://doi.org/10.1029/2022GL100305>
- Smith, D.G. (1994). Glacial lake McConnell: Palaeogeography, age, duration, and associated river deltas, Mackenzie river basin, western Canada. *Quaternary Science*

Reviews, vol. 13(9-10), pp. 829-843. DOI: [https://doi.org/10.1016/0277-3791\(94\)90004-3](https://doi.org/10.1016/0277-3791(94)90004-3)

Smith, G.W. & Hunter, L.E. (1989). Late Wisconsinan deglaciation of coastal Maine. In R.D. Tucker & R.G. Marvinney (eds.): *Studies in Maine Geology*, vol. 6: Quaternary Geology, pp. 13-32. Geological Survey, Augusta, ME.

Smith, G.W. & Hunter, L.E. (1989). Late Wisconsinan Deglaciation of Coastal Maine. Maine Geological Survey. *Studies in Maine Geology*, vol. 6. Retrieved from [https://digitalmaine.com/cgi/viewcontent.cgi?referer=https://www.google.com/&httpsredir=1&article=1100&context=mgs\\_publications](https://digitalmaine.com/cgi/viewcontent.cgi?referer=https://www.google.com/&httpsredir=1&article=1100&context=mgs_publications)

Smith, G.W. (1982). End moraines and the pattern of last ice retreat from central and south coastal Maine. In G.J. Larsen & B.D. Slone (eds.): *Late Wisconsinan Glaciation of New England*, 195-209. Kendall/Hunt Publishing, Dubuque, IA.

Smith, G.W. (1982). End Moraines and the Pattern of Last Ice Retreat from Central and South Coastal Maine. Ohio University, Athens, Ohio, pp. 195- 209

Smith, J.A., Graham, A.G.C., Post, A.L., Hillenbrand, C.-D., Bart, P.J. & Powell, R.D. (2019). The marine geological imprint of Antarctic ice shelves. *Nature Communications*, vol. 10, 5635. DOI: <https://doi.org/10.1038/s41467-019-13496-5>

Smith, M.J. and Clark, C.D. (2005). Methods for the visualization of digital elevation models for landform mapping. *Earth Surf. Process. Landforms*, 30: 885-900. DOI: <https://doi.org/10.1002/esp.1210>

Smith, M.J., Rose, J. & Booth, S. (2006). Geomorphological mapping of glacial landforms from remotely sensed data: An evaluation of the principal data sources and an assessment of their quality. *Geomorphology*, vol. 76(1-2), pp. 148-165. DOI: <https://doi.org/10.1016/j.geomorph.2005.11.001>

Soar, P.J., Wallerstein, N.P. & Thorne, C.R. (2017). Quantifying River Channel Stability at the Basin Scale. *Water*, vol. 9(2), 133. DOI: <https://doi.org/10.3390/w9020133>

Sobota, I., Weckwerth, P. & Nowak, M. (2016). Surge dynamics of Aavatsmarkbreen, Svalbard, inferred from the geomorphological record. *Boreas*, vol. 42(2), pp. 360-376. DOI: <https://doi.org/10.1111/bor.12160>

- Sobota, I., Weckwerth, P. & Nowak, M. (2016). Surge dynamics of Aavatsmarkbreen, Svalbard, inferred from the geomorphological record. *Boreas*, vol. 45, pp. 360-376. DOI: <https://doi.org/10.1111/bor.12160>. ISSN: 0300-9483
- Solheim, A. (1991). The Depositional Environment of Surging Sub-Polar Tidewater Glaciers. A case study of the morphology, sedimentation and sediment properties in a surge-affected marine basin outside Nordaustlandet. *Norsk Polarinstitutt*, vol. 194, pp. 5-97. Oslo. Retrieved from: <https://brage.npolar.no/npolar-xmlui/bitstream/handle/11250/173646/Skrifter194.pdf?sequence=1&isAllowed=y>
- Solheim, A. (1991). The Depositional Environment of Surging Sub-Polar Tidewater Glaciers. A case study of the morphology, sedimentation and sediment properties in a surge-affected marine basin outside Nordaustlandet, Northern Barents Sea. *Norsk Polarinstitutt*. Oslo. Retrieved from <https://brage.npolar.no/npolar-xmlui/bitstream/handle/11250/173646/Skrifter194.pdf?sequence=1&isAllowed=y>
- Sollid, J. L. & Carlson, A. B. 1984: De Geer moraines and eskers in Pasvik, North Norway in Ten Years of Nordic Till Research (L.-K. Königsson, Ed.). *Striae* 20, 55-61.
- Sollid, J. L. (1989). Comments on the genesis of De Geer moraines. *Norsk geografisk Tidsskrift- Norwegian Journal of Geography*, vol. 43 (1), pp. 45-47. Oslo. ISSN: 0029-1951. DOI: <https://doi.org/10.1080/00291958908552217>
- Sollid, J. L. 1989: Comments on the genesis of De Geer moraines. *Norsk Geografisk Tidsskrift – Norwegian Journal of Geography* 43, 45-47, <https://doi.org/10.1080/00291958908552217>.
- Sollid, J.L. & Carlsson, A.B. (1984). De Geer moraines and eskers in Pasvik, North Norway. In Ten Years of Nordic Till Research (L.-K. Königsson, Ed.). *Striae*, vol. 20, pp. 55-61. Uppsala. ISBN: 91-7388-039-6. ISSN: 0345-0074
- Sollid, J.L. (1989). Comments on the genesis of De Geer moraines. *Norsk Geografisk Tidsskrift*
- Sollid, J.L. (1989). Comments on the genesis of De Geer moraines. *Norsk Geografisk Tidsskrift – Norwegian Journal of Geography*, vol. 43(1), pp. 45-47. DOI: <https://doi.org/10.1080/00291958908552217>

- Sookhan, S., Eyles, N. & Bukhari, S. (2022). Drumlins and mega-scale glacial lineations as a continuum of subglacial shear marks: A LiDAR based morphometric study of streamlined surfaces on the bed of a Canadian paleo-ice stream. *Quaternary Science Reviews*, vol. 292. DOI: <https://doi.org/10.1016/j.quascirev.2022.107679>
- Spagnolo, M., Clark, C.D., Ely, J.C., Stokes, C.R., Anderson, J.B., Andreassen, K., Graham, A.G.C. & Kind, E.C. (2014). Size, shape and spatial arrangement of mega-scale glacial lineations from a large and diverse dataset. *Earth Surface Processes and Landforms*. DOI: <https://doi.org/10.1002/esp.3532>
- Stoker, B. J., Livingstone, S. J., Barr, I. D., Ruffell, A., Storrar, R. D. & Roberson, S. 2021: Variations in esker morphology and internal architecture record time-transgressive deposition during ice margin retreat in Northern Ireland. *Proceedings of the Geologists' Association* 132, 409-425, <https://doi.org/10.1016/j.pgeola.2021.03.002>.
- Stoker, B.J., Livingstone, S.J., Barr, I.D., Ruffell, A. Storrar, R.D. & Robertson, S. (2021). Variations in esker morphology and internal architecture record time-transgressive deposition during ice margin retreat in Northern Ireland. *Proceedings of the Geologists' Association*, vol. 132(4), pp. 409-425. DOI: <https://doi.org/10.1016/j.pgeola.2021.03.002>
- Stoker, B.J., Livingstone, S.J., Barr, I.D., Ruffell, A., Storrar, R.D. & Roberson, S. (2021). Variations in esker morphology and internal architecture record time-transgressive deposition during ice margin retreat in Northern Ireland. *Proceedings of the Geologists' Association*, vol. 132(4), pp. 409-425. DOI: <https://doi.org/10.1016/j.pgeola.2021.03.002>
- Stoker, B.J., Livingstone, S.J., Barr, I.D., Ruffell, A., Storrar, R.D. & Robertson, S. (2021). Variations in esker morphology and internal architecture record time-transgressive deposition during ice margin retreat in Northern Ireland. *Proceedings of the Geologists' Association*, vol. 132, pp. 409-425. DOI: <https://doi.org/10.1016.j.pgeola.2021.03.002>
- Stokes, C. R., Tarasov, L., Blomdin, R., Cronin, T. M., Fisher, T. G., Gyllencreutz, R., Hättestrand, C., Heyman, J., Hindmarsh, R. C. A., Hughes, A. L. C., Jakobsson, M., Kirchner, N., Livingstone, S. J., Margold, M., Murton, J. B., Noormets, R., Peltier, W. R.,

- Peteet, D. M., Piper, D. J. W., Preusser, F., Renssen, H., Roberts, D., Roche, D. M., Saint-Ange, F., Stroeve, A. P. & Teller, J. T. 2015: On the reconstruction of palaeo-ice sheets: Recent advances and future challenges. *Quaternary Science Reviews* 125, 15-49, <https://doi.org/10.1016/j.quascirev.2015.07.016>.
- Stokes, C., Clark, C. & Storrar, R. (2009). Major changes in ice stream dynamics during deglaciation of the north-western margin of the Laurentide Ice Sheet. *Quaternary Science Reviews*, vol. 28(7-8), pp. 721-738. DOI: <https://doi.org/10.1016/j.quascirev.2008.07.019>
- Stokes, C.R. & Clark, C.D. (1999). Geomorphological criteria for identifying Pleistocene ice streams. *Annals of Glaciology*, vol. 28, pp. 67-74. DOI: <https://doi.org/10.3189/172756499781821625>
- Stokes, C.R. & Clark, C.D. (2001). Palaeo-ice streams. *Quaternary Science Reviews*, vol. 20, pp. 1437-1457. DOI: [https://doi.org/10.1016/S0277-3791\(01\)00003-8](https://doi.org/10.1016/S0277-3791(01)00003-8)
- Stokes, C.R. & Clark, C.D. (2001). Palaeo-ice streams. *Quaternary Science Reviews*, vol. 20, pp. 1437-1457. ISSN: 0277-3791. PII: S0277-3791(01)00003-8
- Stokes, C.R. (2000). The Geomorphology of Palaeo-Ice Streams: Identification, Characterisation and Implications for Ice Stream Functioning. The University of Sheffield. Retrieved from: <https://core.ac.uk/download/pdf/77023352.pdf>
- Stokes, C.R. (2000). The Geomorphology of Palaeo-Ice Streams: Identification, Characterisation and Implications for Ice Stream Functioning. The University of Sheffield. Retrieved from <https://core.ac.uk/download/pdf/77023352.pdf>
- Stokes, C.R. (2017). Deglaciation of the Laurentide Ice Sheet from The Last Glacial Maximum. *Cuadernos de Investigacion Geografica*, vol. 43 (2), pp. 377-428. DOI: <https://doi.org/10.18172/cig.3237>. ISSN: 0211-6820.
- Stokes, C.R. (2018). Geomorphology under ice streams: Moving from form to process. *Earth Surface Processes and Landforms*, vol. 43(1), pp. 85-123. DOI: <https://doi.org/10.1002/esp.4259>

- Stokes, C.R. (2018). Geomorphology under ice streams: Moving from form to process. *Earth Surface Processes and Landforms*, vol. 43, pp. 85-123. DOI: <https://doi.org/10.1002/esp.4259>
- Stokes, C.R., Clark, C.D., Lian, O.B. & Tulaczyk, S. (2007). Ice stream sticky spots: A review of their identification and influence beneath contemporary and palaeo-ice streams. *Earth-Science Reviews*, vol. 81(3-4), pp. 217-249. DOI: <https://doi.org/10.1016/j.earscirev.2007.01.002>
- Stokes, C.R., Tarasov, L., Blomdin, R., Cronin, T.M., Fisher, T.G., Gyllencreutz, R., Hättestrand, C., Heyman, J., Hindmarsh, R.C.A., Hughes, A.L.C., Jakobsson, M., Kirchner, N., Livingstone, S.J., Margold, M., Murton, J.B., Noormets, R., Peltier, W.R., Peteet, D.M., Piper, D.J.W., Preusser, F. & Teller, J.T. (2015). On the reconstruction of palaeo-ice sheets: Recent advances and future challenges. *Quaternary Science Reviews*, vol. 125, pp. 15-49. DOI: <https://doi.org/10.1016/j.quascirev.2015.07.016>
- Stokes, C.R., Tarasov, L., Blomdin, R., Cronin, T.M., Fisher, T.G., Gyllencreutz, R., Hättestrand, C., Heyman, J., Hindmarsh, R.C.A., Hughes, A.L.C., Jakobsson, M., Kirchner, N., Livingstone, S.J., Margold, M., Murton, J.B., Noormets, R., Peltier, W.R., Peteet, D.M., Piper, D.J.W., Preusser, F., Renssen, H., Roberts, D., Roche, D.M., Saint-Ange, F., Stroeven, A.P. & Teller, J.T. (2015). On the reconstruction of palaeo-ice sheets: Recent advances and future challenges. *Quaternary Science Reviews*, vol. 125, pp. 15-49. DOI: <https://doi.org/10.1016/j.quascirev.2015.07.016>. ISSN: 0277-3791
- Storrar, R.D., Evans, D.J.A., Stokes, C.R. & Ewertowski, M. (2015). Controls on the location, morphology and evolution of complex esker systems at decadal timescales, Breidamerkurjökull, southeast Iceland. *Earth Surf. Process. Landforms* 40, 1421-1438. DOI: <https://doi.org/10.1002/esp.3725>
- Storrar, R.D., Ewertowski, M., Tomczyk, A.M., Barr, I.D., Livingstone, S.J., Ruffell, A., Stoker, B.J. & Evans, D.J.A. (2020). Equifinality and preservation potential of complex eskers. *Boreas*, vol. 49, pp. 211-231. DOI: <https://doi.org/10.1111/bor.12414>
- Storrar, R.D., Stokes, C.R. & Evans, D.J.A. (2014). Morphometry and pattern of a large sample (>20,000) of Canadian eskers and implications for subglacial drainage

beneath ice sheets. *Quaternary Science Reviews*, vol. 105, pp. 1-25. DOI: <https://doi.org/10.1016/j.quascirev.2014.09.013>

Stretch, R.C., Mitchell, N.C. & Portaro, R.A. (2006). A morphometric analysis of the submarine volcanic ridge south-east of Pico Island, Azores. *Journal of Volcanology and Geothermal Research*, Vol. 156(1-2), pp. 35-54. DOI: <https://doi.org/10.1016/j.jvolgeores.2006.03.009>

Streuff, K., Forwick, M., Szczucinski, W., Andreassen, K. & Cofaigh, C.O. (2015). Submarine landform assemblages and sedimentary processes related to glacier surging in Kongsfjorden, Svalbard. *Arktos*, vol. 1 (14). DOI: <https://doi.org/10.1007/s41063-015-0003-y>

Stroeven, A. P., Hättestrand, C., Kleman, J., Keyman, J., Fabel, D., Fredin, O., Goodfellow, B. W., Harbor, J. M., Jansen, J. D., Olsen, L., Caffee, M. W., Fink, D., Lundqvist, J., Rosqvist, G. C., Strömberg, B. & Jansson, K. N. 2016: Deglaciation of Fennoscandia. *Quaternary Science Reviews* 147, 91-121, <https://doi.org/10.1016/j.quascirev.2015.09.016>.

Stroeven, A.P., Hättestrand, C., Kleman, J., Heyman, J., Fabel, D., Fredin, O., Goodfellow, B.W., Harbor, J.M., Jansen, J.D., Olsen, L., Caffee, M.W., Fink, D., Lundqvist, J., Rosqvist, G.C., Strömberg, B. & Jansson, K.N. (2016). Deglaciation of Fennoscandia. *Quaternary Science Reviews*, vol. 147, pp. 91-121. DOI: <https://doi.org/10.1016/j.quascirev.2015.09.016>

Stroeven, A.P., Heyman, J., Fabel, D., Svante, B., Caffee, M.W., Fredin, O. & Harbor, J.M. (2015). A new Scandinavian reference  $^{10}\text{Be}$  production rate. *Quaternary Geochronology*, vol. 29, pp. 104-115. DOI: <https://doi.org/10.1016/j.quascirev.2015.06.011>

Strömberg, B. (1965). Mappings and Geochronological Investigations in Some Moraine Areas of South-Central Sweden. *Geografiska Annaler. Series A, Physical Geography*, vol. 47(2), pp. 73-82. Retrieved from: <https://www.jstor.org/stable/520956>

Strömberg, B. (1965). Mappings and Geochronological Investigations in Some Moraine Areas of South-Central Sweden. *Geografiska Annaler: Series A, Physical Geography*, vol. 47 (2), pp. 73-82. DOI: <https://doi.org/10.1080.04353676.1965.11879715>



- Strömberg, B. (2005). Clay varve chronology and deglaciation in SW Finland. *Annales Academiae Scientiarum Fennicae, Geologica-Geographica*, vol. 167. ISSN: 1239 632X. ISBN: 951-41-0980-5
- Strömberg, B. (2005). Clay varve chronology and deglaciation in SW Finland. *Annales Academiae Scientiarum Fennicae Geologica-Geographica*, vol. 167. ISBN: 9514109805. ISSN: 1239-632X
- Strömberg, B. 1965: Mappings and Geochronological Investigations in Some Moraine Areas of South-Central Sweden. *Geografiska Annaler: Series A, Physical Geography* 47, 73-82, <https://doi.org/10.1080/04353676.1965.11879715>.
- Svendsen, J. I., Alexanderson, H., Astakhov, V. I., Demidov, I., Dowdeswell, J. A., Funder, S., Gataullin, V., Henriksen, M., Hjort, C., Houmark-Nielsen, M., Hubberten, H. W., Ingólfsson, Ó., Jakobsson, M., Kjær, K. H., Larsen, E., Lokrantz, H., Lunkka, J. P., Lyså, A., Mangerud, J., Matiouchkov, A. & Stein, R. 2004: Late Quaternary ice sheet history of northern Eurasia. *Quaternary Science Reviews* 23, 1229-1271, <https://doi.org/10.1016/j.quascirev.2003.12.008>.
- Székely, B. & Karátson, D. (2004). DEM-based morphometry as a tool for reconstructing primary volcanic landforms: examples from the Börzsöny Mountains, Hungary. *Geomorphology*. Vol. 63(1-2), pp. 25-37. DOI: <https://doi.org/10.1016/j.geomorph.2004.03.008>
- Szuman, I., Kalita, J.Z., Ewertowski, M.W., Clark, C.D. & Livingstone, S.J. (2021). Dynamics of the last Scandinavian Ice Sheet's southernmost sector revealed by the pattern of ice streams. *Boreas*, vol. 50, pp. 764-780. DOI: <https://doi.org/10.1111/bor.12512>
- Taylor, C. (2024). Proglacial Glaciofluvial Landforms. *Antarctic Glaciers, Glaciers and Glaciation in Antarctica and beyond*. Retrieved from: <https://www.antarcticglaciers.org/glacial-geology/glacial-landforms/glaciofluvial-landforms/proglacial-glaciofluvial-landforms/>
- Teller, J.T. (2003). Subaquatic landsystems: large proglacial lakes. In Evans, D.J.A. *Glacial Landsystems* (pp. 348-371). Arnold, London.

- Todd, B. J., Valentine, P. C., Longva, O. & Shaw, J. 2007: Glacial landforms on German Bank, Scotian Shelf: evidence for Late Wisconsinan ice-sheet dynamics and implications for the formation of De Geer moraines. *Boreas* 16, 148-169, <https://doi.org/10.1080/03009480600992050>.
- Tschudi, S., Ivy-Ochs, S., Schlüchter, C., Kubik, P. & Rainio, H. (2000). <sup>10</sup>Be dating of Younger Dryas Salpausselkä I formation in Finland. *Boreas*, vol. 29(4), pp. 287-293. DOI: <https://doi.org/10.1111/j.1502-3885.2000.tb01211.x>
- Tschudi, S., Ivy-Ochs, S., Schlüchter, C., Kubik, P. & Rainio, H. 2000: <sup>10</sup>Be dating of Younger Dryas Salpausselkä I formation in Finland. *Boreas* 29, 287-293, <https://doi.org/10.1111/j.1502-3885.2000.tb01211.x>.
- Tschudi, S., Ivy-Ochs, S., Schlüchter, C., Kubik, P. & Rainio, H. (2000). <sup>10</sup>Be dating of the Younger Dryas Salpausselkä I formation in Finland. *Boreas*, vol. 29, pp. 287-293. Oslo. ISSN: 0300-9483. Retrieved from: [https://onlinelibrary.wiley.com/doi/pdf/10.1111/j.1502-3885.2000.tb01211.x?utm\\_campaign=The+Week+in+Botany&utm\\_medium=email&utm\\_source=Revue+newsletter&utm\\_sq=h0khuj5usc](https://onlinelibrary.wiley.com/doi/pdf/10.1111/j.1502-3885.2000.tb01211.x?utm_campaign=The+Week+in+Botany&utm_medium=email&utm_source=Revue+newsletter&utm_sq=h0khuj5usc)
- Valla, P.G., van der Beek, P.A. & Lague, D. (2010). Fluvial incision into bedrock: Insights from morphometric analysis and numerical modeling of gorges incising glacial hanging valleys (Western Alps, France). *JGR Earth Surface*, vol. 115(F2). DOI: <https://doi.org/10.1029/2008JF001079>
- Valters, D.A. (2016). Modelling Geomorphic Systems: Landscape Evolution. *Geomorphological Techniques*, Chap. 5, Sec. 6.12. British Society for Geomorphology. Retrieved from [https://www.geomorphology.org.uk/sites/default/files/chapters/5.6.12\\_LEM.pdf](https://www.geomorphology.org.uk/sites/default/files/chapters/5.6.12_LEM.pdf)
- Van Aalderen, V., Charbit, S., Dumas, C. & Quiquet, A. (2024). Relative importance of the mechanisms triggering the Eurasian ice sheet deglaciation in the GRISLI2.0 ice sheet model. *Climate of the Past*, EGU, vol. 20(1), pp. 187-209. DOI: <https://doi.org/10.5194/cp-20-187-2024>
- Van Asselen, S. & Seijmonsbergen, A.C. (2006). Expert-driven semi-automated geomorphological mapping for a mountainous area using a laser DTM.

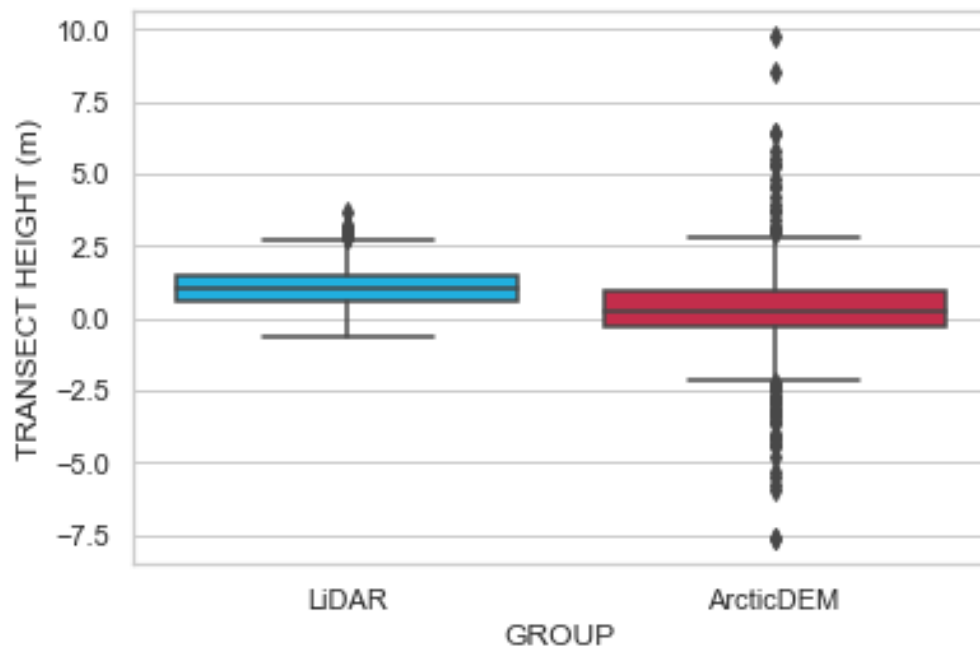
- Geomorphology, vol. 78(3-4), pp. 309-320. DOI: <https://doi.org/10.1016/j.geomorph.2006.01.037>
- Van de Veen, C.J. (2002). Calving glaciers. *Progress in Physical Geography: Earth and Environment*, vol. 26(1), pp. 96-122. DOI: <https://doi.org/10.1191/0309133302pp327ra>
- Van der Veen, C.J. (1996). Tidewater calving. *Journal of Glaciology*, vol. 42(141), pp. 375-385. DOI: <https://doi.org/10.3189/S0022143000004226>
- Vaughn, D.G. (2009). Chapter 22 – Ice Sheets: Indicators and Instruments of Climate Change. *Climate Change, Observed Impacts on Planet Earth*, pp. 391-400. DOI: <https://doi.org/10.1016/B978-0-444-53301-2.00022-1>
- Velay-Vitow, J., Chandan, D. & Peltier, W.R. (2024). Into the Holocene, anatomy of the Younger Dryas cold reversal and preboreal oscillation. *Sci Rep*, vol 14(3134). DOI: <https://doi.org/10.1038/s41598-024-53591-2>
- Vieli, A., Jacek, J. & Lezek, K. (2002). The retreat of a tidewater glacier: Observations and model calculations on Hansbreen, Spitsbergen. *Journal of Glaciology*, vol. 48(163), pp. 592-600. DOI: <https://doi.org/10.3189/172756502781831089>
- Vieli, A., Martin, F. & Heinz, B. (2001). Flow dynamics of tidewater glaciers: A numerical modelling approach. *Journal of Glaciology*, vol. 47(159), pp. 595-606. DOI: <https://doi.org/10.3189/172756501781831747>
- Vinther, B.M., Buchardt, S.L., Clausen, H.B., Dahl-Jensen, D., Johnsen, S.J., Fisher, D.A., Koerner, R.M., Raynaud, D., Lipenkov, V., Andersen, K.K., Blunier, T., Rasmussen, S.O., Steffensen J.P. & Svensson, A.M. (2009). Holocene thinning of the Greenland ice sheet. *Nature*, vol. 461, pp. 385-388. DOI: <https://doi.org/10.1038/nature08355>
- Vollmer, F. W. 2023: Orient Software. Accessed via: <https://www.frederickvollmer.com/orient/index.html>
- Vorren, T.O. & Laberg, J.S. (1997). Trough mouth fans – palaeoclimate and ice-sheet monitors. *Quaternary Science Reviews*, vol. 16(8), pp. 865-881. DOI: [https://doi.org/10.1016/S0277-3791\(97\)00003-6](https://doi.org/10.1016/S0277-3791(97)00003-6)

- Vorren, T.O., Hald, M. & Lebesbye, E. (1988). Late Cenozoic environments in the Barents Sea. *Paleoceanography*, vol. 3(5), pp. 601-612. DOI: <http://doi.org/10.1029/PA003i005p00601>
- Vorren, T.O., Lebesbye, E., Andreassen, K. & Larsen, K.-B. (1989). Glacigenic sediments on a passive continental margin as exemplified by the Barents Sea. *Marine Geology*, vol. 85, pp. 251-272. DOI: [https://doi.org/10.1016/0025-3227\(89\)90156-4](https://doi.org/10.1016/0025-3227(89)90156-4)
- Walker, M. (2005). *Quaternary dating methods*. Wiley-Blackwell. ISBN: 9780470869284
- Walker, M., Head, M.J., Lowe, J., Berkelhammer, M., Björck, S., Cheng, H., Cwynar, L.C., Fisher, D., Gkinis, V., Long, A., Newnham, R., Rasmussen, S.O. & Weiss, H. (2019). Subdividing the Holocene Series/Epoch: formalization of stages/ages and subseries/subepochs, and designation of GSSPs and auxiliary stratotypes. *Journal of Quaternary Science*, vol. 34(3), pp. 173-186. DOI: <https://doi.org/10.1002/jqs.3097>
- Waller, R.I. (2013). Permafrost and periglacial features | Permafrost and Glacier Interactions. *Encyclopedia of Quaternary Science* (second edition), Elsevier, pp. 507-513. DOI: <https://doi.org/10.1016/B978-0-444-53643-3.00107-2>. ISBN: 9780444536426
- Warren, C.R. & Hulton, N.R.J. (1990). Topographic and glaciological controls on Holocene ice-sheet margin dynamics, central West Greenland. *Annals of Glaciology*, vol. 14, pp. 307-310. DOI: <https://doi.org/10.1017/s0260305500008806>
- Warren, C.R. & Kirkbride, M.P. (2003). Calving speed and climatic sensitivity of New Zealand lake-calving glaciers. *Annals of Glaciology*, vol. 36, pp. 173-178. DOI: <https://doi.org/10.3189/172756403781816446>
- Warren, C.R. (1991). Terminal environment, topographic control and fluctuations of West Greenland glaciers. *Boreas*, vol. 20(1), pp. 1-15. DOI: <https://doi.org/10.1111/j.1502-3885.1991.tb00453.x>
- Warren, C.R. (1992). Iceberg calving and the glacioclimatic record. *Progress in Physical Geography: Earth and Environment*, vol. 16(3), 253-282. DOI: <https://doi.org/10.1177/030913339201600301>

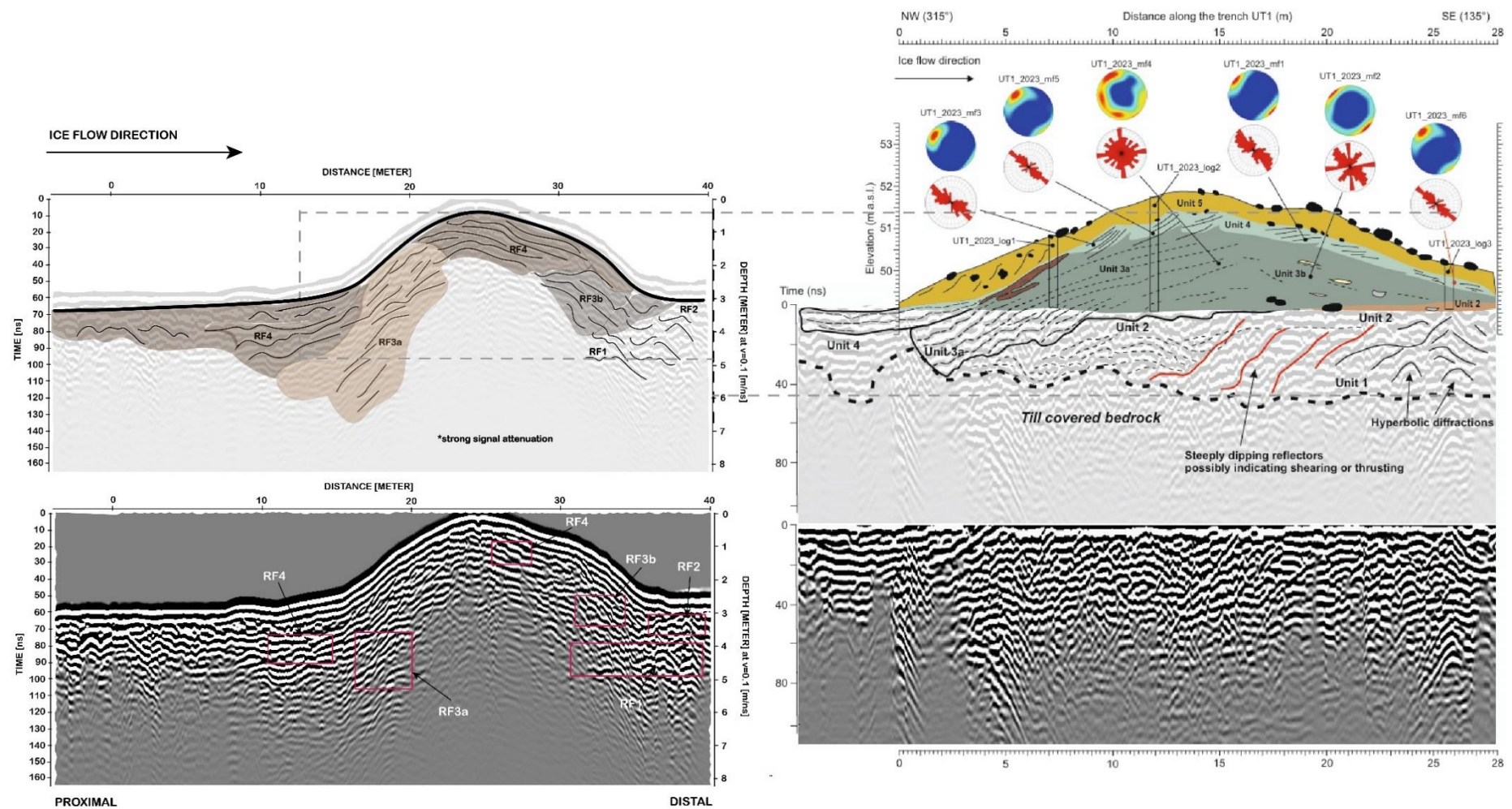
- Warren, C.R., Benn, D., Winchester, V. & Harrison, S. (2001). Buoyancy-driven lacustrine calving, Glaciar Nef, Chilean Patagonia. *Journal of Glaciology*, vol. 47(156), pp. 135-146. DOI: <https://doi.org/10.3189/172756501781832403>
- Weertman, J. (1974). Stability of the Junction of an Ice Sheet and an Ice Shelf. *Journal of Glaciology*, vol. 13(67), pp. 3-11. DOI: <https://doi.org/10.3189/S0022143000023327>
- Weertman, J. (1974). Stability of the Junction of an Ice Sheet and an Ice Shelf. *Journal of Glaciology*, vol. 13(67), pp. 3-11. DOI: <https://doi.org/10.3189/S0022143000023327>
- Whillans, I.M. & van der Veen, C.J. (2001). Transmission of stress between an ice stream and interstream ridge. *Journal of Glaciology*, vol. 47(158), pp. 433-440. DOI: <https://doi.org/10.3189/172756501781832052>
- Whillans, I.M. & van der Veen, C.J. (2001). Transmission of stress between an ice stream and interstream ridge. *Journal of Glaciology*, vol. 47 (158), pp. 433-440. DOI: <https://doi.org/10.3189/172756501781832052>
- White, S.M., Haymon, R.M., Fornari, D.J., Perfit, M.R. & Macdonald, K.C. (2002). Correlation between volcanic and tectonic segmentation of fast-spreading ridges: Evidence from volcanic structures and lava flow morphology on the East Pacific Rise at 9°-10°N. *Journal of Geophysical Research, Solid Earth*. Vol. 107(B8), pp. EPM 7-1-EPM 7-20. DOI: <https://doi.org/10.1029/2001JB000571>
- Winkelmann, D., Jokat, W., Jensen, L. & Schenke, H.-W. (2010). Submarine end moraines on the continental shelf off NE Greenland – Implications for Lateglacial dynamics. *Quaternary Science Reviews*, vol. 29(9-10), pp. 1069-1077. DOI: <https://doi.org/10.1016/j.quascirev.2010.02.002>
- Winsborrow, M.C.M., Andreassen, K., Corner, G.D., Laberg, J.S. (2010). Deglaciation of a marine-based ice sheet: Late Weichselian palaeo-ice dynamics and retreat in the southern Barents Sea reconstructed from onshore and offshore glacial geomorphology. *Quaternary Science Reviews*, vol. 29(3-4), pp. 424-442. DOI: <https://doi.org/10.1016/j.quascirev.2009.10.001>

- Winsborrow, M.C.M., Clark, C.D. & Stokes, C.R. (2010a). What controls the location of ice streams? *Earth-Science Reviews*, vol. 103(1-2), pp. 45-59. DOI: <https://doi.org/10.1016/j.earscirev.2010.07.003>
- Winsborrow, M.C.M., Stokes, C.R. & Andreassen, K. (2012). Ice-stream flow switching during deglaciation of the southwestern Barents Sea. *GSA Bulletin*, vol. 124(3-4), pp. 275-290. DOI: <https://doi.org/10.1130/B30416.1>
- Winter, K., Ross, N., Ferraccioli, F., Jordan, T.A., Corr, H.F.J., Forsberg, R., Matsuoka, K., Olesen, A.V. & Casal, T.G. (2018). *Geophysical Research Letters*, AGU, vol. 45. DOI: <https://doi.org/10.1029/2018GL077504>
- Xie, Z., Huang, H., Yu, G. & Zhang, M. (2018). Quantifying the Effects of Dramatic Changes in Runoff and Sediment on the Channel Morphology of a Large, Wandering River Using Remote Sensing Images. *Water*, vol. 10(12), 1767. DOI: <https://doi.org/10.3390/w10121767>
- Yu, H., Rignot, E., Seroussi, H. & Morlighem, M. (2018). Retreat of Thwaites Glacier, West Antarctica, over the next 100 years using various ice flow models, ice shelf melt scenarios and basal friction laws. *The Cryosphere*, vol. 12(12), pp. 3861-3876. DOI: <https://doi.org/10.5194/tc-12-3861-2018>
- Zilliacus, H. (1989). Genesis of De Geer moraines in Finland. *Sedimentary Geology*, vol. 62(2-4), pp. 309-317. DOI: [https://doi.org/10.1016/0037-0738\(89\)90121-8](https://doi.org/10.1016/0037-0738(89)90121-8)
- Zilliacus, H. (1989). Genesis of De Geer moraines in Finland. *Sedimentary Geology*, vol. 62, pp. 309-317. Elsevier Science Publishers B.V., Amsterdam - Printed in The Netherlands
- Zilliacus, H. 1981: De Geer moränerna på Replot och Björkönen i Vasa skärgård [The De Geer moraines on the islands of Replot and Björkönen in the Vasa archipelago, western Finland]. *Terra* 93, 12-24.
- Zilliacus, H. 1989: Genesis of De Geer moraines in Finland. *Sedimentary Geology* 62, 309-317, [https://doi.org/10.1016/0037-0738\(89\)90121-8](https://doi.org/10.1016/0037-0738(89)90121-8).

## Appendices



**FIGURE 1.** Boxplot presenting calculated transect height difference captured from LiDAR and ArcticDEM data. A sample of 573 transects were compared. A Wilcoxon signed-rank test indicated a significant difference between the two datasets ( $z = -12.8$ ,  $p < .001$ ,  $r = -0.5$ ), with an average difference of 0.79 m. [DEM sources: National Land Survey of Finland, 6/2023; ArcticDEM – Porter et al., 2018].



**FIGURE 2.** Correlation between excavated sediment exposure and neighbouring GPR profile #3 at Site (1) UT1 (see Supplementary FIGURE 1). Radar facies are presented in TABLE 1 within the main manuscript.



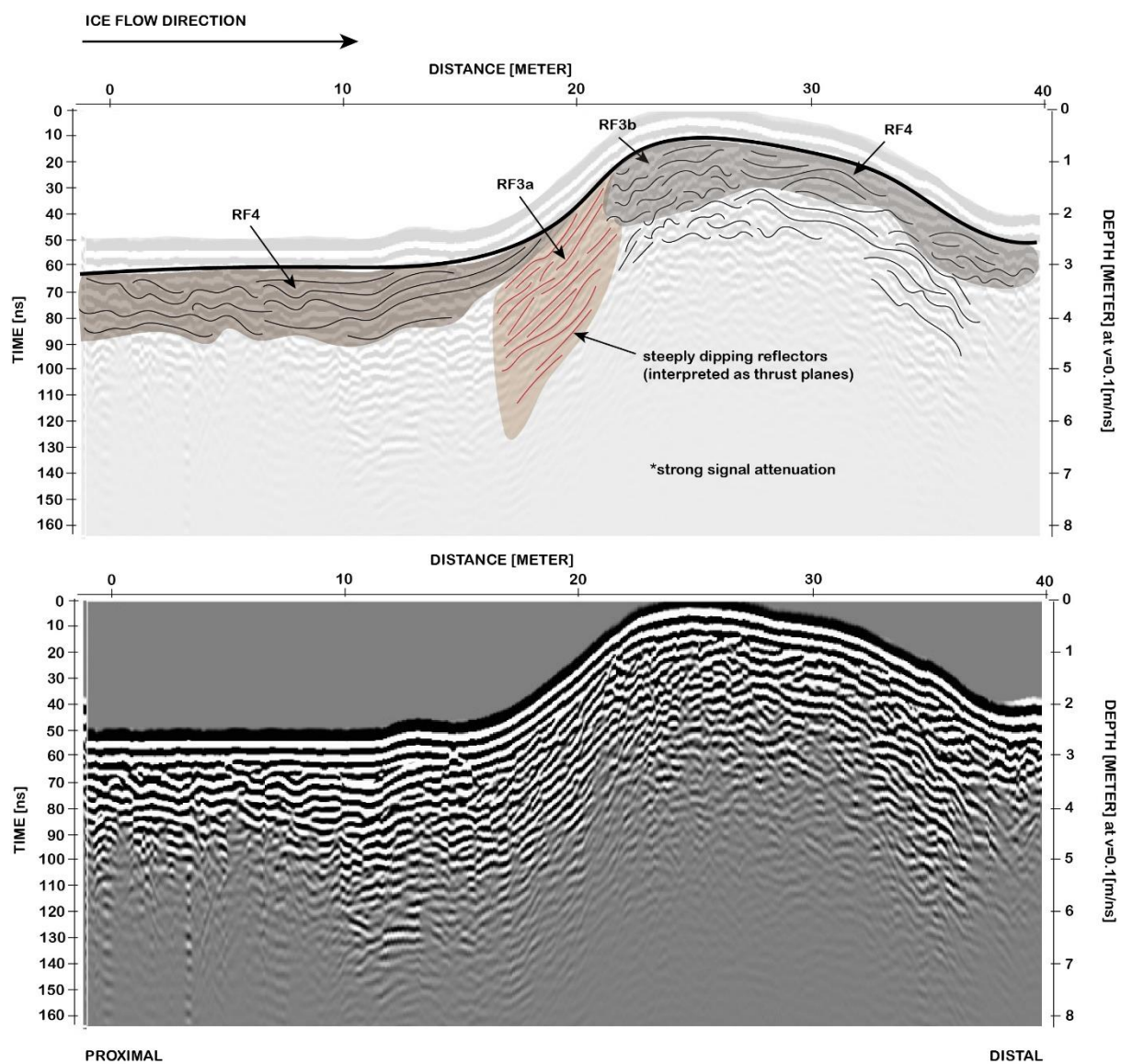


FIGURE 3. Location 1, UT1 GPR Radargram #1.

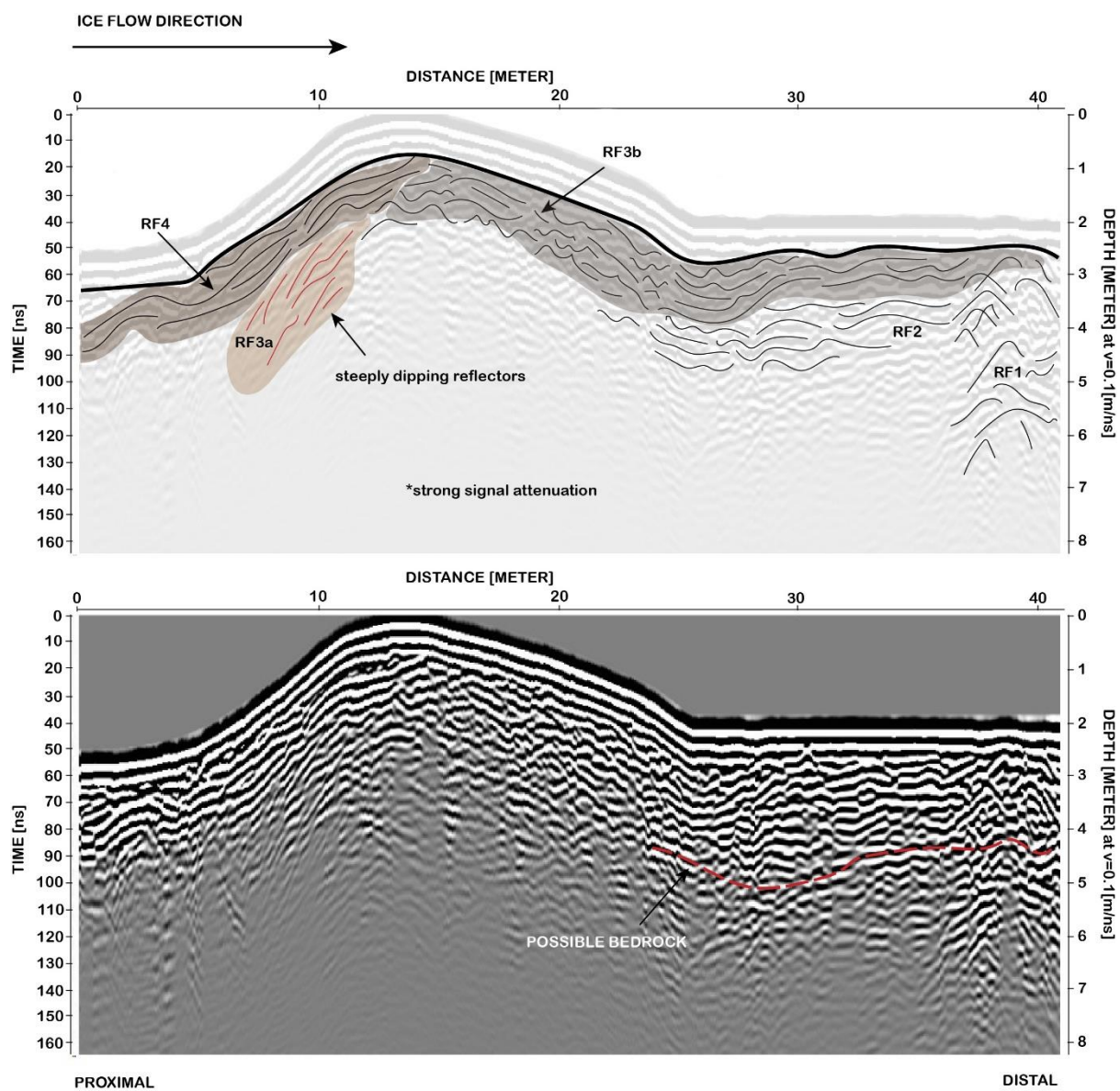


FIGURE 4. Location 1, UT1 GPR Radargram #2.

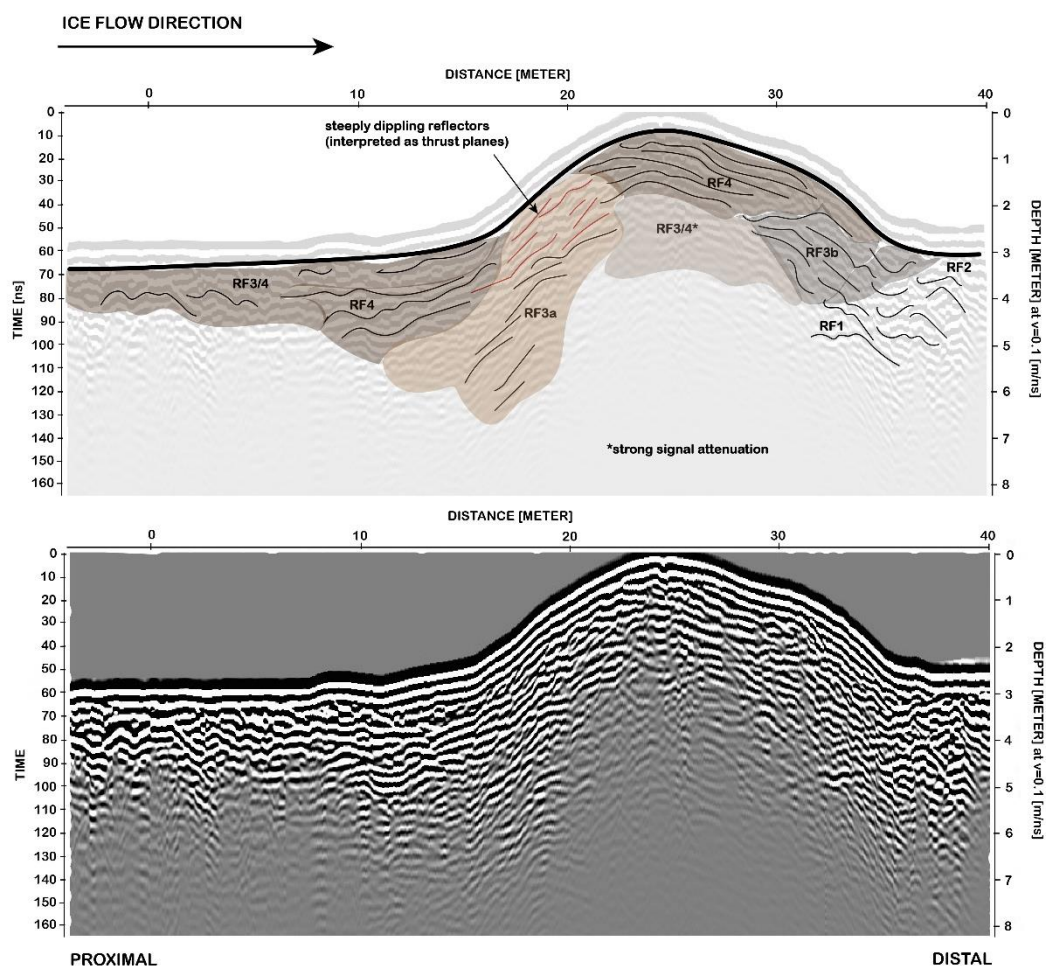


FIGURE 5. Location 1, UT1 GPR Radargram #3.

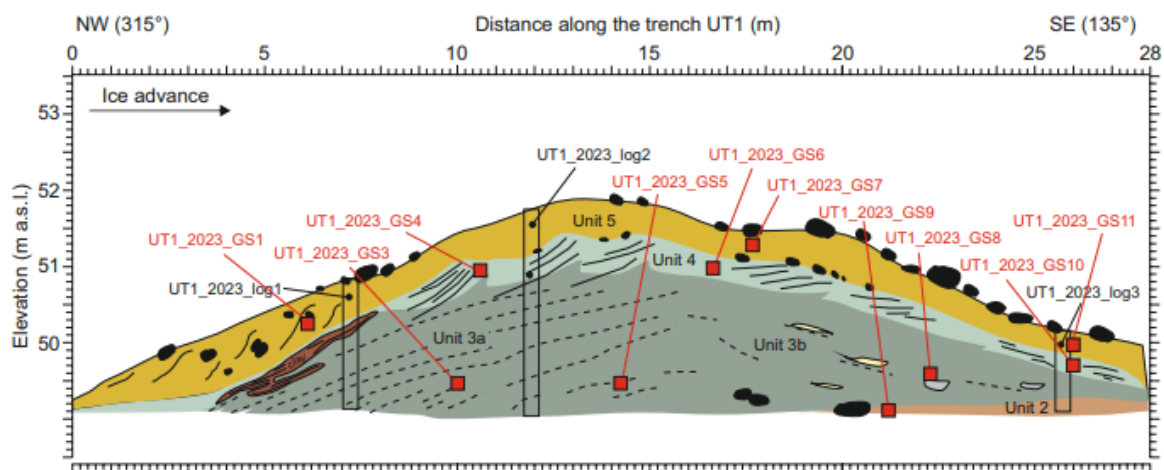
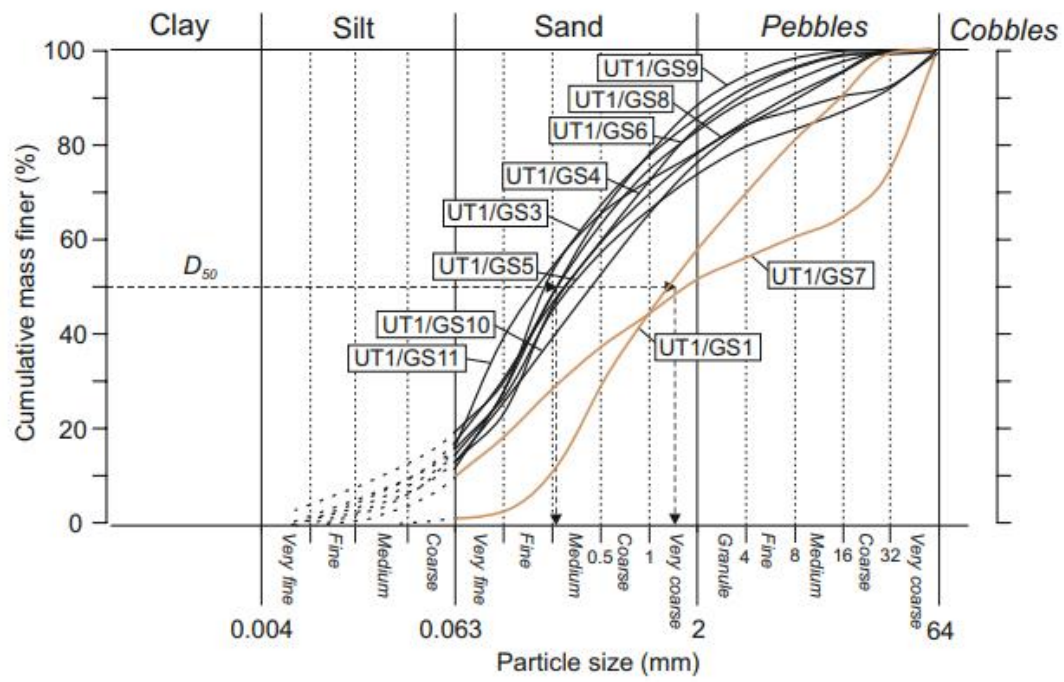
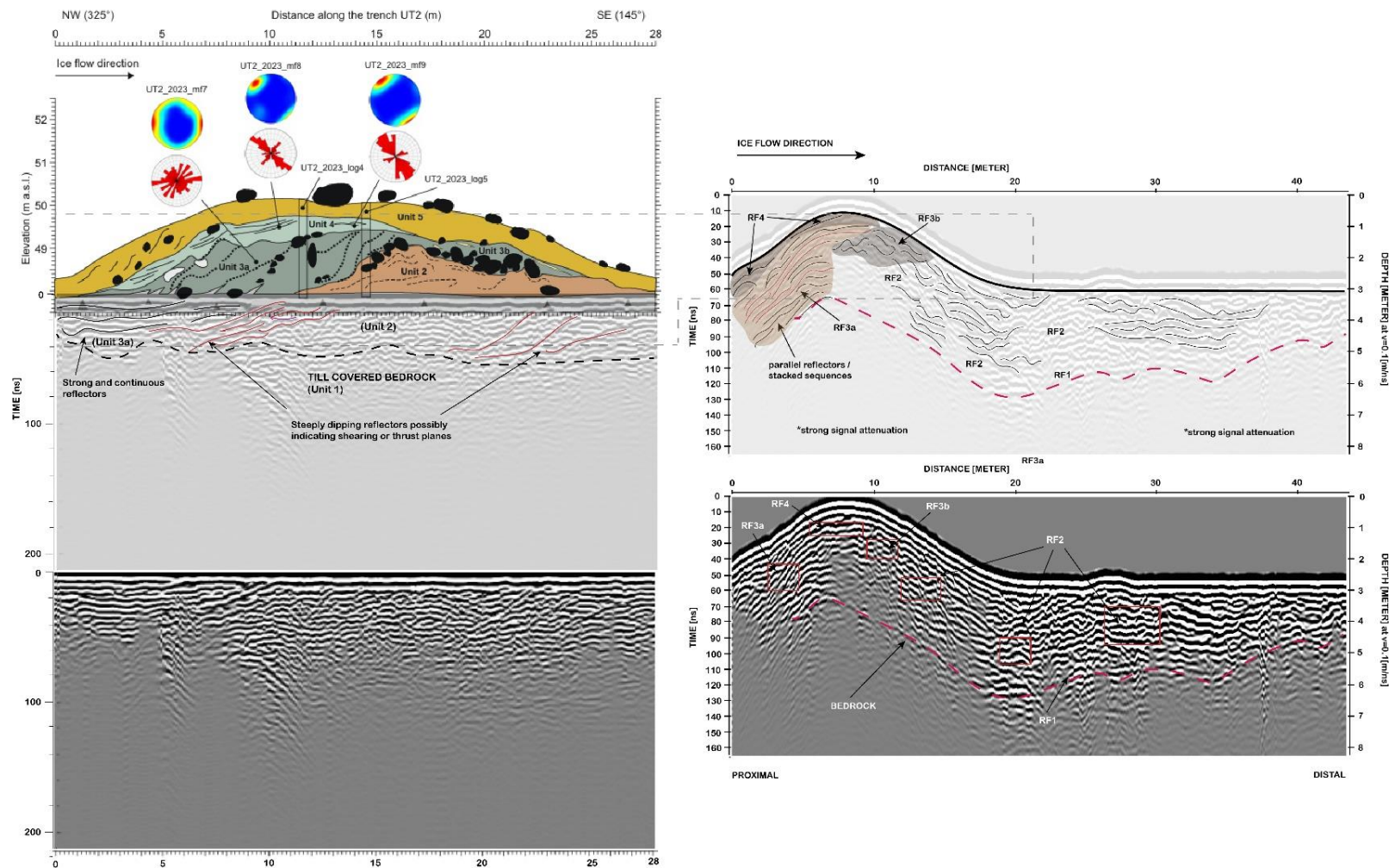


FIGURE 6. Trench locations of grain size curves for location 1, UT1.



**FIGURE 7.** Grain size curves for location 1 UT1. Diamicton curves shown in black. Sand and gravel curves shown in brown.





**FIGURE 8.** Correlation between excavated sediment exposure and neighbouring GPR profile #1 at Site (1) UT2 (see Supplementary FIGURE 8). Comparisons with UT1 show the same lithofacies in the same order within the exposure. This is reflected in the radar facies TABLE 1, presented in the main manuscript.

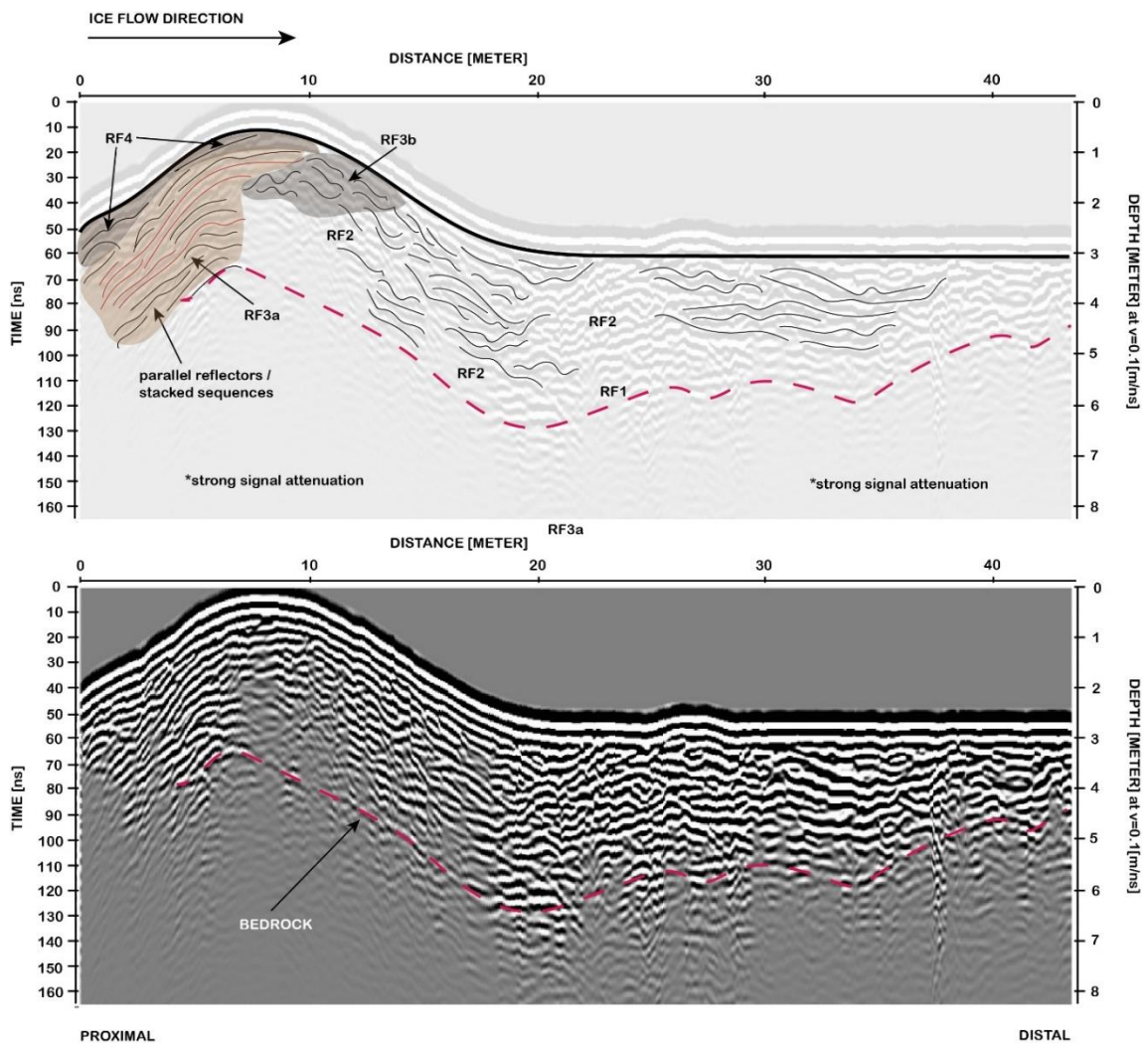


FIGURE 9. Location 1, UT2 GPR Radargram #1.

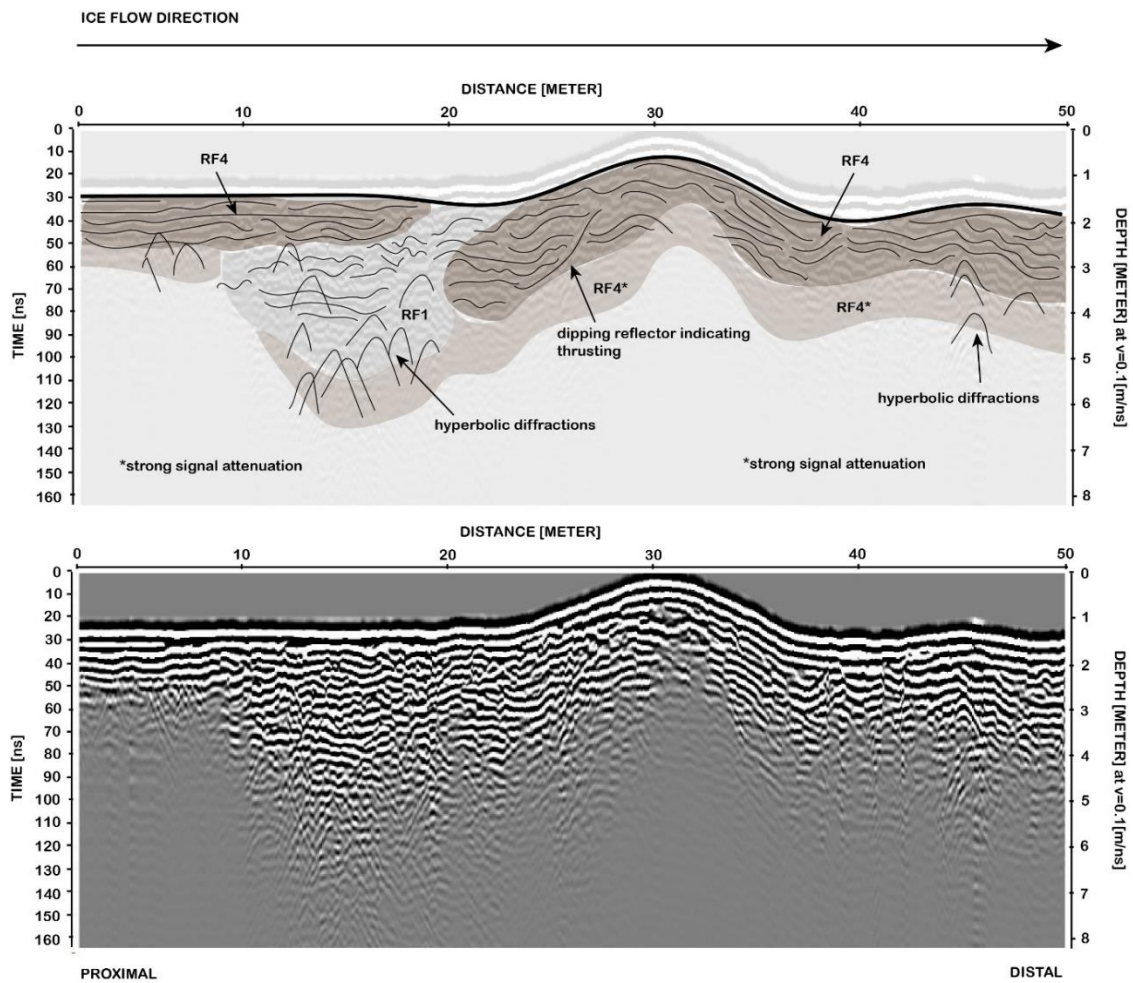


FIGURE 10. Location 1, UT2 GPR Radargram #2



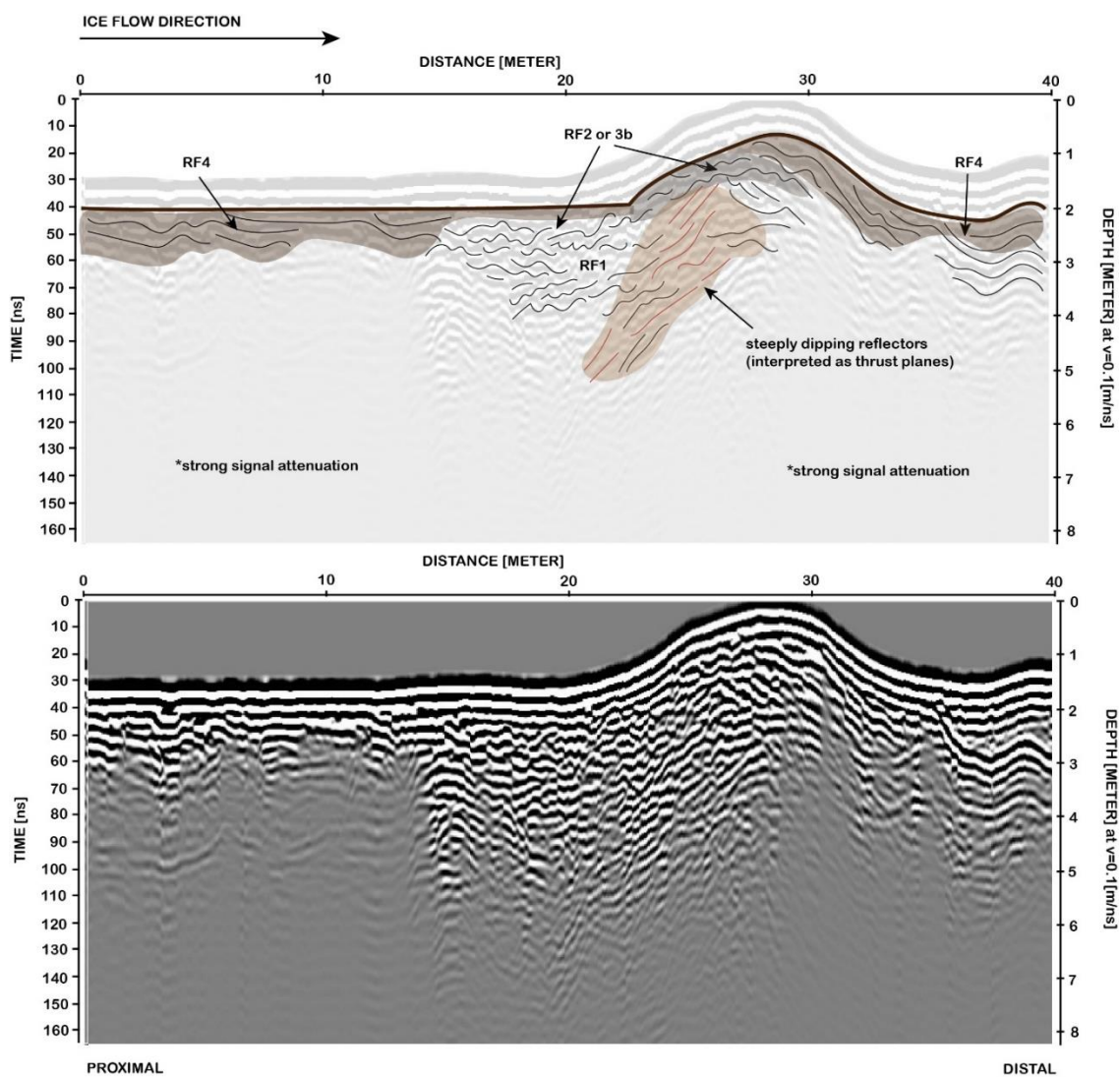


FIGURE 11. Location 1, UT2 GPR Radargram #3.

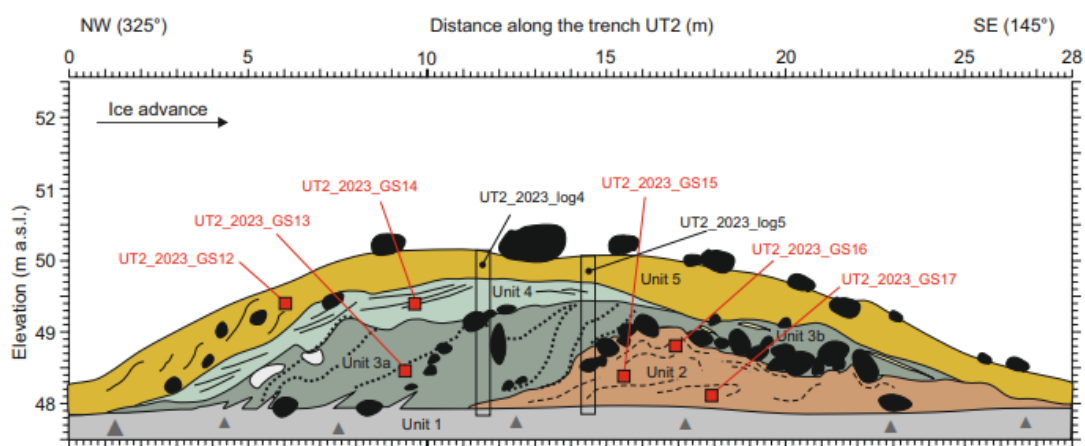


FIGURE 12. Trench locations of grain size curves for location 1 UT2.



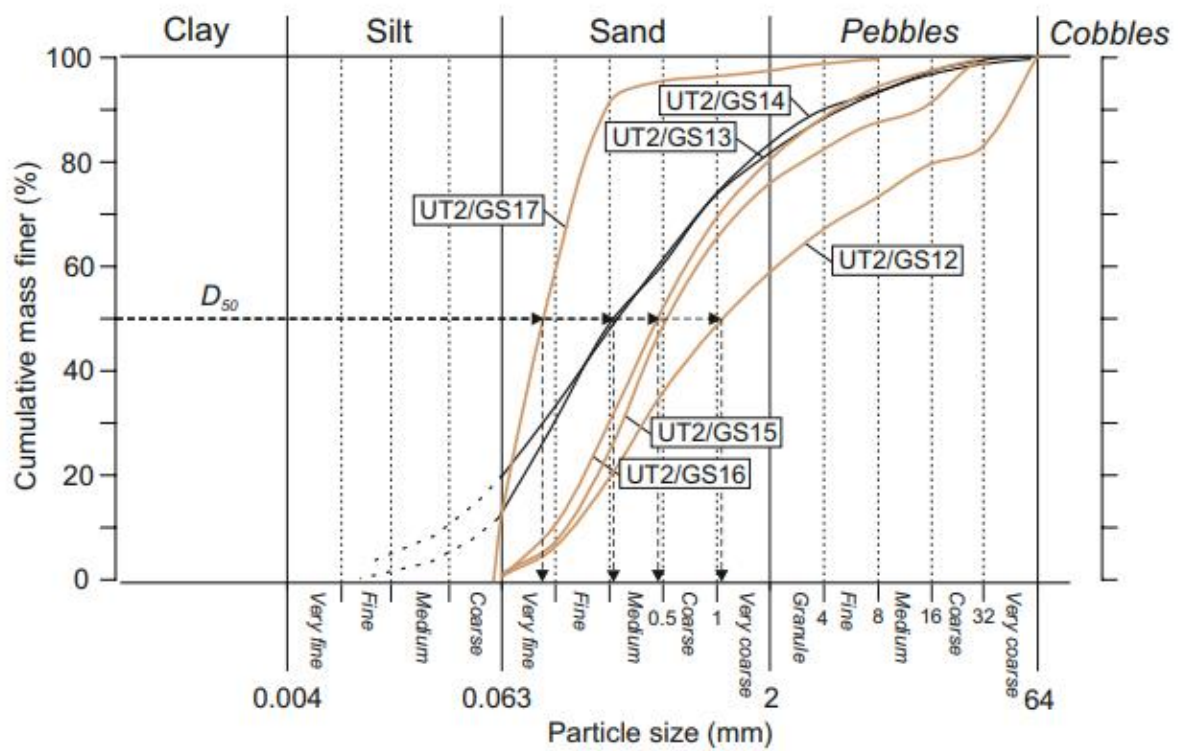


FIGURE 13. Grain size curves for location 1 UT2. Diamicton curves shown in black. Sand and gravel curves shown in brown.

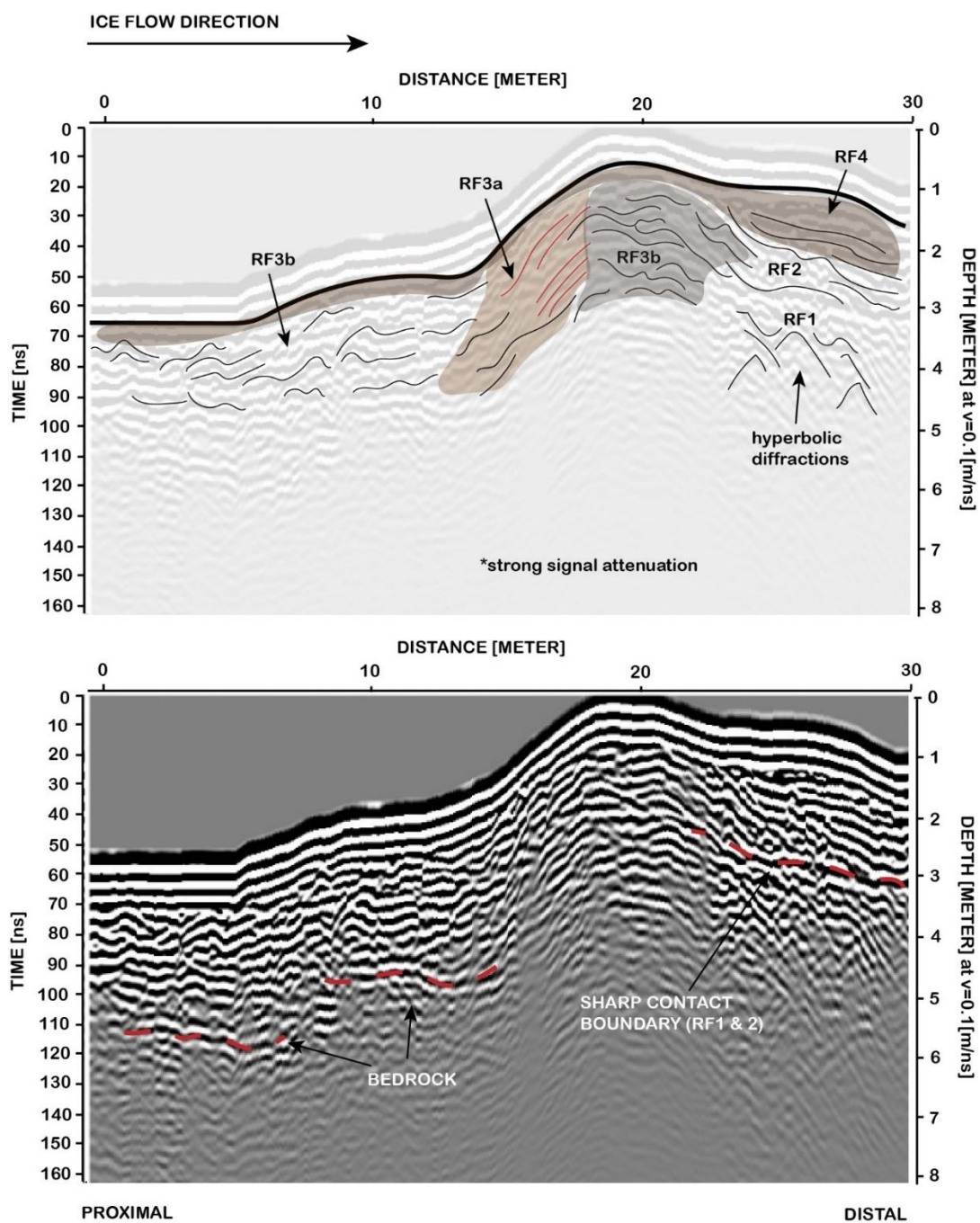


FIGURE 14. Location 2, GPR Radargram #2.

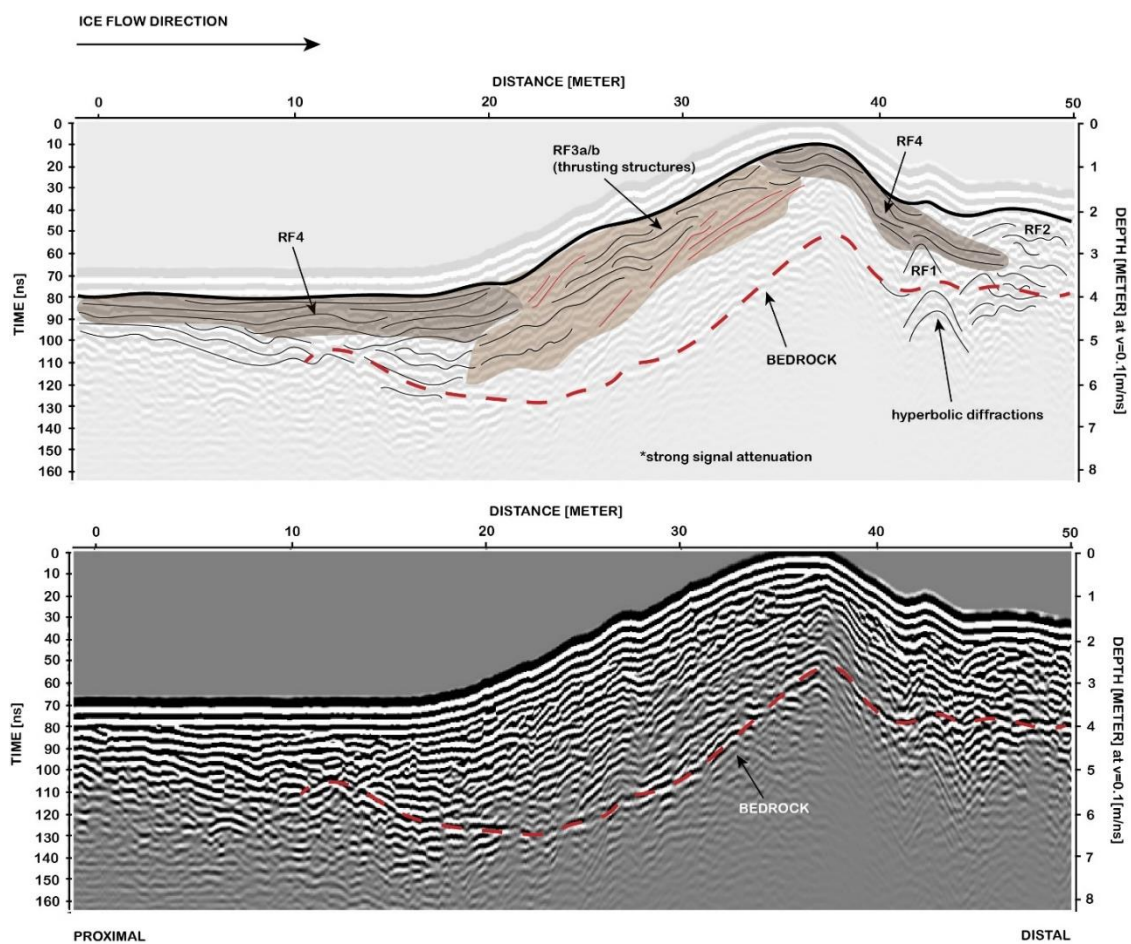


FIGURE 15. Location 2, GPR Radargram #3.

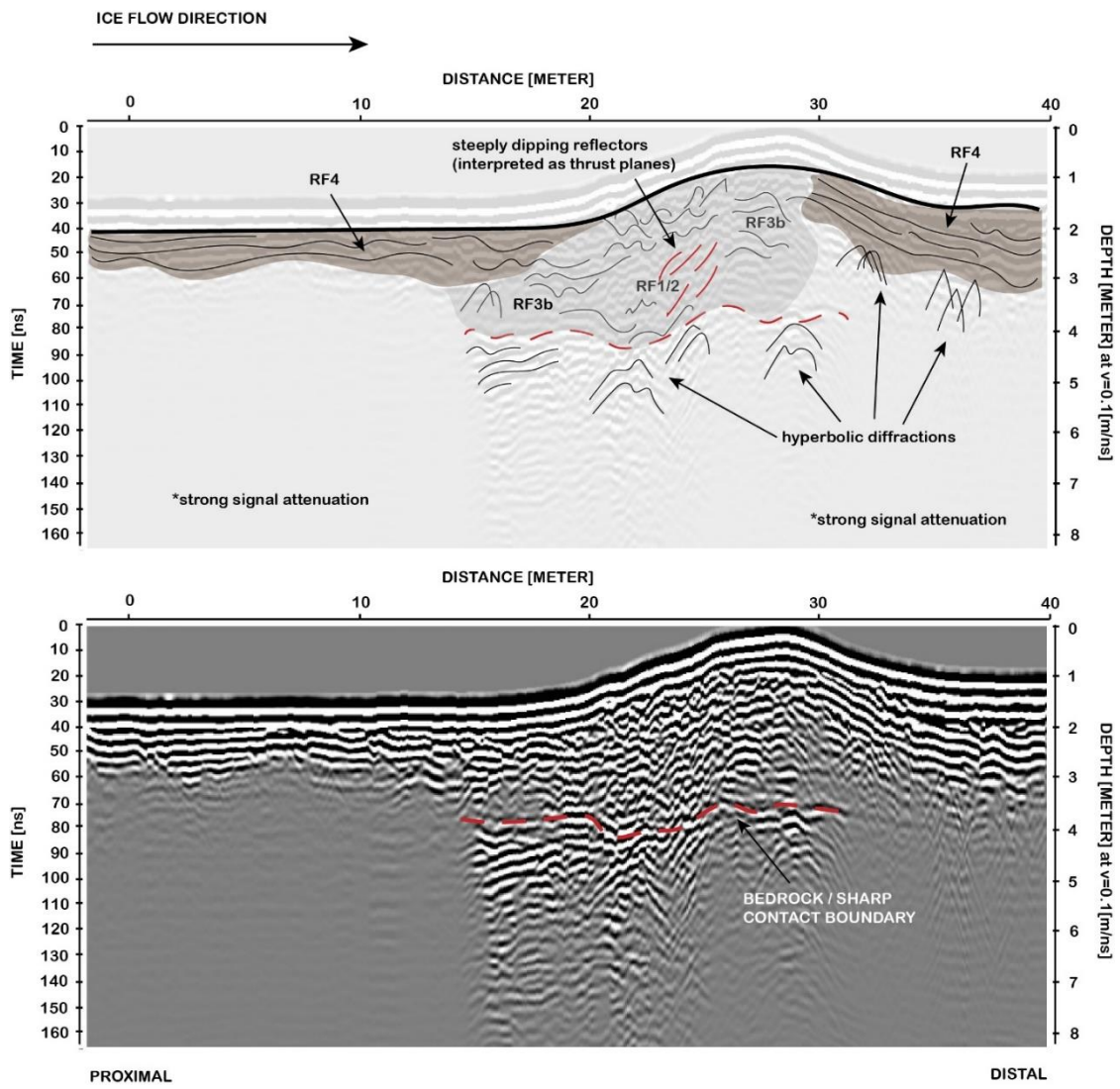


FIGURE 16. Location 3, GPR Radargram #2.



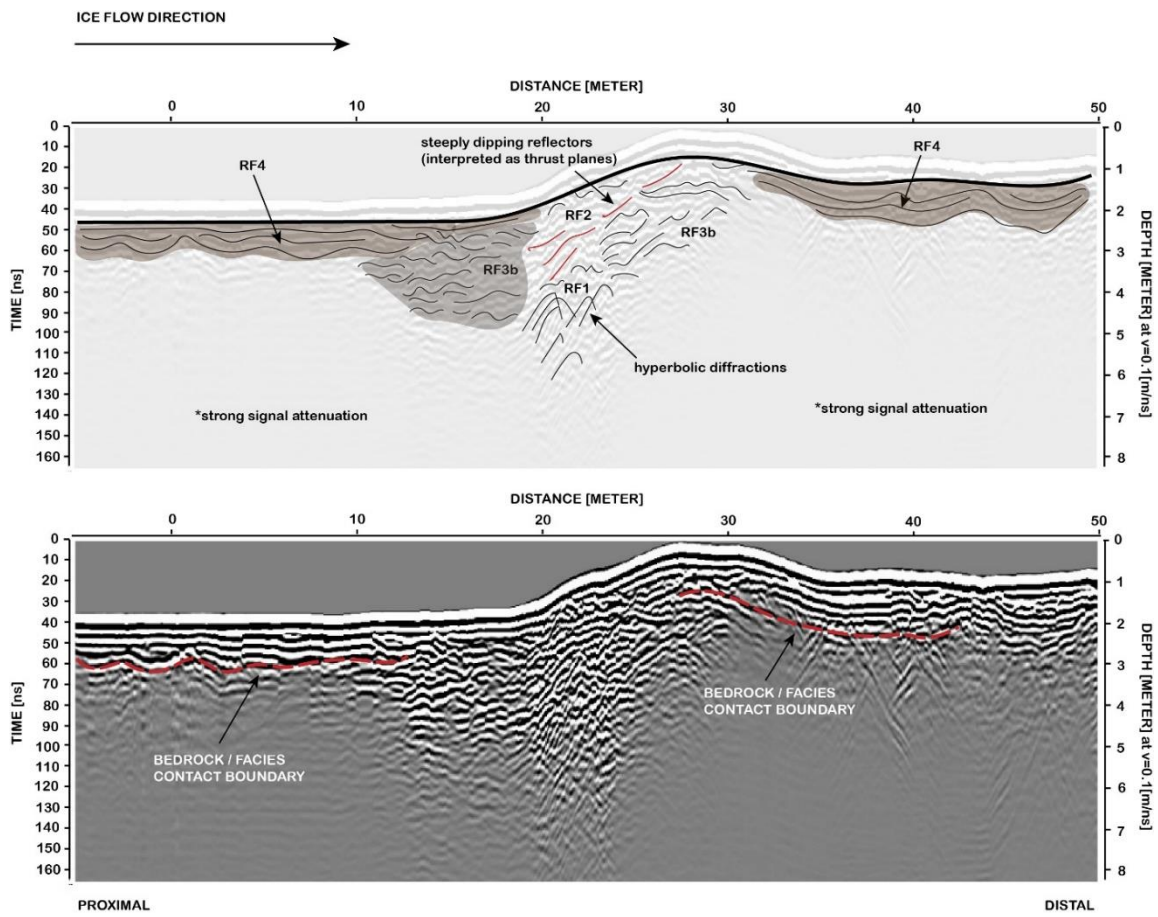


FIGURE 17. Location 3, GPR Radargram #3.

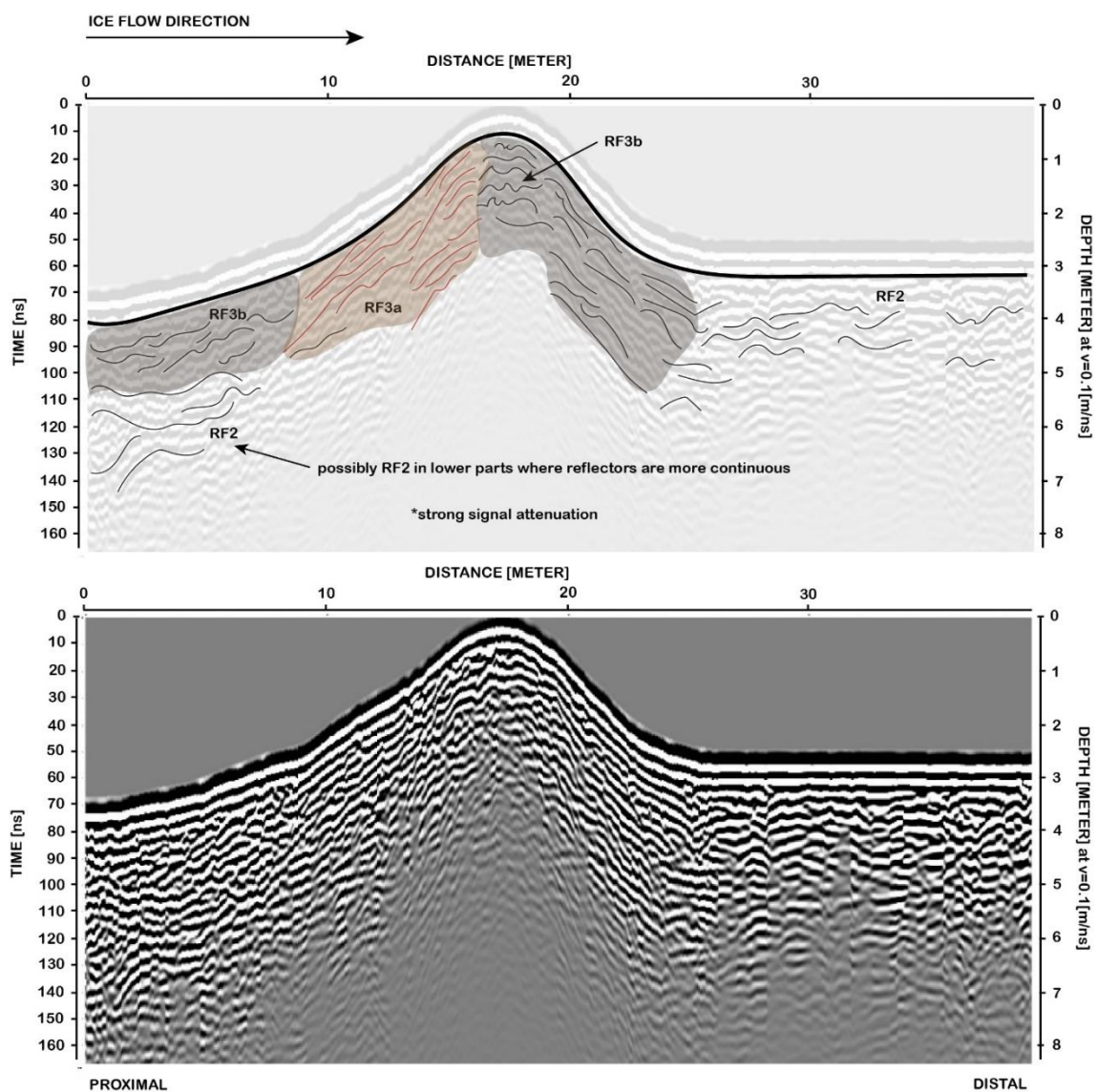


FIGURE 18. Location 4, GPR Radargram #2.

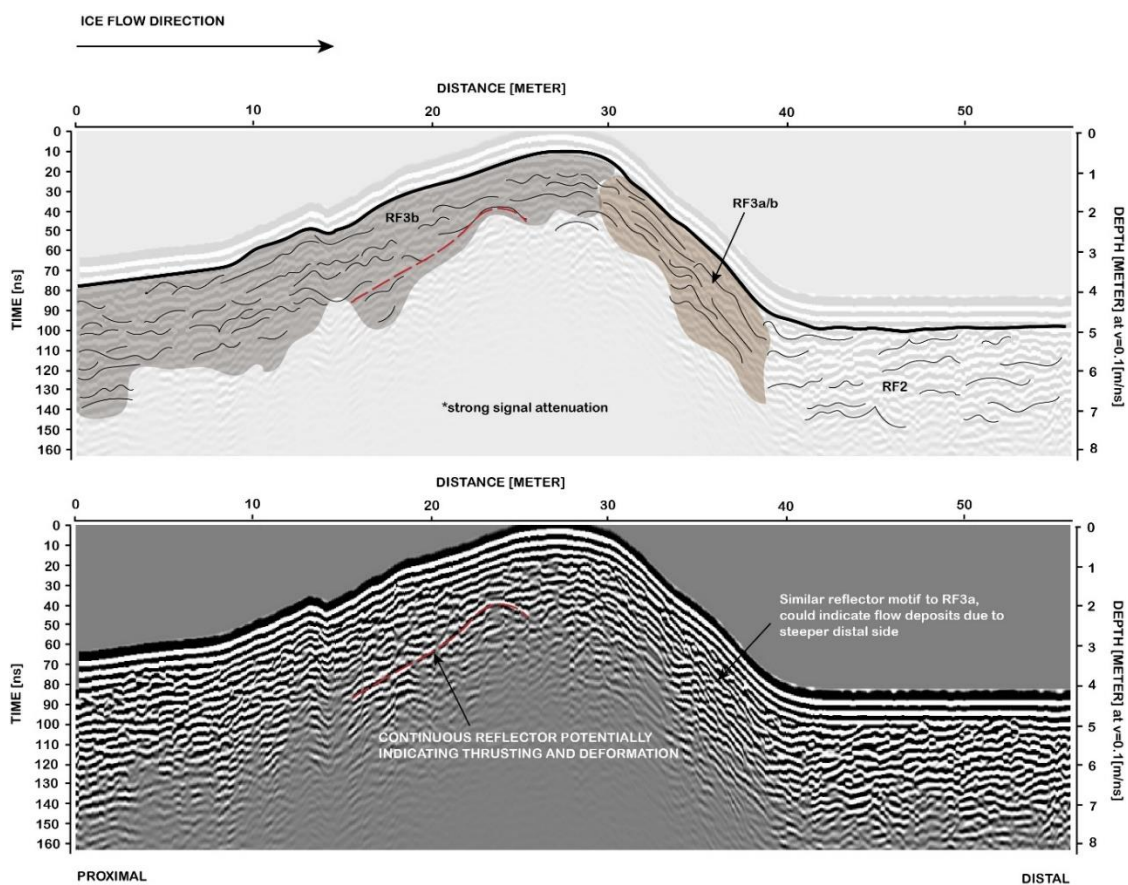


FIGURE 19. Location 4, GPR Radargram #3.

**TABLE 1.** Presenting quantified annual resolution data and descriptive statistics (total (retreat distance only), % change between successive segments in direction of deglaciation, minimum, maximum, median, mean, standard deviation and variance) for retreat distance (m/yr), water depth (m), 20-yr avg. temperature NGRIP (°C), slope (°), and elevation (m), across segments A-E as defined in FIGURE 7.5 (chapter 7).

**RETREAT DISTANCE (m/y**

	TOTAL	CHANGE (%)	MIN	MAX	MED	MEAN	STD. DEV.	VAR
<b>A: 11 615 – 11 531</b>	22 384	-	75	470	274	263.34	91.76	8 420.37
<b>B: 11 530 – 11 350</b>	32 042	-40.15	52	910	164	178.01	87.25	7 611.77
<b>C: 11 349 – 11 150</b>	71 843	101.83	92	1221	331	361.02	182.65	33 361.14
<b>D: 11 149 – 11 000</b>	57 859	-16.62	54	1509	276	388.32	297.85	88 717.02
<b>E: 10 999 – 10 901</b>	76 084	125	191	2773	621	768.53	467.08	218 163



WATER DEPTH (m)

	CHANGE (%)	MIN	MAX	MED	MEAN	STD. DEV.	VAR
A: 11 615 – 11 531	-	118.39	126.36	123.09	122.64	2.64	6.96
B: 11 530 – 11 350	-4.1	117.16	119.66	118.04	118.19	0.78	0.61
C: 11 349 – 11 150	7.64	118.99	136.23	127.07	126.39	4.56	20.78
D: 11 149 – 11 000	12.97	136.49	148.58	143.55	143.57	3.32	11.01
E: 10 999 – 10 901	10.27	148.68	166.99	158.28	157.50	5.11	26.14

TEMP 20-YR AVG. (°C)

	CHANGE (%)	MIN	MAX	MED	MEAN	STD. DEV.	VAR
A: 11 615 – 11 531	-	-3.56	-3.22	-3.29	-3.34	0.14	0.02
B: 11 530 – 11 350	-23.71	-4.48	-3.22	-4.07	-3.87	0.49	0.24
C: 11 349 – 11 150	50	-3.34	-1.74	-2.04	-2.16	0.46	0.21
D: 11 149 – 11 000	22.36	-2.11	-1.36	-1.58	-1.67	0.26	0.07
E: 10 999 – 10 901	13.92	-1.72	-1.01	-1.36	-1.33	0.21	0.04

SLOPE (°)

	CHANGE (%)	MIN	MAX	MED	MEAN	STD. DEV.	VAR
A: 11 615 – 11 531	-	0.01	1.50	0.21	0.31	0.32	0.1
B: 11 530 – 11 350	12.07	0	3.11	0.23	0.40	0.46	0.21
C: 11 349 – 11 150	-38.61	0	1.82	0.14	0.23	0.25	0.06
D: 11 149 – 11 000	-23.19	0	1.95	0.11	0.18	0.22	0.05
E: 10 999 – 10 901	26.67	0	1.2	0.14	0.17	0.17	0.03

ELEVATION (m)

	CHANGE (%)	MIN	MAX	MED	MEAN	STD. DEV.	VAR
A: 11 615 – 11 531	-	44.06	75.25	61.41	59.71	8.15	66.36
B: 11 530 – 11 350	-3.42	21.87	78.14	59.31	58.59	12.54	157.31
C: 11 349 – 11 150	-1.8	44.93	73.75	58.24	58.37	5.4	29.12
D: 11 149 – 11 000	-7.36	38.86	71.93	53.96	52.24	8.38	70.12
E: 10 999 – 10 901	-49.33	13.72	44.33	27.34	27.24	8.69	75.51

*ATTACHMENT 1. Ethics approval*

**Using transverse ridge morphometry to understand ice sheets in high spatiotemporal resolution.**

**Ethics Review ID:** ER38260011

**Workflow Status:** Application Approved

**Type of Ethics Review Template:** No human participants, human tissue or personal data

**Primary Researcher / Principal Investigator**

---

Gwyneth Rivers  
(Faculty of Social Sciences and Humanities)

**Converis Project Application:**

**Q1. Is this project ii) Doctoral research**

**Director of Studies**

---

Robert Storrar  
(Faculty of Social Sciences and Humanities)

**Supervisory Team**

---

Naomi Holmes  
(Natural and Built Environment)